PACIFIC EARTHQUAKE ENGINEERING RESEARCH CENTER

NGA Model for Average Horizontal Component of Peak Ground Motion and Response Spectra

Brian S.-J. Chiou
California Department of Transportation

and

Robert R. Youngs
AMEC Geomatrix

PEER 2008/09
NOVEMBER 2008

NGA Model for Average Horizontal Component of Peak Ground Motion and Response Spectra

Brian S.-J. Chiou
California Department of Transportation
Sacramento, California

and

Robert R. Youngs
AMEC Geomatrix
Oakland, California

PEER Report 2008/09
Pacific Engineering Research Center
College of Engineering
University of California, Berkeley

November 2008

ABSTRACT

We present a model for estimating horizontal ground motion amplitudes caused by shallow crustal earthquakes occurring in active tectonic environments. The model provides predictive relationships for the orientation-independent average horizontal component of ground motions. Relationships are provided for peak acceleration, peak velocity, and 5-percent damped pseudo-spectral acceleration for spectral periods of 0.01–10 sec. The model represents an update of the relationships developed by Sadigh et al. (1997) and includes improved magnitude and distance scaling forms as well as hanging-wall effects. Site effects are represented by smooth functions of average shear-wave velocity of the upper 30 m (V_{S30}) and sediment depth. The new model predicts median ground motion that is similar to Sadigh et al. (1997) at short spectral periods, but lower ground motions at longer periods. The new model produces slightly lower ground motions in the distance range of 10–50 km and larger ground motions at larger distances. The aleatory variability in ground motion amplitude was found to depend on earthquake magnitude and on the degree of nonlinear soil response. For large-magnitude earthquakes, the aleatory variability is larger than found by Sadigh et al. (1997).

ACKNOWLEDGMENTS

This study was sponsored by the Pacific Earthquake Engineering Research (PEER) Center's Program of Applied Earthquake Engineering Research of Lifelines Systems supported by the California Department of Transportation, the California Energy Commission, and the Pacific Gas and Electric Company.

This work made use of the Earthquake Engineering Research Centers Shared Facilities supported by the National Science Foundation under award number EEC-9701568 through the Pacific Earthquake Engineering Research Center. Any opinions, findings, and conclusions or recommendations expressed in this material are those of the authors and do not necessarily reflect those of the National Science Foundation.

We would like to thank all of the members of the PEER-NGA project for many enlightening interactions. We would also like to thank Steve Day, Walt Silva, and Paul Somerville for providing us with ground motion simulation results that helped us in formulating our model. Some of the graphics in this report were prepared using R (R Development Core Team 2006).

CONTENTS

ABSTRACT ..... **iii**
ACKNOWLEDGMENTS ..... **iv**
TABLE OF CONTENTS ..... **v**
LIST OF FIGURES ..... **ix**
LIST OF TABLES ..... **xv**
1 INTRODUCTION **1**
2 EMPIRICAL DATABASE **3**
2.1 Supplemental Metadata 3
2.1.1 Focal Depth, Fault Strike, Fault Dip, and Rake 3
2.1.2 Rupture Distances and Source-Site Geometry 6
2.1.3 Site Average Shear-Wave Velocity 7
2.1.4 Sediment Thickness 9
2.2 Data Selection 11
2.3 Supplemental Strong-Motion Data 16
3 MODEL FORMULATION **17**
3.1 Seismic Source Scaling 17
3.1.1 Effect of Earthquake Size 17
3.1.2 Style of Faulting Effects 21
3.1.3 Other Source Effects 22
3.2 Distance Scaling 23
3.2.1 Near-Source Distance Scaling 24
3.2.2 Distance Scaling at Large Distances 28
3.2.3 Formulation for Distance Attenuation 30
3.2.4 Data Truncation and Estimate of γ 32
3.2.5 Magnitude Dependence of γ 35
3.3 Hanging-Wall Effects 37
3.4 Site Effects 43
3.4.1 Near-Surface Geology 43
3.4.2 Sediment Thickness 51

3.4.2.1 Deep Sediment Sites 51
3.4.2.2 Shallow Sediment Sites 52
3.5 Complete Model for Estimating Ground Motions 53

4 MIXED-EFFECTS MODEL FORMULATION AND VARIANCE MODEL INCORPORATING NONLINEAR SOIL RESPONSE 55

5 MODEL DEVELOPMENT 59

5.1 Estimation of Fixed-Effects Coefficients 59
5.2 Variance Model 64
5.3 Approximate Method for Calculation of Total Variance 66

6 MODEL RESULTS 69

6.1 Inter-Event Residuals 69
6.2 Intra-Event Residuals 70
6.3 Comparisons with Data for Individual Earthquakes 73
6.4 Nonlinear Soil Amplification 73
6.5 Comparison with Previous Model 77

7 EXAMPLE CALCULATIONS 85

8 MODEL APPLICABILITY 89

REFERENCES 91

APPENDIX A: RECORDINGS FROM PEER-NGA FLATFILE VERSION 7.2 USED IN DEVELOPING CHIOU AND YOUNGS'S 2008 EMPIRICAL GROUND MOTION MODEL

APPENDIX B: ESTIMATION OF DISTANCE AND GEOMETRY MEASURES FOR EARTHQUAKES WITHOUT FINITE RUPTURE MODELS

APPENDIX C: ESTIMATION OF V_{S30} AT CWB'S FREE-FIELD SITES

APPENDIX D: SHAKEMAP DATA

APPENDIX E: INDIVIDUAL EARTHQUAKE FITS FOR CHIOU AND YOUNGS'S (2008) GROUND MOTION MODEL

APPENDIX F: MODEL SAO2006—UPDATE OF ATTENUATION MODEL OF SADIGH AND OTHERS (1997), USING PEER-NGA DATASET OF CHIOU AND YOUNGS (2006)

APPENDIX G: RESPONSE TO QUESTIONS BY U.S. GEOLOGICAL SURVEY (USGS) AND CALIFORNIA GEOLOGICAL SURVEY (CGS)

APPENDIX H: FULL SET OF MODEL COEFFICIENTS

LIST OF FIGURES

Fig. 2.1 Ratio of estimated values of R_{JB} and R_{RUP} to R_{EPI} and R_{HYP} for recordings from earthquakes without finite fault models in PEER-NGA database. 7

Fig. 2.2 V_{S30}-magnitude-region distribution of PEER-NGA recordings. Closed symbols indicate measured values, open symbols inferred values. NEHRP site classes indicated along bottom edge. 8

Fig. 2.3 V_{S30}-distance-region distribution of PEER-NGA recordings. Closed symbols indicate measured values, open symbols inferred values. NEHRP site classes indicated along bottom edge. 9

Fig. 2.4 Comparison of $Z_{1.0}$ values from Versions 2 and 4 of SCEC 3-D velocity model 10

Fig. 2.5 Relationship between measured $Z_{1.0}$ and V_{S30} for sites contained in PEER-NGA database. Solid curve is relation used to infer values of missing $Z_{1.0}$ data. 11

Fig. 2.6 (a) Magnitude-distance-region distribution of selected recordings. (b) V_{S30}-magnitude-region distribution of selected recordings. V_{S30} velocity ranges for NEHRP site classes indicated by vertical dashed lines. 15

Fig. 2.7 Reduction of number of usable data as a function of spectral period. 16

Fig. 3.1 Magnitude scaling of pseudo-spectral acceleration at distance of 30 km computed using (a) Sadigh et al. (1997) and (b) stochastic ground motion model, and Atkinson and Silva (1997) source model for California earthquakes. 18

Fig. 3.2 Magnitude scaling predicted by seismic source model of Atkinson and Silva (2000) and the result of fitting Eq. (3.2) to predicted data 19

Fig. 3.3 Peak acceleration data from PEER-NGA database and from ShakeMap (Appendix D) for distance range $30 \le R_{RUP} \le 50$ and velocity range $300 \le V_{S30} \le 400$ fit by alternative function forms of magnitude scaling. 20

Fig. 3.4 Effect of source depth on inter-event residuals. (a) *pga* data fit without Z_{TOR} scaling, (b) *pga* data fit with Z_{TOR} scaling, (c) reduction in inter-event standard error resulting from including Z_{TOR} scaling 23

Fig. 3.5 Illustration of functional forms used to capture magnitude dependence of distance attenuation for distances less than 100 km. All plots are for rupture distance to a vertical strike-slip fault rupturing the surface. Values for Campbell and Bozorgnia (2003) computed using a minimum R_{SEIS} of 3 km. 25

Fig. 3.6 Plots of the instantaneous slope of attenuation curve for the four ground motion models shown in Fig. 3.5. Attenuation rate defined as $\partial \ln(pga) / \partial \ln(R)$ 26
Fig. 3.7 Plots of magnitude scaling at a range of distances produced by form of the attenuation curve for the four ground motion models shown in Fig. 3.5. Magnitude scaling defined as $\partial \ln(pga) / \partial \mathbf{M}$ 27
Fig. 3.8 Coefficients resulting from fits of Eqs. (3.5a), (3.5b), and (3.5c) to the broadband data for earthquakes 0163, 0167, and 0170. T is spectral period in sec. 32
Fig. 3.9 Comparison of fits to expanded data sets and PEER-NGA data only for individual earthquakes using truncated regression. Truncation levels are indicated by horizontal dashed lines for the enhanced and the PEER-NGA only data sets. Hanging-wall sites not included in fits for Northridge. 35
Fig. 3.10 Estimates of γ for individual earthquakes and model fit to California earthquake data. .....
Fig. 3.11 Comparison of the model developed for γ (Eqs. 3.6a–b) versus values of γ obtained from regression without truncation of the PEER-NGA data set. 37
Fig. 3.12 Definition of variable R_X. 39
Fig. 3.13 Map view of example fault rupture. 40
Fig. 3.14 Variation of the term $[1 - R_{JB} / R_{RUP}]$ with location for the three lines shown in Fig. 3.13. Top of rupture is at the ground surface at x=0. 40
Fig. 3.15 Intra-event residuals from fitting a model without a hanging-wall term for sites with R_{JB} = 0 and F_{HW} = 1 plotted against fault dip, δ. 42
Fig. 3.16 Illustration of the hanging-wall geometric factor f_{HW} for sites located directly above or down dip of rupture plane. Left plots are for **M** 5, 6, and 7 earthquakes with Z_{TOR} = 0. Right plots are for **M** 5, 6, and 7 earthquakes with Z_{TOR} = 5 km. Note that locations of the bottom edges of ruptures correspond with peaks in f_{HW} curves. 43
Fig. 3.17 Illustration of functional form for soil amplification effect as a function of $\ln(y_{ref})$. 46
Fig. 3.18 Example site amplification as a function of spectral period, V_{S30}, and level of reference *PSA* 46
Fig. 3.19 Soil amplification for *pga* as a function of rock motion (y_{ref}) from 1-D equivalent linear site response analyses (Silva 2008). 47

Fig. 3.20 Coefficients a and b derived from 1-D site response results of Silva (2008). Dashed lines represent fits using functional form in Eq. (3.9).. 47
Fig. 3.21 Comparison of parameter b dependence on V_{S30} obtained by Choi and Stewart (2003) (Abrahamson and Silva, 1997, reference motions; Sadigh et al., 1997, reference motions) with trend obtained in this study from PEER-NGA data 48
Fig. 3.22 Intra-event residuals plotted as a function of V_{S30}. These residuals are computed using final NGA model without the soil amplification effect. Square and triangle indicate data whose V_{S30} is measured and inferred, respectively. Dot-dashed curve is predicted nonlinear soil amplification factor and solid line is predicted linear amplification factor. Range of reference motion ($y_{ref}\ exp(\eta)$) indicated in lower left corner of each plot. 49
Fig. 3.23 Intra-event residuals plotted against measured $Z_{1.0}$ for 0.01-sec and 1.0-sec PSA. Dashed lines show fits to the residuals using Eq. (3.10). 52
Fig. 3.24 Intra-event residuals plotted against $Z_{1.0}$ for shallow sediment sites for spectral periods of 0.01, 0.10, 0.6, and 6.0 sec. Dashed lines show fits to the residuals using Eq. (3.11).....53
Fig. 4.1 Illustration showing framework of rock surface motion, soil amplification, and soil surface motion, assuming ε_S has the same probability density function for rock and soil surface motions. 56
Fig. 4.2 Intra-event residuals for 0.1-sec PSA plotted against the variance covariate ($1+NL$). Solid squares are bin estimates of standard deviation; dashed lines show fitted variance function. 58
Fig. 5.1 Variation of coefficient c_1 with spectral period. Solid curve is c_1 after bias adjustment. 63
Fig. 5.2 Variation of the derivative of coefficient c_1 with respect to spectral period. Solid curve is smoothed derivative. 63
Fig. 6.1 Main shock inter-event residuals for spectral periods of 0.01 sec (pga), 0.2, 1.0, and 3.0 sec. 70
Fig. 6.2 Intra-event residuals for spectral period of 0.01 sec (pga) plotted against **M**, R_{RUP}, V_{S30}, and y_{ref}. 70
Fig. 6.3 Intra-event residuals for spectral period of 0.2 sec plotted against **M**, R_{RUP}, V_{S30}, and y_{ref}. 71

Fig. 6.4 Intra-event residuals for spectral period of 1.0 sec plotted against **M**, R_{RUP}, V_{S30}, and y_{ref}. 71
Fig. 6.5 Intra-event residuals for spectral period of 3.0 sec plotted against **M**, R_{RUP}, V_{S30}, and y_{ref}. 72
Fig. 6.6 Intra-event residuals for *pga* for the 1994 Northridge, 1998 San Juan Bautista, 1999 Hector Mines, 2000 Yountville, 2001 Mohawk Valley, 2001 Anza, 2002 Baja, 2002 Gilroy, 2002 Yorba Linda, and 2003 Big Bear City earthquakes. 73
Fig. 6.7a Nonlinear soil amplification factor predicted by ground motion model developed in this study compared to those obtained by (a) Silva (2008) and (b) Choi and Stewart, for spectral period of 0.01 sec (*pga*)....74
Fig. 6.7b Nonlinear soil amplification predicted by ground motion model developed in this study compared to those obtained by (a) Silva (2008) and (b) Choi and Stewart, for spectral period of 0.2 sec....75
Fig, 6.7c Nonlinear soil amplification predicted by ground motion model developed in this study compared to those obtained by (a) Silva (2008) and (b) Choi and Stewart, for spectral period of 1.0 sec....76
Fig. 6.7d Nonlinear soil amplification predicted by ground motion model developed in this study compared to those obtained by (a) Silva (2008) and (b) Choi and Stewart, for spectral period of 3.0 sec....77
Fig. 6.8 Magnitude and distance scaling predicted by the model developed in this study and predicted by Sadigh et al. (1997) for horizontal distance from a vertical strike-slip fault and soft rock sites (V_{S30} = 520 m/s). 79
Fig. 6.9 Magnitude and distance scaling predicted by the model developed in this study and predicted by Sadigh et al. (1997) for horizontal distance from a vertical strike-slip fault and firm soil sites (V_{S30} = 310 m/s). 80
Fig. 6.10 Magnitude and distance scaling predicted by the model developed in this study and predicted by Sadigh et al. (1997) for horizontal distance from the top edge of rupture on a reverse fault (δ = 45°) and soft rock sites (V_{S30} = 520 m/s). 81
Fig. 6.11 Median response spectra predicted by the model developed in this study and predicted by Sadigh et al. (1997) for strike-slip earthquakes and soft rock sites (V_{S30} = 520 m/s). Magnitudes are in order of increasing amplitude **M** 5.5, 6.5, 7.5, and 8.5....82

Fig. 6.12 Median response spectra predicted by the model developed in this study and predicted by Sadigh et al. (1997) for strike-slip earthquakes and firm soil sites (V_{S30} = 310 m/s). Magnitudes are in order of increasing amplitude **M** 5.5, 6.5, 7.5, and 8.5.....83

Fig. 6.13 (a) Total standard errors for the model with linear soil response developed in this study and Sadigh et al. (1997). (b) Effect of soil nonlinearity on *pga* total standard error for the model developed in this study. 84

LIST OF TABLES

Table 2.1 Inferred mechanisms, hypocenter depths, fault strikes, and fault dips. 4
Table 2.2 Excluded earthquakes. 12
Table 2.3 Regional distribution of selected recordings. 14
Table 3.1 Estimate of anelastic attenuation parameter γ for individual earthquakes. 38
Table 5.1 Period-independent fixed-effect coefficients for model of ln(y_{ref})—Eq. (3.12a 60
Table 5.2 Period-dependent fixed-effect coefficients for model of ln(y_{ref})—Eq. (3.12a). 61
Table 5.3 Fixed-effect coefficients of site response model for ln(y)—Eq. (3.12b). 62
Table 5.4 Coefficients of variance model—Eqs. (5.1) and (5.2). 66
Table 7.1 Example calculations. 85

1 Introduction

This report presents a ground motion model developed as part of the Pacific Earthquake Engineering Research Center's (PEER) Next Generation Attenuation model (NGA) project. This model is for estimating horizontal ground motion amplitudes caused by shallow crustal earthquakes occurring in active tectonic environments. Our model provides predictive relationships for the orientation-independent average horizontal component of ground motions. Relationships are provided for peak acceleration, peak velocity, and 5-percent damped pseudo-spectral acceleration (*PSA*) for spectral periods of 0.01–10 sec. The model is based on analyses of the PEER-NGA empirical strong-motion database (Chiou et al. 2008). We consider the model presented here to be an update of the set of models developed by Sadigh et al. (1997). As such, we have systematically reviewed the various aspects of the model (e.g., magnitude and distance scaling, site effects, style of faulting effect) and have introduced modifications to the formulation of Sadigh et al. (1997) to incorporate the results of both analyses of empirical data and numerical modeling of earthquake ground motions.

In the following, we first describe the empirical data used to develop the model. We then describe the development of the ground motion model formulation, followed by a description of the process used to define the model coefficients. Finally, we compare the model predictions with those obtained using Sadigh et al. (1997).

2 Empirical Database

The empirical data set used in this study was derived from the PEER-NGA database (Chiou et al. 2008; PEER-NGA flat file Version 7.2). In addition, we supplemented the PEER-NGA flat file with imputed values of missing metadata and with strong-motion data from the California ShakeMap system. These supplemental data, as well as data selection criteria, are discussed in this chapter.

2.1 SUPPLEMENTAL METADATA

The PEER-NGA flat file does not contain the full set of metadata for many of the recordings. The missing data of importance to the ground motion model developed in this study are the following: depth to top of rupture (Z_{TOR}), fault geometry and faulting mechanisms for smaller earthquakes, rupture distances for those earthquakes without published rupture models, and, for many sites, the average shear-wave velocity (V_{S30}) and sediment depth (defined as the depth to shear-wave velocity of 1 km/sec, $Z_{1.0}$). The missing values for these parameters were imputed (estimated) as follows.

2.1.1 Focal Depth, Fault Strike, Fault Dip, and Rake

The PEER-NGA database contains 41 earthquakes with missing parameters defining the characteristics of the earthquake rupture. These earthquakes are listed in Table 2.1 along with estimated values for the missing parameters. The missing values were estimated from other associated events such as the main shock or other aftershocks, or from the tectonic environment. For those earthquakes unassociated with other events, fault dips were assigned based on known or inferred mechanisms as follows, 90º for strike-slip, 40º for reverse (based on average value reported by Sibson and Xie 1998), and 55º for normal (generic value for normal faults and close

to the average of 54º for the normal mechanisms with known dips in the PEER-NGA database). Where the fault strike could not be inferred, it was assumed random. The comments in Table 2.1 indicate the basis for each estimate.

Table 2.1 Inferred mechanisms, hypocenter depths, fault strikes, and fault dips.

EQID	Earthquake	M	Inferred Mechanism[1,2]	Inferred Depth[1]	Inferred Strike[1]	Inferred Dip[1]	Comments
0002	Helena, Montana-02	6	SS	6	268	75	Values assumed equal to event 0001
0003	Humboldt Bay	5.8	SS	10	Random	90	Strike-slip mechanism and nominal depth of 10 km assumed for offshore Gorda plate earthquakes
0004	Imperial Valley-01	5	SS			90	Strike-slip assumed for Imperial Valley earthquakes
0005	Northwest Calif-01	5.5	SS	10	Random	90	Strike-slip mechanism and nominal depth of 10 km assumed for offshore Gorda plate earthquakes
0007	Northwest Calif-02	6.6	SS	10	Random	90	Strike-slip mechanism and nominal depth of 10 km assumed for offshore Gorda plate earthquakes
0008	Northern Calif-01	6.4	SS	10	Random	90	Strike-slip mechanism and nominal depth of 10 km assumed for offshore Gorda plate earthquakes
0009	Borrego	6.5		8	Random		Assumed similar to event 0028
0010	Imperial Valley-03	5.6		9.5			Average depth of other Imperial Valley earthquakes
0011	Northwest Calif-03	5.8	SS	10	Random	90	Strike-slip mechanism and nominal depth of 10 km assumed for offshore Gorda plate earthquakes
0013	Northern Calif-02	5.2	SS	10	Random	90	Strike-slip mechanism and nominal depth of 10 km assumed for offshore Gorda plate earthquakes
0014	Southern California	6	SS	10	Random	90	Assumed similar to event 25
0015	Imperial Valley-04	5.5	SS	9.5	Random	90	Strike-slip assumed for Imperial Valley earthquakes, depth average of similar events
0016	Central Calif-01	5.3	SS	7.4	Random	90	Assumed SS similar to other Hollister earthquakes and depth taken as average of values for events 0034 and 0098
0017	Northern Calif-03	6.5	SS	10	Random	90	Strike-slip mechanism and nominal depth of 10 km assumed for offshore Gorda plate earthquakes

Table 2.1—*Continued*

EQID	Earthquake	M	Inferred Mechanism[1,2]	Inferred Depth[1]	Inferred Strike[1]	Inferred Dip[1]	Comments
0018	Imperial Valley-05	5.4	SS	9.5	Random	90	Strike-slip assumed for Imperial Valley earthquakes, depth average of similar events
0021	Central Calif-02	5	SS	7.4	Random	90	Assumed SS similar to other Hollister earthquakes and depth taken as average of values for events 0034 and 0098
0022	Northern Calif-04	5.7	SS	10	Random	90	Strike-slip mechanism and nominal depth of 10 km assumed for offshore Gorda plate earthquakes
0023	Hollister-01	5.6	SS	7.4	Random	90	Assumed SS similar to other Hollister earthquakes and depth taken as average of values for events 0034 and 0098
0024	Hollister-02	5.5	SS	7.4	Random	90	Assumed SS similar to other Hollister earthquakes and depth taken as average of values for events 0034 and 0098
0026	Northern Calif-05	5.6		10			Nominal depth of 10 km assumed for offshore Gorda plate earthquakes
0027	Northern Calif-06	5.2	SS	7.4	Random	90	Assumed SS similar to other Hollister earthquakes and depth taken as average of values for events 0034 and 0098
0032	Managua, Nicaragua-02	5.2	SS		40	80	Values assumed equal to event 0031
0034	Hollister-03	5.14			Random		
0042	Fruili, Italy-03	5.5	RV		233	16	Average of values for events 0040 and 0043
0044	Izmir, Turkey	5.3	NM		Random	55	Mechanism based on environment
0060	Mammoth Lakes-05	5.7	SS		16	60	Average of values for events 0058–0065 in sequence
0065	Mammoth Lakes-09	4.85	SS		Random	67.5	Average for other SS Mammoth earthquakes
0066	Almiros, Greece	5.2	NM		Random	55	Assumed normal based on environment
0070	Irpinia, Italy-03	4.7	NM		Random	65	Assumed normal similar to events 0068 and 0069, dip average for those events
0089	New Zealand-01	5.5	NM		Random	55	Assumed normal based on environment
0092	Veroia, Greece	5.3	NM		Random	55	Assumed normal based on environment
0093	Pelekanada, Greece	5	NM		Random	55	Assumed normal based on environment

Table 2.1—*Continued*

EQID	Earthquake	M	Inferred Mechanism[1,2]	Inferred Depth[1]	Inferred Strike[1]	Inferred Dip[1]	Comments
0095	Taiwan SMART1(33)	5.8	NM		Random	61.5	Average for focal mechanism planes
0104	Chalfant Valley-03	5.65	SS		Random	90	Assumed SS similar to events 0102 and 0103
0106	Kalamata, Greece-01	6.2	NM		Random	55	Assumed normal based on environment
0107	Kalamata, Greece-02	5.4	NM		Random	55	Assumed normal based on environment
0112	New Zealand-03	5.8	NM		Random	55	Assumed normal based on environment
0124	New Zealand-04	5.7	NM		Random	55	Assumed normal based on environment
0132	Kozani, Greece-03	5.3	NM		Random	42	Assumed normal based on environment
0147	Northridge-02	6.05	RV		Random	40	Assumed mechanism similar to main shock event 127 and other aftershocks
0148	Northridge-03	5.2	RV		Random	40	Assumed mechanism similar to main shock event 127 and other aftershocks

[1] Values not listed are known for specific event

[2] SS—strike-slip, RV— reverse, NM—normal faulting

2.1.2 Rupture Distances and Source-Site Geometry

Of the 173 earthquakes in the PEER-NGA database, 110 do not have associated finite fault models that can be used to compute the standard measures of distance to rupture (e.g., rupture distance R_{RUP} and Joyner-Boore distance, R_{JB}) and the source-site geometry parameters such as hanging-wall and footwall positions and the source-site angle θ_{SITE}. The use of hypocentral distance, R_{HYP}, and epicentral distance, R_{EPI}, for R_{RUP} and R_{JB}, respectively, introduces a bias in the values as in most situations $R_{RUP} < R_{HYP}$ and $R_{JB} < R_{EPI}$, even for small events. The various geometry and distance measures for these earthquakes were estimated by simulating earthquake ruptures using the earthquake size and known or inferred information on the hypocentral depth, fault strike, fault dip, and rupture mechanism. Appendix B describes the simulation process. Figure 2.1 shows the ratios of R_{JB}/R_{EPI} and R_{RUP}/R_{HYP} for the 702 recordings from the 110 earthquakes, and indicates the magnitude of the bias that could be introduced by using R_{EPI} for R_{JB} and R_{HYP} for R_{RUP}. The analysis also provided estimates of the depth to the top of rupture, Z_{TOR}, and rupture width, W, for these earthquakes.

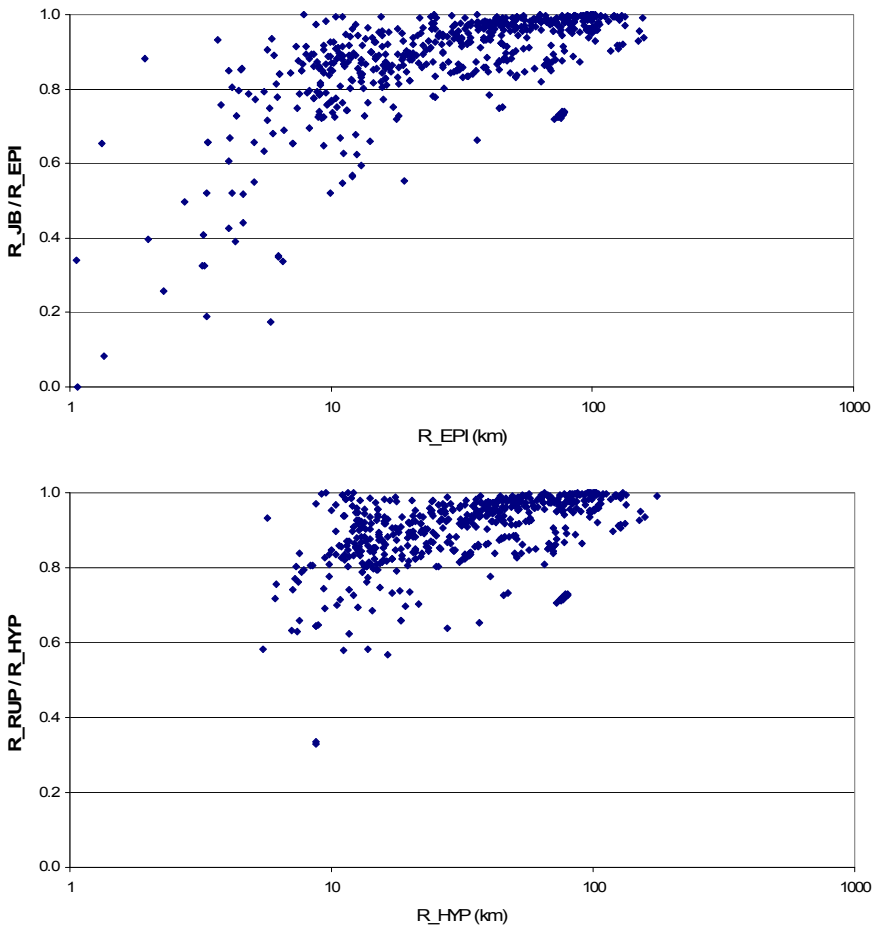

Fig. 2.1 Ratio of estimated values of R_{JB} and R_{RUP} to R_{EPI} and R_{HYP} for recordings from earthquakes without finite fault models in PEER-NGA database.

2.1.3 Site Average Shear-Wave Velocity

Approximately two thirds of the recordings in the PEER-NGA database were obtained at sites without measured values of shear-wave velocity. As part of the database compilation, empirical correlations between the surface geology and the average shear-wave velocity in the top 30 meters, V_{S30}, were developed (Chiou and others 2008). These relationships together with assessments of the surface geology from geologic maps and site descriptions were used to estimate values of V_{S30} at the sites without measured velocities. Additional analysis was performed as part of this study to improve the correlation between surface geology and V_{S30} for the Taiwan sites. This analysis is described in Appendix C.

Figures 2.2 and 2.3 show the measured (solid circles) and estimated (open circles) values of V_{S30} versus magnitude and distance, respectively, for the records in the PEER-NGA database.

Also indicated on the figures are the divisions of the NEHRP site categories A–E. The data distributions plotted in Figures 2.2 and 2.3 indicate that the PEER-NGA database is primarily a soil/soft rock database.

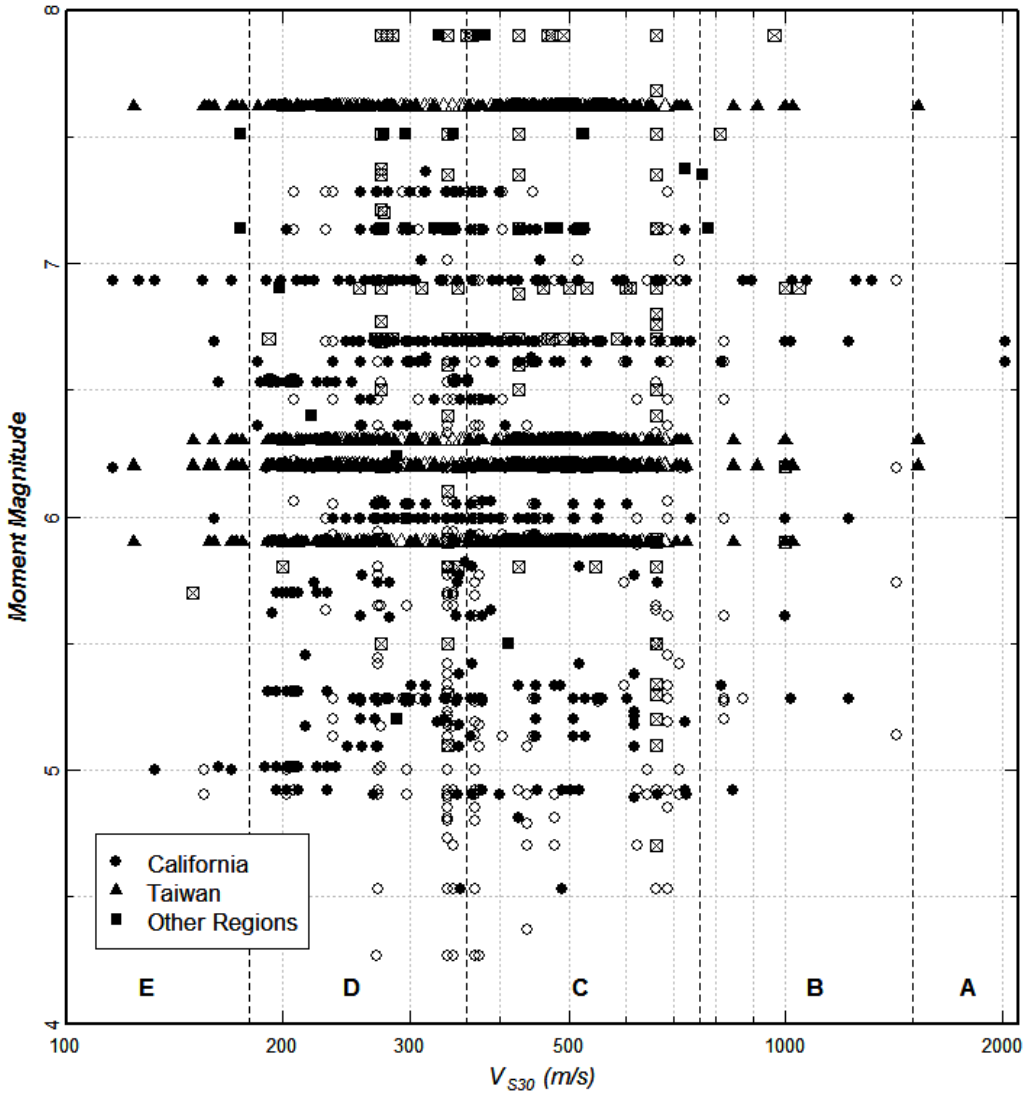

Fig. 2.2 **V_{S30}-magnitude-region distribution of PEER-NGA recordings. Closed symbols indicate measured values, open symbols inferred values. NEHRP site classes are indicated along bottom edge.**

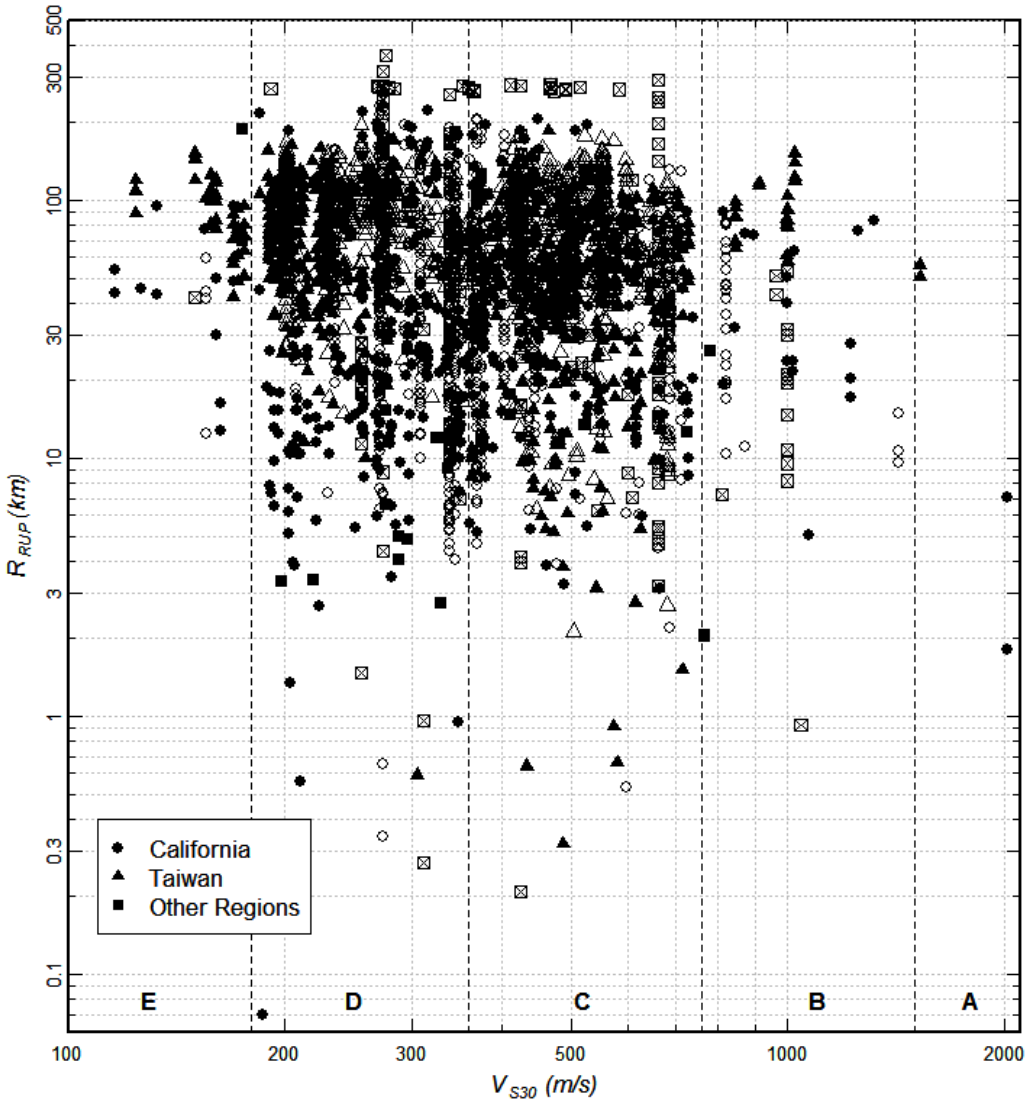

Fig. 2.3 V_{S30}-distance-region distribution of PEER-NGA recordings. Closed symbols indicate measured values, open symbols inferred values. NEHRP site classes are indicated along bottom edge.

2.1.4 Sediment Thickness

The thickness of the near-surface sediments is represented in our NGA model by the depth to a shear-wave velocity of 1.0 km/s, $Z_{1.0}$. These data are available in the PEER-NGA database for sites in the Southern California Earthquake Center 3-D (SCEC-3D) basin model (Magistrale et al. 2000), for sites in the USGS velocity model for the San Francisco Bay area (Boatwright et al. 2004), for sites in the Eel River basin (Graves 1994), and for sites where measured velocities reach this velocity horizon. Note that in our study we updated the $Z_{1.0}$ values from SCEC-3D

Version 2 to those from Version 4 (http://www.data.scec.org/3Dvelocity/). The newly determined V_P-density ratio used by Version 4 produces a new V_S model and hence new $Z_{1.0}$ value. Figure 2.4 shows the relationship between the two $Z_{1.0}$ values for southern California stations. Points on the line of slope 1.52 are sites affected by the new V_P-density ratio. Points off the sloping line are sites in areas such as San Bernardino valley and Salton trough where the V_S model has been improved in Version 4.

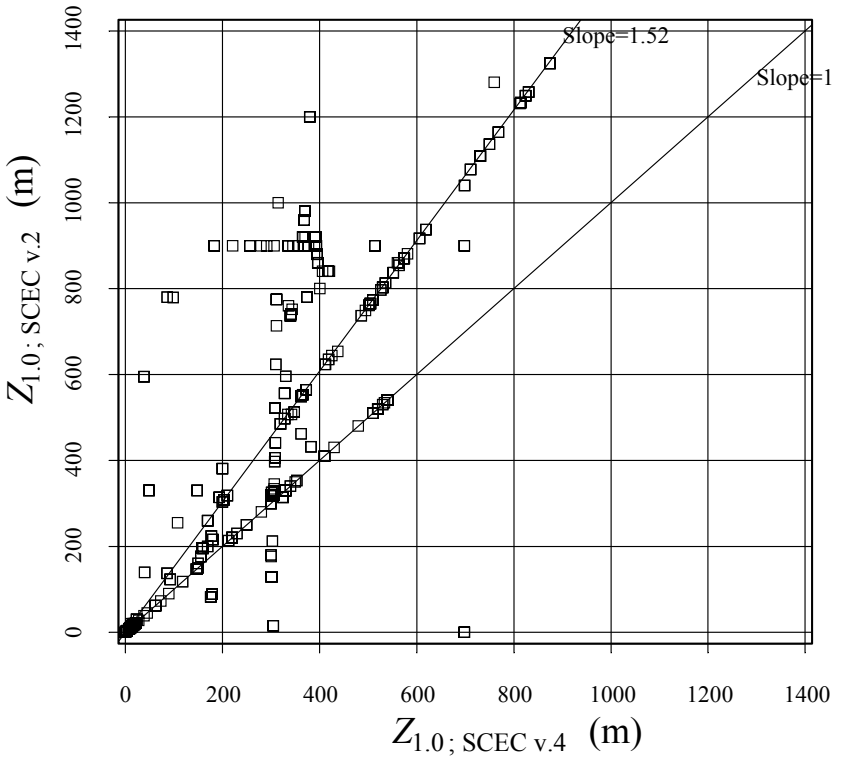

Fig. 2.4 Comparison of $Z_{1.0}$ values from Versions 2 and 4 of SCEC 3-D velocity model.

When $Z_{1.0}$ is not available, it was estimated through the following correlation with V_{S30} developed from the measured (V_{S30}, $Z_{1.0}$) data in the PEER-NGA database (Fig. 2.5):

$$\ln(Z_{1.0}) = 28.5 - \frac{3.82}{8}\ln\left(V_{S30}^{8} + 378.7^{8}\right) \tag{2.1}$$

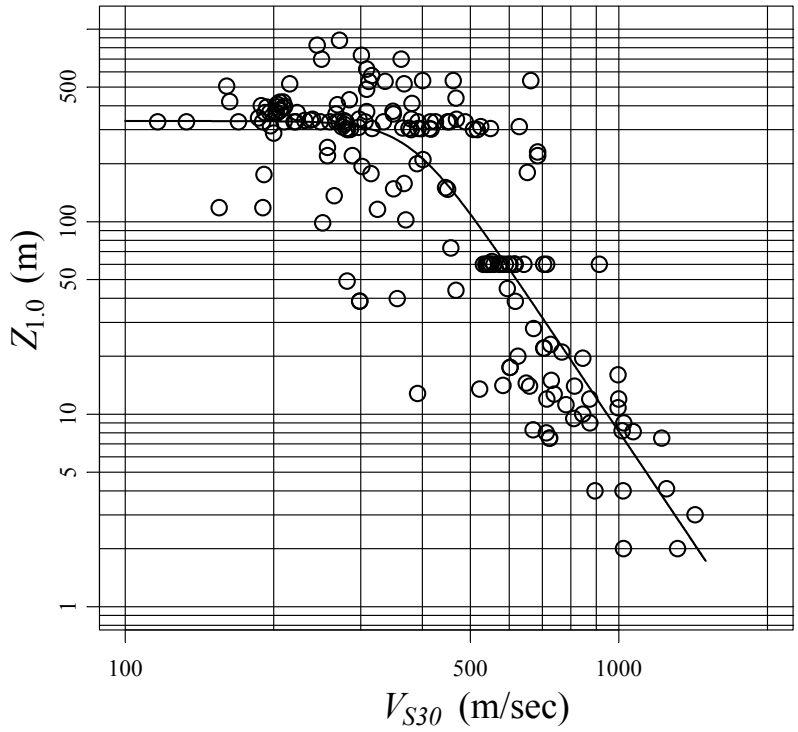

Fig. 2.5 Relationship between measured $Z_{1.0}$ and V_{S30} for sites contained in PEER-NGA database. Solid curve is the relation used to infer values of missing $Z_{1.0}$ data.

2.2 DATA SELECTION

The data set used in this study was selected from the PEER-NGA empirical strong-motion database. Our ground motion model was developed to represent free-field motions from shallow crustal earthquakes in active tectonic regions, principally California. Data from earthquakes that occurred in oceanic crust offshore California and Taiwan (Table 2.2) were excluded because ground motions from these types of events have been found to be more consistent with ground motions from the Wadati-Benioff zone (subduction intraslab) earthquakes than shallow crustal earthquakes (Geomatrix Consultants 1995). Data from the 1992 Cape Mendocino earthquakes were included because the source depth places the event above the likely interface location (Oppenheimer et al. 1993). Four 1997 northwest China earthquakes were excluded because of their moderate depths (≥20 km) and the very limited information about the events and their recordings. Data from the 1979 St. Elias earthquake were excluded because we interpret this earthquake to have occurred on a subduction zone interface based on its depth, dip, and location. Data from the 1985 Nahanni, Canada, and the 1992 Roermond, Netherlands, earthquakes were

included as these earthquakes are interpreted to have occurred at the boundary of stable continental regions (SCR) with active tectonic regions.

Table 2.2 Excluded earthquakes.

EQID	EQNAME	Comment
0003	Humboldt Bay	Gorda plate
0005	Northwest Calif-01	Gorda plate
0007	Northwest Calif-02	Gorda plate
0008	Northern Calif-01	Gorda plate
0011	Northwest Calif-03	Gorda plate
0013	Northern Calif-02	Gorda plate
0017	Northern Calif-03	Gorda plate
0022	Northern Calif-04	Gorda plate
0026	Northern Calif-05	Gorda plate
0035	Northern Calif-07	Gorda plate
0067	Trinidad	Gorda plate
0071	Taiwan SMART1(5)	Deep offshore event
0084	Trinidad offshore	Gorda plate
0086	Taiwan SMART1(25)	Deep offshore event
0093	Pelekanada, Greece	Deep event
0095	Taiwan SMART1(33)	Deep offshore event
0109	Taiwan SMART1(45)	Offshore event
0142	St Elias, Alaska	Subduction interface event
0153	Northwest China-01	Poorly known event
0154	Northwest China-02	Poorly known event of moderate depth
0155	Northwest China-03	Poorly known event of moderate depth
0156	Northwest China-04	Poorly known event of moderate depth

The remaining earthquakes are from a variety of active tectonic regions, as indicated in Table 2.3. Several investigators have shown that ground motion relationships based on California data are consistent with strong motion data in other active tectonic regions [Italy (Sabetta and Pugliese 1996); the Mediterranean basin (Ambraseys et al. 1996); Japan (Fukushima and Tanaka 1990)]. It has also been common to include ground motions from earthquakes such as Gazli, 1976, and Tabas, 1978, in developing ground motion models for application to California (Abrahamson and Silva 1997; Campbell 1997; Sadigh et al. 1997). We start with the hypothesis that the ground motions from these separate active tectonic regions are similar and examine this hypothesis during model development.

Recordings made in large buildings and at depth were removed[1], eliminating several additional earthquakes, notably the 1935 Helena, Montana, and several Imperial Valley, California, earthquakes recorded at the old Imperial Valley Irrigation District site. We kept records from sites that have been characterized as having topographic effects (e.g., Tarzana Cedar Hill nursery, Pacoima dam left abutment). Our rationale for including these records is that the effect of topography has not been systematically studied for all of the records in the database, and many other recording stations may have topographic enhancement or suppression of ground motions. Topographic effects are considered to be part of the variability introduced into ground motions by travel path and site effects.

The ground motion measure used in this model is the orientation-independent ground motion measure GMRotI50 defined by Boore et al. (2006). Use of this ground motion measure eliminates recordings for which only a single horizontal component was obtained, notably the Cholame-Shandon Array #2 recording from the 1966 Parkfield earthquake.

The ground motion model developed in this study explicitly accounts for site conditions. Therefore, recordings from sites for which there is no available information of the local soil conditions were excluded. These data were limited to a few recordings from earthquakes in Greece and Turkey.

[1] These recordings are identified as having "Geomatrix" C1 site code of C, D, E, G, and H (non-abutment sites).

Table 2.3 Regional distribution of selected recordings.[1]

Active Region	# of Earthquakes	# of Recordings
Alaska	3	57
Armenia	1	1
California	81	1311
Canada	1	3
Georgia	1	5
Greece	8	13
Idaho	2	5
Iran	2	14
Israel	1	1
Italy	8	43
Japan	1	22
Netherlands	1	3
New Zealand	4	5
Nicaragua	2	2
Russia	1	1
San Salvador	1	2
Taiwan	6	1753
Turkey	7	56
Totals	**131**	**3297**

[1]Numbers given in this table do not reflect the distance truncation at 70 km.

During the PEER-NGA project, an issue was raised concerning the use of data from aftershocks. We have included data from aftershocks but have allowed for the possibility that there may be systematic differences in the ground motion amplitudes produced by main shocks and aftershocks. Our reason for including the aftershock data is that they provide additional information to constrain the soil amplification model parameters.

As discussed later in the report, we limit the data to recordings within 70 km of the earthquake rupture in order to remove the effects of bias in the strong motion data sample. The combined limitations result in a total data set of 1950 recordings from 125 earthquakes. Figure 2.6 shows the distribution of the selected data in terms of magnitude, distance, and the average shear-wave velocity of the upper 30 m (V_{S30}). The earthquakes and recordings used in the regression analysis are tabulated in Appendix A.

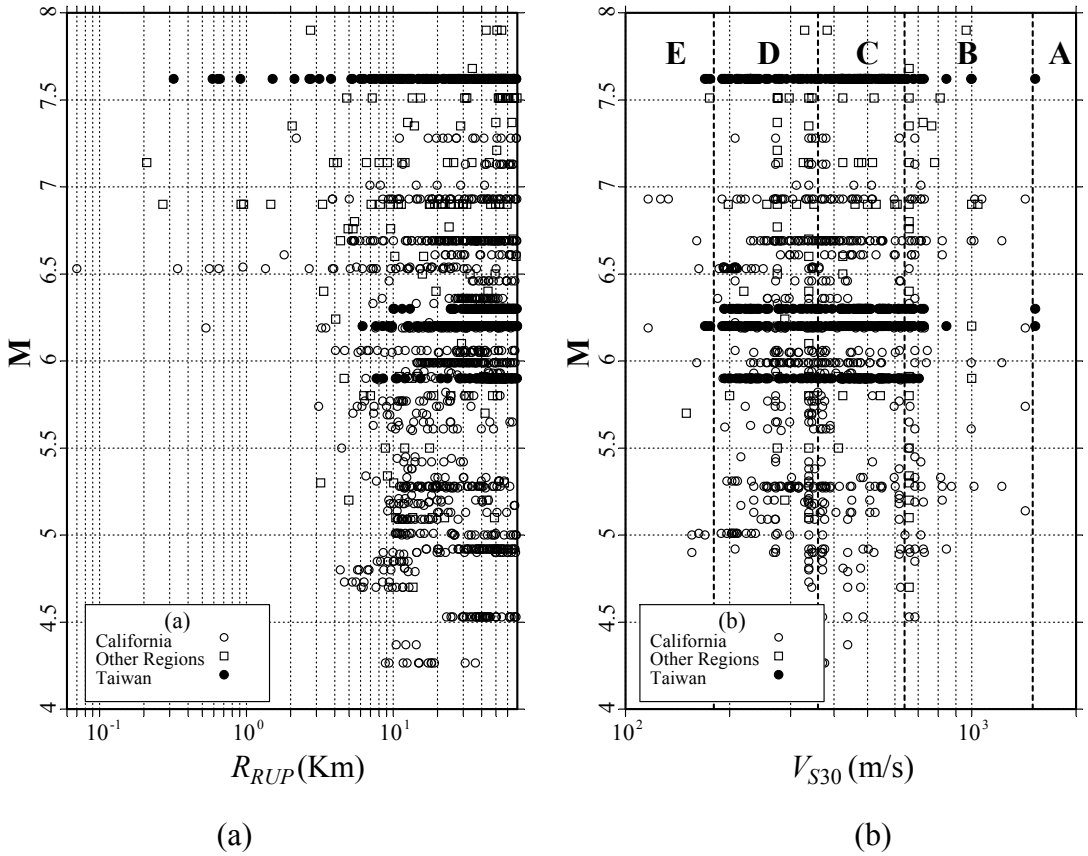

Fig. 2.6 (a) Magnitude-distance-region distribution of selected recordings. (b) V_{S30}-magnitude-region distribution of selected recordings. V_{S30} velocity ranges for NEHRP site classes indicated by vertical dashed lines.

Finally, in the regression of response spectra at a spectral period T, we included only recordings that have a minimum usable spectral frequency that is lower than $1/T$. This selection leads to a decreased data set size as the spectral period increases (Fig. 2.7).

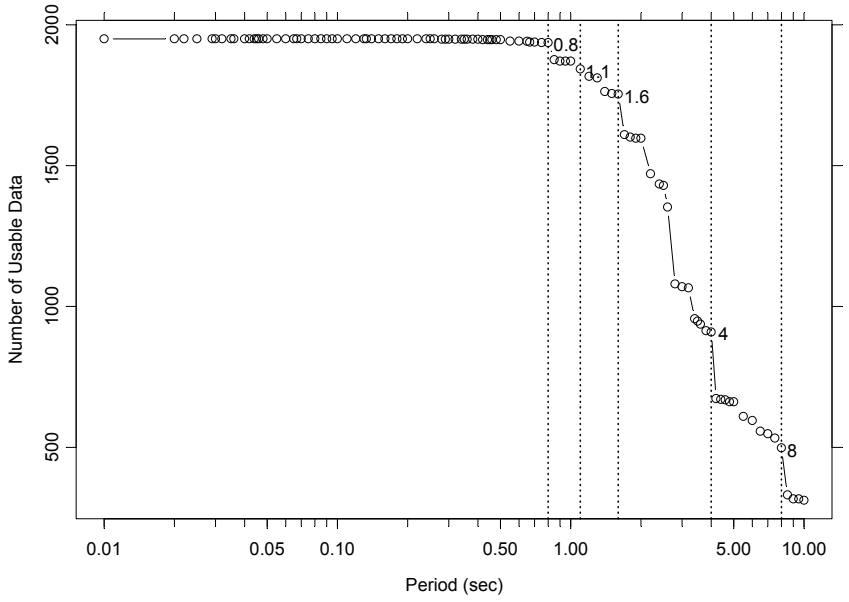

Fig. 2.7 Reduction of number of usable data as a function of spectral period.

2.3 SUPPLEMENTAL STRONG-MOTION DATA

The PEER-NGA strong motion data were supplemented with ground motion data from the California ShakeMap system. Acceleration time histories recorded at ShakeMap's high broadband stations, as well as USGS and CSMIP strong-motion stations, for the 2001 Anza, 2002 Yorba Linda, and 2003 Big Bear City earthquakes were provided by David Boore (written communication, USGS 2005). Peak acceleration values for many other events were supplied by Jack Boatwright and Linda Seekins (written communication, USGS 2005, 2006; see Appendix D) or obtained from the ShakeMap website. Estimates of site conditions at the ShakeMap stations were provided by Chris Wills based on surface geology (Wills and Clahan 2006) and by Jack Boatwright. The supplemental data were used to provide additional guidance on functional forms and provide additional constraints on coefficients of the ground motion model.

3 Model Formulation

Using algebraic expressions to represent the average behavior observed in the empirical strong-motion data, the empirical ground motion model developed here attempts to capture the effects of the amount of energy radiated by the earthquake source, the attenuation of seismic waves along the propagation path due to geometric spreading and energy absorption, and local modification of the seismic waves by the near-surface materials. The form of these expressions is guided by trends in the data, simple seismological models, past experience, and examination of the results of 1-D and 3-D ground motion simulations (Somerville et al. 2006; Day et al. 2008; Silva 2008; Walling 2008) conducted as part of the PEER-NGA project.

3.1 SEISMIC SOURCE SCALING

3.1.1 Effect of Earthquake Size

We use moment magnitude (**M**) as the simplest measure for correlating the amount of energy radiated by an earthquake with the resulting amplitudes of ground motions. Many empirical ground motion models, including Sadigh et al. (1997), use a polynomial function for scaling the ln of ground motions y with magnitude of the form:

$$\ln(y) \propto C_2(T) \times \mathbf{M} + C_3(T) \times (m_C - \mathbf{M})^n \tag{3.1}$$

where coefficients C_3 and possibly C_2 vary with spectral period T, the exponent n is typically in the range of 2–3, and coefficient m_C is independent of T. Figure 3.1(a) shows the magnitude scaling of pseudo-spectral acceleration, y, at a rupture distance of 30 km obtained from the Sadigh et al. (1997) ground motion model.

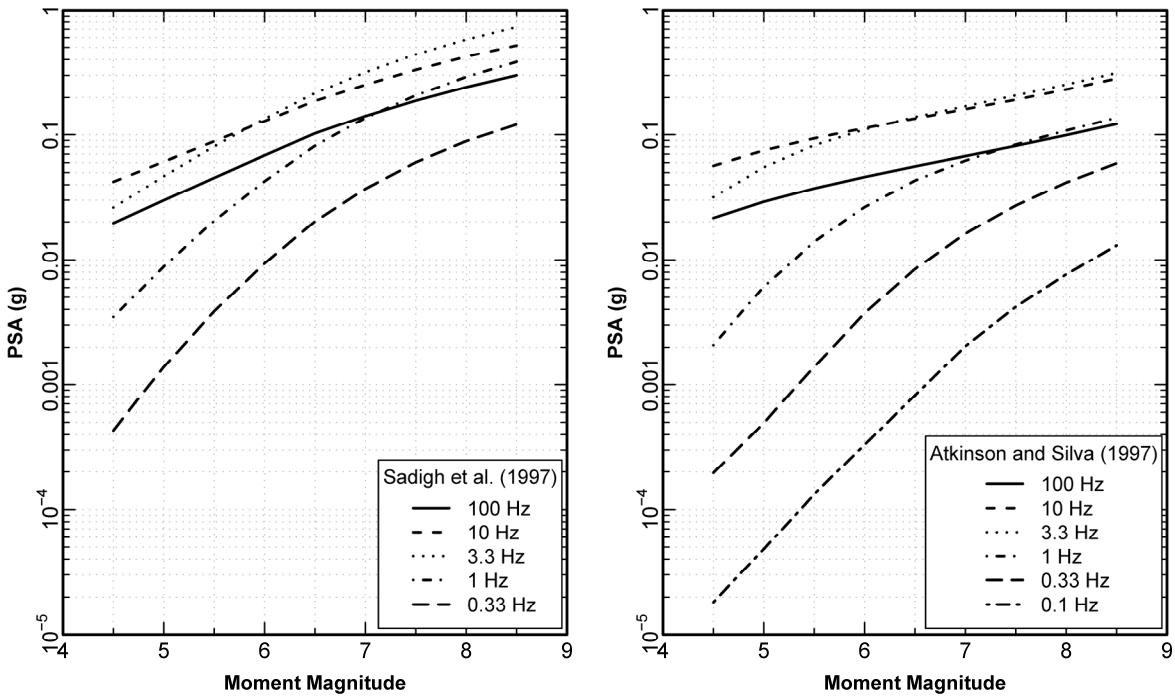

Fig. 3.1 Magnitude scaling of pseudo–spectral acceleration at distance of 30 km computed using (a) Sadigh et al. (1997) and (b) stochastic ground motion model, and Atkinson and Silva (1997) source model for California earthquakes.

In contrast, seismological models for earthquake source spectra suggest an alternative form for magnitude scaling. Figure 3.1(b) shows magnitude scaling relationships at a distance of 30 km, computed using the stochastic ground motion model (Boore 2003) and the Atkinson and Silva (1997) empirical source spectra model for California earthquakes. For spectral frequencies of 10 Hz and higher, the magnitude scaling of ln(y) is approximately linear at a relatively flat slope in the magnitude range of $5 \leq \mathbf{M} \leq 8.5$, representing scaling of the source spectrum above the corner frequency. For frequencies of 0.33 Hz and lower, the magnitude scaling in the range of $5 \leq \mathbf{M} \leq 7$ is again approximately linear, but at a much larger slope than for high-frequency motions, reflecting scaling of the source spectrum below the corner frequency. The transition between the two approximately linear scaling regions occurs over the magnitude range where the corner frequency of the source spectrum is near the spectral frequency of the ground motion. As the spectral frequency of the ground motions decreases, the magnitude range for this transition shifts to larger magnitudes, reflecting the decrease in corner frequency with increasing magnitude.

The shape of the magnitude scaling curves shown in Figure 3.1(b) is modeled by the expression:

$$\ln(y) \propto c_2 \mathbf{M} + \frac{1}{c_n}(c_2 - c_3) \times \ln\left[1 - \exp\left\{c_n\left(c_{\mathbf{M}} - \mathbf{M}\right)\right\}\right] \tag{3.2}$$

Coefficient c_2 is the slope of the magnitude scaling relationship for earthquakes whose theoretical corner frequency is well above the spectral frequency of interest, and c_3 is the slope for earthquakes whose corner frequency is well below the spectral frequency. Coefficient c_n controls the width of the magnitude range over which the transition from c_2 scaling to c_3 scaling occurs. Coefficient $c_{\mathbf{M}}$ is the magnitude at the midpoint of this transition and its value varies with the spectral period of the ground motion parameter y. The function form of Equation (3.2) was tested by fitting a set of ground motion response spectra simulated using the program SMSIM (Boore 2005) and the Atkinson and Silva (2000) stochastic ground motion. Figure 3.2 shows the magnitude scaling obtained from the simulated ground motions. As indicated on the figure, the functional form of Equation (3.2) can provide a close fit to the simulations.

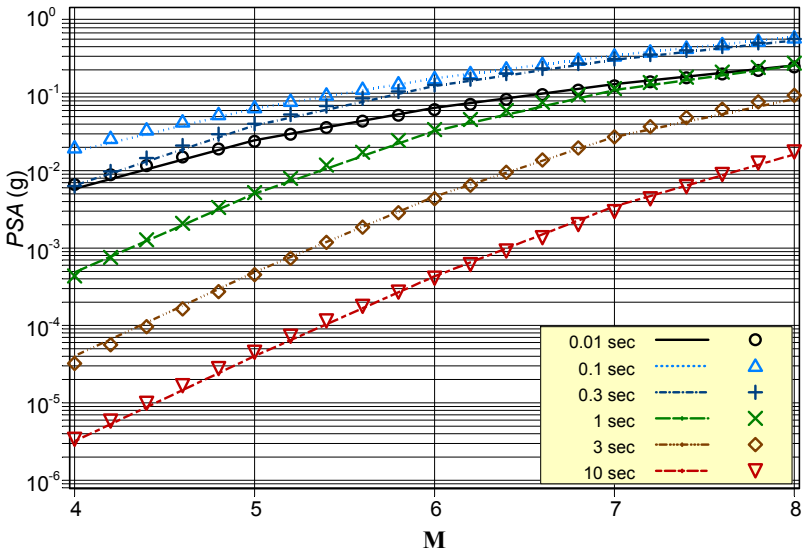

Fig. 3.2 Magnitude scaling predicted by seismic source model of Atkinson and Silva (2000) (points) and result of fitting Eq. (3.2) to predicted data (lines).

To evaluate the utility of Equations (3.1) and (3.2), we put together a set of peak acceleration data in the distance range of 30–50 km and the V_{S30} range of 300–400 m/s from the PEER-NGA database and from the ShakeMap data (Appendix D). These values, shown in Figure 3.3, were fit using three alternative scaling relationships. They are the quadratic form of Equation (3.1) with an exponent n of 2; the Sadigh et al. (1997) form of Equation (3.1) with an n equal to 2.5 and m_C equal to 8.5; and the magnitude scaling defined by Equation (3.2). The fit of the Sadigh et al. (1997) form of Equation (3.1) to the data on Figure 3.3 produced C_2 equal to 1.0. In fitting Equation (3.2) to the data on Figure 3.3, c_2 was constrained to be 1.06, the value obtained from the analysis of spectral accelerations simulated for California earthquakes (see discussions below). All three forms provide essentially equally good fits to the data. The empirical data are not sufficient to distinguish between magnitude-scaling defined by Equation (3.1) or (3.2). We prefer the scaling form of Equation (3.2) because we believe that it better represents our current concept of earthquake source spectra scaling with earthquake magnitude.

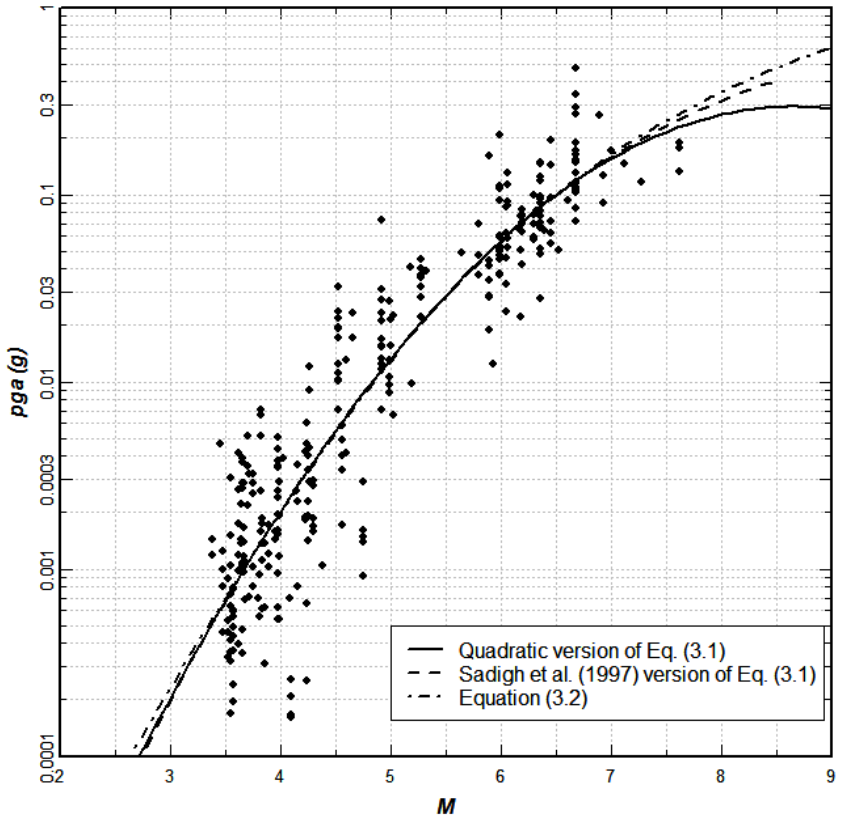

Fig. 3.3 Peak acceleration data from PEER-NGA database and from ShakeMap (Appendix D) for the distance range $30 \le R_{RUP} \le 50$ and the velocity range $300 \le V_{S30} \le 400$ fit by alternative function forms of magnitude scaling.

As explained earlier, in Equation (3.2) c_3 represents scaling of ground motion spectra below the corner frequency where the source spectra are directly proportional to seismic moment, M_0. Because $\mathbf{M} \propto \frac{2}{3}M_0$, theoretically, c_3 should equal 1.5×ln(10) or 3.45 if the magnitude scaling of Fourier amplitude spectra can be directly carried over to the magnitude scaling of response spectra. We decided to fix c_3 at this value. Far-field simulations based on the updated source spectral model for California earthquakes defined by Atkinson and Silva (2000) produces scaling of $\ln(y) \propto 1.06\mathbf{M}$ for spectral period above the source corner frequency. In the Sadigh et al. (1997) form of Equation (3.1), coefficient C_2 also represents the magnitude scaling of the source spectra at distances large enough that the source can be considered a point. The Sadigh et al. (1997) values of C_2 were 1.0–1.1. Therefore, coefficient c_2 was fixed at 1.06. Coefficients c_n and $c_{\mathbf{M}}$ were obtained by fitting the strong motion data.

3.1.2 Style of Faulting Effects

Our exploratory analysis of the NGA data indicated that reverse-faulting earthquakes produce larger high-frequency motions than strike-slip earthquakes. This effect diminishes as the spectral period increases, with the motion from strike-slip earthquakes becoming the larger of the two at long periods, similar to findings by other investigators (Abrahamson and Silva 1997; Campbell and Bozorgnia 2003; Ambraseys et al. 2005). Chiou et al. (2000) showed that when the geometric hanging-wall effect was accounted for by using the R_{RMS} distance measure, reverse-faulting earthquakes still produced statistically significant higher motions than strike-slip earthquakes.

Some empirical models have shown that normal-faulting/extensional regime earthquakes produce lower ground motions than strike-slip earthquakes (Spudich et al. 1999; Ambraseys et al. 2005) while others have included normal faulting and strike slip together in a single class (Abrahamson and Silva 1997; Sadigh et al. 1997; Campbell and Bozorgnia 2003). In our exploratory analysis of NGA data, the style of faulting effect for normal faults was found to be statistically significant (p-values slightly less than 0.05) only when normal faulting was restricted to rake angles, λ, in the range of -120º to -60º; with normal-oblique earthquakes included in the same style-of-faulting class as strike-slip earthquakes.

3.1.3 Other Source Effects

Other source parameters examined include source depth and the difference between aftershocks and main shocks. In the preliminary analyses it was found that the NGA data exhibited a statistically significant dependence on source depth parameterized as the depth to top of rupture, Z_{TOR}. Figure 3.4 shows inter-event residuals for models fit to the *pga* data without and with Z_{TOR} scaling. The inter-event residuals for the fit without Z_{TOR} scaling show a clear trend, while those for the fit with Z_{TOR} scaling do not. Figure 3.4(c) shows the percent reduction in inter-event standard error achieved by including Z_{TOR} scaling.

As indicated earlier in Section 2.2, we include aftershocks in our analyses to provide additional data to help constrain the coefficients of the site response model. We found that aftershocks tend to produce lower motions than main shocks with similar magnitudes. Hence we included this difference in the ground motion model. We also found that the style of faulting effects were much weaker for aftershocks than for main shocks. Furthermore, aftershocks showed a stronger dependence on Z_{TOR} than main shocks. Therefore, the ground motion model incorporates separate depth-dependence for main shocks and aftershocks, and no style of faulting effects for aftershocks.

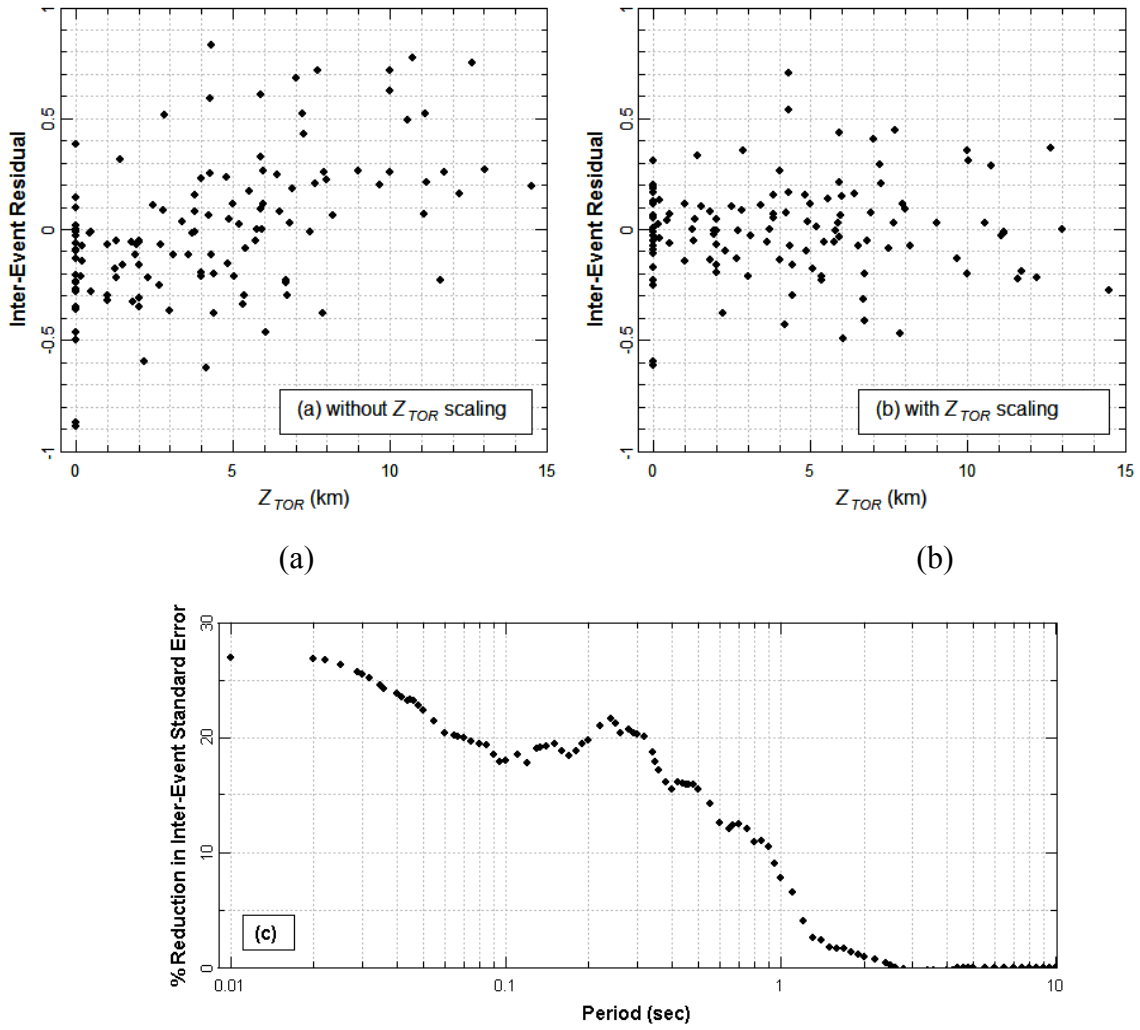

Fig. 3.4 Effect of source depth on inter-event residuals: (a) *pga* data fit without Z_{TOR} scaling, (b) *pga* data fit with Z_{TOR} scaling, (c) reduction in inter-event standard error resulting from including Z_{TOR} scaling.

3.2 DISTANCE SCALING

The scaling or attenuation of ground motion amplitude with distance from the earthquake rupture involves two primary effects, geometric spreading and energy absorption along the travel path due to material damping and wave scattering. In most empirical ground motion models these effects are modeled by the functional form:

$$ln(y) \propto C_{Geometric} \times ln\left[\left(R^n + C^n_{Source_Size}\right)^{1/n}\right] + \gamma \times R \qquad (3.3)$$

where $C_{Geometric}$ nominally defines the rate of attenuation due to geometric spreading, γ defines the rate of anelastic attenuation, typically quantified in terms of the quality factor Q. Coefficient C_{Source_Size} accounts for the effect of the source size on geometric spreading. Coefficient $C_{Geometric}$ interacts with C_{Source_Size} and n to define distance scaling at small distances from the source and interacts with γ to define distance scaling at large distances from the source. These two interactions are examined below.

3.2.1 Near-Source Distance Scaling

Of foremost interest to engineering application in active tectonic regions is the effect of extended source dimensions that leads to magnitude-dependent attenuation rates within the distance range of 0–50 km or more. The consequence of this effect is what has been termed near-source saturation—less magnitude scaling at small source-site distances than at large source-site distances. Two approaches have been used to model this effect within the framework defined by Equation (3.3). One approach uses a magnitude-independent value of $C_{Geometric}$ combined with a magnitude-dependent value for C_{Source_Size} [Sadigh et al. (1997) with exponent n = 1; Campbell (1993) and Campbell and Bozorgnia (2003) with n = 2]. The alternative approach has been to use a magnitude-dependent value for $C_{Geometric}$ combined with a magnitude-independent value for C_{Source_Size} [(Idriss 1991, written communication 2002) with n = 1; (Abrahamson and Silva 1997) with n = 2]. Figure 3.5 illustrates the behavior of these approaches to distance scaling as implemented in recent ground motion models. The attenuation behavior of the four models shown in Figure 3.5 can be illustrated by plotting the attenuation rate, defined as $\partial \ln(y) / \partial \ln(R)$, versus distance. Figure 3.6 shows the results. The effect of the value of the exponent n is seen by comparing the models shown on the left for exponent n = 1 to those shown on the right with n = 2. Use of n = 2 results in the rate of attenuation approaching the value defined by $C_{Geometric}$ at relatively short distances, allowing an interpretation of its value as a direct estimate of the rate of geometric spreading. Use of n = 1 results in the attenuation rate approaching the value of $C_{Geometric}$ slowly and its value cannot be directly equated with the rate of geometric spreading at distances less that 50 km. Figure 3.7 shows the magnitude scaling, defined as $\partial \ln(y) / \partial \mathbf{M}$, for the four ground motion models shown in Figure 3.5. The steps in the values of $\partial \ln(y) / \partial \mathbf{M}$ occur where there are changes in the model parameters for different magnitude ranges. The different implementations of Equation (3.3) also produce differences in

ground motion scaling with magnitude at large distances from the source. The models that use a magnitude-independent $C_{Geometric}$ (top row of Fig. 3.7) approach distance-independent magnitude scaling at large distances, while those that use magnitude-dependent $C_{Geometric}$ produce distant-dependent magnitude scaling at all distances.

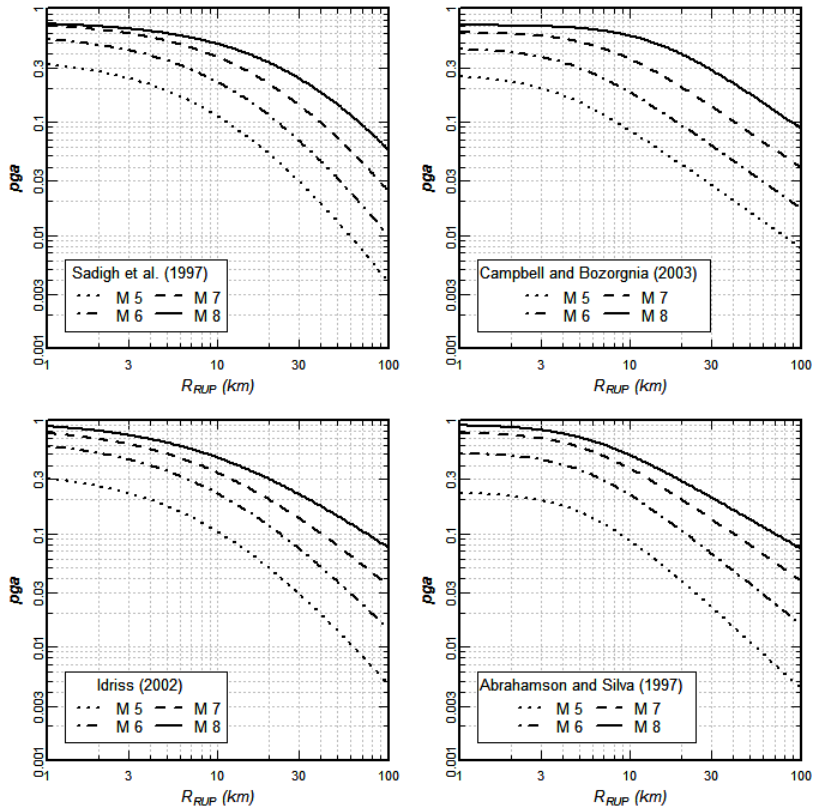

Fig. 3.5 Illustration of functional forms used to capture magnitude-dependence of distance attenuation for distances less than 100 km. All plots are for rupture distance to a vertical strike-slip fault rupturing the surface. Values for Campbell and Bozorgnia (2003) were computed using a minimum R_{SEIS} of 3 km.

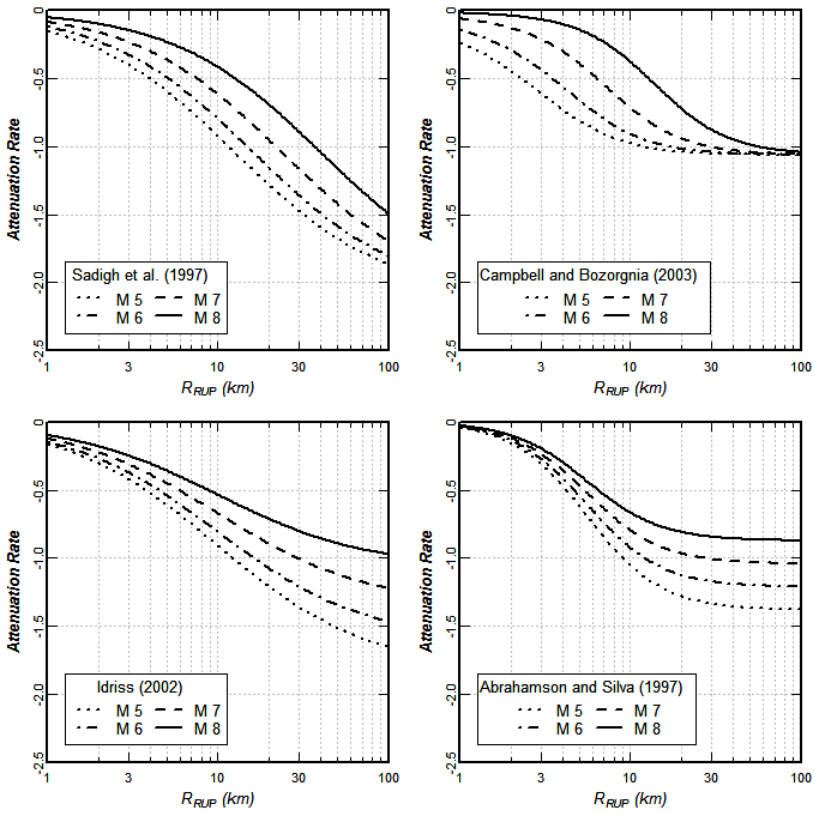

Fig. 3.6 Plots of the instantaneous slope of attenuation curve for the four ground motion models shown in Fig. 3.5. Attenuation rate defined as $\partial \ln(pga) / \partial \ln(R)$.

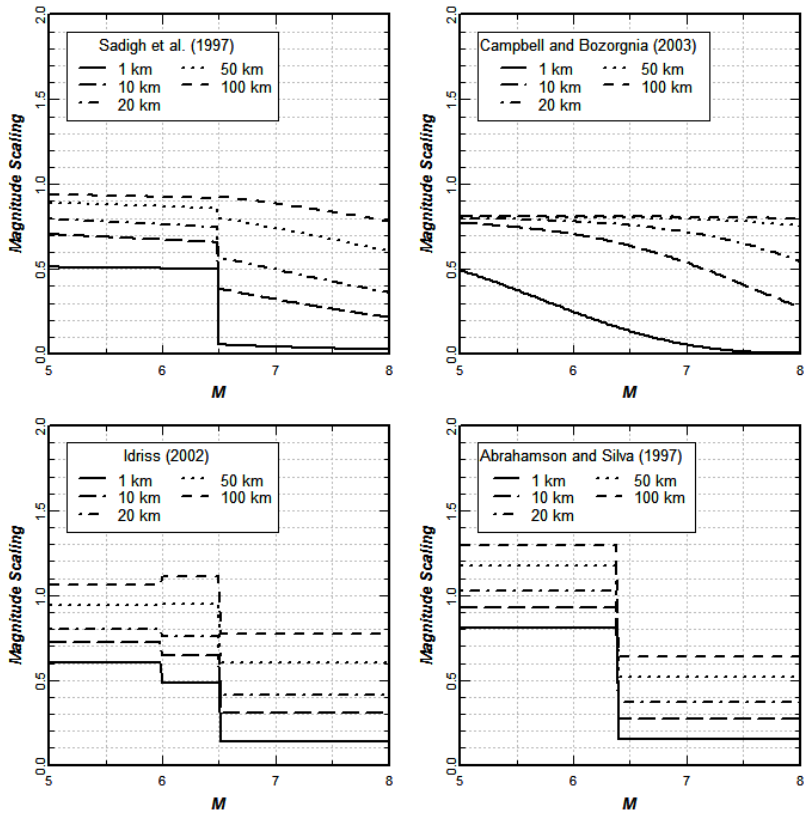

Fig. 3.7 Plots of magnitude scaling at a range of distances produced by form of the attenuation curve for the four ground motion models shown in Fig. 3.5. Magnitude scaling is defined as $\partial \ln(pga) / \partial \mathbf{M}$.

Based on our examination of the alternative forms of Equation (3.3) we conclude that they all provide reasonable fits to the empirical data. Discrimination among them would require a great deal more data at distances less than 10 km. The data show magnitude-dependence in the rate of attenuation at all distances. However, we believe that the mechanisms that cause this behavior may be different at different distances. At distances less than ~50 km, magnitude-dependence is due to the effect of extended sources. This effect can be modeled by all of the functional forms shown in Figure 3.5. However, at large distances, >100 km, we think that another effect may be causing magnitude-dependence in the attenuation of response spectral ordinates—the interaction of path Q with the differences in source Fourier spectra as a function of magnitude. This concept is explored below. We prefer to use a model form that allows for separation of the effect of magnitude scaling at small and large distances, and therefore select the magnitude-independent form of $C_{Geometric}$. This form allows the use of Equation (3.2) to define magnitude scaling at large distances from the source.

We examined the alternatives for the exponent n. As shown by the upper right-hand plot in Figures 3.5 and 3.6, use of $n = 2$ allows the model to approach a constant geometric spreading rate at distances greater than about $2 \times C_{Source_Size}$. After experimenting extensively with this form, we concluded that $n = 2$ resulted in too little distance scaling over the distance range of 0–10 km for large-magnitude earthquakes, and we use exponent $n = 1$, resulting in the form used by Sadigh et al. (1997). Instead of the piece-wise linear model for C_{Source_Size} used by Sadigh et al (1997), we use a smooth function for the magnitude scaling of C_{Source_Size} over the full magnitude range, accomplished by using the relationship:

$$C_{Source_Size}(\mathbf{M}) = c_5 \cosh\{c_6 \max(\mathbf{M} - 3, 0)\} \tag{3.4}$$

The use of Equation (3.4) has the property that C_{Source_Size} varies smoothly from a constant ($C_{Source_Size} = c_5$) at small magnitudes ($\mathbf{M} \leq 3$) to $C_{Source_Size} \propto \exp(c_6 \mathbf{M})$ at large magnitudes.

3.2.2 Distance Scaling at Large Distances

Many studies of the attenuation of ground motion Fourier amplitudes with distance have indicated that there is a change in the rate of geometric spreading from approximately proportional to $1/R$ at short distances to $1/\sqrt{R}$ at large distances, with this transition occurring in the range of 40–70 km. This change has been interpreted to be the combination of the effects of post-critical reflections from the lower crust and transition from direct body wave to *Lg* wave spreading (Atkinson and Mereu 1992). Models of the decay of Fourier spectra with distance in California have found or assumed that the geometric spreading is proportional to $1/\sqrt{R}$ for distances greater than 40 km (Raoof et al. 1999; Erickson et al. 2004) and this form of geometric spreading was used by Atkinson and Silva (2000) to model strong ground motions. Earlier, Atkinson and Silva (1997) used a trilinear form of attenuation similar to that defined by Atkinson and Mereu (1992), but indicated that a bilinear form would also work as well.

We explored this effect by modeling spectral accelerations from 666 broadband recordings from three small Southern California earthquakes (2001 Anza, **M** 4.92; 2002 Yorba Linda, **M** 4.27; and 2003 Big Bear City, **M** 4.92; NGA events 0163, 0167, and 0170,

respectively). These data were fit with three functional forms, a model with a single value of $C_{Geometric}$ at all distances (one-slope model):

$$\ln(y) = C_1 + C_2 F_{BBC} + C_3 F_{YL} + C_4 \ln(R_0) + \gamma R + \phi_1 \ln(V_{S30}/400)$$
$$R_0 = \sqrt{R^2 + 6^2} \tag{3.5a}$$

a model in which $C_{Geometric}$ at large distances becomes one half the value at small distances (two-slope model):

$$\ln(y) = C_1 + C_2 F_{BBC} + C_3 F_{YL} + C_4 \{\ln(R_1) + \ln(R_2)/2\} + \gamma R + \phi_1 \ln(V_{S30}/400)$$
$$R_0 = \sqrt{R^2 + 6^2}, R_1 = \min(R_0, C_8), R_2 = \max(1, R_0/C_8) \tag{3.5b}$$

and a model in which $C_{Geometric}$ is fixed at -0.5 for larger distances (two-slope, second fixed model):

$$\ln(y) = C_1 + C_2 F_{BBC} + C_3 F_{YL} + C_4 \ln(R_1) - 0.5 \ln(R_2) + \gamma R + \phi_1 \ln(V_{S30}/400)$$
$$R_0 = \sqrt{R^2 + 6^2}, R_1 = \min(R_0, C_8), R_2 = \max(1, R_0/C_8) \tag{3.5c}$$

Dummy variables F_{BBC} and F_{YL} along with C_1 were used as earthquake terms; we did not use magnitude scaling with random effect terms because the magnitude range is small (4.33–4.92). The analysis was conducted for spectral periods in the range of 0.01–5 sec. Examination of the recordings indicated that they could be used without processing to periods at least as long as 5 sec.

Figure 3.8 shows the results of fitting the above three equations to the data. At all spectral periods, the two-slope models produced slightly smaller standard errors than the single slope model. The location for the break in slope varied between 40 and 60 km distance. In addition, use of the single-slope model produces unrealistic positive values of the anelastic attenuation term γ for longer period motions, a fact also noted by Atkinson and Silva (1997).

Examination of ShakeMap *pga* data from many of the better-recorded small-magnitude earthquakes shows that there is a decrease in the rate of attenuation at distances in the range of 40–70 km (Appendix D). Tests of the PEER-NGA data also show that a two-slope model is statistically significant with a slope break also in the range of 45–60 km. Examination of the 1-D

rock numerical simulation data (Somerville et al. 2006) also indicate that a two-slope model provides a good fit with a break in slope at about 60 km.

Based on the above observations, we adopted the concept of a change in the rate of attenuation occurring at some transition distance. If one were to use an abrupt change in rate of attenuation, then the best-fit change-point distance may vary from earthquake to earthquake as a function of a number of parameters including source depth, source size, and the local crustal thickness. Instead, we use a smooth transition over a broad distance range to provide a fit to the average behavior of all earthquakes represented in the selected database.

3.2.3 Formulation for Distance Attenuation

Equation (3.5d) defines the formulation used in our study for distance attenuation. It incorporates magnitude-dependent extended source effects, potentially magnitude-dependent wave propagation effects on response spectra at large distances, and a smooth transition from dominance of ground motions by direct waves at small distances, modeled by attenuation coefficient c_4, to dominance by *Lg* waves at large distances, modeled by attenuation coefficient c_{4a}.

$$\ln(y) \propto c_4 \ln\left[R_{RUP} + c_5 \cosh\left\{c_6 \max(\mathbf{M} - 3, 0)\right\}\right] + (c_{4a} - c_4) \ln\sqrt{R_{RUP}^2 + c_{RB}^2} + \gamma(\mathbf{M}) R_{RUP} \qquad (3.5d)$$

Coefficient c_4 was examined by analyses of PEER-NGA data and ShakeMap data. It was concluded that a range of values for c_4 would provide satisfactory fits to the data with adjustments to the rate of near-source attenuation occurring through changes of coefficients c_5 and c_6. Therefore, c_4 was fixed at -2.1, the value obtained originally by Sadigh et al. (1997) for rock sites.

Coefficient c_{RB} defines the midpoint of the transition in rate of attenuation from c_4 to c_{4a}. As discussed above similar transition points were found from analyses of the extended data sets for the three small southern California earthquakes, the NGA data, and the 1-D rock simulations. We therefore, set the value of c_{RB} to be 50 km, the central value of the estimates we obtained from the various data sets.

The appropriate value of the attenuation rate at distances beyond c_{RB}, coefficient c_{4a}, cannot be readily determined from the data because it is highly correlated with the assessment of the anelastic attenuation coefficient γ, as had been noted by many previous investigators (Atkinson 1989; Frankel et al. 1990). Therefore, we assume that c_{4a} equals to -0.5, and let the anelastic attenuation coefficient γ account for departures from this value.

The anelastic attenuation coefficient γ is allowed to be magnitude dependent. Boatwright et al. (2003) found magnitude-dependence in the anelastic attenuation coefficient from their study of *pga* and *pgv* from northern California ShakeMap, with increasing magnitude producing smaller absolute values of γ (less energy absorption). In addition, stochastic simulations of ground motions using a magnitude-independent Q model produce magnitude-dependence in the resulting anelastic attenuation coefficient γ obtained from fits to response spectral ordinates (Campbell 2003). This effect was also noted in our fitting of ground motions simulated using the Atkinson and Silva (2000) ground motion model. The effect is likely due to a shift to lower-frequency ground motion driving the response of a damped oscillator (and driving *pga*, Boatwright et al. 2003) as the size of the earthquake increases. Estimation of $\gamma(\mathbf{M})$ is further discussed in the next section.

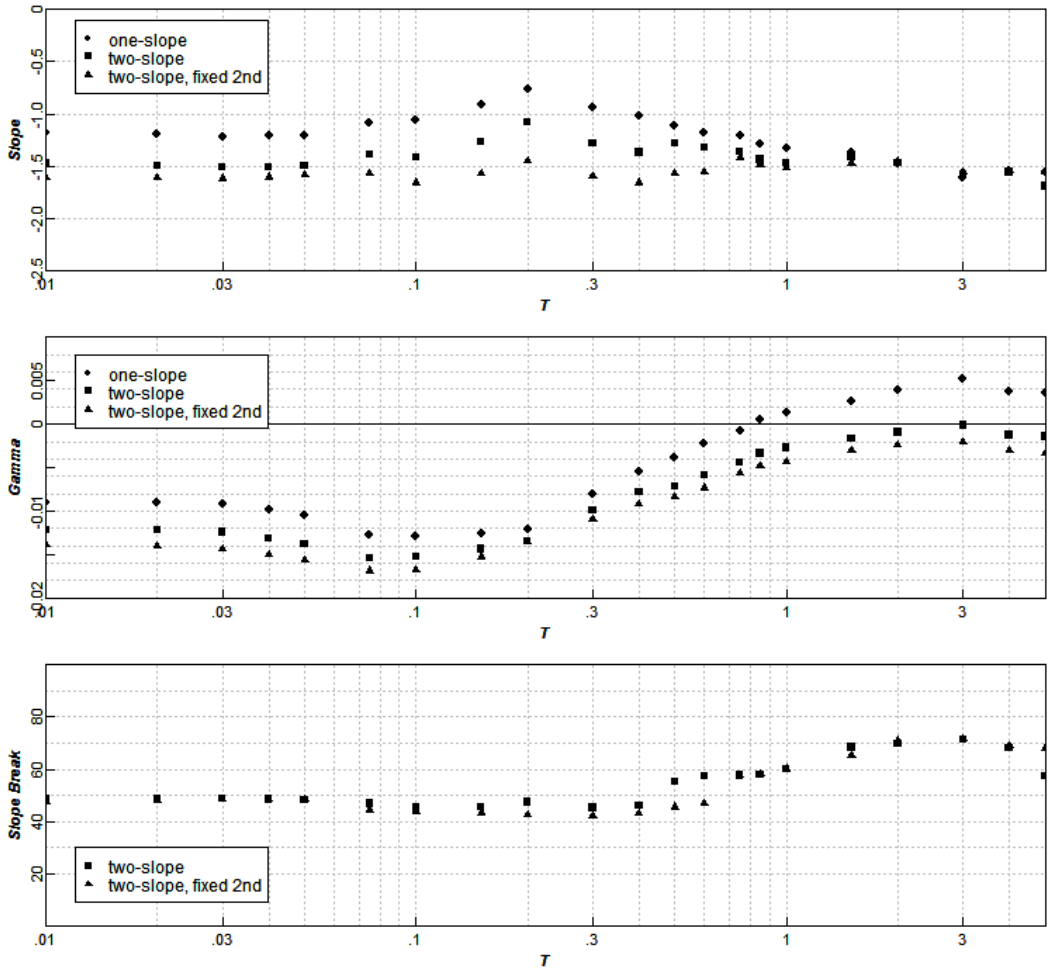

Fig. 3.8 Coefficients resulting from fits of Eqs. (3.5a), (3.5b), and (3.5c) to the broadband data for earthquakes 0163, 0167, and 0170. T is spectral period in sec.

3.2.4 Data Truncation and Estimate of γ

The initial analyses of the PEER-NGA data suggested that the anelastic attenuation coefficient γ in Equation (3.5d) was 50% larger in absolute value for earthquakes in Taiwan than for earthquakes in California or the other active tectonic regions represented in the selected database. This would imply that Q for Taiwan was significantly lower than Q for California or the other regions. However, review of the literature failed to produce studies that confirmed this result. In addition, the estimates of γ obtained from the extensive broadband data for the three southern California earthquakes were inconsistent with the values obtained for California earthquakes from fitting the PEER-NGA data.

These results led us to consideration of the effects of missing response data on the estimation of ground motion model coefficients. There are two forms of missing response data treated in the literature: censoring and truncation. Censoring occurs when a known set of instruments is triggered, but the response is only known to be below $y_{truncation}$. In this case, the number of censored observations and predictor variables for these observations (e.g., **M**, R_{RUP}, and V_{S30}) are known for the censored sample. Truncation occurs when the observed sample is truncated at some response level $y_{truncation}$ such that no responses are reported below this level. The number of missing values and values of the predictor variables for these observations are unknown. The two forms of missing response variables lead to different forms of the sample likelihood function in fitting models by maximum likelihood.

Censoring/truncation of the strong motion database occur due to the occurrence of ground motions below the trigger threshold for the recording instruments and from the selective processing of recordings favoring those with larger amplitudes. Censoring/truncation occurs also from record processing as frequency bands with low signal/noise ratios are filtered out of the processed records. Although the number of possible recordings in a given earthquake is knowable, some instruments may have malfunctioned and there is not a complete accounting of the possible instruments available. Therefore, the truncation model is considered the more appropriate condition for the PEER-NGA database.

Evidence of truncation of the PEER-NGA data is shown in Figure 3.9. The solid data points are *pga* values for the processed acceleration time histories in the PEER-NGA database. The open data points are additional *pga* values obtained from other recordings. The PEER-NGA data and the extended data for each earthquake were fit using a truncated regression model (Toro 1981; Bragato 2004), and the truncation levels are shown by the dotted and dash-dotted lines, respectively, in Figure 3.9. For the Northridge earthquake, similar estimates of γ were obtained from the PEER-NGA and the extended data set. However, for the other three earthquakes, the estimate of γ obtained from the PEER-NGA data set were approximately 2/3 of the values obtained from the extended data sets, indicating that truncated regression using the PEER-NGA data set tends to underestimate the appropriate absolute value of γ.

To further investigate the underestimation of γ, extended *pga* and *pgv* data sets were developed for 11 earthquakes in the PEER-NGA database plus three additional recent California earthquakes (Table 3.1). The PEER-NGA set of earthquakes was supplemented by data from the Feb 2, 2000, Loma Linda; Dec 23, 2003, San Simeon; and the Sept 28, 2004, Parkfield

earthquakes. In addition, an extended data set was developed for the 1995 Kobe earthquake using the data presented in Fukushima et al. (2000). Additional *pga* data for Northridge (EQID 0127) were supplied by Vladimir Graizer (personal communication 2006). The remaining California data were obtained from the ShakeMap web pages, of which only the high broadband data were used. For each of these earthquakes, estimates of γ were made using truncated regression and using Equation (3.5d) to model distance attenuation with coefficient c_{4a} fixed at -0.5. To remove the influence of hanging-wall effects, hanging-wall and footwall sites were removed. As indicated by the results in Table 3.1, the absolute values of γ computed using only PEER-NGA data were typically smaller than those obtained from the extended data. The few cases where the PEER-NGA data produced larger (and often unrealistic) values of γ are for earthquakes with very limited samples in the PEER-NGA database (e.g., San Juan Bautista, Mohawk Valley).

Based on the above analyses we conclude that regression analyses using the PEER-NGA data will tend to underestimate the rate of anelastic attenuation due to data truncation and that the problem cannot be solved using truncated regression. Our solution is to estimate the anelastic attenuation coefficient γ from the extended data sets developed for individual earthquakes. We then estimate the remaining model coefficients from the PEER-NGA data truncated at a maximum distance of 70 km. This distance was selected by visual inspection as the point where, on average, data truncation may begin to affect the distribution of recordings in the PEER-NGA database. We believe that this (short-term) solution should provide an appropriate model for California earthquake ground motions. We also believe that the model properly represents the attenuation of ground motion at larger distances in California. The issue we have raised points out the need to systematically collect and process all recordings from moderate to large earthquakes in order to correctly model the attenuation of ground motions at large distances.

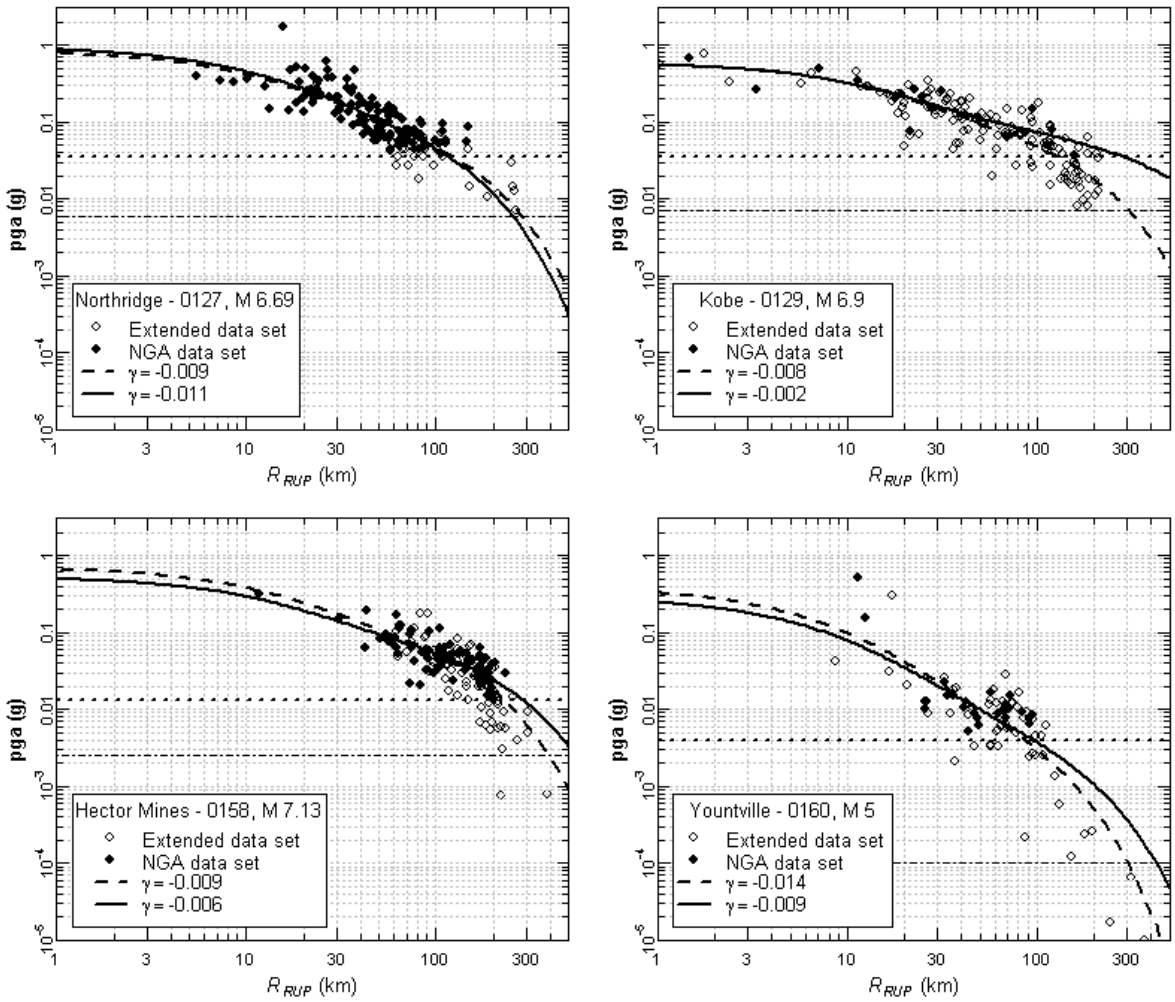

Fig. 3.9 Comparison of fits to expanded data sets (open plus solid points, dashed curve) and PEER-NGA data only (solid points, solid curve) for individual earthquakes using truncated regression. Truncation levels are indicated by the horizontal dashed lines for enhanced (dash-dotted) and PEER-NGA only (dotted) data sets. Hanging-wall sites were not included in fits for Northridge.

3.2.5 Magnitude Dependence of γ

The values of γ obtained from the extended data sets (shown in Fig. 3.10) show that γ decreases in absolute value with increasing magnitude, similar to results reported by others from analysis of empirical data (Campbell 1993) and stochastic ground motion simulations (Campbell 2003).

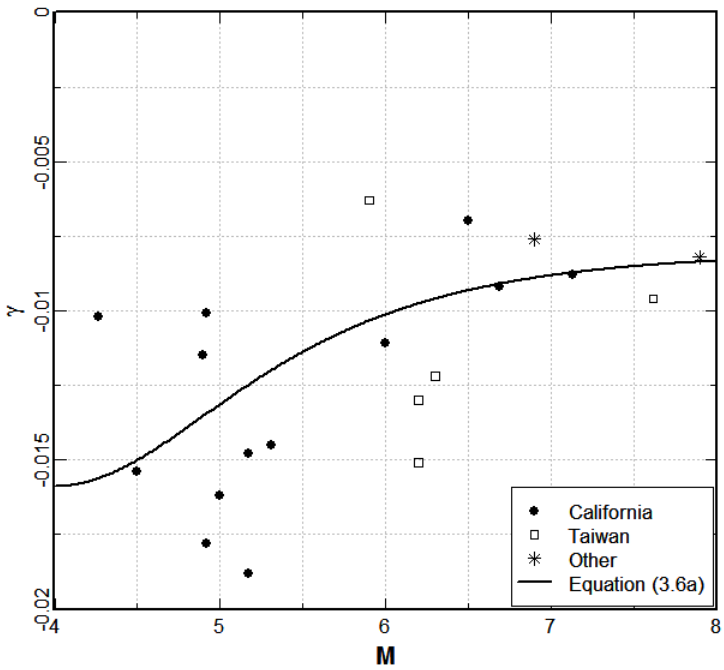

Fig. 3.10 Estimates of γ for individual earthquakes and model fit to California earthquake data.

Because we are interested primarily in modeling earthquake ground motions in the western United States, we develop a model for γ from the results for the 13 California earthquakes for which we developed extended data sets. The resulting relationship is:

$$\gamma(pga)_{California} = -0.00804 - 0.00785 / \cosh\{\max(\mathbf{M} - 4, 0)\} \tag{3.6a}$$

This relationship is plotted in Figure 3.10. The limited data for earthquakes from other regions (Kobe, Japan; Denali, Alaska; Chi-Chi main shock and aftershocks, Taiwan) are generally consistent with this relationship. The data indicate that the value of γ for Taiwan may be slightly greater than that for California, but the difference is much less than the 50-percent larger values for Taiwan obtained from the initial regressions using the full PEER-NGA database. Equation (3.6a) provides a relationship for γ at *pga*. The relationships for other spectral periods were constructed by scaling the period-dependent γ estimated from the broadband data for the three small southern California earthquakes ($\gamma(T)_{Anza\text{-}YL\text{-}BBC}$) by the relative difference in γ at *pga*, that is:

$$\gamma(T)_{California} = \gamma(T)_{Anza-YL-BBC} \times \frac{\gamma(pga)_{California}}{\gamma(pga)_{Anza-YL-BBC}} \tag{3.6b}$$

Figure 3.11 compares the model developed for γ with values obtained from direct regression of the PEER-NGA data without imposing any distance truncation and without using truncated regression. The variation of γ with spectral period T is similar.

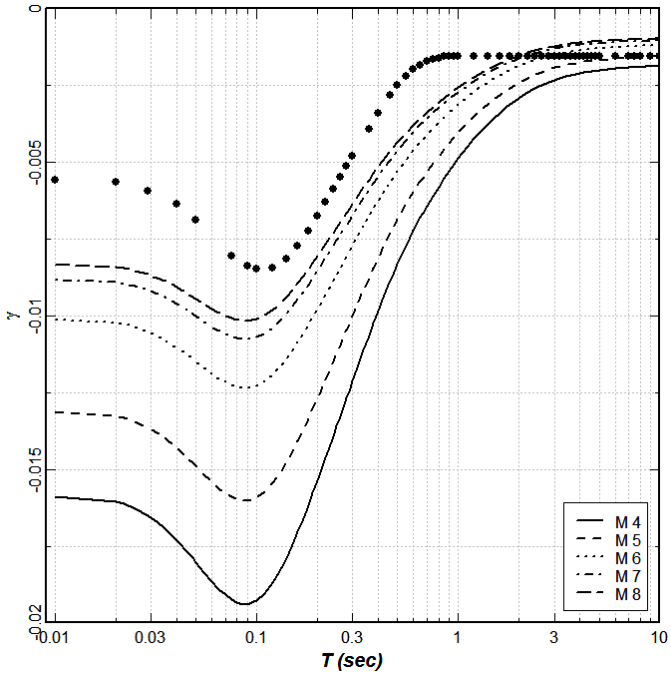

Fig. 3.11 Comparison of the model developed for γ (Eqs. 3.6a–b) versus values of γ obtained from regression without truncation (solid circles) of PEER-NGA data set.

3.3 HANGING-WALL EFFECTS

Based on analyses of ground motions from reverse earthquakes, Somerville and Abrahamson (1995) and Abrahamson and Somerville (1996) proposed the so-called hanging-wall effect in which ground motions are enhanced in the hanging wall of reverse earthquakes. The effect was attributed to the inability of the R_{RUP} distance measure to capture the general proximity of a hanging-wall site to rupture on the fault plane dipping beneath it. Chiou et al. (2000) performed extensive analyses of empirical and numerical modeling data for reverse fault ruptures and reached the same conclusion. They were able to remove the hanging-wall effect by using a root-

mean-squared distance measure, R_{RMS}. The hanging-wall effect is also seen in the 1-D rock ground motion simulations conducted for the PEER-NGA project (Somerville et al. 2006).

Table 3.1 Estimate of anelastic attenuation parameter γ for individual earthquakes.

EQID	Earthquake	M	PEER-NGA Data Set		Expanded Data Set		Region
			γ	Number of Recordings	γ	Number of Recordings	
0127	Northridge	6.69	-0.0108	122	-0.0092	154	California
0129	Kobe	6.9	-0.0020	22	-0.0076	157	Japan
0137	Chi-Chi	7.62	-0.0096	305			Taiwan
0157	San Juan Bautista	5.17	-0.0392	2	-0.0188	23	California
0158	Hector Mines	7.13	-0.0056	82	-0.0088	163	California
0160	Yountville	5	-0.0088	24	-0.0162	76	California
0162	Mohawk Val, Portola	5.17	-0.0191	6	-0.0148	36	California
0163	Anza-02	4.92	-0.0164	72	-0.0178	193	California
0165	CA/Baja Border Area	5.31	-0.0433	9	-0.0145	142	California
0166	Gilroy	4.9	-0.0054	34	-0.0115	136	California
0167	Yorba Linda	4.265	-0.0851	12	-0.0102	207	California
0169	Denali	7.9	-0.0082	23			Alaska
0170	Big Bear City	4.92	-0.0004	35	-0.0101	262	California
0171	Chi-Chi, Taiwan-02	5.9	-0.0063	277			Taiwan
0172	Chi-Chi, Taiwan-03	6.2	-0.0151	225			Taiwan
0173	Chi-Chi, Taiwan-04	6.2	-0.0130	241			Taiwan
0174	Chi-Chi, Taiwan-05	6.2	-0.0130	310			Taiwan
0175	Chi-Chi, Taiwan-06	6.3	-0.0122	260			Taiwan
	Loma Linda	4.5			-0.0154	93	California
	Parkfield	6			-0.0111	308	California
	San Simeon	6.5			-0.0070	225	California

Abrahamson and Silva (1997) included the hanging-wall effect in their empirical ground motion model as a distance-dependent term with an abrupt switch from no effect to full effect as one crosses into the hanging-wall region. Boore et al. (1997) conclude that their use of R_{JB} implicitly accounts for the hanging-wall effect in that all sites directly above the rupture have R_{JB} = 0. Campbell and Bozorgnia (2003) introduces a smooth variation in the hanging-wall effect by tapering the effect from a maximum at R_{JB} = 0 to zero for R_{JB} > 5 km. We use the following model to represent the hanging-wall effect:

$$f_{HW} = F_{HW} \times tanh\left(\frac{R_X \cos^2 \delta}{c_{9a}}\right) \times \left[1 - \frac{\sqrt{R_{JB}^2 + Z_{TOR}^2}}{R_{RUP} + 0.001}\right] \tag{3.7}$$

where δ is fault dip and R_X represents the site coordinate (in km) measured perpendicular to the fault strike from the surface projection of the up-dip edge of the fault plane, as illustrated in Figure 3.12. Note that R_X is negative for sites on the footwall side of the fault trace. Parameter F_{HW} is 1 for $R_X \geq 0$ and 0 for $R_X < 0$. Generalization of R_X's definition to the case of a multi-segment fault can be found in Spudich and Chiou (2008).

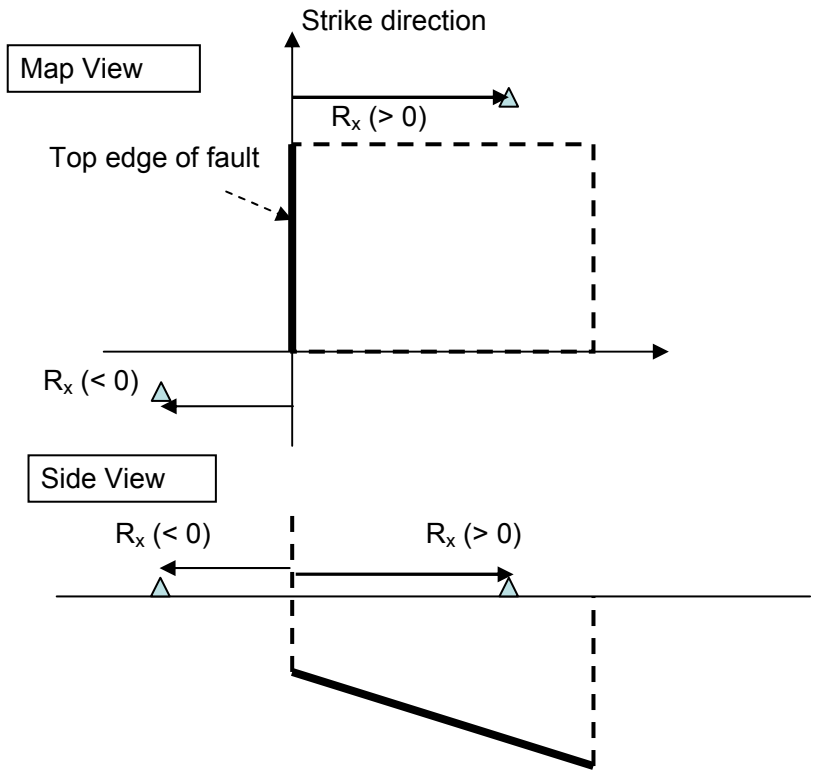

Fig. 3.12 Definition of variable R_X.

The motivation for Equation (3.7) is as follows. The third term of Equation (3.7) is motivated by the modeling of Boore et al. (1997) and Campbell and Bozorgnia (2003) in that f_{HW} decreases as R_{JB} increases. Placing R_{RUP} in the denominator produces a smooth transition in the spatial extent of the hanging-wall effect at various locations in the hanging wall. This behavior is demonstrated by the examples shown in Figures 3.13–3.14. Figure 3.13 shows a map view of a fault rupture with the top of rupture located at x=0 and the fault dipping toward positive x. Figure 3.14 shows the variation of $[1 - R_{JB} / R_{RUP}]$ with location along three lines for the case of $Z_{TOR} = 0$ (i.e., the top of rupture is at the ground surface). Line 1 runs from negative x values in the footwall to positive x values in the hanging wall. Lines 2 and 3 show the variation of

$[1 - R_{JB} / R_{RUP}]$ as one moves away from the rupture along strike. For hanging-wall sites not directly above but near the top of the rupture (Line 2) R_{RUP} is only slightly larger than R_{JB} and $[1 - R_{JB} / R_{RUP}]$ decreases rapidly as one move away from the rupture. For sites near the bottom edge of the rupture (Line 3) $R_{RUP} >> R_{JB}$ and $[1 - R_{JB} / R_{RUP}]$ decreases more slowly as one moves away from the rupture. The function $[1 - R_{JB} / R_{RUP}]$ decays much more rapidly for Line 2 than for Line 3. Most of Line 2 lies outside of the hanging-wall region defined by Abrahamson and Somerville (1996) as subject to the hanging-wall effect, while much of Line 3 for small values of y lies near the hanging-wall region. The functional form $[1 - R_{JB} / R_{RUP}]$ gives similar spatial extent of the hanging-wall region to that defined by Abrahamson and Somerville (1996), but provides for a smooth transition in the level of the hanging-wall effect along the strike region.

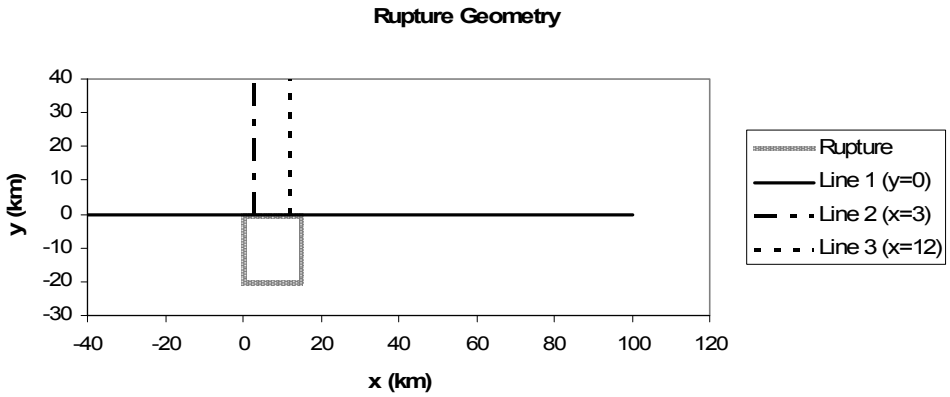

Fig. 3.13 Map view of example fault rupture.

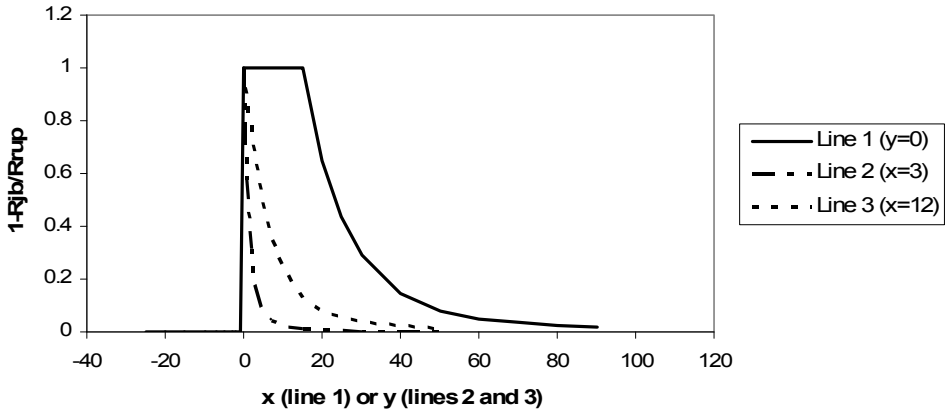

Fig. 3.14 Variation of the term $[1 - R_{JB} / R_{RUP}]$ with location for the three lines shown in Fig. 3.13. Top of rupture is at the ground surface at *x*=0.

The value of 0.001 km is added to provide numerical stability when R_{RUP} equals 0. Assuming the hanging-wall effect is a geometric effect, as the same size rupture is moved to deeper depths, we would expect the hanging-wall effect to be less. This trend has been observed in the PEER-NGA data and in the study by Chiou et al. (2000). The Z^2_{TOR} in $\sqrt{R^2_{JB} + Z^2_{TOR}}$ is used to model the decrease in the hanging-wall effect with increasing depth of rupture.

The second term of Equation (3.7) modifies the third term to capture several additional geometric aspects of the hanging-wall effect. Examination of the simulation results presented in Chiou et al. (2000) and those conducted for the NGA project (Somerville et al. 2006) indicated that the hanging-wall effect decreases to near zero as one approaches the up-dip edge of the rupture (R_X approaches 0). To model this behavior, the $\tanh(R_X/c_{9a})$ function tapers the hanging-wall effect on and near the up-dip edge of rupture. The simulated data also show that the hanging-wall effect decreases with increasing dip angle. Assuming that the hanging-wall effect is a geometric effect, this trend with δ is expected. Figure 3.15 shows residuals for sites on the hanging wall of reverse faults (R_{JB} = 0) plotted versus δ. The data indicate increasing motion with decreasing δ, consistent with the trend seen in simulations. In Figure 3.15 the trend was modeled with linear functions 90º - δ, $\cos(\delta)$, and $\cos^2(\delta)$. All three functions show a significant trend with the residuals, with $\cos^2(\delta)$ providing a slightly better fit than the other two models. Similar results were found for data from sites with $[1 - R_{JB} / R_{RUP}] > 0.8$ and for data from sites with $R_{JB} < 5$ km. We use $\cos^2(\delta)$ in our model to represent the dependence on δ. Finally, we expect that smaller overall ruptures would produce less effect than larger rupture, given the same values of R_{JB} and R_{RUP}. Previous implementations of the hanging-wall effect in empirical models have reduced the effect to 0 for magnitudes less than **M** 6. Equation (3.7), combined with the fact that the fault rupture width decreases as the magnitude decreases, automatically produces a decrease in the hanging-wall effect with decreasing magnitude.

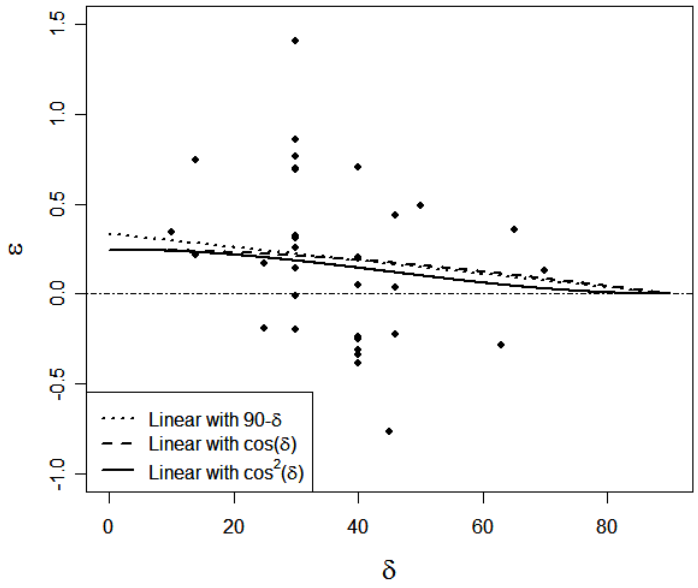

Fig. 3.15 Intra-event residuals from fitting a model without a hanging-wall term for sites with $R_{JB} = 0$ and $F_{HW} = 1$ plotted against fault dip, δ.

The behavior of f_{HW} defined in Equation (3.7) is illustrated in Figure 3.16 for three magnitudes and two values of Z_{TOR}. The plots show the value of f_{HW} for sites located directly above or down dip of the rupture surface. Note that the locations of the bottom edge of the ruptures correspond with the peaks in the f_{HW} curves.

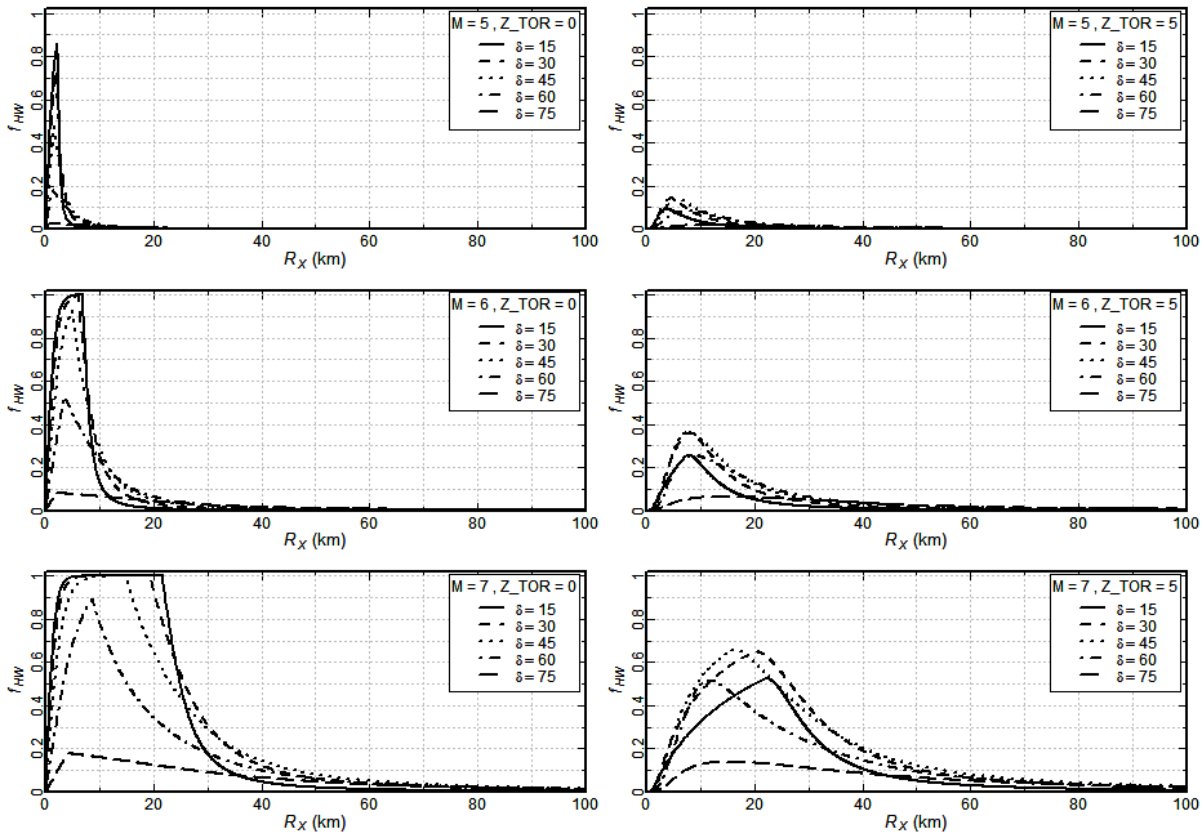

Fig. 3.16 Illustration of the hanging-wall geometric factor f_{HW} for sites located directly above or down dip of rupture plane. Left plots are for M 5, 6, and 7 earthquakes with $Z_{TOR} = 0$. Right plots are for M 5, 6, and 7 earthquakes with $Z_{TOR} = 5$ km. Note that locations of the bottom edges of ruptures correspond with peaks in f_{HW} curves.

3.4 SITE EFFECTS

3.4.1 Near-Surface Geology

The incorporation of the effects of near-surface geology or site classification has gone through an evolution in the past 10 years. At the beginning of this period, ground motion models typically contained a scaling parameter based on site classification (Boore et al. 1993), or presented different models for "rock" and "soil" sites (Campbell 1993; Sadigh et al. 1997). Classification of recording sites into rock or soil sites varied among investigators. Boore et al. (1997) introduced the explicit use of the average shear-wave velocity in the upper 30 meters, V_{S30}, in the ground motion model. Abrahamson and Silva (1997) building on an earlier model by Youngs (1993) introduced the explicit modeling of nonlinear site effects in the ground motion model.

The model we have developed for incorporating near-surface geology combines these concepts using the formulation:

$$ln(y) = ln(y_{ref}) + f_{site}(V_{S30}, y_{ref}, \eta) \tag{3.8}$$

Parameter y_{ref} is the population median motion on the reference site condition derived from the source and path scaling models described in the previous sections; see also Equation (3.12a) below. Parameter η is the earthquake effect term (also called the random-effect term), representing the deviation of the median reference motion for a given earthquake from the population median. Note that y_{ref} and η are combined to form the event-specific median reference motion $y_{ref}\, e^{\eta}$ that drives the nonlinear part of f_{site} (see Eq. 3.12.b and explanation in Chapter 4). In the discussions below, we sometimes drop the event term η and the word 'event-specific' for convenience of discussion.

The reference site V_{S30} was chosen to be 1130 m/sec because it is expected that there will not be significant nonlinear site response at this velocity. In addition, there are very few data with values of V_{S30} greater than 1100 m/sec in the PEER-NGA database. The reference motion is defined to be the spectral acceleration at the spectral period of interest for two reasons. Bazzurro and Cornell (2004) indicate that the spectral acceleration at spectral period T is "the single most helpful parameter" for the prediction of site amplification at that period. In addition, estimation of the coefficients of ground motion model is performed using random (mixed) effects regression in which the reference motion includes the random event term. Use of the reference spectral acceleration at period T to estimate surface ground motions at the same period eliminates the need to include the correlation in the random effects between those at period T and those at another period or *pga*.

The function form for the site response model f_{site} with y_{ref} computed at V_{S30} equal to 1130 m/sec is given by:

$$f_{site}(V_{S30}, T, y_{ref}) = a(V_{S30}, T) + b(V_{S30}, T) \ln\left[\frac{y_{ref}(T) + c(T)}{c(T)}\right]$$

$$a(V_{S30}, T) = \phi_1(T) \ln\left[\frac{V_{S30}}{1130}\right] \tag{3.9}$$

$$b(V_{S30}, T) = \phi_2(T)\left[\exp\{\phi_3(T) \times (\min(V_{S30}, 1130) - 360)\} - \exp\{\phi_3(T) \times (1130 - 360)\}\right]$$

$$c(T) = \phi_4(T)$$

The interpretation of coefficients *a*, *b*, and *c* is as follows (Fig. 3.17). Coefficient *a* represents the linear soil amplification factor that occurs at a small level of y_{ref}. It is modeled as a linear function of ln(V_{S30}), consistent with previous representations (Boore et al. 1997). Coefficient *c* represents the reference ground motion level in the middle of the transition from linear to nonlinear behavior. Coefficient *b* represents the nonlinear behavior in terms of the rate of decrease in site amplification, f_{site}, with increasing amplitude of y_{ref}. In general, a stronger nonlinearity in soil response corresponds to a more negative value for *b* (stronger dependence on y_{ref}). It is expected that the degree of nonlinearity is a function of the stiffness of the site soils, and this dependence is represented by making *b* a function of V_{S30}. The last term of the equation for *b* is used to produce linear response (*b* = 0) for V_{S30} = 1,130 m/sec. Figure 3.18 shows several examples of f_{site} obtained from fitting the PEER-NGA data.

The functional form of Equation (3.9) is able to represent other models of nonlinear site response, such as that developed by Choi and Stewart (2005) as well as the results of site response analyses conducted for the NGA project by Silva (2008; Walling et al. 2008). The ability of Equation (3.9) to represent nonlinear soil response derived from Silva's simulations is illustrated in Figures 3.19–3.20. Figure 3.19 shows soil amplification factors for *pga* derived from Silva's (2008) simulations. Two soil property models were used by Silva (2008; Walling et al. 2008), the EPRI (1993) set of soil modulus and damping relationships and the less nonlinear Peninsular Range set developed by Silva et al. (1996). The solid lines shown on the figure are the result of fitting Equation (3.9) to the combined amplification factors for the two soil model sets and indicate that the function form can well represent the behavior implied by nonlinear (equivalent-linear) soil response. Figure 3.20 shows the values of parameters *a* and *b* derived from the results of Silva (2008). The dashed lines show that the function forms for *a* and *b* in Equation (3.9) provide a good match to the site response results.

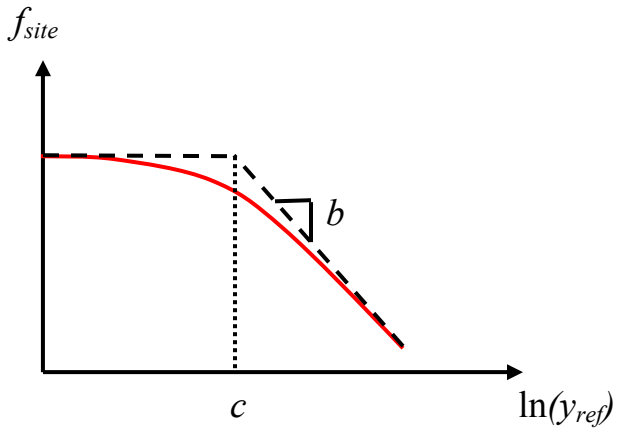

Fig. 3.17 Illustration of functional form for soil amplification effect as a function of ln(y_{ref}).

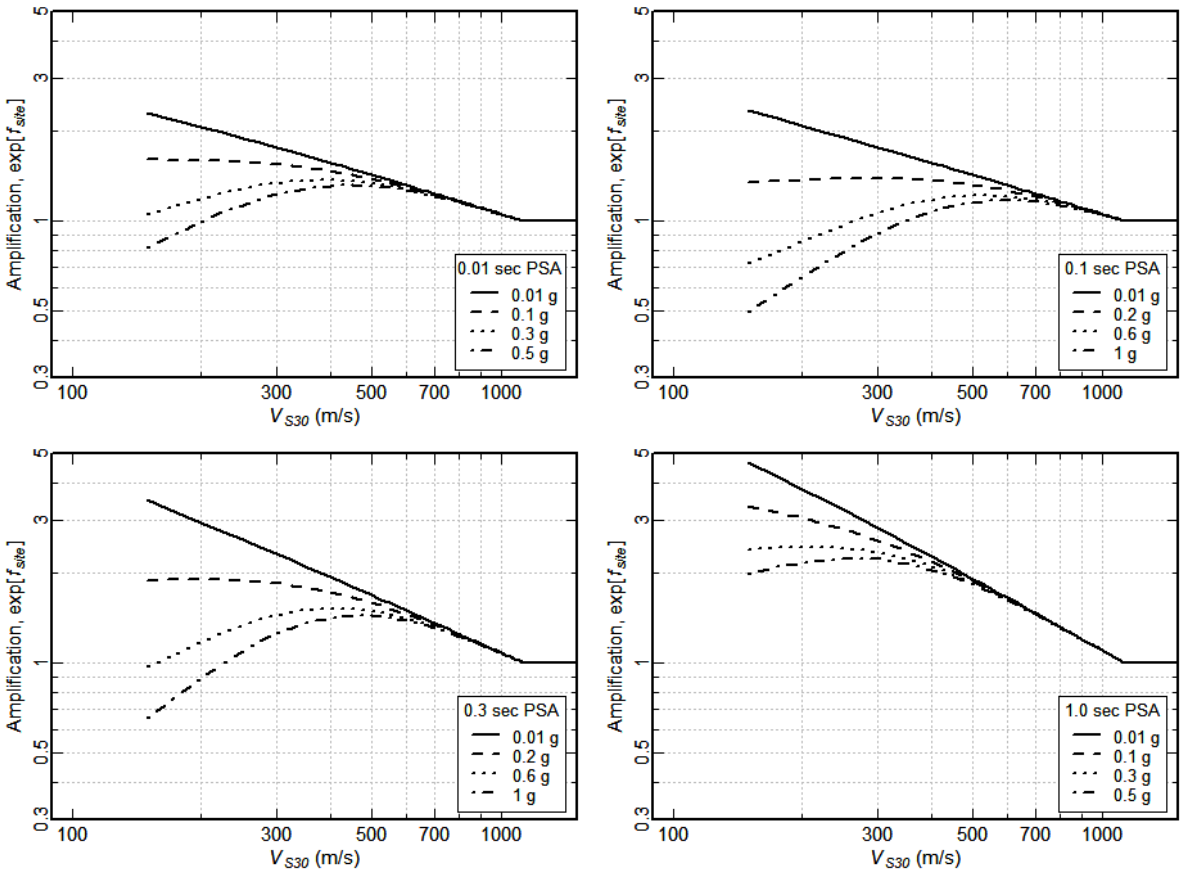

Fig. 3.18 Example site amplification as a function of spectral period, V_{S30}, and level of reference *PSA*.

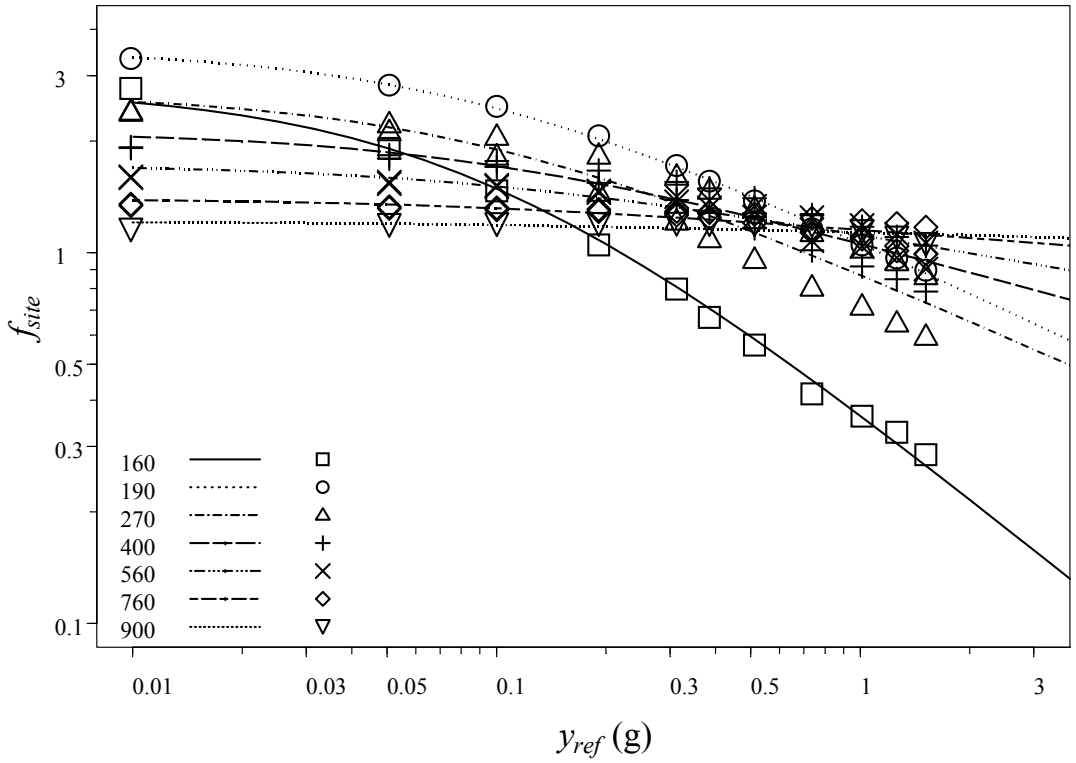

Fig. 3.19 Soil amplification for *pga* as a function of rock motion (y_{ref}) from 1-D equivalent linear site response analyses (Silva 2008).

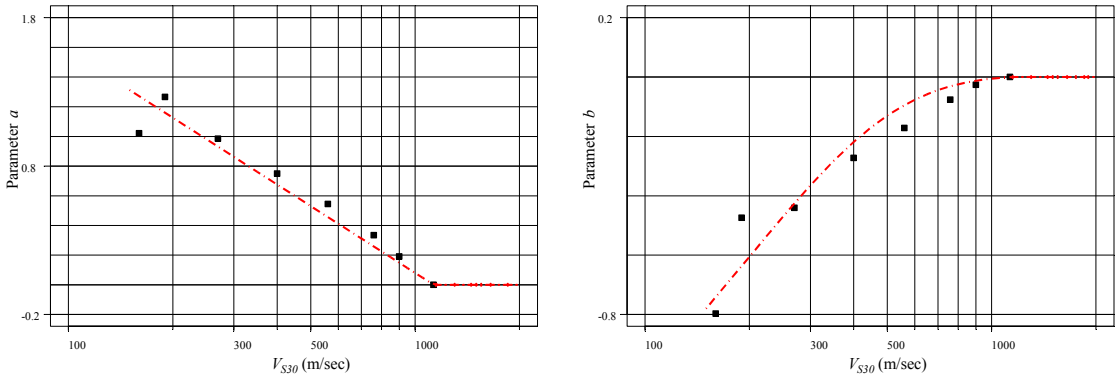

Fig. 3.20 Coefficients a and b derived from 1-D site response results of Silva (2008). Dashed lines represent fits using functional form in Eq. (3.9).

Choi and Stewart (2005) developed a model for the dependence of nonlinear soil amplification on V_{S30} and the level of input rock *pga*. Figure 3.21 compares the variation of the parameter b computed from their models with results obtained from fitting Equation (3.9) to the PEER-NGA *pga* data selected for use in this study. The functional form of Equation (3.9) provides a good match to the general behavior of the models developed by Choi and Stewart (2003).

To demonstrate the validity of Equation (3.9) in modeling the nonlinear soil amplification implied by the NGA data, we compute the intra-event residuals with respect to our final NGA model without the soil amplification effect (i.e., for a V_{S30} of 1130 m/sec). The residuals computed this way can be interpreted as soil amplification data relative to the event-specific median reference motion. The residuals for *PSA* at 0.2-sec period, grouped by the level of event-specific median reference motion, are plotted against V_{S30} in Figure 3.22. The average soil amplification factor predicted from our final NGA model is also shown in Figure 3.22 as the dot-dashed curve. For low-V_{S30} recordings subjecting to large reference motion, there are clearly defined deviations from the linear soil amplification (shown as the solid line) in a manner that is consistent with Equation (3.9).

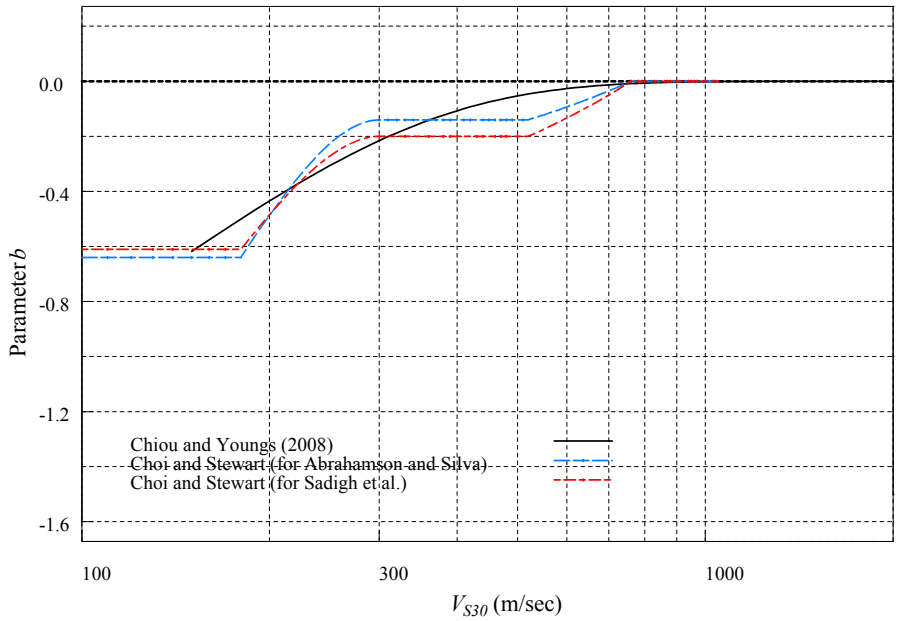

Fig. 3.21 Comparison of parameter *b* dependence on V_{S30} obtained by Choi and Stewart (2003) (dashed curve—Abrahamson and Silva 1997, reference motions; dot-dashed curve—Sadigh et al. 1997, reference motions) with trend obtained in this study from PEER-NGA data (solid line).

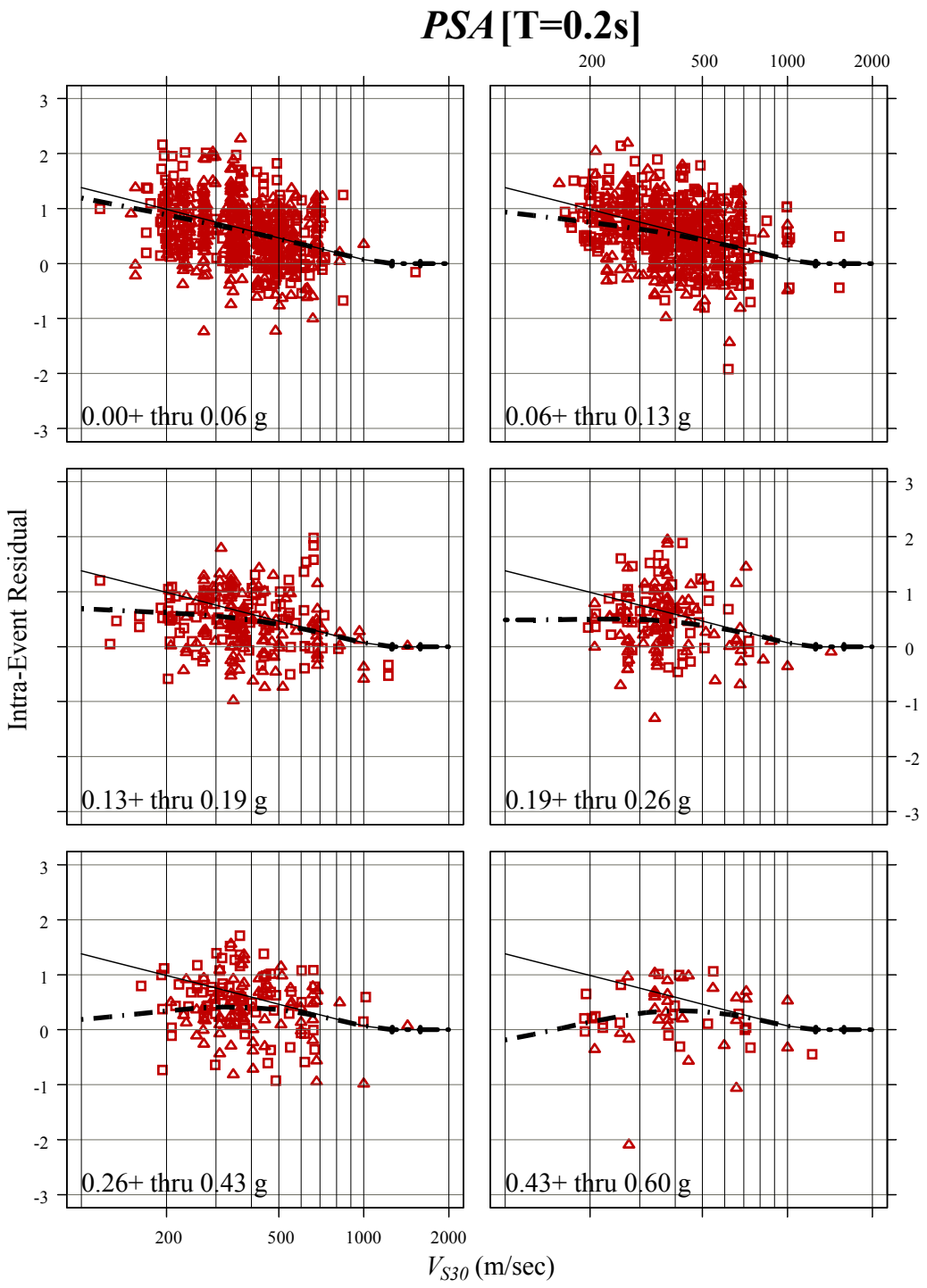

Fig. 3.22 Intra-event residuals plotted as a function of V_{S30}. These residuals are computed using the final NA model without the soil amplification effect. Square and triangle indicate data whose V_{S30} is measured and inferred, respectively. The dot-dashed curve is the predicted nonlinear soil amplification factor and the solid line is the predicted linear amplification factor. The range of event-specific median reference motion ($y_{ref}\ exp(\eta)$) is indicated in the lower left corner of each plot.

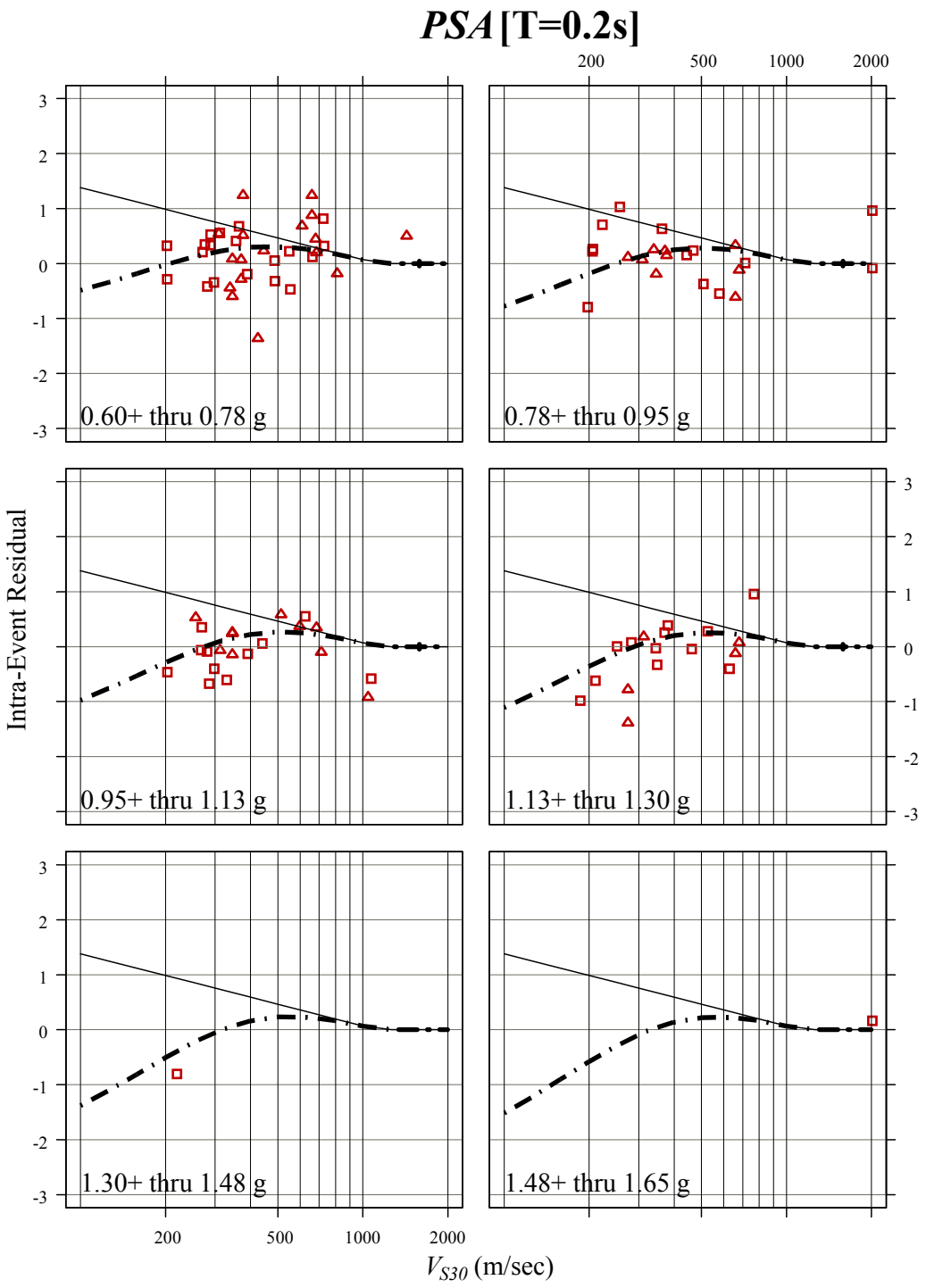

Fig. 3.22—*Continued*

3.4.2 Sediment Thickness

Most empirical ground motion models have used either a simple classification scheme (Abrahamson and Silva 1997, Sadigh et al. 1997) or V_{S30} (Boore et al. 1997) to represent soil amplification in ground motions. The success of these models suggests that surface geology or V_{S30} is often highly correlated with other site properties important to the quantification of site amplification. However, a single parameter such as V_{S30} cannot be expected to completely represent the effects of local site conditions on earthquake ground motions. Campbell (1989) found that adding a parameter for depth to basement rock improved the predictive ability of empirical ground motion models. Other investigators had proposed including basin depth to improve empirical ground motion models (Joyner 2000; Field 2000; Choi et al. 2005). In addition, successful numerical modeling of ground motions on a variety of site conditions typically incorporate a much more detailed characterization of the site velocity profile (Silva et al. 1996; Boore and Joyner 1997).

To improve the modeling in environments such as deep sedimentary basins, we add sediment thickness as a second predictor of site amplification. We define sediment thickness as the depth to a material (bedrock) with a shear-wave velocity (V_S) of 1 km/sec or greater. Shear-wave velocities of 1.5 km/sec and 2.5 km/sec have also been used to define the appropriate velocity horizon (Field 2000; Day et al. 2006). We prefer 1 km/sec because it is similar to values commonly used in practice for rock. It is also close to the reference V_{S30} (1130 m/sec) used in the V_{S30}-scaling of soil amplification. Finally, the depth to this velocity is more likely to be available as a part of site characterization than depths to higher velocity horizons. Boreholes at 54 sites in the PEER-NGA database penetrated the V_S = 1 km/sec horizon.

For the majority of NGA strong-motion sites there is a correlation between V_{S30} and $Z_{1.0}$. The intent of Equations (3.10) and (3.11), described below, is to capture departures from the general V_{S30} scaling defined by Equation (3.9).

3.4.2.1 Deep Sediment Sites

Figure 3.23 shows residuals from an interim model without a sediment depth effect plotted versus $Z_{1.0}$ for sites in the PEER-NGA database. We find that the trend can be adequately modeled by the functional form:

$$\ln(y) \propto \phi_5 \left(1 - \frac{1}{\cosh[\phi_6 \times \max(0, Z_{1.0} - \phi_7)]} \right) \tag{3.10}$$

This functional form produces behavior similar to the model developed by Day et al. (2006, 2008), allowing for the fact that Day et al. (2006) modeled the combined effect of V_{S30} and sediment depth using only sediment depth, while the residuals shown in Figure 3.23 are computed from a model that incorporates V_{S30} scaling. The main difference from the functional form of Day et al. (2006, 2008) is that we allow the affected $Z_{1.0}$ range ($Z_{1.0} > \phi_7$) to vary with spectral period, motivated by observing this trend in the residuals (Fig. 3.23). The fitted models are also shown on Figure 3.23.

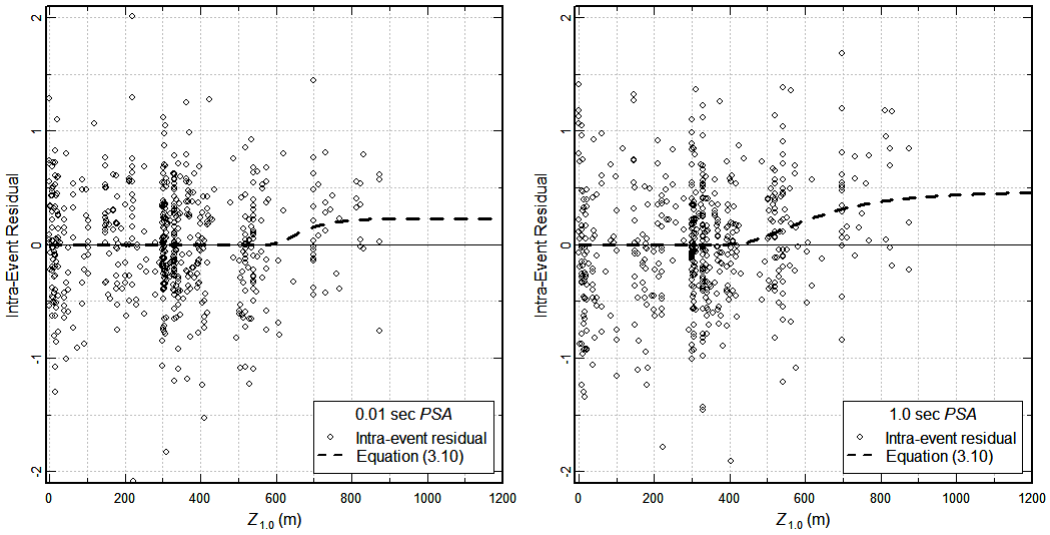

Fig. 3.23 Intra-event residuals plotted against measured $Z_{1.0}$ for 0.01-sec and 1.0-sec *PSA*. Dashed lines show fits to the residuals using Eq. (3.10).

3.4.2.2 Shallow Sediment Sites

Focusing on the shallow $Z_{1.0}$ range, we find negative average residuals in the $Z_{1.0}$ range of 5–25m for spectral periods between 0.3 and 1 sec and positive residuals at other periods (Fig. 3.24). Because of the limited data available to determine the $Z_{1.0}$ at which average residual is back to 0, we judged a value of 40 m to be reasonable, and use the following functional form to model the $Z_{1.0}$ effect on shallow rock sites:

$$\ln(y) \propto \frac{\phi_8}{\cosh(0.15 \times \max(0, Z_{1.0} - 15)} \tag{3.11}$$

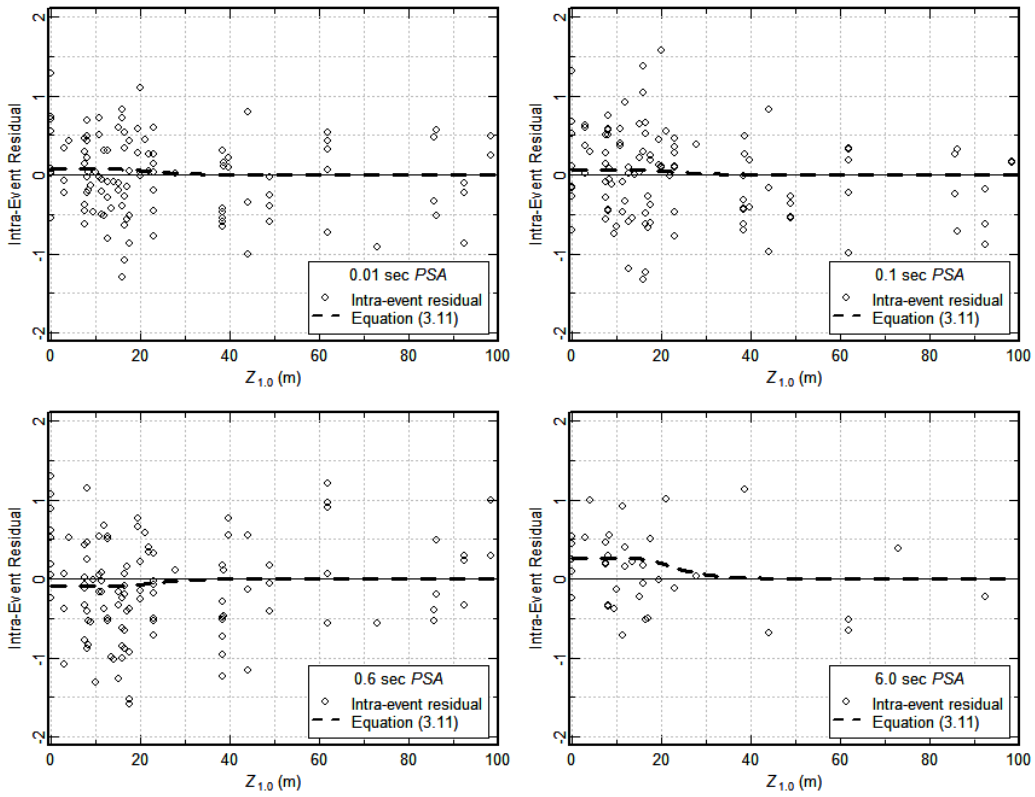

Fig. 3.24 Intra-event residuals plotted against $Z_{1.0}$ for shallow sediment sites for spectral periods of 0.01, 0.10, 0.6, and 6.0 sec. Dashed lines show fits to the residuals using Eq. (3.11).

3.5 COMPLETE MODEL FOR ESTIMATING GROUND MOTIONS

The above considerations are combined to form the final complete model formulation:

$$\begin{aligned}\ln\left(y_{ref_{ij}}\right) = {} & c_1 + \left[c_{1a}F_{RVi} + c_{1b}F_{NMi} + c_7\left(Z_{TORi} - 4\right)\right]\left(1 - AS_i\right) + \left[c_{10} + c_{7a}\left(Z_{TORi} - 4\right)\right]AS_i \\ & + c_2\left(\mathbf{M}_i - 6\right) + \frac{c_2 - c_3}{c_n}\ln\left(1 + e^{c_n\left(c_M - \mathbf{M}_i\right)}\right) \\ & + c_4\ln\left[R_{RUPij} + c_5\cosh\left\{c_6\max\left(\mathbf{M}_i - c_{HM}, 0\right)\right\}\right] \\ & + \left(c_{4a} - c_4\right)\ln\left(\sqrt{R^2{}_{RUPij} + c_{RB}{}^2}\right) \\ & + \left\{c_{\gamma 1} + \frac{c_{\gamma 2}}{\cosh\left[\max\left(\mathbf{M}_i - c_{\gamma 3},\ 0\right)\right]}\right\}R_{RUPij} \\ & + c_9F_{HWij}\tanh\left(\frac{R_{Xij}\cos^2\delta_i}{c_{9a}}\right)\left\{1 - \frac{\sqrt{R^2_{JBij} + Z^2_{TORi}}}{R_{RUPij} + 0.001}\right\}\end{aligned} \tag{3.12a}$$

and

$$\ln(y_{ij}) = \ln(y_{ref_{ij}}) + \phi_1 \cdot \min\left(\ln\left(\frac{V_{S30\,j}}{1130}\right), 0\right) + \phi_2\left\{e^{\phi_3(\min(V_{S30\,j},\,1130)-360)} - e^{\phi_3(1130-360)}\right\}\ln\left(\frac{y_{ref_{ij}} e^{\eta_i} + \phi_4}{\phi_4}\right) + \phi_5\left(1 - \frac{1}{\cosh[\phi_6 \cdot \max(0, Z_{1.0} - \phi_7)]}\right) + \frac{\phi_8}{\cosh[0.15 \cdot \max(0,\ Z_{1.0} - 15)]} + \eta_i + \varepsilon_{ij} \quad (3.12b)$$

The predictor variables for fixed effects are:

M = Moment magnitude

R_{RUP} = Closest distance to the rupture plane (km)

R_{JB} = Joyner-Boore distance to the rupture plane (km)

R_X = Site coordinate (km) measured perpendicular to the fault strike from the surface projection of the up-dip edge of the fault rupture, with the down-dip direction being positive (See Fig. 3.12)

F_{HW} = Hanging-wall flag: 1 for $R_X \geq 0$ and 0 for $R_X < 0$

δ = Fault dip angle

Z_{TOR} = Depth to top of rupture (km)

F_{RV} = Reverse-faulting flag: 1 for $30^o \leq \lambda \leq 150^o$ (combined reverse and reverse-oblique), 0 otherwise; λ is the rake angle.

F_{NM} = Normal faulting flag: 1 for $-120^o \leq \lambda \leq -60^o$ (excludes normal-oblique), 0 otherwise.

AS = Aftershock flag: 1 if the event is an aftershock, 0 otherwise

V_{S30} = Average shear-wave velocity for top 30 m (m/s)

$Z_{1.0}$ = Depth to shear-wave velocity of 1.0 km/s (m).

The variability in ground motion is represented in Equation (3.12b) by random variables η_i and ε_{ij}. Models for the variance of these two random variables are described in the next Chapter. Note that the random earthquake effect η_i appears on the 3rd line of Equation (3.12b) as well as inside the logarithmic function on the 2nd line. The reason for this formulation is also explained in the next Chapter.

4 Mixed-Effects Model Formulation and Variance Model Incorporating Nonlinear Soil Response

Equations (3.12a) and (3.12b) are a mixed-effects regression model (Brillinger and Preisler 1984; Abrahamson and Youngs 1992; Pinheiro and Bates 2000). The mixed-effects model incorporates fixed effects to model the expected amplitude of ln(y) as a function of magnitude, distance, V_{S30}, etc., and random effects to represent a random shift of all observations for an individual earthquake from this expected amplitude. Just as fixed effects described in the previous Chapter are grouped into three components representing the physical processes of source, path, and site, the random errors in our mixed-effects model are divided into four independent components of source (η_i), path (ε_{Pij}), site (ε_{Sj}), and the remaining modeling errors ε_{Xij}. The first component, η_i, represents the random earthquake effect (Brillinger and Preisler 1984; Abrahamson and Youngs 1992). This random effect, also called the inter-event residual, is attributed to the individual earthquake such that all recordings from the *i-th* earthquake deviate from the global population mean, μ, by a value η_i. The inter-event residuals are assumed to be independent and normally distributed with a zero mean and a variance τ^2.

Each of the three remaining error components is also assumed to be independent and normally distributed with a zero mean and variances σ_P^2, σ_S^2, and σ_X^2, respectively. In practice, these three error components are lumped into a combined intra-event residual ε_{ij}. Individual recording at station j from the *i-th* earthquake deviate from the earthquake-specific mean, $\mu+\eta_i$, by intra-event residuals, ε_{ij}, that are assumed to be normally distributed with variance σ^2. In the following we show that due to nonlinear soil response the variance σ^2 is a function of soil nonlinearity.

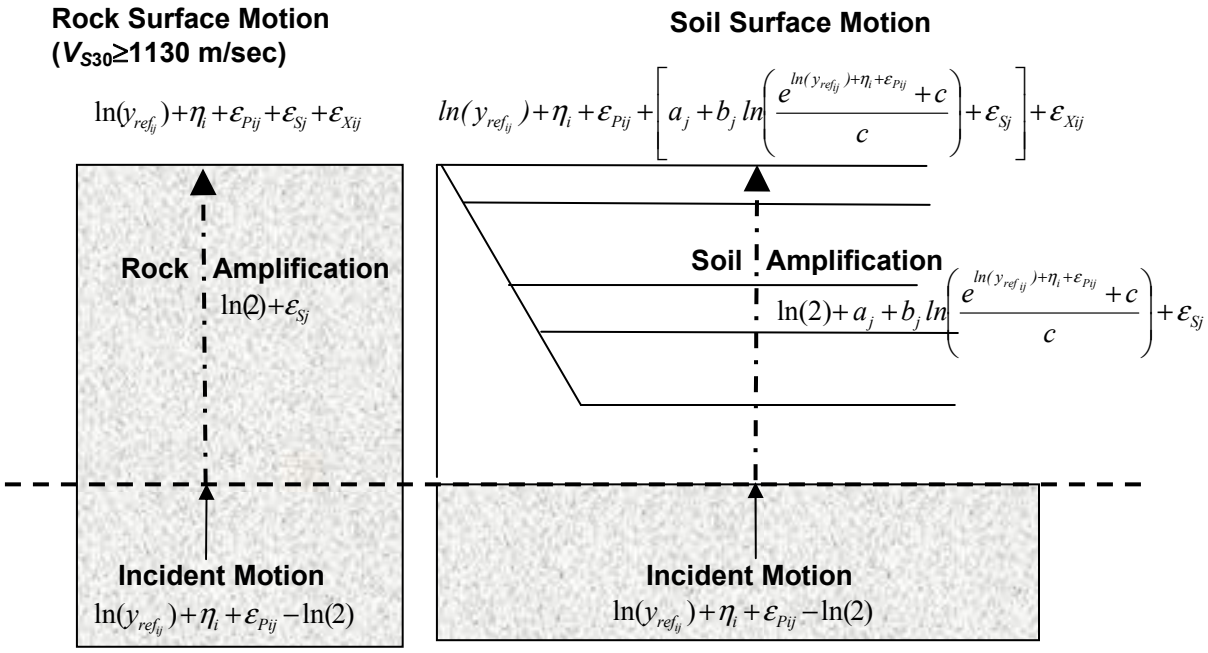

Fig. 4.1 Illustration showing framework of rock surface motion, soil amplification, and soil surface motion, assuming ε_S has the same probability density function for rock and soil surface motions.

Using the formulation of soil amplification described in Section 3.4.1 and the geotechnical framework illustrated in Figure 4.1, the surface motion $\ln(y_{ij})$ is written as:

$$ln(y_{ij}) = ln(y_{ref_{ij}}) + \eta_i + \varepsilon_{Pij} + a_j + b_j\, ln\left(\frac{e^{(ln(y_{refij})+\eta_i+\varepsilon_{Pij})}+c}{c}\right) + \varepsilon_{Sj} + \varepsilon_{Xij}, \qquad (4.1)$$

where y_{refij} is the reference motion specified by Equation (3.12a). The sum of $\ln(y_{refij})$, the earthquake term η_i, and the path error ε_{Pij} [the first three terms of Eq. (4.1)] represents the logarithm of the incident motion to the bedrock-soil column interface beneath a site. This incident motion drives the soil column and determines the average soil amplification factor for surface motion. Note that the intra-event components ε_{Sj} and ε_{Xij} are not part of the incident motion and hence they do not affect the average soil amplification factor.

Though Equation (4.1) represents fully our conceptual model of nonlinear soil amplification, its use in regression analysis of empirical data is made difficult by the lack of repeatedly sampled paths and limited repeatedly sampled sites; and by the unavailability of a

statistical inference method capable of handling the complicated data structure induced by the path error ε_{Pij} being part of the incident motion that drives the soil nonlinear response. To get around these difficulties, we move ε_{Pij} outside of $ln\left[\left(y_{ref_{ij}} e^{\eta_i+\varepsilon_{Pij}} + c\right)/c\right]$ by replacing the logarithm with the first two terms of its Taylor series expansion (a first-order approximation):

$$\ln(y_{ij}) = \ln(y_{ref_{ij}}) + \eta_i + \varepsilon_{Pij} + a_j + b_j \left(\ln\left(\frac{y_{ref_{ij}} e^{\eta_i} + c}{c} \right) + \frac{y_{ref_{ij}} e^{\eta_i}}{y_{ref_{ij}} e^{\eta_i} + c} \varepsilon_{Pij} \right) + \varepsilon_{Sj} + \varepsilon_{Xij} \tag{4.2}$$

Combining the error terms (not including η_i) into a single intra-event error ε_{ij} produces:

$$\varepsilon_{ij} = \varepsilon_{Pij} + \left[b_j \frac{y_{ref_{ij}} e^{\eta_i}}{y_{ref_{ij}} e^{\eta_i} + c} \right] \varepsilon_{Pij} + \varepsilon_{Sj} + \varepsilon_{Xij} \tag{4.3}$$

Substituting Equation (4.3) into (4.2), we obtain the mixed-effects regression model that Equation (3.12b) used in our regression analysis:

$$\ln(y_{ij}) = \ln(y_{ref_{ij}}) + \eta_i + a_j + b_j \ln\left(\frac{y_{ref_{ij}} e^{\eta_i} + c}{c}\right) + \varepsilon_{ij} \tag{4.4}$$

In Equation (4.4) the effect of η_i on nonlinear soil de-amplification is being carried exactly. The approximate effect of ε_{Pij} on soil nonlinear response is now part of the intra-event error ε_{ij}, the 2nd term of Equation (4.3).

From Equation (4.3), the variance of the intra-event error is given by:

$$\sigma^2 = \sigma_S^2 + \sigma_X^2 + \left(1 + b_j \frac{y_{ref_{ij}} e^{\eta_i}}{y_{ref_{ij}} e^{\eta_i} + c} \right)^2 \sigma_P^2 \tag{4.5}$$

It is important to note that the intra-event variance decreases with decreasing value of $\left|1 + b_j y_{ref_{ij}} e^{\eta_i} / \left(y_{ref_{ij}} e^{\eta_i} + c\right)\right|$. Therefore, the introduction of nonlinear soil response into our ground

motion prediction equation directly leads to a heteroscedastic (non-constant) intra-event variance that is dependent on the values of b (hence, V_{S30}), $y_{ref}\, exp(\eta)$, and c. The variable $NL_{ij} = \left| b_j y_{ref_{ij}} e^{\eta_i} / \left(y_{ref_{ij}} e^{\eta_i} + c \right) \right|$, which is always less than or equal to 0 because the sign of b_j is negative, can be interpreted as a measure of soil nonlinearity affecting a strong-motion recording, with a value of 0 indicating linear soil response.

One way to explore the degree of intra-event heteroscedasticity in our NGA data set is to plot intra-event residuals against $1+NL_{ij}$. Intra-event residuals for the spectral period of 0.1 sec are plotted against $(1+NL_{ij})$ in Figure 4.2. The quantities b_j, η_i, and c needed for the calculation of NL_{ij} are taken from the fitted model for T=0.1 sec. To help illustrate the variation of intra-event variance as a function of $(1+NL_{ij})$, intra-event standard errors computed for several non-overlapping intervals of $(1+NL_{ij})$ are plotted as solid squares. The dashed curves in Figure 4.2 show the fitted variance model based on Equation (4.5). They clearly show a dependency of intra-event variance on $(1+NL_{ij})$ that is consistent with Equation (4.5).

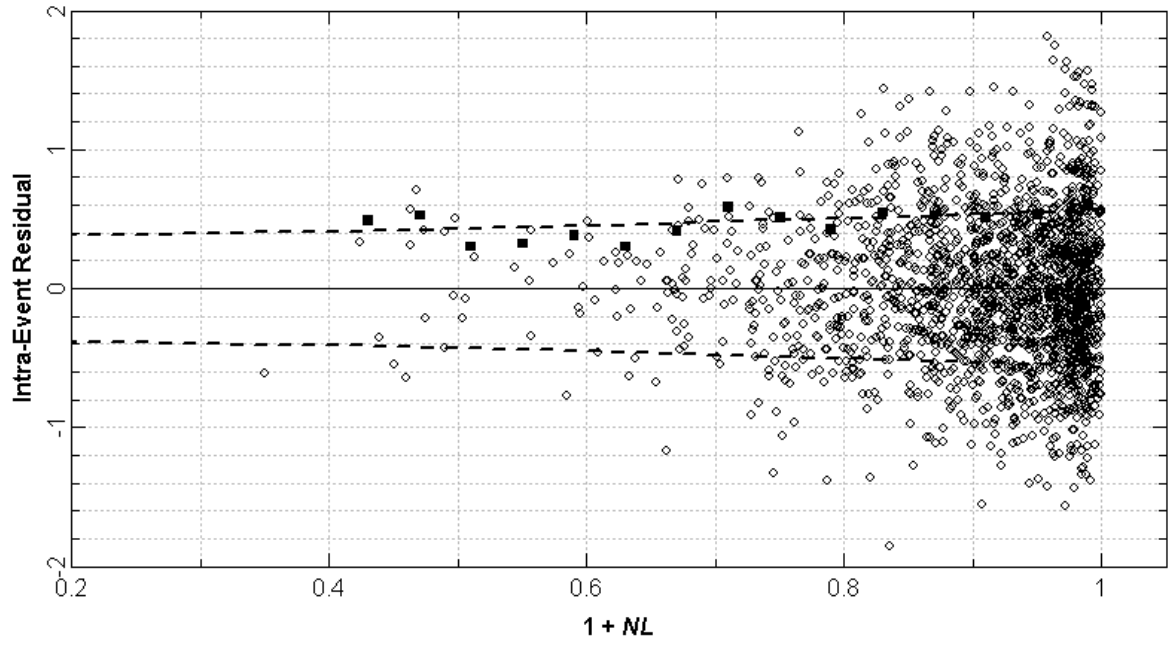

Fig. 4.2 Intra-event residuals for 0.1-sec *PSA* plotted against variance covariate (*1+NL*). Solid squares are bin estimates of standard deviation; dashed lines show fitted variance function.

5 Model Development

5.1 ESTIMATION OF FIXED-EFFECTS COEFFICIENTS

The fixed-effects coefficients of the ground motion model [Eqs. (3.12a) and (3.13b)]) were estimated using the nonlinear mixed-effects method *nlme* (Pinheiro and Bates 2000) implemented in the statistical packages **S-PLUS** and **R**. The coefficients were developed through an iterative process of performing regressions for the entire spectral period range with some parts of the model fixed, developing smoothing models for these coefficients with period, and then repeating the analysis to examine the variation of the remaining coefficients. All analyses were performed using the selected PEER-NGA data truncated at a maximum distance of R_{RUP} = 70 km. The resulting coefficients are listed in Tables 5.1–5.3 for selected spectral periods. Appendix H lists the complete set of coefficients for 105 spectral periods.

After extensive exploratory analysis of the data, we concluded that the PEER-NGA data set does not sample a sufficiently wide range of motion and V_{S30} to allow the simultaneous estimation of all 3 nonlinear soil parameters (ϕ_2, ϕ_3, and ϕ_4). We thus decided to fix ϕ_4 through other supporting information in the initial steps of regressions. Both our preliminary analysis of the PEER-NGA data and analyses of the simulated soil amplification factors from Silva (2008) and Bazzurro and Cornell (2004) suggested that ϕ_4 is about 0.1g in the case of *pga*. The empirical study of Choi and Stewart (2005) also indicated that 0.1g is a viable value for ϕ_4. We thus fix *pga*'s ϕ_4 at 0.1g. To fix ϕ_4 of other periods, we anchored the rock spectral shape of **M** 6.5 at 10 km (Silva et al. 1997) at 0.1g *pga*. The remaining two nonlinear parameters ϕ_2 and ϕ_3 were then estimated by the regression of data. Once the values of ϕ_2 and ϕ_3 were determined, we revised the estimate of ϕ_4 with coefficients ϕ_2 and ϕ_3 fixed to their estimated values. This process was repeated a few times. The final ϕ_4 for *pga* is slightly larger than 0.1g.

Coefficient c_{1a} (reverse-faulting effect) was found to decrease with increasing spectral period, becoming 0 at a period of 2.0 sec and then decreasing to about -0.1 at long periods. This is consistent with the trends observed in previous empirical models (Abrahamson and Silva 1997; Campbell and Bozorgnia 2003; the soil model of Sadigh et al. 1997). At high frequency, the positive c_{1a} value is consistent with an interpretation of higher stress drops (stress parameters) for reverse-faulting earthquakes than for strike-slip earthquakes. However, the negative value of c_{1a} at long periods is not consistent with this concept, indicating that other factors may also be influencing the difference between the motions produced by the two styles of faulting. For normal faulting, the value of c_{1b} was approximately -0.25 for short-period *PSA* and decreased in absolute value as the spectral period decreased. For spectral periods greater than about 1.0 sec, the value of c_{1b} becomes very uncertain. If one speculates that the negative value of c_{1a} for reverse-faulting earthquakes at long periods is due to more compact dip-slip earthquakes being less efficient at producing long-period motions than long strike-slip earthquakes, then perhaps the values of c_{1a} and c_{1b} should be similar in this period range. We have made this assumption in developing the period dependence of c_{1b}.

Table 5.1 Period-independent fixed-effect coefficients for model of ln(y_{ref})—Eq. (3.12a).

c_2	c_3	c_4	c_{4a}	c_{RB}	c_{HM}	$c_{\gamma 3}$
1.06	3.45	-2.1	-0.5	50	3	4

Table 5.2 Period-dependent fixed-effect coefficients for model of ln(y_{ref})—Eq. (3.12a)[1].

Spectral Period (sec)	c_1	c_{1a}	c_{1b}	c_n	c_M	c_5	c_6	c_7	c_{7a}	c_9	c_{9a}	c_{10}	$c_{\gamma 1}$	$c_{\gamma 2}$
pga	-1.2687	0.1	-0.2550	2.996	4.1840	6.1600	0.4893	0.0512	0.0860	0.7900	1.5005	-0.3218	-0.00804	-0.00785
pgv	2.2884	0.1094	-0.0626	1.648	4.2979	5.1700	0.4407	0.0207	0.0437	0.3079	2.6690	-0.1166	-0.00275	-0.00625
0.01	-1.2687	0.1	-0.2550	2.996	4.1840	6.1600	0.4893	0.0512	0.0860	0.7900	1.5005	-0.3218	-0.00804	-0.00785
0.02	-1.2515	0.1	-0.2550	3.292	4.1879	6.1580	0.4892	0.0512	0.0860	0.8129	1.5028	-0.3323	-0.00811	-0.00792
0.03	-1.1744	0.1	-0.2550	3.514	4.1556	6.1550	0.4890	0.0511	0.0860	0.8439	1.5071	-0.3394	-0.00839	-0.00819
0.04	-1.0671	0.1	-0.2550	3.563	4.1226	6.1508	0.4888	0.0508	0.0860	0.8740	1.5138	-0.3453	-0.00875	-0.00855
0.05	-0.9464	0.1	-0.2550	3.547	4.1011	6.1441	0.4884	0.0504	0.0860	0.8996	1.5230	-0.3502	-0.00912	-0.00891
0.075	-0.7051	0.1	-0.2540	3.448	4.0860	6.1200	0.4872	0.0495	0.0860	0.9442	1.5597	-0.3579	-0.00973	-0.00950
0.1	-0.5747	0.1	-0.2530	3.312	4.1030	6.0850	0.4854	0.0489	0.0860	0.9677	1.6104	-0.3604	-0.00975	-0.00952
0.15	-0.5309	0.1	-0.2500	3.044	4.1717	5.9871	0.4808	0.0479	0.0860	0.9660	1.7549	-0.3565	-0.00883	-0.00862
0.2	-0.6352	0.1	-0.2449	2.831	4.2476	5.8699	0.4755	0.0471	0.0860	0.9334	1.9157	-0.3470	-0.00778	-0.00759
0.25	-0.7766	0.1	-0.2382	2.658	4.3184	5.7547	0.4706	0.0464	0.0860	0.8946	2.0709	-0.3379	-0.00688	-0.00671
0.3	-0.9278	0.0999	-0.2313	2.505	4.3844	5.6527	0.4665	0.0458	0.0860	0.8590	2.2005	-0.3314	-0.00612	-0.00598
0.4	-1.2176	0.0997	-0.2146	2.261	4.4979	5.4997	0.4607	0.0445	0.0850	0.8019	2.3886	-0.3256	-0.00498	-0.00486
0.5	-1.4695	0.0991	-0.1972	2.087	4.5881	5.4029	0.4571	0.0429	0.0830	0.7578	2.5000	-0.3189	-0.00420	-0.00410
0.75	-1.9278	0.0936	-0.1620	1.812	4.7571	5.2900	0.4531	0.0387	0.0690	0.6788	2.6224	-0.2702	-0.00308	-0.00301
1	-2.2453	0.0766	-0.1400	1.648	4.8820	5.2480	0.4517	0.0350	0.0450	0.6196	2.6690	-0.2059	-0.00246	-0.00241
1.5	-2.7307	0.0022	-0.1184	1.511	5.0697	5.2194	0.4507	0.0280	0.0134	0.5101	2.6985	-0.0852	-0.00180	-0.00176
2	-3.1413	-0.0591	-0.1100	1.470	5.2173	5.2099	0.4504	0.0213	0.0040	0.3917	2.7085	0.0160	-0.00147	-0.00143
3	-3.7413	-0.0931	-0.1040	1.456	5.4385	5.2040	0.4501	0.0106	0.0010	0.1244	2.7145	0.1876	-0.00117	-0.00115
4	-4.1814	-0.0982	-0.1020	1.465	5.5977	5.2020	0.4501	0.0041	0	0.0086	2.7164	0.3378	-0.00107	-0.00104
5	-4.5187	-0.0994	-0.1010	1.478	5.7276	5.2010	0.4500	0.0010	0	0	2.7172	0.4579	-0.00102	-0.00099
7.5	-5.1224	-0.0999	-0.1010	1.498	5.9891	5.2000	0.4500	0	0	0	2.7177	0.7514	-0.00096	-0.00094
10	-5.5872	-0.1	-0.1000	1.502	6.1930	5.2000	0.4500	0	0	0	2.7180	1.1856	-0.00094	-0.00091

[1]Units are g's for *pga* and *PSA* , and cm/sec for *pgv*

Table 5.3 Fixed-effect coefficients of site response model for ln(y)—Eq. (3.12b).

Spectral Period (sec)	ϕ_1	ϕ_2	ϕ_3	ϕ_4	ϕ_5	ϕ_6	ϕ_7	ϕ_8
pga	-0.4417	-0.1417	-0.007010	0.102151	0.2289	0.014996	580.0	0.0700
pgv	-0.7861	-0.0699	-0.008444	5.41000	0.2899	0.006718	459.0	0.1138
0.01	-0.4417	-0.1417	-0.007010	0.102151	0.2289	0.014996	580.0	0.0700
0.02	-0.4340	-0.1364	-0.007279	0.108360	0.2289	0.014996	580.0	0.0699
0.03	-0.4177	-0.1403	-0.007354	0.119888	0.2289	0.014996	580.0	0.0701
0.04	-0.4000	-0.1591	-0.006977	0.133641	0.2289	0.014996	579.9	0.0702
0.05	-0.3903	-0.1862	-0.006467	0.148927	0.2290	0.014996	579.9	0.0701
0.075	-0.4040	-0.2538	-0.005734	0.190596	0.2292	0.014996	579.6	0.0686
0.1	-0.4423	-0.2943	-0.005604	0.230662	0.2297	0.014996	579.2	0.0646
0.15	-0.5162	-0.3113	-0.005845	0.266468	0.2326	0.014988	577.2	0.0494
0.2	-0.5697	-0.2927	-0.006141	0.255253	0.2386	0.014964	573.9	-0.0019
0.25	-0.6109	-0.2662	-0.006439	0.231541	0.2497	0.014881	568.5	-0.0479
0.3	-0.6444	-0.2405	-0.006704	0.207277	0.2674	0.014639	560.5	-0.0756
0.4	-0.6931	-0.1975	-0.007125	0.165464	0.3120	0.013493	540.0	-0.0960
0.5	-0.7246	-0.1633	-0.007435	0.133828	0.3610	0.011133	512.9	-0.0998
0.75	-0.7708	-0.1028	-0.008120	0.085153	0.4353	0.006739	441.9	-0.0765
1	-0.7990	-0.0699	-0.008444	0.058595	0.4629	0.005749	391.8	-0.0412
1.5	-0.8382	-0.0425	-0.007707	0.031787	0.4756	0.005544	348.1	0.0140
2	-0.8663	-0.0302	-0.004792	0.019716	0.4785	0.005521	332.5	0.0544
3	-0.9032	-0.0129	-0.001828	0.009643	0.4796	0.005517	324.1	0.1232
4	-0.9231	-0.0016	-0.001523	0.005379	0.4799	0.005517	321.7	0.1859
5	-0.9222	0.0000	-0.001440	0.003223	0.4799	0.005517	320.9	0.2295
7.5	-0.8346	0.0000	-0.001369	0.001134	0.4800	0.005517	320.3	0.2660
10	-0.7332	0.0000	-0.001361	0.000515	0.4800	0.005517	320.1	0.2682

The estimated values of coefficient c_1 exhibited noticeable steps at periods of 0.8, 1.1, 1.6, 4, and 8 sec (Fig. 5.1). These steps occur at spectral periods where there are large reductions in the number of usable data (see Fig. 2.7), defined by the record's minimum usable frequency (Chiou et al. 2008). This suggested that the estimated values of c_1 may be biased by the systematic removal of weaker motions from the data set, which would tend to leave larger ground motion amplitudes in the remaining data. To correct this bias and to smooth c_1, we imposed a smooth variation in the slope of c_1 with respect to period. The slope of c_1 was computed numerically and is shown in Figure 5.2. We examined the shapes of resulting displacement spectra for large-magnitude earthquakes (**M** $\geq$ 6.5) to verify that constant

displacement is reached at spectral periods that are consistent with the model presented in BSSC (2004). The difference between the values of c_1 obtained from regression and the smoothed values reported after bias adjustment was incorporated into the assessment of the inter-event variance. The estimated values of c_1 before smoothing/bias correction are listed in Appendix H.

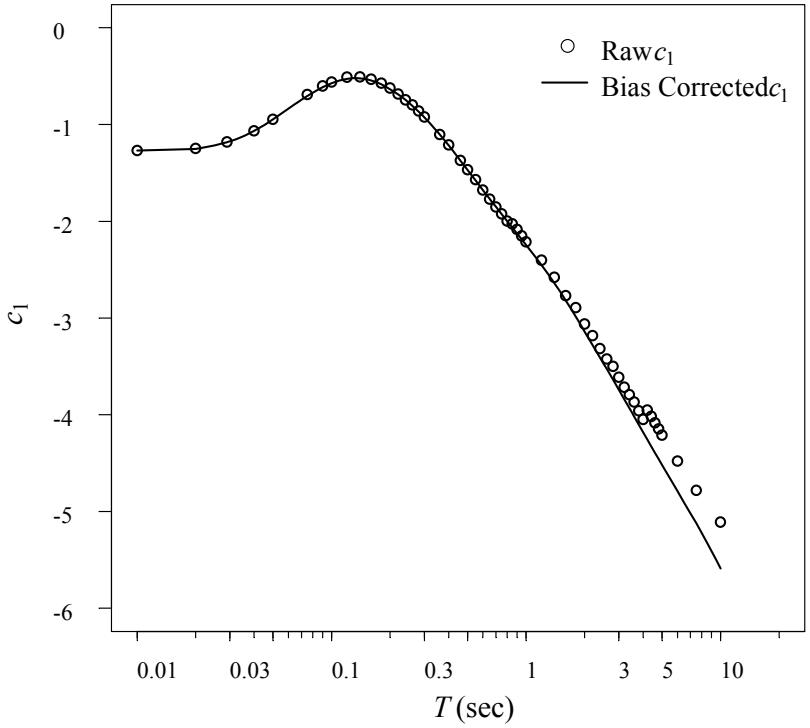

Fig. 5.1 Variation of coefficient c_1 with spectral period. Solid curve is c_1 after bias adjustment.

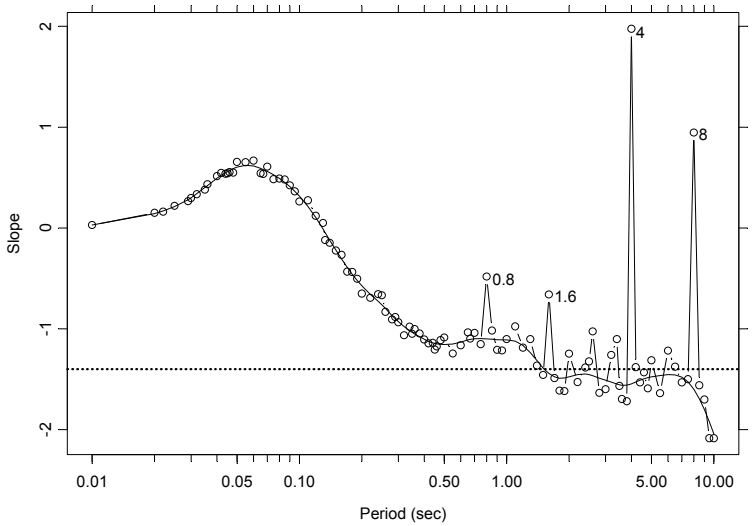

Fig. 5.2 Variation of the derivative of coefficient c_1 with respect to spectral period. Solid curve is smoothed derivative.

5.2 VARIANCE MODEL

During the first stages of model development, the results suggested that the residual standard errors did not depend upon earthquake magnitude, in contrast to the previous Sadigh et al. (1997) models. This was based on visual inspection of the residuals. However, statistical analysis of the residuals indicated that a statistically significant dependence on magnitude is present, although the amplitude of the effect is less than that found by Sadigh et al. (1997). The employed statistical test followed that used by Youngs et al. (1995). We first computed the log-likelihood for a model assuming magnitude-independent variance terms and after that for another model with the trilinear magnitude-dependent variance used by Youngs et al. (1995). We then used the likelihood ratio test to check the significance of the increase in log-likelihood found assuming magnitude-dependent variance. Magnitude-dependence in the variance was found to be statistically significant (p-values < 0.05) for periods up to about 1 sec. For longer periods the results showed less statistical significance, but at the same time there is a large reduction in the size of the data set, particularly in data from smaller-magnitude earthquakes.

We performed two additional checks on possible contributions to the observed magnitude dependence. We found that value of the intra-event standard deviation for the aftershock data is approximately 0.08 larger than that for the main shock data. When this was accounted for in the variance model, magnitude-dependence in the main-shock residuals was still found to be statistically significant. Similar estimates of inter-event variability were obtained for main shocks and aftershocks. Secondly, the reduction in intra-event variance due to nonlinear soil response could also contribute to the observed magnitude dependence, as larger earthquakes tend to produce larger motions, and thus induce greater nonlinear response. This effect was explored by Youngs et al. (1995), who found that it was not a major contributing factor. We tested the influence of soil nonlinearity by comparing the log-likelihoods obtained for data sets restricted to nonlinearity factors $NL > -0.15$ and again found that magnitude-dependence of the variance terms is statistically significant over much of the period range. Restricting the degree of nonlinearity further to $NL > -0.05$ resulted in greatly reducing the size of the data set to the level where there is large uncertainty in estimating the variances.

The model for the inter-event standard error τ is given by:

$$\tau = \tau_1 + \frac{\tau_2 - \tau_1}{2} \times \left[min\{max(\mathbf{M},5),7\} - 5 \right] \tag{5.1}$$

The smoothed values of τ_1 and τ_2 are listed in Table 5.4. Magnitude-dependence in τ is much weaker than was estimated in the Sadigh et al. (1997) models and disappears for periods longer than 2 sec. The inter-event residuals also display increased variability near a spectral period of 0.1 sec compared to those for larger and smaller periods.

The intra-event residuals display stronger magnitude dependence than the inter-event residuals. The variability is also affected by the degree of nonlinearity in the soil, as defined by Equation (4.5). In addition, greater variability is observed in the residuals for sites with inferred values of V_{S30} than for sites with measured values of V_{S30}. The model for the intra-event standard deviation that incorporates these observations is give by:

$$\sigma = \left[\sigma_1 + \frac{\sigma_2 - \sigma_1}{2} \left(\min\{\max(\mathbf{M}, 5), 7\} - 5 \right) + \sigma_4 \times AS \right] \times \sqrt{(\sigma_3 F_{Inferred} + 0.7 F_{Measured}) + (1 + NL)^2} \tag{5.2}$$

with

$$NL = \left(b \frac{y_{ref} e^{\eta}}{y_{ref} e^{\eta} + c} \right)$$

where $F_{Inferred}$ equals 1, if V_{S30} is inferred from geology, and 0 otherwise; $F_{Measured}$ equals 1, if V_{S30} is measured, and 0 otherwise; and AS equals 1 if the event is an aftershock, and 0 otherwise. Coefficients σ_1, σ_2, σ_3, and σ_4 are listed in Table 5.4.

Table 5.4 Coefficients of variance model—Eqs. (5.1) and (5.2).

Spectral Period (sec)	τ_1	τ_2	σ_1	σ_2	σ_3	σ_4
pga	0.3437	0.2637	0.4458	0.3459	0.8	0.0663
pgv	0.2539	0.2381	0.4496	0.3554	0.7504	0.0133
0.01	0.3437	0.2637	0.4458	0.3459	0.8	0.0663
0.02	0.3471	0.2671	0.4458	0.3459	0.8	0.0663
0.03	0.3603	0.2803	0.4535	0.3537	0.8	0.0663
0.04	0.3718	0.2918	0.4589	0.3592	0.8	0.0663
0.05	0.3848	0.3048	0.4630	0.3635	0.8	0.0663
0.075	0.3878	0.3129	0.4702	0.3713	0.8	0.0663
0.1	0.3835	0.3152	0.4747	0.3769	0.8	0.0663
0.15	0.3719	0.3128	0.4798	0.3847	0.8	0.0612
0.2	0.3601	0.3076	0.4816	0.3902	0.8	0.0530
0.25	0.3522	0.3047	0.4815	0.3946	0.7999	0.0457
0.3	0.3438	0.3005	0.4801	0.3981	0.7997	0.0398
0.4	0.3351	0.2984	0.4758	0.4036	0.7988	0.0312
0.5	0.3353	0.3036	0.4710	0.4079	0.7966	0.0255
0.75	0.3429	0.3205	0.4621	0.4157	0.7792	0.0175
1	0.3577	0.3419	0.4581	0.4213	0.7504	0.0133
1.5	0.3769	0.3703	0.4493	0.4213	0.7136	0.0090
2	0.4023	0.4023	0.4459	0.4213	0.7035	0.0068
3	0.4406	0.4406	0.4433	0.4213	0.7006	0.0045
4	0.4784	0.4784	0.4424	0.4213	0.7001	0.0034
5	0.5074	0.5074	0.4420	0.4213	0.7000	0.0027
7.5	0.5328	0.5328	0.4416	0.4213	0.7000	0.0018
10	0.5542	0.5542	0.4414	0.4213	0.7000	0.0014

5.3 APPROXIMATE METHOD FOR CALCULATION OF TOTAL VARIANCE

The total variance for ln(y) is the sum of the inter-event and intra-event variances. Based on Equation (5.2), the intra-event variance σ^2 is a function of the random effect η such that the calculation of the total variance σ_T^2 requires integration over the random variable η. In the following we provide an approximate method that does not require integration. Taking the first two terms (first-order approximation) of the Taylor series expansion for σ_T^2 evaluated at $\eta = 0$ yields the expression:

$$\sigma_T^2 = (1 + NL_0)^2 \tau^2 + \sigma_{NL_0}^2$$

with (5.3)

$$NL_0 = \left(b \frac{y_{ref}}{y_{ref} + c} \right)$$

In Equation (5.3), τ is obtained from Equation (5.1), and $\sigma_{NL_0}^2$ is evaluated using Equation (5.2) with $\eta = 0$. We compared the performance of Equation (5.3) to numerical integration over η and to Monte-Carlo simulation and found that it produces results that are, in most cases, within a few percent of the more exact calculations, with the values obtained from Equation (5.3) slightly larger than the more exact solutions. Therefore, we recommend the use of Equation (5.3) for calculating the total variance of ln(y) about the population mean evaluated by Equation (3.12a, 3.12b) with $\eta = 0$.

6 Model Results

6.1 INTER-EVENT RESIDUALS

Figure 6.1 shows the inter-event residuals, η_i, for main shocks. The residuals do not exhibit a trend with magnitude. The values for California and non-California earthquakes do not show any trends with respect to the population mean, indicating that both sets of earthquakes are consistent with the model. These results indicate that the data from the other active tectonic regions are consistent with ground motions from California earthquakes. The inter-event term for the Chi-Chi main shock is approximately $2\times\tau$ below the population mean for *pga* (0.01 sec spectral acceleration), and becomes positive for periods longer than 1.0 sec.

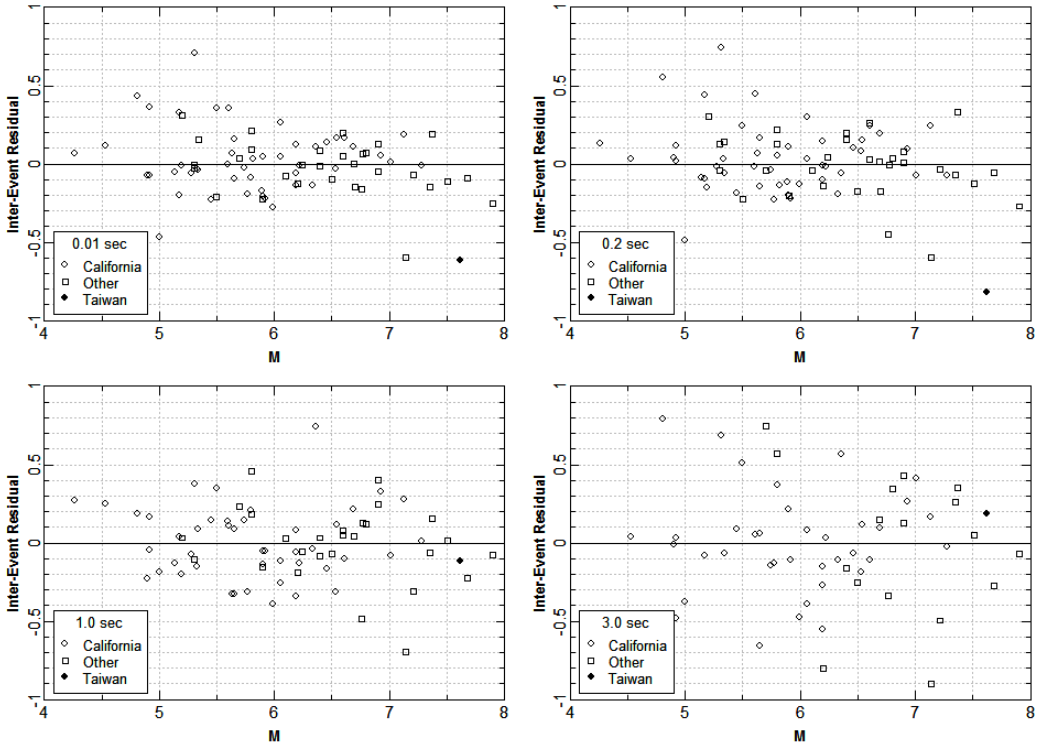

Fig. 6.1 Main shock inter-event residuals for spectral periods of 0.01 sec (*pga*), 0.2, 1.0, and 3.0 sec.

6.2 INTRA-EVENT RESIDUALS

Figures 6.2–6.5 show the intra-event residuals plotted versus **M**, R_{RUP}, V_{S30}, and y_{ref} for spectral periods of 0.01 (*pga*), 0.2, 1.0 and 3.0 sec, respectively. The residuals do not exhibit any trends with respect to **M**, R_{RUP}, V_{S30}, and y_{ref}. The site response model we have developed (Eq. 3.9) assumes that there is no deamplification of ground motions relative to y_{ref} for sites with V_{S30} greater that 1130 m/sec. Although there is very little data in the PEER-NGA database for such sites, the limited data, if anything, suggest a slight upward trend in the residuals. The site amplification model developed here does not account for the effect of the lower kappa expected for hard rock sites, which would lead to increases in high-frequency ground motions.

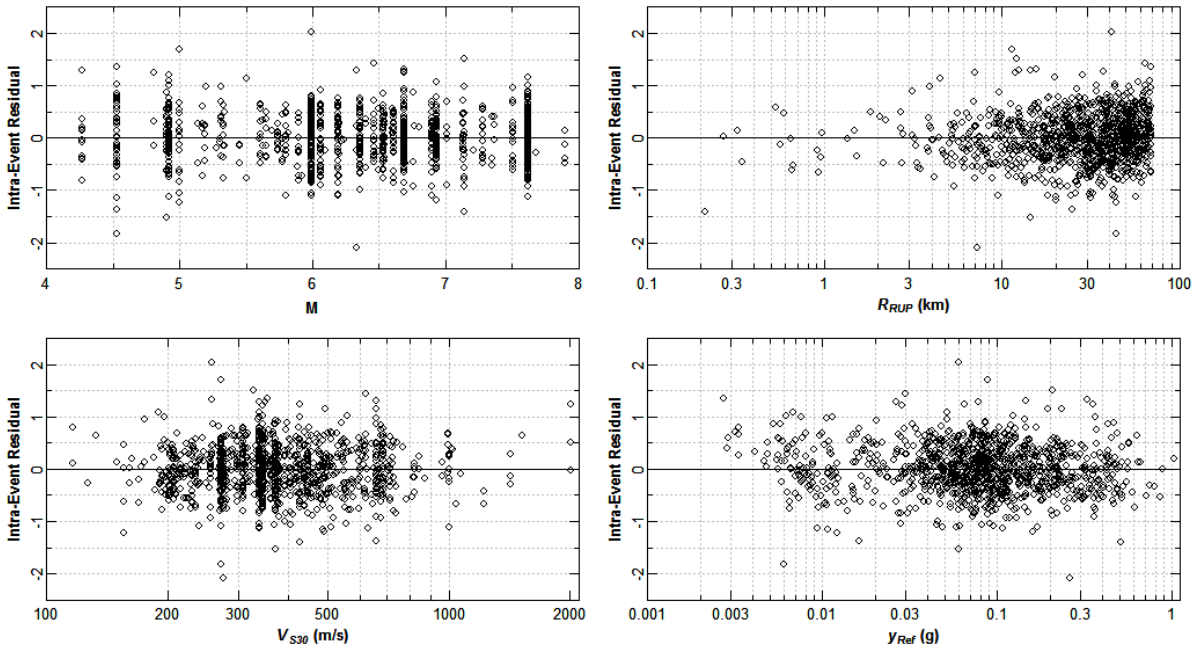

Fig. 6.2 Intra-event residuals for spectral period of 0.01 sec (*pga*) plotted against M, R_{RUP}, V_{S30}, and y_{ref}.

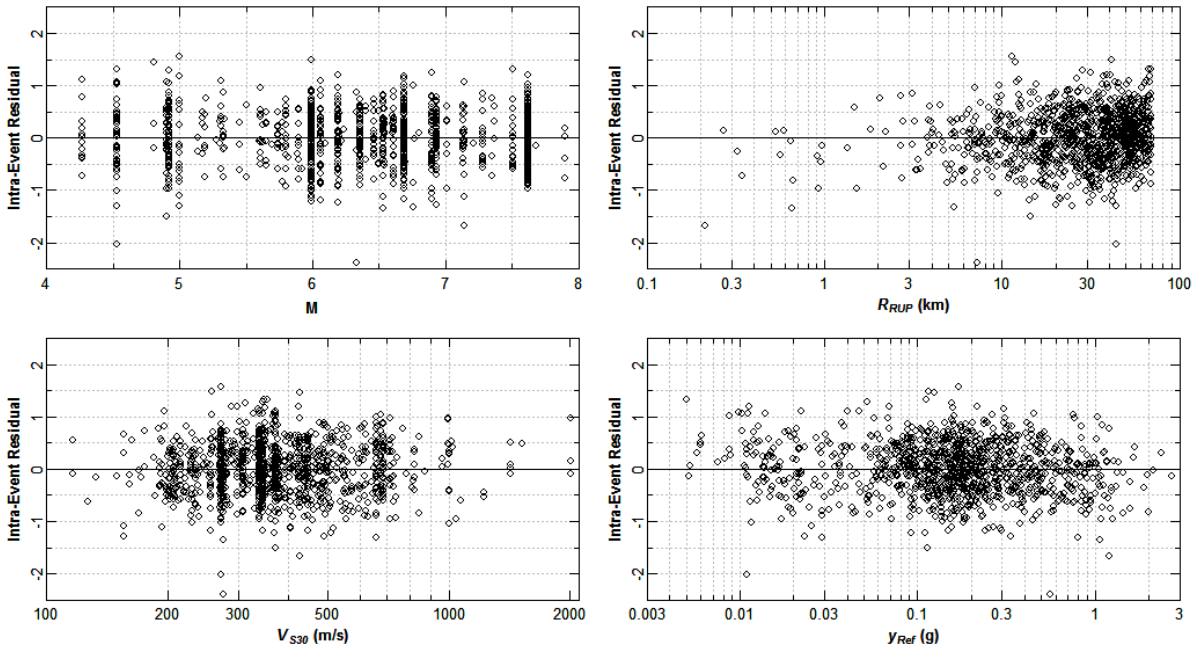

Fig. 6.3 Intra-event residuals for spectral period of 0.2 sec plotted against M, R_{RUP}, V_{S30}, and y_{ref}.

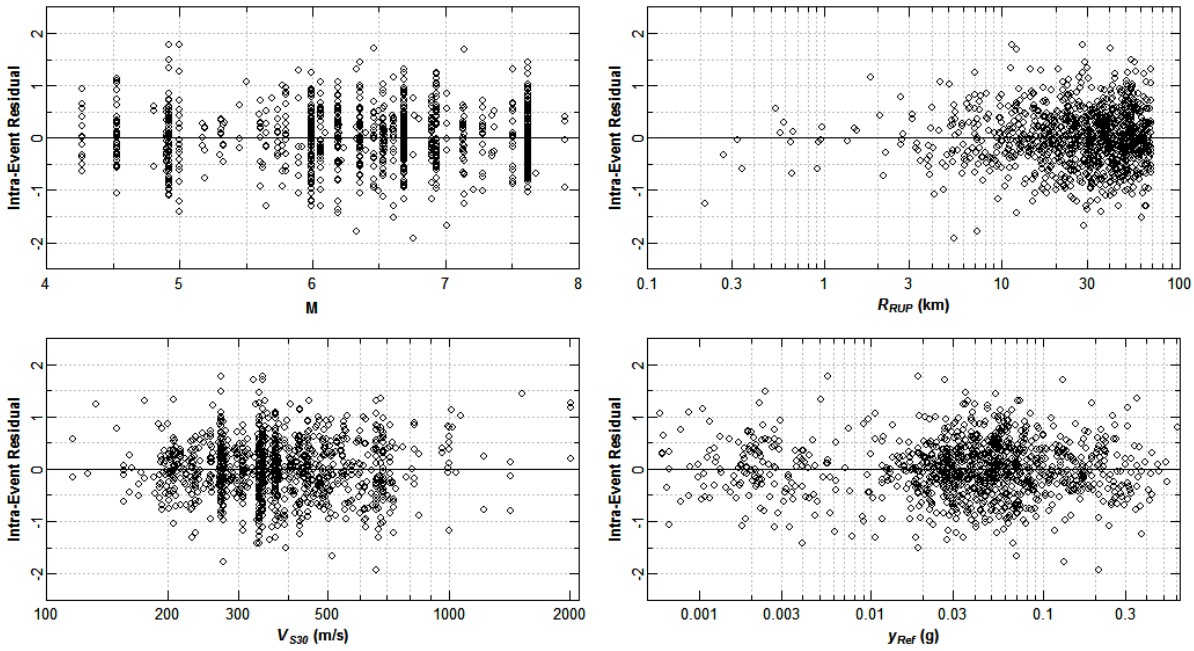

Fig. 6.4 Intra-event residuals for spectral period of 1.0 sec plotted against M, R_{RUP}, V_{S30}, and y_{ref}.

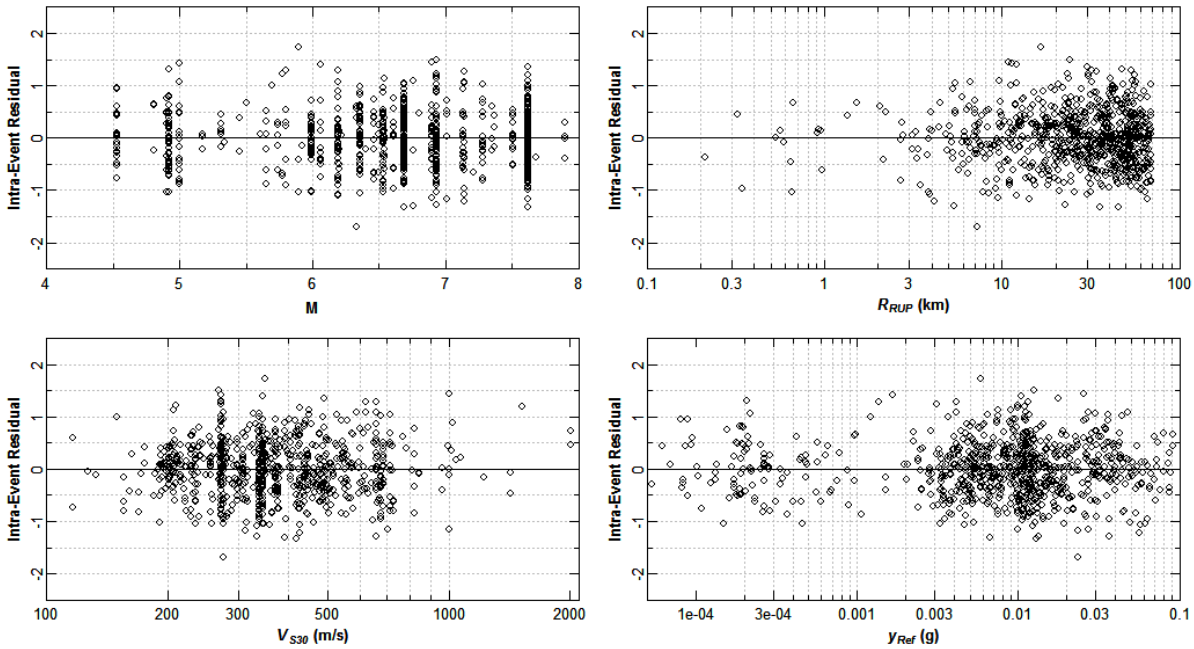

Fig. 6.5 Intra-event residuals for spectral period of 3.0 sec plotted against M, R_{RUP}, V_{S30}, and y_{ref}.

Figure 6.6 shows intra-event residuals plotted against R_{RUP} for the 10 earthquakes in the NGA database for which we developed extended *pga* data sets. The intra-event residuals are computed using the inter-event term calculated from just the NGA data within 70 km as part of our overall fit to the NGA model. These results show that the model provides a good fit at distances greater than 70 km. Also shown is the bias in the NGA data set at larger distances.

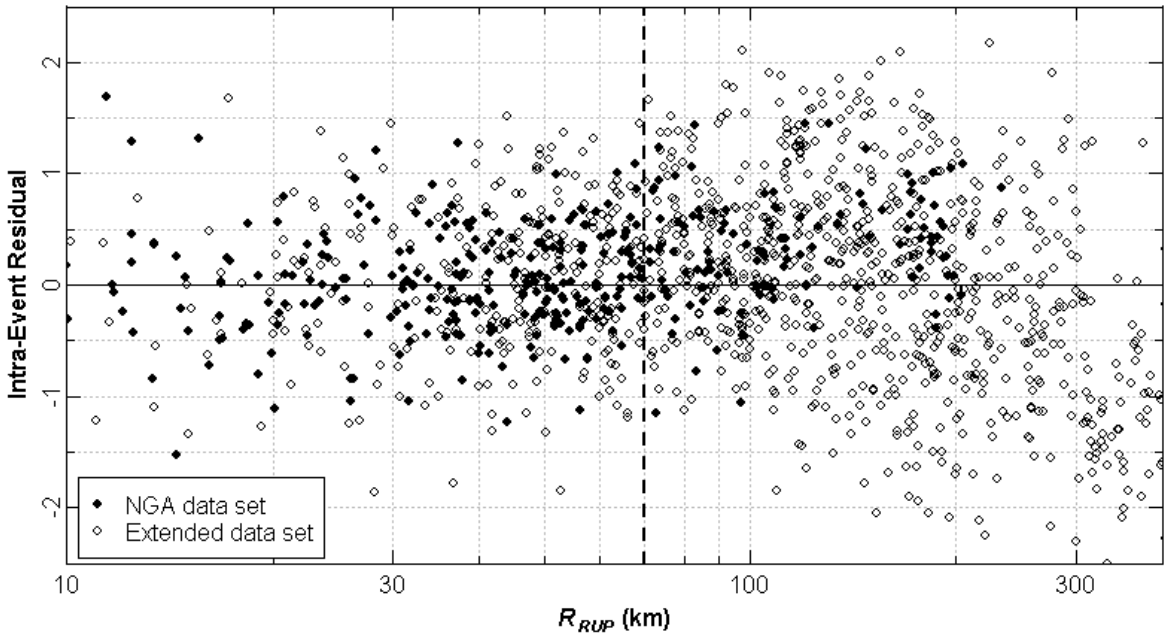

Fig. 6.6 Intra-event residuals for *pga* for the 1994 Northridge, 1998 San Juan Bautista, 1999 Hector Mines, 2000 Yountville, 2001 Mohawk Valley, 2001 Anza, 2002 Baja, 2002 Gilroy, 2002 Yorba Linda, and 2003 Big Bear City earthquakes.

6.3 COMPARISONS WITH DATA FOR INDIVIDUAL EARTHQUAKES

Appendix E contains plots showing the model fit to the data for individual earthquakes. The prediction curves in these plots are earthquake specific, meaning they include the inter-event random effect.

6.4 NONLINEAR SOIL AMPLIFICATION

Figure 6.7 compares the soil amplifications versus V_{S30} predicted by the nonlinear soil model developed as part of our ground motion model with the site amplifications computed by Silva (2008) using equivalent linear site response analyses and by Choi and Stewart (2003) using empirical ground motion data. The soil amplification model developed in this study compares well with the site response results computed by Silva (2008) for spectral periods of 0.01, 0.2, and 1.0 sec and shows greater amplification at the spectral period of 3.0 sec. Our model also compares well to Choi and Stewart's results at spectral periods of 0.01 and 1.0 sec, is more nonlinear at the spectral period of 0.2 sec, and shows greater amplification at the period of 3.0 sec.

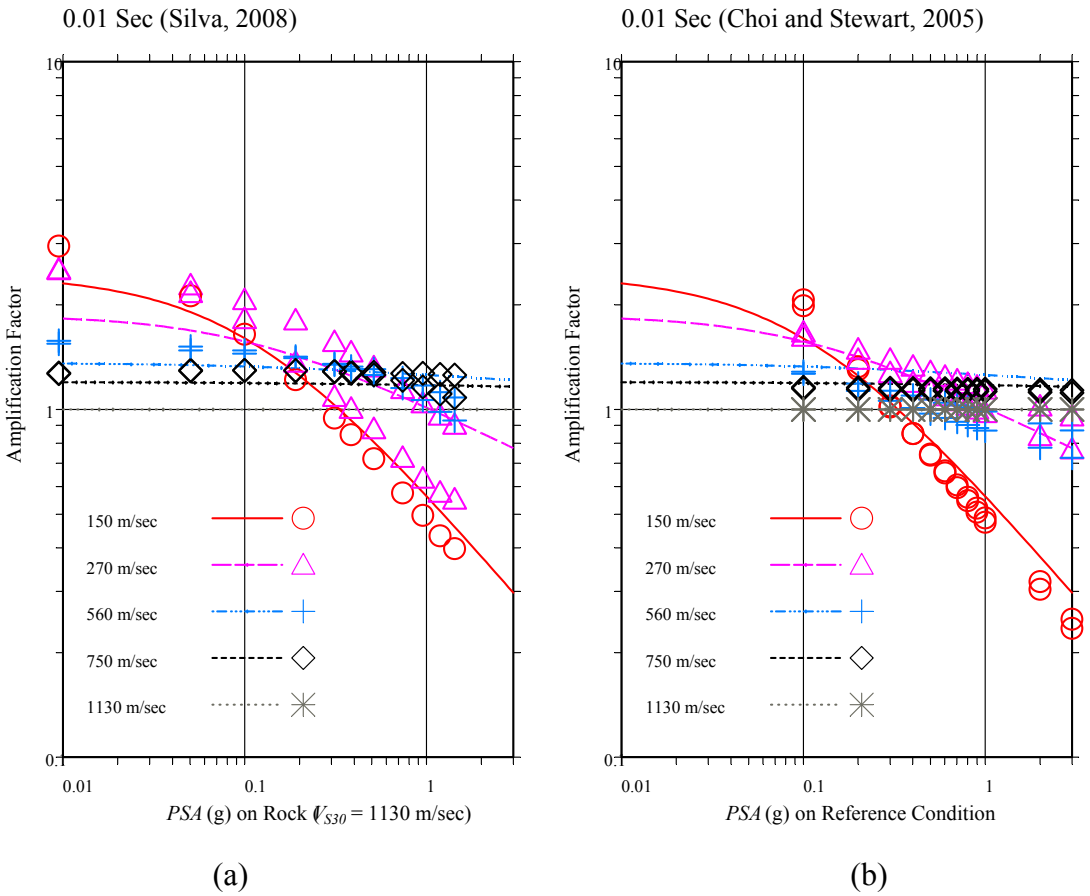

Fig. 6.7a Nonlinear soil amplification factor predicted by ground motion model developed in this study (lines) compared to those obtained by (a) Silva (2008) and (b) Choi and Stewart (symbols), for spectral period of 0.01 sec (*pga*).

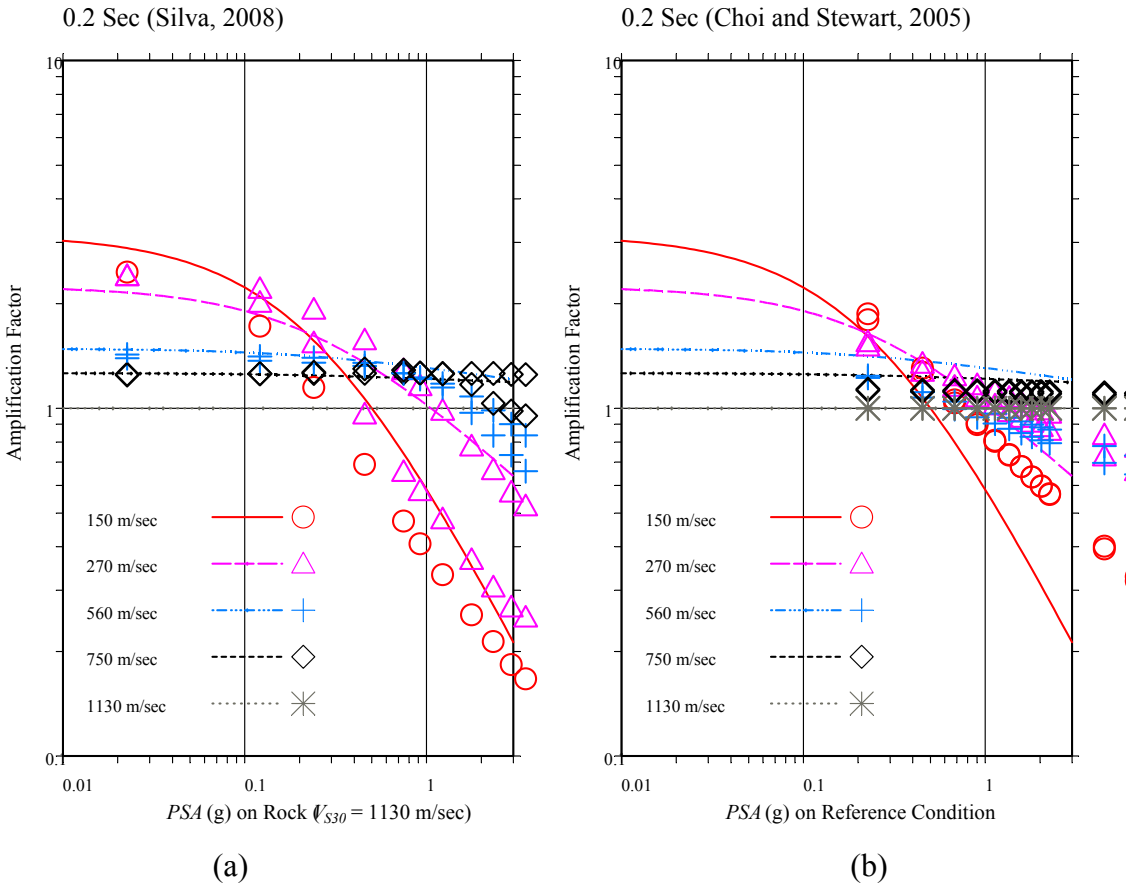

Fig. 6.7b Nonlinear soil amplification predicted by ground motion model developed in this study (lines) compared to those obtained by (a) Silva (2008) and (b) Choi and Stewart (symbols), for spectral period of 0.2 sec.

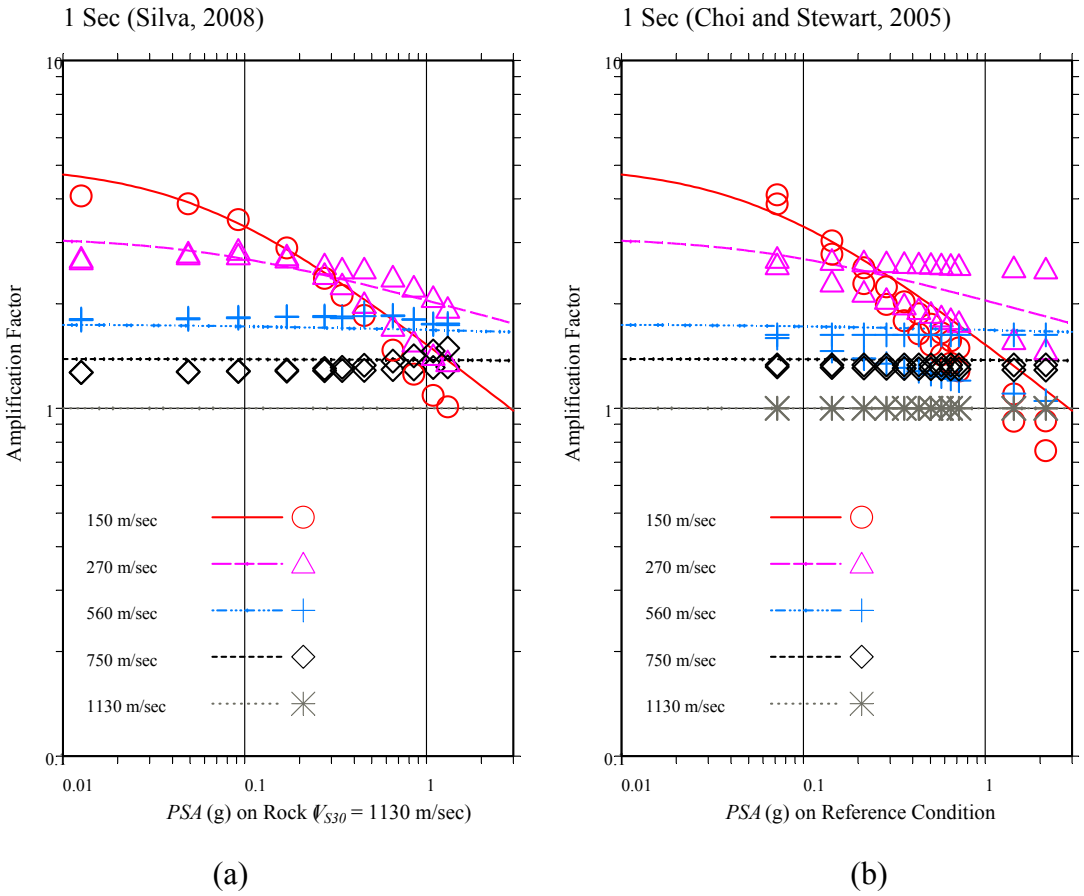

Fig. 6.7c Nonlinear soil amplification predicted by ground motion model developed in this study (lines) compared to those obtained by (a) Silva (2008) and (b) Choi and Stewart, for spectral period of 1.0 sec.

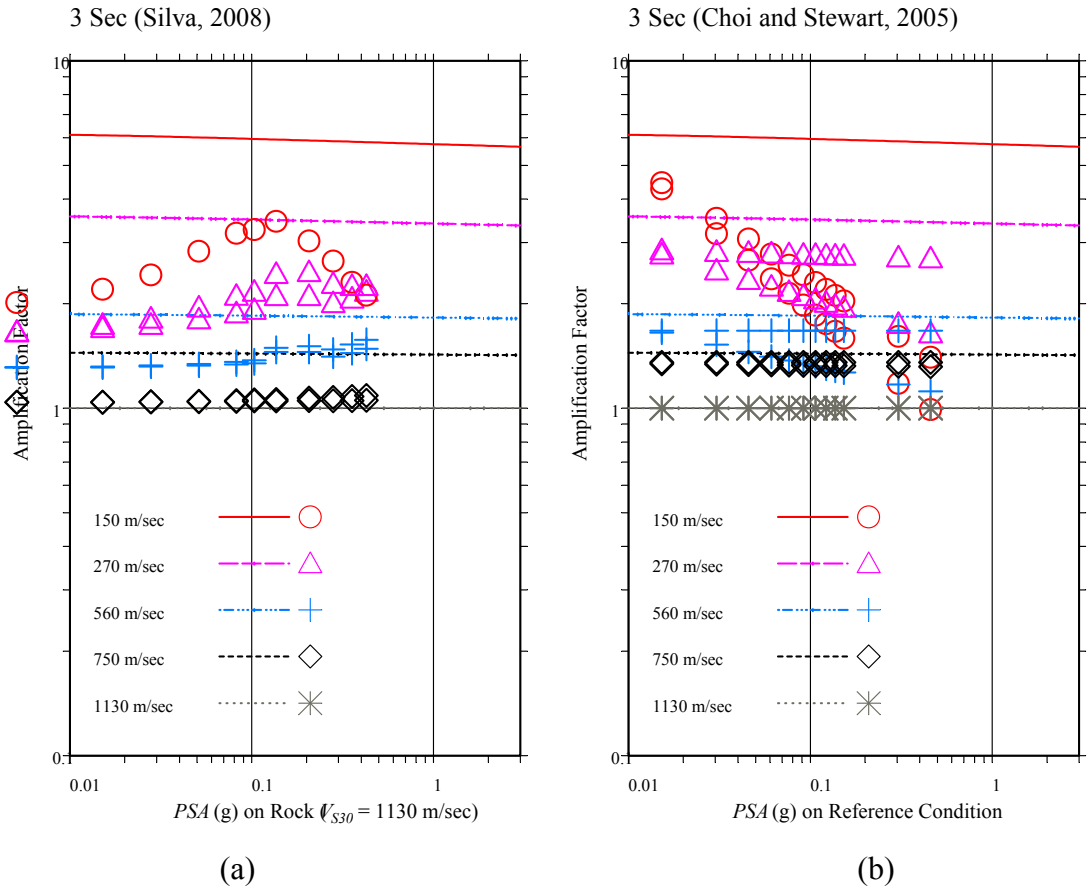

Fig. 6.7d Nonlinear soil amplification predicted by ground motion model developed in this study (lines) compared to those obtained by (a) Silva (2008) and (b) Choi and Stewart (symbols), for spectral period of 3.0 sec.

6.5 COMPARISON WITH PREVIOUS MODEL

Figures 6.8–6.10 compare magnitude and distance scaling produced by the new model with that predicted by the models developed by Sadigh et al. (1997). The comparisons require an assessment of V_{S30} representative of the Sadigh et al. (1997) relationships. For soil, we have used a value of 310 m/s, the velocity suggested by Boore et al. (1997) as representative of generic soil. This value is also approximately the geometric mean of V_{S30} for sites in the PEER-NGA database that would have been included in the Sadigh et al. (1997) soil database (see also Appendix F). For generic rock, Boore et al. (1997) suggested a value of 620 m/s. However, we think that this may be higher than the average for the data used by Sadigh et al. (1997), which included recordings from many sites that are now classified as NEHRP C, and have used a V_{S30} of 520 m/s for the comparisons.

The bulk of the ground motion data are for soil sites and at distances between 20 and 50 km and the two models produce generally similar results for these conditions and short-period motions. The models are more similar for soil than for rock, which is to be expected given that the majority of ground motion data is recorded on soil sites. The difference between the two models increases for longer period motions, with the new model generally indicating lower motions. This difference is attributed largely to the much larger spectral acceleration database available to constrain the model coefficients compared to the amount of data available for use by the Sadigh et al. (1997). This claim is also supported by the findings of Appendix F. Differences in the model formulations account for the differences in predicted ground motions at the edges of the data. The distance scaling formulations are quite different, resulting in differences in the shape of the attenuation curves beyond 70 km, especially for long-period motions. The introduction of the hanging-wall effect results in increases in the model predictions over those of Sadigh et al. (1997) for sites located in the hanging wall and reductions at other sites. The style of faulting effect for reverse earthquakes is now smaller and reduces with increasing spectral period. Differences in the predictions also occur for smaller magnitudes at close distances due to the revised scaling formulations.

Figures 6.11–6.12 compare median response spectra for the two models. The spectral shapes generated by the two models are similar, but as indicated in Figures 6.8–6.10, the updated model produces lower long-period motions.

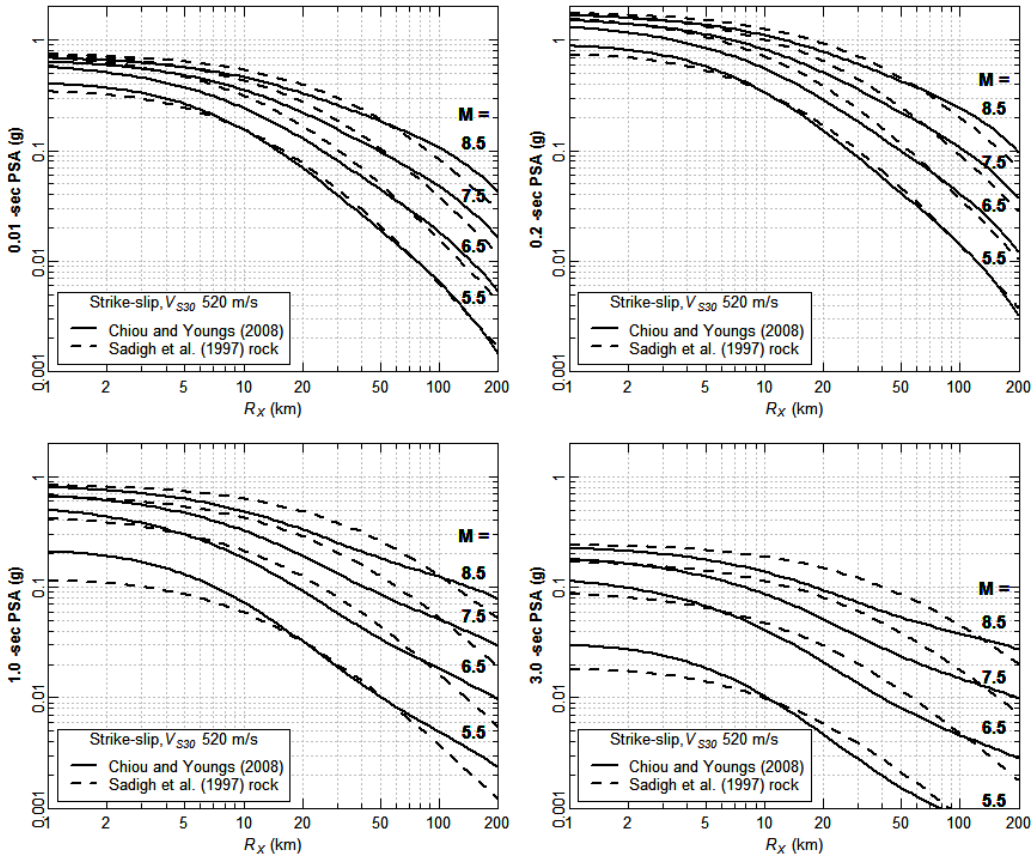

Fig. 6.8 Magnitude and distance scaling predicted by the model developed in this study and predicted by Sadigh et al. (1997) for horizontal distance from a vertical strike-slip fault and soft rock sites (V_{S30} = 520 m/s).

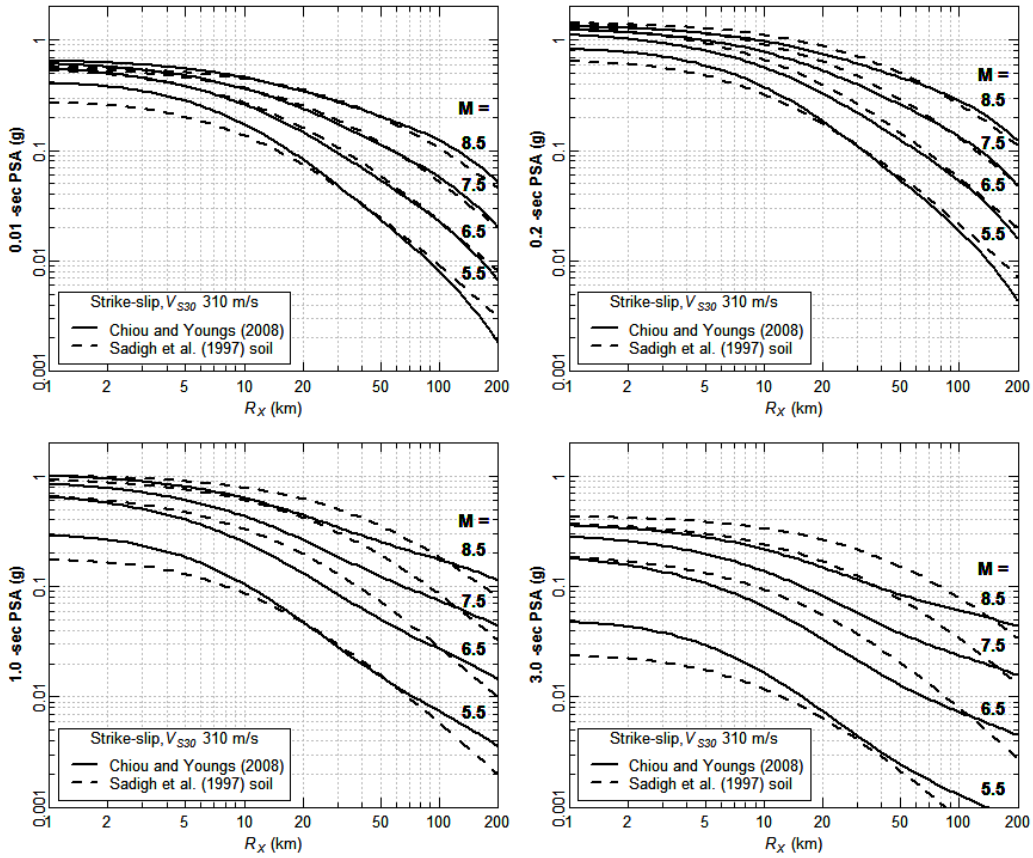

Fig. 6.9 Magnitude and distance scaling predicted by the model developed in this study and predicted by Sadigh et al. (1997) for horizontal distance from a vertical strike-slip fault and firm soil sites (V_{S30} = 310 m/s).

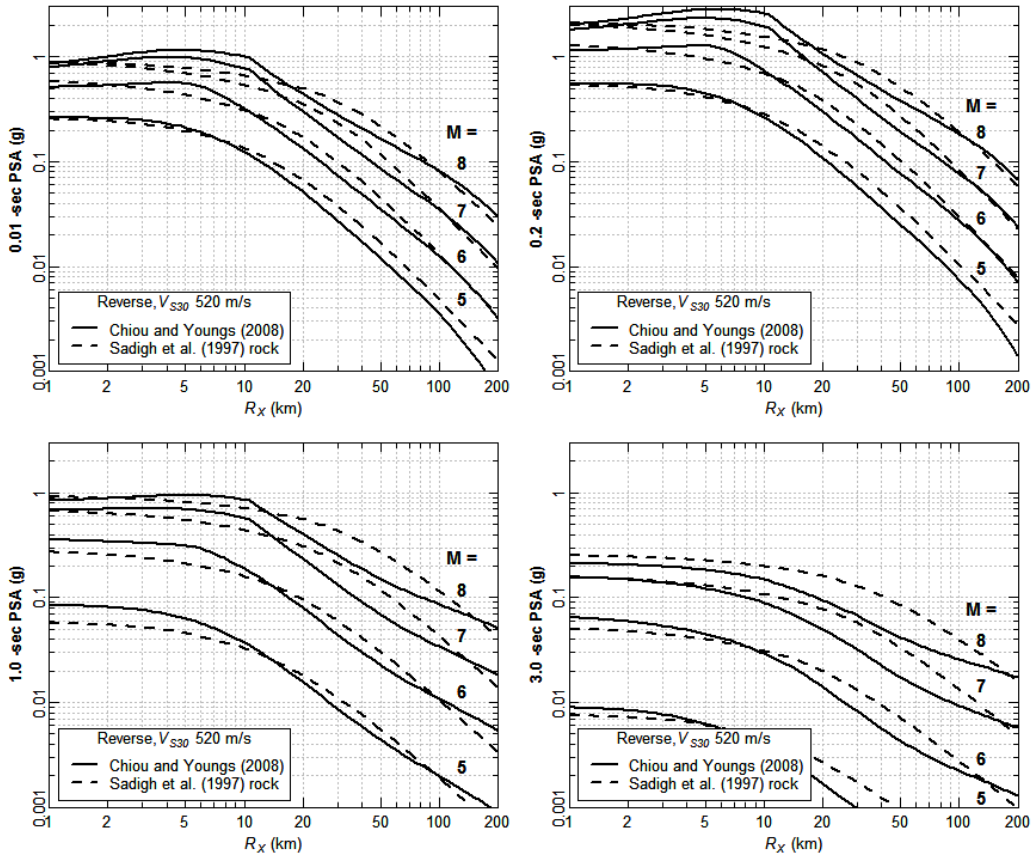

Fig. 6.10 Magnitude and distance scaling predicted by the model developed in this study and predicted by Sadigh et al. (1997) for horizontal distance from top edge of rupture on a reverse fault (δ = 45°) and soft rock sites (V_{S30} = 520 m/s).

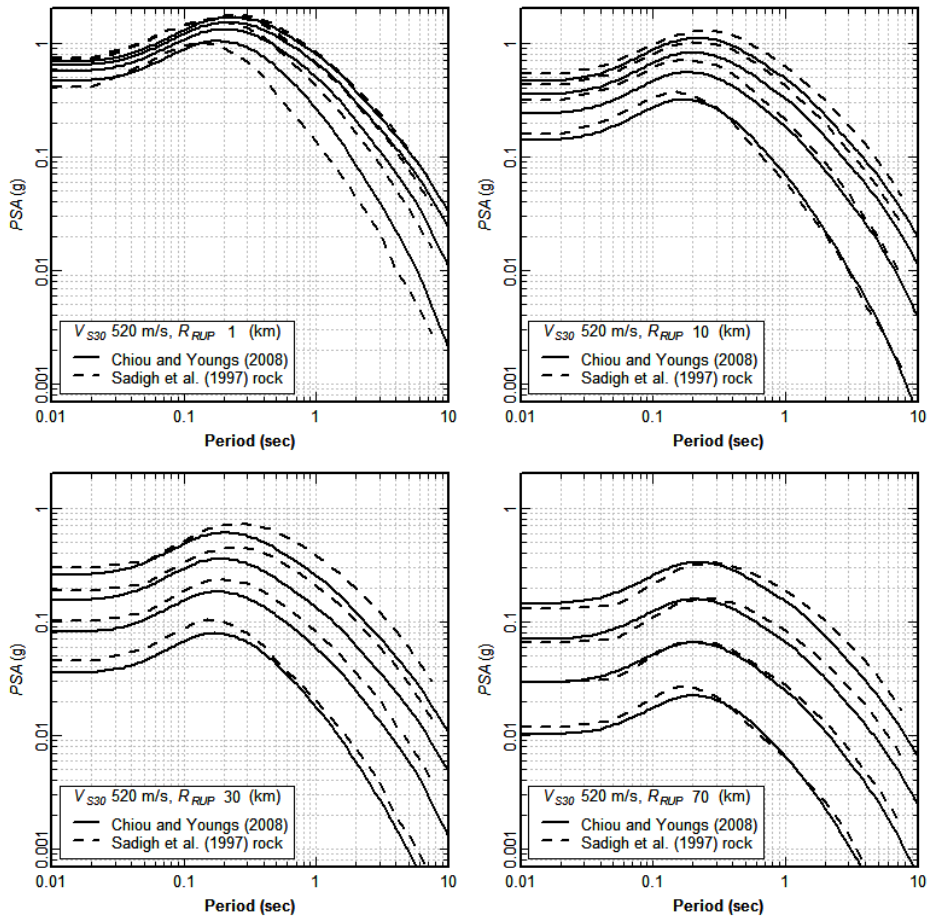

Fig. 6.11 Median response spectra predicted by the model developed in this study and predicted by Sadigh et al. (1997) for strike-slip earthquakes and soft rock sites (V_{S30} = 520 m/s). Magnitudes are in order of increasing amplitude M 5.5, 6.5, 7.5, and 8.5.

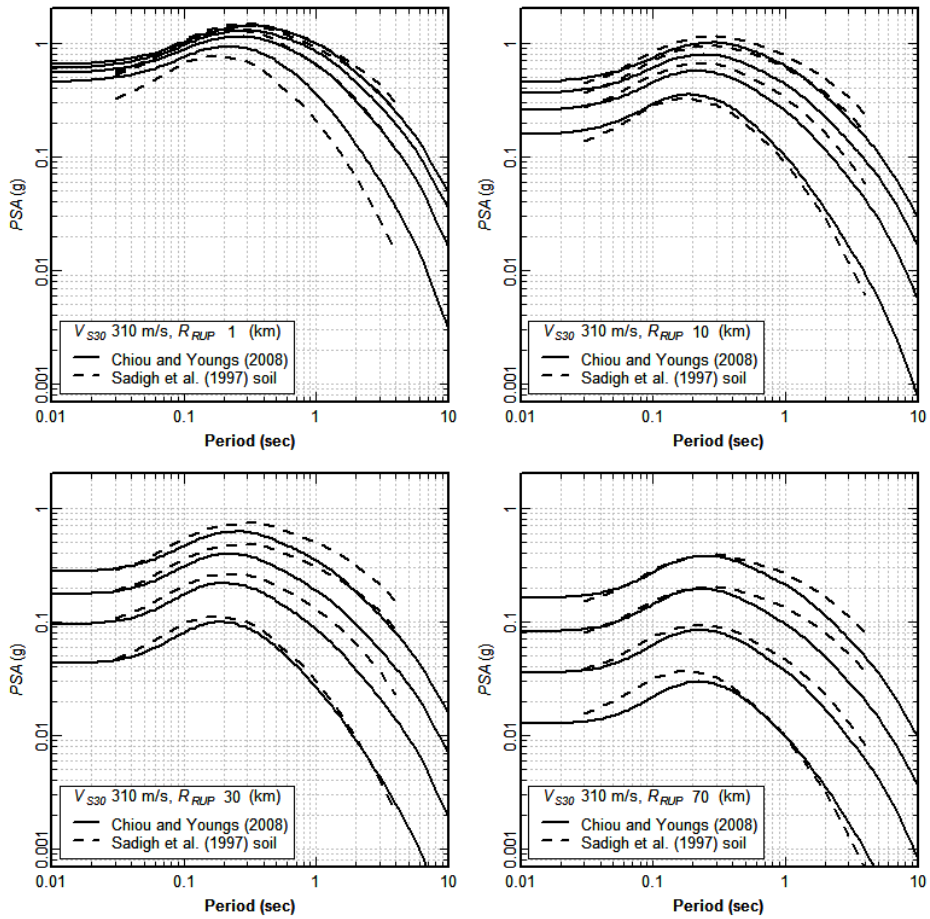

Fig. 6.12 Median response spectra predicted by the model developed in this study and predicted by Sadigh et al. (1997) for strike-slip earthquakes and firm soil sites (V_{S30} = 310 m/s). Magnitudes are in order of increasing amplitude M 5.5, 6.5, 7.5, and 8.5.

Figure 6.13(a) compares the total standard errors for the updated model with linear soil response compared to those for the Sadigh et al. (1997) models. The total standard errors for **M** 5 earthquakes are similar but the updated standard errors for **M** 7 earthquakes are larger. Figure 6.13(b) shows the effect of soil nonlinearity on the total standard errors of *pga*.

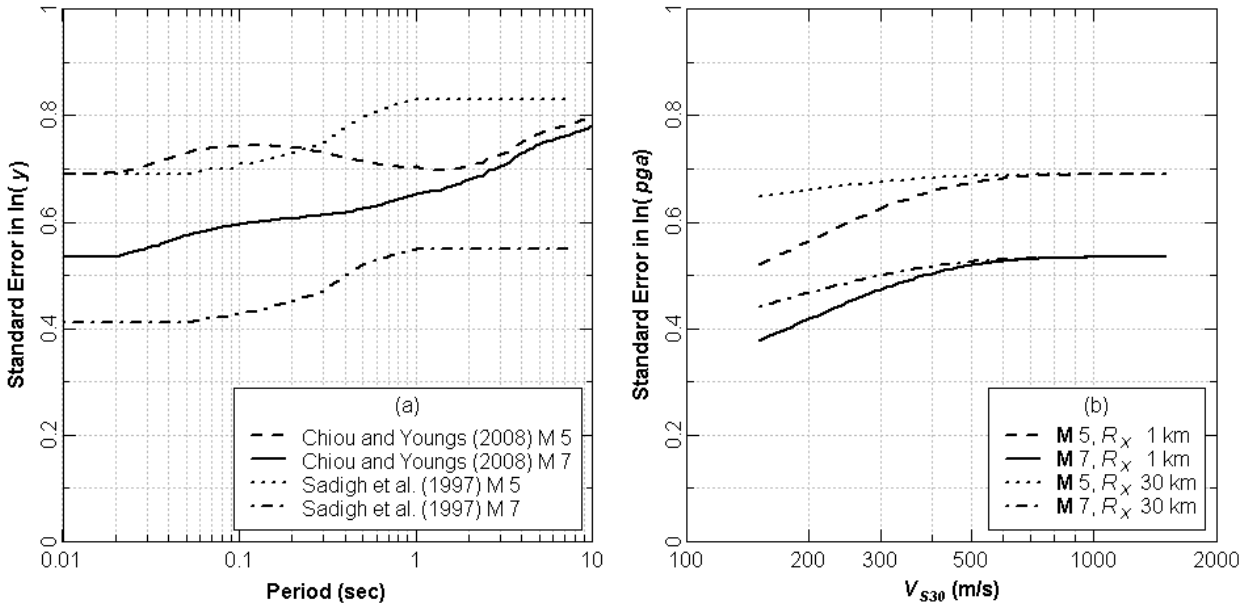

(a) (b)

Fig. 6.13 (a) Total standard errors for the model with linear soil response developed in this study and Sadigh et al. (1997). (b) Effect of soil nonlinearity on *pga* total standard error for the model developed in this study.

7 Example Calculations

FORTRAN routine CY2008.FOR (http://peer.berkeley.edu/products/Chiou_Youngs_NGA.html) is provided to implement the model developed in this study. Example input and output files are provided for four scenarios: **M** 5 and **M** 7 strike-slip earthquakes and **M** 5 and **M** 7 reverse-faulting earthquakes. The required input variables are indicated by the header record in the example input files. The routine accepts its main input and writes the output to the console. After invoking at the command prompt, the routine loops over prompts for the input and output files.

Table 7.1 list the computed median spectral accelerations (y) for the four example scenarios for spectral periods of 0.01, 0.2, 1.0, 3.0 sec. The total standard deviation (σ_{total}) is computed by the approximate method of Equation (5.3) for the case of $F_{Inferred} = 0$ (i.e., measured V_{S30}).

Table 7.1 Example calculations.

Period (sec)	M	R_{RUP}	R_{JB}	R_X	V_{S30} (m/s)	$Z_{1.0}$ (m)	F_{RV}	F_{NM}	Z_{TOR}	δ (°)	y_{ref} (g)	y (g)	σ_{total}
M 5 Strike Slip													
0.01	5	5	0	0	760	23.5	0	0	5	90	0.1761	0.2159	0.6729
0.01	5	10	8.66	8.66	760	23.5	0	0	5	90	0.0901	0.1108	0.6735
0.01	5	15	14.14	14.14	760	23.5	0	0	5	90	0.0541	0.0666	0.6740
0.01	5	30	29.58	29.58	760	23.5	0	0	5	90	0.0194	0.0239	0.6747
0.01	5	50	49.75	49.75	760	23.5	0	0	5	90	0.0086	0.0106	0.6750
0.01	5	100	99.87	99.87	760	23.5	0	0	5	90	0.0026	0.0032	0.6752
0.01	5	200	199.94	199.94	760	23.5	0	0	5	90	0.0005	0.0006	0.6752
0.2	5	5	0	0	760	23.5	0	0	5	90	0.3533	0.4339	0.7173
0.2	5	10	8.66	8.66	760	23.5	0	0	5	90	0.1768	0.2188	0.7193
0.2	5	15	14.14	14.14	760	23.5	0	0	5	90	0.1048	0.1303	0.7206
0.2	5	30	29.58	29.58	760	23.5	0	0	5	90	0.0370	0.0462	0.7224
0.2	5	50	49.75	49.75	760	23.5	0	0	5	90	0.0163	0.0204	0.7232
0.2	5	100	99.87	99.87	760	23.5	0	0	5	90	0.0049	0.0062	0.7236
0.2	5	200	199.94	199.94	760	23.5	0	0	5	90	0.0009	0.0012	0.7238

Table 7.1–*Continued*

Period (sec)	M	R_{RUP}	R_{JB}	R_X	V_{S30} (m/s)	$Z_{1.0}$ (m)	F_{RV}	F_{NM}	Z_{TOR}	δ (°)	y_{ref} (g)	y (g)	σ_{total}
1	5	5	0	0	760	23.5	0	0	5	90	0.0406	0.0544	0.6958
1	5	10	8.66	8.66	760	23.5	0	0	5	90	0.0201	0.0270	0.6959
1	5	15	14.14	14.14	760	23.5	0	0	5	90	0.0121	0.0162	0.6960
1	5	30	29.58	29.58	760	23.5	0	0	5	90	0.0047	0.0063	0.6961
1	5	50	49.75	49.75	760	23.5	0	0	5	90	0.0024	0.0032	0.6962
1	5	100	99.87	99.87	760	23.5	0	0	5	90	0.0011	0.0015	0.6962
1	5	200	199.94	199.94	760	23.5	0	0	5	90	0.0005	0.0007	0.6962
3	5	5	0	0	760	23.5	0	0	5	90	0.0038	0.0058	0.7263
3	5	10	8.66	8.66	760	23.5	0	0	5	90	0.0019	0.0029	0.7265
3	5	15	14.14	14.14	760	23.5	0	0	5	90	0.0011	0.0018	0.7266
3	5	30	29.58	29.58	760	23.5	0	0	5	90	0.0005	0.0007	0.7267
3	5	50	49.75	49.75	760	23.5	0	0	5	90	0.0002	0.0004	0.7267
3	5	100	99.87	99.87	760	23.5	0	0	5	90	0.0001	0.0002	0.7268
3	5	200	199.94	199.94	760	23.5	0	0	5	90	0.0001	0.0001	0.7268
M 5 Reverse													
0.01	5	5	0	0	760	23.5	1	0	5	45	0.1946	0.2385	0.6728
0.01	5	10	7.03	9.14	760	23.5	1	0	5	45	0.1110	0.1363	0.6733
0.01	5	15	13.21	15.32	760	23.5	1	0	5	45	0.0626	0.0771	0.6739
0.01	5	30	29.15	31.25	760	23.5	1	0	5	45	0.0216	0.0267	0.6746
0.01	5	50	49.49	51.6	760	23.5	1	0	5	45	0.0095	0.0117	0.6749
0.01	5	100	99.75	101.85	760	23.5	1	0	5	45	0.0028	0.0035	0.6752
0.01	5	200	199.87	201.98	760	23.5	1	0	5	45	0.0005	0.0006	0.6752
0.2	5	5	0	0	760	23.5	1	0	5	45	0.3905	0.4789	0.7171
0.2	5	10	7.03	9.14	760	23.5	1	0	5	45	0.2217	0.2737	0.7186
0.2	5	15	13.21	15.32	760	23.5	1	0	5	45	0.1223	0.1519	0.7202
0.2	5	30	29.15	31.25	760	23.5	1	0	5	45	0.0414	0.0517	0.7223
0.2	5	50	49.49	51.6	760	23.5	1	0	5	45	0.0181	0.0226	0.7231
0.2	5	100	99.75	101.85	760	23.5	1	0	5	45	0.0055	0.0068	0.7236
0.2	5	200	199.87	201.98	760	23.5	1	0	5	45	0.0010	0.0013	0.7238
1	5	5	0	0	760	23.5	1	0	5	45	0.0438	0.0588	0.6957
1	5	10	7.03	9.14	760	23.5	1	0	5	45	0.0235	0.0316	0.6959
1	5	15	13.21	15.32	760	23.5	1	0	5	45	0.0135	0.0182	0.6960
1	5	30	29.15	31.25	760	23.5	1	0	5	45	0.0051	0.0068	0.6961
1	5	50	49.49	51.6	760	23.5	1	0	5	45	0.0026	0.0035	0.6962
1	5	100	99.75	101.85	760	23.5	1	0	5	45	0.0012	0.0016	0.6962
1	5	200	199.87	201.98	760	23.5	1	0	5	45	0.0005	0.0007	0.6962
3	5	5	0	0	760	23.5	1	0	5	45	0.0035	0.0053	0.7263
3	5	10	7.03	9.14	760	23.5	1	0	5	45	0.0018	0.0027	0.7265
3	5	15	13.21	15.32	760	23.5	1	0	5	45	0.0011	0.0016	0.7266
3	5	30	29.15	31.25	760	23.5	1	0	5	45	0.0004	0.0006	0.7267
3	5	50	49.49	51.6	760	23.5	1	0	5	45	0.0002	0.0003	0.7267
3	5	100	99.75	101.85	760	23.5	1	0	5	45	0.0001	0.0002	0.7268
3	5	200	199.87	201.98	760	23.5	1	0	5	45	0.0001	0.0001	0.7268

Table 7.1—*Continued*

Period (sec)	M	R_{RUP}	R_{JB}	R_X	V_{S30} (m/s)	$Z_{1.0}$ (m)	F_{RV}	F_{NM}	Z_{TOR}	δ (°)	y_{ref} (g)	y (g)	σ_{total}
M 7 Strike Slip													
0.01	7	1	1	1	760	23.5	0	0	0	90	0.4634	0.5648	0.5201
0.01	7	3	3	3	760	23.5	0	0	0	90	0.3838	0.4683	0.5202
0.01	7	5	5	5	760	23.5	0	0	0	90	0.3229	0.3945	0.5203
0.01	7	10	10	10	760	23.5	0	0	0	90	0.2220	0.2718	0.5205
0.01	7	15	15	15	760	23.5	0	0	0	90	0.1630	0.1998	0.5207
0.01	7	30	30	30	760	23.5	0	0	0	90	0.0837	0.1029	0.5211
0.01	7	50	50	50	760	23.5	0	0	0	90	0.0484	0.0596	0.5215
0.01	7	100	100	100	760	23.5	0	0	0	90	0.0215	0.0265	0.5219
0.01	7	200	200	200	760	23.5	0	0	0	90	0.0067	0.0083	0.5223
0.2	7	1	1	1	760	23.5	0	0	0	90	1.0872	1.3115	0.5870
0.2	7	3	3	3	760	23.5	0	0	0	90	0.8859	1.0727	0.5873
0.2	7	5	5	5	760	23.5	0	0	0	90	0.7353	0.8932	0.5876
0.2	7	10	10	10	760	23.5	0	0	0	90	0.4925	0.6021	0.5884
0.2	7	15	15	15	760	23.5	0	0	0	90	0.3549	0.4358	0.5891
0.2	7	30	30	30	760	23.5	0	0	0	90	0.1765	0.2185	0.5907
0.2	7	50	50	50	760	23.5	0	0	0	90	0.1001	0.1244	0.5919
0.2	7	100	100	100	760	23.5	0	0	0	90	0.0439	0.0548	0.5931
0.2	7	200	200	200	760	23.5	0	0	0	90	0.0139	0.0174	0.5940
1	7	1	1	1	760	23.5	0	0	0	90	0.3288	0.4400	0.6461
1	7	3	3	3	760	23.5	0	0	0	90	0.2610	0.3494	0.6462
1	7	5	5	5	760	23.5	0	0	0	90	0.2123	0.2844	0.6462
1	7	10	10	10	760	23.5	0	0	0	90	0.1380	0.1850	0.6463
1	7	15	15	15	760	23.5	0	0	0	90	0.0982	0.1317	0.6464
1	7	30	30	30	760	23.5	0	0	0	90	0.0496	0.0666	0.6465
1	7	50	50	50	760	23.5	0	0	0	90	0.0302	0.0405	0.6467
1	7	100	100	100	760	23.5	0	0	0	90	0.0169	0.0227	0.6468
1	7	200	200	200	760	23.5	0	0	0	90	0.0093	0.0125	0.6469
3	7	1	1	1	760	23.5	0	0	0	90	0.0744	0.1128	0.7028
3	7	3	3	3	760	23.5	0	0	0	90	0.0591	0.0895	0.7028
3	7	5	5	5	760	23.5	0	0	0	90	0.0481	0.0729	0.7028
3	7	10	10	10	760	23.5	0	0	0	90	0.0313	0.0476	0.7029
3	7	15	15	15	760	23.5	0	0	0	90	0.0224	0.0340	0.7031
3	7	30	30	30	760	23.5	0	0	0	90	0.0115	0.0175	0.7033
3	7	50	50	50	760	23.5	0	0	0	90	0.0072	0.0109	0.7035
3	7	100	100	100	760	23.5	0	0	0	90	0.0043	0.0065	0.7037
3	7	200	200	200	760	23.5	0	0	0	90	0.0027	0.0042	0.7038
M 7 Reverse													
0.01	7	1	0	1.41	760	23.5	1	0	0	45	0.7238	0.8796	0.5199
0.01	7	3	0	4.24	760	23.5	1	0	0	45	0.8555	1.0383	0.5199
0.01	7	5	0	7.07	760	23.5	1	0	0	45	0.7753	0.9417	0.5199
0.01	7	10	0	14.14	760	23.5	1	0	0	45	0.5406	0.6582	0.5200
0.01	7	15	6.21	21.21	760	23.5	1	0	0	45	0.2861	0.3498	0.5203

Table 7.1—*Continued*

Period (sec)	M	R_{RUP}	R_{JB}	R_X	V_{S30} (m/s)	$Z_{1.0}$ (m)	F_{RV}	F_{NM}	Z_{TOR}	δ (°)	y_{ref} (g)	y (g)	σ_{total}
0.01	7	30	25.98	40.98	760	23.5	1	0	0	45	0.1029	0.1264	0.5210
0.01	7	50	47.7	62.7	760	23.5	1	0	0	45	0.0554	0.0683	0.5214
0.01	7	100	98.87	113.87	760	23.5	1	0	0	45	0.0239	0.0295	0.5219
0.01	7	200	199.44	214.43	760	23.5	1	0	0	45	0.0075	0.0092	0.5222
0.2	7	1	0	1.41	760	23.5	1	0	0	45	1.6693	1.9975	0.5864
0.2	7	3	0	4.24	760	23.5	1	0	0	45	2.0716	2.4683	0.5862
0.2	7	5	0	7.07	760	23.5	1	0	0	45	1.9748	2.3553	0.5863
0.2	7	10	0	14.14	760	23.5	1	0	0	45	1.3827	1.6606	0.5867
0.2	7	15	6.21	21.21	760	23.5	1	0	0	45	0.6777	0.8243	0.5877
0.2	7	30	25.98	40.98	760	23.5	1	0	0	45	0.2211	0.2730	0.5902
0.2	7	50	47.7	62.7	760	23.5	1	0	0	45	0.1155	0.1434	0.5916
0.2	7	100	98.87	113.87	760	23.5	1	0	0	45	0.0490	0.0611	0.5930
0.2	7	200	199.44	214.43	760	23.5	1	0	0	45	0.0155	0.0193	0.5940
1	7	1	0	1.41	760	23.5	1	0	0	45	0.4166	0.5572	0.6461
1	7	3	0	4.24	760	23.5	1	0	0	45	0.4243	0.5675	0.6461
1	7	5	0	7.07	760	23.5	1	0	0	45	0.3925	0.5250	0.6461
1	7	10	0	14.14	760	23.5	1	0	0	45	0.2752	0.3683	0.6462
1	7	15	6.21	21.21	760	23.5	1	0	0	45	0.1525	0.2043	0.6463
1	7	30	25.98	40.98	760	23.5	1	0	0	45	0.0582	0.0781	0.6465
1	7	50	47.7	62.7	760	23.5	1	0	0	45	0.0335	0.0450	0.6466
1	7	100	98.87	113.87	760	23.5	1	0	0	45	0.0183	0.0246	0.6468
1	7	200	199.44	214.43	760	23.5	1	0	0	45	0.0101	0.0135	0.6469
3	7	1	0	1.41	760	23.5	1	0	0	45	0.0700	0.1061	0.7028
3	7	3	0	4.24	760	23.5	1	0	0	45	0.0584	0.0885	0.7028
3	7	5	0	7.07	760	23.5	1	0	0	45	0.0488	0.0740	0.7028
3	7	10	0	14.14	760	23.5	1	0	0	45	0.0323	0.0490	0.7029
3	7	15	6.21	21.21	760	23.5	1	0	0	45	0.0219	0.0333	0.7031
3	7	30	25.98	40.98	760	23.5	1	0	0	45	0.0106	0.0162	0.7033
3	7	50	47.7	62.7	760	23.5	1	0	0	45	0.0066	0.0100	0.7035
3	7	100	98.87	113.87	760	23.5	1	0	0	45	0.0039	0.0060	0.7037
3	7	200	199.44	214.43	760	23.5	1	0	0	45	0.0025	0.0038	0.7038

8 Model Applicability

The model developed in this study is considered to be applicable for estimating pseudo–spectral accelerations (5% damping) and peak motions for earthquakes in active tectonic regions in which the following conditions apply:

- $4 \leq \mathbf{M} \leq 8.5$ for strike-slip earthquakes
- $4 \leq \mathbf{M} \leq 8.0$ for reverse and normal faulting earthquakes
- $0 \leq R_{RUP} \leq 200$ km
- 150 m/sec $\leq V_{S30} \leq 1500$ m/sec

The model was developed using the anelastic attenuation coefficient γ constrained by data from California earthquakes. For application in other regions where earthquakes at distances greater than about 50 km are a major contributor to the hazard, adjustments to the $\gamma(\mathbf{M})$ coefficients $c_{\gamma 1}$ and $c_{\gamma 2}$ may be warranted. These adjustments can be made using the hybrid approach developed by Campbell (2003). In making such adjustments, we stress the need for the user to obtain estimates of Q for the two regions that are based on consistent geometric spreading models.

The site response portion of the ground motion model was constrained such that all ground motion amplification factors are 1 for V_{S30} greater than 1130 m/s. As the rock velocity increases we expect shallow crustal damping (i.e., "kappa") to decrease, resulting in increases in high-frequency motion. Data for such sites are not present in the PEER-NGA database in sufficient quantity to estimate this effect, and it is not captured in our model. Such effects should be considered if the model is to be applied to sites with V_{S30} greater than 1500 m/sec.

The model was developed using recordings from earthquakes with a maximum depth to top of rupture of 15 km and a maximum hypocentral depth of 19 km. The model predicts a linear increase in $\ln(y_{ref})$ with increasing Z_{TOR} over this depth range for most spectral periods.

Application of the model in regions with very thick crust (e.g., >> 20 km) is an extrapolation outside of the range of data used to develop the model coefficients.

The ground motion model presented here is sensitive to the value of sediment depth, $Z_{1.0}$, for the site. We have used data from the SCEC-3D Version 4 model for southern California and users should use this version to estimate values of $Z_{1.0}$ at sites in southern California. For general application, we recommend that the user estimate $Z_{1.0}$ from Equation (2.1) unless there is site-specific data to provide a better estimate (e.g., a site velocity profile). Note also that large values of $Z_{1.0}$ may produce numerical overflow of the cosh function in some compilers and the user may need to determine the appropriate limits in implementing our model in computer programs.

REFERENCES

Abrahamson, N.A., and W.J. Silva, 1997, Empirical response spectral attenuation relations for shallow crustal earthquakes, *Seismological Research Letters*, v. 68, p. 94–127.

Abrahamson, N.A., and P.G. Somerville, 1996, Effects of the hanging wall and footwall on the ground motions recorded during the Northridge earthquake, *Bulletin of the Seismological Society of America*, v. 86, p. S93–S99.

Abrahamson, N.A., and R.R., Youngs, R.R., 1992, A stable algorithm for regression analyses using the random effects model, *Bulletin of the Seismological Society of America*, v. 82, p. 505–510.

Ambraseys, N.N, Simpson, K.A., and Bommer, J.J, 1996, Prediction of horizontal response spectra in Europe, *Earthquake Engineering and Structural Dynamics*, v. 25, p. 371–400.

Ambraseys, N.N., J Douglas, S.K. Sarmal, and P.M. Smit, 2005, Equations for the estimation of strong ground motions from shallow crustal earthquakes using data from Europe and the Middle East: Horizontal peak ground acceleration and spectral acceleration, *Bulletin of Earthquake Engineering*, v 3, p. 1–35.

BSSC, 2004, *NEHRP Recommended Provisions for Seismic Regulations for New Buildings and Other Structures*, 2003 Edition, FEMA Publication 450, Building Seismic Safety Council, Washington, D.C.

Atkinson, G.M., 1989, Attenuation of the Lg phase and site response for the Eastern Canada Telemetered Network, *Seismological Research Letters*, v.60 (2), p. 59–69.

Atkinson, G.M. and R. Mereu, 1992, The shape of ground motion attenuation curves in southeastern Canada, *Bulletin of the Seismological Society of America*, v.82, p. 2014–2031.

Atkinson, G.M. and W. Silva, 1997, An empirical study of earthquake source spectra for California earthquakes, *Bulletin of the Seismological Society of America*, v.87, p. 97–113.

Atkinson, G.M. and W. Silva, 2000, Stochastic modeling of California ground motions, *Bulletin of the Seismological Society of America*, v.90, p. 255–274.

Bazzurro, P. and C.A. Cornell, 2004, Ground-motion amplification in nonlinear soil sites with uncertain properties, *Bulletin of the Seismological Society of America*, v.94, p. 2090–2109.

Boatwright, J., H. Bundock, J. Luetgert, L. Seekins, L. Gee, and P. Lombard, 2003, The dependence of PGA and PGV on distance and magnitude inferred from northern California ShakeMap data, *Bulletin of the Seismological Society of America*, v. 93, p. 2043–2055.

Boatwright, J., L. Blair, R. Catchings, M. Goldman, F. Perosi, and C. Steedman, 2004, *Using Twelve Years of USGS Refraction Lines to Calibrate the Brocher and Others (1997) 3D Velocity Model of the Bay Area*, U.S. Geological Survey Open File Report 2004–1282.

Boore, D.M., 2003, Simulation of ground motion using the stochastic method, *Pure and Applied Geophysics*, v. 160, p. 635–676.

Boore, D.M., 2005, SMSIM – Fortran programs for simulating ground motions from earthquakes: Version 2.3-A revision of OFR 96-80-A: U.S. Geological Survey Open File Report 00-509, 15 August, 55 p.

Boore, D.M. and W.B. Joyner, 1997, Site amplification for generic rock sites, *Bulletin of the Seismological Society of America*, v.87, p. 327341.

Boore, D.M., W.B, Joyner, and T.E. Fumal, 1993, Estimation of response spectra and peak accelerations from western North American earthquakes: An interim report, U.S. Geological Survey Open-File Report 93-509, 72 pp.

Boore, D.M., W.B, Joyner, and T.E. Fumal, 1997, Equations for estimating horizontal response spectra and peak acceleration from western North American earthquakes–A summary of recent work, *Seismological Research Letters*, v. 68, p. 128153.

Boore, D.M., J. Watson-Lamprey, and N.A. Abrahamson, 2006, GMRotD and GMRotI: Orientation-independent measures of ground motion, *Bulletin of the Seismological Society of America*, v. 96, p. 1202–1511.

Bragato, P.L., 2004, Regression analysis with truncated samples and its application to ground-motion attenuation studies, *Bulletin of the Seismological Society of America*, v. 94, p. 1369–1378.

Brillinger, D.R., and H.K. Preisler, 1984, An exploratory analysis of the Joyner-Boore attenuation data, *Bulletin of the Seismological Society of America*, v. 74, p. 1441–1450.

Brune, J., 1970, Tectonic stress and the spectra of seismic shear waves from earthquakes, *Journal of Geophysical Research*, v. 75, p. 4997–5009.

Brune, J., 1971, Correction, *Journal of Geophysical Research*, v. 76, p. 5002.

Campbell, K.W., 1989, Empirical Prediction of Near-Source Ground Motion for the Diablo Canyon Power Plant site, San Luis Obispo County, California, U.S. Geological Survey Open-File Report 89-484.

Campbell, K.W., 1993, Empirical prediction of near-source ground motion from large earthquakes, *Proceedings International Workshop on Earthquake Hazards and Large Dams in the Himalaya*, January 15-16, New Deli India.

Campbell, K.W., 1997, Empirical near-source attenuation relationships for horizontal and vertical components of peak ground acceleration, peak ground velocity, and pseudo-absolute acceleration response spectra, *Seismological Research Letters*, v. 68, p. 154–179.

Campbell, K.W., 2003, Prediction of strong ground motion using the hybrid empirical method and its use in the development of ground motion (attenuation) relations in eastern North America, *Bulletin of the Seismological Society of America*, v. 93, p. 1012–1033.

Campbell, K.W., and Y. Bozorgnia, 2003, Updated near-source ground-motion (attenuation) relations for the horizontal and vertical components of peak ground acceleration and acceleration response spectra, *Bulletin of the Seismological Society of America*, v.93, p. 314–331.

Chiou, B. S.-J., R. Darragh, N. Gregor, and W. Silva, 2008, NGA project strong-motion database, *Earthquake Spectra*, v. 24, p. 23 – 44.

Chiou, S.-J., F.I. Makdisi, and R.R. Youngs, 2000, Style-of-Faulting and Footwall/Hanging Wall Effects on Strong Ground Motion, FY 1995 NEHRP Award Number 1434-95-G-2614, final report, 21 pp.

Chiou, B. S.-J., and R.R. Youngs, 2006, Chiou and Youngs PEER-NGA empirical ground motion model for the average horizontal component of peak acceleration, peak velocity, and pseudo-spectral acceleration for spectral periods of 0.01–10 sec, interim report submitted to PEER, July 2006.

Choi, Y., and J.P. Stewart, 2005, Nonlinear site amplification as function of 30 m shear wave velocity, *Earthquake Spectra*, v. 21, p. 1–30.

Choi, Y., J.P. Stewart, and R.W. Graves, 2005, Empirical model for basin effect accounting for basin depth and source location, *Bulletin of the Seismological Society of America*, v. 95, p. 1412 – 1427.

Day, S.M., J. Bielak, D. Dreger, R. Graves, S. Larsen, K.B. Olsen, A. Pitarka, and L. Ramirez-Guzman, 2006, Numerical simulation of basin effects on long-period ground motion, *Proceedings of the 8th National Conference on Earthquake Engineering*, April 18–22, San Francisco, California, paper No. 1857.

Day, S.M., R. Graves, J. Bielak, D. Dreger, S. Larsen, K.B. Olsen, A. Pitarka, and L. Ramirez-Guzman, 2008, Model for basin effects on long-period response spectra in southern California, *Earthquake Spectra*, v. 24, p. 257 – 277.

EPRI, 1993, Guidelines for determining design basis ground motions, Electric Power Research Institute Report EPRI TR-102293, Vol. 1.

Erickson, D., D.E. McNamara, and H.M. Benz, 2004, Frequency-dependent Lg Q within the continental United States, *Bulletin of the Seismological Society of America*, v.94, p. 1630–1643.

Field, E.H., 2000, A modified ground motion attenuation relationship for southern California that accounts for detailed site classification and a basin depth effect, *Bulletin of the Seismological Society of America,* v. 90**,** p. S209–S221.

Frankel, A., A. McGarr, J. Bicknell, J. Mori, L. Seeber, and E. Cranswick, 1990, Attenuation of high-frequency shear waves in the crust, measurements from New York State, South Africa, and southern California, *Journal of Geophysical Research*, v. 95, p. 17,441–17,457.

Fukushima, Y., and T. Tanaka, 1990, A new attenuation relation for peak horizontal acceleration of strong earthquake ground motion in Japan, *Bulletin of the Seismological Society of America*, v. 80, p. 757–783.

Fukushima, Y., K. Irikura, T. Uetake, and H. Matsumoto, 2000, Characteristics of observed peak amplitude for strong ground motion from the 1995 Hyogoken Nanbu (Kobe) earthquake, *Bulletin of the Seismological Society of America*, v. 90, p. 545–565.

Geomatrix Consultants, 1995, *Seismic design mapping State of Oregon*, report prepared for the Oregon Department of Transportation, Personal Services Contract 11688, Geomatrix Consultants Project No. 2442, January.

Graves, R.W., 1994, Simulating the 3D Basin Response in the Portland and Puget Sound Regions from Large Subduction Zone Earthquakes, USGS Award 1434-93-G-2327, Annual Technical Report.

Idriss, I.M., 1991, *Procedures for Selecting Earthquake Ground Motions at Rock Sites*, National Institute of Standards and Technology, Report No. NIST GCR 93-625.

Idriss, I.M., (2002) Personal Communication.

Joyner, W. B., 2000, Strong motion from surface waves in deep sedimentary basins, *Bulletin of the Seismological Society of America*, v. 90, p. S95–S112.

Magistrale, H., S.M. Day, R. Clayton, and R.W. Graves, 2000, The SCEC southern California reference three-dimensional seismic velocity model version 2, *Bulletin of the Seismological Society of America*, v. 90, p. S65-S76.

Mai, P.M., P. Spudich, and J. Boatwright, 2005, Hypocenter locations in finite-source rupture models, Bulletin of the Seismological Society of America, v. 95, p. 965-980.

Oppenheimer, D., G. Beroza, G. Carver, L. Dengler, J. Eaton, L. Gee, F. Gonzalez, A. Jayko, W.H. Li, M. Lisowski, M. Magee, G. Marshall, M. Murray, R. McPherson, B. Romanowicz, K. Satake, R. Simpson, P. Somerville, R. Stein, R., and D. Valentine, 1993, The Cape Mendocino, California Earthquakes of April 1992: Subduction at the Triple Junction, *Science*, v. 261, p. 433-438.

Pinheiro, J., and D. Bates, 2000, *Mixed Effects Models in S and S-Plus*, Springer, 528 pp.

R Development Core Team, 2006, R: *A Language and Environment for Statistical Computing, R Foundation for Statistical Computing*, Vienna, Austria. ISBN 3-900051-07-0, http://www.R-project.org.

Raoof, M., R. Herrmann, and L. Malagnini, 1999, Attenuation and excitation of three-component ground motion in southern California, *Bulletin of the Seismological Society of America*, v.89, p. 888-902.

Sabetta, F., and Pugliese, A., 1996, Estimation of response spectra and simulation of nonstationary earthquake ground motions, *Bulletin of the Seismological Society of America*, v. 86, p. 337-352.

Sadigh, K., Chang, C.-Y., Egan, J.A., Makdisi, F.I., and Youngs, R.R., 1997, Attenuation relationships for shallow crustal earthquakes based on California strong motion data, *Seismological Research Letters*, v. 68, p. 180-189.

Sibson, R. H., and Xie, G., 1998, Dip range for intracontinental reverse fault ruptures: Truth not stranger than friction, *Bulletin of the Seismological Society of America*, v. 88, p. 1014-1022.

Silva, W., 2008, Site response simulations for the PEER-NGA project, report prepared for the Pacific Earthquake Engineering Research Center.

Silva, W.C., Abrahamson, N., Toro, G., and Costantino, C., 1996, *Description and Validation of the Stochastic Ground Motion Model*, report submitted to Brookhaven National Laboratory, Associated Universities, Inc., New York (available at www.pacificengineering.org).

Somerville, P.G., and N.A. Abrahamson, 1995, *Prediction of Ground Motions for Thrust Earthquakes*, report to the California Strong Motion Instrumentation Program (CSMIP).

Somerville, P., N. Collins, R. Graves, A. Pitarka, W. Silva, and Y. Zeng, 2006, Simulation of ground motion scaling characteristics for the NGA-E project, *Proceedings of the 8th National Conference on Earthquake Engineering*, April 18-22, San Francisco, California, USA, paper No. 1789.

Spudich, P., W.B. Joyner, A.G. Lindh, D.M. Boore, B.M. Margaris, and J.B. Fletcher, 1999, SEA99: a revised ground motion prediction relation for use in extensional tectonic regimes, *Bulletin of the Seismological Society of America*, v. 89, p. 1156-1170.

Spudich, P and B. Chiou, 2008, Directivity in NGA earthquake ground motions: analysis using isochrone theory, *Earthquake Spectra*, v. 24, p. 279 – 298.

Toro G.R., 1981, *Biases in Seismic Ground Motion Prediction*, Ph.D. Thesis, Dept. of Civil Eng., Massachusetts Inst. of Technology, 133 pp.

Walling, M., W. Silva, and N.A. Abrahamson, 2008, Non-linear site amplification factors for constraining the NGA models, *Earthquake Spectra*, v. 24, p 243 - 255.

Wells, D.L., and Coppersmith, K.J., 1994, New empirical relationships among magnitude, rupture length, rupture width, rupture area, and surface displacement, *Bulletin of the Seismological Society of America*, v. 84, p. 974-1002.

Wills, C.J., and L.B. Clahan, 2006, Developing a map of geologically defined site-condition categories for California, *Bulletin of the Seismological Society of America*, v. 96(4A), p. 1483-1501.

Youngs, R.R., 1993, Soil amplification and vertical to horizontal ratios for analysis of strong motion data from active tectonic regions, Appendix 2C in *Guidelines for Determining Design Basis Ground Motions, Vol. 2: Appendices for Ground Motion Estimation*, EPRI Report TR-102293.

Youngs, R.R, N. Abrahamson, F. Makdisi, and K. Sadigh, 1995, Magnitude Dependent Variance of Peak Ground Acceleration, *Bulletin of the Seismological Society of America*, v. 85, p. 1161-1176.

Appendix A: Recordings from PEER-NGA Flatfile Version 7.2 Used in Developing Chiou and Youngs's 2008 Empirical Ground Motion Model

RSN	EQID	Earthquake	M	Station No.	Station
23	0020	San Francisco	5.28	1117	Golden Gate Park
28	0025	Parkfield	6.19	1016	Cholame - Shandon Array #12
30	0025	Parkfield	6.19	1014	Cholame - Shandon Array #5
31	0025	Parkfield	6.19	1015	Cholame - Shandon Array #8
33	0025	Parkfield	6.19	1438	Temblor pre-1969
42	0029	Lytle Creek	5.33	112	Cedar Springs Pumphouse
43	0029	Lytle Creek	5.33	111	Cedar Springs, Allen Ranch
44	0029	Lytle Creek	5.33	113	Colton - So Cal Edison
45	0029	Lytle Creek	5.33	620	Devil's Canyon
48	0029	Lytle Creek	5.33	278	Puddingstone Dam (Abutment)
49	0029	Lytle Creek	5.33	104	Santa Anita Dam
50	0029	Lytle Creek	5.33	290	Wrightwood - 6074 Park Dr
51	0030	San Fernando	6.61	411	2516 Via Tejon PV
56	0030	San Fernando	6.61	108	Carbon Canyon Dam
57	0030	San Fernando	6.61	24278	Castaic - Old Ridge Route
63	0030	San Fernando	6.61	121	Fairmont Dam
64	0030	San Fernando	6.61	998	Fort Tejon
65	0030	San Fernando	6.61	994	Gormon - Oso Pump Plant
68	0030	San Fernando	6.61	24303	LA - Hollywood Stor FF
70	0030	San Fernando	6.61	24271	Lake Hughes #1
71	0030	San Fernando	6.61	128	Lake Hughes #12
72	0030	San Fernando	6.61	126	Lake Hughes #4
73	0030	San Fernando	6.61	127	Lake Hughes #9
77	0030	San Fernando	6.61	279	Pacoima Dam (upper left abut)
78	0030	San Fernando	6.61	262	Palmdale Fire Station
81	0030	San Fernando	6.61	269	Pearblossom Pump
82	0030	San Fernando	6.61	272	Port Hueneme
83	0030	San Fernando	6.61	278	Puddingstone Dam (Abutment)
87	0030	San Fernando	6.61	104	Santa Anita Dam
88	0030	San Fernando	6.61	285	Santa Felita Dam (Outlet)
89	0030	San Fernando	6.61	1027	Tehachapi Pump
91	0030	San Fernando	6.61	287	Upland - San Antonio Dam
93	0030	San Fernando	6.61	289	Whittier Narrows Dam
94	0030	San Fernando	6.61	290	Wrightwood - 6074 Park Dr
95	0031	Managua, Nicaragua-01	6.24	3501	Managua, ESSO
96	0032	Managua, Nicaragua-02	5.2	3501	Managua, ESSO
97	0033	Point Mugu	5.65	272	Port Hueneme
98	0034	Hollister-03	5.14	47379	Gilroy Array #1
100	0034	Hollister-03	5.14	47126	San Juan Bautista, 24 Polk St
106	0036	Oroville-01	5.89	1051	Oroville Seismograph Station
107	0037	Oroville-02	4.79	1545	Oroville Airport
108	0037	Oroville-02	4.79	1546	Up & Down Cafe (OR1)
109	0038	Oroville-04	4.37	1544	Medical Center
110	0038	Oroville-04	4.37	1545	Oroville Airport
111	0038	Oroville-04	4.37	1546	Up & Down Cafe (OR1)
112	0039	Oroville-03	4.7	1542	Broadbeck Residence
113	0039	Oroville-03	4.7	1543	DWR Garage
114	0039	Oroville-03	4.7	1550	Duffy Residence (OR5)
115	0039	Oroville-03	4.7	1493	Johnson Ranch
116	0039	Oroville-03	4.7	1496	Nelson Ranch (OR7)
117	0039	Oroville-03	4.7	1545	Oroville Airport
118	0039	Oroville-03	4.7	1549	Pacific Heights Rd (OR4)
119	0039	Oroville-03	4.7	1551	Summit Ave (OR6)
120	0039	Oroville-03	4.7	1546	Up & Down Cafe (OR1)

RSN	EQID	Earthquake	M	Station No.	Station
121	0040	Friuli, Italy-01	6.5	8002	Barcis
122	0040	Friuli, Italy-01	6.5	8004	Codroipo
125	0040	Friuli, Italy-01	6.5	8012	Tolmezzo
126	0041	Gazli, USSR	6.8	9201	Karakyr
127	0042	Fruili, Italy-03	5.5	8023	Buia
128	0042	Fruili, Italy-03	5.5	8014	Forgaria Cornino
129	0042	Fruili, Italy-03	5.5	8022	San Rocco
130	0043	Friuli, Italy-02	5.91	8023	Buia
131	0043	Friuli, Italy-02	5.91	8004	Codroipo
132	0043	Friuli, Italy-02	5.91	8014	Forgaria Cornino
133	0043	Friuli, Italy-02	5.91	8022	San Rocco
134	0044	Izmir, Turkey	5.3	99999	Izmir
135	0045	Santa Barbara	5.92	106	Cachuma Dam Toe
138	0046	Tabas, Iran	7.35	70	Boshrooyeh
139	0046	Tabas, Iran	7.35	9102	Dayhook
143	0046	Tabas, Iran	7.35	9101	Tabas
144	0047	Dursunbey, Turkey	5.34	99999	Dursunbey
145	0048	Coyote Lake	5.74	57217	Coyote Lake Dam (SW Abut)
146	0048	Coyote Lake	5.74	47379	Gilroy Array #1
147	0048	Coyote Lake	5.74	47380	Gilroy Array #2
148	0048	Coyote Lake	5.74	47381	Gilroy Array #3
149	0048	Coyote Lake	5.74	57382	Gilroy Array #4
150	0048	Coyote Lake	5.74	57383	Gilroy Array #6
151	0048	Coyote Lake	5.74	57191	Halls Valley
152	0048	Coyote Lake	5.74	47315	SJB Overpass, Bent 3 g.l.
153	0048	Coyote Lake	5.74	47315	SJB Overpass, Bent 5 g.l.
154	0048	Coyote Lake	5.74	47126	San Juan Bautista, 24 Polk St
155	0049	Norcia, Italy	5.9	99999	Bevagna
156	0049	Norcia, Italy	5.9	99999	Cascia
157	0049	Norcia, Italy	5.9	99999	Spoleto
158	0050	Imperial Valley-06	6.53	6616	Aeropuerto Mexicali
159	0050	Imperial Valley-06	6.53	6618	Agrarias
160	0050	Imperial Valley-06	6.53	5054	Bonds Corner
161	0050	Imperial Valley-06	6.53	5060	Brawley Airport
162	0050	Imperial Valley-06	6.53	5053	Calexico Fire Station
163	0050	Imperial Valley-06	6.53	5061	Calipatria Fire Station
164	0050	Imperial Valley-06	6.53	6604	Cerro Prieto
165	0050	Imperial Valley-06	6.53	6621	Chihuahua
166	0050	Imperial Valley-06	6.53	5066	Coachella Canal #4
167	0050	Imperial Valley-06	6.53	6622	Compuertas
169	0050	Imperial Valley-06	6.53	6605	Delta
170	0050	Imperial Valley-06	6.53	01136	EC County Center FF
171	0050	Imperial Valley-06	6.53	1336	EC Meloland Overpass FF
172	0050	Imperial Valley-06	6.53	5056	El Centro Array #1
173	0050	Imperial Valley-06	6.53	412	El Centro Array #10
174	0050	Imperial Valley-06	6.53	5058	El Centro Array #11
175	0050	Imperial Valley-06	6.53	931	El Centro Array #12
176	0050	Imperial Valley-06	6.53	5059	El Centro Array #13
178	0050	Imperial Valley-06	6.53	5057	El Centro Array #3
179	0050	Imperial Valley-06	6.53	955	El Centro Array #4
180	0050	Imperial Valley-06	6.53	952	El Centro Array #5
181	0050	Imperial Valley-06	6.53	5158	El Centro Array #6
182	0050	Imperial Valley-06	6.53	5028	El Centro Array #7
183	0050	Imperial Valley-06	6.53	958	El Centro Array #8
184	0050	Imperial Valley-06	6.53	5165	El Centro Differential Array

RSN	EQID	Earthquake	M	Station No.	Station
185	0050	Imperial Valley-06	6.53	5055	Holtville Post Office
186	0050	Imperial Valley-06	6.53	11023	Niland Fire Station
187	0050	Imperial Valley-06	6.53	5051	Parachute Test Site
188	0050	Imperial Valley-06	6.53	5052	Plaster City
189	0050	Imperial Valley-06	6.53	6619	SAHOP Casa Flores
190	0050	Imperial Valley-06	6.53	286	Superstition Mtn Camera
191	0050	Imperial Valley-06	6.53	6610	Victoria
192	0050	Imperial Valley-06	6.53	11369	Westmorland Fire Sta
193	0051	Imperial Valley-07	5.01	5054	Bonds Corner
194	0051	Imperial Valley-07	5.01	5060	Brawley Airport
195	0051	Imperial Valley-07	5.01	5053	Calexico Fire Station
196	0051	Imperial Valley-07	5.01	6605	Delta
197	0051	Imperial Valley-07	5.01	5056	El Centro Array #1
198	0051	Imperial Valley-07	5.01	412	El Centro Array #10
199	0051	Imperial Valley-07	5.01	5058	El Centro Array #11
200	0051	Imperial Valley-07	5.01	5115	El Centro Array #2
201	0051	Imperial Valley-07	5.01	5057	El Centro Array #3
202	0051	Imperial Valley-07	5.01	955	El Centro Array #4
203	0051	Imperial Valley-07	5.01	952	El Centro Array #5
204	0051	Imperial Valley-07	5.01	5158	El Centro Array #6
205	0051	Imperial Valley-07	5.01	5028	El Centro Array #7
206	0051	Imperial Valley-07	5.01	958	El Centro Array #8
207	0051	Imperial Valley-07	5.01	5165	El Centro Differential Array
208	0051	Imperial Valley-07	5.01	5055	Holtville Post Office
209	0052	Imperial Valley-08	5.62	11369	Westmorland Fire Sta
210	0053	Livermore-01	5.8	58219	APEEL 3E Hayward CSUH
212	0053	Livermore-01	5.8	1265	Del Valle Dam (Toe)
213	0053	Livermore-01	5.8	57064	Fremont - Mission San Jose
214	0053	Livermore-01	5.8	57187	San Ramon - Eastman Kodak
215	0053	Livermore-01	5.8	57134	San Ramon Fire Station
216	0053	Livermore-01	5.8	57063	Tracy - Sewage Treatm Plant
217	0054	Livermore-02	5.42	58219	APEEL 3E Hayward CSUH
219	0054	Livermore-02	5.42	1265	Del Valle Dam (Toe)
220	0054	Livermore-02	5.42	57064	Fremont - Mission San Jose
221	0054	Livermore-02	5.42	57T01	Livermore - Fagundas Ranch
222	0054	Livermore-02	5.42	57T02	Livermore - Morgan Terr Park
223	0054	Livermore-02	5.42	57187	San Ramon - Eastman Kodak
224	0054	Livermore-02	5.42	57134	San Ramon Fire Station
225	0055	Anza (Horse Canyon)-01	5.19	5044	Anza - Pinyon Flat
226	0055	Anza (Horse Canyon)-01	5.19	5045	Anza - Terwilliger Valley
227	0055	Anza (Horse Canyon)-01	5.19	5160	Anza Fire Station
228	0055	Anza (Horse Canyon)-01	5.19	5049	Borrego Air Ranch
229	0055	Anza (Horse Canyon)-01	5.19	5047	Rancho De Anza
230	0056	Mammoth Lakes-01	6.06	54099	Convict Creek
231	0056	Mammoth Lakes-01	6.06	54214	Long Valley Dam (Upr L Abut)
232	0056	Mammoth Lakes-01	6.06	54301	Mammoth Lakes H. S.
233	0057	Mammoth Lakes-02	5.69	54099	Convict Creek
234	0057	Mammoth Lakes-02	5.69	54214	Long Valley Dam (Upr L Abut)
235	0057	Mammoth Lakes-02	5.69	54301	Mammoth Lakes H. S.
236	0058	Mammoth Lakes-03	5.91	54099	Convict Creek
237	0058	Mammoth Lakes-03	5.91	54214	Long Valley Dam (Downst)
238	0058	Mammoth Lakes-03	5.91	54214	Long Valley Dam (L Abut)
239	0058	Mammoth Lakes-03	5.91	54214	Long Valley Dam (Upr L Abut)
240	0059	Mammoth Lakes-04	5.7	54099	Convict Creek
241	0059	Mammoth Lakes-04	5.7	54214	Long Valley Dam (Downst)

RSN	EQID	Earthquake	M	Station No.	Station
242	0059	Mammoth Lakes-04	5.7	54214	Long Valley Dam (L Abut)
243	0059	Mammoth Lakes-04	5.7	54214	Long Valley Dam (Upr L Abut)
244	0060	Mammoth Lakes-05	5.7	54099	Convict Creek
245	0060	Mammoth Lakes-05	5.7	54214	Long Valley Dam (Upr L Abut)
246	0061	Mammoth Lakes-06	5.94	54100	Benton
247	0061	Mammoth Lakes-06	5.94	54424	Bishop - Paradise Lodge
248	0061	Mammoth Lakes-06	5.94	54099	Convict Creek
249	0061	Mammoth Lakes-06	5.94	43	Fish & Game (FIS)
250	0061	Mammoth Lakes-06	5.94	54214	Long Valley Dam (Upr L Abut)
251	0062	Mammoth Lakes-07	4.73	43	Fish & Game (FIS)
252	0062	Mammoth Lakes-07	4.73	3	Green Church
253	0062	Mammoth Lakes-07	4.73	35	Long Valley Fire Sta
254	0062	Mammoth Lakes-07	4.73	36	Mammoth Elem School
255	0062	Mammoth Lakes-07	4.73	34	USC Cash Baugh Ranch
256	0062	Mammoth Lakes-07	4.73	37	USC McGee Creek Inn
257	0063	Mammoth Lakes-08	4.8	41	Cashbaugh (CBR)
258	0063	Mammoth Lakes-08	4.8	42	Convict Lakes (CON)
259	0063	Mammoth Lakes-08	4.8	43	Fish & Game (FIS)
261	0063	Mammoth Lakes-08	4.8	35	Long Valley Fire Sta
262	0063	Mammoth Lakes-08	4.8	36	Mammoth Elem School
263	0063	Mammoth Lakes-08	4.8	40	USC Convict Lakes
264	0063	Mammoth Lakes-08	4.8	37	USC McGee Creek Inn
265	0064	Victoria, Mexico	6.33	6604	Cerro Prieto
266	0064	Victoria, Mexico	6.33	6621	Chihuahua
268	0064	Victoria, Mexico	6.33	6619	SAHOP Casa Flores
269	0064	Victoria, Mexico	6.33	6624	Victoria Hospital Sotano
270	0065	Mammoth Lakes-09	4.85	42	Convict Lakes (CON)
271	0065	Mammoth Lakes-09	4.85	43	Fish & Game (FIS)
272	0065	Mammoth Lakes-09	4.85	3	Green Church
273	0065	Mammoth Lakes-09	4.85	44	Hot Creek (HCF)
274	0065	Mammoth Lakes-09	4.85	35	Long Valley Fire Sta
275	0065	Mammoth Lakes-09	4.85	36	Mammoth Elem School
276	0065	Mammoth Lakes-09	4.85	45	McGee Creek (MGE)
277	0065	Mammoth Lakes-09	4.85	40	USC Convict Lakes
278	0065	Mammoth Lakes-09	4.85	52	USC McGee Creek
283	0068	Irpinia, Italy-01	6.9	99999	Arienzo
284	0068	Irpinia, Italy-01	6.9	99999	Auletta
285	0068	Irpinia, Italy-01	6.9	99999	Bagnoli Irpinio
286	0068	Irpinia, Italy-01	6.9	99999	Bisaccia
287	0068	Irpinia, Italy-01	6.9	99999	Bovino
288	0068	Irpinia, Italy-01	6.9	99999	Brienza
289	0068	Irpinia, Italy-01	6.9	99999	Calitri
290	0068	Irpinia, Italy-01	6.9	99999	Mercato San Severino
291	0068	Irpinia, Italy-01	6.9	99999	Rionero In Vulture
292	0068	Irpinia, Italy-01	6.9	99999	Sturno
293	0068	Irpinia, Italy-01	6.9	99999	Torre Del Greco
294	0068	Irpinia, Italy-01	6.9	99999	Tricarico
295	0069	Irpinia, Italy-02	6.2	99999	Auletta
296	0069	Irpinia, Italy-02	6.2	99999	Bagnoli Irpinio
297	0069	Irpinia, Italy-02	6.2	99999	Bisaccia
298	0069	Irpinia, Italy-02	6.2	99999	Bovino
299	0069	Irpinia, Italy-02	6.2	99999	Brienza
300	0069	Irpinia, Italy-02	6.2	99999	Calitri
301	0069	Irpinia, Italy-02	6.2	99999	Mercato San Severino
302	0069	Irpinia, Italy-02	6.2	99999	Rionero In Vulture

RSN	EQID	Earthquake	M	Station No.	Station
303	0069	Irpinia, Italy-02	6.2	99999	Sturno
304	0069	Irpinia, Italy-02	6.2	99999	Tricarico
305	0070	Irpinia, Italy-03	4.7	99999	Conza (Base)
313	0072	Corinth, Greece	6.6	99999	Corinth
314	0073	Westmorland	5.9	5060	Brawley Airport
315	0073	Westmorland	5.9	11023	Niland Fire Station
316	0073	Westmorland	5.9	5051	Parachute Test Site
317	0073	Westmorland	5.9	5062	Salton Sea Wildlife Refuge
318	0073	Westmorland	5.9	286	Superstition Mtn Camera
319	0073	Westmorland	5.9	11369	Westmorland Fire Sta
320	0074	Mammoth Lakes-10	5.34	54099	Convict Creek
321	0075	Mammoth Lakes-11	5.31	54099	Convict Creek
322	0076	Coalinga-01	6.36	46314	Cantua Creek School
323	0076	Coalinga-01	6.36	36229	Parkfield - Cholame 12W
324	0076	Coalinga-01	6.36	36452	Parkfield - Cholame 1E
325	0076	Coalinga-01	6.36	36230	Parkfield - Cholame 2E
326	0076	Coalinga-01	6.36	36228	Parkfield - Cholame 2WA
327	0076	Coalinga-01	6.36	36450	Parkfield - Cholame 3E
328	0076	Coalinga-01	6.36	36410	Parkfield - Cholame 3W
329	0076	Coalinga-01	6.36	36412	Parkfield - Cholame 4AW
330	0076	Coalinga-01	6.36	36411	Parkfield - Cholame 4W
331	0076	Coalinga-01	6.36	36227	Parkfield - Cholame 5W
332	0076	Coalinga-01	6.36	36451	Parkfield - Cholame 6W
333	0076	Coalinga-01	6.36	36226	Parkfield - Cholame 8W
334	0076	Coalinga-01	6.36	36407	Parkfield - Fault Zone 1
335	0076	Coalinga-01	6.36	36444	Parkfield - Fault Zone 10
336	0076	Coalinga-01	6.36	36453	Parkfield - Fault Zone 11
337	0076	Coalinga-01	6.36	36138	Parkfield - Fault Zone 12
338	0076	Coalinga-01	6.36	36456	Parkfield - Fault Zone 14
339	0076	Coalinga-01	6.36	36445	Parkfield - Fault Zone 15
340	0076	Coalinga-01	6.36	36457	Parkfield - Fault Zone 16
341	0076	Coalinga-01	6.36	36413	Parkfield - Fault Zone 2
342	0076	Coalinga-01	6.36	36408	Parkfield - Fault Zone 3
343	0076	Coalinga-01	6.36	36414	Parkfield - Fault Zone 4
344	0076	Coalinga-01	6.36	36454	Parkfield - Fault Zone 6
345	0076	Coalinga-01	6.36	36431	Parkfield - Fault Zone 7
346	0076	Coalinga-01	6.36	36449	Parkfield - Fault Zone 8
347	0076	Coalinga-01	6.36	36443	Parkfield - Fault Zone 9
348	0076	Coalinga-01	6.36	36415	Parkfield - Gold Hill 1W
349	0076	Coalinga-01	6.36	36421	Parkfield - Gold Hill 2E
350	0076	Coalinga-01	6.36	36416	Parkfield - Gold Hill 2W
351	0076	Coalinga-01	6.36	36439	Parkfield - Gold Hill 3E
352	0076	Coalinga-01	6.36	36420	Parkfield - Gold Hill 3W
353	0076	Coalinga-01	6.36	36433	Parkfield - Gold Hill 4W
354	0076	Coalinga-01	6.36	36434	Parkfield - Gold Hill 5W
355	0076	Coalinga-01	6.36	36432	Parkfield - Gold Hill 6W
356	0076	Coalinga-01	6.36	36422	Parkfield - Stone Corral 2E
357	0076	Coalinga-01	6.36	36437	Parkfield - Stone Corral 3E
358	0076	Coalinga-01	6.36	36438	Parkfield - Stone Corral 4E
359	0076	Coalinga-01	6.36	36455	Parkfield - Vineyard Cany 1E
360	0076	Coalinga-01	6.36	36448	Parkfield - Vineyard Cany 1W
362	0076	Coalinga-01	6.36	36447	Parkfield - Vineyard Cany 2W
363	0076	Coalinga-01	6.36	36176	Parkfield - Vineyard Cany 3W
364	0076	Coalinga-01	6.36	36446	Parkfield - Vineyard Cany 4W
366	0076	Coalinga-01	6.36	36441	Parkfield - Vineyard Cany 6W

RSN	EQID	Earthquake	M	Station No.	Station
368	0076	Coalinga-01	6.36	1162	Pleasant Valley P.P. - yard
369	0076	Coalinga-01	6.36	46175	Slack Canyon
370	0077	Coalinga-02	5.09	4	ALP (temp)
371	0077	Coalinga-02	5.09	46T05	Anticline Ridge - Palmer Ave
372	0077	Coalinga-02	5.09	1607	Anticline Ridge Free-Field
373	0077	Coalinga-02	5.09	1607	Anticline Ridge Pad
374	0077	Coalinga-02	5.09	1606	Burnett Construction
375	0077	Coalinga-02	5.09	46617	Coalinga-14th & Elm (Old CHP)
376	0077	Coalinga-02	5.09	46T07	Harris Ranch - Hdqtrs (temp)
377	0077	Coalinga-02	5.09	5	LLN (temp)
379	0077	Coalinga-02	5.09	1604	Oil City
380	0077	Coalinga-02	5.09	46T06	Oil Fields - Skunk Hollow
381	0077	Coalinga-02	5.09	1608	Oil Fields Fire Station
382	0077	Coalinga-02	5.09	1609	Palmer Ave
383	0077	Coalinga-02	5.09	1162	Pleasant Valley P.P. - yard
384	0077	Coalinga-02	5.09	7	SGT (temp)
385	0077	Coalinga-02	5.09	8	SUB (temp)
386	0077	Coalinga-02	5.09	1605	Skunk Hollow
387	0077	Coalinga-02	5.09	47T03	Sulphur Baths (temp)
388	0077	Coalinga-02	5.09	9	TRA (temp)
389	0077	Coalinga-02	5.09	10	VEW (temp)
390	0077	Coalinga-02	5.09	11	YUB (temp)
391	0078	Coalinga-03	5.38	1606	Burnett Construction
392	0078	Coalinga-03	5.38	46617	Coalinga-14th & Elm (Old CHP)
393	0078	Coalinga-03	5.38	47T03	Sulphur Baths (temp)
394	0079	Coalinga-04	5.18	1607	Anticline Ridge Free-Field
395	0079	Coalinga-04	5.18	1607	Anticline Ridge Pad
396	0079	Coalinga-04	5.18	1606	Burnett Construction
397	0079	Coalinga-04	5.18	46617	Coalinga-14th & Elm (Old CHP)
398	0079	Coalinga-04	5.18	1604	Oil City
399	0079	Coalinga-04	5.18	1608	Oil Fields Fire Station - FF
400	0079	Coalinga-04	5.18	1608	Oil Fields Fire Station - Pad
401	0079	Coalinga-04	5.18	1609	Palmer Ave
402	0079	Coalinga-04	5.18	1605	Skunk Hollow
403	0079	Coalinga-04	5.18	47T03	Sulphur Baths (temp)
404	0079	Coalinga-04	5.18	1651	Transmitter Hill
405	0080	Coalinga-05	5.77	1606	Burnett Construction
406	0080	Coalinga-05	5.77	46617	Coalinga-14th & Elm (Old CHP)
407	0080	Coalinga-05	5.77	1604	Oil City
408	0080	Coalinga-05	5.77	1608	Oil Fields Fire Station - FF
409	0080	Coalinga-05	5.77	1608	Oil Fields Fire Station - Pad
410	0080	Coalinga-05	5.77	1609	Palmer Ave
411	0080	Coalinga-05	5.77	1162	Pleasant Valley P.P. - FF
412	0080	Coalinga-05	5.77	1162	Pleasant Valley P.P. - yard
413	0080	Coalinga-05	5.77	1605	Skunk Hollow
414	0080	Coalinga-05	5.77	47T03	Sulphur Baths (temp)
415	0080	Coalinga-05	5.77	1651	Transmitter Hill
416	0081	Coalinga-06	4.89	46617	Coalinga-14th & Elm (Old CHP)
417	0081	Coalinga-06	4.89	47T03	Sulphur Baths (temp)
418	0082	Coalinga-07	5.21	46617	Coalinga-14th & Elm (Old CHP)
419	0082	Coalinga-07	5.21	47T03	Sulphur Baths (temp)
420	0083	Ierissos, Greece	6.7	99999	Ierissos
423	0085	Coalinga-08	5.23	46617	Coalinga-14th & Elm (Old CHP)
424	0085	Coalinga-08	5.23	47T03	Sulphur Baths (temp)
442	0088	Borah Peak, ID-02	5.1	99999	BOR

RSN	EQID	Earthquake	M	Station No.	Station
443	0088	Borah Peak, ID-02	5.1	99999	CEM
444	0088	Borah Peak, ID-02	5.1	99999	HAU
445	0089	New Zealand-01	5.5	081A	Turangi Telephone Exchange
446	0090	Morgan Hill	6.19	58376	APEEL 1E - Hayward
447	0090	Morgan Hill	6.19	57066	Agnews State Hospital
448	0090	Morgan Hill	6.19	1652	Anderson Dam (Downstream)
449	0090	Morgan Hill	6.19	47125	Capitola
450	0090	Morgan Hill	6.19	57007	Corralitos
451	0090	Morgan Hill	6.19	57217	Coyote Lake Dam (SW Abut)
452	0090	Morgan Hill	6.19	58375	Foster City - APEEL 1
453	0090	Morgan Hill	6.19	57064	Fremont - Mission San Jose
454	0090	Morgan Hill	6.19	47006	Gilroy - Gavilan Coll.
455	0090	Morgan Hill	6.19	47379	Gilroy Array #1
456	0090	Morgan Hill	6.19	47380	Gilroy Array #2
457	0090	Morgan Hill	6.19	47381	Gilroy Array #3
458	0090	Morgan Hill	6.19	57382	Gilroy Array #4
459	0090	Morgan Hill	6.19	57383	Gilroy Array #6
460	0090	Morgan Hill	6.19	57425	Gilroy Array #7
461	0090	Morgan Hill	6.19	57191	Halls Valley
463	0090	Morgan Hill	6.19	1656	Hollister Diff Array #1
464	0090	Morgan Hill	6.19	1656	Hollister Diff Array #3
465	0090	Morgan Hill	6.19	1656	Hollister Diff Array #4
466	0090	Morgan Hill	6.19	1656	Hollister Diff Array #5
467	0090	Morgan Hill	6.19	1656	Hollister Diff. Array
468	0090	Morgan Hill	6.19	56012	Los Banos
470	0090	Morgan Hill	6.19	47126	San Juan Bautista, 24 Polk St
471	0090	Morgan Hill	6.19	1655	San Justo Dam (L Abut)
472	0090	Morgan Hill	6.19	1655	San Justo Dam (R Abut)
476	0090	Morgan Hill	6.19	58135	UCSC Lick Observatory
477	0091	Lazio-Abruzzo, Italy	5.8	99999	Atina
478	0091	Lazio-Abruzzo, Italy	5.8	99999	Garigliano-Centrale Nucleare
479	0091	Lazio-Abruzzo, Italy	5.8	99999	Isernia-Sant'Agapito
480	0091	Lazio-Abruzzo, Italy	5.8	99999	Pontecorvo
481	0091	Lazio-Abruzzo, Italy	5.8	99999	Roccamonfina
485	0094	Bishop (Rnd Val)	5.82	1661	McGee Creek - Surface
494	0096	Drama, Greece	5.2	99999	Kavala
495	0097	Nahanni, Canada	6.76	6097	Site 1
496	0097	Nahanni, Canada	6.76	6098	Site 2
497	0097	Nahanni, Canada	6.76	6099	Site 3
498	0098	Hollister-04	5.45	1656	Hollister Diff Array #1
499	0098	Hollister-04	5.45	1656	Hollister Diff Array #3
501	0098	Hollister-04	5.45	47189	SAGO South - Surface
502	0099	Mt. Lewis	5.6	57191	Halls Valley
511	0101	N. Palm Springs	6.06	5224	Anza - Red Mountain
512	0101	N. Palm Springs	6.06	5231	Anza - Tule Canyon
513	0101	N. Palm Springs	6.06	5160	Anza Fire Station
514	0101	N. Palm Springs	6.06	5073	Cabazon
515	0101	N. Palm Springs	6.06	754	Colton Interchange - Vault
516	0101	N. Palm Springs	6.06	5157	Cranston Forest Station
517	0101	N. Palm Springs	6.06	12149	Desert Hot Springs
518	0101	N. Palm Springs	6.06	5069	Fun Valley
519	0101	N. Palm Springs	6.06	12331	Hemet Fire Station
521	0101	N. Palm Springs	6.06	5043	Hurkey Creek Park
522	0101	N. Palm Springs	6.06	5067	Indio
523	0101	N. Palm Springs	6.06	12026	Indio - Coachella Canal

RSN	EQID	Earthquake	M	Station No.	Station
524	0101	N. Palm Springs	6.06	22170	Joshua Tree
525	0101	N. Palm Springs	6.06	707	Lake Mathews Dike Toe
526	0101	N. Palm Springs	6.06	22T13	Landers Fire Station
527	0101	N. Palm Springs	6.06	5071	Morongo Valley
528	0101	N. Palm Springs	6.06	13198	Murrieta Hot Springs
529	0101	N. Palm Springs	6.06	5070	North Palm Springs
530	0101	N. Palm Springs	6.06	12025	Palm Springs Airport
531	0101	N. Palm Springs	6.06	12168	Puerta La Cruz
533	0101	N. Palm Springs	6.06	13123	Riverside Airport
534	0101	N. Palm Springs	6.06	12204	San Jacinto - Soboba
535	0101	N. Palm Springs	6.06	12202	San Jacinto - Valley Cemetery
536	0101	N. Palm Springs	6.06	5230	Santa Rosa Mountain
537	0101	N. Palm Springs	6.06	12206	Silent Valley - Poppet Flat
538	0101	N. Palm Springs	6.06	5038	Sunnymead
539	0101	N. Palm Springs	6.06	13172	Temecula - 6th & Mercedes
540	0101	N. Palm Springs	6.06	5072	Whitewater Trout Farm
541	0101	N. Palm Springs	6.06	13199	Winchester Bergman Ran
542	0101	N. Palm Springs	6.06	13201	Winchester Page Bros R
543	0102	Chalfant Valley-01	5.77	54100	Benton
544	0102	Chalfant Valley-01	5.77	54171	Bishop - LADWP South St
545	0102	Chalfant Valley-01	5.77	54424	Bishop - Paradise Lodge
546	0102	Chalfant Valley-01	5.77	54T03	Lake Crowley - Shehorn Res.
547	0102	Chalfant Valley-01	5.77	54428	Zack Brothers Ranch
548	0103	Chalfant Valley-02	6.19	54100	Benton
549	0103	Chalfant Valley-02	6.19	54171	Bishop - LADWP South St
550	0103	Chalfant Valley-02	6.19	54424	Bishop - Paradise Lodge
551	0103	Chalfant Valley-02	6.19	54099	Convict Creek
552	0103	Chalfant Valley-02	6.19	54T03	Lake Crowley - Shehorn Res.
553	0103	Chalfant Valley-02	6.19	54214	Long Valley Dam (Downst)
554	0103	Chalfant Valley-02	6.19	54214	Long Valley Dam (L Abut)
555	0103	Chalfant Valley-02	6.19	54T04	Mammoth Lakes Sheriff Subst.
556	0103	Chalfant Valley-02	6.19	1661	McGee Creek - Surface
557	0103	Chalfant Valley-02	6.19	54101	Tinemaha Res. Free Field
558	0103	Chalfant Valley-02	6.19	54428	Zack Brothers Ranch
559	0104	Chalfant Valley-03	5.65	54171	Bishop - LADWP South St
560	0104	Chalfant Valley-03	5.65	54424	Bishop - Paradise Lodge
561	0104	Chalfant Valley-03	5.65	54428	Zack Brothers Ranch
562	0105	Chalfant Valley-04	5.44	54171	Bishop - LADWP South St
563	0105	Chalfant Valley-04	5.44	54428	Zack Brothers Ranch
568	0108	San Salvador	5.8	99999	Geotech Investig Center
569	0108	San Salvador	5.8	99999	National Geografical Inst
585	0110	Baja California	5.5	6604	Cerro Prieto
586	0111	New Zealand-02	6.6	113A	Maraenui Primary School
587	0111	New Zealand-02	6.6	99999	Matahina Dam
588	0112	New Zealand-03	5.8	99999	Matahina Dam
589	0113	Whittier Narrows-01	5.99	24461	Alhambra - Fremont School
590	0113	Whittier Narrows-01	5.99	24402	Altadena - Eaton Canyon
591	0113	Whittier Narrows-01	5.99	90088	Anaheim - W Ball Rd
592	0113	Whittier Narrows-01	5.99	90093	Arcadia - Campus Dr
593	0113	Whittier Narrows-01	5.99	24087	Arleta - Nordhoff Fire Sta
594	0113	Whittier Narrows-01	5.99	90069	Baldwin Park - N Holly
595	0113	Whittier Narrows-01	5.99	90094	Bell Gardens - Jaboneria
596	0113	Whittier Narrows-01	5.99	90014	Beverly Hills - 12520 Mulhol
597	0113	Whittier Narrows-01	5.99	90013	Beverly Hills - 14145 Mulhol
598	0113	Whittier Narrows-01	5.99	90061	Big Tujunga, Angeles Nat F

RSN	EQID	Earthquake	M	Station No.	Station
600	0113	Whittier Narrows-01	5.99	951	Brea Dam (Downstream)
601	0113	Whittier Narrows-01	5.99	951	Brea Dam (L Abut)
602	0113	Whittier Narrows-01	5.99	90012	Burbank - N Buena Vista
603	0113	Whittier Narrows-01	5.99	90052	Calabasas - N Las Virg
604	0113	Whittier Narrows-01	5.99	90053	Canoga Park - Topanga Can
605	0113	Whittier Narrows-01	5.99	90057	Canyon Country - W Lost Cany
606	0113	Whittier Narrows-01	5.99	108	Carbon Canyon Dam
607	0113	Whittier Narrows-01	5.99	90040	Carson - Catskill Ave
608	0113	Whittier Narrows-01	5.99	90081	Carson - Water St
609	0113	Whittier Narrows-01	5.99	24277	Castaic - Hasley Canyon
611	0113	Whittier Narrows-01	5.99	90078	Compton - Castlegate St
612	0113	Whittier Narrows-01	5.99	90068	Covina - S Grand Ave
613	0113	Whittier Narrows-01	5.99	90070	Covina - W Badillo
614	0113	Whittier Narrows-01	5.99	90079	Downey - Birchdale
615	0113	Whittier Narrows-01	5.99	14368	Downey - Co Maint Bldg
616	0113	Whittier Narrows-01	5.99	90066	El Monte - Fairview Av
617	0113	Whittier Narrows-01	5.99	13122	Featherly Park - Maint
618	0113	Whittier Narrows-01	5.99	90002	Fountain Valley - Euclid
619	0113	Whittier Narrows-01	5.99	709	Garvey Res. - Control Bldg
620	0113	Whittier Narrows-01	5.99	90063	Glendale - Las Palmas
621	0113	Whittier Narrows-01	5.99	90065	Glendora - N Oakbank
622	0113	Whittier Narrows-01	5.99	90073	Hacienda Heights - Colima
624	0113	Whittier Narrows-01	5.99	13197	Huntington Beach - Lake St
625	0113	Whittier Narrows-01	5.99	14196	Inglewood - Union Oil
626	0113	Whittier Narrows-01	5.99	14403	LA - 116th St School
627	0113	Whittier Narrows-01	5.99	24157	LA - Baldwin Hills
628	0113	Whittier Narrows-01	5.99	90054	LA - Centinela St
629	0113	Whittier Narrows-01	5.99	24389	LA - Century City CC North
630	0113	Whittier Narrows-01	5.99	24390	LA - Century City CC South
631	0113	Whittier Narrows-01	5.99	90015	LA - Chalon Rd
632	0113	Whittier Narrows-01	5.99	90033	LA - Cypress Ave
634	0113	Whittier Narrows-01	5.99	90034	LA - Fletcher Dr
635	0113	Whittier Narrows-01	5.99	24303	LA - Hollywood Stor FF
636	0113	Whittier Narrows-01	5.99	90016	LA - N Faring Rd
637	0113	Whittier Narrows-01	5.99	90032	LA - N Figueroa St
638	0113	Whittier Narrows-01	5.99	90021	LA - N Westmoreland
639	0113	Whittier Narrows-01	5.99	24400	LA - Obregon Park
640	0113	Whittier Narrows-01	5.99	90022	LA - S Grand Ave
641	0113	Whittier Narrows-01	5.99	90091	LA - Saturn St
642	0113	Whittier Narrows-01	5.99	90023	LA - W 70th St
643	0113	Whittier Narrows-01	5.99	90017	LA - Wonderland Ave
644	0113	Whittier Narrows-01	5.99	14395	LB - Harbor Admin FF
645	0113	Whittier Narrows-01	5.99	90080	LB - Orange Ave
646	0113	Whittier Narrows-01	5.99	14242	LB - Rancho Los Cerritos
647	0113	Whittier Narrows-01	5.99	14241	LB - Recreation Park
648	0113	Whittier Narrows-01	5.99	90060	La Crescenta - New York
649	0113	Whittier Narrows-01	5.99	90074	La Habra - Briarcliff
650	0113	Whittier Narrows-01	5.99	90072	La Puente - Rimgrove Av
652	0113	Whittier Narrows-01	5.99	90084	Lakewood - Del Amo Blvd
653	0113	Whittier Narrows-01	5.99	24526	Lancaster - Med Off FF
654	0113	Whittier Narrows-01	5.99	90045	Lawndale - Osage Ave
655	0113	Whittier Narrows-01	5.99	24055	Leona Valley #5 - Ritter
656	0113	Whittier Narrows-01	5.99	24309	Leona Valley #6
657	0113	Whittier Narrows-01	5.99	90050	Malibu - Las Flores Canyon
658	0113	Whittier Narrows-01	5.99	24396	Malibu - Point Dume Sch

RSN	EQID	Earthquake	M	Station No.	Station
659	0113	Whittier Narrows-01	5.99	90051	Malibu - W Pacific Cst Hwy
661	0113	Whittier Narrows-01	5.99	90062	Mill Creek, Angeles Nat For
663	0113	Whittier Narrows-01	5.99	24399	Mt Wilson - CIT Seis Sta
664	0113	Whittier Narrows-01	5.99	90009	N Hollywood - Coldwater Can
665	0113	Whittier Narrows-01	5.99	24279	Newhall - Fire Sta
666	0113	Whittier Narrows-01	5.99	90056	Newhall - W Pico Canyon Rd.
667	0113	Whittier Narrows-01	5.99	90003	Northridge - 17645 Saticoy St
668	0113	Whittier Narrows-01	5.99	634	Norwalk - Imp Hwy, S Grnd
669	0113	Whittier Narrows-01	5.99	697	Orange Co. Reservoir
670	0113	Whittier Narrows-01	5.99	90049	Pacific Palisades - Sunset
671	0113	Whittier Narrows-01	5.99	24088	Pacoima Kagel Canyon
672	0113	Whittier Narrows-01	5.99	90005	Pacoima Kagel Canyon USC
673	0113	Whittier Narrows-01	5.99	90007	Panorama City - Roscoe
674	0113	Whittier Narrows-01	5.99	80046	Pasadena - Brown Gym
677	0113	Whittier Narrows-01	5.99	80047	Pasadena - CIT Calif Blvd
678	0113	Whittier Narrows-01	5.99	80051	Pasadena - CIT Indust. Rel
681	0113	Whittier Narrows-01	5.99	80048	Pasadena - CIT Lura St
683	0113	Whittier Narrows-01	5.99	90095	Pasadena - Old House Rd
684	0113	Whittier Narrows-01	5.99	90047	Playa Del Rey - Saran
685	0113	Whittier Narrows-01	5.99	23525	Pomona - 4th & Locust FF
686	0113	Whittier Narrows-01	5.99	23497	Rancho Cucamonga - FF
687	0113	Whittier Narrows-01	5.99	90044	Rancho Palos Verdes - Luconia
688	0113	Whittier Narrows-01	5.99	13123	Riverside Airport
690	0113	Whittier Narrows-01	5.99	90019	San Gabriel - E Grand Ave
691	0113	Whittier Narrows-01	5.99	24401	San Marino - SW Academy
692	0113	Whittier Narrows-01	5.99	90077	Santa Fe Springs - E.Joslin
693	0113	Whittier Narrows-01	5.99	90048	Santa Monica - Second St
694	0113	Whittier Narrows-01	5.99	90010	Studio City - Coldwater Can
695	0113	Whittier Narrows-01	5.99	90006	Sun Valley - Roscoe Blvd
696	0113	Whittier Narrows-01	5.99	90008	Sun Valley - Sunland
697	0113	Whittier Narrows-01	5.99	90058	Sunland - Mt Gleason Ave
698	0113	Whittier Narrows-01	5.99	24514	Sylmar - Olive View Med FF
699	0113	Whittier Narrows-01	5.99	90001	Sylmar - Sayre St
700	0113	Whittier Narrows-01	5.99	24436	Tarzana - Cedar Hill
701	0113	Whittier Narrows-01	5.99	90082	Terminal Island - S Seaside
702	0113	Whittier Narrows-01	5.99	90038	Torrance - W 226th St
703	0113	Whittier Narrows-01	5.99	24047	Vasquez Rocks Park
704	0113	Whittier Narrows-01	5.99	90090	Villa Park - Serrano Ave
705	0113	Whittier Narrows-01	5.99	90071	West Covina - S Orange Ave
706	0113	Whittier Narrows-01	5.99	289	Whittier Narrows Dam upstream
707	0114	Whittier Narrows-02	5.27	24461	Alhambra - Fremont School
708	0114	Whittier Narrows-02	5.27	24402	Altadena - Eaton Canyon
709	0114	Whittier Narrows-02	5.27	14368	Downey - Co Maint Bldg
710	0114	Whittier Narrows-02	5.27	14196	Inglewood - Union Oil
711	0114	Whittier Narrows-02	5.27	14403	LA - 116th St School
712	0114	Whittier Narrows-02	5.27	24157	LA - Baldwin Hills
713	0114	Whittier Narrows-02	5.27	24303	LA - Hollywood Stor FF
714	0114	Whittier Narrows-02	5.27	24400	LA - Obregon Park
715	0114	Whittier Narrows-02	5.27	24399	Mt Wilson - CIT Seis Sta
716	0114	Whittier Narrows-02	5.27	24401	San Marino - SW Academy
717	0114	Whittier Narrows-02	5.27	24436	Tarzana - Cedar Hill
718	0115	Superstition Hills-01	6.22	5210	Wildlife Liquef. Array
719	0116	Superstition Hills-02	6.54	5060	Brawley Airport
720	0116	Superstition Hills-02	6.54	5061	Calipatria Fire Station
721	0116	Superstition Hills-02	6.54	1335	El Centro Imp. Co. Cent

RSN	EQID	Earthquake	M	Station No.	Station
722	0116	Superstition Hills-02	6.54	9401	Kornbloom Road (temp)
723	0116	Superstition Hills-02	6.54	5051	Parachute Test Site
724	0116	Superstition Hills-02	6.54	5052	Plaster City
725	0116	Superstition Hills-02	6.54	9400	Poe Road (temp)
726	0116	Superstition Hills-02	6.54	5062	Salton Sea Wildlife Refuge
727	0116	Superstition Hills-02	6.54	286	Superstition Mtn Camera
728	0116	Superstition Hills-02	6.54	11369	Westmorland Fire Sta
729	0116	Superstition Hills-02	6.54	5210	Wildlife Liquef. Array
730	0117	Spitak, Armenia	6.77	12	Gukasian
731	0118	Loma Prieta	6.93	58373	APEEL 10 - Skyline
732	0118	Loma Prieta	6.93	1002	APEEL 2 - Redwood City
733	0118	Loma Prieta	6.93	58393	APEEL 2E Hayward Muir Sch
734	0118	Loma Prieta	6.93	58219	APEEL 3E Hayward CSUH
735	0118	Loma Prieta	6.93	58378	APEEL 7 - Pulgas
736	0118	Loma Prieta	6.93	1161	APEEL 9 - Crystal Springs Res
737	0118	Loma Prieta	6.93	57066	Agnews State Hospital
739	0118	Loma Prieta	6.93	1652	Anderson Dam (Downstream)
740	0118	Loma Prieta	6.93	1652	Anderson Dam (L Abut)
741	0118	Loma Prieta	6.93	13	BRAN
742	0118	Loma Prieta	6.93	1210	Bear Valley #1, Fire Station
743	0118	Loma Prieta	6.93	1479	Bear Valley #10, Webb Residence
744	0118	Loma Prieta	6.93	1481	Bear Valley #12, Williams Ranch
746	0118	Loma Prieta	6.93	1474	Bear Valley #5, Callens Ranch
747	0118	Loma Prieta	6.93	1476	Bear Valley #7, Pinnacles
751	0118	Loma Prieta	6.93	1687	Calaveras Reservoir
752	0118	Loma Prieta	6.93	47125	Capitola
753	0118	Loma Prieta	6.93	57007	Corralitos
754	0118	Loma Prieta	6.93	57504	Coyote Lake Dam (Downst)
755	0118	Loma Prieta	6.93	57217	Coyote Lake Dam (SW Abut)
756	0118	Loma Prieta	6.93	1689	Dublin - Fire Station
757	0118	Loma Prieta	6.93	58664	Dumbarton Bridge West End FF
759	0118	Loma Prieta	6.93	58375	Foster City - APEEL 1
760	0118	Loma Prieta	6.93	1515	Foster City - Menhaden Court
761	0118	Loma Prieta	6.93	1686	Fremont - Emerson Court
762	0118	Loma Prieta	6.93	57064	Fremont - Mission San Jose
763	0118	Loma Prieta	6.93	47006	Gilroy - Gavilan Coll.
764	0118	Loma Prieta	6.93	57476	Gilroy - Historic Bldg.
765	0118	Loma Prieta	6.93	47379	Gilroy Array #1
766	0118	Loma Prieta	6.93	47380	Gilroy Array #2
767	0118	Loma Prieta	6.93	47381	Gilroy Array #3
768	0118	Loma Prieta	6.93	57382	Gilroy Array #4
769	0118	Loma Prieta	6.93	57383	Gilroy Array #6
770	0118	Loma Prieta	6.93	57425	Gilroy Array #7
772	0118	Loma Prieta	6.93	57191	Halls Valley
773	0118	Loma Prieta	6.93	58498	Hayward - BART Sta
776	0118	Loma Prieta	6.93	47524	Hollister - South & Pine
778	0118	Loma Prieta	6.93	1656	Hollister Diff. Array
779	0118	Loma Prieta	6.93	16	LGPC
781	0118	Loma Prieta	6.93	58233	Lower Crystal Springs Dam dwnst
782	0118	Loma Prieta	6.93	47377	Monterey City Hall
786	0118	Loma Prieta	6.93	58264	Palo Alto - 1900 Embarc.
787	0118	Loma Prieta	6.93	1601	Palo Alto - SLAC Lab
791	0118	Loma Prieta	6.93	47189	SAGO South - Surface
792	0118	Loma Prieta	6.93	1675	SF - 1295 Shafter
799	0118	Loma Prieta	6.93	58223	SF Intern. Airport

RSN	EQID	Earthquake	M	Station No.	Station
800	0118	Loma Prieta	6.93	47179	Salinas - John & Work
801	0118	Loma Prieta	6.93	57563	San Jose - Santa Teresa Hills
802	0118	Loma Prieta	6.93	58065	Saratoga - Aloha Ave
803	0118	Loma Prieta	6.93	58235	Saratoga - W Valley Coll.
804	0118	Loma Prieta	6.93	58539	So. San Francisco, Sierra Pt.
806	0118	Loma Prieta	6.93	1695	Sunnyvale - Colton Ave.
807	0118	Loma Prieta	6.93	1688	Sunol - Forest Fire Station
809	0118	Loma Prieta	6.93	15	UCSC
810	0118	Loma Prieta	6.93	58135	UCSC Lick Observatory
811	0118	Loma Prieta	6.93	14	WAHO
812	0118	Loma Prieta	6.93	58127	Woodside
3548	0118	Loma Prieta	6.93	57180	Los Gatos - Lexington Dam
815	0119	Griva, Greece	6.1	99999	Kilkis
816	0120	Georgia, USSR	6.2	18	Ambralauri
817	0120	Georgia, USSR	6.2	21	Baz
818	0120	Georgia, USSR	6.2	19	Iri
819	0120	Georgia, USSR	6.2	20	Oni
820	0120	Georgia, USSR	6.2	22	Zem
821	0121	Erzican, Turkey	6.69	95	Erzincan
822	0122	Roermond, Netherlands	5.3	99999	GSH
825	0123	Cape Mendocino	7.01	89005	Cape Mendocino
826	0123	Cape Mendocino	7.01	89509	Eureka - Myrtle & West
827	0123	Cape Mendocino	7.01	89486	Fortuna - Fortuna Blvd
828	0123	Cape Mendocino	7.01	89156	Petrolia
829	0123	Cape Mendocino	7.01	89324	Rio Dell Overpass - FF
830	0123	Cape Mendocino	7.01	89530	Shelter Cove Airport
831	0124	New Zealand-04	5.7	930A	Edgecumbe Substation Electric
832	0125	Landers	7.28	21081	Amboy
838	0125	Landers	7.28	23559	Barstow
848	0125	Landers	7.28	23	Coolwater
850	0125	Landers	7.28	12149	Desert Hot Springs
855	0125	Landers	7.28	24577	Fort Irwin
860	0125	Landers	7.28	12331	Hemet Fire Station
862	0125	Landers	7.28	12026	Indio - Coachella Canal
864	0125	Landers	7.28	22170	Joshua Tree
879	0125	Landers	7.28	24	Lucerne
880	0125	Landers	7.28	100	Mission Creek Fault
881	0125	Landers	7.28	5071	Morongo Valley
882	0125	Landers	7.28	5070	North Palm Springs
884	0125	Landers	7.28	12025	Palm Springs Airport
891	0125	Landers	7.28	12206	Silent Valley - Poppet Flat
897	0125	Landers	7.28	22161	Twentynine Palms
900	0125	Landers	7.28	22074	Yermo Fire Station
901	0126	Big Bear-01	6.46	22561	Big Bear Lake - Civic Center
902	0126	Big Bear-01	6.46	12149	Desert Hot Springs
906	0126	Big Bear-01	6.46	12331	Hemet Fire Station
907	0126	Big Bear-01	6.46	23583	Hesperia - 4th & Palm
910	0126	Big Bear-01	6.46	22170	Joshua Tree
917	0126	Big Bear-01	6.46	23572	Mt Baldy - Elementary Sch
921	0126	Big Bear-01	6.46	12025	Palm Springs Airport
923	0126	Big Bear-01	6.46	23597	Phelan - Wilson Ranch
925	0126	Big Bear-01	6.46	23598	Rancho Cucamonga - Deer Can
926	0126	Big Bear-01	6.46	23497	Rancho Cucamonga - FF
927	0126	Big Bear-01	6.46	13123	Riverside Airport
928	0126	Big Bear-01	6.46	12636	Sage - Fire Station

RSN	EQID	Earthquake	M	Station No.	Station
931	0126	Big Bear-01	6.46	23542	San Bernardino - E & Hospitality
932	0126	Big Bear-01	6.46	12202	San Jacinto - Valley Cemetery
934	0126	Big Bear-01	6.46	12206	Silent Valley - Poppet Flat
935	0126	Big Bear-01	6.46	12630	Snow Creek
938	0126	Big Bear-01	6.46	13199	Winchester Bergman Ran
939	0126	Big Bear-01	6.46	23573	Wrightwood - Nielson Ranch
942	0127	Northridge-01	6.69	24461	Alhambra - Fremont School
943	0127	Northridge-01	6.69	25169	Anacapa Island
944	0127	Northridge-01	6.69	90088	Anaheim - W Ball Rd
945	0127	Northridge-01	6.69	24576	Anaverde Valley - City R
946	0127	Northridge-01	6.69	24310	Antelope Buttes
947	0127	Northridge-01	6.69	90099	Arcadia - Arcadia Av
948	0127	Northridge-01	6.69	90093	Arcadia - Campus Dr
949	0127	Northridge-01	6.69	24087	Arleta - Nordhoff Fire Sta
950	0127	Northridge-01	6.69	90069	Baldwin Park - N Holly
951	0127	Northridge-01	6.69	90094	Bell Gardens - Jaboneria
952	0127	Northridge-01	6.69	90014	Beverly Hills - 12520 Mulhol
953	0127	Northridge-01	6.69	90013	Beverly Hills - 14145 Mulhol
954	0127	Northridge-01	6.69	90061	Big Tujunga, Angeles Nat F
955	0127	Northridge-01	6.69	90087	Brea - S Flower Av
956	0127	Northridge-01	6.69	90086	Buena Park - La Palma
957	0127	Northridge-01	6.69	90059	Burbank - Howard Rd.
958	0127	Northridge-01	6.69	25282	Camarillo
959	0127	Northridge-01	6.69	90053	Canoga Park - Topanga Can
960	0127	Northridge-01	6.69	90057	Canyon Country - W Lost Cany
961	0127	Northridge-01	6.69	90040	Carson - Catskill Ave
962	0127	Northridge-01	6.69	90081	Carson - Water St
963	0127	Northridge-01	6.69	24278	Castaic - Old Ridge Route
964	0127	Northridge-01	6.69	90078	Compton - Castlegate St
965	0127	Northridge-01	6.69	90068	Covina - S Grand Ave
966	0127	Northridge-01	6.69	90070	Covina - W Badillo
967	0127	Northridge-01	6.69	90079	Downey - Birchdale
968	0127	Northridge-01	6.69	14368	Downey - Co Maint Bldg
969	0127	Northridge-01	6.69	90067	Duarte - Mel Canyon Rd.
970	0127	Northridge-01	6.69	90066	El Monte - Fairview Av
971	0127	Northridge-01	6.69	24575	Elizabeth Lake
973	0127	Northridge-01	6.69	90085	Garden Grove - Santa Rita
974	0127	Northridge-01	6.69	90063	Glendale - Las Palmas
975	0127	Northridge-01	6.69	90065	Glendora - N Oakbank
976	0127	Northridge-01	6.69	90073	Hacienda Heights - Colima
978	0127	Northridge-01	6.69	90018	Hollywood - Willoughby Ave
979	0127	Northridge-01	6.69	90083	Huntington Bch - Waikiki
981	0127	Northridge-01	6.69	14196	Inglewood - Union Oil
983	0127	Northridge-01	6.69	655	Jensen Filter Plant Generator
984	0127	Northridge-01	6.69	14403	LA - 116th St School
985	0127	Northridge-01	6.69	24157	LA - Baldwin Hills
986	0127	Northridge-01	6.69	638	LA - Brentwood VA Hospital
987	0127	Northridge-01	6.69	90054	LA - Centinela St
988	0127	Northridge-01	6.69	24389	LA - Century City CC North
989	0127	Northridge-01	6.69	90015	LA - Chalon Rd
990	0127	Northridge-01	6.69	24592	LA - City Terrace
991	0127	Northridge-01	6.69	90033	LA - Cypress Ave
993	0127	Northridge-01	6.69	90034	LA - Fletcher Dr
994	0127	Northridge-01	6.69	141	LA - Griffith Park Observatory
995	0127	Northridge-01	6.69	24303	LA - Hollywood Stor FF

RSN	EQID	Earthquake	M	Station No.	Station
996	0127	Northridge-01	6.69	90016	LA - N Faring Rd
997	0127	Northridge-01	6.69	90032	LA - N Figueroa St
998	0127	Northridge-01	6.69	90021	LA - N Westmoreland
999	0127	Northridge-01	6.69	24400	LA - Obregon Park
1000	0127	Northridge-01	6.69	24612	LA - Pico & Sentous
1001	0127	Northridge-01	6.69	90022	LA - S Grand Ave
1003	0127	Northridge-01	6.69	90091	LA - Saturn St
1004	0127	Northridge-01	6.69	637	LA - Sepulveda VA Hospital
1005	0127	Northridge-01	6.69	24611	LA - Temple & Hope
1006	0127	Northridge-01	6.69	24688	LA - UCLA Grounds
1007	0127	Northridge-01	6.69	24605	LA - Univ. Hospital
1008	0127	Northridge-01	6.69	90020	LA - W 15th St
1009	0127	Northridge-01	6.69	5082	LA - Wadsworth VA Hospital North
1010	0127	Northridge-01	6.69	5082	LA - Wadsworth VA Hospital South
1011	0127	Northridge-01	6.69	90017	LA - Wonderland Ave
1012	0127	Northridge-01	6.69	99999	LA 00
1013	0127	Northridge-01	6.69	0	LA Dam
1014	0127	Northridge-01	6.69	14560	LB - City Hall
1015	0127	Northridge-01	6.69	14242	LB - Rancho Los Cerritos
1016	0127	Northridge-01	6.69	90060	La Crescenta - New York
1017	0127	Northridge-01	6.69	90074	La Habra - Briarcliff
1018	0127	Northridge-01	6.69	90072	La Puente - Rimgrove Av
1019	0127	Northridge-01	6.69	24271	Lake Hughes #1
1020	0127	Northridge-01	6.69	24607	Lake Hughes #12A
1021	0127	Northridge-01	6.69	24469	Lake Hughes #4 - Camp Mend
1022	0127	Northridge-01	6.69	24523	Lake Hughes #4B - Camp Mend
1023	0127	Northridge-01	6.69	127	Lake Hughes #9
1024	0127	Northridge-01	6.69	90084	Lakewood - Del Amo Blvd
1025	0127	Northridge-01	6.69	24475	Lancaster - Fox Airfield Grnd
1026	0127	Northridge-01	6.69	90045	Lawndale - Osage Ave
1027	0127	Northridge-01	6.69	24305	Leona Valley #1
1028	0127	Northridge-01	6.69	24306	Leona Valley #2
1029	0127	Northridge-01	6.69	24307	Leona Valley #3
1030	0127	Northridge-01	6.69	24308	Leona Valley #4
1031	0127	Northridge-01	6.69	24055	Leona Valley #5 - Ritter
1032	0127	Northridge-01	6.69	24309	Leona Valley #6
1033	0127	Northridge-01	6.69	23595	Littlerock - Brainard Can
1034	0127	Northridge-01	6.69	24396	Malibu - Point Dume Sch
1035	0127	Northridge-01	6.69	90046	Manhattan Beach - Manhattan
1038	0127	Northridge-01	6.69	90011	Montebello - Bluff Rd.
1039	0127	Northridge-01	6.69	24283	Moorpark - Fire Sta
1041	0127	Northridge-01	6.69	24399	Mt Wilson - CIT Seis Sta
1042	0127	Northridge-01	6.69	90009	N Hollywood - Coldwater Can
1043	0127	Northridge-01	6.69	24586	Neenach - Sacatara Ck
1044	0127	Northridge-01	6.69	24279	Newhall - Fire Sta
1045	0127	Northridge-01	6.69	90056	Newhall - W Pico Canyon Rd.
1048	0127	Northridge-01	6.69	90003	Northridge - 17645 Saticoy St
1049	0127	Northridge-01	6.69	90049	Pacific Palisades - Sunset
1050	0127	Northridge-01	6.69	24207	Pacoima Dam (downstr)
1051	0127	Northridge-01	6.69	24207	Pacoima Dam (upper left)
1052	0127	Northridge-01	6.69	24088	Pacoima Kagel Canyon
1053	0127	Northridge-01	6.69	24521	Palmdale - Hwy 14 & Palmdale
1054	0127	Northridge-01	6.69	99999	Pardee - SCE
1055	0127	Northridge-01	6.69	90095	Pasadena - N Sierra Madre
1057	0127	Northridge-01	6.69	90047	Playa Del Rey - Saran

RSN	EQID	Earthquake	M	Station No.	Station
1058	0127	Northridge-01	6.69	25148	Point Mugu - Laguna Peak
1059	0127	Northridge-01	6.69	25281	Port Hueneme - Naval Lab.
1061	0127	Northridge-01	6.69	14404	Rancho Palos Verdes - Hawth
1062	0127	Northridge-01	6.69	90044	Rancho Palos Verdes - Luconia
1063	0127	Northridge-01	6.69	77	Rinaldi Receiving Sta
1065	0127	Northridge-01	6.69	14405	Rolling Hills Est-Rancho Vista
1066	0127	Northridge-01	6.69	24092	Rosamond - Airport
1070	0127	Northridge-01	6.69	90019	San Gabriel - E Grand Ave
1072	0127	Northridge-01	6.69	24401	San Marino - SW Academy
1073	0127	Northridge-01	6.69	14159	San Pedro - Palos Verdes
1074	0127	Northridge-01	6.69	24644	Sandberg - Bald Mtn
1076	0127	Northridge-01	6.69	90077	Santa Fe Springs - E.Joslin
1077	0127	Northridge-01	6.69	24538	Santa Monica City Hall
1078	0127	Northridge-01	6.69	5108	Santa Susana Ground
1079	0127	Northridge-01	6.69	14578	Seal Beach - Office Bldg
1080	0127	Northridge-01	6.69	90055	Simi Valley - Katherine Rd
1082	0127	Northridge-01	6.69	90006	Sun Valley - Roscoe Blvd
1083	0127	Northridge-01	6.69	90058	Sunland - Mt Gleason Ave
1084	0127	Northridge-01	6.69	74	Sylmar - Converter Sta
1085	0127	Northridge-01	6.69	75	Sylmar - Converter Sta East
1086	0127	Northridge-01	6.69	24514	Sylmar - Olive View Med FF
1087	0127	Northridge-01	6.69	24436	Tarzana - Cedar Hill A
1088	0127	Northridge-01	6.69	90082	Terminal Island - S Seaside
1089	0127	Northridge-01	6.69	5081	Topanga - Fire Sta
1091	0127	Northridge-01	6.69	24047	Vasquez Rocks Park
1092	0127	Northridge-01	6.69	25340	Ventura - Harbor & California
1094	0127	Northridge-01	6.69	90071	West Covina - S Orange Ave
1095	0127	Northridge-01	6.69	90075	Whittier - S. Alta Dr
1096	0127	Northridge-01	6.69	23590	Wrightwood - Jackson Flat
3549	0127	Northridge-01	6.69	5080	Monte Nido Fire Station
1099	0128	Double Springs	5.9	65398	Woodfords
1100	0129	Kobe, Japan	6.9	99999	Abeno
1101	0129	Kobe, Japan	6.9	99999	Amagasaki
1102	0129	Kobe, Japan	6.9	99999	Chihaya
1104	0129	Kobe, Japan	6.9	99999	Fukushima
1106	0129	Kobe, Japan	6.9	99999	KJMA
1107	0129	Kobe, Japan	6.9	99999	Kakogawa
1108	0129	Kobe, Japan	6.9	99999	Kobe University
1110	0129	Kobe, Japan	6.9	99999	Morigawachi
1111	0129	Kobe, Japan	6.9	99999	Nishi-Akashi
1113	0129	Kobe, Japan	6.9	99999	OSAJ
1114	0129	Kobe, Japan	6.9	99999	Port Island (0 m)
1115	0129	Kobe, Japan	6.9	99999	Sakai
1116	0129	Kobe, Japan	6.9	99999	Shin-Osaka
1118	0129	Kobe, Japan	6.9	99999	Tadoka
1119	0129	Kobe, Japan	6.9	99999	Takarazuka
1120	0129	Kobe, Japan	6.9	99999	Takatori
1121	0129	Kobe, Japan	6.9	99999	Yae
1126	0130	Kozani, Greece-01	6.4	99999	Kozani
1129	0131	Kozani, Greece-02	5.1	99999	Chromio Anapsiktirio
1131	0132	Kozani, Greece-03	5.3	99999	Chromio Anapsiktirio
1135	0133	Kozani, Greece-04	5.1	99999	Karpero
1139	0134	Dinar, Turkey	6.4	99999	Cardak
1141	0134	Dinar, Turkey	6.4	99999	Dinar
1147	0136	Kocaeli, Turkey	7.51	99999	Ambarli

RSN	EQID	Earthquake	M	Station No.	Station
1148	0136	Kocaeli, Turkey	7.51	99999	Arcelik
1149	0136	Kocaeli, Turkey	7.51	99999	Atakoy
1154	0136	Kocaeli, Turkey	7.51	99999	Bursa Sivil
1155	0136	Kocaeli, Turkey	7.51	99999	Bursa Tofas
1157	0136	Kocaeli, Turkey	7.51	99999	Cekmece
1158	0136	Kocaeli, Turkey	7.51	99999	Duzce
1160	0136	Kocaeli, Turkey	7.51	99999	Fatih
1162	0136	Kocaeli, Turkey	7.51	99999	Goynuk
1163	0136	Kocaeli, Turkey	7.51	99999	Hava Alani
1164	0136	Kocaeli, Turkey	7.51	99999	Istanbul
1165	0136	Kocaeli, Turkey	7.51	99999	Izmit
1166	0136	Kocaeli, Turkey	7.51	99999	Iznik
1169	0136	Kocaeli, Turkey	7.51	99999	Maslak
1170	0136	Kocaeli, Turkey	7.51	99999	Mecidiyekoy
1176	0136	Kocaeli, Turkey	7.51	99999	Yarimca
1177	0136	Kocaeli, Turkey	7.51	99999	Zeytinburnu
1180	0137	Chi-Chi, Taiwan	7.62	99999	CHY002
1181	0137	Chi-Chi, Taiwan	7.62	99999	CHY004
1182	0137	Chi-Chi, Taiwan	7.62	99999	CHY006
1183	0137	Chi-Chi, Taiwan	7.62	99999	CHY008
1184	0137	Chi-Chi, Taiwan	7.62	99999	CHY010
1185	0137	Chi-Chi, Taiwan	7.62	99999	CHY012
1186	0137	Chi-Chi, Taiwan	7.62	99999	CHY014
1187	0137	Chi-Chi, Taiwan	7.62	99999	CHY015
1188	0137	Chi-Chi, Taiwan	7.62	99999	CHY016
1189	0137	Chi-Chi, Taiwan	7.62	99999	CHY017
1190	0137	Chi-Chi, Taiwan	7.62	99999	CHY019
1191	0137	Chi-Chi, Taiwan	7.62	99999	CHY022
1193	0137	Chi-Chi, Taiwan	7.62	99999	CHY024
1194	0137	Chi-Chi, Taiwan	7.62	99999	CHY025
1195	0137	Chi-Chi, Taiwan	7.62	99999	CHY026
1196	0137	Chi-Chi, Taiwan	7.62	99999	CHY027
1197	0137	Chi-Chi, Taiwan	7.62	99999	CHY028
1198	0137	Chi-Chi, Taiwan	7.62	99999	CHY029
1199	0137	Chi-Chi, Taiwan	7.62	99999	CHY032
1200	0137	Chi-Chi, Taiwan	7.62	99999	CHY033
1201	0137	Chi-Chi, Taiwan	7.62	99999	CHY034
1202	0137	Chi-Chi, Taiwan	7.62	99999	CHY035
1203	0137	Chi-Chi, Taiwan	7.62	99999	CHY036
1204	0137	Chi-Chi, Taiwan	7.62	99999	CHY039
1205	0137	Chi-Chi, Taiwan	7.62	99999	CHY041
1206	0137	Chi-Chi, Taiwan	7.62	99999	CHY042
1207	0137	Chi-Chi, Taiwan	7.62	99999	CHY044
1208	0137	Chi-Chi, Taiwan	7.62	99999	CHY046
1209	0137	Chi-Chi, Taiwan	7.62	99999	CHY047
1210	0137	Chi-Chi, Taiwan	7.62	99999	CHY050
1211	0137	Chi-Chi, Taiwan	7.62	99999	CHY052
1212	0137	Chi-Chi, Taiwan	7.62	99999	CHY054
1213	0137	Chi-Chi, Taiwan	7.62	99999	CHY055
1214	0137	Chi-Chi, Taiwan	7.62	99999	CHY057
1215	0137	Chi-Chi, Taiwan	7.62	99999	CHY058
1217	0137	Chi-Chi, Taiwan	7.62	99999	CHY060
1218	0137	Chi-Chi, Taiwan	7.62	99999	CHY061
1227	0137	Chi-Chi, Taiwan	7.62	99999	CHY074
1228	0137	Chi-Chi, Taiwan	7.62	99999	CHY076

RSN	EQID	Earthquake	M	Station No.	Station
1230	0137	Chi-Chi, Taiwan	7.62	99999	CHY079
1231	0137	Chi-Chi, Taiwan	7.62	99999	CHY080
1232	0137	Chi-Chi, Taiwan	7.62	99999	CHY081
1233	0137	Chi-Chi, Taiwan	7.62	99999	CHY082
1234	0137	Chi-Chi, Taiwan	7.62	99999	CHY086
1235	0137	Chi-Chi, Taiwan	7.62	99999	CHY087
1236	0137	Chi-Chi, Taiwan	7.62	99999	CHY088
1237	0137	Chi-Chi, Taiwan	7.62	99999	CHY090
1238	0137	Chi-Chi, Taiwan	7.62	99999	CHY092
1239	0137	Chi-Chi, Taiwan	7.62	99999	CHY093
1240	0137	Chi-Chi, Taiwan	7.62	99999	CHY094
1242	0137	Chi-Chi, Taiwan	7.62	99999	CHY099
1243	0137	Chi-Chi, Taiwan	7.62	99999	CHY100
1244	0137	Chi-Chi, Taiwan	7.62	99999	CHY101
1245	0137	Chi-Chi, Taiwan	7.62	99999	CHY102
1246	0137	Chi-Chi, Taiwan	7.62	99999	CHY104
1247	0137	Chi-Chi, Taiwan	7.62	99999	CHY107
1248	0137	Chi-Chi, Taiwan	7.62	9999917	CHY109
1256	0137	Chi-Chi, Taiwan	7.62	99999	HWA002
1257	0137	Chi-Chi, Taiwan	7.62	99999	HWA003
1258	0137	Chi-Chi, Taiwan	7.62	99999	HWA005
1259	0137	Chi-Chi, Taiwan	7.62	99999	HWA006
1260	0137	Chi-Chi, Taiwan	7.62	99999	HWA007
1261	0137	Chi-Chi, Taiwan	7.62	99999	HWA009
1262	0137	Chi-Chi, Taiwan	7.62	99999	HWA011
1263	0137	Chi-Chi, Taiwan	7.62	99999	HWA012
1264	0137	Chi-Chi, Taiwan	7.62	99999	HWA013
1265	0137	Chi-Chi, Taiwan	7.62	99999	HWA014
1266	0137	Chi-Chi, Taiwan	7.62	99999	HWA015
1267	0137	Chi-Chi, Taiwan	7.62	99999	HWA016
1268	0137	Chi-Chi, Taiwan	7.62	99999	HWA017
1269	0137	Chi-Chi, Taiwan	7.62	99999	HWA019
1270	0137	Chi-Chi, Taiwan	7.62	99999	HWA020
1271	0137	Chi-Chi, Taiwan	7.62	99999	HWA022
1272	0137	Chi-Chi, Taiwan	7.62	99999	HWA023
1273	0137	Chi-Chi, Taiwan	7.62	99999	HWA024
1274	0137	Chi-Chi, Taiwan	7.62	99999	HWA025
1275	0137	Chi-Chi, Taiwan	7.62	99999	HWA026
1276	0137	Chi-Chi, Taiwan	7.62	99999	HWA027
1277	0137	Chi-Chi, Taiwan	7.62	99999	HWA028
1278	0137	Chi-Chi, Taiwan	7.62	99999	HWA029
1279	0137	Chi-Chi, Taiwan	7.62	99999	HWA030
1280	0137	Chi-Chi, Taiwan	7.62	99999	HWA031
1281	0137	Chi-Chi, Taiwan	7.62	99999	HWA032
1282	0137	Chi-Chi, Taiwan	7.62	99999	HWA033
1283	0137	Chi-Chi, Taiwan	7.62	99999	HWA034
1284	0137	Chi-Chi, Taiwan	7.62	99999	HWA035
1285	0137	Chi-Chi, Taiwan	7.62	99999	HWA036
1286	0137	Chi-Chi, Taiwan	7.62	99999	HWA037
1287	0137	Chi-Chi, Taiwan	7.62	99999	HWA038
1288	0137	Chi-Chi, Taiwan	7.62	99999	HWA039
1289	0137	Chi-Chi, Taiwan	7.62	99999	HWA041
1290	0137	Chi-Chi, Taiwan	7.62	99999	HWA043
1291	0137	Chi-Chi, Taiwan	7.62	99999	HWA044
1292	0137	Chi-Chi, Taiwan	7.62	99999	HWA045

RSN	EQID	Earthquake	M	Station No.	Station
1293	0137	Chi-Chi, Taiwan	7.62	99999	HWA046
1294	0137	Chi-Chi, Taiwan	7.62	99999	HWA048
1295	0137	Chi-Chi, Taiwan	7.62	99999	HWA049
1296	0137	Chi-Chi, Taiwan	7.62	99999	HWA050
1297	0137	Chi-Chi, Taiwan	7.62	99999	HWA051
1300	0137	Chi-Chi, Taiwan	7.62	99999	HWA055
1301	0137	Chi-Chi, Taiwan	7.62	99999	HWA056
1302	0137	Chi-Chi, Taiwan	7.62	99999	HWA057
1303	0137	Chi-Chi, Taiwan	7.62	99999	HWA058
1304	0137	Chi-Chi, Taiwan	7.62	99999	HWA059
1305	0137	Chi-Chi, Taiwan	7.62	99999	HWA060
1322	0137	Chi-Chi, Taiwan	7.62	99999	ILA024
1338	0137	Chi-Chi, Taiwan	7.62	99999	ILA050
1347	0137	Chi-Chi, Taiwan	7.62	99999	ILA063
1350	0137	Chi-Chi, Taiwan	7.62	99999	ILA067
1351	0137	Chi-Chi, Taiwan	7.62	99999	KAU001
1375	0137	Chi-Chi, Taiwan	7.62	99999	KAU047
1377	0137	Chi-Chi, Taiwan	7.62	99999	KAU050
1380	0137	Chi-Chi, Taiwan	7.62	99999	KAU054
1471	0137	Chi-Chi, Taiwan	7.62	99999	TCU015
1472	0137	Chi-Chi, Taiwan	7.62	99999	TCU017
1473	0137	Chi-Chi, Taiwan	7.62	99999	TCU018
1475	0137	Chi-Chi, Taiwan	7.62	99999	TCU026
1476	0137	Chi-Chi, Taiwan	7.62	99999	TCU029
1477	0137	Chi-Chi, Taiwan	7.62	99999	TCU031
1478	0137	Chi-Chi, Taiwan	7.62	99999	TCU033
1479	0137	Chi-Chi, Taiwan	7.62	99999	TCU034
1480	0137	Chi-Chi, Taiwan	7.62	99999	TCU036
1481	0137	Chi-Chi, Taiwan	7.62	99999	TCU038
1482	0137	Chi-Chi, Taiwan	7.62	99999	TCU039
1483	0137	Chi-Chi, Taiwan	7.62	99999	TCU040
1484	0137	Chi-Chi, Taiwan	7.62	99999	TCU042
1486	0137	Chi-Chi, Taiwan	7.62	99999	TCU046
1488	0137	Chi-Chi, Taiwan	7.62	99999	TCU048
1489	0137	Chi-Chi, Taiwan	7.62	99999	TCU049
1490	0137	Chi-Chi, Taiwan	7.62	99999	TCU050
1491	0137	Chi-Chi, Taiwan	7.62	99999	TCU051
1492	0137	Chi-Chi, Taiwan	7.62	99999	TCU052
1493	0137	Chi-Chi, Taiwan	7.62	99999	TCU053
1494	0137	Chi-Chi, Taiwan	7.62	99999	TCU054
1495	0137	Chi-Chi, Taiwan	7.62	99999	TCU055
1496	0137	Chi-Chi, Taiwan	7.62	99999	TCU056
1497	0137	Chi-Chi, Taiwan	7.62	99999	TCU057
1498	0137	Chi-Chi, Taiwan	7.62	99999	TCU059
1499	0137	Chi-Chi, Taiwan	7.62	99999	TCU060
1500	0137	Chi-Chi, Taiwan	7.62	99999	TCU061
1501	0137	Chi-Chi, Taiwan	7.62	99999	TCU063
1502	0137	Chi-Chi, Taiwan	7.62	99999	TCU064
1503	0137	Chi-Chi, Taiwan	7.62	99999	TCU065
1504	0137	Chi-Chi, Taiwan	7.62	99999	TCU067
1505	0137	Chi-Chi, Taiwan	7.62	99999	TCU068
1506	0137	Chi-Chi, Taiwan	7.62	99999	TCU070
1507	0137	Chi-Chi, Taiwan	7.62	99999	TCU071
1508	0137	Chi-Chi, Taiwan	7.62	99999	TCU072
1509	0137	Chi-Chi, Taiwan	7.62	99999	TCU074

RSN	EQID	Earthquake	M	Station No.	Station
1510	0137	Chi-Chi, Taiwan	7.62	99999	TCU075
1511	0137	Chi-Chi, Taiwan	7.62	99999	TCU076
1512	0137	Chi-Chi, Taiwan	7.62	99999	TCU078
1513	0137	Chi-Chi, Taiwan	7.62	99999	TCU079
1515	0137	Chi-Chi, Taiwan	7.62	99999	TCU082
1517	0137	Chi-Chi, Taiwan	7.62	99999	TCU084
1518	0137	Chi-Chi, Taiwan	7.62	99999	TCU085
1519	0137	Chi-Chi, Taiwan	7.62	99999	TCU087
1520	0137	Chi-Chi, Taiwan	7.62	99999	TCU088
1521	0137	Chi-Chi, Taiwan	7.62	99999	TCU089
1523	0137	Chi-Chi, Taiwan	7.62	99999	TCU094
1525	0137	Chi-Chi, Taiwan	7.62	99999	TCU096
1526	0137	Chi-Chi, Taiwan	7.62	99999	TCU098
1527	0137	Chi-Chi, Taiwan	7.62	99999	TCU100
1528	0137	Chi-Chi, Taiwan	7.62	99999	TCU101
1529	0137	Chi-Chi, Taiwan	7.62	99999	TCU102
1530	0137	Chi-Chi, Taiwan	7.62	99999	TCU103
1531	0137	Chi-Chi, Taiwan	7.62	99999	TCU104
1532	0137	Chi-Chi, Taiwan	7.62	99999	TCU105
1533	0137	Chi-Chi, Taiwan	7.62	99999	TCU106
1534	0137	Chi-Chi, Taiwan	7.62	99999	TCU107
1535	0137	Chi-Chi, Taiwan	7.62	99999	TCU109
1536	0137	Chi-Chi, Taiwan	7.62	99999	TCU110
1537	0137	Chi-Chi, Taiwan	7.62	99999	TCU111
1538	0137	Chi-Chi, Taiwan	7.62	99999	TCU112
1539	0137	Chi-Chi, Taiwan	7.62	99999	TCU113
1540	0137	Chi-Chi, Taiwan	7.62	99999	TCU115
1541	0137	Chi-Chi, Taiwan	7.62	99999	TCU116
1542	0137	Chi-Chi, Taiwan	7.62	99999	TCU117
1543	0137	Chi-Chi, Taiwan	7.62	99999	TCU118
1544	0137	Chi-Chi, Taiwan	7.62	99999	TCU119
1545	0137	Chi-Chi, Taiwan	7.62	99999	TCU120
1546	0137	Chi-Chi, Taiwan	7.62	99999	TCU122
1547	0137	Chi-Chi, Taiwan	7.62	99999	TCU123
1548	0137	Chi-Chi, Taiwan	7.62	99999	TCU128
1550	0137	Chi-Chi, Taiwan	7.62	99999	TCU136
1551	0137	Chi-Chi, Taiwan	7.62	99999	TCU138
1552	0137	Chi-Chi, Taiwan	7.62	99999	TCU140
1553	0137	Chi-Chi, Taiwan	7.62	99999	TCU141
1554	0137	Chi-Chi, Taiwan	7.62	99999	TCU145
1557	0137	Chi-Chi, Taiwan	7.62	99999	TTN001
1558	0137	Chi-Chi, Taiwan	7.62	99999	TTN002
1560	0137	Chi-Chi, Taiwan	7.62	99999	TTN004
1569	0137	Chi-Chi, Taiwan	7.62	99999	TTN014
1573	0137	Chi-Chi, Taiwan	7.62	99999	TTN020
1574	0137	Chi-Chi, Taiwan	7.62	99999	TTN022
1575	0137	Chi-Chi, Taiwan	7.62	99999	TTN023
1576	0137	Chi-Chi, Taiwan	7.62	99999	TTN024
1577	0137	Chi-Chi, Taiwan	7.62	99999	TTN025
1581	0137	Chi-Chi, Taiwan	7.62	99999	TTN031
1582	0137	Chi-Chi, Taiwan	7.62	99999	TTN032
1583	0137	Chi-Chi, Taiwan	7.62	99999	TTN033
1585	0137	Chi-Chi, Taiwan	7.62	99999	TTN040
1586	0137	Chi-Chi, Taiwan	7.62	99999	TTN041
1587	0137	Chi-Chi, Taiwan	7.62	99999	TTN042

RSN	EQID	Earthquake	M	Station No.	Station
1588	0137	Chi-Chi, Taiwan	7.62	99999	TTN044
1589	0137	Chi-Chi, Taiwan	7.62	99999	TTN045
1590	0137	Chi-Chi, Taiwan	7.62	99999	TTN046
1594	0137	Chi-Chi, Taiwan	7.62	99999	TTN051
1602	0138	Duzce, Turkey	7.14	99999	Bolu
1605	0138	Duzce, Turkey	7.14	99999	Duzce
1611	0138	Duzce, Turkey	7.14	1058	Lamont 1058
1612	0138	Duzce, Turkey	7.14	1059	Lamont 1059
1613	0138	Duzce, Turkey	7.14	1060	Lamont 1060
1614	0138	Duzce, Turkey	7.14	1061	Lamont 1061
1615	0138	Duzce, Turkey	7.14	1062	Lamont 1062
1616	0138	Duzce, Turkey	7.14	362	Lamont 362
1617	0138	Duzce, Turkey	7.14	375	Lamont 375
1618	0138	Duzce, Turkey	7.14	531	Lamont 531
1619	0138	Duzce, Turkey	7.14	99999	Mudurnu
1620	0138	Duzce, Turkey	7.14	99999	Sakarya
1622	0139	Stone Canyon	4.81	1210	Bear Valley #1, Fire Station
1623	0139	Stone Canyon	4.81	1211	Melendy Ranch
1624	0139	Stone Canyon	4.81	1343	Stone Canyon Geophys Obs
1626	0140	Sitka, Alaska	7.68	2714	Sitka Observatory
1627	0141	Caldiran, Turkey	7.21	37	Maku
1631	0143	Upland	5.63	23525	Pomona - 4th & Locust FF
1632	0143	Upland	5.63	23497	Rancho Cucamonga - FF
1633	0144	Manjil, Iran	7.37	99999	Abbar
1636	0144	Manjil, Iran	7.37	99999	Qazvin
1637	0144	Manjil, Iran	7.37	99999	Rudsar
1641	0145	Sierra Madre	5.61	24402	Altadena - Eaton Canyon
1642	0145	Sierra Madre	5.61	23210	Cogswell Dam - Right Abutment
1643	0145	Sierra Madre	5.61	24592	LA - City Terrace
1644	0145	Sierra Madre	5.61	24400	LA - Obregon Park
1645	0145	Sierra Madre	5.61	24399	Mt Wilson - CIT Seis Sta
1646	0145	Sierra Madre	5.61	5296	Pasadena - USGS/NSMP Office
1647	0145	Sierra Madre	5.61	24401	San Marino - SW Academy
1648	0145	Sierra Madre	5.61	24436	Tarzana - Cedar Hill A
1649	0145	Sierra Madre	5.61	24047	Vasquez Rocks Park
1650	0147	Northridge-02	6.05	24576	Anaverde Valley - City R
1651	0147	Northridge-02	6.05	24087	Arleta - Nordhoff Fire Sta
1652	0147	Northridge-02	6.05	24278	Castaic - Old Ridge Route
1653	0147	Northridge-02	6.05	14368	Downey - Co Maint Bldg
1654	0147	Northridge-02	6.05	24575	Elizabeth Lake
1655	0147	Northridge-02	6.05	14196	Inglewood - Union Oil
1656	0147	Northridge-02	6.05	14403	LA - 116th St School
1657	0147	Northridge-02	6.05	24157	LA - Baldwin Hills
1658	0147	Northridge-02	6.05	24389	LA - Century City CC North
1659	0147	Northridge-02	6.05	24592	LA - City Terrace
1660	0147	Northridge-02	6.05	24303	LA - Hollywood Stor FF
1661	0147	Northridge-02	6.05	24400	LA - Obregon Park
1662	0147	Northridge-02	6.05	24611	LA - Temple & Hope
1663	0147	Northridge-02	6.05	24605	LA - Univ. Hospital
1664	0147	Northridge-02	6.05	24607	Lake Hughes #12A
1665	0147	Northridge-02	6.05	24279	Newhall - Fire Sta
1666	0147	Northridge-02	6.05	24088	Pacoima Kagel Canyon
1667	0147	Northridge-02	6.05	24521	Palmdale - Hwy 14 & Palmdale
1668	0148	Northridge-03	5.2	24278	Castaic - Old Ridge Route
1669	0148	Northridge-03	5.2	24575	Elizabeth Lake

RSN	EQID	Earthquake	M	Station No.	Station
1670	0148	Northridge-03	5.2	24279	Newhall - Fire Sta
1671	0148	Northridge-03	5.2	24088	Pacoima Kagel Canyon
1672	0148	Northridge-03	5.2	24644	Sandberg - Bald Mtn
1673	0148	Northridge-03	5.2	24538	Santa Monica City Hall
1674	0148	Northridge-03	5.2	24436	Tarzana - Cedar Hill A
1675	0149	Northridge-04	5.93	24576	Anaverde Valley - City R
1676	0149	Northridge-04	5.93	24278	Castaic - Old Ridge Route
1677	0149	Northridge-04	5.93	24575	Elizabeth Lake
1678	0149	Northridge-04	5.93	24592	LA - City Terrace
1679	0149	Northridge-04	5.93	24611	LA - Temple & Hope
1680	0149	Northridge-04	5.93	24605	LA - Univ. Hospital
1681	0149	Northridge-04	5.93	24283	Moorpark - Fire Sta
1682	0150	Northridge-05	5.13	24576	Anaverde Valley - City R
1683	0150	Northridge-05	5.13	24278	Castaic - Old Ridge Route
1684	0150	Northridge-05	5.13	24575	Elizabeth Lake
1686	0150	Northridge-05	5.13	655	Jensen Filter Plant Generator
1687	0150	Northridge-05	5.13	24592	LA - City Terrace
1688	0150	Northridge-05	5.13	24283	Moorpark - Fire Sta
1689	0150	Northridge-05	5.13	24088	Pacoima Kagel Canyon
1690	0150	Northridge-05	5.13	24763	Sylmar - County Hospital Grounds
1692	0151	Northridge-06	5.28	24576	Anaverde Valley - City R
1693	0151	Northridge-06	5.28	24087	Arleta - Nordhoff Fire Sta
1694	0151	Northridge-06	5.28	90014	Beverly Hills - 12520 Mulhol
1695	0151	Northridge-06	5.28	90061	Big Tujunga, Angeles Nat F
1696	0151	Northridge-06	5.28	90059	Burbank - Howard Rd.
1697	0151	Northridge-06	5.28	90012	Burbank - N Buena Vista
1698	0151	Northridge-06	5.28	90052	Calabasas - N Las Virg
1699	0151	Northridge-06	5.28	24278	Castaic - Old Ridge Route
1700	0151	Northridge-06	5.28	24575	Elizabeth Lake
1701	0151	Northridge-06	5.28	90018	Hollywood - Willoughby Ave
1702	0151	Northridge-06	5.28	14196	Inglewood - Union Oil
1704	0151	Northridge-06	5.28	655	Jensen Filter Plant Generator
1705	0151	Northridge-06	5.28	14403	LA - 116th St School
1706	0151	Northridge-06	5.28	24157	LA - Baldwin Hills
1707	0151	Northridge-06	5.28	24389	LA - Century City CC North
1708	0151	Northridge-06	5.28	24592	LA - City Terrace
1709	0151	Northridge-06	5.28	141	LA - Griffith Park Observatory
1710	0151	Northridge-06	5.28	24303	LA - Hollywood Stor FF
1711	0151	Northridge-06	5.28	90016	LA - N Faring Rd
1712	0151	Northridge-06	5.28	24611	LA - Temple & Hope
1713	0151	Northridge-06	5.28	24605	LA - Univ. Hospital
1714	0151	Northridge-06	5.28	90023	LA - W 70th St
1715	0151	Northridge-06	5.28	90017	LA - Wonderland Ave
1716	0151	Northridge-06	5.28	90060	La Crescenta - New York
1717	0151	Northridge-06	5.28	24607	Lake Hughes #12A
1718	0151	Northridge-06	5.28	23595	Littlerock - Brainard Can
1719	0151	Northridge-06	5.28	24396	Malibu - Point Dume Sch
1720	0151	Northridge-06	5.28	90062	Mill Creek, Angeles Nat For
1721	0151	Northridge-06	5.28	24279	Newhall - Fire Sta
1722	0151	Northridge-06	5.28	90003	Northridge - 17645 Saticoy St
1723	0151	Northridge-06	5.28	24088	Pacoima Kagel Canyon
1724	0151	Northridge-06	5.28	24521	Palmdale - Hwy 14 & Palmdale
1725	0151	Northridge-06	5.28	90007	Panorama City - Roscoe
1726	0151	Northridge-06	5.28	5296	Pasadena - USGS/NSMP Office
1728	0151	Northridge-06	5.28	77	Rinaldi Receiving Sta

RSN	EQID	Earthquake	M	Station No.	Station
1729	0151	Northridge-06	5.28	24401	San Marino - SW Academy
1730	0151	Northridge-06	5.28	24538	Santa Monica City Hall
1731	0151	Northridge-06	5.28	14578	Seal Beach - Office Bldg
1732	0151	Northridge-06	5.28	90055	Simi Valley - Katherine Rd
1733	0151	Northridge-06	5.28	90006	Sun Valley - Roscoe Blvd
1734	0151	Northridge-06	5.28	90008	Sun Valley - Sunland
1735	0151	Northridge-06	5.28	90058	Sunland - Mt Gleason Ave
1736	0151	Northridge-06	5.28	74	Sylmar - Converter Sta
1737	0151	Northridge-06	5.28	75	Sylmar - Converter Sta East
1738	0151	Northridge-06	5.28	90001	Sylmar - Sayre St
1739	0151	Northridge-06	5.28	24436	Tarzana - Cedar Hill A
1740	0152	Little Skull Mtn,NV	5.65	99999	Station #1-Lathrop Wells
1741	0152	Little Skull Mtn,NV	5.65	99999	Station #2-NTS Control Pt. 1
1742	0152	Little Skull Mtn,NV	5.65	99999	Station #3-Beaty
1743	0152	Little Skull Mtn,NV	5.65	99999	Station #4-Pahrump 2
1744	0152	Little Skull Mtn,NV	5.65	99999	Station #5-Pahrump 1
1758	0157	San Juan Bautista	5.17	1656	Hollister Diff. Array
1762	0158	Hector Mine	7.13	21081	Amboy
1766	0158	Hector Mine	7.13	32075	Baker Fire Station
1768	0158	Hector Mine	7.13	23559	Barstow
1770	0158	Hector Mine	7.13	22791	Big Bear Lake - Fire Station
1776	0158	Hector Mine	7.13	12149	Desert Hot Springs
1783	0158	Hector Mine	7.13	24577	Fort Irwin
1785	0158	Hector Mine	7.13	5069	Fun Valley
1786	0158	Hector Mine	7.13	22T04	Heart Bar State Park
1787	0158	Hector Mine	7.13	99999	Hector
1794	0158	Hector Mine	7.13	22170	Joshua Tree
1795	0158	Hector Mine	7.13	12647	Joshua Tree N.M. - Keys View
1813	0158	Hector Mine	7.13	5071	Morongo Valley
1816	0158	Hector Mine	7.13	5295	North Palm Springs Fire Sta #36
1836	0158	Hector Mine	7.13	22161	Twentynine Palms
1838	0158	Hector Mine	7.13	5072	Whitewater Trout Farm
1845	0160	Yountville	5	1755	Alameda Fire Station #1
1846	0160	Yountville	5	1760	Benicia Fire Station #1
1849	0160	Yountville	5	1737	El Cerrito - Mira Vista Country
1851	0160	Yountville	5	1678	Golden Gate Bridge
1852	0160	Yountville	5	1590	Larkspur Ferry Terminal (FF)
1853	0160	Yountville	5	1765	Napa Fire Station #3
1854	0160	Yountville	5	1762	Novato Fire Station #1
1855	0160	Yountville	5	1751	Novato Fire Station #4
1856	0160	Yountville	5	1743	Petaluma Fire Station
1857	0160	Yountville	5	1768	Petaluma Fire Station #1
1858	0160	Yountville	5	1691	Pleasant Hill Fire Station #2
1860	0160	Yountville	5	1749	Richmond - Point Molate
1861	0160	Yountville	5	1722	Richmond Rod & Gun Club
1862	0160	Yountville	5	1735	San Francisco - 9th Circuit Crt
1863	0160	Yountville	5	1774	San Francisco - Fire Station #2
1865	0160	Yountville	5	1767	Santa Rosa Fire Station #1
1866	0160	Yountville	5	1761	Sonoma Fire Station #1
1867	0160	Yountville	5	1759	Vallejo Fire Station #1
1868	0161	Big Bear-02	4.53	23788	Colton - Hospital Complex FF
1869	0161	Big Bear-02	4.53	5341	Colton - Kaiser Medical Clinic
1870	0161	Big Bear-02	4.53	5265	Devore - Devore Water Company
1871	0161	Big Bear-02	4.53	5075	Forest Falls Post Office
1872	0161	Big Bear-02	4.53	23957	Helendale - Helendale & Vista

RSN	EQID	Earthquake	M	Station No.	Station
1873	0161	Big Bear-02	4.53	12331	Hemet Fire Station
1874	0161	Big Bear-02	4.53	23583	Hesperia - 4th & Palm
1875	0161	Big Bear-02	4.53	5161	Highland Fire Station
1876	0161	Big Bear-02	4.53	13924	Homeland - Hwy 74 & Sultanas
1879	0161	Big Bear-02	4.53	22959	Landers - Hwy 247 & Jesse
1881	0161	Big Bear-02	4.53	5409	Lytle Creek Fire Station
1882	0161	Big Bear-02	4.53	5162	Mentone Fire Station #9
1883	0161	Big Bear-02	4.53	5076	Mill Creek Ranger Station
1884	0161	Big Bear-02	4.53	13927	Moreno Valley - Alessandro&More
1885	0161	Big Bear-02	4.53	13925	Moreno Valley - Indian & Kennedy
1886	0161	Big Bear-02	4.53	5071	Morongo Valley
1887	0161	Big Bear-02	4.53	5295	North Palm Springs Fire Sta #36
1888	0161	Big Bear-02	4.53	23958	Pinon Hills - Hwy 138 & Mtn Road
1889	0161	Big Bear-02	4.53	5037	Reche Canyon - Olive Dell Ranch
1890	0161	Big Bear-02	4.53	13915	Riverside - I215 & 3rd
1891	0161	Big Bear-02	4.53	5331	San Bernardino - Del Rosa Wk Sta
1892	0161	Big Bear-02	4.53	23542	San Bernardino - E & Hospitality
1893	0161	Big Bear-02	4.53	5339	San Bernardino - Fire Sta. #10
1894	0161	Big Bear-02	4.53	5329	San Bernardino - Fire Sta. #11
1895	0161	Big Bear-02	4.53	5337	San Bernardino - Fire Sta. #4
1896	0161	Big Bear-02	4.53	5327	San Bernardino - Fire Sta. #7
1897	0161	Big Bear-02	4.53	5330	San Bernardino - Fire Sta. #9
1898	0161	Big Bear-02	4.53	5373	San Bernardino - Lincoln School
1899	0161	Big Bear-02	4.53	23898	San Bernardino - Medical Center
1900	0161	Big Bear-02	4.53	5328	San Bernardino - Mont. Mem Pk
1901	0161	Big Bear-02	4.53	23780	San Bernardino - Mtn Vw & Clstr
1902	0161	Big Bear-02	4.53	5336	San Bernardino - Serrano School
1903	0161	Big Bear-02	4.53	5300	Seven Oaks Dam Downstream Surf.
1904	0161	Big Bear-02	4.53	5300	Seven Oaks Dam Right Abt.
1905	0161	Big Bear-02	4.53	13930	Sun City - I215 & McCall Blvd
1907	0161	Big Bear-02	4.53	5072	Whitewater Trout Farm
1908	0161	Big Bear-02	4.53	5282	Wrightwood Post Office
1909	0161	Big Bear-02	4.53	22074	Yermo Fire Station
1910	0161	Big Bear-02	4.53	23920	Yucaipa Valley - Calimesa & Cnty
1912	0162	Mohawk Val, Portola	5.17	1133	Martis Creek Dam (Dwn Stream)
1913	0162	Mohawk Val, Portola	5.17	1133	Martis Creek Dam (Left Abtmnt)
1914	0162	Mohawk Val, Portola	5.17	1133	Martis Creek Dam (Right Abtmnt)
1918	0163	Anza-02	4.92	5044	Anza - Pinyon Flat
1919	0163	Anza-02	4.92	5222	Anza - Tripp Flats Training
1920	0163	Anza-02	4.92	5160	Anza Fire Station
1921	0163	Anza-02	4.92	12919	Beaumont - 6th & Maple
1923	0163	Anza-02	4.92	5220	Borrego Springs - Scripps Clinic
1924	0163	Anza-02	4.92	5073	Cabazon
1927	0163	Anza-02	4.92	12076	Coachella - 6th & Palm
1934	0163	Anza-02	4.92	5069	Fun Valley
1935	0163	Anza-02	4.92	12923	Hemet - Acacia & Stanford
1936	0163	Anza-02	4.92	13093	Hemet - Cawston & Devonshire
1937	0163	Anza-02	4.92	12331	Hemet Fire Station
1940	0163	Anza-02	4.92	13924	Homeland - Hwy 74 & Sultanas
1941	0163	Anza-02	4.92	5043	Hurkey Creek Park
1942	0163	Anza-02	4.92	12116	Idyllwild - Hwy 243 & Pine Crest
1943	0163	Anza-02	4.92	5232	Idyllwild - Keenwild Fire Sta.
1944	0163	Anza-02	4.92	5372	Idyllwild - Kenworthy Fire Sta.
1945	0163	Anza-02	4.92	12966	Indian Wells - Hwy111 & El Dorad
1946	0163	Anza-02	4.92	5294	Indio - Jackson Road

RSN	EQID	Earthquake	M	Station No.	Station
1948	0163	Anza-02	4.92	12951	La Quinta - Bermudas & Durango
1950	0163	Anza-02	4.92	5270	Mecca Fire Station
1951	0163	Anza-02	4.92	13929	Menifee Valley - Murrieta&Scott
1957	0163	Anza-02	4.92	5071	Morongo Valley
1958	0163	Anza-02	4.92	5223	Mountain Center - Pine Mtn Rnch
1960	0163	Anza-02	4.92	5295	North Palm Springs Fire Sta #36
1962	0163	Anza-02	4.92	5375	Ocotillo Wells - Veh. Rec. Area
1963	0163	Anza-02	4.92	12952	Palm Desert - Country Club & Por
1966	0163	Anza-02	4.92	12092	Radec - Sage & Cottonwood School
1967	0163	Anza-02	4.92	12953	Rancho Mirage - G Ford & B Hope
1974	0163	Anza-02	4.92	12636	Sage - Fire Station
1983	0163	Anza-02	4.92	5289	San Jacinto - MWD West Portal
1984	0163	Anza-02	4.92	12102	San Jacinto CDF Fire Station 25
1986	0163	Anza-02	4.92	13930	Sun City - I215 & McCall Blvd
1987	0163	Anza-02	4.92	13172	Temecula - 6th & Mercedes
1989	0163	Anza-02	4.92	5072	Whitewater Trout Farm
2003	0165	CA/Baja Border Area	5.31	5053	Calexico Fire Station
2005	0165	CA/Baja Border Area	5.31	464	El Centro - Meadows Union School
2006	0165	CA/Baja Border Area	5.31	412	El Centro Array #10
2007	0165	CA/Baja Border Area	5.31	5058	El Centro Array #11
2008	0165	CA/Baja Border Area	5.31	5028	El Centro Array #7
2009	0165	CA/Baja Border Area	5.31	5055	Holtville Post Office
2014	0166	Gilroy	4.9	1720	Cupertino - Sunnyvale Rod & Gun
2018	0166	Gilroy	4.9	57064	Fremont - Mission San Jose
2019	0166	Gilroy	4.9	47006	Gilroy - Gavilan Coll.
2020	0166	Gilroy	4.9	47381	Gilroy Array #3
2021	0166	Gilroy	4.9	57383	Gilroy Array #6
2024	0166	Gilroy	4.9	1797	Hollister - Airport Bldg #3
2026	0166	Gilroy	4.9	47524	Hollister - South & Pine
2027	0166	Gilroy	4.9	1697	Los Gatos - Los Altos Rod & Gun
2030	0166	Gilroy	4.9	1758	Morgan Hill - El Toro Fire Sta
2033	0166	Gilroy	4.9	47762	Salinas - County Hospital Gnds
2036	0166	Gilroy	4.9	57600	San Jose - Emory & Bellrose
2037	0166	Gilroy	4.9	57604	San Jose - S Clara Co Bldg Grnd
2038	0166	Gilroy	4.9	1742	San Jose - Weather Station
2039	0166	Gilroy	4.9	47126	San Juan Bautista, 24 Polk St
2040	0166	Gilroy	4.9	57748	Santa Clara - Hwy 237/Alviso OVP
2041	0166	Gilroy	4.9	48906	Santa Cruz - Co Office Bldg Gnds
2042	0166	Gilroy	4.9	1695	Sunnyvale - Colton Ave.
2044	0166	Gilroy	4.9	1684	Sunol - Ohlone Wilderness Reg Pk
2047	0167	Yorba Linda	4.265	13066	Anaheim - Brookhurst & Crescent
2048	0167	Yorba Linda	4.265	13068	Anaheim - Hwy 91 & Weir Cyn Rd
2049	0167	Yorba Linda	4.265	13849	Anaheim - Lakeview & Riverdale
2050	0167	Yorba Linda	4.265	13873	Brea - Central Ave Caltrans Yard
2051	0167	Yorba Linda	4.265	24941	City of Commerce - Whittier &
2052	0167	Yorba Linda	4.265	13099	Corona - 6th & Smith
2053	0167	Yorba Linda	4.265	13100	Corona - Green River & Cyn Crest
2054	0167	Yorba Linda	4.265	13878	Fullerton - CSU Fullerton Grnds
2055	0167	Yorba Linda	4.265	13880	Fullerton - Hermosa & Harbor
2056	0167	Yorba Linda	4.265	13879	Fullerton - Valencia&Brookhurst
2057	0167	Yorba Linda	4.265	13881	La Habra - La Habra&Monte Vista
2058	0167	Yorba Linda	4.265	13079	Riverside - Hwy 91 & Van Buren
2107	0169	Denali, Alaska	7.9	Carl	Carlo (temp)
2111	0169	Denali, Alaska	7.9	R109	R109 (temp)
2113	0169	Denali, Alaska	7.9	ps09	TAPS Pump Station #09

RSN	EQID	Earthquake	M	Station No.	Station
2114	0169	Denali, Alaska	7.9	ps10	TAPS Pump Station #10
2120	0170	Big Bear City	4.92	5073	Cabazon
2121	0170	Big Bear City	4.92	5341	Colton - Kaiser Medical Clinic
2122	0170	Big Bear City	4.92	5265	Devore - Devore Water Company
2123	0170	Big Bear City	4.92	5075	Forest Falls Post Office
2124	0170	Big Bear City	4.92	5161	Highland Fire Station
2129	0170	Big Bear City	4.92	5162	Mentone Fire Station #9
2130	0170	Big Bear City	4.92	5076	Mill Creek Ranger Station
2131	0170	Big Bear City	4.92	5071	Morongo Valley
2132	0170	Big Bear City	4.92	5295	North Palm Springs Fire Sta #36
2137	0170	Big Bear City	4.92	5245	San Bernardino - Co Service Bldg - Freefield
2138	0170	Big Bear City	4.92	5331	San Bernardino - Del Rosa Wk Sta
2139	0170	Big Bear City	4.92	5339	San Bernardino - Fire Sta. #10
2140	0170	Big Bear City	4.92	5329	San Bernardino - Fire Sta. #11
2141	0170	Big Bear City	4.92	5337	San Bernardino - Fire Sta. #4
2142	0170	Big Bear City	4.92	5327	San Bernardino - Fire Sta. #7
2143	0170	Big Bear City	4.92	5330	San Bernardino - Fire Sta. #9
2144	0170	Big Bear City	4.92	5373	San Bernardino - Lincoln School
2145	0170	Big Bear City	4.92	5328	San Bernardino - Mont. Mem Pk
2146	0170	Big Bear City	4.92	5371	San Bernardino - N Verdemont Sch
2147	0170	Big Bear City	4.92	5336	San Bernardino - Serrano School
2148	0170	Big Bear City	4.92	5036	San Bernardino - Sycamore FS
2149	0170	Big Bear City	4.92	5300	Seven Oaks Dam Downstream Surf.
2150	0170	Big Bear City	4.92	5300	Seven Oaks Dam Right Abt.
2151	0170	Big Bear City	4.92	5435	Sky Valley - Fire Station #56
2154	0170	Big Bear City	4.92	5072	Whitewater Trout Farm
2159	0171	Chi-Chi, Taiwan-02	5.9	99999	CHY024
2160	0171	Chi-Chi, Taiwan-02	5.9	99999	CHY025
2161	0171	Chi-Chi, Taiwan-02	5.9	99999	CHY026
2163	0171	Chi-Chi, Taiwan-02	5.9	99999	CHY028
2164	0171	Chi-Chi, Taiwan-02	5.9	99999	CHY029
2167	0171	Chi-Chi, Taiwan-02	5.9	99999	CHY034
2168	0171	Chi-Chi, Taiwan-02	5.9	99999	CHY035
2169	0171	Chi-Chi, Taiwan-02	5.9	99999	CHY036
2171	0171	Chi-Chi, Taiwan-02	5.9	99999	CHY041
2174	0171	Chi-Chi, Taiwan-02	5.9	99999	CHY046
2175	0171	Chi-Chi, Taiwan-02	5.9	99999	CHY047
2190	0171	Chi-Chi, Taiwan-02	5.9	99999	CHY074
2195	0171	Chi-Chi, Taiwan-02	5.9	99999	CHY080
2197	0171	Chi-Chi, Taiwan-02	5.9	99999	CHY082
2201	0171	Chi-Chi, Taiwan-02	5.9	99999	CHY092
2203	0171	Chi-Chi, Taiwan-02	5.9	99999	CHY094
2206	0171	Chi-Chi, Taiwan-02	5.9	99999	CHY101
2208	0171	Chi-Chi, Taiwan-02	5.9	99999	CHY104
2215	0171	Chi-Chi, Taiwan-02	5.9	99999	HWA002
2216	0171	Chi-Chi, Taiwan-02	5.9	99999	HWA005
2217	0171	Chi-Chi, Taiwan-02	5.9	99999	HWA006
2218	0171	Chi-Chi, Taiwan-02	5.9	99999	HWA007
2219	0171	Chi-Chi, Taiwan-02	5.9	99999	HWA009
2220	0171	Chi-Chi, Taiwan-02	5.9	99999	HWA011
2221	0171	Chi-Chi, Taiwan-02	5.9	99999	HWA012
2222	0171	Chi-Chi, Taiwan-02	5.9	99999	HWA013
2223	0171	Chi-Chi, Taiwan-02	5.9	99999	HWA014
2224	0171	Chi-Chi, Taiwan-02	5.9	99999	HWA015
2225	0171	Chi-Chi, Taiwan-02	5.9	99999	HWA016

RSN	EQID	Earthquake	M	Station No.	Station
2226	0171	Chi-Chi, Taiwan-02	5.9	99999	HWA017
2227	0171	Chi-Chi, Taiwan-02	5.9	99999	HWA019
2228	0171	Chi-Chi, Taiwan-02	5.9	99999	HWA020
2230	0171	Chi-Chi, Taiwan-02	5.9	99999	HWA023
2231	0171	Chi-Chi, Taiwan-02	5.9	99999	HWA024
2232	0171	Chi-Chi, Taiwan-02	5.9	99999	HWA025
2233	0171	Chi-Chi, Taiwan-02	5.9	99999	HWA026
2234	0171	Chi-Chi, Taiwan-02	5.9	99999	HWA027
2235	0171	Chi-Chi, Taiwan-02	5.9	99999	HWA028
2236	0171	Chi-Chi, Taiwan-02	5.9	99999	HWA029
2237	0171	Chi-Chi, Taiwan-02	5.9	99999	HWA030
2238	0171	Chi-Chi, Taiwan-02	5.9	99999	HWA031
2239	0171	Chi-Chi, Taiwan-02	5.9	99999	HWA032
2240	0171	Chi-Chi, Taiwan-02	5.9	99999	HWA033
2241	0171	Chi-Chi, Taiwan-02	5.9	99999	HWA034
2242	0171	Chi-Chi, Taiwan-02	5.9	99999	HWA035
2243	0171	Chi-Chi, Taiwan-02	5.9	99999	HWA036
2244	0171	Chi-Chi, Taiwan-02	5.9	99999	HWA037
2245	0171	Chi-Chi, Taiwan-02	5.9	99999	HWA038
2246	0171	Chi-Chi, Taiwan-02	5.9	99999	HWA039
2248	0171	Chi-Chi, Taiwan-02	5.9	99999	HWA043
2249	0171	Chi-Chi, Taiwan-02	5.9	99999	HWA044
2251	0171	Chi-Chi, Taiwan-02	5.9	99999	HWA046
2252	0171	Chi-Chi, Taiwan-02	5.9	99999	HWA048
2253	0171	Chi-Chi, Taiwan-02	5.9	99999	HWA049
2254	0171	Chi-Chi, Taiwan-02	5.9	99999	HWA050
2255	0171	Chi-Chi, Taiwan-02	5.9	99999	HWA051
2256	0171	Chi-Chi, Taiwan-02	5.9	99999	HWA055
2257	0171	Chi-Chi, Taiwan-02	5.9	99999	HWA056
2258	0171	Chi-Chi, Taiwan-02	5.9	99999	HWA057
2259	0171	Chi-Chi, Taiwan-02	5.9	99999	HWA058
2260	0171	Chi-Chi, Taiwan-02	5.9	99999	HWA059
2261	0171	Chi-Chi, Taiwan-02	5.9	99999	HWA060
2299	0171	Chi-Chi, Taiwan-02	5.9	99999	ILA067
2357	0171	Chi-Chi, Taiwan-02	5.9	99999	TCU029
2362	0171	Chi-Chi, Taiwan-02	5.9	99999	TCU036
2363	0171	Chi-Chi, Taiwan-02	5.9	99999	TCU038
2364	0171	Chi-Chi, Taiwan-02	5.9	99999	TCU039
2365	0171	Chi-Chi, Taiwan-02	5.9	99999	TCU040
2366	0171	Chi-Chi, Taiwan-02	5.9	99999	TCU042
2367	0171	Chi-Chi, Taiwan-02	5.9	99999	TCU045
2368	0171	Chi-Chi, Taiwan-02	5.9	99999	TCU046
2369	0171	Chi-Chi, Taiwan-02	5.9	99999	TCU048
2370	0171	Chi-Chi, Taiwan-02	5.9	99999	TCU050
2371	0171	Chi-Chi, Taiwan-02	5.9	99999	TCU051
2372	0171	Chi-Chi, Taiwan-02	5.9	99999	TCU052
2373	0171	Chi-Chi, Taiwan-02	5.9	99999	TCU053
2374	0171	Chi-Chi, Taiwan-02	5.9	99999	TCU054
2375	0171	Chi-Chi, Taiwan-02	5.9	99999	TCU055
2376	0171	Chi-Chi, Taiwan-02	5.9	99999	TCU056
2377	0171	Chi-Chi, Taiwan-02	5.9	99999	TCU057
2378	0171	Chi-Chi, Taiwan-02	5.9	99999	TCU059
2379	0171	Chi-Chi, Taiwan-02	5.9	99999	TCU060
2380	0171	Chi-Chi, Taiwan-02	5.9	99999	TCU061
2381	0171	Chi-Chi, Taiwan-02	5.9	99999	TCU063

RSN	EQID	Earthquake	M	Station No.	Station
2382	0171	Chi-Chi, Taiwan-02	5.9	99999	TCU065
2383	0171	Chi-Chi, Taiwan-02	5.9	99999	TCU067
2384	0171	Chi-Chi, Taiwan-02	5.9	99999	TCU068
2385	0171	Chi-Chi, Taiwan-02	5.9	99999	TCU071
2386	0171	Chi-Chi, Taiwan-02	5.9	99999	TCU073
2387	0171	Chi-Chi, Taiwan-02	5.9	99999	TCU074
2388	0171	Chi-Chi, Taiwan-02	5.9	99999	TCU075
2389	0171	Chi-Chi, Taiwan-02	5.9	99999	TCU076
2390	0171	Chi-Chi, Taiwan-02	5.9	99999	TCU078
2391	0171	Chi-Chi, Taiwan-02	5.9	99999	TCU079
2393	0171	Chi-Chi, Taiwan-02	5.9	99999	TCU082
2395	0171	Chi-Chi, Taiwan-02	5.9	99999	TCU084
2397	0171	Chi-Chi, Taiwan-02	5.9	99999	TCU087
2398	0171	Chi-Chi, Taiwan-02	5.9	99999	TCU088
2399	0171	Chi-Chi, Taiwan-02	5.9	99999	TCU089
2403	0171	Chi-Chi, Taiwan-02	5.9	99999	TCU100
2404	0171	Chi-Chi, Taiwan-02	5.9	99999	TCU103
2405	0171	Chi-Chi, Taiwan-02	5.9	99999	TCU104
2406	0171	Chi-Chi, Taiwan-02	5.9	99999	TCU105
2407	0171	Chi-Chi, Taiwan-02	5.9	99999	TCU106
2408	0171	Chi-Chi, Taiwan-02	5.9	99999	TCU107
2409	0171	Chi-Chi, Taiwan-02	5.9	99999	TCU109
2410	0171	Chi-Chi, Taiwan-02	5.9	99999	TCU110
2411	0171	Chi-Chi, Taiwan-02	5.9	99999	TCU111
2412	0171	Chi-Chi, Taiwan-02	5.9	99999	TCU112
2413	0171	Chi-Chi, Taiwan-02	5.9	99999	TCU113
2414	0171	Chi-Chi, Taiwan-02	5.9	99999	TCU115
2415	0171	Chi-Chi, Taiwan-02	5.9	99999	TCU116
2416	0171	Chi-Chi, Taiwan-02	5.9	99999	TCU117
2417	0171	Chi-Chi, Taiwan-02	5.9	99999	TCU118
2418	0171	Chi-Chi, Taiwan-02	5.9	99999	TCU119
2419	0171	Chi-Chi, Taiwan-02	5.9	99999	TCU120
2420	0171	Chi-Chi, Taiwan-02	5.9	99999	TCU122
2421	0171	Chi-Chi, Taiwan-02	5.9	99999	TCU123
2422	0171	Chi-Chi, Taiwan-02	5.9	99999	TCU128
2423	0171	Chi-Chi, Taiwan-02	5.9	9999936	TCU129
2424	0171	Chi-Chi, Taiwan-02	5.9	99999	TCU131
2425	0171	Chi-Chi, Taiwan-02	5.9	99999	TCU136
2426	0171	Chi-Chi, Taiwan-02	5.9	99999	TCU137
2427	0171	Chi-Chi, Taiwan-02	5.9	99999	TCU138
2428	0171	Chi-Chi, Taiwan-02	5.9	99999	TCU140
2429	0171	Chi-Chi, Taiwan-02	5.9	99999	TCU141
2430	0171	Chi-Chi, Taiwan-02	5.9	99999	TCU145
2452	0172	Chi-Chi, Taiwan-03	6.2	99999	CHY015
2457	0172	Chi-Chi, Taiwan-03	6.2	99999	CHY024
2458	0172	Chi-Chi, Taiwan-03	6.2	99999	CHY025
2459	0172	Chi-Chi, Taiwan-03	6.2	99999	CHY026
2460	0172	Chi-Chi, Taiwan-03	6.2	99999	CHY027
2461	0172	Chi-Chi, Taiwan-03	6.2	99999	CHY028
2462	0172	Chi-Chi, Taiwan-03	6.2	99999	CHY029
2463	0172	Chi-Chi, Taiwan-03	6.2	99999	CHY032
2464	0172	Chi-Chi, Taiwan-03	6.2	99999	CHY033
2465	0172	Chi-Chi, Taiwan-03	6.2	99999	CHY034
2466	0172	Chi-Chi, Taiwan-03	6.2	99999	CHY035
2467	0172	Chi-Chi, Taiwan-03	6.2	99999	CHY036

RSN	EQID	Earthquake	M	Station No.	Station
2468	0172	Chi-Chi, Taiwan-03	6.2	99999	CHY039
2469	0172	Chi-Chi, Taiwan-03	6.2	99999	CHY041
2470	0172	Chi-Chi, Taiwan-03	6.2	99999	CHY042
2472	0172	Chi-Chi, Taiwan-03	6.2	99999	CHY046
2473	0172	Chi-Chi, Taiwan-03	6.2	99999	CHY047
2474	0172	Chi-Chi, Taiwan-03	6.2	99999	CHY050
2475	0172	Chi-Chi, Taiwan-03	6.2	99999	CHY052
2490	0172	Chi-Chi, Taiwan-03	6.2	99999	CHY074
2492	0172	Chi-Chi, Taiwan-03	6.2	99999	CHY076
2494	0172	Chi-Chi, Taiwan-03	6.2	99999	CHY079
2495	0172	Chi-Chi, Taiwan-03	6.2	99999	CHY080
2496	0172	Chi-Chi, Taiwan-03	6.2	99999	CHY081
2497	0172	Chi-Chi, Taiwan-03	6.2	99999	CHY082
2498	0172	Chi-Chi, Taiwan-03	6.2	99999	CHY086
2499	0172	Chi-Chi, Taiwan-03	6.2	99999	CHY087
2500	0172	Chi-Chi, Taiwan-03	6.2	99999	CHY088
2502	0172	Chi-Chi, Taiwan-03	6.2	99999	CHY093
2503	0172	Chi-Chi, Taiwan-03	6.2	99999	CHY094
2507	0172	Chi-Chi, Taiwan-03	6.2	99999	CHY101
2508	0172	Chi-Chi, Taiwan-03	6.2	99999	CHY102
2509	0172	Chi-Chi, Taiwan-03	6.2	99999	CHY104
2514	0172	Chi-Chi, Taiwan-03	6.2	99999	HWA002
2515	0172	Chi-Chi, Taiwan-03	6.2	99999	HWA005
2516	0172	Chi-Chi, Taiwan-03	6.2	99999	HWA006
2522	0172	Chi-Chi, Taiwan-03	6.2	99999	HWA015
2523	0172	Chi-Chi, Taiwan-03	6.2	99999	HWA016
2524	0172	Chi-Chi, Taiwan-03	6.2	99999	HWA017
2526	0172	Chi-Chi, Taiwan-03	6.2	99999	HWA020
2528	0172	Chi-Chi, Taiwan-03	6.2	99999	HWA024
2533	0172	Chi-Chi, Taiwan-03	6.2	99999	HWA030
2534	0172	Chi-Chi, Taiwan-03	6.2	99999	HWA031
2535	0172	Chi-Chi, Taiwan-03	6.2	99999	HWA032
2536	0172	Chi-Chi, Taiwan-03	6.2	99999	HWA033
2537	0172	Chi-Chi, Taiwan-03	6.2	99999	HWA034
2538	0172	Chi-Chi, Taiwan-03	6.2	99999	HWA035
2539	0172	Chi-Chi, Taiwan-03	6.2	99999	HWA036
2540	0172	Chi-Chi, Taiwan-03	6.2	99999	HWA037
2541	0172	Chi-Chi, Taiwan-03	6.2	99999	HWA038
2542	0172	Chi-Chi, Taiwan-03	6.2	99999	HWA039
2543	0172	Chi-Chi, Taiwan-03	6.2	99999	HWA041
2544	0172	Chi-Chi, Taiwan-03	6.2	99999	HWA043
2545	0172	Chi-Chi, Taiwan-03	6.2	99999	HWA044
2549	0172	Chi-Chi, Taiwan-03	6.2	99999	HWA049
2551	0172	Chi-Chi, Taiwan-03	6.2	99999	HWA051
2554	0172	Chi-Chi, Taiwan-03	6.2	99999	HWA058
2555	0172	Chi-Chi, Taiwan-03	6.2	99999	HWA059
2567	0172	Chi-Chi, Taiwan-03	6.2	99999	KAU001
2573	0172	Chi-Chi, Taiwan-03	6.2	99999	KAU050
2574	0172	Chi-Chi, Taiwan-03	6.2	99999	KAU054
2596	0172	Chi-Chi, Taiwan-03	6.2	99999	TCU036
2599	0172	Chi-Chi, Taiwan-03	6.2	99999	TCU040
2602	0172	Chi-Chi, Taiwan-03	6.2	99999	TCU046
2604	0172	Chi-Chi, Taiwan-03	6.2	99999	TCU048
2605	0172	Chi-Chi, Taiwan-03	6.2	99999	TCU049
2606	0172	Chi-Chi, Taiwan-03	6.2	99999	TCU050

RSN	EQID	Earthquake	M	Station No.	Station
2607	0172	Chi-Chi, Taiwan-03	6.2	99999	TCU051
2608	0172	Chi-Chi, Taiwan-03	6.2	99999	TCU052
2609	0172	Chi-Chi, Taiwan-03	6.2	99999	TCU053
2610	0172	Chi-Chi, Taiwan-03	6.2	99999	TCU054
2611	0172	Chi-Chi, Taiwan-03	6.2	99999	TCU056
2612	0172	Chi-Chi, Taiwan-03	6.2	99999	TCU057
2613	0172	Chi-Chi, Taiwan-03	6.2	99999	TCU059
2614	0172	Chi-Chi, Taiwan-03	6.2	99999	TCU060
2615	0172	Chi-Chi, Taiwan-03	6.2	99999	TCU061
2616	0172	Chi-Chi, Taiwan-03	6.2	99999	TCU063
2617	0172	Chi-Chi, Taiwan-03	6.2	99999	TCU064
2618	0172	Chi-Chi, Taiwan-03	6.2	99999	TCU065
2619	0172	Chi-Chi, Taiwan-03	6.2	99999	TCU067
2620	0172	Chi-Chi, Taiwan-03	6.2	99999	TCU068
2621	0172	Chi-Chi, Taiwan-03	6.2	99999	TCU070
2622	0172	Chi-Chi, Taiwan-03	6.2	99999	TCU071
2623	0172	Chi-Chi, Taiwan-03	6.2	99999	TCU072
2624	0172	Chi-Chi, Taiwan-03	6.2	99999	TCU073
2625	0172	Chi-Chi, Taiwan-03	6.2	99999	TCU074
2626	0172	Chi-Chi, Taiwan-03	6.2	99999	TCU075
2627	0172	Chi-Chi, Taiwan-03	6.2	99999	TCU076
2628	0172	Chi-Chi, Taiwan-03	6.2	99999	TCU078
2629	0172	Chi-Chi, Taiwan-03	6.2	99999	TCU079
2631	0172	Chi-Chi, Taiwan-03	6.2	99999	TCU082
2632	0172	Chi-Chi, Taiwan-03	6.2	99999	TCU084
2634	0172	Chi-Chi, Taiwan-03	6.2	99999	TCU087
2635	0172	Chi-Chi, Taiwan-03	6.2	99999	TCU089
2639	0172	Chi-Chi, Taiwan-03	6.2	99999	TCU100
2640	0172	Chi-Chi, Taiwan-03	6.2	99999	TCU102
2641	0172	Chi-Chi, Taiwan-03	6.2	99999	TCU103
2642	0172	Chi-Chi, Taiwan-03	6.2	99999	TCU104
2643	0172	Chi-Chi, Taiwan-03	6.2	99999	TCU105
2644	0172	Chi-Chi, Taiwan-03	6.2	99999	TCU106
2645	0172	Chi-Chi, Taiwan-03	6.2	99999	TCU107
2646	0172	Chi-Chi, Taiwan-03	6.2	99999	TCU109
2647	0172	Chi-Chi, Taiwan-03	6.2	99999	TCU112
2648	0172	Chi-Chi, Taiwan-03	6.2	99999	TCU113
2649	0172	Chi-Chi, Taiwan-03	6.2	99999	TCU115
2650	0172	Chi-Chi, Taiwan-03	6.2	99999	TCU116
2651	0172	Chi-Chi, Taiwan-03	6.2	99999	TCU117
2652	0172	Chi-Chi, Taiwan-03	6.2	99999	TCU118
2653	0172	Chi-Chi, Taiwan-03	6.2	99999	TCU119
2654	0172	Chi-Chi, Taiwan-03	6.2	99999	TCU120
2655	0172	Chi-Chi, Taiwan-03	6.2	99999	TCU122
2656	0172	Chi-Chi, Taiwan-03	6.2	99999	TCU123
2657	0172	Chi-Chi, Taiwan-03	6.2	99999	TCU128
2658	0172	Chi-Chi, Taiwan-03	6.2	9999936	TCU129
2660	0172	Chi-Chi, Taiwan-03	6.2	99999	TCU136
2661	0172	Chi-Chi, Taiwan-03	6.2	99999	TCU138
2662	0172	Chi-Chi, Taiwan-03	6.2	99999	TCU140
2663	0172	Chi-Chi, Taiwan-03	6.2	99999	TCU141
2664	0172	Chi-Chi, Taiwan-03	6.2	99999	TCU145
2693	0172	Chi-Chi, Taiwan-03	6.2	99999	TTN051
2694	0173	Chi-Chi, Taiwan-04	6.2	99999	CHY015
2697	0173	Chi-Chi, Taiwan-04	6.2	99999	CHY019

RSN	EQID	Earthquake	M	Station No.	Station
2698	0173	Chi-Chi, Taiwan-04	6.2	99999	CHY022
2699	0173	Chi-Chi, Taiwan-04	6.2	99999	CHY024
2700	0173	Chi-Chi, Taiwan-04	6.2	99999	CHY025
2701	0173	Chi-Chi, Taiwan-04	6.2	99999	CHY026
2702	0173	Chi-Chi, Taiwan-04	6.2	99999	CHY027
2703	0173	Chi-Chi, Taiwan-04	6.2	99999	CHY028
2704	0173	Chi-Chi, Taiwan-04	6.2	99999	CHY029
2705	0173	Chi-Chi, Taiwan-04	6.2	99999	CHY030
2706	0173	Chi-Chi, Taiwan-04	6.2	99999	CHY032
2707	0173	Chi-Chi, Taiwan-04	6.2	99999	CHY033
2708	0173	Chi-Chi, Taiwan-04	6.2	99999	CHY034
2709	0173	Chi-Chi, Taiwan-04	6.2	99999	CHY035
2710	0173	Chi-Chi, Taiwan-04	6.2	99999	CHY036
2711	0173	Chi-Chi, Taiwan-04	6.2	99999	CHY039
2712	0173	Chi-Chi, Taiwan-04	6.2	99999	CHY042
2713	0173	Chi-Chi, Taiwan-04	6.2	99999	CHY044
2714	0173	Chi-Chi, Taiwan-04	6.2	99999	CHY046
2715	0173	Chi-Chi, Taiwan-04	6.2	99999	CHY047
2716	0173	Chi-Chi, Taiwan-04	6.2	99999	CHY050
2717	0173	Chi-Chi, Taiwan-04	6.2	99999	CHY052
2718	0173	Chi-Chi, Taiwan-04	6.2	99999	CHY054
2719	0173	Chi-Chi, Taiwan-04	6.2	99999	CHY055
2721	0173	Chi-Chi, Taiwan-04	6.2	99999	CHY057
2722	0173	Chi-Chi, Taiwan-04	6.2	99999	CHY058
2725	0173	Chi-Chi, Taiwan-04	6.2	99999	CHY061
2726	0173	Chi-Chi, Taiwan-04	6.2	99999	CHY062
2734	0173	Chi-Chi, Taiwan-04	6.2	99999	CHY074
2736	0173	Chi-Chi, Taiwan-04	6.2	99999	CHY076
2738	0173	Chi-Chi, Taiwan-04	6.2	99999	CHY079
2739	0173	Chi-Chi, Taiwan-04	6.2	99999	CHY080
2740	0173	Chi-Chi, Taiwan-04	6.2	99999	CHY081
2741	0173	Chi-Chi, Taiwan-04	6.2	99999	CHY082
2742	0173	Chi-Chi, Taiwan-04	6.2	99999	CHY086
2743	0173	Chi-Chi, Taiwan-04	6.2	99999	CHY087
2744	0173	Chi-Chi, Taiwan-04	6.2	99999	CHY088
2746	0173	Chi-Chi, Taiwan-04	6.2	99999	CHY092
2747	0173	Chi-Chi, Taiwan-04	6.2	99999	CHY093
2748	0173	Chi-Chi, Taiwan-04	6.2	99999	CHY094
2751	0173	Chi-Chi, Taiwan-04	6.2	99999	CHY100
2752	0173	Chi-Chi, Taiwan-04	6.2	99999	CHY101
2753	0173	Chi-Chi, Taiwan-04	6.2	99999	CHY102
2754	0173	Chi-Chi, Taiwan-04	6.2	99999	CHY104
2755	0173	Chi-Chi, Taiwan-04	6.2	99999	CHY107
2759	0173	Chi-Chi, Taiwan-04	6.2	99999	HWA002
2760	0173	Chi-Chi, Taiwan-04	6.2	99999	HWA005
2761	0173	Chi-Chi, Taiwan-04	6.2	99999	HWA006
2771	0173	Chi-Chi, Taiwan-04	6.2	99999	HWA020
2772	0173	Chi-Chi, Taiwan-04	6.2	99999	HWA024
2778	0173	Chi-Chi, Taiwan-04	6.2	99999	HWA030
2779	0173	Chi-Chi, Taiwan-04	6.2	99999	HWA031
2780	0173	Chi-Chi, Taiwan-04	6.2	99999	HWA032
2781	0173	Chi-Chi, Taiwan-04	6.2	99999	HWA033
2782	0173	Chi-Chi, Taiwan-04	6.2	99999	HWA034
2783	0173	Chi-Chi, Taiwan-04	6.2	99999	HWA035
2784	0173	Chi-Chi, Taiwan-04	6.2	99999	HWA036

RSN	EQID	Earthquake	M	Station No.	Station
2785	0173	Chi-Chi, Taiwan-04	6.2	99999	HWA037
2786	0173	Chi-Chi, Taiwan-04	6.2	99999	HWA038
2787	0173	Chi-Chi, Taiwan-04	6.2	99999	HWA039
2788	0173	Chi-Chi, Taiwan-04	6.2	99999	HWA041
2790	0173	Chi-Chi, Taiwan-04	6.2	99999	HWA044
2797	0173	Chi-Chi, Taiwan-04	6.2	99999	HWA055
2804	0173	Chi-Chi, Taiwan-04	6.2	99999	KAU001
2820	0173	Chi-Chi, Taiwan-04	6.2	99999	KAU050
2821	0173	Chi-Chi, Taiwan-04	6.2	99999	KAU054
2854	0173	Chi-Chi, Taiwan-04	6.2	99999	TCU048
2855	0173	Chi-Chi, Taiwan-04	6.2	99999	TCU049
2856	0173	Chi-Chi, Taiwan-04	6.2	99999	TCU050
2857	0173	Chi-Chi, Taiwan-04	6.2	99999	TCU051
2858	0173	Chi-Chi, Taiwan-04	6.2	99999	TCU052
2859	0173	Chi-Chi, Taiwan-04	6.2	99999	TCU053
2860	0173	Chi-Chi, Taiwan-04	6.2	99999	TCU054
2861	0173	Chi-Chi, Taiwan-04	6.2	99999	TCU056
2862	0173	Chi-Chi, Taiwan-04	6.2	99999	TCU057
2864	0173	Chi-Chi, Taiwan-04	6.2	99999	TCU060
2865	0173	Chi-Chi, Taiwan-04	6.2	99999	TCU061
2867	0173	Chi-Chi, Taiwan-04	6.2	99999	TCU067
2868	0173	Chi-Chi, Taiwan-04	6.2	99999	TCU068
2869	0173	Chi-Chi, Taiwan-04	6.2	99999	TCU070
2870	0173	Chi-Chi, Taiwan-04	6.2	99999	TCU082
2871	0173	Chi-Chi, Taiwan-04	6.2	99999	TCU084
2873	0173	Chi-Chi, Taiwan-04	6.2	99999	TCU089
2876	0173	Chi-Chi, Taiwan-04	6.2	99999	TCU100
2877	0173	Chi-Chi, Taiwan-04	6.2	99999	TCU102
2879	0173	Chi-Chi, Taiwan-04	6.2	99999	TCU104
2880	0173	Chi-Chi, Taiwan-04	6.2	99999	TCU105
2881	0173	Chi-Chi, Taiwan-04	6.2	99999	TCU106
2882	0173	Chi-Chi, Taiwan-04	6.2	99999	TCU107
2883	0173	Chi-Chi, Taiwan-04	6.2	99999	TCU109
2884	0173	Chi-Chi, Taiwan-04	6.2	99999	TCU110
2885	0173	Chi-Chi, Taiwan-04	6.2	99999	TCU112
2886	0173	Chi-Chi, Taiwan-04	6.2	99999	TCU113
2887	0173	Chi-Chi, Taiwan-04	6.2	99999	TCU115
2888	0173	Chi-Chi, Taiwan-04	6.2	99999	TCU116
2889	0173	Chi-Chi, Taiwan-04	6.2	99999	TCU117
2890	0173	Chi-Chi, Taiwan-04	6.2	99999	TCU118
2891	0173	Chi-Chi, Taiwan-04	6.2	99999	TCU119
2892	0173	Chi-Chi, Taiwan-04	6.2	99999	TCU120
2893	0173	Chi-Chi, Taiwan-04	6.2	99999	TCU122
2894	0173	Chi-Chi, Taiwan-04	6.2	99999	TCU123
2896	0173	Chi-Chi, Taiwan-04	6.2	99999	TCU136
2897	0173	Chi-Chi, Taiwan-04	6.2	99999	TCU138
2898	0173	Chi-Chi, Taiwan-04	6.2	99999	TCU140
2899	0173	Chi-Chi, Taiwan-04	6.2	99999	TCU141
2900	0173	Chi-Chi, Taiwan-04	6.2	99999	TCU145
2901	0173	Chi-Chi, Taiwan-04	6.2	99999	TTN001
2912	0173	Chi-Chi, Taiwan-04	6.2	99999	TTN014
2915	0173	Chi-Chi, Taiwan-04	6.2	99999	TTN020
2916	0173	Chi-Chi, Taiwan-04	6.2	99999	TTN022
2917	0173	Chi-Chi, Taiwan-04	6.2	99999	TTN023
2918	0173	Chi-Chi, Taiwan-04	6.2	99999	TTN024

RSN	EQID	Earthquake	M	Station No.	Station
2919	0173	Chi-Chi, Taiwan-04	6.2	99999	TTN025
2923	0173	Chi-Chi, Taiwan-04	6.2	99999	TTN031
2924	0173	Chi-Chi, Taiwan-04	6.2	99999	TTN032
2925	0173	Chi-Chi, Taiwan-04	6.2	99999	TTN033
2927	0173	Chi-Chi, Taiwan-04	6.2	99999	TTN040
2928	0173	Chi-Chi, Taiwan-04	6.2	99999	TTN041
2929	0173	Chi-Chi, Taiwan-04	6.2	99999	TTN042
2930	0173	Chi-Chi, Taiwan-04	6.2	99999	TTN044
2931	0173	Chi-Chi, Taiwan-04	6.2	99999	TTN045
2932	0173	Chi-Chi, Taiwan-04	6.2	99999	TTN046
2935	0173	Chi-Chi, Taiwan-04	6.2	99999	TTN051
2942	0174	Chi-Chi, Taiwan-05	6.2	99999	CHY024
2943	0174	Chi-Chi, Taiwan-05	6.2	99999	CHY025
2944	0174	Chi-Chi, Taiwan-05	6.2	99999	CHY026
2946	0174	Chi-Chi, Taiwan-05	6.2	99999	CHY029
2947	0174	Chi-Chi, Taiwan-05	6.2	99999	CHY030
2950	0174	Chi-Chi, Taiwan-05	6.2	99999	CHY035
2952	0174	Chi-Chi, Taiwan-05	6.2	99999	CHY042
2980	0174	Chi-Chi, Taiwan-05	6.2	99999	CHY086
2995	0174	Chi-Chi, Taiwan-05	6.2	99999	HWA002
2996	0174	Chi-Chi, Taiwan-05	6.2	99999	HWA003
2997	0174	Chi-Chi, Taiwan-05	6.2	99999	HWA005
2998	0174	Chi-Chi, Taiwan-05	6.2	99999	HWA007
2999	0174	Chi-Chi, Taiwan-05	6.2	99999	HWA009
3000	0174	Chi-Chi, Taiwan-05	6.2	99999	HWA011
3001	0174	Chi-Chi, Taiwan-05	6.2	99999	HWA012
3002	0174	Chi-Chi, Taiwan-05	6.2	99999	HWA013
3003	0174	Chi-Chi, Taiwan-05	6.2	99999	HWA014
3004	0174	Chi-Chi, Taiwan-05	6.2	99999	HWA015
3005	0174	Chi-Chi, Taiwan-05	6.2	99999	HWA016
3006	0174	Chi-Chi, Taiwan-05	6.2	99999	HWA017
3007	0174	Chi-Chi, Taiwan-05	6.2	99999	HWA019
3008	0174	Chi-Chi, Taiwan-05	6.2	99999	HWA020
3010	0174	Chi-Chi, Taiwan-05	6.2	99999	HWA023
3011	0174	Chi-Chi, Taiwan-05	6.2	99999	HWA024
3012	0174	Chi-Chi, Taiwan-05	6.2	99999	HWA025
3013	0174	Chi-Chi, Taiwan-05	6.2	99999	HWA026
3014	0174	Chi-Chi, Taiwan-05	6.2	99999	HWA027
3015	0174	Chi-Chi, Taiwan-05	6.2	99999	HWA028
3016	0174	Chi-Chi, Taiwan-05	6.2	99999	HWA029
3017	0174	Chi-Chi, Taiwan-05	6.2	99999	HWA030
3018	0174	Chi-Chi, Taiwan-05	6.2	99999	HWA031
3019	0174	Chi-Chi, Taiwan-05	6.2	99999	HWA032
3020	0174	Chi-Chi, Taiwan-05	6.2	99999	HWA033
3021	0174	Chi-Chi, Taiwan-05	6.2	99999	HWA034
3022	0174	Chi-Chi, Taiwan-05	6.2	99999	HWA035
3023	0174	Chi-Chi, Taiwan-05	6.2	99999	HWA036
3024	0174	Chi-Chi, Taiwan-05	6.2	99999	HWA037
3025	0174	Chi-Chi, Taiwan-05	6.2	99999	HWA038
3026	0174	Chi-Chi, Taiwan-05	6.2	99999	HWA039
3027	0174	Chi-Chi, Taiwan-05	6.2	99999	HWA041
3028	0174	Chi-Chi, Taiwan-05	6.2	99999	HWA043
3029	0174	Chi-Chi, Taiwan-05	6.2	99999	HWA044
3031	0174	Chi-Chi, Taiwan-05	6.2	99999	HWA046
3032	0174	Chi-Chi, Taiwan-05	6.2	99999	HWA048

RSN	EQID	Earthquake	M	Station No.	Station
3033	0174	Chi-Chi, Taiwan-05	6.2	99999	HWA049
3034	0174	Chi-Chi, Taiwan-05	6.2	99999	HWA050
3035	0174	Chi-Chi, Taiwan-05	6.2	99999	HWA051
3036	0174	Chi-Chi, Taiwan-05	6.2	99999	HWA056
3037	0174	Chi-Chi, Taiwan-05	6.2	99999	HWA057
3038	0174	Chi-Chi, Taiwan-05	6.2	99999	HWA058
3039	0174	Chi-Chi, Taiwan-05	6.2	99999	HWA059
3040	0174	Chi-Chi, Taiwan-05	6.2	99999	HWA060
3095	0174	Chi-Chi, Taiwan-05	6.2	99999	KAU054
3171	0174	Chi-Chi, Taiwan-05	6.2	99999	TCU044
3173	0174	Chi-Chi, Taiwan-05	6.2	99999	TCU046
3174	0174	Chi-Chi, Taiwan-05	6.2	99999	TCU048
3175	0174	Chi-Chi, Taiwan-05	6.2	99999	TCU049
3176	0174	Chi-Chi, Taiwan-05	6.2	99999	TCU050
3177	0174	Chi-Chi, Taiwan-05	6.2	99999	TCU051
3178	0174	Chi-Chi, Taiwan-05	6.2	99999	TCU052
3179	0174	Chi-Chi, Taiwan-05	6.2	99999	TCU053
3180	0174	Chi-Chi, Taiwan-05	6.2	99999	TCU054
3181	0174	Chi-Chi, Taiwan-05	6.2	99999	TCU055
3182	0174	Chi-Chi, Taiwan-05	6.2	99999	TCU056
3183	0174	Chi-Chi, Taiwan-05	6.2	99999	TCU057
3184	0174	Chi-Chi, Taiwan-05	6.2	99999	TCU059
3185	0174	Chi-Chi, Taiwan-05	6.2	99999	TCU060
3186	0174	Chi-Chi, Taiwan-05	6.2	99999	TCU061
3187	0174	Chi-Chi, Taiwan-05	6.2	99999	TCU064
3188	0174	Chi-Chi, Taiwan-05	6.2	99999	TCU067
3189	0174	Chi-Chi, Taiwan-05	6.2	99999	TCU068
3190	0174	Chi-Chi, Taiwan-05	6.2	99999	TCU070
3192	0174	Chi-Chi, Taiwan-05	6.2	99999	TCU082
3195	0174	Chi-Chi, Taiwan-05	6.2	99999	TCU087
3201	0174	Chi-Chi, Taiwan-05	6.2	99999	TCU101
3202	0174	Chi-Chi, Taiwan-05	6.2	99999	TCU102
3203	0174	Chi-Chi, Taiwan-05	6.2	99999	TCU103
3204	0174	Chi-Chi, Taiwan-05	6.2	99999	TCU104
3205	0174	Chi-Chi, Taiwan-05	6.2	99999	TCU105
3206	0174	Chi-Chi, Taiwan-05	6.2	99999	TCU106
3207	0174	Chi-Chi, Taiwan-05	6.2	99999	TCU107
3208	0174	Chi-Chi, Taiwan-05	6.2	99999	TCU109
3209	0174	Chi-Chi, Taiwan-05	6.2	99999	TCU112
3210	0174	Chi-Chi, Taiwan-05	6.2	99999	TCU113
3211	0174	Chi-Chi, Taiwan-05	6.2	99999	TCU115
3212	0174	Chi-Chi, Taiwan-05	6.2	99999	TCU117
3213	0174	Chi-Chi, Taiwan-05	6.2	99999	TCU118
3215	0174	Chi-Chi, Taiwan-05	6.2	99999	TCU123
3216	0174	Chi-Chi, Taiwan-05	6.2	99999	TCU128
3217	0174	Chi-Chi, Taiwan-05	6.2	9999936	TCU129
3219	0174	Chi-Chi, Taiwan-05	6.2	99999	TCU136
3220	0174	Chi-Chi, Taiwan-05	6.2	99999	TCU138
3222	0174	Chi-Chi, Taiwan-05	6.2	99999	TCU141
3224	0174	Chi-Chi, Taiwan-05	6.2	99999	TTN001
3245	0174	Chi-Chi, Taiwan-05	6.2	99999	TTN031
3246	0174	Chi-Chi, Taiwan-05	6.2	99999	TTN032
3247	0174	Chi-Chi, Taiwan-05	6.2	99999	TTN033
3249	0174	Chi-Chi, Taiwan-05	6.2	99999	TTN040
3250	0174	Chi-Chi, Taiwan-05	6.2	99999	TTN041

RSN	EQID	Earthquake	M	Station No.	Station
3257	0174	Chi-Chi, Taiwan-05	6.2	99999	TTN051
3258	0175	Chi-Chi, Taiwan-06	6.3	99999	CHY014
3259	0175	Chi-Chi, Taiwan-06	6.3	99999	CHY015
3264	0175	Chi-Chi, Taiwan-06	6.3	99999	CHY024
3265	0175	Chi-Chi, Taiwan-06	6.3	99999	CHY025
3266	0175	Chi-Chi, Taiwan-06	6.3	99999	CHY026
3267	0175	Chi-Chi, Taiwan-06	6.3	99999	CHY027
3268	0175	Chi-Chi, Taiwan-06	6.3	99999	CHY028
3269	0175	Chi-Chi, Taiwan-06	6.3	99999	CHY029
3270	0175	Chi-Chi, Taiwan-06	6.3	99999	CHY030
3271	0175	Chi-Chi, Taiwan-06	6.3	99999	CHY032
3273	0175	Chi-Chi, Taiwan-06	6.3	99999	CHY034
3274	0175	Chi-Chi, Taiwan-06	6.3	99999	CHY035
3275	0175	Chi-Chi, Taiwan-06	6.3	99999	CHY036
3276	0175	Chi-Chi, Taiwan-06	6.3	99999	CHY037
3277	0175	Chi-Chi, Taiwan-06	6.3	99999	CHY039
3278	0175	Chi-Chi, Taiwan-06	6.3	99999	CHY041
3279	0175	Chi-Chi, Taiwan-06	6.3	99999	CHY042
3281	0175	Chi-Chi, Taiwan-06	6.3	99999	CHY046
3282	0175	Chi-Chi, Taiwan-06	6.3	99999	CHY047
3284	0175	Chi-Chi, Taiwan-06	6.3	99999	CHY052
3300	0175	Chi-Chi, Taiwan-06	6.3	99999	CHY074
3305	0175	Chi-Chi, Taiwan-06	6.3	99999	CHY081
3306	0175	Chi-Chi, Taiwan-06	6.3	99999	CHY082
3307	0175	Chi-Chi, Taiwan-06	6.3	99999	CHY086
3308	0175	Chi-Chi, Taiwan-06	6.3	99999	CHY087
3309	0175	Chi-Chi, Taiwan-06	6.3	99999	CHY088
3311	0175	Chi-Chi, Taiwan-06	6.3	99999	CHY092
3313	0175	Chi-Chi, Taiwan-06	6.3	99999	CHY094
3317	0175	Chi-Chi, Taiwan-06	6.3	99999	CHY101
3318	0175	Chi-Chi, Taiwan-06	6.3	99999	CHY102
3320	0175	Chi-Chi, Taiwan-06	6.3	99999	CHY111
3324	0175	Chi-Chi, Taiwan-06	6.3	99999	HWA002
3325	0175	Chi-Chi, Taiwan-06	6.3	99999	HWA003
3326	0175	Chi-Chi, Taiwan-06	6.3	99999	HWA007
3327	0175	Chi-Chi, Taiwan-06	6.3	99999	HWA009
3328	0175	Chi-Chi, Taiwan-06	6.3	99999	HWA011
3329	0175	Chi-Chi, Taiwan-06	6.3	99999	HWA012
3330	0175	Chi-Chi, Taiwan-06	6.3	99999	HWA014
3331	0175	Chi-Chi, Taiwan-06	6.3	99999	HWA015
3332	0175	Chi-Chi, Taiwan-06	6.3	99999	HWA016
3333	0175	Chi-Chi, Taiwan-06	6.3	99999	HWA019
3334	0175	Chi-Chi, Taiwan-06	6.3	99999	HWA020
3336	0175	Chi-Chi, Taiwan-06	6.3	99999	HWA023
3337	0175	Chi-Chi, Taiwan-06	6.3	99999	HWA024
3338	0175	Chi-Chi, Taiwan-06	6.3	99999	HWA025
3339	0175	Chi-Chi, Taiwan-06	6.3	99999	HWA026
3340	0175	Chi-Chi, Taiwan-06	6.3	99999	HWA027
3341	0175	Chi-Chi, Taiwan-06	6.3	99999	HWA028
3342	0175	Chi-Chi, Taiwan-06	6.3	99999	HWA029
3343	0175	Chi-Chi, Taiwan-06	6.3	99999	HWA030
3344	0175	Chi-Chi, Taiwan-06	6.3	99999	HWA031
3345	0175	Chi-Chi, Taiwan-06	6.3	99999	HWA033
3346	0175	Chi-Chi, Taiwan-06	6.3	99999	HWA034
3347	0175	Chi-Chi, Taiwan-06	6.3	99999	HWA035

RSN	EQID	Earthquake	M	Station No.	Station
3348	0175	Chi-Chi, Taiwan-06	6.3	99999	HWA036
3349	0175	Chi-Chi, Taiwan-06	6.3	99999	HWA037
3350	0175	Chi-Chi, Taiwan-06	6.3	99999	HWA038
3351	0175	Chi-Chi, Taiwan-06	6.3	99999	HWA041
3352	0175	Chi-Chi, Taiwan-06	6.3	99999	HWA043
3353	0175	Chi-Chi, Taiwan-06	6.3	99999	HWA044
3355	0175	Chi-Chi, Taiwan-06	6.3	99999	HWA046
3356	0175	Chi-Chi, Taiwan-06	6.3	99999	HWA050
3357	0175	Chi-Chi, Taiwan-06	6.3	99999	HWA051
3358	0175	Chi-Chi, Taiwan-06	6.3	99999	HWA055
3359	0175	Chi-Chi, Taiwan-06	6.3	99999	HWA056
3360	0175	Chi-Chi, Taiwan-06	6.3	99999	HWA057
3361	0175	Chi-Chi, Taiwan-06	6.3	99999	HWA058
3362	0175	Chi-Chi, Taiwan-06	6.3	99999	HWA059
3363	0175	Chi-Chi, Taiwan-06	6.3	99999	HWA060
3404	0175	Chi-Chi, Taiwan-06	6.3	99999	KAU054
3445	0175	Chi-Chi, Taiwan-06	6.3	99999	TCU029
3446	0175	Chi-Chi, Taiwan-06	6.3	99999	TCU031
3447	0175	Chi-Chi, Taiwan-06	6.3	99999	TCU032
3448	0175	Chi-Chi, Taiwan-06	6.3	99999	TCU036
3449	0175	Chi-Chi, Taiwan-06	6.3	99999	TCU038
3450	0175	Chi-Chi, Taiwan-06	6.3	99999	TCU039
3451	0175	Chi-Chi, Taiwan-06	6.3	99999	TCU040
3452	0175	Chi-Chi, Taiwan-06	6.3	99999	TCU042
3453	0175	Chi-Chi, Taiwan-06	6.3	99999	TCU044
3454	0175	Chi-Chi, Taiwan-06	6.3	99999	TCU046
3455	0175	Chi-Chi, Taiwan-06	6.3	99999	TCU048
3456	0175	Chi-Chi, Taiwan-06	6.3	99999	TCU049
3457	0175	Chi-Chi, Taiwan-06	6.3	99999	TCU050
3458	0175	Chi-Chi, Taiwan-06	6.3	99999	TCU051
3459	0175	Chi-Chi, Taiwan-06	6.3	99999	TCU052
3460	0175	Chi-Chi, Taiwan-06	6.3	99999	TCU053
3461	0175	Chi-Chi, Taiwan-06	6.3	99999	TCU056
3462	0175	Chi-Chi, Taiwan-06	6.3	99999	TCU057
3463	0175	Chi-Chi, Taiwan-06	6.3	99999	TCU059
3464	0175	Chi-Chi, Taiwan-06	6.3	99999	TCU060
3465	0175	Chi-Chi, Taiwan-06	6.3	99999	TCU061
3466	0175	Chi-Chi, Taiwan-06	6.3	99999	TCU064
3467	0175	Chi-Chi, Taiwan-06	6.3	99999	TCU065
3468	0175	Chi-Chi, Taiwan-06	6.3	99999	TCU067
3469	0175	Chi-Chi, Taiwan-06	6.3	99999	TCU068
3470	0175	Chi-Chi, Taiwan-06	6.3	99999	TCU072
3471	0175	Chi-Chi, Taiwan-06	6.3	99999	TCU075
3472	0175	Chi-Chi, Taiwan-06	6.3	99999	TCU076
3473	0175	Chi-Chi, Taiwan-06	6.3	99999	TCU078
3474	0175	Chi-Chi, Taiwan-06	6.3	99999	TCU079
3475	0175	Chi-Chi, Taiwan-06	6.3	99999	TCU080
3477	0175	Chi-Chi, Taiwan-06	6.3	99999	TCU082
3480	0175	Chi-Chi, Taiwan-06	6.3	99999	TCU086
3481	0175	Chi-Chi, Taiwan-06	6.3	99999	TCU087
3488	0175	Chi-Chi, Taiwan-06	6.3	99999	TCU100
3489	0175	Chi-Chi, Taiwan-06	6.3	99999	TCU102
3490	0175	Chi-Chi, Taiwan-06	6.3	99999	TCU103
3491	0175	Chi-Chi, Taiwan-06	6.3	99999	TCU104
3492	0175	Chi-Chi, Taiwan-06	6.3	99999	TCU105

RSN	EQID	Earthquake	M	Station No.	Station
3493	0175	Chi-Chi, Taiwan-06	6.3	99999	TCU107
3494	0175	Chi-Chi, Taiwan-06	6.3	99999	TCU108
3495	0175	Chi-Chi, Taiwan-06	6.3	99999	TCU109
3496	0175	Chi-Chi, Taiwan-06	6.3	99999	TCU110
3497	0175	Chi-Chi, Taiwan-06	6.3	99999	TCU112
3498	0175	Chi-Chi, Taiwan-06	6.3	99999	TCU113
3499	0175	Chi-Chi, Taiwan-06	6.3	99999	TCU115
3500	0175	Chi-Chi, Taiwan-06	6.3	99999	TCU118
3501	0175	Chi-Chi, Taiwan-06	6.3	99999	TCU119
3502	0175	Chi-Chi, Taiwan-06	6.3	99999	TCU120
3503	0175	Chi-Chi, Taiwan-06	6.3	99999	TCU122
3504	0175	Chi-Chi, Taiwan-06	6.3	99999	TCU123
3505	0175	Chi-Chi, Taiwan-06	6.3	99999	TCU125
3506	0175	Chi-Chi, Taiwan-06	6.3	99999	TCU128
3507	0175	Chi-Chi, Taiwan-06	6.3	9999936	TCU129
3508	0175	Chi-Chi, Taiwan-06	6.3	99999	TCU136
3509	0175	Chi-Chi, Taiwan-06	6.3	99999	TCU138
3510	0175	Chi-Chi, Taiwan-06	6.3	99999	TCU139
3511	0175	Chi-Chi, Taiwan-06	6.3	99999	TCU140
3512	0175	Chi-Chi, Taiwan-06	6.3	99999	TCU141
3513	0175	Chi-Chi, Taiwan-06	6.3	99999	TCU145
3515	0175	Chi-Chi, Taiwan-06	6.3	99999	TTN001
3536	0175	Chi-Chi, Taiwan-06	6.3	99999	TTN031
3537	0175	Chi-Chi, Taiwan-06	6.3	99999	TTN032
3540	0175	Chi-Chi, Taiwan-06	6.3	99999	TTN040
3541	0175	Chi-Chi, Taiwan-06	6.3	99999	TTN041
23	0020	San Francisco	5.28	1117	Golden Gate Park
28	0025	Parkfield	6.19	1016	Cholame - Shandon Array #12
30	0025	Parkfield	6.19	1014	Cholame - Shandon Array #5
31	0025	Parkfield	6.19	1015	Cholame - Shandon Array #8
33	0025	Parkfield	6.19	1438	Temblor pre-1969
42	0029	Lytle Creek	5.33	112	Cedar Springs Pumphouse
43	0029	Lytle Creek	5.33	111	Cedar Springs, Allen Ranch
44	0029	Lytle Creek	5.33	113	Colton - So Cal Edison
45	0029	Lytle Creek	5.33	620	Devil's Canyon
48	0029	Lytle Creek	5.33	278	Puddingstone Dam (Abutment)
49	0029	Lytle Creek	5.33	104	Santa Anita Dam
50	0029	Lytle Creek	5.33	290	Wrightwood - 6074 Park Dr
51	0030	San Fernando	6.61	411	2516 Via Tejon PV
56	0030	San Fernando	6.61	108	Carbon Canyon Dam
57	0030	San Fernando	6.61	24278	Castaic - Old Ridge Route
63	0030	San Fernando	6.61	121	Fairmont Dam
64	0030	San Fernando	6.61	998	Fort Tejon
65	0030	San Fernando	6.61	994	Gormon - Oso Pump Plant
68	0030	San Fernando	6.61	24303	LA - Hollywood Stor FF
70	0030	San Fernando	6.61	24271	Lake Hughes #1
71	0030	San Fernando	6.61	128	Lake Hughes #12
72	0030	San Fernando	6.61	126	Lake Hughes #4
73	0030	San Fernando	6.61	127	Lake Hughes #9
77	0030	San Fernando	6.61	279	Pacoima Dam (upper left abut)
78	0030	San Fernando	6.61	262	Palmdale Fire Station
81	0030	San Fernando	6.61	269	Pearblossom Pump
82	0030	San Fernando	6.61	272	Port Hueneme
83	0030	San Fernando	6.61	278	Puddingstone Dam (Abutment)
87	0030	San Fernando	6.61	104	Santa Anita Dam

RSN	EQID	Earthquake	M	Station No.	Station
88	0030	San Fernando	6.61	285	Santa Felita Dam (Outlet)
89	0030	San Fernando	6.61	1027	Tehachapi Pump
91	0030	San Fernando	6.61	287	Upland - San Antonio Dam
93	0030	San Fernando	6.61	289	Whittier Narrows Dam
94	0030	San Fernando	6.61	290	Wrightwood - 6074 Park Dr
95	0031	Managua, Nicaragua-01	6.24	3501	Managua, ESSO
96	0032	Managua, Nicaragua-02	5.2	3501	Managua, ESSO
97	0033	Point Mugu	5.65	272	Port Hueneme
98	0034	Hollister-03	5.14	47379	Gilroy Array #1
100	0034	Hollister-03	5.14	47126	San Juan Bautista, 24 Polk St
106	0036	Oroville-01	5.89	1051	Oroville Seismograph Station
107	0037	Oroville-02	4.79	1545	Oroville Airport
108	0037	Oroville-02	4.79	1546	Up & Down Cafe (OR1)
109	0038	Oroville-04	4.37	1544	Medical Center
110	0038	Oroville-04	4.37	1545	Oroville Airport
111	0038	Oroville-04	4.37	1546	Up & Down Cafe (OR1)
112	0039	Oroville-03	4.7	1542	Broadbeck Residence
113	0039	Oroville-03	4.7	1543	DWR Garage
114	0039	Oroville-03	4.7	1550	Duffy Residence (OR5)
115	0039	Oroville-03	4.7	1493	Johnson Ranch
116	0039	Oroville-03	4.7	1496	Nelson Ranch (OR7)
117	0039	Oroville-03	4.7	1545	Oroville Airport
118	0039	Oroville-03	4.7	1549	Pacific Heights Rd (OR4)
119	0039	Oroville-03	4.7	1551	Summit Ave (OR6)
120	0039	Oroville-03	4.7	1546	Up & Down Cafe (OR1)
121	0040	Friuli, Italy-01	6.5	8002	Barcis
122	0040	Friuli, Italy-01	6.5	8004	Codroipo
125	0040	Friuli, Italy-01	6.5	8012	Tolmezzo
126	0041	Gazli, USSR	6.8	9201	Karakyr
127	0042	Fruili, Italy-03	5.5	8023	Buia
128	0042	Fruili, Italy-03	5.5	8014	Forgaria Cornino
129	0042	Fruili, Italy-03	5.5	8022	San Rocco
130	0043	Friuli, Italy-02	5.91	8023	Buia
131	0043	Friuli, Italy-02	5.91	8004	Codroipo
132	0043	Friuli, Italy-02	5.91	8014	Forgaria Cornino
133	0043	Friuli, Italy-02	5.91	8022	San Rocco
134	0044	Izmir, Turkey	5.3	99999	Izmir
135	0045	Santa Barbara	5.92	106	Cachuma Dam Toe
138	0046	Tabas, Iran	7.35	70	Boshrooyeh
139	0046	Tabas, Iran	7.35	9102	Dayhook
143	0046	Tabas, Iran	7.35	9101	Tabas
144	0047	Dursunbey, Turkey	5.34	99999	Dursunbey
145	0048	Coyote Lake	5.74	57217	Coyote Lake Dam (SW Abut)
146	0048	Coyote Lake	5.74	47379	Gilroy Array #1
147	0048	Coyote Lake	5.74	47380	Gilroy Array #2
148	0048	Coyote Lake	5.74	47381	Gilroy Array #3
149	0048	Coyote Lake	5.74	57382	Gilroy Array #4
150	0048	Coyote Lake	5.74	57383	Gilroy Array #6
151	0048	Coyote Lake	5.74	57191	Halls Valley
152	0048	Coyote Lake	5.74	47315	SJB Overpass, Bent 3 g.l.
153	0048	Coyote Lake	5.74	47315	SJB Overpass, Bent 5 g.l.
154	0048	Coyote Lake	5.74	47126	San Juan Bautista, 24 Polk St
155	0049	Norcia, Italy	5.9	99999	Bevagna
156	0049	Norcia, Italy	5.9	99999	Cascia
157	0049	Norcia, Italy	5.9	99999	Spoleto

RSN	EQID	Earthquake	M	Station No.	Station
158	0050	Imperial Valley-06	6.53	6616	Aeropuerto Mexicali
159	0050	Imperial Valley-06	6.53	6618	Agrarias
160	0050	Imperial Valley-06	6.53	5054	Bonds Corner
161	0050	Imperial Valley-06	6.53	5060	Brawley Airport
162	0050	Imperial Valley-06	6.53	5053	Calexico Fire Station
163	0050	Imperial Valley-06	6.53	5061	Calipatria Fire Station
164	0050	Imperial Valley-06	6.53	6604	Cerro Prieto
165	0050	Imperial Valley-06	6.53	6621	Chihuahua
166	0050	Imperial Valley-06	6.53	5066	Coachella Canal #4
167	0050	Imperial Valley-06	6.53	6622	Compuertas
169	0050	Imperial Valley-06	6.53	6605	Delta
170	0050	Imperial Valley-06	6.53	01136	EC County Center FF
171	0050	Imperial Valley-06	6.53	1336	EC Meloland Overpass FF
172	0050	Imperial Valley-06	6.53	5056	El Centro Array #1
173	0050	Imperial Valley-06	6.53	412	El Centro Array #10
174	0050	Imperial Valley-06	6.53	5058	El Centro Array #11
175	0050	Imperial Valley-06	6.53	931	El Centro Array #12
176	0050	Imperial Valley-06	6.53	5059	El Centro Array #13
178	0050	Imperial Valley-06	6.53	5057	El Centro Array #3
179	0050	Imperial Valley-06	6.53	955	El Centro Array #4
180	0050	Imperial Valley-06	6.53	952	El Centro Array #5
181	0050	Imperial Valley-06	6.53	5158	El Centro Array #6
182	0050	Imperial Valley-06	6.53	5028	El Centro Array #7
183	0050	Imperial Valley-06	6.53	958	El Centro Array #8
184	0050	Imperial Valley-06	6.53	5165	El Centro Differential Array
185	0050	Imperial Valley-06	6.53	5055	Holtville Post Office
186	0050	Imperial Valley-06	6.53	11023	Niland Fire Station
187	0050	Imperial Valley-06	6.53	5051	Parachute Test Site
188	0050	Imperial Valley-06	6.53	5052	Plaster City
189	0050	Imperial Valley-06	6.53	6619	SAHOP Casa Flores
190	0050	Imperial Valley-06	6.53	286	Superstition Mtn Camera
191	0050	Imperial Valley-06	6.53	6610	Victoria
192	0050	Imperial Valley-06	6.53	11369	Westmorland Fire Sta
193	0051	Imperial Valley-07	5.01	5054	Bonds Corner
194	0051	Imperial Valley-07	5.01	5060	Brawley Airport
195	0051	Imperial Valley-07	5.01	5053	Calexico Fire Station
196	0051	Imperial Valley-07	5.01	6605	Delta
197	0051	Imperial Valley-07	5.01	5056	El Centro Array #1
198	0051	Imperial Valley-07	5.01	412	El Centro Array #10
199	0051	Imperial Valley-07	5.01	5058	El Centro Array #11
200	0051	Imperial Valley-07	5.01	5115	El Centro Array #2
201	0051	Imperial Valley-07	5.01	5057	El Centro Array #3
202	0051	Imperial Valley-07	5.01	955	El Centro Array #4
203	0051	Imperial Valley-07	5.01	952	El Centro Array #5
204	0051	Imperial Valley-07	5.01	5158	El Centro Array #6
205	0051	Imperial Valley-07	5.01	5028	El Centro Array #7
206	0051	Imperial Valley-07	5.01	958	El Centro Array #8
207	0051	Imperial Valley-07	5.01	5165	El Centro Differential Array
208	0051	Imperial Valley-07	5.01	5055	Holtville Post Office
209	0052	Imperial Valley-08	5.62	11369	Westmorland Fire Sta
210	0053	Livermore-01	5.8	58219	APEEL 3E Hayward CSUH
212	0053	Livermore-01	5.8	1265	Del Valle Dam (Toe)
213	0053	Livermore-01	5.8	57064	Fremont - Mission San Jose
214	0053	Livermore-01	5.8	57187	San Ramon - Eastman Kodak
215	0053	Livermore-01	5.8	57134	San Ramon Fire Station

RSN	EQID	Earthquake	M	Station No.	Station
216	0053	Livermore-01	5.8	57063	Tracy - Sewage Treatm Plant
217	0054	Livermore-02	5.42	58219	APEEL 3E Hayward CSUH
219	0054	Livermore-02	5.42	1265	Del Valle Dam (Toe)
220	0054	Livermore-02	5.42	57064	Fremont - Mission San Jose
221	0054	Livermore-02	5.42	57T01	Livermore - Fagundas Ranch
222	0054	Livermore-02	5.42	57T02	Livermore - Morgan Terr Park
223	0054	Livermore-02	5.42	57187	San Ramon - Eastman Kodak
224	0054	Livermore-02	5.42	57134	San Ramon Fire Station
225	0055	Anza (Horse Canyon)-01	5.19	5044	Anza - Pinyon Flat
226	0055	Anza (Horse Canyon)-01	5.19	5045	Anza - Terwilliger Valley
227	0055	Anza (Horse Canyon)-01	5.19	5160	Anza Fire Station
228	0055	Anza (Horse Canyon)-01	5.19	5049	Borrego Air Ranch
229	0055	Anza (Horse Canyon)-01	5.19	5047	Rancho De Anza
230	0056	Mammoth Lakes-01	6.06	54099	Convict Creek
231	0056	Mammoth Lakes-01	6.06	54214	Long Valley Dam (Upr L Abut)
232	0056	Mammoth Lakes-01	6.06	54301	Mammoth Lakes H. S.
233	0057	Mammoth Lakes-02	5.69	54099	Convict Creek
234	0057	Mammoth Lakes-02	5.69	54214	Long Valley Dam (Upr L Abut)
235	0057	Mammoth Lakes-02	5.69	54301	Mammoth Lakes H. S.
236	0058	Mammoth Lakes-03	5.91	54099	Convict Creek
237	0058	Mammoth Lakes-03	5.91	54214	Long Valley Dam (Downst)
238	0058	Mammoth Lakes-03	5.91	54214	Long Valley Dam (L Abut)
239	0058	Mammoth Lakes-03	5.91	54214	Long Valley Dam (Upr L Abut)
240	0059	Mammoth Lakes-04	5.7	54099	Convict Creek
241	0059	Mammoth Lakes-04	5.7	54214	Long Valley Dam (Downst)
242	0059	Mammoth Lakes-04	5.7	54214	Long Valley Dam (L Abut)
243	0059	Mammoth Lakes-04	5.7	54214	Long Valley Dam (Upr L Abut)
244	0060	Mammoth Lakes-05	5.7	54099	Convict Creek
245	0060	Mammoth Lakes-05	5.7	54214	Long Valley Dam (Upr L Abut)
246	0061	Mammoth Lakes-06	5.94	54100	Benton
247	0061	Mammoth Lakes-06	5.94	54424	Bishop - Paradise Lodge
248	0061	Mammoth Lakes-06	5.94	54099	Convict Creek
249	0061	Mammoth Lakes-06	5.94	43	Fish & Game (FIS)
250	0061	Mammoth Lakes-06	5.94	54214	Long Valley Dam (Upr L Abut)
251	0062	Mammoth Lakes-07	4.73	43	Fish & Game (FIS)
252	0062	Mammoth Lakes-07	4.73	3	Green Church
253	0062	Mammoth Lakes-07	4.73	35	Long Valley Fire Sta
254	0062	Mammoth Lakes-07	4.73	36	Mammoth Elem School
255	0062	Mammoth Lakes-07	4.73	34	USC Cash Baugh Ranch
256	0062	Mammoth Lakes-07	4.73	37	USC McGee Creek Inn
257	0063	Mammoth Lakes-08	4.8	41	Cashbaugh (CBR)
258	0063	Mammoth Lakes-08	4.8	42	Convict Lakes (CON)
259	0063	Mammoth Lakes-08	4.8	43	Fish & Game (FIS)
261	0063	Mammoth Lakes-08	4.8	35	Long Valley Fire Sta
262	0063	Mammoth Lakes-08	4.8	36	Mammoth Elem School
263	0063	Mammoth Lakes-08	4.8	40	USC Convict Lakes
264	0063	Mammoth Lakes-08	4.8	37	USC McGee Creek Inn
265	0064	Victoria, Mexico	6.33	6604	Cerro Prieto
266	0064	Victoria, Mexico	6.33	6621	Chihuahua
268	0064	Victoria, Mexico	6.33	6619	SAHOP Casa Flores
269	0064	Victoria, Mexico	6.33	6624	Victoria Hospital Sotano
270	0065	Mammoth Lakes-09	4.85	42	Convict Lakes (CON)
271	0065	Mammoth Lakes-09	4.85	43	Fish & Game (FIS)
272	0065	Mammoth Lakes-09	4.85	3	Green Church
273	0065	Mammoth Lakes-09	4.85	44	Hot Creek (HCF)

RSN	EQID	Earthquake	M	Station No.	Station
274	0065	Mammoth Lakes-09	4.85	35	Long Valley Fire Sta
275	0065	Mammoth Lakes-09	4.85	36	Mammoth Elem School
276	0065	Mammoth Lakes-09	4.85	45	McGee Creek (MGE)
277	0065	Mammoth Lakes-09	4.85	40	USC Convict Lakes
278	0065	Mammoth Lakes-09	4.85	52	USC McGee Creek
283	0068	Irpinia, Italy-01	6.9	99999	Arienzo
284	0068	Irpinia, Italy-01	6.9	99999	Auletta
285	0068	Irpinia, Italy-01	6.9	99999	Bagnoli Irpinio
286	0068	Irpinia, Italy-01	6.9	99999	Bisaccia
287	0068	Irpinia, Italy-01	6.9	99999	Bovino
288	0068	Irpinia, Italy-01	6.9	99999	Brienza
289	0068	Irpinia, Italy-01	6.9	99999	Calitri
290	0068	Irpinia, Italy-01	6.9	99999	Mercato San Severino
291	0068	Irpinia, Italy-01	6.9	99999	Rionero In Vulture
292	0068	Irpinia, Italy-01	6.9	99999	Sturno
293	0068	Irpinia, Italy-01	6.9	99999	Torre Del Greco
294	0068	Irpinia, Italy-01	6.9	99999	Tricarico
295	0069	Irpinia, Italy-02	6.2	99999	Auletta
296	0069	Irpinia, Italy-02	6.2	99999	Bagnoli Irpinio
297	0069	Irpinia, Italy-02	6.2	99999	Bisaccia
298	0069	Irpinia, Italy-02	6.2	99999	Bovino
299	0069	Irpinia, Italy-02	6.2	99999	Brienza
300	0069	Irpinia, Italy-02	6.2	99999	Calitri
301	0069	Irpinia, Italy-02	6.2	99999	Mercato San Severino
302	0069	Irpinia, Italy-02	6.2	99999	Rionero In Vulture
303	0069	Irpinia, Italy-02	6.2	99999	Sturno
304	0069	Irpinia, Italy-02	6.2	99999	Tricarico
305	0070	Irpinia, Italy-03	4.7	99999	Conza (Base)
313	0072	Corinth, Greece	6.6	99999	Corinth
314	0073	Westmorland	5.9	5060	Brawley Airport
315	0073	Westmorland	5.9	11023	Niland Fire Station
316	0073	Westmorland	5.9	5051	Parachute Test Site
317	0073	Westmorland	5.9	5062	Salton Sea Wildlife Refuge
318	0073	Westmorland	5.9	286	Superstition Mtn Camera
319	0073	Westmorland	5.9	11369	Westmorland Fire Sta
320	0074	Mammoth Lakes-10	5.34	54099	Convict Creek
321	0075	Mammoth Lakes-11	5.31	54099	Convict Creek
322	0076	Coalinga-01	6.36	46314	Cantua Creek School
323	0076	Coalinga-01	6.36	36229	Parkfield - Cholame 12W
324	0076	Coalinga-01	6.36	36452	Parkfield - Cholame 1E
325	0076	Coalinga-01	6.36	36230	Parkfield - Cholame 2E
326	0076	Coalinga-01	6.36	36228	Parkfield - Cholame 2WA
327	0076	Coalinga-01	6.36	36450	Parkfield - Cholame 3E
328	0076	Coalinga-01	6.36	36410	Parkfield - Cholame 3W
329	0076	Coalinga-01	6.36	36412	Parkfield - Cholame 4AW
330	0076	Coalinga-01	6.36	36411	Parkfield - Cholame 4W
331	0076	Coalinga-01	6.36	36227	Parkfield - Cholame 5W
332	0076	Coalinga-01	6.36	36451	Parkfield - Cholame 6W
333	0076	Coalinga-01	6.36	36226	Parkfield - Cholame 8W
334	0076	Coalinga-01	6.36	36407	Parkfield - Fault Zone 1
335	0076	Coalinga-01	6.36	36444	Parkfield - Fault Zone 10
336	0076	Coalinga-01	6.36	36453	Parkfield - Fault Zone 11
337	0076	Coalinga-01	6.36	36138	Parkfield - Fault Zone 12
338	0076	Coalinga-01	6.36	36456	Parkfield - Fault Zone 14
339	0076	Coalinga-01	6.36	36445	Parkfield - Fault Zone 15

RSN	EQID	Earthquake	M	Station No.	Station
340	0076	Coalinga-01	6.36	36457	Parkfield - Fault Zone 16
341	0076	Coalinga-01	6.36	36413	Parkfield - Fault Zone 2
342	0076	Coalinga-01	6.36	36408	Parkfield - Fault Zone 3
343	0076	Coalinga-01	6.36	36414	Parkfield - Fault Zone 4
344	0076	Coalinga-01	6.36	36454	Parkfield - Fault Zone 6
345	0076	Coalinga-01	6.36	36431	Parkfield - Fault Zone 7
346	0076	Coalinga-01	6.36	36449	Parkfield - Fault Zone 8
347	0076	Coalinga-01	6.36	36443	Parkfield - Fault Zone 9
348	0076	Coalinga-01	6.36	36415	Parkfield - Gold Hill 1W
349	0076	Coalinga-01	6.36	36421	Parkfield - Gold Hill 2E
350	0076	Coalinga-01	6.36	36416	Parkfield - Gold Hill 2W
351	0076	Coalinga-01	6.36	36439	Parkfield - Gold Hill 3E
352	0076	Coalinga-01	6.36	36420	Parkfield - Gold Hill 3W
353	0076	Coalinga-01	6.36	36433	Parkfield - Gold Hill 4W
354	0076	Coalinga-01	6.36	36434	Parkfield - Gold Hill 5W
355	0076	Coalinga-01	6.36	36432	Parkfield - Gold Hill 6W
356	0076	Coalinga-01	6.36	36422	Parkfield - Stone Corral 2E
357	0076	Coalinga-01	6.36	36437	Parkfield - Stone Corral 3E
358	0076	Coalinga-01	6.36	36438	Parkfield - Stone Corral 4E
359	0076	Coalinga-01	6.36	36455	Parkfield - Vineyard Cany 1E
360	0076	Coalinga-01	6.36	36448	Parkfield - Vineyard Cany 1W
362	0076	Coalinga-01	6.36	36447	Parkfield - Vineyard Cany 2W
363	0076	Coalinga-01	6.36	36176	Parkfield - Vineyard Cany 3W
364	0076	Coalinga-01	6.36	36446	Parkfield - Vineyard Cany 4W
366	0076	Coalinga-01	6.36	36441	Parkfield - Vineyard Cany 6W
368	0076	Coalinga-01	6.36	1162	Pleasant Valley P.P. - yard
369	0076	Coalinga-01	6.36	46175	Slack Canyon
370	0077	Coalinga-02	5.09	4	ALP (temp)
371	0077	Coalinga-02	5.09	46T05	Anticline Ridge - Palmer Ave
372	0077	Coalinga-02	5.09	1607	Anticline Ridge Free-Field
373	0077	Coalinga-02	5.09	1607	Anticline Ridge Pad
374	0077	Coalinga-02	5.09	1606	Burnett Construction
375	0077	Coalinga-02	5.09	46617	Coalinga-14th & Elm (Old CHP)
376	0077	Coalinga-02	5.09	46T07	Harris Ranch - Hdqtrs (temp)
377	0077	Coalinga-02	5.09	5	LLN (temp)
379	0077	Coalinga-02	5.09	1604	Oil City
380	0077	Coalinga-02	5.09	46T06	Oil Fields - Skunk Hollow
381	0077	Coalinga-02	5.09	1608	Oil Fields Fire Station
382	0077	Coalinga-02	5.09	1609	Palmer Ave
383	0077	Coalinga-02	5.09	1162	Pleasant Valley P.P. - yard
384	0077	Coalinga-02	5.09	7	SGT (temp)
385	0077	Coalinga-02	5.09	8	SUB (temp)
386	0077	Coalinga-02	5.09	1605	Skunk Hollow
387	0077	Coalinga-02	5.09	47T03	Sulphur Baths (temp)
388	0077	Coalinga-02	5.09	9	TRA (temp)
389	0077	Coalinga-02	5.09	10	VEW (temp)
390	0077	Coalinga-02	5.09	11	YUB (temp)
391	0078	Coalinga-03	5.38	1606	Burnett Construction
392	0078	Coalinga-03	5.38	46617	Coalinga-14th & Elm (Old CHP)
393	0078	Coalinga-03	5.38	47T03	Sulphur Baths (temp)
394	0079	Coalinga-04	5.18	1607	Anticline Ridge Free-Field
395	0079	Coalinga-04	5.18	1607	Anticline Ridge Pad
396	0079	Coalinga-04	5.18	1606	Burnett Construction
397	0079	Coalinga-04	5.18	46617	Coalinga-14th & Elm (Old CHP)
398	0079	Coalinga-04	5.18	1604	Oil City

RSN	EQID	Earthquake	M	Station No.	Station
399	0079	Coalinga-04	5.18	1608	Oil Fields Fire Station - FF
400	0079	Coalinga-04	5.18	1608	Oil Fields Fire Station - Pad
401	0079	Coalinga-04	5.18	1609	Palmer Ave
402	0079	Coalinga-04	5.18	1605	Skunk Hollow
403	0079	Coalinga-04	5.18	47T03	Sulphur Baths (temp)
404	0079	Coalinga-04	5.18	1651	Transmitter Hill
405	0080	Coalinga-05	5.77	1606	Burnett Construction
406	0080	Coalinga-05	5.77	46617	Coalinga-14th & Elm (Old CHP)
407	0080	Coalinga-05	5.77	1604	Oil City
408	0080	Coalinga-05	5.77	1608	Oil Fields Fire Station - FF
409	0080	Coalinga-05	5.77	1608	Oil Fields Fire Station - Pad
410	0080	Coalinga-05	5.77	1609	Palmer Ave
411	0080	Coalinga-05	5.77	1162	Pleasant Valley P.P. - FF
412	0080	Coalinga-05	5.77	1162	Pleasant Valley P.P. - yard
413	0080	Coalinga-05	5.77	1605	Skunk Hollow
414	0080	Coalinga-05	5.77	47T03	Sulphur Baths (temp)
415	0080	Coalinga-05	5.77	1651	Transmitter Hill
416	0081	Coalinga-06	4.89	46617	Coalinga-14th & Elm (Old CHP)
417	0081	Coalinga-06	4.89	47T03	Sulphur Baths (temp)
418	0082	Coalinga-07	5.21	46617	Coalinga-14th & Elm (Old CHP)
419	0082	Coalinga-07	5.21	47T03	Sulphur Baths (temp)
420	0083	Ierissos, Greece	6.7	99999	Ierissos
423	0085	Coalinga-08	5.23	46617	Coalinga-14th & Elm (Old CHP)
424	0085	Coalinga-08	5.23	47T03	Sulphur Baths (temp)
442	0088	Borah Peak, ID-02	5.1	99999	BOR
443	0088	Borah Peak, ID-02	5.1	99999	CEM
444	0088	Borah Peak, ID-02	5.1	99999	HAU
445	0089	New Zealand-01	5.5	081A	Turangi Telephone Exchange
446	0090	Morgan Hill	6.19	58376	APEEL 1E - Hayward
447	0090	Morgan Hill	6.19	57066	Agnews State Hospital
448	0090	Morgan Hill	6.19	1652	Anderson Dam (Downstream)
449	0090	Morgan Hill	6.19	47125	Capitola
450	0090	Morgan Hill	6.19	57007	Corralitos
451	0090	Morgan Hill	6.19	57217	Coyote Lake Dam (SW Abut)
452	0090	Morgan Hill	6.19	58375	Foster City - APEEL 1
453	0090	Morgan Hill	6.19	57064	Fremont - Mission San Jose
454	0090	Morgan Hill	6.19	47006	Gilroy - Gavilan Coll.
455	0090	Morgan Hill	6.19	47379	Gilroy Array #1
456	0090	Morgan Hill	6.19	47380	Gilroy Array #2
457	0090	Morgan Hill	6.19	47381	Gilroy Array #3
458	0090	Morgan Hill	6.19	57382	Gilroy Array #4
459	0090	Morgan Hill	6.19	57383	Gilroy Array #6
460	0090	Morgan Hill	6.19	57425	Gilroy Array #7
461	0090	Morgan Hill	6.19	57191	Halls Valley
463	0090	Morgan Hill	6.19	1656	Hollister Diff Array #1
464	0090	Morgan Hill	6.19	1656	Hollister Diff Array #3
465	0090	Morgan Hill	6.19	1656	Hollister Diff Array #4
466	0090	Morgan Hill	6.19	1656	Hollister Diff Array #5
467	0090	Morgan Hill	6.19	1656	Hollister Diff. Array
468	0090	Morgan Hill	6.19	56012	Los Banos
470	0090	Morgan Hill	6.19	47126	San Juan Bautista, 24 Polk St
471	0090	Morgan Hill	6.19	1655	San Justo Dam (L Abut)
472	0090	Morgan Hill	6.19	1655	San Justo Dam (R Abut)
476	0090	Morgan Hill	6.19	58135	UCSC Lick Observatory
477	0091	Lazio-Abruzzo, Italy	5.8	99999	Atina

RSN	EQID	Earthquake	M	Station No.	Station
478	0091	Lazio-Abruzzo, Italy	5.8	99999	Garigliano-Centrale Nucleare
479	0091	Lazio-Abruzzo, Italy	5.8	99999	Isernia-Sant'Agapito
480	0091	Lazio-Abruzzo, Italy	5.8	99999	Pontecorvo
481	0091	Lazio-Abruzzo, Italy	5.8	99999	Roccamonfina
485	0094	Bishop (Rnd Val)	5.82	1661	McGee Creek - Surface
494	0096	Drama, Greece	5.2	99999	Kavala
495	0097	Nahanni, Canada	6.76	6097	Site 1
496	0097	Nahanni, Canada	6.76	6098	Site 2
497	0097	Nahanni, Canada	6.76	6099	Site 3
498	0098	Hollister-04	5.45	1656	Hollister Diff Array #1
499	0098	Hollister-04	5.45	1656	Hollister Diff Array #3
501	0098	Hollister-04	5.45	47189	SAGO South - Surface
502	0099	Mt. Lewis	5.6	57191	Halls Valley
511	0101	N. Palm Springs	6.06	5224	Anza - Red Mountain
512	0101	N. Palm Springs	6.06	5231	Anza - Tule Canyon
513	0101	N. Palm Springs	6.06	5160	Anza Fire Station
514	0101	N. Palm Springs	6.06	5073	Cabazon
515	0101	N. Palm Springs	6.06	754	Colton Interchange - Vault
516	0101	N. Palm Springs	6.06	5157	Cranston Forest Station
517	0101	N. Palm Springs	6.06	12149	Desert Hot Springs
518	0101	N. Palm Springs	6.06	5069	Fun Valley
519	0101	N. Palm Springs	6.06	12331	Hemet Fire Station
521	0101	N. Palm Springs	6.06	5043	Hurkey Creek Park
522	0101	N. Palm Springs	6.06	5067	Indio
523	0101	N. Palm Springs	6.06	12026	Indio - Coachella Canal
524	0101	N. Palm Springs	6.06	22170	Joshua Tree
525	0101	N. Palm Springs	6.06	707	Lake Mathews Dike Toe
526	0101	N. Palm Springs	6.06	22T13	Landers Fire Station
527	0101	N. Palm Springs	6.06	5071	Morongo Valley
528	0101	N. Palm Springs	6.06	13198	Murrieta Hot Springs
529	0101	N. Palm Springs	6.06	5070	North Palm Springs
530	0101	N. Palm Springs	6.06	12025	Palm Springs Airport
531	0101	N. Palm Springs	6.06	12168	Puerta La Cruz
533	0101	N. Palm Springs	6.06	13123	Riverside Airport
534	0101	N. Palm Springs	6.06	12204	San Jacinto - Soboba
535	0101	N. Palm Springs	6.06	12202	San Jacinto - Valley Cemetery
536	0101	N. Palm Springs	6.06	5230	Santa Rosa Mountain
537	0101	N. Palm Springs	6.06	12206	Silent Valley - Poppet Flat
538	0101	N. Palm Springs	6.06	5038	Sunnymead
539	0101	N. Palm Springs	6.06	13172	Temecula - 6th & Mercedes
540	0101	N. Palm Springs	6.06	5072	Whitewater Trout Farm
541	0101	N. Palm Springs	6.06	13199	Winchester Bergman Ran
542	0101	N. Palm Springs	6.06	13201	Winchester Page Bros R
543	0102	Chalfant Valley-01	5.77	54100	Benton
544	0102	Chalfant Valley-01	5.77	54171	Bishop - LADWP South St
545	0102	Chalfant Valley-01	5.77	54424	Bishop - Paradise Lodge
546	0102	Chalfant Valley-01	5.77	54T03	Lake Crowley - Shehorn Res.
547	0102	Chalfant Valley-01	5.77	54428	Zack Brothers Ranch
548	0103	Chalfant Valley-02	6.19	54100	Benton
549	0103	Chalfant Valley-02	6.19	54171	Bishop - LADWP South St
550	0103	Chalfant Valley-02	6.19	54424	Bishop - Paradise Lodge
551	0103	Chalfant Valley-02	6.19	54099	Convict Creek
552	0103	Chalfant Valley-02	6.19	54T03	Lake Crowley - Shehorn Res.
553	0103	Chalfant Valley-02	6.19	54214	Long Valley Dam (Downst)
554	0103	Chalfant Valley-02	6.19	54214	Long Valley Dam (L Abut)

RSN	EQID	Earthquake	M	Station No.	Station
555	0103	Chalfant Valley-02	6.19	54T04	Mammoth Lakes Sheriff Subst.
556	0103	Chalfant Valley-02	6.19	1661	McGee Creek - Surface
557	0103	Chalfant Valley-02	6.19	54101	Tinemaha Res. Free Field
558	0103	Chalfant Valley-02	6.19	54428	Zack Brothers Ranch
559	0104	Chalfant Valley-03	5.65	54171	Bishop - LADWP South St
560	0104	Chalfant Valley-03	5.65	54424	Bishop - Paradise Lodge
561	0104	Chalfant Valley-03	5.65	54428	Zack Brothers Ranch
562	0105	Chalfant Valley-04	5.44	54171	Bishop - LADWP South St
563	0105	Chalfant Valley-04	5.44	54428	Zack Brothers Ranch
568	0108	San Salvador	5.8	99999	Geotech Investig Center
569	0108	San Salvador	5.8	99999	National Geografical Inst
585	0110	Baja California	5.5	6604	Cerro Prieto
586	0111	New Zealand-02	6.6	113A	Maraenui Primary School
587	0111	New Zealand-02	6.6	99999	Matahina Dam
588	0112	New Zealand-03	5.8	99999	Matahina Dam
589	0113	Whittier Narrows-01	5.99	24461	Alhambra - Fremont School
590	0113	Whittier Narrows-01	5.99	24402	Altadena - Eaton Canyon
591	0113	Whittier Narrows-01	5.99	90088	Anaheim - W Ball Rd
592	0113	Whittier Narrows-01	5.99	90093	Arcadia - Campus Dr
593	0113	Whittier Narrows-01	5.99	24087	Arleta - Nordhoff Fire Sta
594	0113	Whittier Narrows-01	5.99	90069	Baldwin Park - N Holly
595	0113	Whittier Narrows-01	5.99	90094	Bell Gardens - Jaboneria
596	0113	Whittier Narrows-01	5.99	90014	Beverly Hills - 12520 Mulhol
597	0113	Whittier Narrows-01	5.99	90013	Beverly Hills - 14145 Mulhol
598	0113	Whittier Narrows-01	5.99	90061	Big Tujunga, Angeles Nat F
600	0113	Whittier Narrows-01	5.99	951	Brea Dam (Downstream)
601	0113	Whittier Narrows-01	5.99	951	Brea Dam (L Abut)
602	0113	Whittier Narrows-01	5.99	90012	Burbank - N Buena Vista
603	0113	Whittier Narrows-01	5.99	90052	Calabasas - N Las Virg
604	0113	Whittier Narrows-01	5.99	90053	Canoga Park - Topanga Can
605	0113	Whittier Narrows-01	5.99	90057	Canyon Country - W Lost Cany
606	0113	Whittier Narrows-01	5.99	108	Carbon Canyon Dam
607	0113	Whittier Narrows-01	5.99	90040	Carson - Catskill Ave
608	0113	Whittier Narrows-01	5.99	90081	Carson - Water St
609	0113	Whittier Narrows-01	5.99	24277	Castaic - Hasley Canyon
611	0113	Whittier Narrows-01	5.99	90078	Compton - Castlegate St
612	0113	Whittier Narrows-01	5.99	90068	Covina - S Grand Ave
613	0113	Whittier Narrows-01	5.99	90070	Covina - W Badillo
614	0113	Whittier Narrows-01	5.99	90079	Downey - Birchdale
615	0113	Whittier Narrows-01	5.99	14368	Downey - Co Maint Bldg
616	0113	Whittier Narrows-01	5.99	90066	El Monte - Fairview Av
617	0113	Whittier Narrows-01	5.99	13122	Featherly Park - Maint
618	0113	Whittier Narrows-01	5.99	90002	Fountain Valley - Euclid
619	0113	Whittier Narrows-01	5.99	709	Garvey Res. - Control Bldg
620	0113	Whittier Narrows-01	5.99	90063	Glendale - Las Palmas
621	0113	Whittier Narrows-01	5.99	90065	Glendora - N Oakbank
622	0113	Whittier Narrows-01	5.99	90073	Hacienda Heights - Colima
624	0113	Whittier Narrows-01	5.99	13197	Huntington Beach - Lake St
625	0113	Whittier Narrows-01	5.99	14196	Inglewood - Union Oil
626	0113	Whittier Narrows-01	5.99	14403	LA - 116th St School
627	0113	Whittier Narrows-01	5.99	24157	LA - Baldwin Hills
628	0113	Whittier Narrows-01	5.99	90054	LA - Centinela St
629	0113	Whittier Narrows-01	5.99	24389	LA - Century City CC North
630	0113	Whittier Narrows-01	5.99	24390	LA - Century City CC South
631	0113	Whittier Narrows-01	5.99	90015	LA - Chalon Rd

RSN	EQID	Earthquake	M	Station No.	Station
632	0113	Whittier Narrows-01	5.99	90033	LA - Cypress Ave
634	0113	Whittier Narrows-01	5.99	90034	LA - Fletcher Dr
635	0113	Whittier Narrows-01	5.99	24303	LA - Hollywood Stor FF
636	0113	Whittier Narrows-01	5.99	90016	LA - N Faring Rd
637	0113	Whittier Narrows-01	5.99	90032	LA - N Figueroa St
638	0113	Whittier Narrows-01	5.99	90021	LA - N Westmoreland
639	0113	Whittier Narrows-01	5.99	24400	LA - Obregon Park
640	0113	Whittier Narrows-01	5.99	90022	LA - S Grand Ave
641	0113	Whittier Narrows-01	5.99	90091	LA - Saturn St
642	0113	Whittier Narrows-01	5.99	90023	LA - W 70th St
643	0113	Whittier Narrows-01	5.99	90017	LA - Wonderland Ave
644	0113	Whittier Narrows-01	5.99	14395	LB - Harbor Admin FF
645	0113	Whittier Narrows-01	5.99	90080	LB - Orange Ave
646	0113	Whittier Narrows-01	5.99	14242	LB - Rancho Los Cerritos
647	0113	Whittier Narrows-01	5.99	14241	LB - Recreation Park
648	0113	Whittier Narrows-01	5.99	90060	La Crescenta - New York
649	0113	Whittier Narrows-01	5.99	90074	La Habra - Briarcliff
650	0113	Whittier Narrows-01	5.99	90072	La Puente - Rimgrove Av
652	0113	Whittier Narrows-01	5.99	90084	Lakewood - Del Amo Blvd
653	0113	Whittier Narrows-01	5.99	24526	Lancaster - Med Off FF
654	0113	Whittier Narrows-01	5.99	90045	Lawndale - Osage Ave
655	0113	Whittier Narrows-01	5.99	24055	Leona Valley #5 - Ritter
656	0113	Whittier Narrows-01	5.99	24309	Leona Valley #6
657	0113	Whittier Narrows-01	5.99	90050	Malibu - Las Flores Canyon
658	0113	Whittier Narrows-01	5.99	24396	Malibu - Point Dume Sch
659	0113	Whittier Narrows-01	5.99	90051	Malibu - W Pacific Cst Hwy
661	0113	Whittier Narrows-01	5.99	90062	Mill Creek, Angeles Nat For
663	0113	Whittier Narrows-01	5.99	24399	Mt Wilson - CIT Seis Sta
664	0113	Whittier Narrows-01	5.99	90009	N Hollywood - Coldwater Can
665	0113	Whittier Narrows-01	5.99	24279	Newhall - Fire Sta
666	0113	Whittier Narrows-01	5.99	90056	Newhall - W Pico Canyon Rd.
667	0113	Whittier Narrows-01	5.99	90003	Northridge - 17645 Saticoy St
668	0113	Whittier Narrows-01	5.99	634	Norwalk - Imp Hwy, S Grnd
669	0113	Whittier Narrows-01	5.99	697	Orange Co. Reservoir
670	0113	Whittier Narrows-01	5.99	90049	Pacific Palisades - Sunset
671	0113	Whittier Narrows-01	5.99	24088	Pacoima Kagel Canyon
672	0113	Whittier Narrows-01	5.99	90005	Pacoima Kagel Canyon USC
673	0113	Whittier Narrows-01	5.99	90007	Panorama City - Roscoe
674	0113	Whittier Narrows-01	5.99	80046	Pasadena - Brown Gym
677	0113	Whittier Narrows-01	5.99	80047	Pasadena - CIT Calif Blvd
678	0113	Whittier Narrows-01	5.99	80051	Pasadena - CIT Indust. Rel
681	0113	Whittier Narrows-01	5.99	80048	Pasadena - CIT Lura St
683	0113	Whittier Narrows-01	5.99	90095	Pasadena - Old House Rd
684	0113	Whittier Narrows-01	5.99	90047	Playa Del Rey - Saran
685	0113	Whittier Narrows-01	5.99	23525	Pomona - 4th & Locust FF
686	0113	Whittier Narrows-01	5.99	23497	Rancho Cucamonga - FF
687	0113	Whittier Narrows-01	5.99	90044	Rancho Palos Verdes - Luconia
688	0113	Whittier Narrows-01	5.99	13123	Riverside Airport
690	0113	Whittier Narrows-01	5.99	90019	San Gabriel - E Grand Ave
691	0113	Whittier Narrows-01	5.99	24401	San Marino - SW Academy
692	0113	Whittier Narrows-01	5.99	90077	Santa Fe Springs - E.Joslin
693	0113	Whittier Narrows-01	5.99	90048	Santa Monica - Second St
694	0113	Whittier Narrows-01	5.99	90010	Studio City - Coldwater Can
695	0113	Whittier Narrows-01	5.99	90006	Sun Valley - Roscoe Blvd
696	0113	Whittier Narrows-01	5.99	90008	Sun Valley - Sunland

RSN	EQID	Earthquake	M	Station No.	Station
697	0113	Whittier Narrows-01	5.99	90058	Sunland - Mt Gleason Ave
698	0113	Whittier Narrows-01	5.99	24514	Sylmar - Olive View Med FF
699	0113	Whittier Narrows-01	5.99	90001	Sylmar - Sayre St
700	0113	Whittier Narrows-01	5.99	24436	Tarzana - Cedar Hill
701	0113	Whittier Narrows-01	5.99	90082	Terminal Island - S Seaside
702	0113	Whittier Narrows-01	5.99	90038	Torrance - W 226th St
703	0113	Whittier Narrows-01	5.99	24047	Vasquez Rocks Park
704	0113	Whittier Narrows-01	5.99	90090	Villa Park - Serrano Ave
705	0113	Whittier Narrows-01	5.99	90071	West Covina - S Orange Ave
706	0113	Whittier Narrows-01	5.99	289	Whittier Narrows Dam upstream
707	0114	Whittier Narrows-02	5.27	24461	Alhambra - Fremont School
708	0114	Whittier Narrows-02	5.27	24402	Altadena - Eaton Canyon
709	0114	Whittier Narrows-02	5.27	14368	Downey - Co Maint Bldg
710	0114	Whittier Narrows-02	5.27	14196	Inglewood - Union Oil
711	0114	Whittier Narrows-02	5.27	14403	LA - 116th St School
712	0114	Whittier Narrows-02	5.27	24157	LA - Baldwin Hills
713	0114	Whittier Narrows-02	5.27	24303	LA - Hollywood Stor FF
714	0114	Whittier Narrows-02	5.27	24400	LA - Obregon Park
715	0114	Whittier Narrows-02	5.27	24399	Mt Wilson - CIT Seis Sta
716	0114	Whittier Narrows-02	5.27	24401	San Marino - SW Academy
717	0114	Whittier Narrows-02	5.27	24436	Tarzana - Cedar Hill
718	0115	Superstition Hills-01	6.22	5210	Wildlife Liquef. Array
719	0116	Superstition Hills-02	6.54	5060	Brawley Airport
720	0116	Superstition Hills-02	6.54	5061	Calipatria Fire Station
721	0116	Superstition Hills-02	6.54	1335	El Centro Imp. Co. Cent
722	0116	Superstition Hills-02	6.54	9401	Kornbloom Road (temp)
723	0116	Superstition Hills-02	6.54	5051	Parachute Test Site
724	0116	Superstition Hills-02	6.54	5052	Plaster City
725	0116	Superstition Hills-02	6.54	9400	Poe Road (temp)
726	0116	Superstition Hills-02	6.54	5062	Salton Sea Wildlife Refuge
727	0116	Superstition Hills-02	6.54	286	Superstition Mtn Camera
728	0116	Superstition Hills-02	6.54	11369	Westmorland Fire Sta
729	0116	Superstition Hills-02	6.54	5210	Wildlife Liquef. Array
730	0117	Spitak, Armenia	6.77	12	Gukasian
731	0118	Loma Prieta	6.93	58373	APEEL 10 - Skyline
732	0118	Loma Prieta	6.93	1002	APEEL 2 - Redwood City
733	0118	Loma Prieta	6.93	58393	APEEL 2E Hayward Muir Sch
734	0118	Loma Prieta	6.93	58219	APEEL 3E Hayward CSUH
735	0118	Loma Prieta	6.93	58378	APEEL 7 - Pulgas
736	0118	Loma Prieta	6.93	1161	APEEL 9 - Crystal Springs Res
737	0118	Loma Prieta	6.93	57066	Agnews State Hospital
739	0118	Loma Prieta	6.93	1652	Anderson Dam (Downstream)
740	0118	Loma Prieta	6.93	1652	Anderson Dam (L Abut)
741	0118	Loma Prieta	6.93	13	BRAN
742	0118	Loma Prieta	6.93	1210	Bear Valley #1, Fire Station
743	0118	Loma Prieta	6.93	1479	Bear Valley #10, Webb Residence
744	0118	Loma Prieta	6.93	1481	Bear Valley #12, Williams Ranch
746	0118	Loma Prieta	6.93	1474	Bear Valley #5, Callens Ranch
747	0118	Loma Prieta	6.93	1476	Bear Valley #7, Pinnacles
751	0118	Loma Prieta	6.93	1687	Calaveras Reservoir
752	0118	Loma Prieta	6.93	47125	Capitola
753	0118	Loma Prieta	6.93	57007	Corralitos
754	0118	Loma Prieta	6.93	57504	Coyote Lake Dam (Downst)
755	0118	Loma Prieta	6.93	57217	Coyote Lake Dam (SW Abut)
756	0118	Loma Prieta	6.93	1689	Dublin - Fire Station

RSN	EQID	Earthquake	M	Station No.	Station
757	0118	Loma Prieta	6.93	58664	Dumbarton Bridge West End FF
759	0118	Loma Prieta	6.93	58375	Foster City - APEEL 1
760	0118	Loma Prieta	6.93	1515	Foster City - Menhaden Court
761	0118	Loma Prieta	6.93	1686	Fremont - Emerson Court
762	0118	Loma Prieta	6.93	57064	Fremont - Mission San Jose
763	0118	Loma Prieta	6.93	47006	Gilroy - Gavilan Coll.
764	0118	Loma Prieta	6.93	57476	Gilroy - Historic Bldg.
765	0118	Loma Prieta	6.93	47379	Gilroy Array #1
766	0118	Loma Prieta	6.93	47380	Gilroy Array #2
767	0118	Loma Prieta	6.93	47381	Gilroy Array #3
768	0118	Loma Prieta	6.93	57382	Gilroy Array #4
769	0118	Loma Prieta	6.93	57383	Gilroy Array #6
770	0118	Loma Prieta	6.93	57425	Gilroy Array #7
772	0118	Loma Prieta	6.93	57191	Halls Valley
773	0118	Loma Prieta	6.93	58498	Hayward - BART Sta
776	0118	Loma Prieta	6.93	47524	Hollister - South & Pine
778	0118	Loma Prieta	6.93	1656	Hollister Diff. Array
779	0118	Loma Prieta	6.93	16	LGPC
781	0118	Loma Prieta	6.93	58233	Lower Crystal Springs Dam dwnst
782	0118	Loma Prieta	6.93	47377	Monterey City Hall
786	0118	Loma Prieta	6.93	58264	Palo Alto - 1900 Embarc.
787	0118	Loma Prieta	6.93	1601	Palo Alto - SLAC Lab
791	0118	Loma Prieta	6.93	47189	SAGO South - Surface
792	0118	Loma Prieta	6.93	1675	SF - 1295 Shafter
799	0118	Loma Prieta	6.93	58223	SF Intern. Airport
800	0118	Loma Prieta	6.93	47179	Salinas - John & Work
801	0118	Loma Prieta	6.93	57563	San Jose - Santa Teresa Hills
802	0118	Loma Prieta	6.93	58065	Saratoga - Aloha Ave
803	0118	Loma Prieta	6.93	58235	Saratoga - W Valley Coll.
804	0118	Loma Prieta	6.93	58539	So. San Francisco, Sierra Pt.
806	0118	Loma Prieta	6.93	1695	Sunnyvale - Colton Ave.
807	0118	Loma Prieta	6.93	1688	Sunol - Forest Fire Station
809	0118	Loma Prieta	6.93	15	UCSC
810	0118	Loma Prieta	6.93	58135	UCSC Lick Observatory
811	0118	Loma Prieta	6.93	14	WAHO
812	0118	Loma Prieta	6.93	58127	Woodside
3548	0118	Loma Prieta	6.93	57180	Los Gatos - Lexington Dam
815	0119	Griva, Greece	6.1	99999	Kilkis
816	0120	Georgia, USSR	6.2	18	Ambralauri
817	0120	Georgia, USSR	6.2	21	Baz
818	0120	Georgia, USSR	6.2	19	Iri
819	0120	Georgia, USSR	6.2	20	Oni
820	0120	Georgia, USSR	6.2	22	Zem
821	0121	Erzican, Turkey	6.69	95	Erzincan
822	0122	Roermond, Netherlands	5.3	99999	GSH
825	0123	Cape Mendocino	7.01	89005	Cape Mendocino
826	0123	Cape Mendocino	7.01	89509	Eureka - Myrtle & West
827	0123	Cape Mendocino	7.01	89486	Fortuna - Fortuna Blvd
828	0123	Cape Mendocino	7.01	89156	Petrolia
829	0123	Cape Mendocino	7.01	89324	Rio Dell Overpass - FF
830	0123	Cape Mendocino	7.01	89530	Shelter Cove Airport
831	0124	New Zealand-04	5.7	930A	Edgecumbe Substation Electric
832	0125	Landers	7.28	21081	Amboy
838	0125	Landers	7.28	23559	Barstow
848	0125	Landers	7.28	23	Coolwater

RSN	EQID	Earthquake	M	Station No.	Station
850	0125	Landers	7.28	12149	Desert Hot Springs
855	0125	Landers	7.28	24577	Fort Irwin
860	0125	Landers	7.28	12331	Hemet Fire Station
862	0125	Landers	7.28	12026	Indio - Coachella Canal
864	0125	Landers	7.28	22170	Joshua Tree
879	0125	Landers	7.28	24	Lucerne
880	0125	Landers	7.28	100	Mission Creek Fault
881	0125	Landers	7.28	5071	Morongo Valley
882	0125	Landers	7.28	5070	North Palm Springs
884	0125	Landers	7.28	12025	Palm Springs Airport
891	0125	Landers	7.28	12206	Silent Valley - Poppet Flat
897	0125	Landers	7.28	22161	Twentynine Palms
900	0125	Landers	7.28	22074	Yermo Fire Station
901	0126	Big Bear-01	6.46	22561	Big Bear Lake - Civic Center
902	0126	Big Bear-01	6.46	12149	Desert Hot Springs
906	0126	Big Bear-01	6.46	12331	Hemet Fire Station
907	0126	Big Bear-01	6.46	23583	Hesperia - 4th & Palm
910	0126	Big Bear-01	6.46	22170	Joshua Tree
917	0126	Big Bear-01	6.46	23572	Mt Baldy - Elementary Sch
921	0126	Big Bear-01	6.46	12025	Palm Springs Airport
923	0126	Big Bear-01	6.46	23597	Phelan - Wilson Ranch
925	0126	Big Bear-01	6.46	23598	Rancho Cucamonga - Deer Can
926	0126	Big Bear-01	6.46	23497	Rancho Cucamonga - FF
927	0126	Big Bear-01	6.46	13123	Riverside Airport
928	0126	Big Bear-01	6.46	12636	Sage - Fire Station
931	0126	Big Bear-01	6.46	23542	San Bernardino - E & Hospitality
932	0126	Big Bear-01	6.46	12202	San Jacinto - Valley Cemetery
934	0126	Big Bear-01	6.46	12206	Silent Valley - Poppet Flat
935	0126	Big Bear-01	6.46	12630	Snow Creek
938	0126	Big Bear-01	6.46	13199	Winchester Bergman Ran
939	0126	Big Bear-01	6.46	23573	Wrightwood - Nielson Ranch
942	0127	Northridge-01	6.69	24461	Alhambra - Fremont School
943	0127	Northridge-01	6.69	25169	Anacapa Island
944	0127	Northridge-01	6.69	90088	Anaheim - W Ball Rd
945	0127	Northridge-01	6.69	24576	Anaverde Valley - City R
946	0127	Northridge-01	6.69	24310	Antelope Buttes
947	0127	Northridge-01	6.69	90099	Arcadia - Arcadia Av
948	0127	Northridge-01	6.69	90093	Arcadia - Campus Dr
949	0127	Northridge-01	6.69	24087	Arleta - Nordhoff Fire Sta
950	0127	Northridge-01	6.69	90069	Baldwin Park - N Holly
951	0127	Northridge-01	6.69	90094	Bell Gardens - Jaboneria
952	0127	Northridge-01	6.69	90014	Beverly Hills - 12520 Mulhol
953	0127	Northridge-01	6.69	90013	Beverly Hills - 14145 Mulhol
954	0127	Northridge-01	6.69	90061	Big Tujunga, Angeles Nat F
955	0127	Northridge-01	6.69	90087	Brea - S Flower Av
956	0127	Northridge-01	6.69	90086	Buena Park - La Palma
957	0127	Northridge-01	6.69	90059	Burbank - Howard Rd.
958	0127	Northridge-01	6.69	25282	Camarillo
959	0127	Northridge-01	6.69	90053	Canoga Park - Topanga Can
960	0127	Northridge-01	6.69	90057	Canyon Country - W Lost Cany
961	0127	Northridge-01	6.69	90040	Carson - Catskill Ave
962	0127	Northridge-01	6.69	90081	Carson - Water St
963	0127	Northridge-01	6.69	24278	Castaic - Old Ridge Route
964	0127	Northridge-01	6.69	90078	Compton - Castlegate St
965	0127	Northridge-01	6.69	90068	Covina - S Grand Ave

RSN	EQID	Earthquake	M	Station No.	Station
966	0127	Northridge-01	6.69	90070	Covina - W Badillo
967	0127	Northridge-01	6.69	90079	Downey - Birchdale
968	0127	Northridge-01	6.69	14368	Downey - Co Maint Bldg
969	0127	Northridge-01	6.69	90067	Duarte - Mel Canyon Rd.
970	0127	Northridge-01	6.69	90066	El Monte - Fairview Av
971	0127	Northridge-01	6.69	24575	Elizabeth Lake
973	0127	Northridge-01	6.69	90085	Garden Grove - Santa Rita
974	0127	Northridge-01	6.69	90063	Glendale - Las Palmas
975	0127	Northridge-01	6.69	90065	Glendora - N Oakbank
976	0127	Northridge-01	6.69	90073	Hacienda Heights - Colima
978	0127	Northridge-01	6.69	90018	Hollywood - Willoughby Ave
979	0127	Northridge-01	6.69	90083	Huntington Bch - Waikiki
981	0127	Northridge-01	6.69	14196	Inglewood - Union Oil
983	0127	Northridge-01	6.69	655	Jensen Filter Plant Generator
984	0127	Northridge-01	6.69	14403	LA - 116th St School
985	0127	Northridge-01	6.69	24157	LA - Baldwin Hills
986	0127	Northridge-01	6.69	638	LA - Brentwood VA Hospital
987	0127	Northridge-01	6.69	90054	LA - Centinela St
988	0127	Northridge-01	6.69	24389	LA - Century City CC North
989	0127	Northridge-01	6.69	90015	LA - Chalon Rd
990	0127	Northridge-01	6.69	24592	LA - City Terrace
991	0127	Northridge-01	6.69	90033	LA - Cypress Ave
993	0127	Northridge-01	6.69	90034	LA - Fletcher Dr
994	0127	Northridge-01	6.69	141	LA - Griffith Park Observatory
995	0127	Northridge-01	6.69	24303	LA - Hollywood Stor FF
996	0127	Northridge-01	6.69	90016	LA - N Faring Rd
997	0127	Northridge-01	6.69	90032	LA - N Figueroa St
998	0127	Northridge-01	6.69	90021	LA - N Westmoreland
999	0127	Northridge-01	6.69	24400	LA - Obregon Park
1000	0127	Northridge-01	6.69	24612	LA - Pico & Sentous
1001	0127	Northridge-01	6.69	90022	LA - S Grand Ave
1003	0127	Northridge-01	6.69	90091	LA - Saturn St
1004	0127	Northridge-01	6.69	637	LA - Sepulveda VA Hospital
1005	0127	Northridge-01	6.69	24611	LA - Temple & Hope
1006	0127	Northridge-01	6.69	24688	LA - UCLA Grounds
1007	0127	Northridge-01	6.69	24605	LA - Univ. Hospital
1008	0127	Northridge-01	6.69	90020	LA - W 15th St
1009	0127	Northridge-01	6.69	5082	LA - Wadsworth VA Hospital North
1010	0127	Northridge-01	6.69	5082	LA - Wadsworth VA Hospital South
1011	0127	Northridge-01	6.69	90017	LA - Wonderland Ave
1012	0127	Northridge-01	6.69	99999	LA 00
1013	0127	Northridge-01	6.69	0	LA Dam
1014	0127	Northridge-01	6.69	14560	LB - City Hall
1015	0127	Northridge-01	6.69	14242	LB - Rancho Los Cerritos
1016	0127	Northridge-01	6.69	90060	La Crescenta - New York
1017	0127	Northridge-01	6.69	90074	La Habra - Briarcliff
1018	0127	Northridge-01	6.69	90072	La Puente - Rimgrove Av
1019	0127	Northridge-01	6.69	24271	Lake Hughes #1
1020	0127	Northridge-01	6.69	24607	Lake Hughes #12A
1021	0127	Northridge-01	6.69	24469	Lake Hughes #4 - Camp Mend
1022	0127	Northridge-01	6.69	24523	Lake Hughes #4B - Camp Mend
1023	0127	Northridge-01	6.69	127	Lake Hughes #9
1024	0127	Northridge-01	6.69	90084	Lakewood - Del Amo Blvd
1025	0127	Northridge-01	6.69	24475	Lancaster - Fox Airfield Grnd
1026	0127	Northridge-01	6.69	90045	Lawndale - Osage Ave

RSN	EQID	Earthquake	M	Station No.	Station
1027	0127	Northridge-01	6.69	24305	Leona Valley #1
1028	0127	Northridge-01	6.69	24306	Leona Valley #2
1029	0127	Northridge-01	6.69	24307	Leona Valley #3
1030	0127	Northridge-01	6.69	24308	Leona Valley #4
1031	0127	Northridge-01	6.69	24055	Leona Valley #5 - Ritter
1032	0127	Northridge-01	6.69	24309	Leona Valley #6
1033	0127	Northridge-01	6.69	23595	Littlerock - Brainard Can
1034	0127	Northridge-01	6.69	24396	Malibu - Point Dume Sch
1035	0127	Northridge-01	6.69	90046	Manhattan Beach - Manhattan
1038	0127	Northridge-01	6.69	90011	Montebello - Bluff Rd.
1039	0127	Northridge-01	6.69	24283	Moorpark - Fire Sta
1041	0127	Northridge-01	6.69	24399	Mt Wilson - CIT Seis Sta
1042	0127	Northridge-01	6.69	90009	N Hollywood - Coldwater Can
1043	0127	Northridge-01	6.69	24586	Neenach - Sacatara Ck
1044	0127	Northridge-01	6.69	24279	Newhall - Fire Sta
1045	0127	Northridge-01	6.69	90056	Newhall - W Pico Canyon Rd.
1048	0127	Northridge-01	6.69	90003	Northridge - 17645 Saticoy St
1049	0127	Northridge-01	6.69	90049	Pacific Palisades - Sunset
1050	0127	Northridge-01	6.69	24207	Pacoima Dam (downstr)
1051	0127	Northridge-01	6.69	24207	Pacoima Dam (upper left)
1052	0127	Northridge-01	6.69	24088	Pacoima Kagel Canyon
1053	0127	Northridge-01	6.69	24521	Palmdale - Hwy 14 & Palmdale
1054	0127	Northridge-01	6.69	99999	Pardee - SCE
1055	0127	Northridge-01	6.69	90095	Pasadena - N Sierra Madre
1057	0127	Northridge-01	6.69	90047	Playa Del Rey - Saran
1058	0127	Northridge-01	6.69	25148	Point Mugu - Laguna Peak
1059	0127	Northridge-01	6.69	25281	Port Hueneme - Naval Lab.
1061	0127	Northridge-01	6.69	14404	Rancho Palos Verdes - Hawth
1062	0127	Northridge-01	6.69	90044	Rancho Palos Verdes - Luconia
1063	0127	Northridge-01	6.69	77	Rinaldi Receiving Sta
1065	0127	Northridge-01	6.69	14405	Rolling Hills Est-Rancho Vista
1066	0127	Northridge-01	6.69	24092	Rosamond - Airport
1070	0127	Northridge-01	6.69	90019	San Gabriel - E Grand Ave
1072	0127	Northridge-01	6.69	24401	San Marino - SW Academy
1073	0127	Northridge-01	6.69	14159	San Pedro - Palos Verdes
1074	0127	Northridge-01	6.69	24644	Sandberg - Bald Mtn
1076	0127	Northridge-01	6.69	90077	Santa Fe Springs - E.Joslin
1077	0127	Northridge-01	6.69	24538	Santa Monica City Hall
1078	0127	Northridge-01	6.69	5108	Santa Susana Ground
1079	0127	Northridge-01	6.69	14578	Seal Beach - Office Bldg
1080	0127	Northridge-01	6.69	90055	Simi Valley - Katherine Rd
1082	0127	Northridge-01	6.69	90006	Sun Valley - Roscoe Blvd
1083	0127	Northridge-01	6.69	90058	Sunland - Mt Gleason Ave
1084	0127	Northridge-01	6.69	74	Sylmar - Converter Sta
1085	0127	Northridge-01	6.69	75	Sylmar - Converter Sta East
1086	0127	Northridge-01	6.69	24514	Sylmar - Olive View Med FF
1087	0127	Northridge-01	6.69	24436	Tarzana - Cedar Hill A
1088	0127	Northridge-01	6.69	90082	Terminal Island - S Seaside
1089	0127	Northridge-01	6.69	5081	Topanga - Fire Sta
1091	0127	Northridge-01	6.69	24047	Vasquez Rocks Park
1092	0127	Northridge-01	6.69	25340	Ventura - Harbor & California
1094	0127	Northridge-01	6.69	90071	West Covina - S Orange Ave
1095	0127	Northridge-01	6.69	90075	Whittier - S. Alta Dr
1096	0127	Northridge-01	6.69	23590	Wrightwood - Jackson Flat
3549	0127	Northridge-01	6.69	5080	Monte Nido Fire Station

RSN	EQID	Earthquake	M	Station No.	Station
1099	0128	Double Springs	5.9	65398	Woodfords
1100	0129	Kobe, Japan	6.9	99999	Abeno
1101	0129	Kobe, Japan	6.9	99999	Amagasaki
1102	0129	Kobe, Japan	6.9	99999	Chihaya
1104	0129	Kobe, Japan	6.9	99999	Fukushima
1106	0129	Kobe, Japan	6.9	99999	KJMA
1107	0129	Kobe, Japan	6.9	99999	Kakogawa
1108	0129	Kobe, Japan	6.9	99999	Kobe University
1110	0129	Kobe, Japan	6.9	99999	Morigawachi
1111	0129	Kobe, Japan	6.9	99999	Nishi-Akashi
1113	0129	Kobe, Japan	6.9	99999	OSAJ
1114	0129	Kobe, Japan	6.9	99999	Port Island (0 m)
1115	0129	Kobe, Japan	6.9	99999	Sakai
1116	0129	Kobe, Japan	6.9	99999	Shin-Osaka
1118	0129	Kobe, Japan	6.9	99999	Tadoka
1119	0129	Kobe, Japan	6.9	99999	Takarazuka
1120	0129	Kobe, Japan	6.9	99999	Takatori
1121	0129	Kobe, Japan	6.9	99999	Yae
1126	0130	Kozani, Greece-01	6.4	99999	Kozani
1129	0131	Kozani, Greece-02	5.1	99999	Chromio Anapsiktirio
1131	0132	Kozani, Greece-03	5.3	99999	Chromio Anapsiktirio
1135	0133	Kozani, Greece-04	5.1	99999	Karpero
1139	0134	Dinar, Turkey	6.4	99999	Cardak
1141	0134	Dinar, Turkey	6.4	99999	Dinar
1147	0136	Kocaeli, Turkey	7.51	99999	Ambarli
1148	0136	Kocaeli, Turkey	7.51	99999	Arcelik
1149	0136	Kocaeli, Turkey	7.51	99999	Atakoy
1154	0136	Kocaeli, Turkey	7.51	99999	Bursa Sivil
1155	0136	Kocaeli, Turkey	7.51	99999	Bursa Tofas
1157	0136	Kocaeli, Turkey	7.51	99999	Cekmece
1158	0136	Kocaeli, Turkey	7.51	99999	Duzce
1160	0136	Kocaeli, Turkey	7.51	99999	Fatih
1162	0136	Kocaeli, Turkey	7.51	99999	Goynuk
1163	0136	Kocaeli, Turkey	7.51	99999	Hava Alani
1164	0136	Kocaeli, Turkey	7.51	99999	Istanbul
1165	0136	Kocaeli, Turkey	7.51	99999	Izmit
1166	0136	Kocaeli, Turkey	7.51	99999	Iznik
1169	0136	Kocaeli, Turkey	7.51	99999	Maslak
1170	0136	Kocaeli, Turkey	7.51	99999	Mecidiyekoy
1176	0136	Kocaeli, Turkey	7.51	99999	Yarimca
1177	0136	Kocaeli, Turkey	7.51	99999	Zeytinburnu
1180	0137	Chi-Chi, Taiwan	7.62	99999	CHY002
1181	0137	Chi-Chi, Taiwan	7.62	99999	CHY004
1182	0137	Chi-Chi, Taiwan	7.62	99999	CHY006
1183	0137	Chi-Chi, Taiwan	7.62	99999	CHY008
1184	0137	Chi-Chi, Taiwan	7.62	99999	CHY010
1185	0137	Chi-Chi, Taiwan	7.62	99999	CHY012
1186	0137	Chi-Chi, Taiwan	7.62	99999	CHY014
1187	0137	Chi-Chi, Taiwan	7.62	99999	CHY015
1188	0137	Chi-Chi, Taiwan	7.62	99999	CHY016
1189	0137	Chi-Chi, Taiwan	7.62	99999	CHY017
1190	0137	Chi-Chi, Taiwan	7.62	99999	CHY019
1191	0137	Chi-Chi, Taiwan	7.62	99999	CHY022
1193	0137	Chi-Chi, Taiwan	7.62	99999	CHY024
1194	0137	Chi-Chi, Taiwan	7.62	99999	CHY025

RSN	EQID	Earthquake	M	Station No.	Station
1195	0137	Chi-Chi, Taiwan	7.62	99999	CHY026
1196	0137	Chi-Chi, Taiwan	7.62	99999	CHY027
1197	0137	Chi-Chi, Taiwan	7.62	99999	CHY028
1198	0137	Chi-Chi, Taiwan	7.62	99999	CHY029
1199	0137	Chi-Chi, Taiwan	7.62	99999	CHY032
1200	0137	Chi-Chi, Taiwan	7.62	99999	CHY033
1201	0137	Chi-Chi, Taiwan	7.62	99999	CHY034
1202	0137	Chi-Chi, Taiwan	7.62	99999	CHY035
1203	0137	Chi-Chi, Taiwan	7.62	99999	CHY036
1204	0137	Chi-Chi, Taiwan	7.62	99999	CHY039
1205	0137	Chi-Chi, Taiwan	7.62	99999	CHY041
1206	0137	Chi-Chi, Taiwan	7.62	99999	CHY042
1207	0137	Chi-Chi, Taiwan	7.62	99999	CHY044
1208	0137	Chi-Chi, Taiwan	7.62	99999	CHY046
1209	0137	Chi-Chi, Taiwan	7.62	99999	CHY047
1210	0137	Chi-Chi, Taiwan	7.62	99999	CHY050
1211	0137	Chi-Chi, Taiwan	7.62	99999	CHY052
1212	0137	Chi-Chi, Taiwan	7.62	99999	CHY054
1213	0137	Chi-Chi, Taiwan	7.62	99999	CHY055
1214	0137	Chi-Chi, Taiwan	7.62	99999	CHY057
1215	0137	Chi-Chi, Taiwan	7.62	99999	CHY058
1217	0137	Chi-Chi, Taiwan	7.62	99999	CHY060
1218	0137	Chi-Chi, Taiwan	7.62	99999	CHY061
1227	0137	Chi-Chi, Taiwan	7.62	99999	CHY074
1228	0137	Chi-Chi, Taiwan	7.62	99999	CHY076
1230	0137	Chi-Chi, Taiwan	7.62	99999	CHY079
1231	0137	Chi-Chi, Taiwan	7.62	99999	CHY080
1232	0137	Chi-Chi, Taiwan	7.62	99999	CHY081
1233	0137	Chi-Chi, Taiwan	7.62	99999	CHY082
1234	0137	Chi-Chi, Taiwan	7.62	99999	CHY086
1235	0137	Chi-Chi, Taiwan	7.62	99999	CHY087
1236	0137	Chi-Chi, Taiwan	7.62	99999	CHY088
1237	0137	Chi-Chi, Taiwan	7.62	99999	CHY090
1238	0137	Chi-Chi, Taiwan	7.62	99999	CHY092
1239	0137	Chi-Chi, Taiwan	7.62	99999	CHY093
1240	0137	Chi-Chi, Taiwan	7.62	99999	CHY094
1242	0137	Chi-Chi, Taiwan	7.62	99999	CHY099
1243	0137	Chi-Chi, Taiwan	7.62	99999	CHY100
1244	0137	Chi-Chi, Taiwan	7.62	99999	CHY101
1245	0137	Chi-Chi, Taiwan	7.62	99999	CHY102
1246	0137	Chi-Chi, Taiwan	7.62	99999	CHY104
1247	0137	Chi-Chi, Taiwan	7.62	99999	CHY107
1248	0137	Chi-Chi, Taiwan	7.62	9999917	CHY109
1256	0137	Chi-Chi, Taiwan	7.62	99999	HWA002
1257	0137	Chi-Chi, Taiwan	7.62	99999	HWA003
1258	0137	Chi-Chi, Taiwan	7.62	99999	HWA005
1259	0137	Chi-Chi, Taiwan	7.62	99999	HWA006
1260	0137	Chi-Chi, Taiwan	7.62	99999	HWA007
1261	0137	Chi-Chi, Taiwan	7.62	99999	HWA009
1262	0137	Chi-Chi, Taiwan	7.62	99999	HWA011
1263	0137	Chi-Chi, Taiwan	7.62	99999	HWA012
1264	0137	Chi-Chi, Taiwan	7.62	99999	HWA013
1265	0137	Chi-Chi, Taiwan	7.62	99999	HWA014
1266	0137	Chi-Chi, Taiwan	7.62	99999	HWA015
1267	0137	Chi-Chi, Taiwan	7.62	99999	HWA016

RSN	EQID	Earthquake	M	Station No.	Station
1268	0137	Chi-Chi, Taiwan	7.62	99999	HWA017
1269	0137	Chi-Chi, Taiwan	7.62	99999	HWA019
1270	0137	Chi-Chi, Taiwan	7.62	99999	HWA020
1271	0137	Chi-Chi, Taiwan	7.62	99999	HWA022
1272	0137	Chi-Chi, Taiwan	7.62	99999	HWA023
1273	0137	Chi-Chi, Taiwan	7.62	99999	HWA024
1274	0137	Chi-Chi, Taiwan	7.62	99999	HWA025
1275	0137	Chi-Chi, Taiwan	7.62	99999	HWA026
1276	0137	Chi-Chi, Taiwan	7.62	99999	HWA027
1277	0137	Chi-Chi, Taiwan	7.62	99999	HWA028
1278	0137	Chi-Chi, Taiwan	7.62	99999	HWA029
1279	0137	Chi-Chi, Taiwan	7.62	99999	HWA030
1280	0137	Chi-Chi, Taiwan	7.62	99999	HWA031
1281	0137	Chi-Chi, Taiwan	7.62	99999	HWA032
1282	0137	Chi-Chi, Taiwan	7.62	99999	HWA033
1283	0137	Chi-Chi, Taiwan	7.62	99999	HWA034
1284	0137	Chi-Chi, Taiwan	7.62	99999	HWA035
1285	0137	Chi-Chi, Taiwan	7.62	99999	HWA036
1286	0137	Chi-Chi, Taiwan	7.62	99999	HWA037
1287	0137	Chi-Chi, Taiwan	7.62	99999	HWA038
1288	0137	Chi-Chi, Taiwan	7.62	99999	HWA039
1289	0137	Chi-Chi, Taiwan	7.62	99999	HWA041
1290	0137	Chi-Chi, Taiwan	7.62	99999	HWA043
1291	0137	Chi-Chi, Taiwan	7.62	99999	HWA044
1292	0137	Chi-Chi, Taiwan	7.62	99999	HWA045
1293	0137	Chi-Chi, Taiwan	7.62	99999	HWA046
1294	0137	Chi-Chi, Taiwan	7.62	99999	HWA048
1295	0137	Chi-Chi, Taiwan	7.62	99999	HWA049
1296	0137	Chi-Chi, Taiwan	7.62	99999	HWA050
1297	0137	Chi-Chi, Taiwan	7.62	99999	HWA051
1300	0137	Chi-Chi, Taiwan	7.62	99999	HWA055
1301	0137	Chi-Chi, Taiwan	7.62	99999	HWA056
1302	0137	Chi-Chi, Taiwan	7.62	99999	HWA057
1303	0137	Chi-Chi, Taiwan	7.62	99999	HWA058
1304	0137	Chi-Chi, Taiwan	7.62	99999	HWA059
1305	0137	Chi-Chi, Taiwan	7.62	99999	HWA060
1322	0137	Chi-Chi, Taiwan	7.62	99999	ILA024
1338	0137	Chi-Chi, Taiwan	7.62	99999	ILA050
1347	0137	Chi-Chi, Taiwan	7.62	99999	ILA063
1350	0137	Chi-Chi, Taiwan	7.62	99999	ILA067
1351	0137	Chi-Chi, Taiwan	7.62	99999	KAU001
1375	0137	Chi-Chi, Taiwan	7.62	99999	KAU047
1377	0137	Chi-Chi, Taiwan	7.62	99999	KAU050
1380	0137	Chi-Chi, Taiwan	7.62	99999	KAU054
1471	0137	Chi-Chi, Taiwan	7.62	99999	TCU015
1472	0137	Chi-Chi, Taiwan	7.62	99999	TCU017
1473	0137	Chi-Chi, Taiwan	7.62	99999	TCU018
1475	0137	Chi-Chi, Taiwan	7.62	99999	TCU026
1476	0137	Chi-Chi, Taiwan	7.62	99999	TCU029
1477	0137	Chi-Chi, Taiwan	7.62	99999	TCU031
1478	0137	Chi-Chi, Taiwan	7.62	99999	TCU033
1479	0137	Chi-Chi, Taiwan	7.62	99999	TCU034
1480	0137	Chi-Chi, Taiwan	7.62	99999	TCU036
1481	0137	Chi-Chi, Taiwan	7.62	99999	TCU038
1482	0137	Chi-Chi, Taiwan	7.62	99999	TCU039

RSN	EQID	Earthquake	M	Station No.	Station
1483	0137	Chi-Chi, Taiwan	7.62	99999	TCU040
1484	0137	Chi-Chi, Taiwan	7.62	99999	TCU042
1486	0137	Chi-Chi, Taiwan	7.62	99999	TCU046
1488	0137	Chi-Chi, Taiwan	7.62	99999	TCU048
1489	0137	Chi-Chi, Taiwan	7.62	99999	TCU049
1490	0137	Chi-Chi, Taiwan	7.62	99999	TCU050
1491	0137	Chi-Chi, Taiwan	7.62	99999	TCU051
1492	0137	Chi-Chi, Taiwan	7.62	99999	TCU052
1493	0137	Chi-Chi, Taiwan	7.62	99999	TCU053
1494	0137	Chi-Chi, Taiwan	7.62	99999	TCU054
1495	0137	Chi-Chi, Taiwan	7.62	99999	TCU055
1496	0137	Chi-Chi, Taiwan	7.62	99999	TCU056
1497	0137	Chi-Chi, Taiwan	7.62	99999	TCU057
1498	0137	Chi-Chi, Taiwan	7.62	99999	TCU059
1499	0137	Chi-Chi, Taiwan	7.62	99999	TCU060
1500	0137	Chi-Chi, Taiwan	7.62	99999	TCU061
1501	0137	Chi-Chi, Taiwan	7.62	99999	TCU063
1502	0137	Chi-Chi, Taiwan	7.62	99999	TCU064
1503	0137	Chi-Chi, Taiwan	7.62	99999	TCU065
1504	0137	Chi-Chi, Taiwan	7.62	99999	TCU067
1505	0137	Chi-Chi, Taiwan	7.62	99999	TCU068
1506	0137	Chi-Chi, Taiwan	7.62	99999	TCU070
1507	0137	Chi-Chi, Taiwan	7.62	99999	TCU071
1508	0137	Chi-Chi, Taiwan	7.62	99999	TCU072
1509	0137	Chi-Chi, Taiwan	7.62	99999	TCU074
1510	0137	Chi-Chi, Taiwan	7.62	99999	TCU075
1511	0137	Chi-Chi, Taiwan	7.62	99999	TCU076
1512	0137	Chi-Chi, Taiwan	7.62	99999	TCU078
1513	0137	Chi-Chi, Taiwan	7.62	99999	TCU079
1515	0137	Chi-Chi, Taiwan	7.62	99999	TCU082
1517	0137	Chi-Chi, Taiwan	7.62	99999	TCU084
1518	0137	Chi-Chi, Taiwan	7.62	99999	TCU085
1519	0137	Chi-Chi, Taiwan	7.62	99999	TCU087
1520	0137	Chi-Chi, Taiwan	7.62	99999	TCU088
1521	0137	Chi-Chi, Taiwan	7.62	99999	TCU089
1523	0137	Chi-Chi, Taiwan	7.62	99999	TCU094
1525	0137	Chi-Chi, Taiwan	7.62	99999	TCU096
1526	0137	Chi-Chi, Taiwan	7.62	99999	TCU098
1527	0137	Chi-Chi, Taiwan	7.62	99999	TCU100
1528	0137	Chi-Chi, Taiwan	7.62	99999	TCU101
1529	0137	Chi-Chi, Taiwan	7.62	99999	TCU102
1530	0137	Chi-Chi, Taiwan	7.62	99999	TCU103
1531	0137	Chi-Chi, Taiwan	7.62	99999	TCU104
1532	0137	Chi-Chi, Taiwan	7.62	99999	TCU105
1533	0137	Chi-Chi, Taiwan	7.62	99999	TCU106
1534	0137	Chi-Chi, Taiwan	7.62	99999	TCU107
1535	0137	Chi-Chi, Taiwan	7.62	99999	TCU109
1536	0137	Chi-Chi, Taiwan	7.62	99999	TCU110
1537	0137	Chi-Chi, Taiwan	7.62	99999	TCU111
1538	0137	Chi-Chi, Taiwan	7.62	99999	TCU112
1539	0137	Chi-Chi, Taiwan	7.62	99999	TCU113
1540	0137	Chi-Chi, Taiwan	7.62	99999	TCU115
1541	0137	Chi-Chi, Taiwan	7.62	99999	TCU116
1542	0137	Chi-Chi, Taiwan	7.62	99999	TCU117
1543	0137	Chi-Chi, Taiwan	7.62	99999	TCU118

RSN	EQID	Earthquake	M	Station No.	Station
1544	0137	Chi-Chi, Taiwan	7.62	99999	TCU119
1545	0137	Chi-Chi, Taiwan	7.62	99999	TCU120
1546	0137	Chi-Chi, Taiwan	7.62	99999	TCU122
1547	0137	Chi-Chi, Taiwan	7.62	99999	TCU123
1548	0137	Chi-Chi, Taiwan	7.62	99999	TCU128
1550	0137	Chi-Chi, Taiwan	7.62	99999	TCU136
1551	0137	Chi-Chi, Taiwan	7.62	99999	TCU138
1552	0137	Chi-Chi, Taiwan	7.62	99999	TCU140
1553	0137	Chi-Chi, Taiwan	7.62	99999	TCU141
1554	0137	Chi-Chi, Taiwan	7.62	99999	TCU145
1557	0137	Chi-Chi, Taiwan	7.62	99999	TTN001
1558	0137	Chi-Chi, Taiwan	7.62	99999	TTN002
1560	0137	Chi-Chi, Taiwan	7.62	99999	TTN004
1569	0137	Chi-Chi, Taiwan	7.62	99999	TTN014
1573	0137	Chi-Chi, Taiwan	7.62	99999	TTN020
1574	0137	Chi-Chi, Taiwan	7.62	99999	TTN022
1575	0137	Chi-Chi, Taiwan	7.62	99999	TTN023
1576	0137	Chi-Chi, Taiwan	7.62	99999	TTN024
1577	0137	Chi-Chi, Taiwan	7.62	99999	TTN025
1581	0137	Chi-Chi, Taiwan	7.62	99999	TTN031
1582	0137	Chi-Chi, Taiwan	7.62	99999	TTN032
1583	0137	Chi-Chi, Taiwan	7.62	99999	TTN033
1585	0137	Chi-Chi, Taiwan	7.62	99999	TTN040
1586	0137	Chi-Chi, Taiwan	7.62	99999	TTN041
1587	0137	Chi-Chi, Taiwan	7.62	99999	TTN042
1588	0137	Chi-Chi, Taiwan	7.62	99999	TTN044
1589	0137	Chi-Chi, Taiwan	7.62	99999	TTN045
1590	0137	Chi-Chi, Taiwan	7.62	99999	TTN046
1594	0137	Chi-Chi, Taiwan	7.62	99999	TTN051
1602	0138	Duzce, Turkey	7.14	99999	Bolu
1605	0138	Duzce, Turkey	7.14	99999	Duzce
1611	0138	Duzce, Turkey	7.14	1058	Lamont 1058
1612	0138	Duzce, Turkey	7.14	1059	Lamont 1059
1613	0138	Duzce, Turkey	7.14	1060	Lamont 1060
1614	0138	Duzce, Turkey	7.14	1061	Lamont 1061
1615	0138	Duzce, Turkey	7.14	1062	Lamont 1062
1616	0138	Duzce, Turkey	7.14	362	Lamont 362
1617	0138	Duzce, Turkey	7.14	375	Lamont 375
1618	0138	Duzce, Turkey	7.14	531	Lamont 531
1619	0138	Duzce, Turkey	7.14	99999	Mudurnu
1620	0138	Duzce, Turkey	7.14	99999	Sakarya
1622	0139	Stone Canyon	4.81	1210	Bear Valley #1, Fire Station
1623	0139	Stone Canyon	4.81	1211	Melendy Ranch
1624	0139	Stone Canyon	4.81	1343	Stone Canyon Geophys Obs
1626	0140	Sitka, Alaska	7.68	2714	Sitka Observatory
1627	0141	Caldiran, Turkey	7.21	37	Maku
1631	0143	Upland	5.63	23525	Pomona - 4th & Locust FF
1632	0143	Upland	5.63	23497	Rancho Cucamonga - FF
1633	0144	Manjil, Iran	7.37	99999	Abbar
1636	0144	Manjil, Iran	7.37	99999	Qazvin
1637	0144	Manjil, Iran	7.37	99999	Rudsar
1641	0145	Sierra Madre	5.61	24402	Altadena - Eaton Canyon
1642	0145	Sierra Madre	5.61	23210	Cogswell Dam - Right Abutment
1643	0145	Sierra Madre	5.61	24592	LA - City Terrace
1644	0145	Sierra Madre	5.61	24400	LA - Obregon Park

RSN	EQID	Earthquake	M	Station No.	Station
1645	0145	Sierra Madre	5.61	24399	Mt Wilson - CIT Seis Sta
1646	0145	Sierra Madre	5.61	5296	Pasadena - USGS/NSMP Office
1647	0145	Sierra Madre	5.61	24401	San Marino - SW Academy
1648	0145	Sierra Madre	5.61	24436	Tarzana - Cedar Hill A
1649	0145	Sierra Madre	5.61	24047	Vasquez Rocks Park
1650	0147	Northridge-02	6.05	24576	Anaverde Valley - City R
1651	0147	Northridge-02	6.05	24087	Arleta - Nordhoff Fire Sta
1652	0147	Northridge-02	6.05	24278	Castaic - Old Ridge Route
1653	0147	Northridge-02	6.05	14368	Downey - Co Maint Bldg
1654	0147	Northridge-02	6.05	24575	Elizabeth Lake
1655	0147	Northridge-02	6.05	14196	Inglewood - Union Oil
1656	0147	Northridge-02	6.05	14403	LA - 116th St School
1657	0147	Northridge-02	6.05	24157	LA - Baldwin Hills
1658	0147	Northridge-02	6.05	24389	LA - Century City CC North
1659	0147	Northridge-02	6.05	24592	LA - City Terrace
1660	0147	Northridge-02	6.05	24303	LA - Hollywood Stor FF
1661	0147	Northridge-02	6.05	24400	LA - Obregon Park
1662	0147	Northridge-02	6.05	24611	LA - Temple & Hope
1663	0147	Northridge-02	6.05	24605	LA - Univ. Hospital
1664	0147	Northridge-02	6.05	24607	Lake Hughes #12A
1665	0147	Northridge-02	6.05	24279	Newhall - Fire Sta
1666	0147	Northridge-02	6.05	24088	Pacoima Kagel Canyon
1667	0147	Northridge-02	6.05	24521	Palmdale - Hwy 14 & Palmdale
1668	0148	Northridge-03	5.2	24278	Castaic - Old Ridge Route
1669	0148	Northridge-03	5.2	24575	Elizabeth Lake
1670	0148	Northridge-03	5.2	24279	Newhall - Fire Sta
1671	0148	Northridge-03	5.2	24088	Pacoima Kagel Canyon
1672	0148	Northridge-03	5.2	24644	Sandberg - Bald Mtn
1673	0148	Northridge-03	5.2	24538	Santa Monica City Hall
1674	0148	Northridge-03	5.2	24436	Tarzana - Cedar Hill A
1675	0149	Northridge-04	5.93	24576	Anaverde Valley - City R
1676	0149	Northridge-04	5.93	24278	Castaic - Old Ridge Route
1677	0149	Northridge-04	5.93	24575	Elizabeth Lake
1678	0149	Northridge-04	5.93	24592	LA - City Terrace
1679	0149	Northridge-04	5.93	24611	LA - Temple & Hope
1680	0149	Northridge-04	5.93	24605	LA - Univ. Hospital
1681	0149	Northridge-04	5.93	24283	Moorpark - Fire Sta
1682	0150	Northridge-05	5.13	24576	Anaverde Valley - City R
1683	0150	Northridge-05	5.13	24278	Castaic - Old Ridge Route
1684	0150	Northridge-05	5.13	24575	Elizabeth Lake
1686	0150	Northridge-05	5.13	655	Jensen Filter Plant Generator
1687	0150	Northridge-05	5.13	24592	LA - City Terrace
1688	0150	Northridge-05	5.13	24283	Moorpark - Fire Sta
1689	0150	Northridge-05	5.13	24088	Pacoima Kagel Canyon
1690	0150	Northridge-05	5.13	24763	Sylmar - County Hospital Grounds
1692	0151	Northridge-06	5.28	24576	Anaverde Valley - City R
1693	0151	Northridge-06	5.28	24087	Arleta - Nordhoff Fire Sta
1694	0151	Northridge-06	5.28	90014	Beverly Hills - 12520 Mulhol
1695	0151	Northridge-06	5.28	90061	Big Tujunga, Angeles Nat F
1696	0151	Northridge-06	5.28	90059	Burbank - Howard Rd.
1697	0151	Northridge-06	5.28	90012	Burbank - N Buena Vista
1698	0151	Northridge-06	5.28	90052	Calabasas - N Las Virg
1699	0151	Northridge-06	5.28	24278	Castaic - Old Ridge Route
1700	0151	Northridge-06	5.28	24575	Elizabeth Lake
1701	0151	Northridge-06	5.28	90018	Hollywood - Willoughby Ave

RSN	EQID	Earthquake	M	Station No.	Station
1702	0151	Northridge-06	5.28	14196	Inglewood - Union Oil
1704	0151	Northridge-06	5.28	655	Jensen Filter Plant Generator
1705	0151	Northridge-06	5.28	14403	LA - 116th St School
1706	0151	Northridge-06	5.28	24157	LA - Baldwin Hills
1707	0151	Northridge-06	5.28	24389	LA - Century City CC North
1708	0151	Northridge-06	5.28	24592	LA - City Terrace
1709	0151	Northridge-06	5.28	141	LA - Griffith Park Observatory
1710	0151	Northridge-06	5.28	24303	LA - Hollywood Stor FF
1711	0151	Northridge-06	5.28	90016	LA - N Faring Rd
1712	0151	Northridge-06	5.28	24611	LA - Temple & Hope
1713	0151	Northridge-06	5.28	24605	LA - Univ. Hospital
1714	0151	Northridge-06	5.28	90023	LA - W 70th St
1715	0151	Northridge-06	5.28	90017	LA - Wonderland Ave
1716	0151	Northridge-06	5.28	90060	La Crescenta - New York
1717	0151	Northridge-06	5.28	24607	Lake Hughes #12A
1718	0151	Northridge-06	5.28	23595	Littlerock - Brainard Can
1719	0151	Northridge-06	5.28	24396	Malibu - Point Dume Sch
1720	0151	Northridge-06	5.28	90062	Mill Creek, Angeles Nat For
1721	0151	Northridge-06	5.28	24279	Newhall - Fire Sta
1722	0151	Northridge-06	5.28	90003	Northridge - 17645 Saticoy St
1723	0151	Northridge-06	5.28	24088	Pacoima Kagel Canyon
1724	0151	Northridge-06	5.28	24521	Palmdale - Hwy 14 & Palmdale
1725	0151	Northridge-06	5.28	90007	Panorama City - Roscoe
1726	0151	Northridge-06	5.28	5296	Pasadena - USGS/NSMP Office
1728	0151	Northridge-06	5.28	77	Rinaldi Receiving Sta
1729	0151	Northridge-06	5.28	24401	San Marino - SW Academy
1730	0151	Northridge-06	5.28	24538	Santa Monica City Hall
1731	0151	Northridge-06	5.28	14578	Seal Beach - Office Bldg
1732	0151	Northridge-06	5.28	90055	Simi Valley - Katherine Rd
1733	0151	Northridge-06	5.28	90006	Sun Valley - Roscoe Blvd
1734	0151	Northridge-06	5.28	90008	Sun Valley - Sunland
1735	0151	Northridge-06	5.28	90058	Sunland - Mt Gleason Ave
1736	0151	Northridge-06	5.28	74	Sylmar - Converter Sta
1737	0151	Northridge-06	5.28	75	Sylmar - Converter Sta East
1738	0151	Northridge-06	5.28	90001	Sylmar - Sayre St
1739	0151	Northridge-06	5.28	24436	Tarzana - Cedar Hill A
1740	0152	Little Skull Mtn,NV	5.65	99999	Station #1-Lathrop Wells
1741	0152	Little Skull Mtn,NV	5.65	99999	Station #2-NTS Control Pt. 1
1742	0152	Little Skull Mtn,NV	5.65	99999	Station #3-Beaty
1743	0152	Little Skull Mtn,NV	5.65	99999	Station #4-Pahrump 2
1744	0152	Little Skull Mtn,NV	5.65	99999	Station #5-Pahrump 1
1758	0157	San Juan Bautista	5.17	1656	Hollister Diff. Array
1762	0158	Hector Mine	7.13	21081	Amboy
1766	0158	Hector Mine	7.13	32075	Baker Fire Station
1768	0158	Hector Mine	7.13	23559	Barstow
1770	0158	Hector Mine	7.13	22791	Big Bear Lake - Fire Station
1776	0158	Hector Mine	7.13	12149	Desert Hot Springs
1783	0158	Hector Mine	7.13	24577	Fort Irwin
1785	0158	Hector Mine	7.13	5069	Fun Valley
1786	0158	Hector Mine	7.13	22T04	Heart Bar State Park
1787	0158	Hector Mine	7.13	99999	Hector
1794	0158	Hector Mine	7.13	22170	Joshua Tree
1795	0158	Hector Mine	7.13	12647	Joshua Tree N.M. - Keys View
1813	0158	Hector Mine	7.13	5071	Morongo Valley
1816	0158	Hector Mine	7.13	5295	North Palm Springs Fire Sta #36

RSN	EQID	Earthquake	M	Station No.	Station
1836	0158	Hector Mine	7.13	22161	Twentynine Palms
1838	0158	Hector Mine	7.13	5072	Whitewater Trout Farm
1845	0160	Yountville	5	1755	Alameda Fire Station #1
1846	0160	Yountville	5	1760	Benicia Fire Station #1
1849	0160	Yountville	5	1737	El Cerrito - Mira Vista Country
1851	0160	Yountville	5	1678	Golden Gate Bridge
1852	0160	Yountville	5	1590	Larkspur Ferry Terminal (FF)
1853	0160	Yountville	5	1765	Napa Fire Station #3
1854	0160	Yountville	5	1762	Novato Fire Station #1
1855	0160	Yountville	5	1751	Novato Fire Station #4
1856	0160	Yountville	5	1743	Petaluma Fire Station
1857	0160	Yountville	5	1768	Petaluma Fire Station #1
1858	0160	Yountville	5	1691	Pleasant Hill Fire Station #2
1860	0160	Yountville	5	1749	Richmond - Point Molate
1861	0160	Yountville	5	1722	Richmond Rod & Gun Club
1862	0160	Yountville	5	1735	San Francisco - 9th Circuit Crt
1863	0160	Yountville	5	1774	San Francisco - Fire Station #2
1865	0160	Yountville	5	1767	Santa Rosa Fire Station #1
1866	0160	Yountville	5	1761	Sonoma Fire Station #1
1867	0160	Yountville	5	1759	Vallejo Fire Station #1
1868	0161	Big Bear-02	4.53	23788	Colton - Hospital Complex FF
1869	0161	Big Bear-02	4.53	5341	Colton - Kaiser Medical Clinic
1870	0161	Big Bear-02	4.53	5265	Devore - Devore Water Company
1871	0161	Big Bear-02	4.53	5075	Forest Falls Post Office
1872	0161	Big Bear-02	4.53	23957	Helendale - Helendale & Vista
1873	0161	Big Bear-02	4.53	12331	Hemet Fire Station
1874	0161	Big Bear-02	4.53	23583	Hesperia - 4th & Palm
1875	0161	Big Bear-02	4.53	5161	Highland Fire Station
1876	0161	Big Bear-02	4.53	13924	Homeland - Hwy 74 & Sultanas
1879	0161	Big Bear-02	4.53	22959	Landers - Hwy 247 & Jesse
1881	0161	Big Bear-02	4.53	5409	Lytle Creek Fire Station
1882	0161	Big Bear-02	4.53	5162	Mentone Fire Station #9
1883	0161	Big Bear-02	4.53	5076	Mill Creek Ranger Station
1884	0161	Big Bear-02	4.53	13927	Moreno Valley - Alessandro&More
1885	0161	Big Bear-02	4.53	13925	Moreno Valley - Indian & Kennedy
1886	0161	Big Bear-02	4.53	5071	Morongo Valley
1887	0161	Big Bear-02	4.53	5295	North Palm Springs Fire Sta #36
1888	0161	Big Bear-02	4.53	23958	Pinon Hills - Hwy 138 & Mtn Road
1889	0161	Big Bear-02	4.53	5037	Reche Canyon - Olive Dell Ranch
1890	0161	Big Bear-02	4.53	13915	Riverside - I215 & 3rd
1891	0161	Big Bear-02	4.53	5331	San Bernardino - Del Rosa Wk Sta
1892	0161	Big Bear-02	4.53	23542	San Bernardino - E & Hospitality
1893	0161	Big Bear-02	4.53	5339	San Bernardino - Fire Sta. #10
1894	0161	Big Bear-02	4.53	5329	San Bernardino - Fire Sta. #11
1895	0161	Big Bear-02	4.53	5337	San Bernardino - Fire Sta. #4
1896	0161	Big Bear-02	4.53	5327	San Bernardino - Fire Sta. #7
1897	0161	Big Bear-02	4.53	5330	San Bernardino - Fire Sta. #9
1898	0161	Big Bear-02	4.53	5373	San Bernardino - Lincoln School
1899	0161	Big Bear-02	4.53	23898	San Bernardino - Medical Center
1900	0161	Big Bear-02	4.53	5328	San Bernardino - Mont. Mem Pk
1901	0161	Big Bear-02	4.53	23780	San Bernardino - Mtn Vw & Clstr
1902	0161	Big Bear-02	4.53	5336	San Bernardino - Serrano School
1903	0161	Big Bear-02	4.53	5300	Seven Oaks Dam Downstream Surf.
1904	0161	Big Bear-02	4.53	5300	Seven Oaks Dam Right Abt.
1905	0161	Big Bear-02	4.53	13930	Sun City - I215 & McCall Blvd

RSN	EQID	Earthquake	M	Station No.	Station
1907	0161	Big Bear-02	4.53	5072	Whitewater Trout Farm
1908	0161	Big Bear-02	4.53	5282	Wrightwood Post Office
1909	0161	Big Bear-02	4.53	22074	Yermo Fire Station
1910	0161	Big Bear-02	4.53	23920	Yucaipa Valley - Calimesa & Cnty
1912	0162	Mohawk Val, Portola	5.17	1133	Martis Creek Dam (Dwn Stream)
1913	0162	Mohawk Val, Portola	5.17	1133	Martis Creek Dam (Left Abtmnt)
1914	0162	Mohawk Val, Portola	5.17	1133	Martis Creek Dam (Right Abtmnt)
1918	0163	Anza-02	4.92	5044	Anza - Pinyon Flat
1919	0163	Anza-02	4.92	5222	Anza - Tripp Flats Training
1920	0163	Anza-02	4.92	5160	Anza Fire Station
1921	0163	Anza-02	4.92	12919	Beaumont - 6th & Maple
1923	0163	Anza-02	4.92	5220	Borrego Springs - Scripps Clinic
1924	0163	Anza-02	4.92	5073	Cabazon
1927	0163	Anza-02	4.92	12076	Coachella - 6th & Palm
1934	0163	Anza-02	4.92	5069	Fun Valley
1935	0163	Anza-02	4.92	12923	Hemet - Acacia & Stanford
1936	0163	Anza-02	4.92	13093	Hemet - Cawston & Devonshire
1937	0163	Anza-02	4.92	12331	Hemet Fire Station
1940	0163	Anza-02	4.92	13924	Homeland - Hwy 74 & Sultanas
1941	0163	Anza-02	4.92	5043	Hurkey Creek Park
1942	0163	Anza-02	4.92	12116	Idyllwild - Hwy 243 & Pine Crest
1943	0163	Anza-02	4.92	5232	Idyllwild - Keenwild Fire Sta.
1944	0163	Anza-02	4.92	5372	Idyllwild - Kenworthy Fire Sta.
1945	0163	Anza-02	4.92	12966	Indian Wells - Hwy111 & El Dorad
1946	0163	Anza-02	4.92	5294	Indio - Jackson Road
1948	0163	Anza-02	4.92	12951	La Quinta - Bermudas & Durango
1950	0163	Anza-02	4.92	5270	Mecca Fire Station
1951	0163	Anza-02	4.92	13929	Menifee Valley - Murrieta&Scott
1957	0163	Anza-02	4.92	5071	Morongo Valley
1958	0163	Anza-02	4.92	5223	Mountain Center - Pine Mtn Rnch
1960	0163	Anza-02	4.92	5295	North Palm Springs Fire Sta #36
1962	0163	Anza-02	4.92	5375	Ocotillo Wells - Veh. Rec. Area
1963	0163	Anza-02	4.92	12952	Palm Desert - Country Club & Por
1966	0163	Anza-02	4.92	12092	Radec - Sage & Cottonwood School
1967	0163	Anza-02	4.92	12953	Rancho Mirage - G Ford & B Hope
1974	0163	Anza-02	4.92	12636	Sage - Fire Station
1983	0163	Anza-02	4.92	5289	San Jacinto - MWD West Portal
1984	0163	Anza-02	4.92	12102	San Jacinto CDF Fire Station 25
1986	0163	Anza-02	4.92	13930	Sun City - I215 & McCall Blvd
1987	0163	Anza-02	4.92	13172	Temecula - 6th & Mercedes
1989	0163	Anza-02	4.92	5072	Whitewater Trout Farm
2003	0165	CA/Baja Border Area	5.31	5053	Calexico Fire Station
2005	0165	CA/Baja Border Area	5.31	464	El Centro - Meadows Union School
2006	0165	CA/Baja Border Area	5.31	412	El Centro Array #10
2007	0165	CA/Baja Border Area	5.31	5058	El Centro Array #11
2008	0165	CA/Baja Border Area	5.31	5028	El Centro Array #7
2009	0165	CA/Baja Border Area	5.31	5055	Holtville Post Office
2014	0166	Gilroy	4.9	1720	Cupertino - Sunnyvale Rod & Gun
2018	0166	Gilroy	4.9	57064	Fremont - Mission San Jose
2019	0166	Gilroy	4.9	47006	Gilroy - Gavilan Coll.
2020	0166	Gilroy	4.9	47381	Gilroy Array #3
2021	0166	Gilroy	4.9	57383	Gilroy Array #6
2024	0166	Gilroy	4.9	1797	Hollister - Airport Bldg #3
2026	0166	Gilroy	4.9	47524	Hollister - South & Pine
2027	0166	Gilroy	4.9	1697	Los Gatos - Los Altos Rod & Gun

RSN	EQID	Earthquake	M	Station No.	Station
2030	0166	Gilroy	4.9	1758	Morgan Hill - El Toro Fire Sta
2033	0166	Gilroy	4.9	47762	Salinas - County Hospital Gnds
2036	0166	Gilroy	4.9	57600	San Jose - Emory & Bellrose
2037	0166	Gilroy	4.9	57604	San Jose - S Clara Co Bldg Grnd
2038	0166	Gilroy	4.9	1742	San Jose - Weather Station
2039	0166	Gilroy	4.9	47126	San Juan Bautista, 24 Polk St
2040	0166	Gilroy	4.9	57748	Santa Clara - Hwy 237/Alviso OVP
2041	0166	Gilroy	4.9	48906	Santa Cruz - Co Office Bldg Gnds
2042	0166	Gilroy	4.9	1695	Sunnyvale - Colton Ave.
2044	0166	Gilroy	4.9	1684	Sunol - Ohlone Wilderness Reg Pk
2047	0167	Yorba Linda	4.265	13066	Anaheim - Brookhurst & Crescent
2048	0167	Yorba Linda	4.265	13068	Anaheim - Hwy 91 & Weir Cyn Rd
2049	0167	Yorba Linda	4.265	13849	Anaheim - Lakeview & Riverdale
2050	0167	Yorba Linda	4.265	13873	Brea - Central Ave Caltrans Yard
2051	0167	Yorba Linda	4.265	24941	City of Commerce - Whittier &
2052	0167	Yorba Linda	4.265	13099	Corona - 6th & Smith
2053	0167	Yorba Linda	4.265	13100	Corona - Green River & Cyn Crest
2054	0167	Yorba Linda	4.265	13878	Fullerton - CSU Fullerton Grnds
2055	0167	Yorba Linda	4.265	13880	Fullerton - Hermosa & Harbor
2056	0167	Yorba Linda	4.265	13879	Fullerton - Valencia&Brookhurst
2057	0167	Yorba Linda	4.265	13881	La Habra - La Habra&Monte Vista
2058	0167	Yorba Linda	4.265	13079	Riverside - Hwy 91 & Van Buren
2107	0169	Denali, Alaska	7.9	Carl	Carlo (temp)
2111	0169	Denali, Alaska	7.9	R109	R109 (temp)
2113	0169	Denali, Alaska	7.9	ps09	TAPS Pump Station #09
2114	0169	Denali, Alaska	7.9	ps10	TAPS Pump Station #10
2120	0170	Big Bear City	4.92	5073	Cabazon
2121	0170	Big Bear City	4.92	5341	Colton - Kaiser Medical Clinic
2122	0170	Big Bear City	4.92	5265	Devore - Devore Water Company
2123	0170	Big Bear City	4.92	5075	Forest Falls Post Office
2124	0170	Big Bear City	4.92	5161	Highland Fire Station
2129	0170	Big Bear City	4.92	5162	Mentone Fire Station #9
2130	0170	Big Bear City	4.92	5076	Mill Creek Ranger Station
2131	0170	Big Bear City	4.92	5071	Morongo Valley
2132	0170	Big Bear City	4.92	5295	North Palm Springs Fire Sta #36
2137	0170	Big Bear City	4.92	5245	San Bernardino - Co Service Bldg – Free field
2138	0170	Big Bear City	4.92	5331	San Bernardino - Del Rosa Wk Sta
2139	0170	Big Bear City	4.92	5339	San Bernardino - Fire Sta. #10
2140	0170	Big Bear City	4.92	5329	San Bernardino - Fire Sta. #11
2141	0170	Big Bear City	4.92	5337	San Bernardino - Fire Sta. #4
2142	0170	Big Bear City	4.92	5327	San Bernardino - Fire Sta. #7
2143	0170	Big Bear City	4.92	5330	San Bernardino - Fire Sta. #9
2144	0170	Big Bear City	4.92	5373	San Bernardino - Lincoln School
2145	0170	Big Bear City	4.92	5328	San Bernardino - Mont. Mem Pk
2146	0170	Big Bear City	4.92	5371	San Bernardino - N Verdemont Sch
2147	0170	Big Bear City	4.92	5336	San Bernardino - Serrano School
2148	0170	Big Bear City	4.92	5036	San Bernardino - Sycamore FS
2149	0170	Big Bear City	4.92	5300	Seven Oaks Dam Downstream Surf.
2150	0170	Big Bear City	4.92	5300	Seven Oaks Dam Right Abt.
2151	0170	Big Bear City	4.92	5435	Sky Valley - Fire Station #56
2154	0170	Big Bear City	4.92	5072	Whitewater Trout Farm
2159	0171	Chi-Chi, Taiwan-02	5.9	99999	CHY024
2160	0171	Chi-Chi, Taiwan-02	5.9	99999	CHY025

Appendix B: Estimation of Distance and Geometry Measures for Earthquakes without Finite Rupture Models

B.1 APPROACH

There are 110 earthquakes in the NGA data set that do not have finite fault models, and therefore have only epicentral and hypocentral distances listed in the flat file. Rupture distances and source-site geometry parameters were estimated for the recordings from these earthquakes by simulating 101 possible rupture planes for each earthquake, computing the distance measures for each site for each simulation, and then taking the median of these values for use in completing the metadata in the PEER-NGA database. The estimated parameters include R_{RUP}, R_{JB}, R_{SEIS}, R_{RMS}, the source-site angle θ_{SITE}, the hanging-wall and footwall indicators F_{HW} and F_{FW}, and the fault rupture width W and depth to top of rupture, Z_{TOR}.

B.2 SIMULATION PROCESS

The first step was to simulate the fault rupture dimensions. The rupture area, A, was simulated using the Wells and Coppersmith (1994) relationship for all fault types:

$$log(A) = -3.49 + 0.91\mathbf{M}, \quad \sigma_{log(Area)} = 0.24 \tag{B.1}$$

Figure B.1 shows the data for rupture area versus M for the finite rupture models in the PEER-NGA database. The black lines show a linear fit to the data (solid = mean, dashed = 90% confidence on mean). The blue line, from Wells and Coppersmith (1994), falls within the 90% confidence interval and provides a closer fit to the data for smaller-magnitude earthquakes of

primary interest in the simulation, as those earthquakes without finite fault models are principally of magnitude < **M** 6.

The aspect ratio of the rupture was then simulated using the relationship:

$$\log(AR) = (0.01752 - 0.00472F_{NM} - 0.01099F_{RV}) * (\mathbf{M} - 4)^{3.097} \quad \sigma_{\log(AR)} = 0.16 \quad \text{(B.2)}$$

where F_{NM} and F_{RV} are (0,1) dummy variables for normal and revere earthquakes, respectively. This relationship was defined by fitting the aspect ratio data for the PEER-NGA finite fault model data set (Fig. B.2). Correlation in the residuals between rupture area and aspect ratio was low (<0.3), and it was assumed that they were independent in the simulation.

Using the simulated values of A and AR, the rupture width W and rupture length L were computed assuming a rectangular fault rupture.

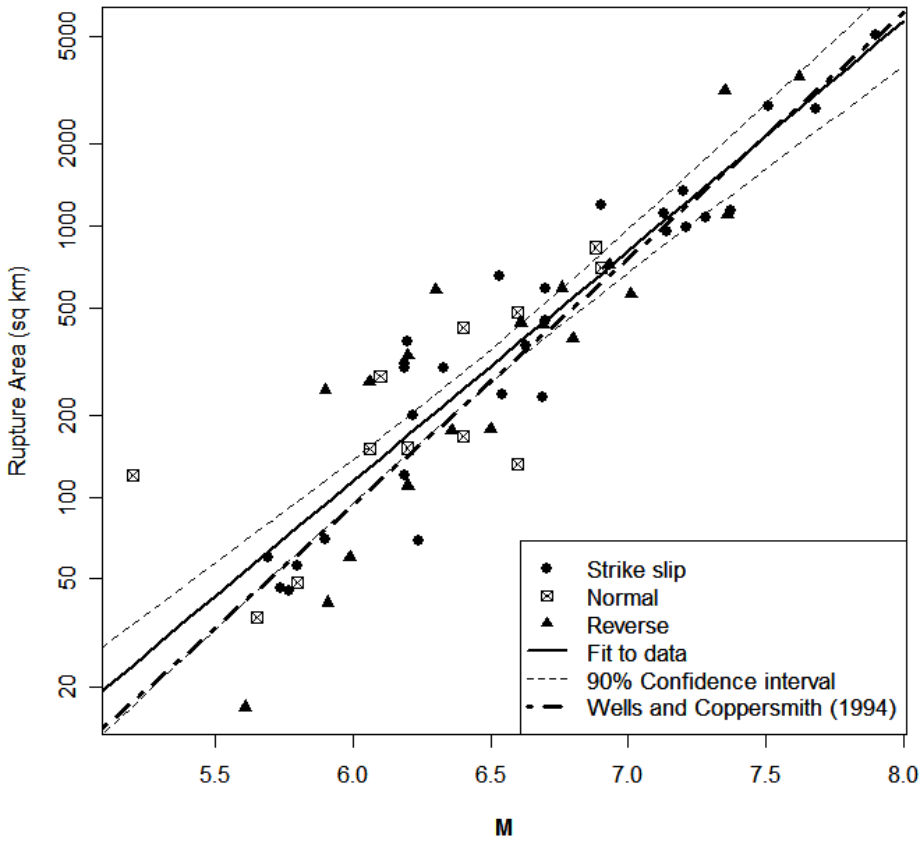

Fig. B.1 Data for M versus rupture area from PEER-NGA finite fault model dataset. Lines show fit to data and Wells and Coppersmith (1994) relationship for all slip types.

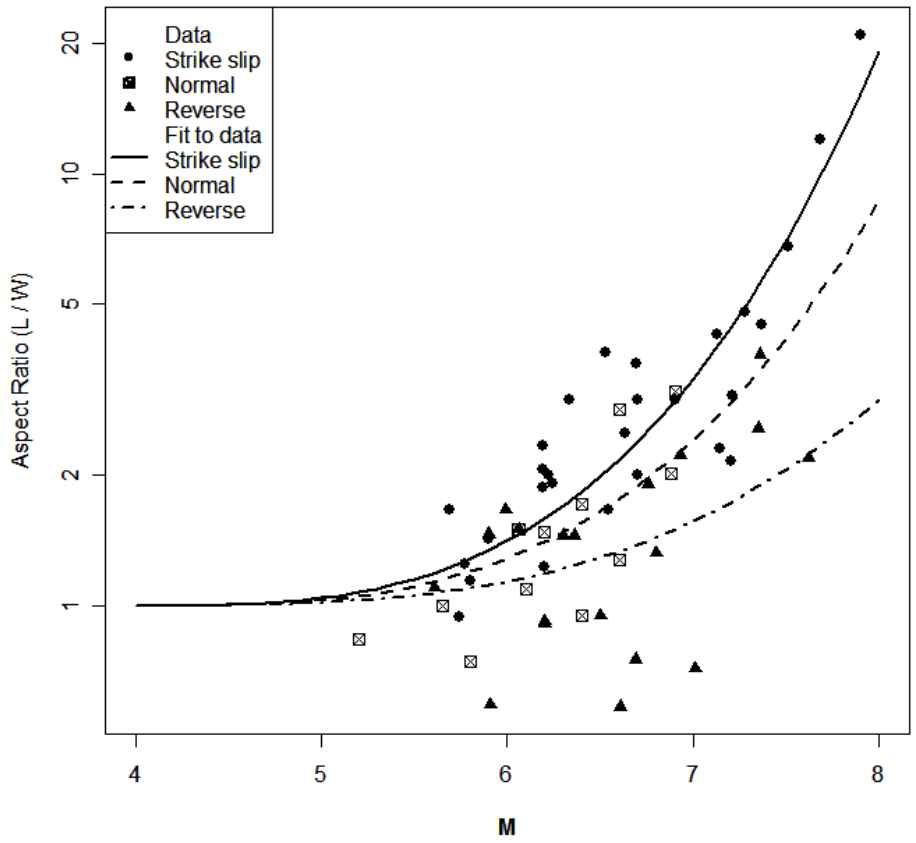

Fig. B.2 Data for M versus aspect ratio from PEER-NGA finite fault model dataset.

The next step was to locate the rupture plane in space. The vertical location of the simulated rupture with respect to the hypocenter was simulated using empirical distributions for the hypocenter location derived from the PEER-NGA set of rupture models. The observed and smoothed empirical distributions are shown in Figure B.3. If the top of the simulated rupture plane extended above 0 depth, it was placed at 0 depth. The rupture plane dip was fixed at the value assigned to the earthquake.

The location of the hypocenter along strike was simulated using data from Mai et al. (2005) for earthquakes ≤ **M** 6.5. This distribution is shown in Figure B.4.

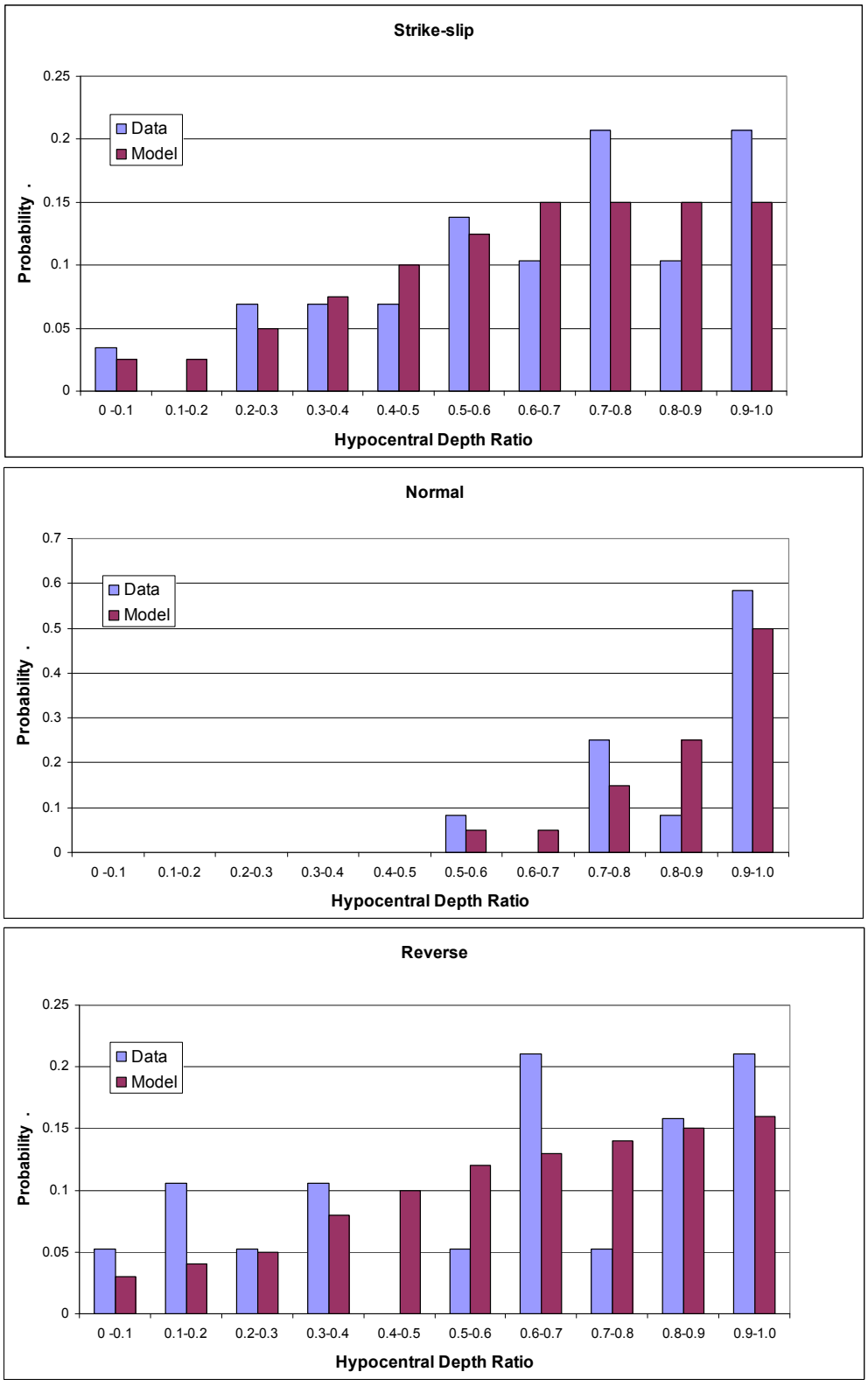

Fig. B.3 Empirical distributions for vertical location of hypocenter in rupture plane derived from the PEER-NGA rupture model data set ("Data") and smoothed for use in simulations ("Model").

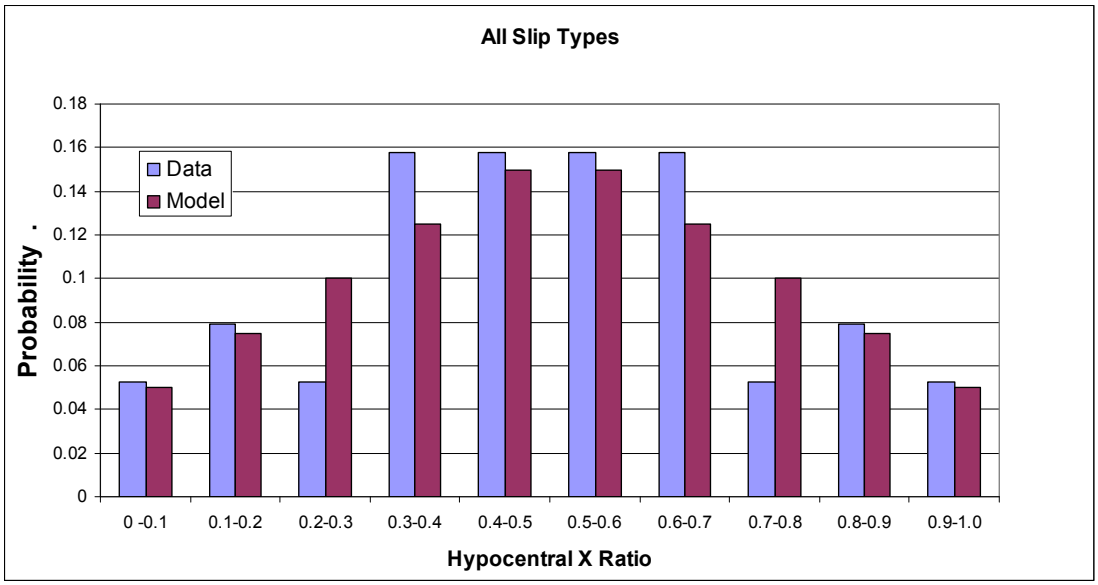

Fig. B.4 Distributions for horizontal location of hypocenter in rupture plane derived from data for M ≤ 6.5 earthquakes presented in Mai et al. (2005) ("Data") and smoothed for use in simulations ("Model").

For each simulated rupture plane, the distance to all sites was computed in terms of R_{JB}, R_{SEIS} (assuming a minimum seismogenic depth of 3 km), R_{RMS} distance, and closest distance to rupture, R_{RUP}. The depth to top of rupture, Z_{TOR} and the source-site angle were also computed.

The values selected for use were the median values for each site from the 101 simulations. The median was chosen because most of the values enter regressions as logs.

Figure 2.3 in the main text shows the ratio of the estimated values of the Joyner-Boore distance to the epicentral distance and the ratio of the estimated rupture distance to hypocentral distance for the 702 sites associated with the 110 earthquakes analyzed.

Ken Campbell provided the distances he obtained for the 1992 Big Bear **M** 6.46 earthquake based on a rupture model he developed for that event. Figure B.5 compares his estimates of R_{JB} and R_{RUP} to those obtained from this exercise. The values are close, indicating that the process provides reasonable estimates of rupture distance measures.

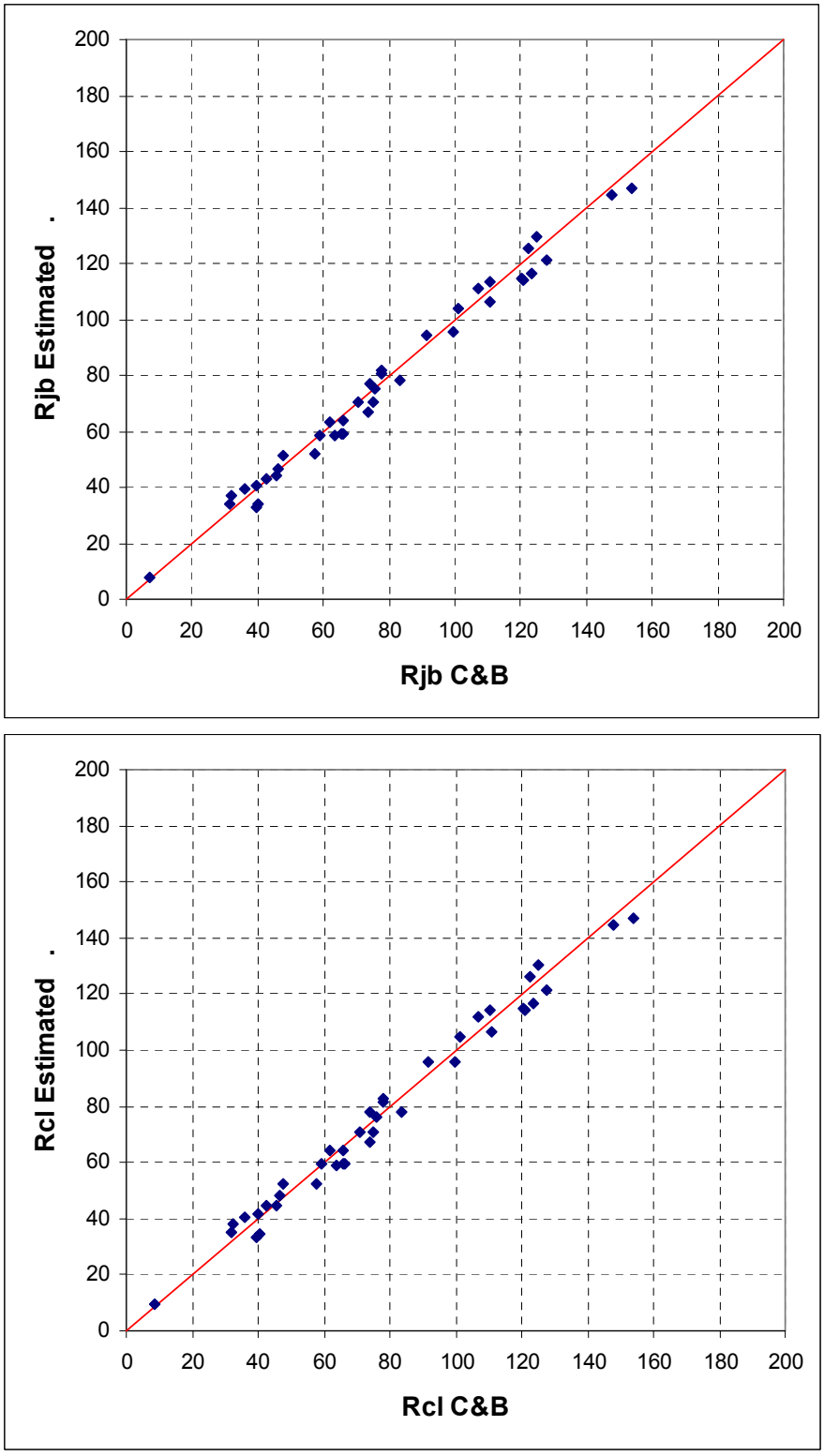

Fig. B.5 Comparison of estimated Joyner-Boore distances (R_{JB}) closest distance to rupture (R_{RUP}) obtained in this analysis to those obtained by Ken Campbell and used in Campbell and Bozorgnia (2003).

Appendix C: Estimation of V_{S30} at CWB's Free-Field Sites

Brian Chiou and K.L. Wen[2]

(June 08, 2006)

C.1 INTRODUCTION

When a site's V_{S30} measurement is missing, it is typically estimated using an empirical relationship between V_{S30} and other site information, such as surface geology or Geomatrix's 3rd letter (C_3). This approach has been used by the PEER-NGA project and has also been widely used in California (Wills and Silva 1998; Wills and others 2000; Wills and Clahan 2004) and other regions. This short note reports our efforts to establish an empirical V_{S30} - C_3 relationship for CWB's strong-motion sites in Taiwan. The Taiwan-specific relationship uses C_3 as the main predictor. It also uses station elevation to capture the within-category variation of V_{S30}. Using elevation as a V_{S30} predictor leads to a significant improvement of mapping accuracy within a site category, particularly for Geomatrix's category D.

C.2 DATA

V_{S30} data used in this study were derived from the *P*-*S* logging information provided by NCREE, who has been conducting site investigation of strong-motion stations in Taiwan[3]. During the period of 2000–2004 a total of 231 holes were drilled and logged. The site investigation project is still on going and more *P*-*S* logging data will become available in the next several years.

For each drill hole, Dr. Walt Silva (PE&A) reviewed the *P*-*S* logging data, smoothed the velocity profile, and computed V_{S30} from the smoothed profile. We used the resulting V_{S30} at 165

[2] Professor, Department of Geophysics, National Central University, Taiwan.
[3] Plots of the drilling logs are available on CWB's website (http://www.cwb.gov.tw/).

sites for our study. The other 66 strong-motion sites were not used because either the drill hole is less than 20 m deep or a Geomatrix C_3 classification has not been assigned yet.

Other collected site data are: (1) Geomatrix's 2nd and 3rd letters (D. Wells, pers. comm., 2004); (2) The site classification (PSC) by Lee et al. (2001); and (3) Station elevation (Lee et al. 2001).

C.3 VARIATION OF V_{S30} WITHIN A SITE CATEGORY

Histogram of the 165 V_{S30} data, grouped by C_3, is shown in Figure C.1. This figure illustrates two challenges in using Geomatrix's C_3 to map V_{S30} in Taiwan. First, categories A, B, and C are not distinguishable as far as V_{S30} is concerned. Second, the most populous category (D) is bimodal. It has been suggested that, due to the active tectonic in Taiwan, the higher the elevation the stiffer the surface material tends to be (Lee et al. 2001). To explore if elevation could be used to explain the V_{S30} variation, V_{S30} data are plotted as a function of station elevation in Figure C.2. Except for a few outliers, a strong correlation of V_{S30} with the station elevation is clearly seen, particularly for the Geomatrix-D category. The bimodal distribution observed in Figure C.1 can be adequately modeled by the station elevation.

C.4 MAPPING V_{S30} BY C_3 AND ELEVATION

Based on the trends noted in Figure C.2, the following functional form is used to model V_{S30} as a function of station elevation (*Elv*, in meters),

$$ln(V_{S30}) = ln(\phi_1) + \frac{ln(\phi_2) - ln(\phi_1)}{1 + e^{(ln(\phi_3) - ln(Elv))/\phi_4}}.$$

Interpretations of the model coefficients are as follows: ϕ_1 and ϕ_2 are the asymptotic V_{S30} as the elevation approaches 0 and ∞, respectively; at the elevation of ϕ_3 meters, V_{S30} is the (geometric) average of the two asymptotes.

The above functional form was used to fit V_{S30} data for each of the five Geomatrix categories. The resulting coefficients (ϕ_i, $i=1, 4$) are listed in Table C.1 and the fitted curves are shown in the left hand plot of Figure C.3.

To illustrate the difference in inferred V_{S30} due to different mapping schemes, V_{S30} estimates for the non-measurement CWB sites are plotted in the right panel of Figure C.3. The solid lines represent estimated V_{S30} using the new model for Taiwan; circles are V_{S30} estimated using California's model (Silva 2004; see Note #34 in the site file NGA_Site_V017.XLS). Difference in estimated V_{S30} is not large, with the exception of Geomatrix-D category at elevation higher than 70m, which is expected.

REFERENCES:

Lee, C.T., Cheng, C.T., Liao, C.W., and Tsai, T.B., 2001, Site classification of Taiwan free-field strong-motion stations: *Bulletin of the Seismological Society of America*, v. 91, no. 5, p 1283-1297.

Wills, C.J., Petersen, M.D., Bryant, W.A., Reichle, M.S., Saucedo, G.J., Tan, S.S, Taylor, G.C, and Treiman J.A., 2000, A site conditions map for California based on geology and shear wave velocity: *Bulletin of the Seismological Society of America*, v. 90, no. 6b, p S187-S208.

Wills, C.J. and Silva, W., 1998, Shear wave velocity characteristics of geologic units in California: *Earthquake Spectra*, v. 14, p. 533-556.

Wills C.J. and Clahan K., 2005, NGA site condition metadata from geology, report to PEER-LL, 2005.

Table C.1 Estimated coefficients.

Geomatrix 3rd Letter	ϕ_1	ϕ_2	ϕ_3	ϕ_4	σ	Number of Data Points
A	552	680[1]	244	0.1154	0.3174	15
B	418	579	107.1	0.3850	0.2294	35
C	-	-	-	-	-	4[2]
D	228	509	39.4	0.373	0.2953	91
E	201	405	38.2	0.087	0.1810	18

Total = 163 [3]

[1] This parameter is fixed by judgment.

[2] There is insufficient number of data to derive a relationship. To estimate V_{S30} of category C site, one could use the relationship for category D.

[3] Two data points in Geomatrix-B category were removed.

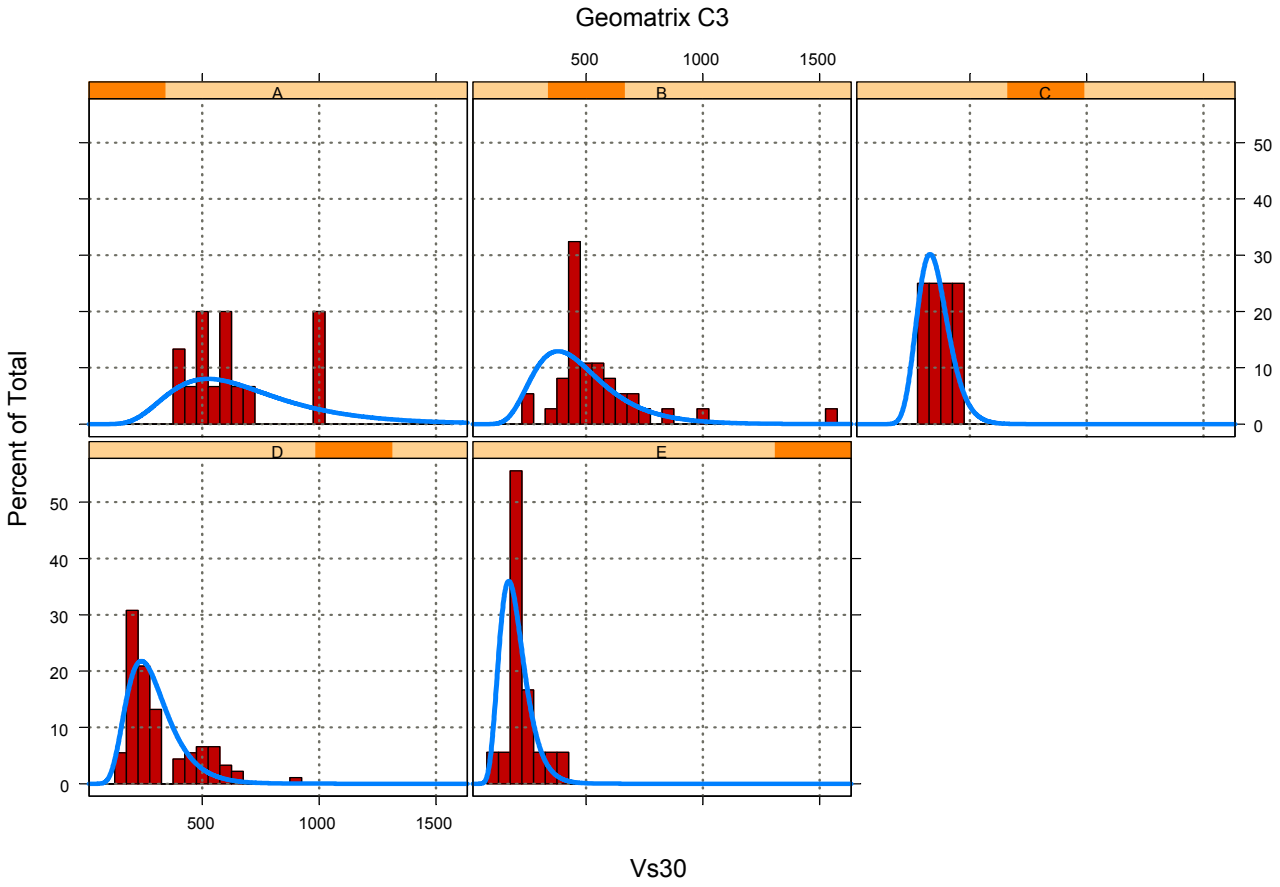

Fig. C.1 Histogram of measured V_{S30} grouped by Geomatrix's 3rd letter (C_3). Thick blue line is V_{S30} distribution of California strong-motion stations (Silva 2004).

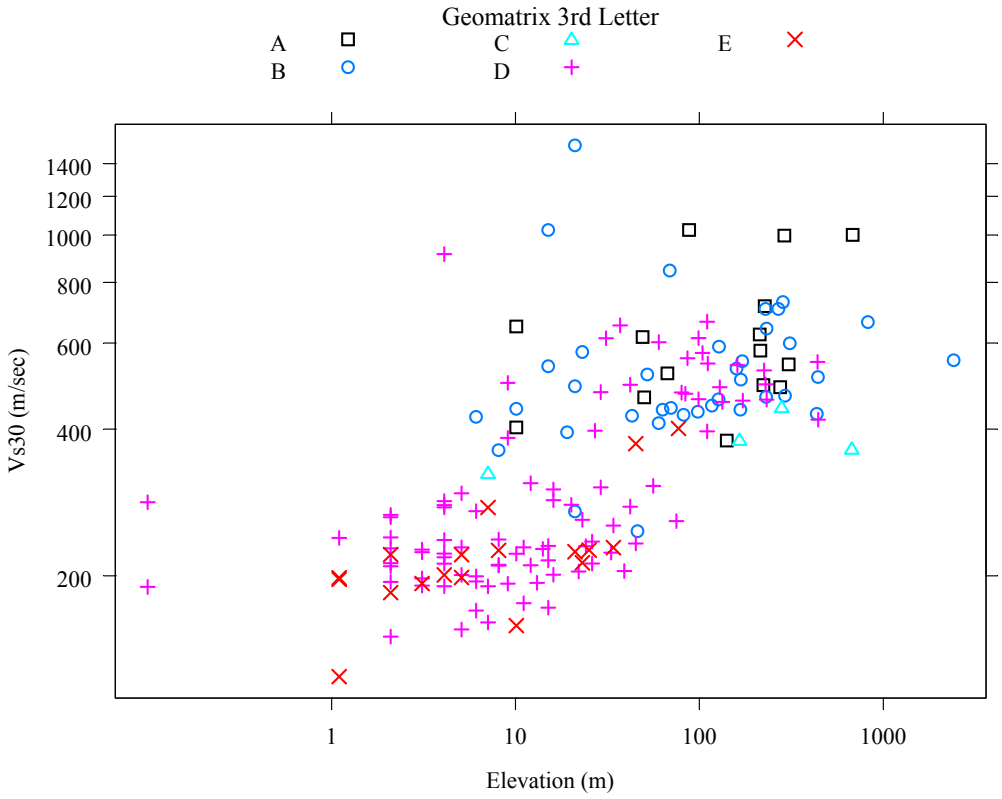

Fig. C.2 Variation of measured V_{S30} with station's elevation.

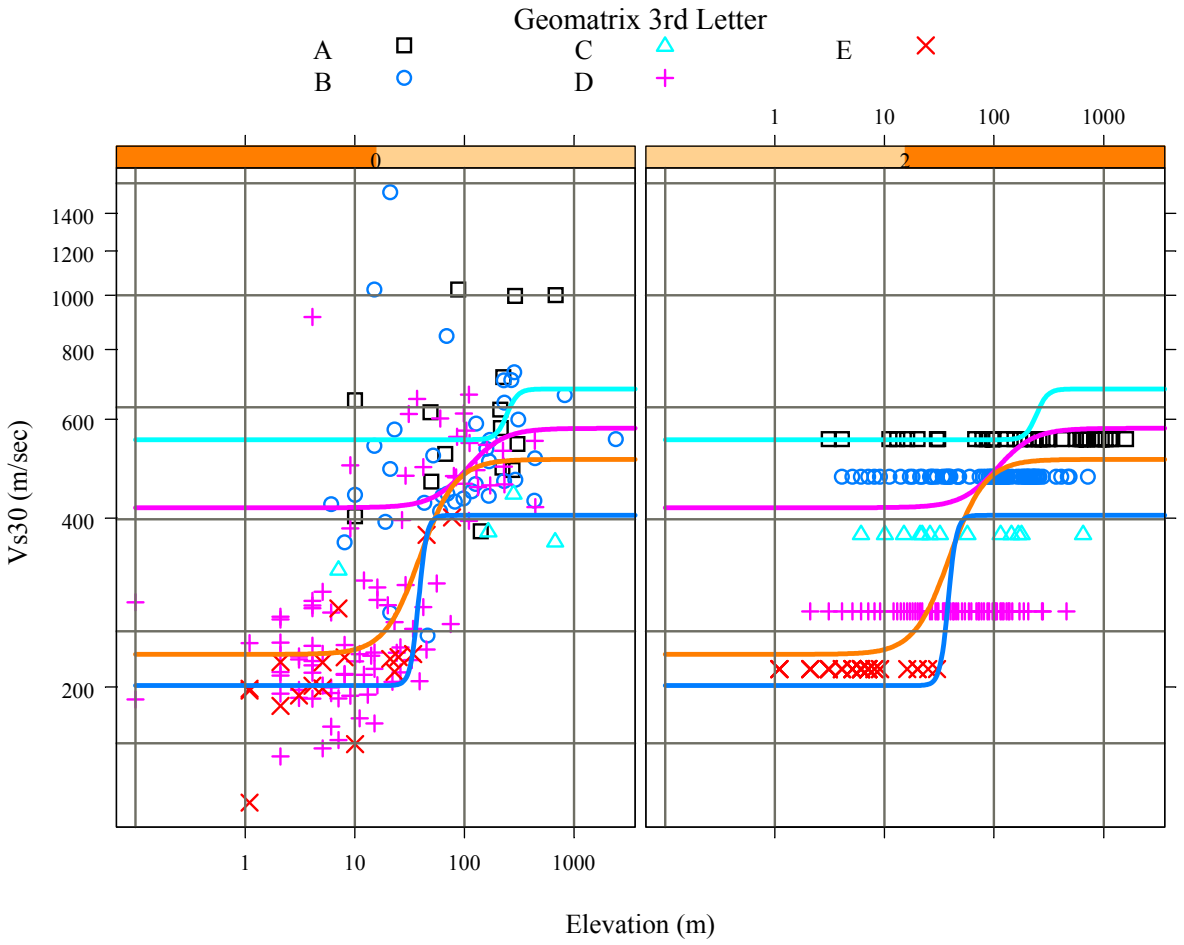

Fig. C.3 (Left) Measured V_{S30} data and fits to the data. (Right) Comparison of V_{S30} estimated by two different approaches. Solid lines are V_{S30} estimated by the Taiwan-specific model developed in this study; circles are V_{S30} estimated by the California model (Silva, 2004).

Appendix D: ShakeMap Data

D.1 DATASET

The ground motion dataset described in this appendix was compiled from the southern California ShakeMap system by Boatwright and his colleagues at USGS (per. communication). It includes *pga* (in units of %g) and *pgv* (in units of cm/sec) from 252 earthquakes (Fig. D.1). Because only the larger of the tow horizontal components is provided, we divide the listed *pga* value by 1.1 to adjust the value down to the expected level of average horizontal component. Epicenter location, focal depth, and local magnitude M_L of each earthquake are obtained from the SCSN (Southern California Seismic Network) earthquake catalog. Moment magnitude (**M**) is based on the moment from the SCSN moment tensor solution catalog.

Since most earthquakes are without a finite source model, rupture distance is imputed using the same procedure as described in Appendix B. For site conditions, we used the V_{S30} value in the NGA database or estimated it using the correlation between V_{S30} and surface geological unit as was used in NGA project. Surface geological unit at the station coordinates is provided by Chris Wills using the recently refined CGS site-conditions map (Wills et al. 2006). For stations without a geological unit and a NGA V_{S30} value, we used the site category (C) given in the USGS data file to infer V_{S30} (Wills et al. 2001):

C=1: V_{S30} = 674 (m/sec)

C=2: V_{S30} = 423 (m/sec)

C=3: V_{S30} = 281 (m/sec)

C=4: V_{S30} = 165 (m/sec).

$Z_{1.0}$ is estimated from the V_{S30} value using equation (2.1) of the main text.

D.2 DATA SELECTION

We did not include any earthquake whose epicenter is outside or near the network boundary of the southern California ShakeMap system. The quality of *pga* data degrades as distance increases. A full quality control is not feasible; instead we removed *pga* from beyond the cutoff distance of 130 x (**M** - 2) km. Our cutoff distance is slightly more generous than the cutoff distance of 100 x (**M** - 2) km recommended by Boatwright et al. (2003) for northern California earthquakes. To get a reliable estimate of event term, we removed earthquakes with less than 20 data points. We also removed data that are obviously in errors. The final data subset includes 9060 *pga* data points from 102 earthquakes, ranging in magnitude from 3.39 to 5.17., *pga* values are in the range of 0.0007–24.5% g.

D.3 COMPARISON TO CHIOU AND YOUNGS (2008)

Plots of *pga* vs. distance are presented in Figure D.2 for each of the selected earthquakes. A similar comparison has been made using the preliminary model published in Chiou and Youngs (2006). Dashed line in each plot represents the population median prediction by Chiou and Youngs (2008) and the solid line represents the event-specific median (population median times e^{η}, η is the event term). Both predictions are evaluated from the mean V_{S30} of the recording stations. The event term of an earthquake is computed as the mean residual of data from that earthquake.

Figure D.3 shows all the event terms as a function of earthquake magnitude. A significant trend with magnitude is noted, suggesting that the magnitude scaling in Chiou and Youngs (2008) does not apply to earthquakes smaller than **M** 4.5. To improve the misfits, coefficients c_3 and $c_{\mathbf{M}}$ of Chiou and Youngs (2008) must be revised. Since such revision will not affect the predictions of ground motion for large magnitude, we leave this revision to a future study.

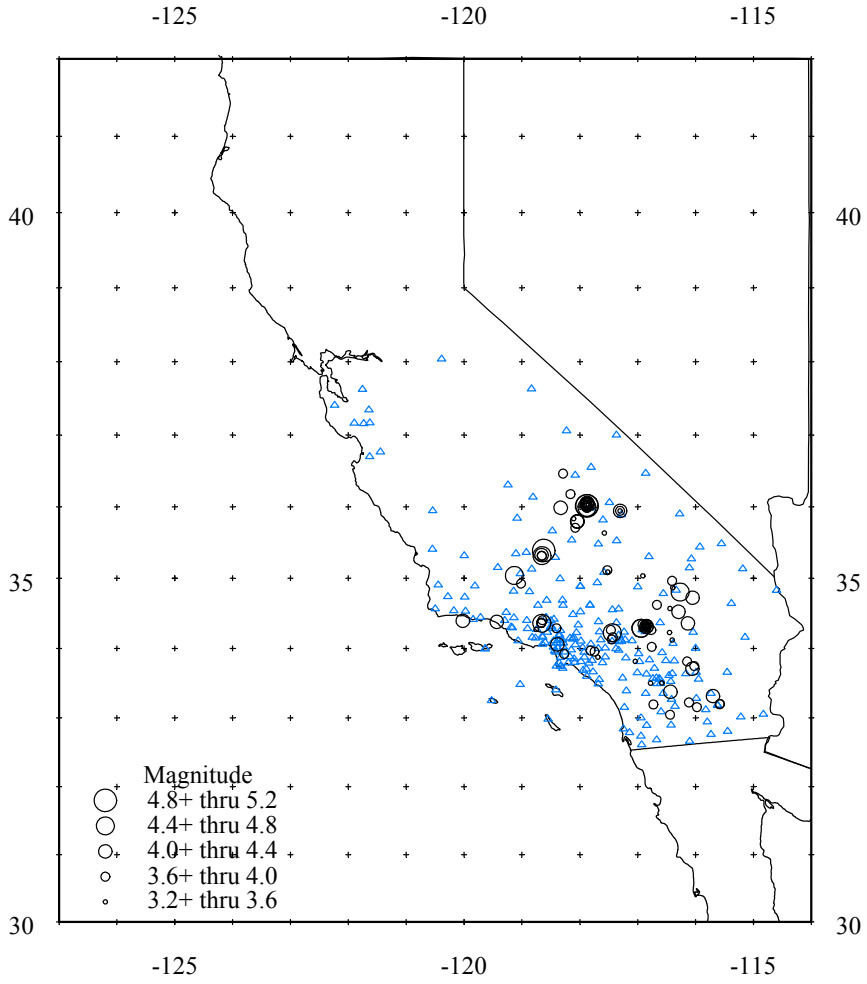

Fig. D.1 Earthquake epicenter distribution of southern California ShakeMap dataset. triangles indicate locations of recording stations.

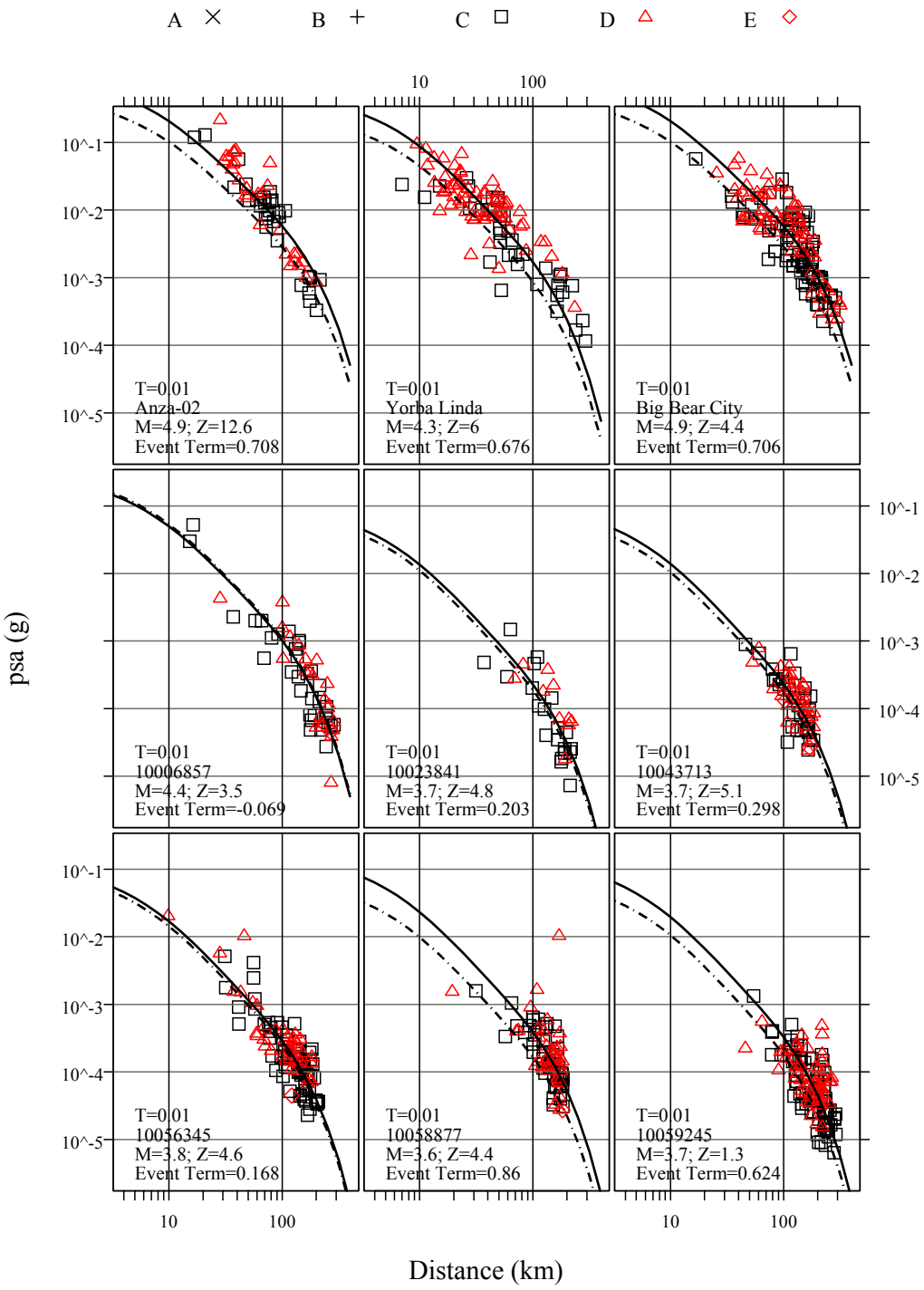

Fig. D.2 Comparison of TriNet/ShakeMap *pga* data to predictions by Chiou and Youngs (2008).

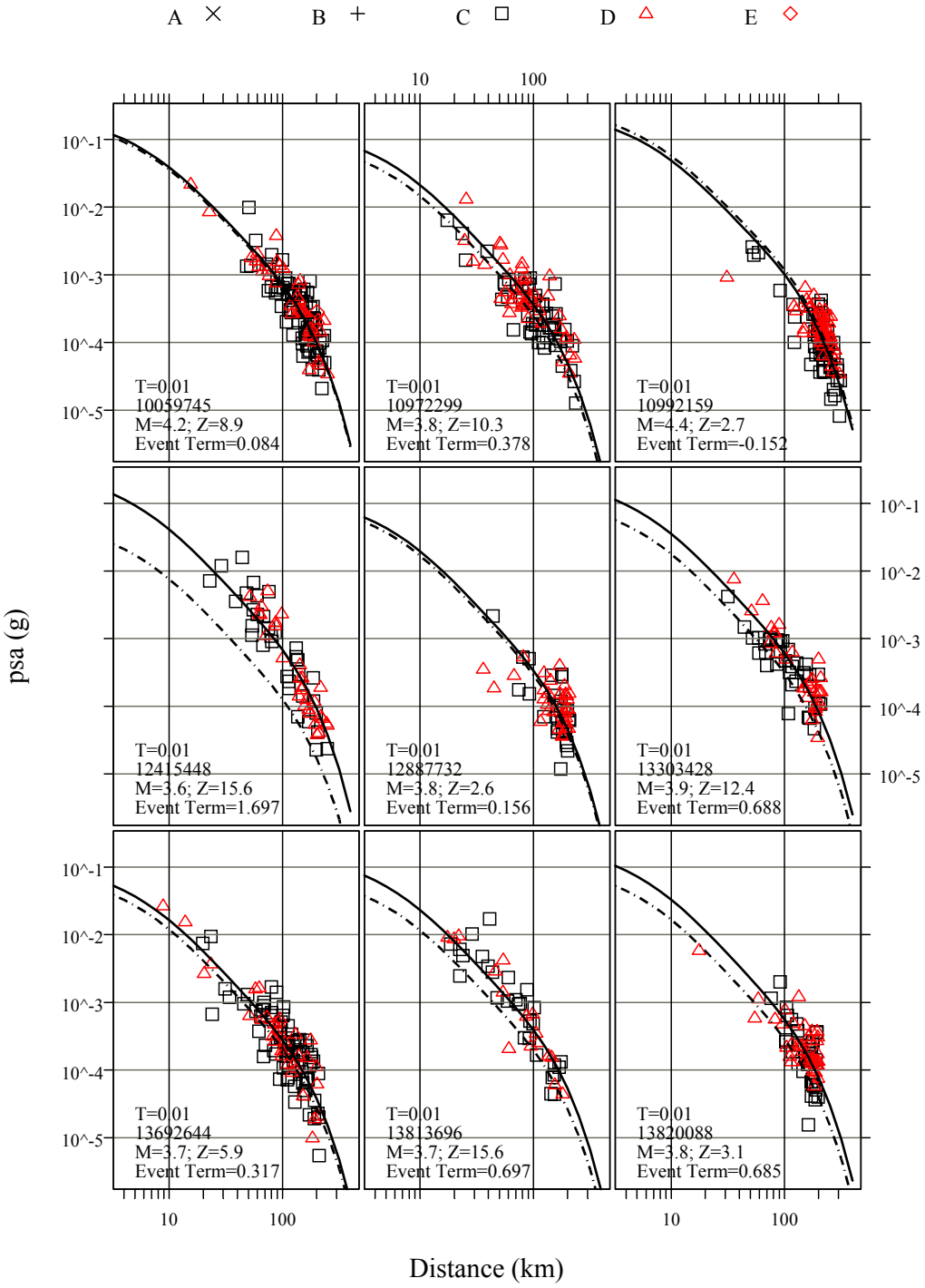

Fig. D.2—*Continued*

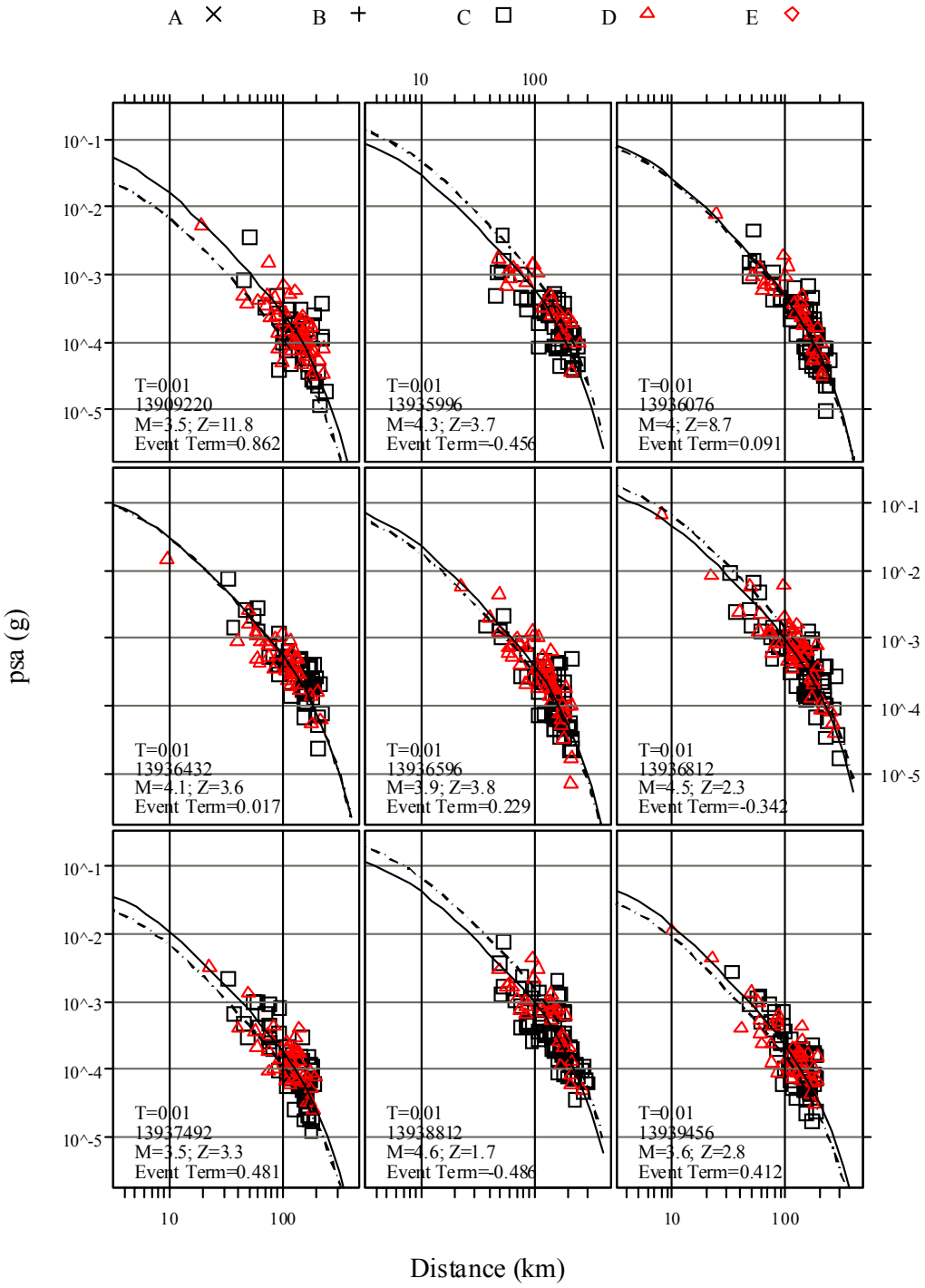

Fig. D.2—*Continued*

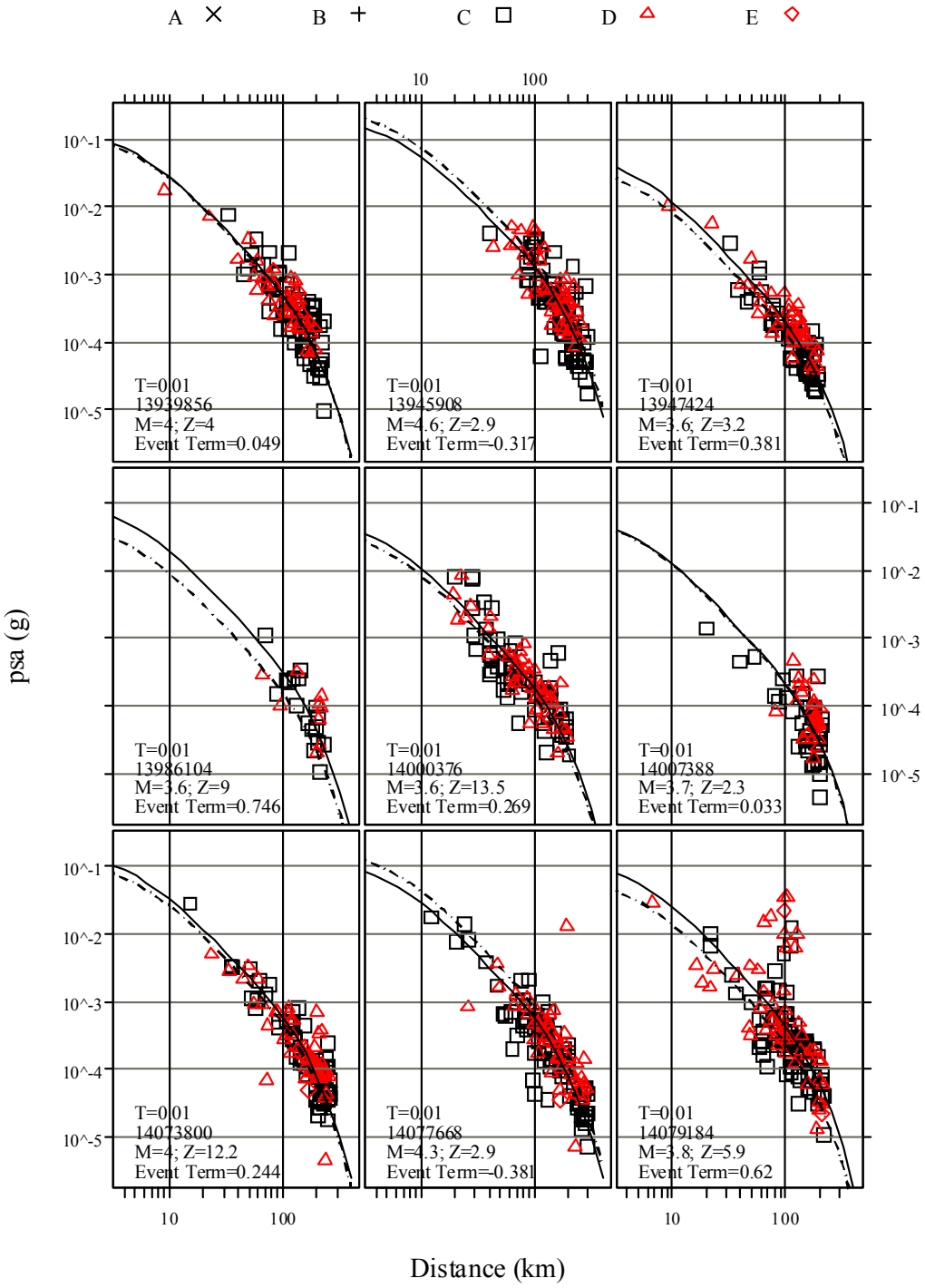

Fig. D.2—*Continued*

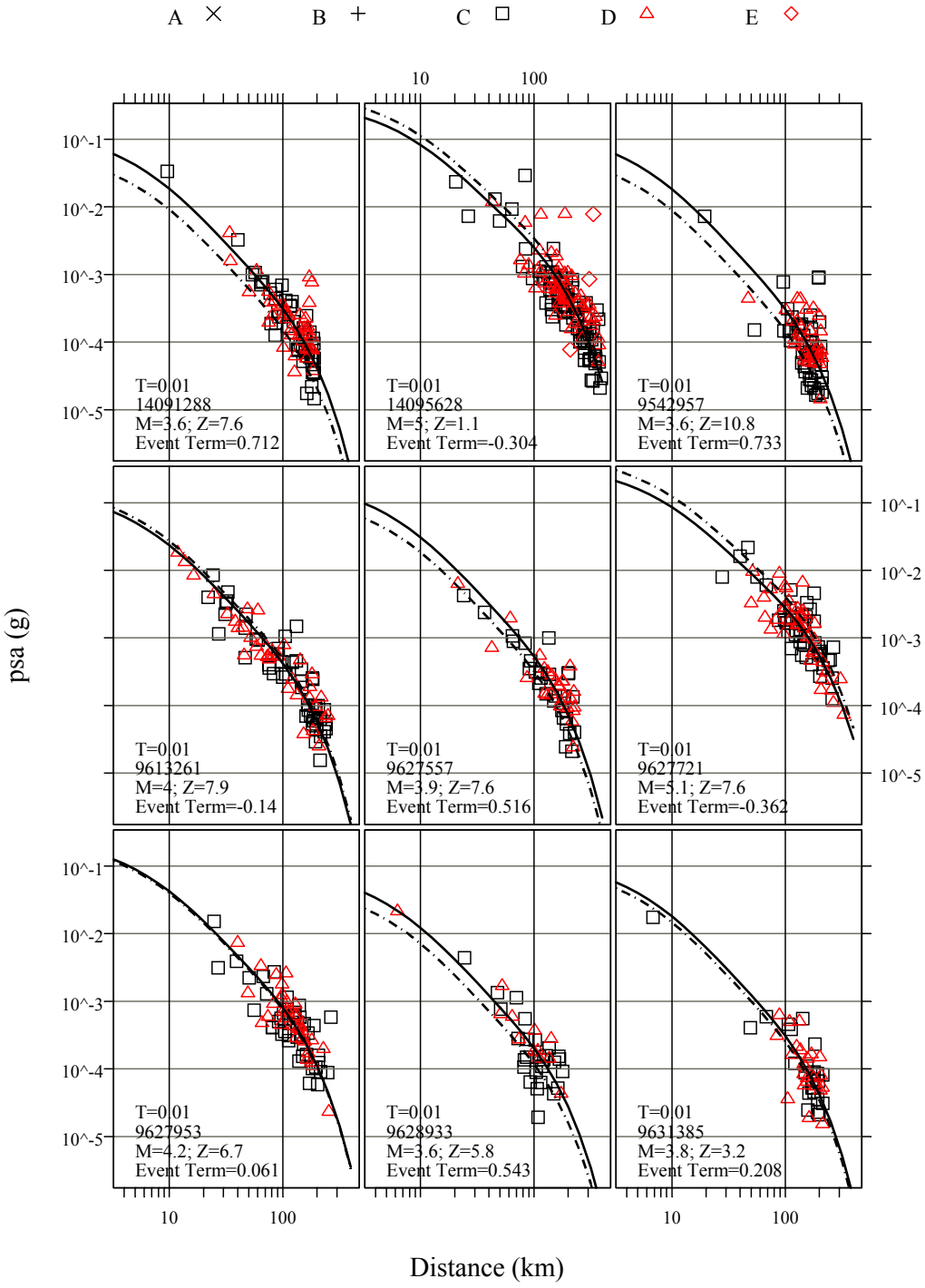

Fig. D.2—*Continued*

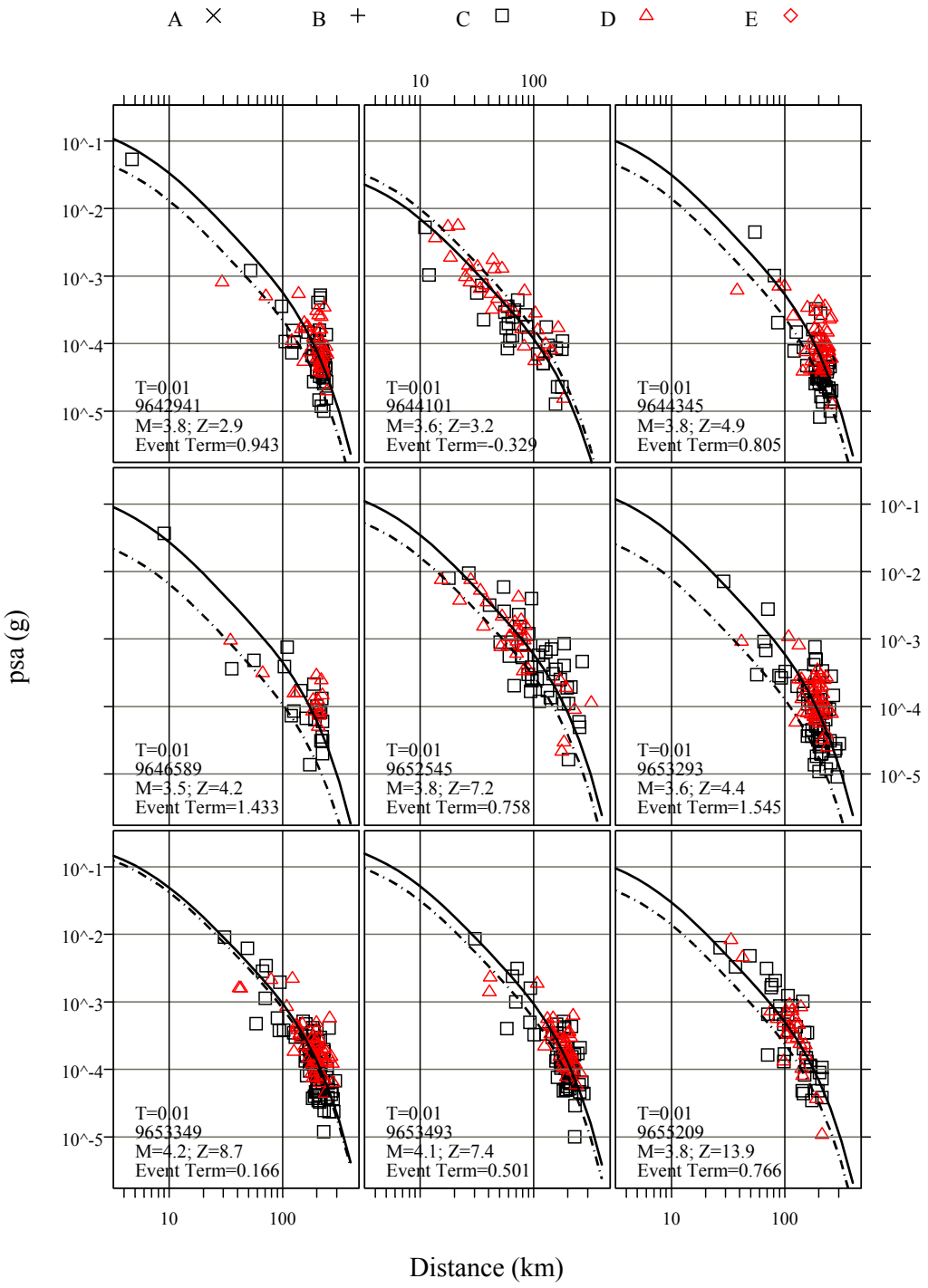

Figure D.2—*Continued*

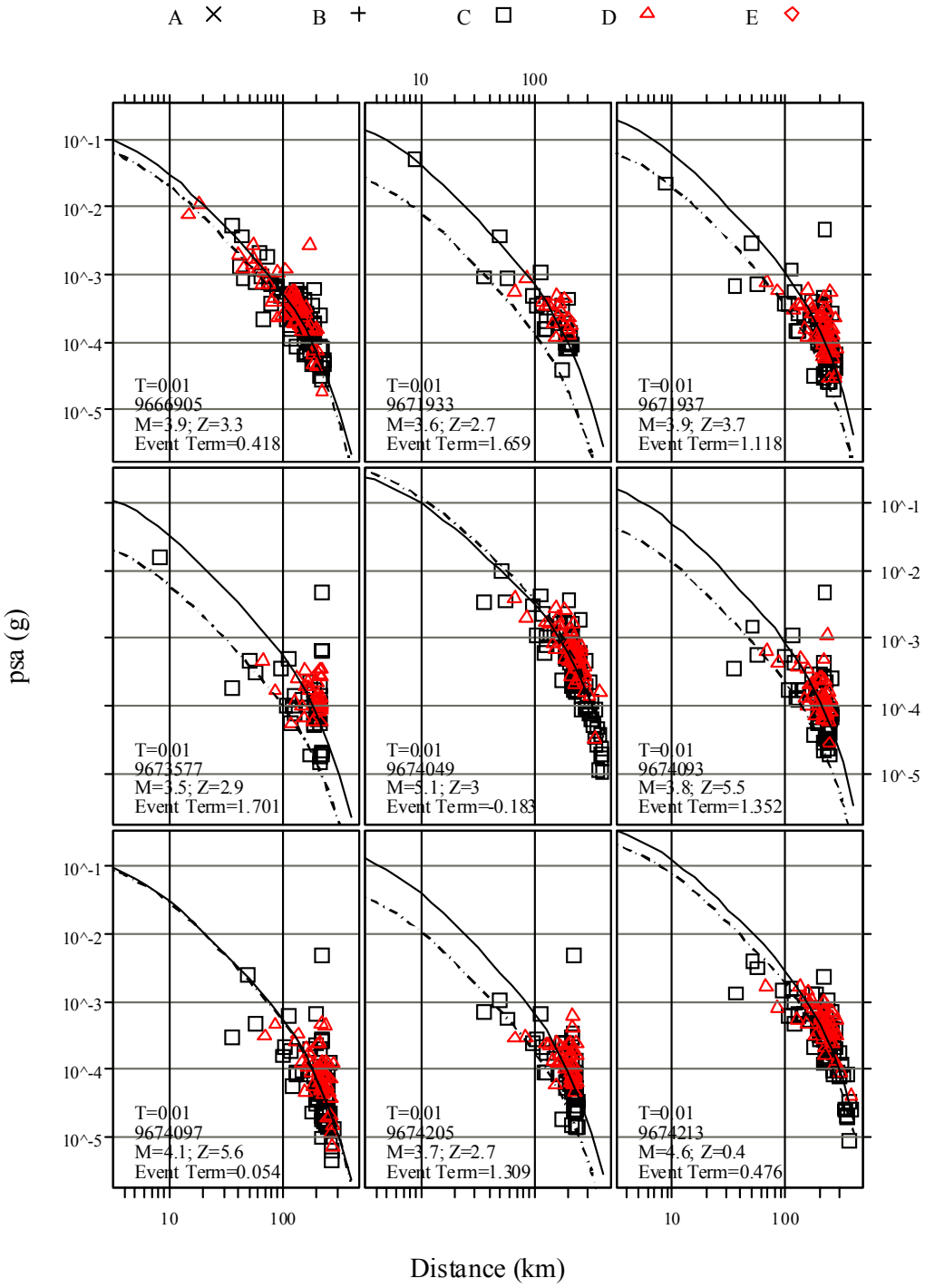

Figure D.2—*Continued*

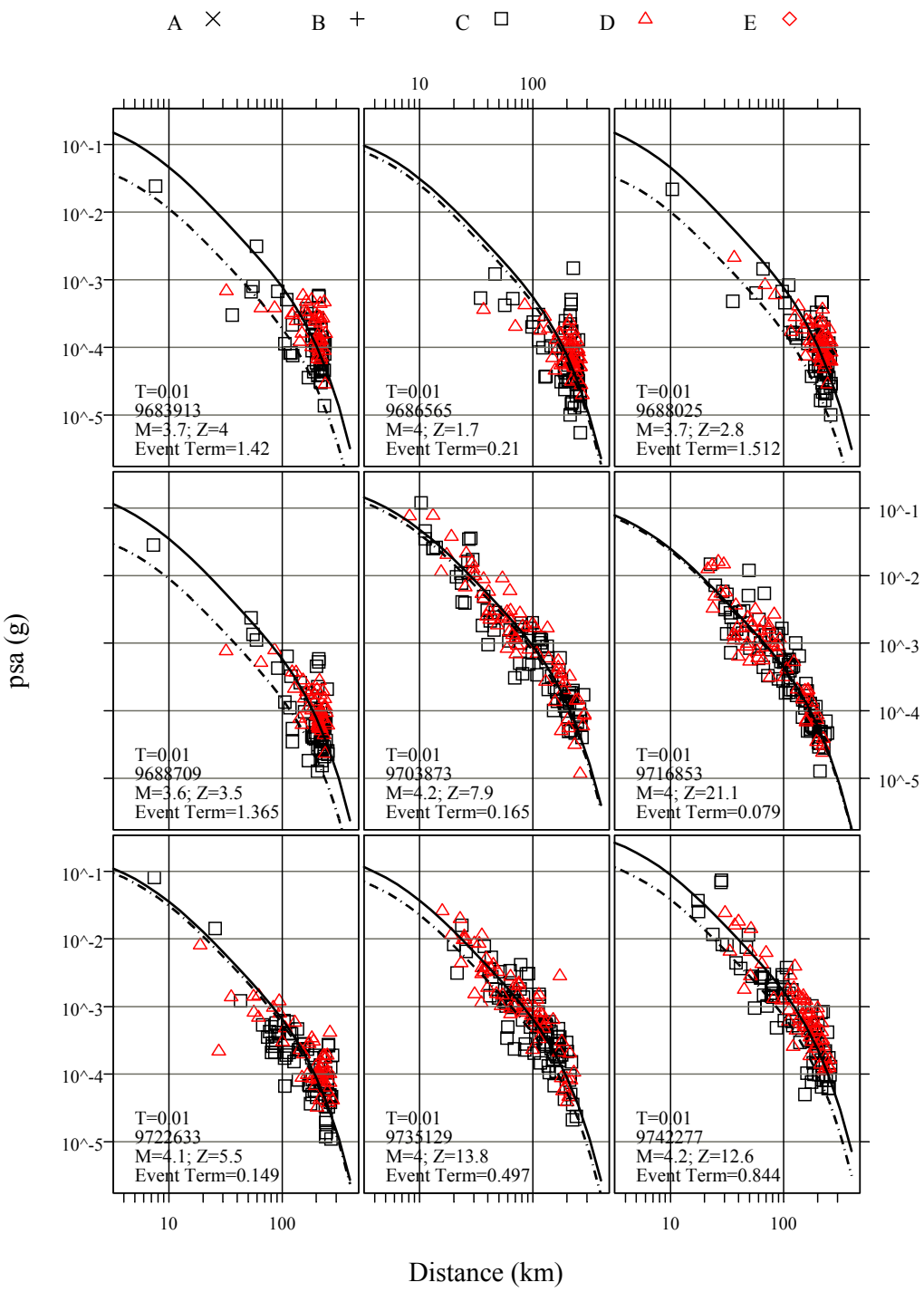

Figure D.2—*Continued*

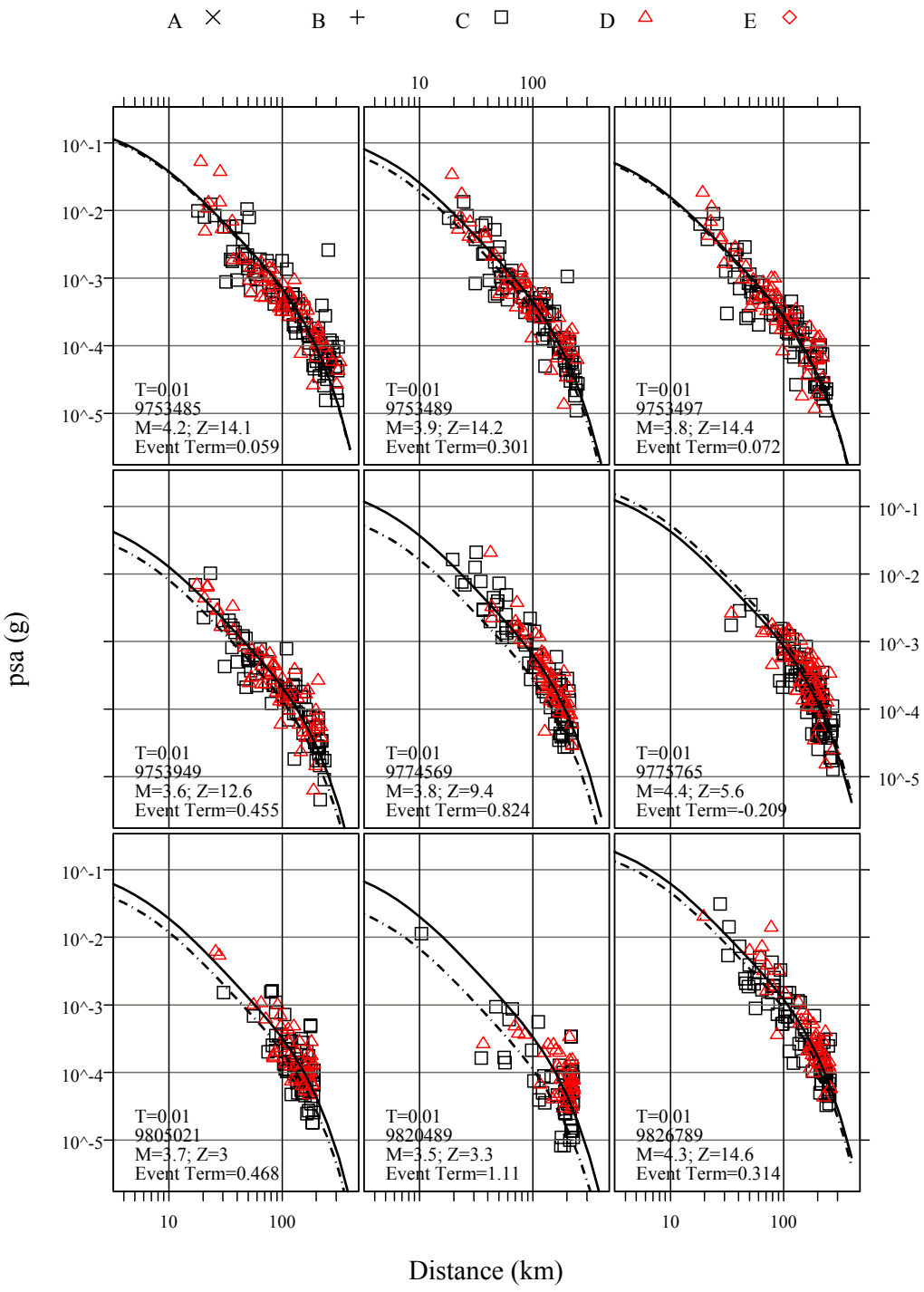

Figure D.2—*Continued*

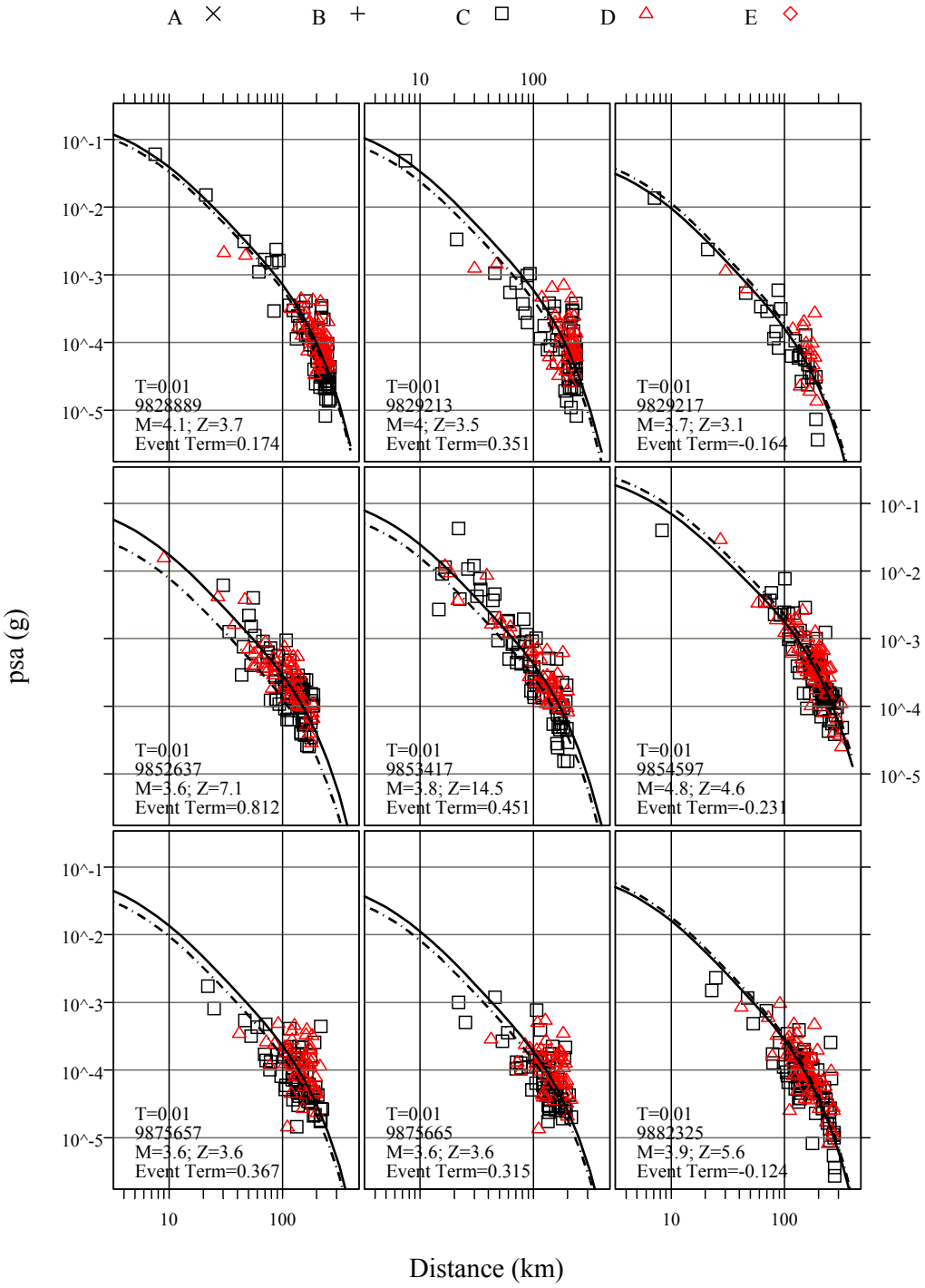

Figure D.2—*Continued*

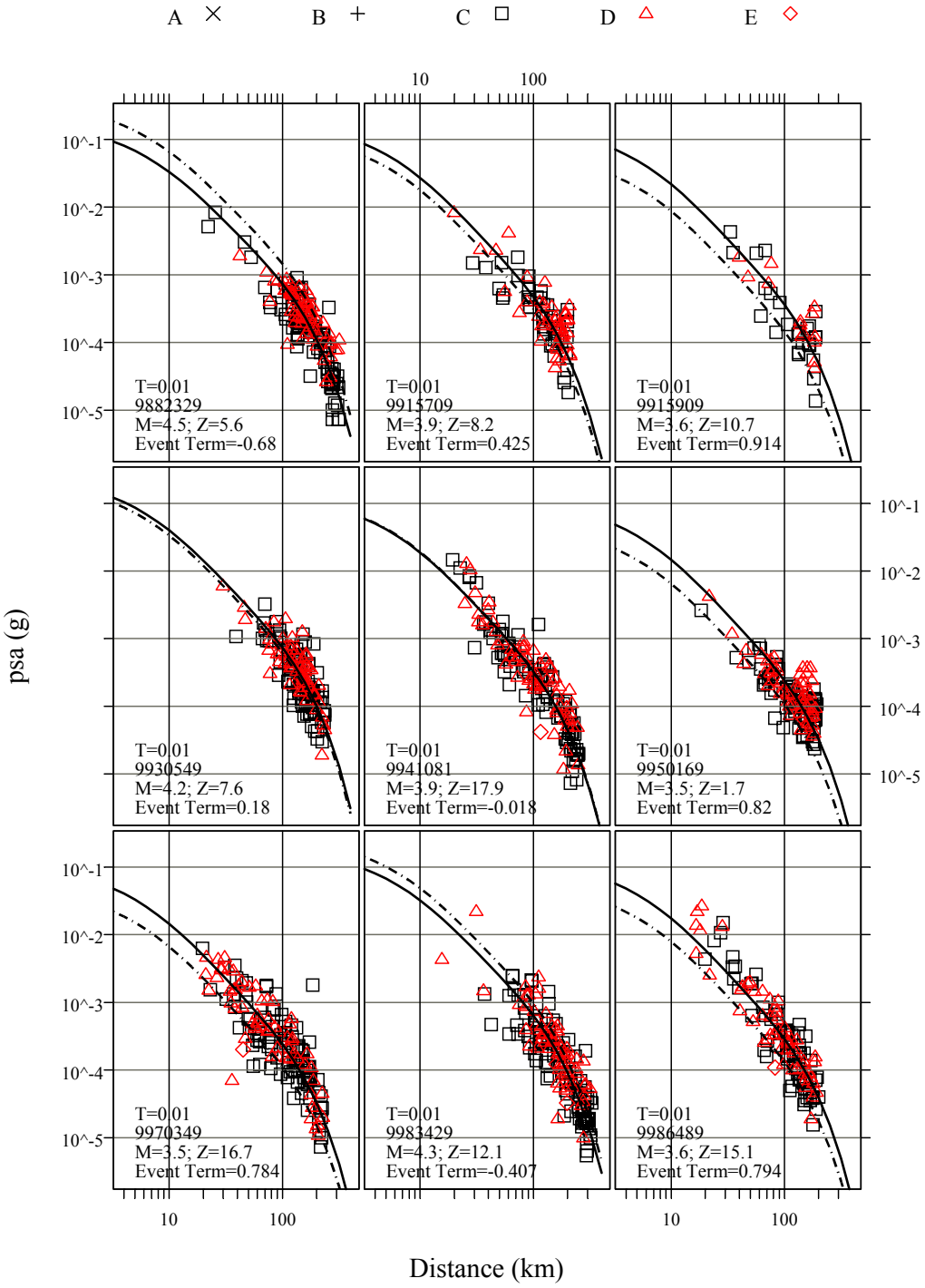

Figure D.2—*Continued*

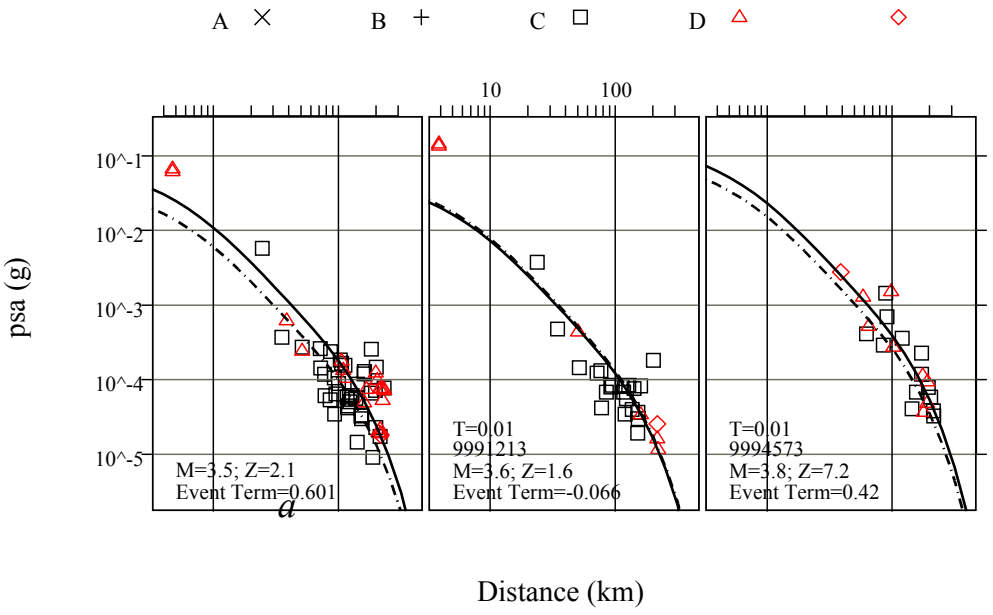

Figure D.2—*Continued*

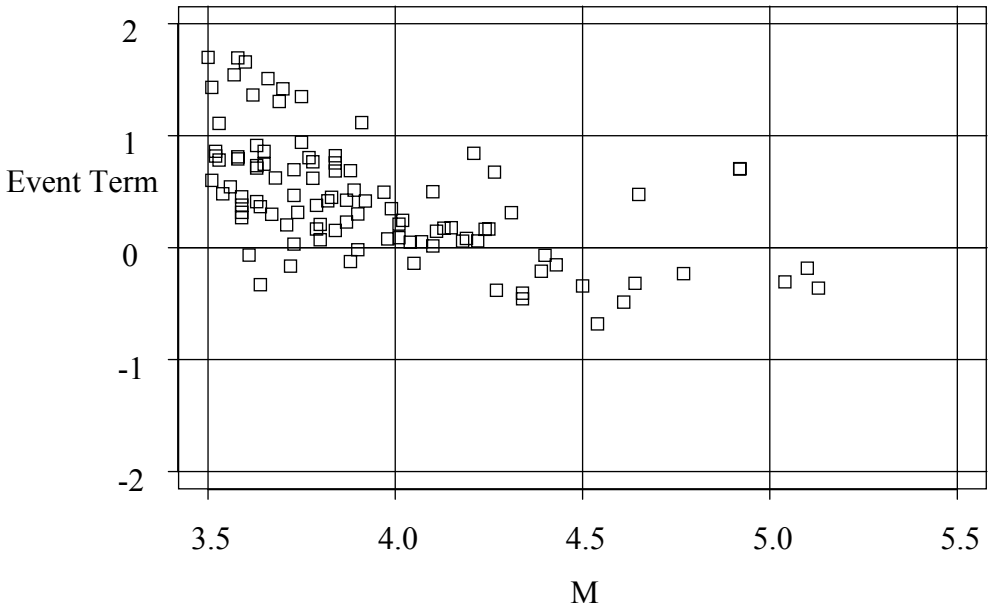

Fig. D.3 Event terms of southern California earthquakes in TriNet/ShakeMap dataset.

Appendix E: Individual Earthquake Fits for Chiou and Youngs's (2008) Ground Motion Model

Plots in this appendix show the fits of Chiou and Youngs's (2008) model to empirical data for each earthquake used in the regressions analysis. Predictions are evaluated without hanging-wall effect. The predicted curves are color coded to indicate the V_{S30} values used in making the ground motion prediction, and the ground motion data are color coded by the recording site's NEHRP site class. The results are shown for the ground motion parameters of pseudo spectral acceleration at spectral periods of 0.01 (*pga*), 0.2, 1.0, and 3.0 sec.

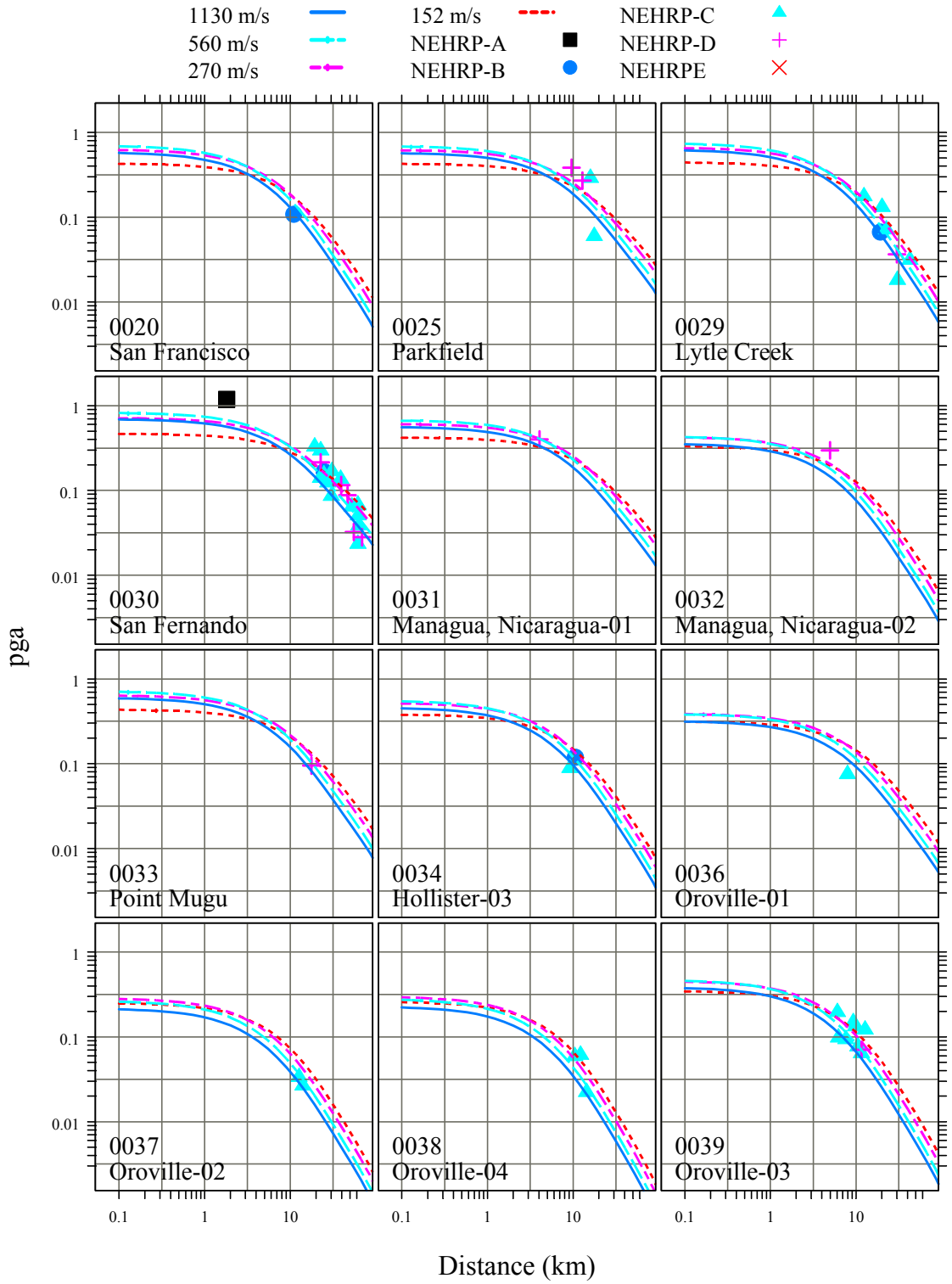
1130 m/s
560 m/s
270 m/s
152 m/s
NEHRP-A
NEHRP-B
NEHRP-C
NEHRP-D
NEHRPE
pga
Distance (km)
0020
San Francisco
0025
Parkfield
0029
Lytle Creek
0030
San Fernando
0031
Managua, Nicaragua-01
0032
Managua, Nicaragua-02
0033
Point Mugu
0034
Hollister-03
0036
Oroville-01
0037
Oroville-02
0038
Oroville-04
0039
Oroville-03

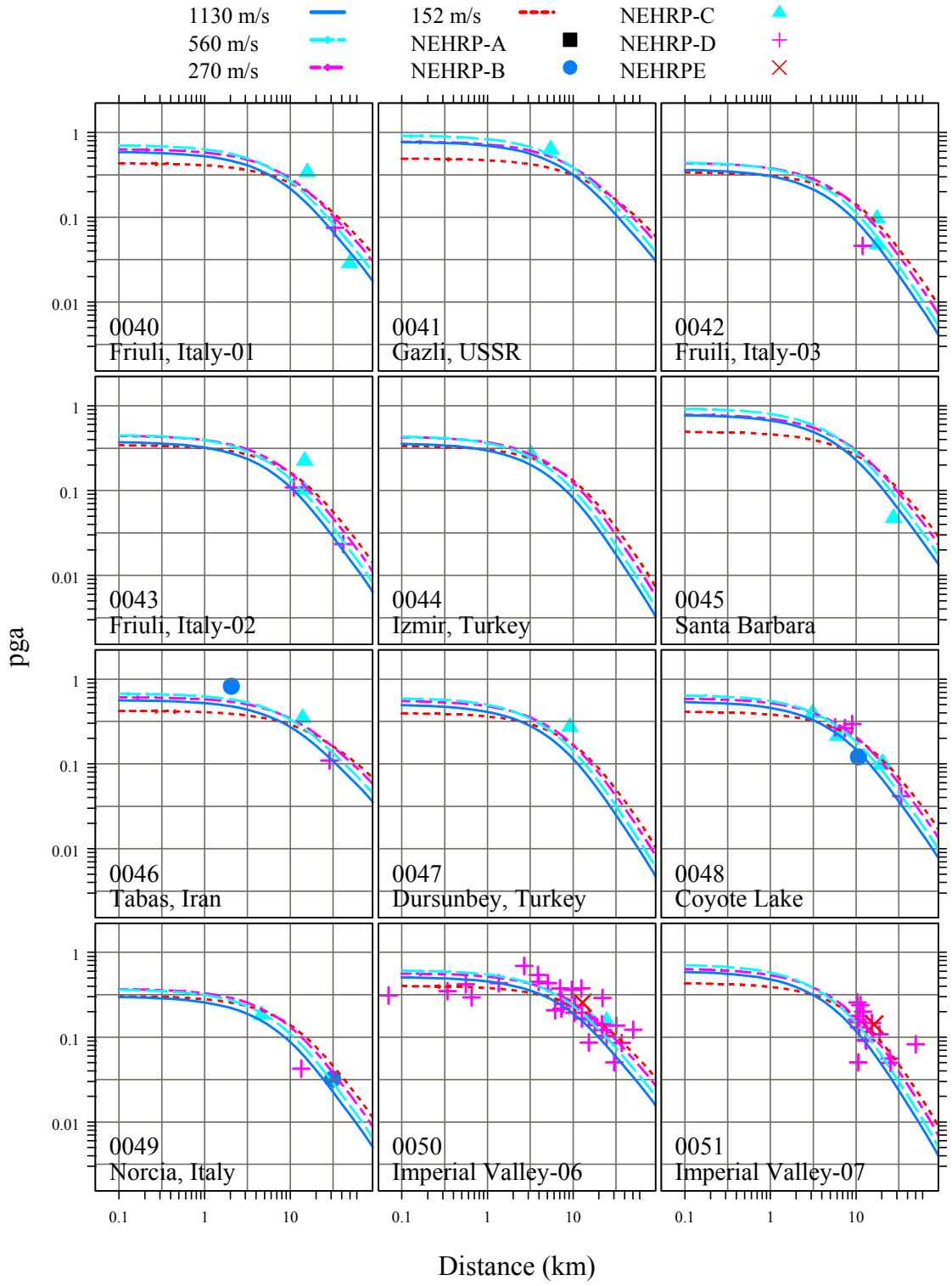
1130 m/s
560 m/s
270 m/s
152 m/s
NEHRP-A
NEHRP-B
NEHRP-C
NEHRP-D
NEHRPE
pga
Distance (km)
0040
Friuli, Italy-01
0041
Gazli, USSR
0042
Fruili, Italy-03
0043
Friuli, Italy-02
0044
Izmir, Turkey
0045
Santa Barbara
0046
Tabas, Iran
0047
Dursunbey, Turkey
0048
Coyote Lake
0049
Norcia, Italy
0050
Imperial Valley-06
0051
Imperial Valley-07

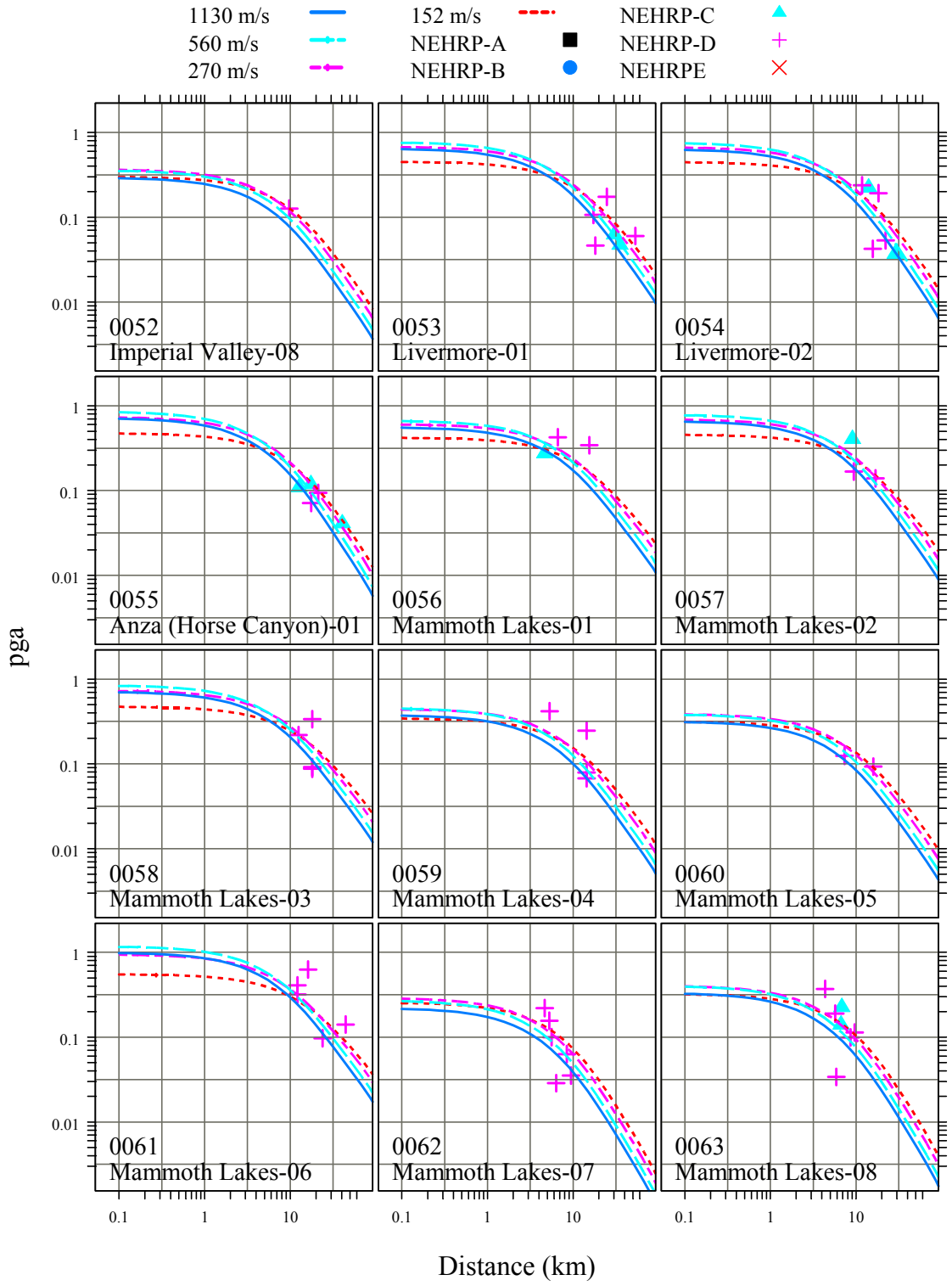
1130 m/s
560 m/s
270 m/s
152 m/s
NEHRP-A
NEHRP-B
NEHRP-C
NEHRP-D
NEHRPE
pga
Distance (km)
0052
Imperial Valley-08
0053
Livermore-01
0054
Livermore-02
0055
Anza (Horse Canyon)-01
0056
Mammoth Lakes-01
0057
Mammoth Lakes-02
0058
Mammoth Lakes-03
0059
Mammoth Lakes-04
0060
Mammoth Lakes-05
0061
Mammoth Lakes-06
0062
Mammoth Lakes-07
0063
Mammoth Lakes-08

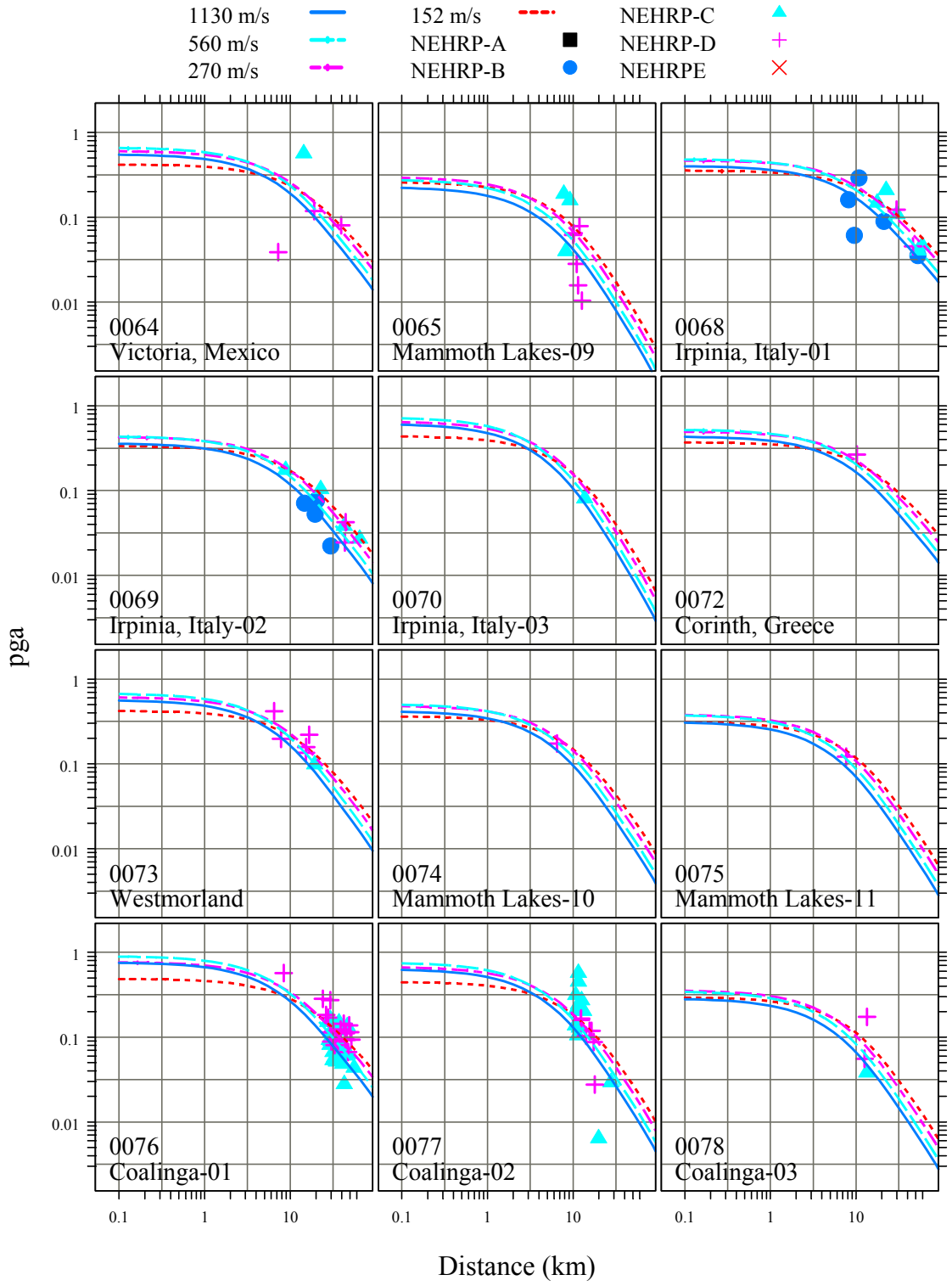
1130 m/s
560 m/s
270 m/s
152 m/s
NEHRP-A
NEHRP-B
NEHRP-C
NEHRP-D
NEHRPE
pga
Distance (km)
0064
Victoria, Mexico
0065
Mammoth Lakes-09
0068
Irpinia, Italy-01
0069
Irpinia, Italy-02
0070
Irpinia, Italy-03
0072
Corinth, Greece
0073
Westmorland
0074
Mammoth Lakes-10
0075
Mammoth Lakes-11
0076
Coalinga-01
0077
Coalinga-02
0078
Coalinga-03

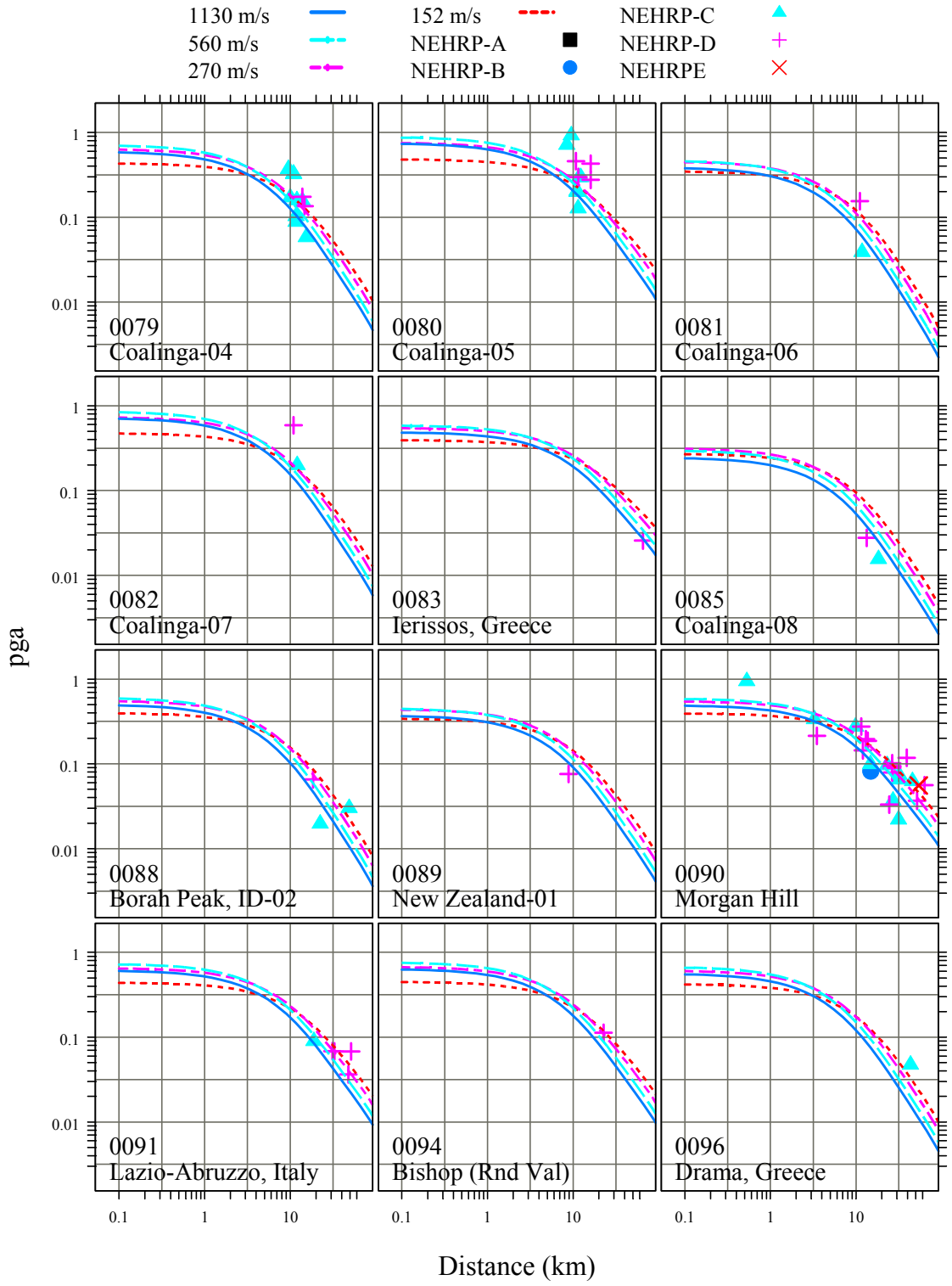
1130 m/s
560 m/s
270 m/s
152 m/s
NEHRP-A
NEHRP-B
NEHRP-C
NEHRP-D
NEHRPE
pga
Distance (km)
0079
Coalinga-04
0080
Coalinga-05
0081
Coalinga-06
0082
Coalinga-07
0083
Ierissos, Greece
0085
Coalinga-08
0088
Borah Peak, ID-02
0089
New Zealand-01
0090
Morgan Hill
0091
Lazio-Abruzzo, Italy
0094
Bishop (Rnd Val)
0096
Drama, Greece

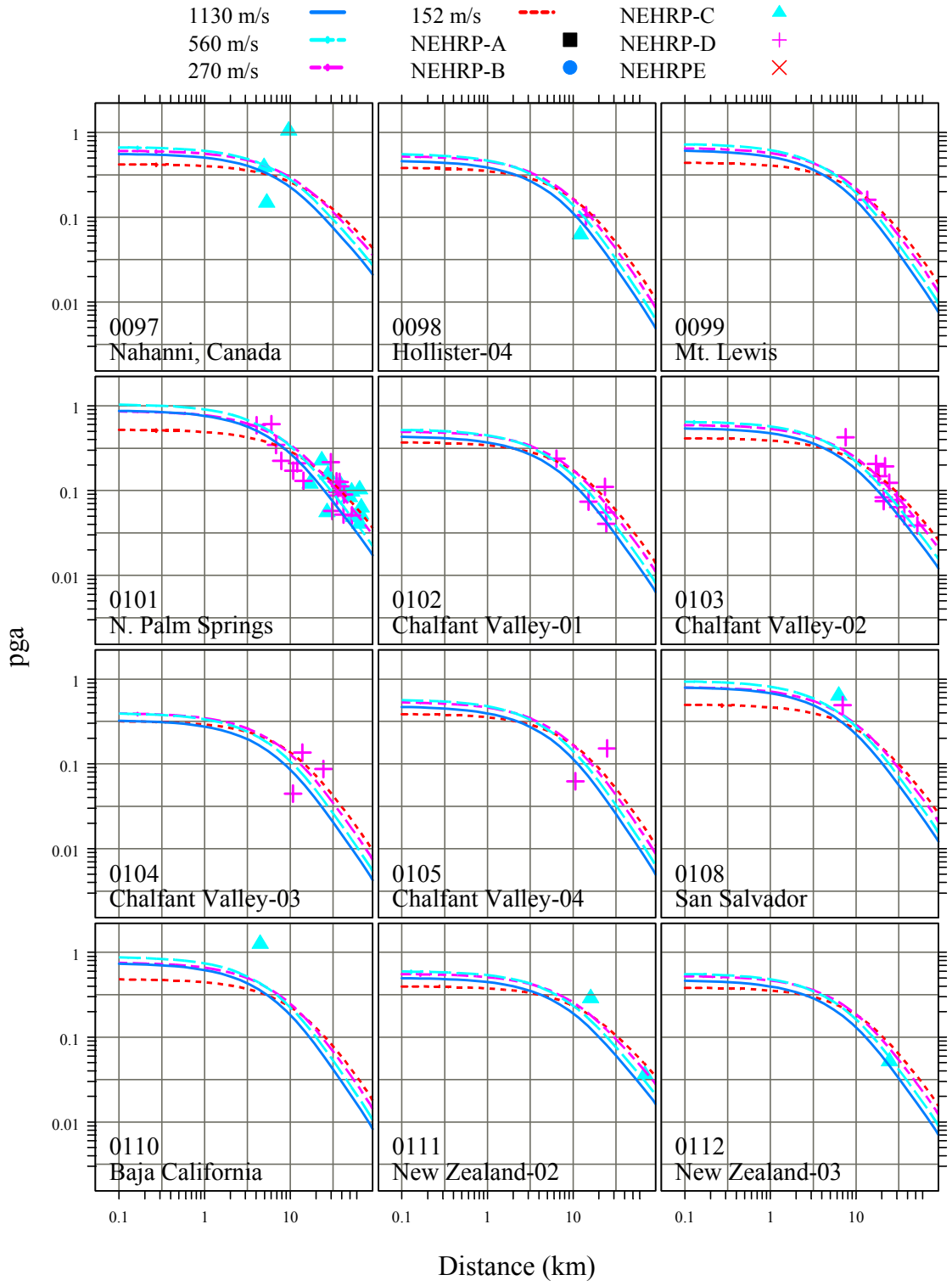
1130 m/s
560 m/s
270 m/s
152 m/s
NEHRP-A
NEHRP-B
NEHRP-C
NEHRP-D
NEHRPE
pga
Distance (km)
0097
Nahanni, Canada
0098
Hollister-04
0099
Mt. Lewis
0101
N. Palm Springs
0102
Chalfant Valley-01
0103
Chalfant Valley-02
0104
Chalfant Valley-03
0105
Chalfant Valley-04
0108
San Salvador
0110
Baja California
0111
New Zealand-02
0112
New Zealand-03

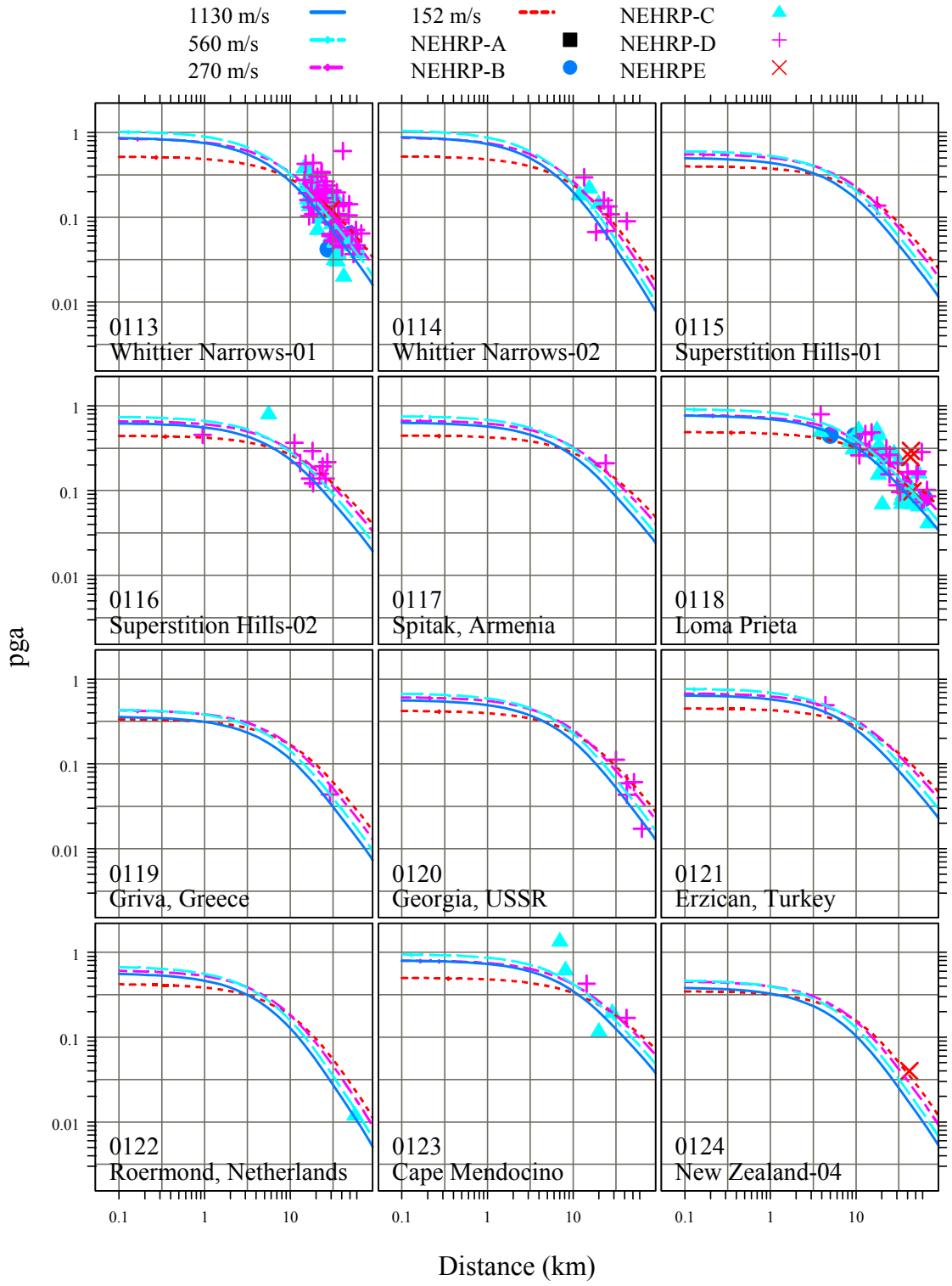
1130 m/s
560 m/s
270 m/s
152 m/s
NEHRP-A
NEHRP-B
NEHRP-C
NEHRP-D
NEHRPE
pga
1
0.1
0.01
0113
Whittier Narrows-01
0114
Whittier Narrows-02
0115
Superstition Hills-01
0116
Superstition Hills-02
0117
Spitak, Armenia
0118
Loma Prieta
0119
Griva, Greece
0120
Georgia, USSR
0121
Erzican, Turkey
0122
Roermond, Netherlands
0123
Cape Mendocino
0124
New Zealand-04
0.1
1
10
Distance (km)

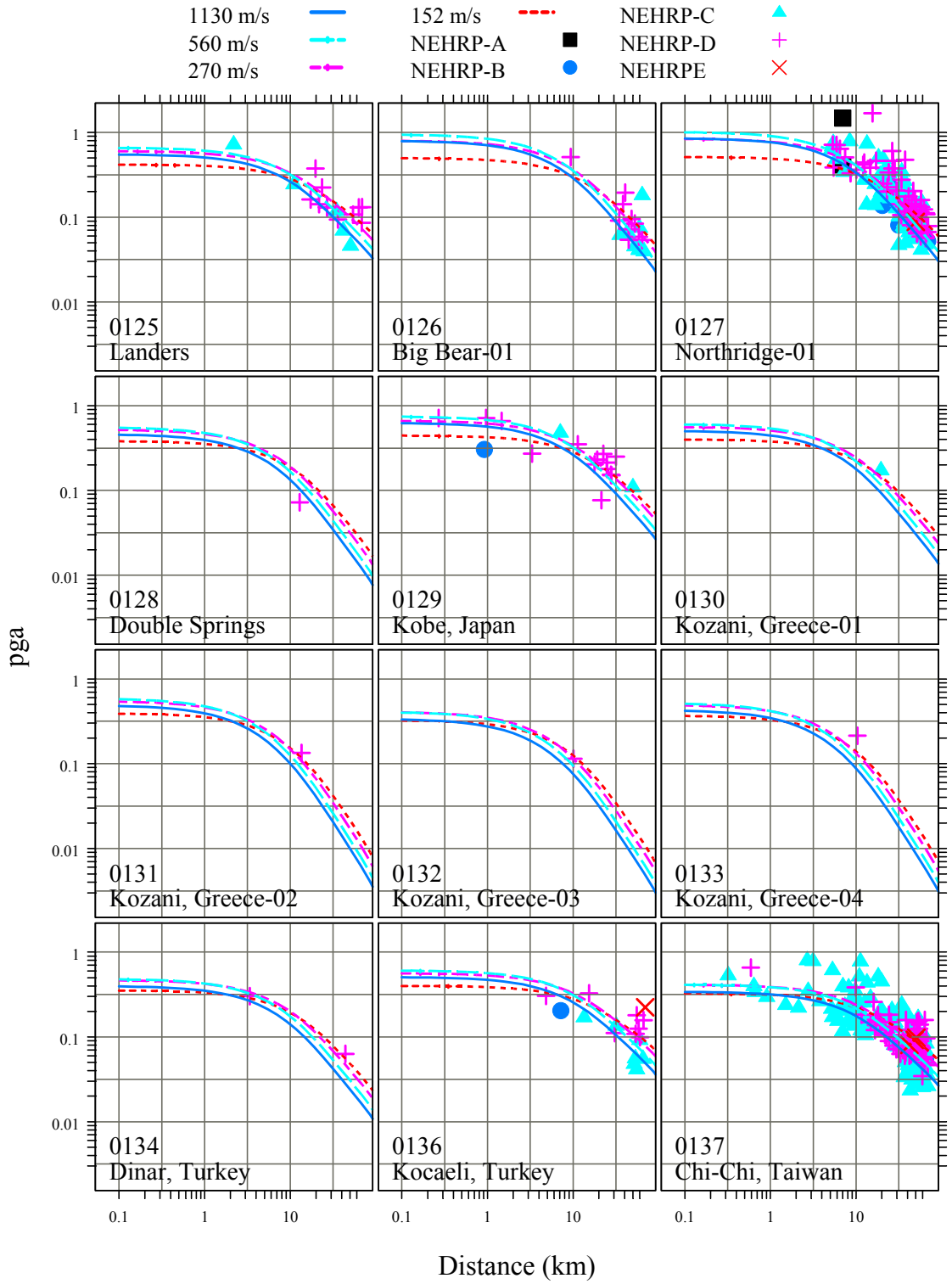
1130 m/s
560 m/s
270 m/s
152 m/s
NEHRP-A
NEHRP-B
NEHRP-C
NEHRP-D
NEHRPE
pga
Distance (km)
0125
Landers
0126
Big Bear-01
0127
Northridge-01
0128
Double Springs
0129
Kobe, Japan
0130
Kozani, Greece-01
0131
Kozani, Greece-02
0132
Kozani, Greece-03
0133
Kozani, Greece-04
0134
Dinar, Turkey
0136
Kocaeli, Turkey
0137
Chi-Chi, Taiwan

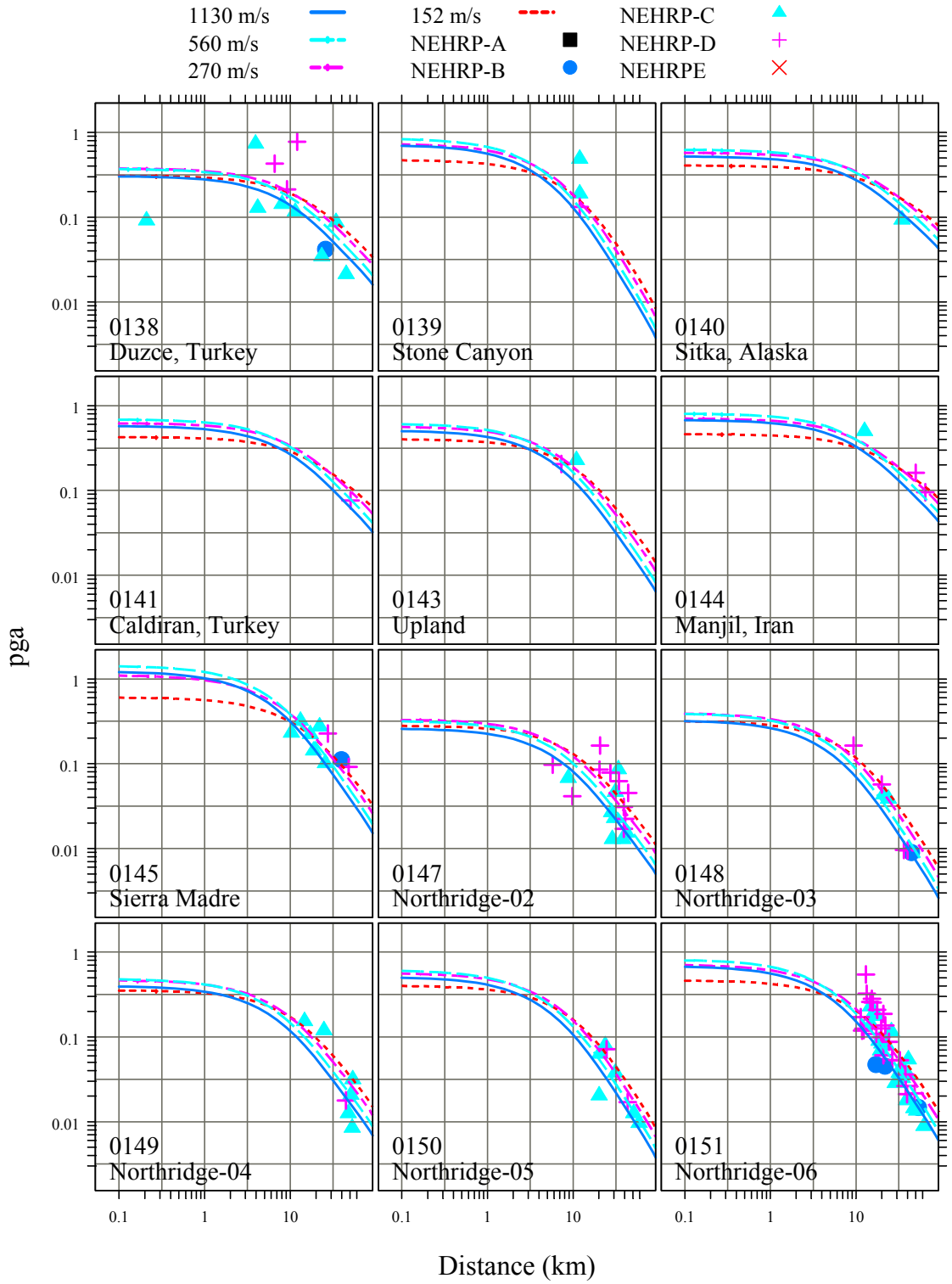
1130 m/s
560 m/s
270 m/s
152 m/s
NEHRP-A
NEHRP-B
NEHRP-C
NEHRP-D
NEHRPE
pga
Distance (km)
0138
Duzce, Turkey
0139
Stone Canyon
0140
Sitka, Alaska
0141
Caldiran, Turkey
0143
Upland
0144
Manjil, Iran
0145
Sierra Madre
0147
Northridge-02
0148
Northridge-03
0149
Northridge-04
0150
Northridge-05
0151
Northridge-06

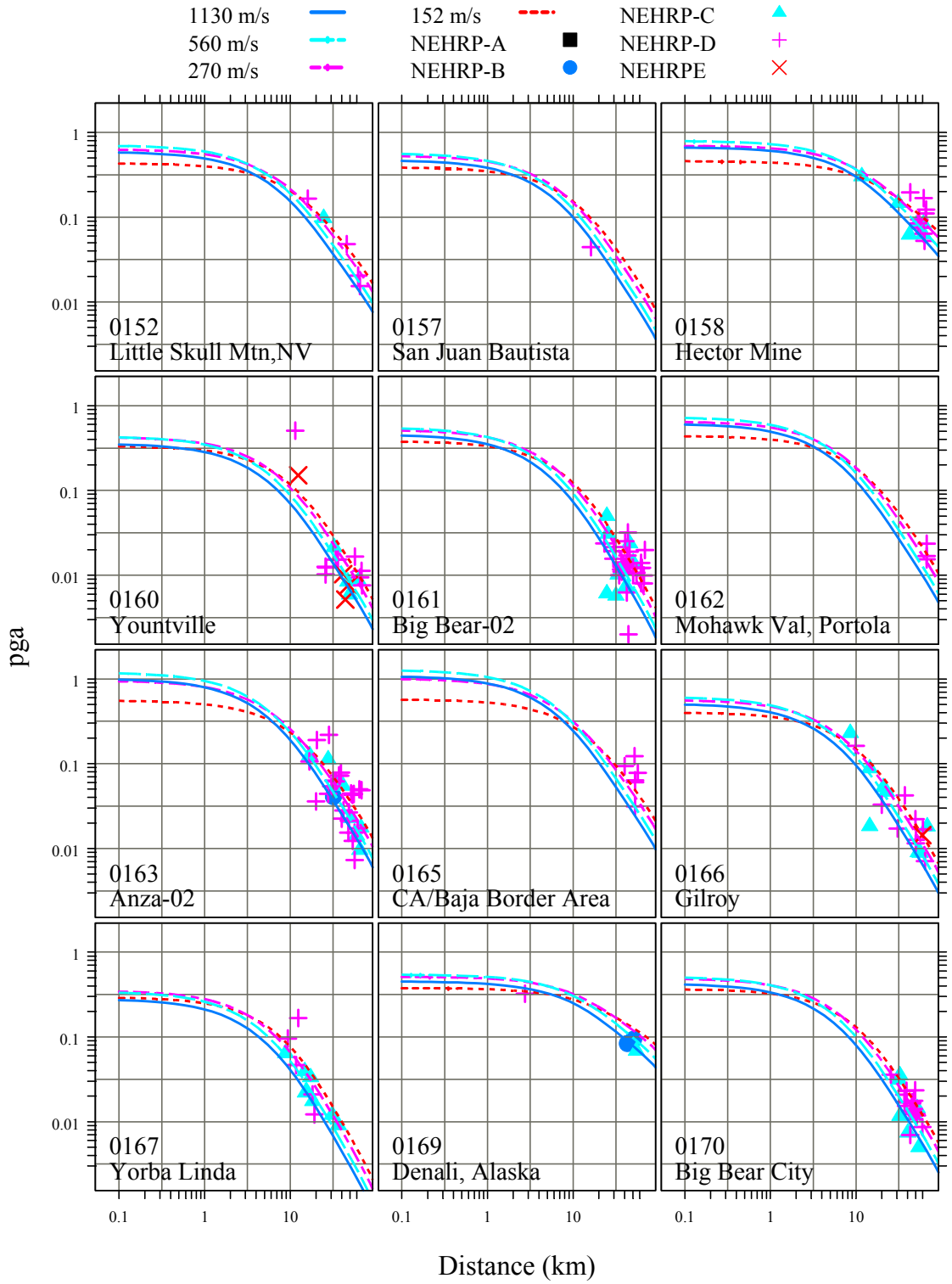
1130 m/s
560 m/s
270 m/s
152 m/s
NEHRP-A
NEHRP-B
NEHRP-C
NEHRP-D
NEHRPE
pga
Distance (km)
0152
Little Skull Mtn,NV
0157
San Juan Bautista
0158
Hector Mine
0160
Yountville
0161
Big Bear-02
0162
Mohawk Val, Portola
0163
Anza-02
0165
CA/Baja Border Area
0166
Gilroy
0167
Yorba Linda
0169
Denali, Alaska
0170
Big Bear City

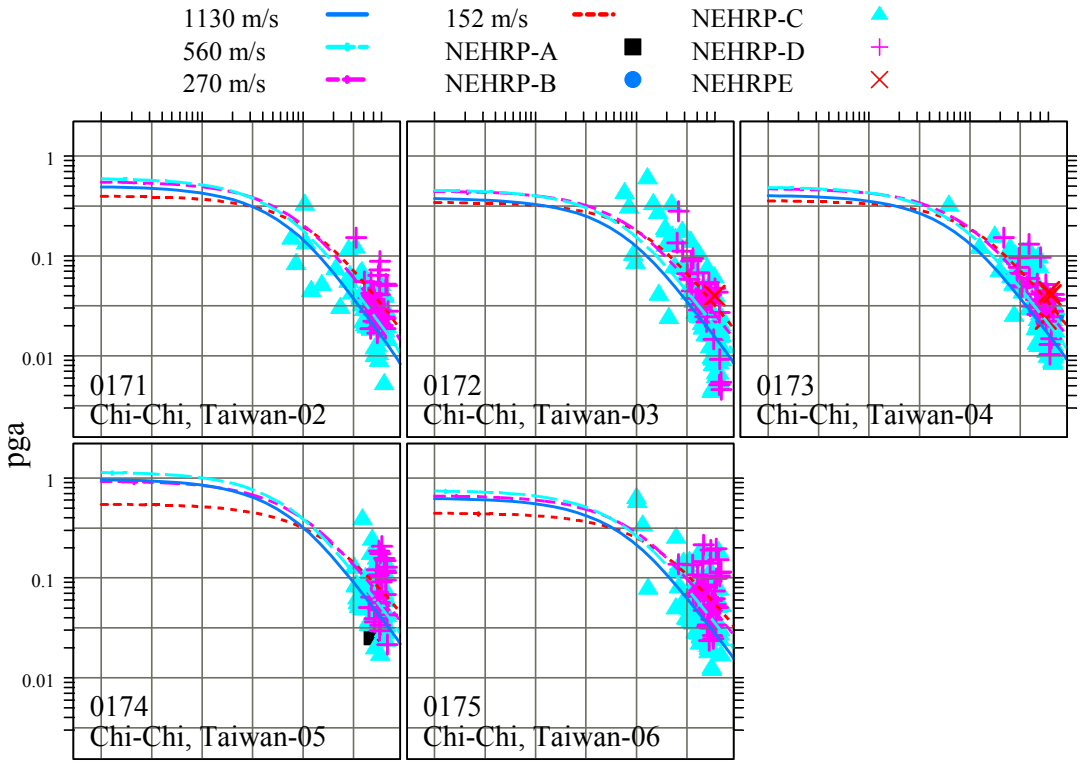
1130 m/s
560 m/s
270 m/s
152 m/s
NEHRP-A
NEHRP-B
NEHRP-C
NEHRP-D
NEHRPE
pga
1
0.1
0.01
0171
Chi-Chi, Taiwan-02
0172
Chi-Chi, Taiwan-03
0173
Chi-Chi, Taiwan-04
0174
Chi-Chi, Taiwan-05
0175
Chi-Chi, Taiwan-06
Distance (km)

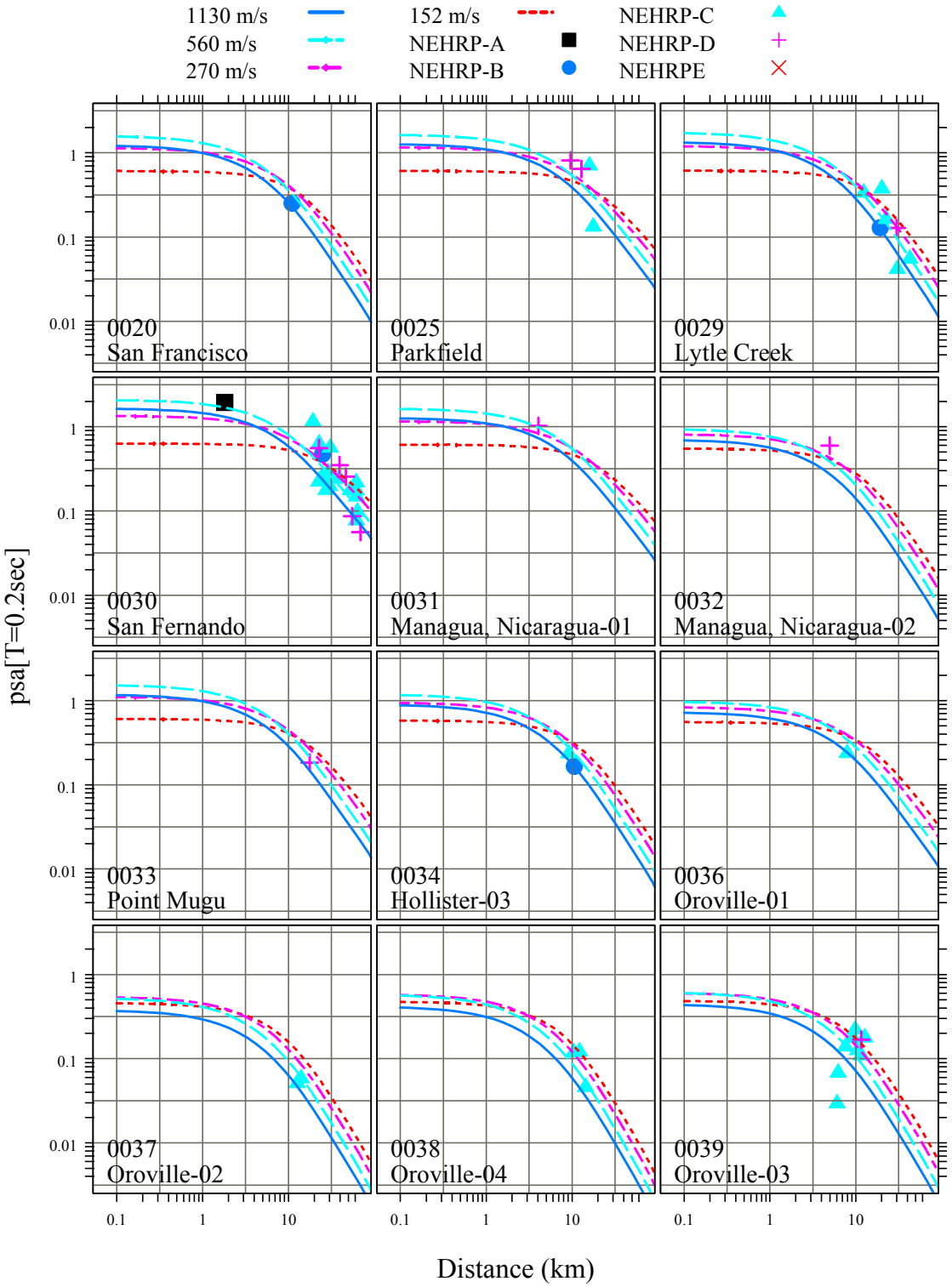
1130 m/s
560 m/s
270 m/s
152 m/s
NEHRP-A
NEHRP-B
NEHRP-C
NEHRP-D
NEHRPE
psa[T=0.2sec]
Distance (km)
0020
San Francisco
0025
Parkfield
0029
Lytle Creek
0030
San Fernando
0031
Managua, Nicaragua-01
0032
Managua, Nicaragua-02
0033
Point Mugu
0034
Hollister-03
0036
Oroville-01
0037
Oroville-02
0038
Oroville-04
0039
Oroville-03

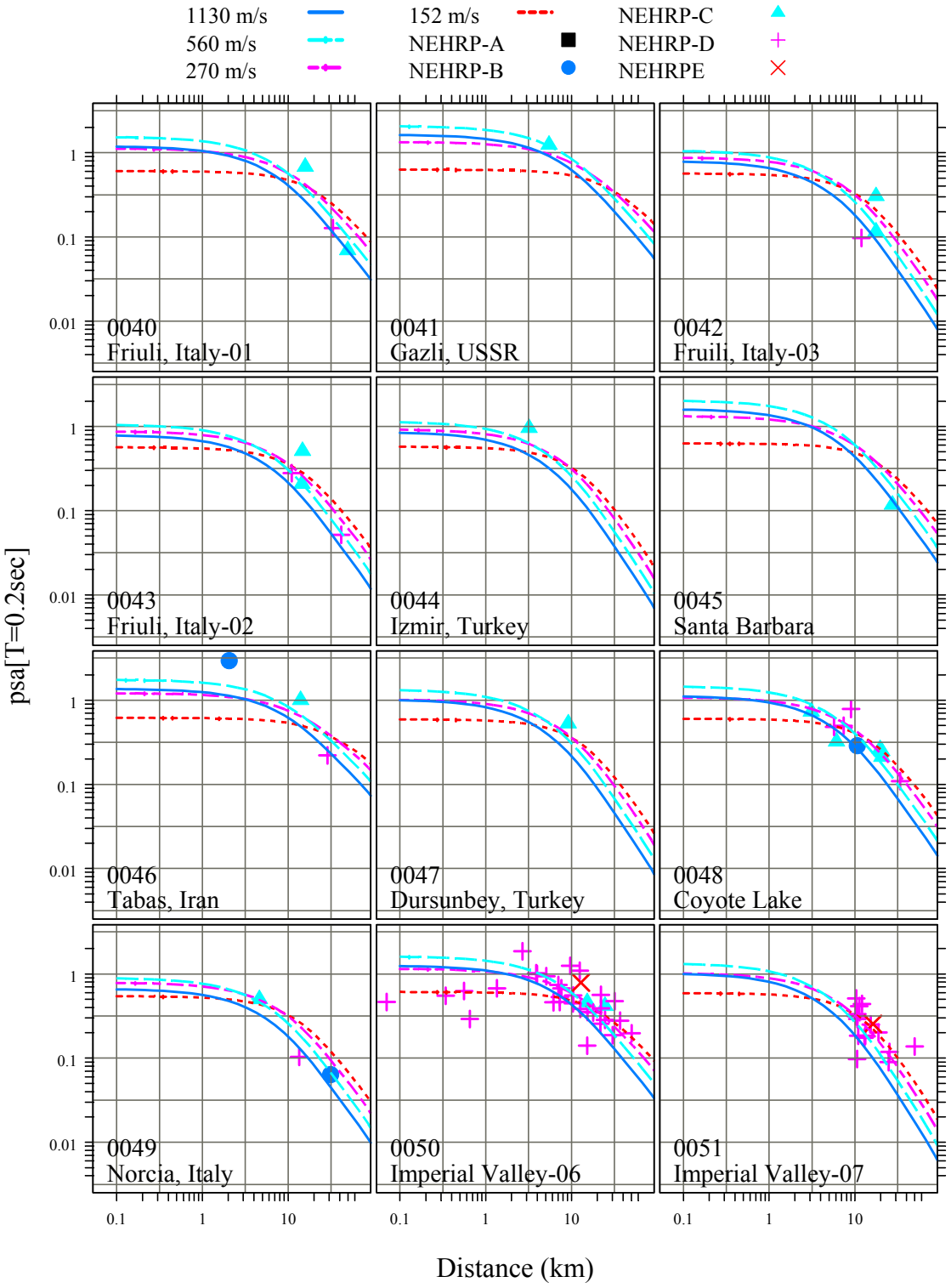
1130 m/s
560 m/s
270 m/s
152 m/s
NEHRP-A
NEHRP-B
NEHRP-C
NEHRP-D
NEHRPE
psa[T=0.2sec]
0040
Friuli, Italy-01
0041
Gazli, USSR
0042
Fruili, Italy-03
0043
Friuli, Italy-02
0044
Izmir, Turkey
0045
Santa Barbara
0046
Tabas, Iran
0047
Dursunbey, Turkey
0048
Coyote Lake
0049
Norcia, Italy
0050
Imperial Valley-06
0051
Imperial Valley-07
1
0.1
0.01
0.1
1
10
Distance (km)

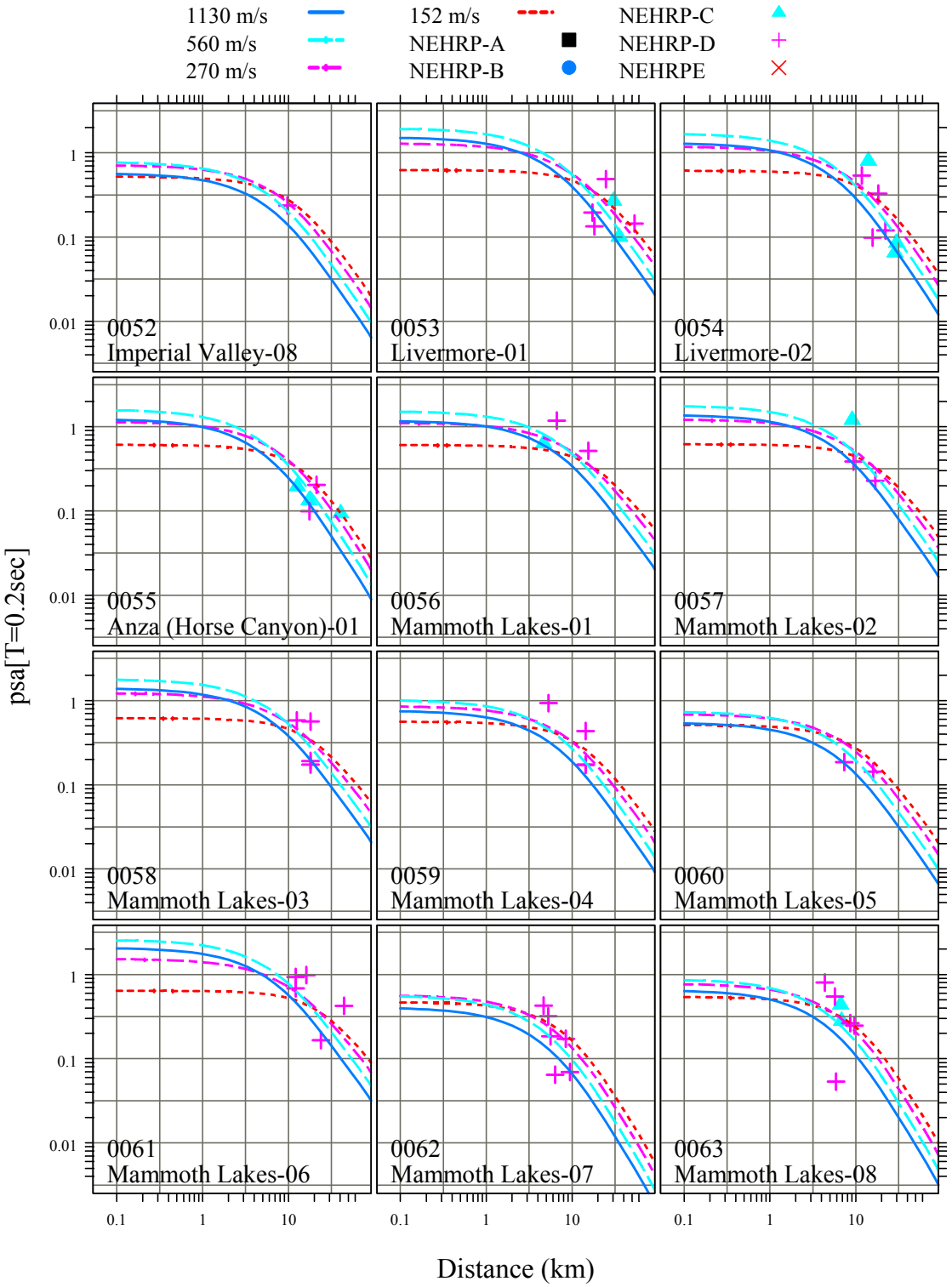
1130 m/s
560 m/s
270 m/s
152 m/s
NEHRP-A
NEHRP-B
NEHRP-C
NEHRP-D
NEHRPE
psa[T=0.2sec]
0052
Imperial Valley-08
0053
Livermore-01
0054
Livermore-02
0055
Anza (Horse Canyon)-01
0056
Mammoth Lakes-01
0057
Mammoth Lakes-02
0058
Mammoth Lakes-03
0059
Mammoth Lakes-04
0060
Mammoth Lakes-05
0061
Mammoth Lakes-06
0062
Mammoth Lakes-07
0063
Mammoth Lakes-08
1
0.1
0.01
0.1
1
10
Distance (km)

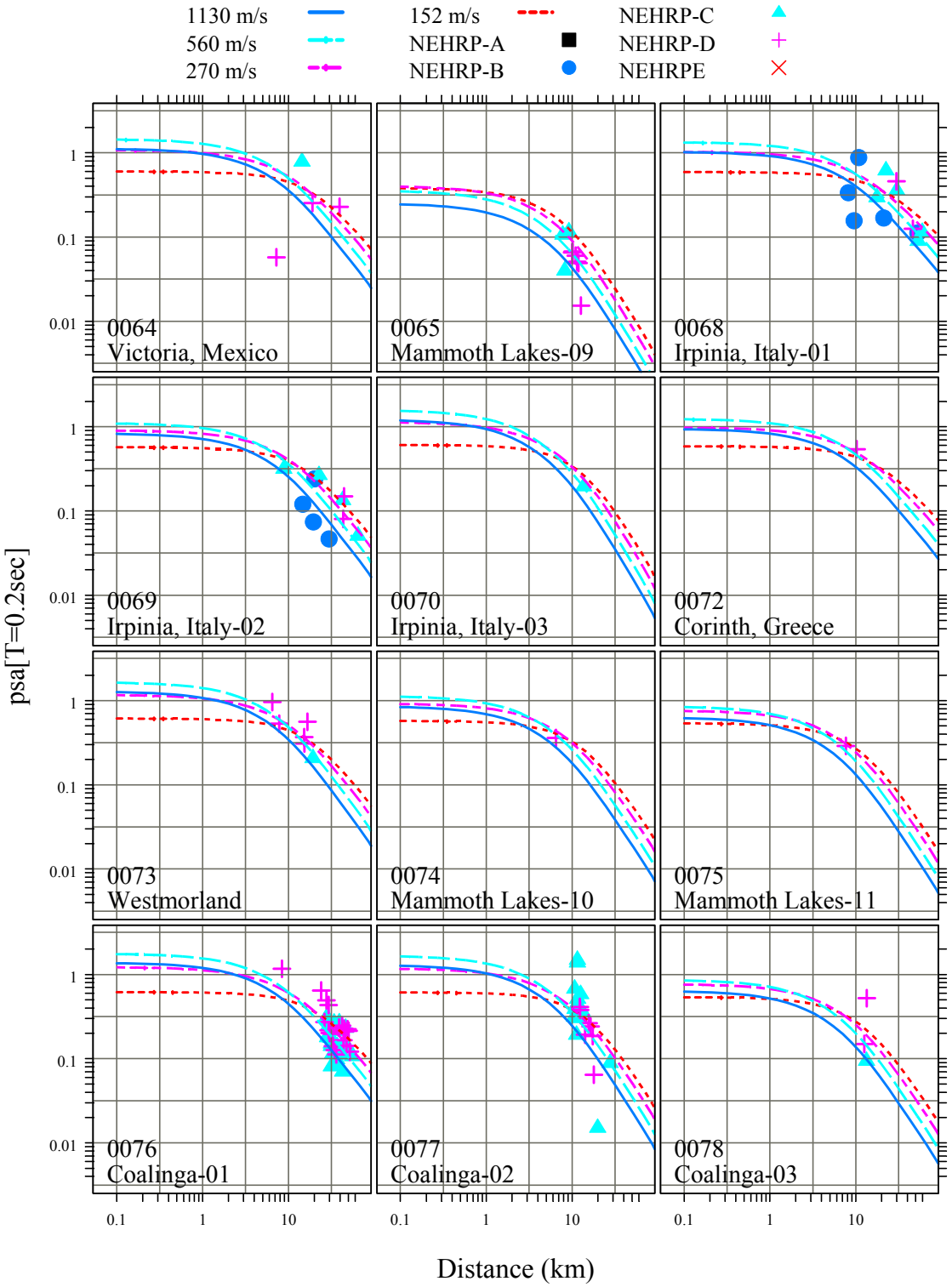
1130 m/s
560 m/s
270 m/s
152 m/s
NEHRP-A
NEHRP-B
NEHRP-C
NEHRP-D
NEHRPE
psa[T=0.2sec]
Distance (km)
0064
Victoria, Mexico
0065
Mammoth Lakes-09
0068
Irpinia, Italy-01
0069
Irpinia, Italy-02
0070
Irpinia, Italy-03
0072
Corinth, Greece
0073
Westmorland
0074
Mammoth Lakes-10
0075
Mammoth Lakes-11
0076
Coalinga-01
0077
Coalinga-02
0078
Coalinga-03

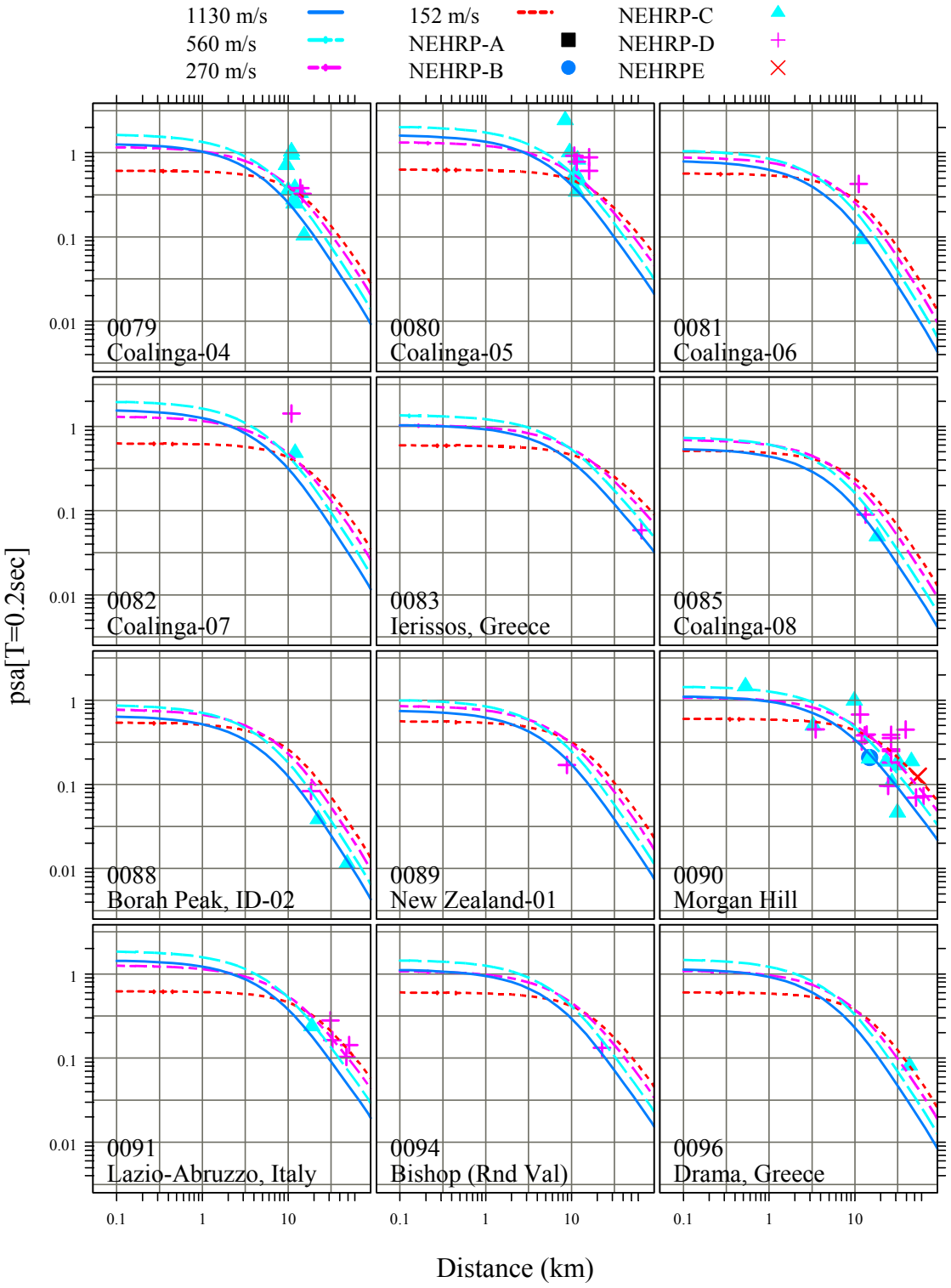
1130 m/s
560 m/s
270 m/s
152 m/s
NEHRP-A
NEHRP-B
NEHRP-C
NEHRP-D
NEHRPE
psa[T=0.2sec]
Distance (km)
0079
Coalinga-04
0080
Coalinga-05
0081
Coalinga-06
0082
Coalinga-07
0083
Ierissos, Greece
0085
Coalinga-08
0088
Borah Peak, ID-02
0089
New Zealand-01
0090
Morgan Hill
0091
Lazio-Abruzzo, Italy
0094
Bishop (Rnd Val)
0096
Drama, Greece

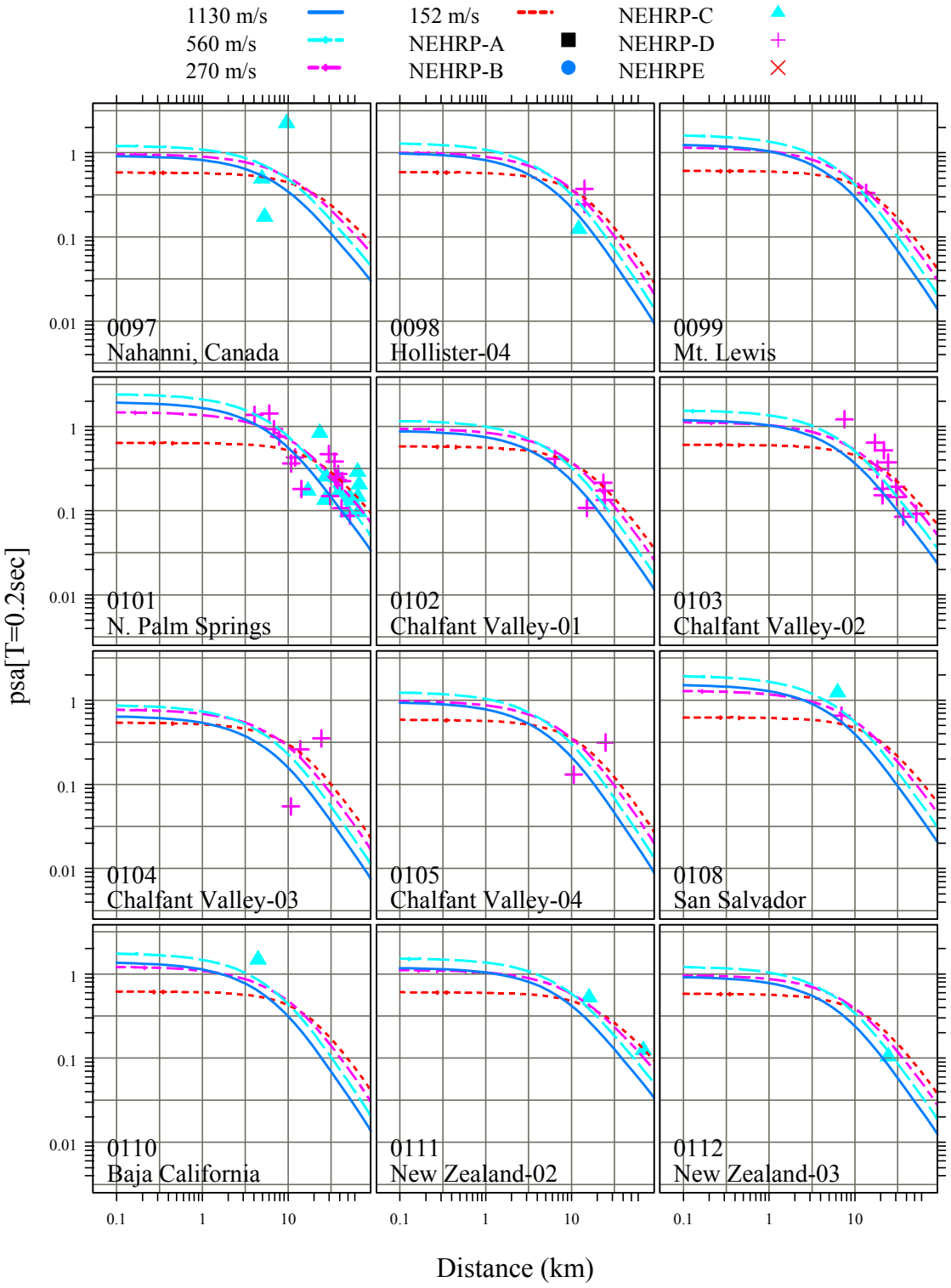
1130 m/s
560 m/s
270 m/s
152 m/s
NEHRP-A
NEHRP-B
NEHRP-C
NEHRP-D
NEHRPE
psa[T=0.2sec]
Distance (km)
0097
Nahanni, Canada
0098
Hollister-04
0099
Mt. Lewis
0101
N. Palm Springs
0102
Chalfant Valley-01
0103
Chalfant Valley-02
0104
Chalfant Valley-03
0105
Chalfant Valley-04
0108
San Salvador
0110
Baja California
0111
New Zealand-02
0112
New Zealand-03

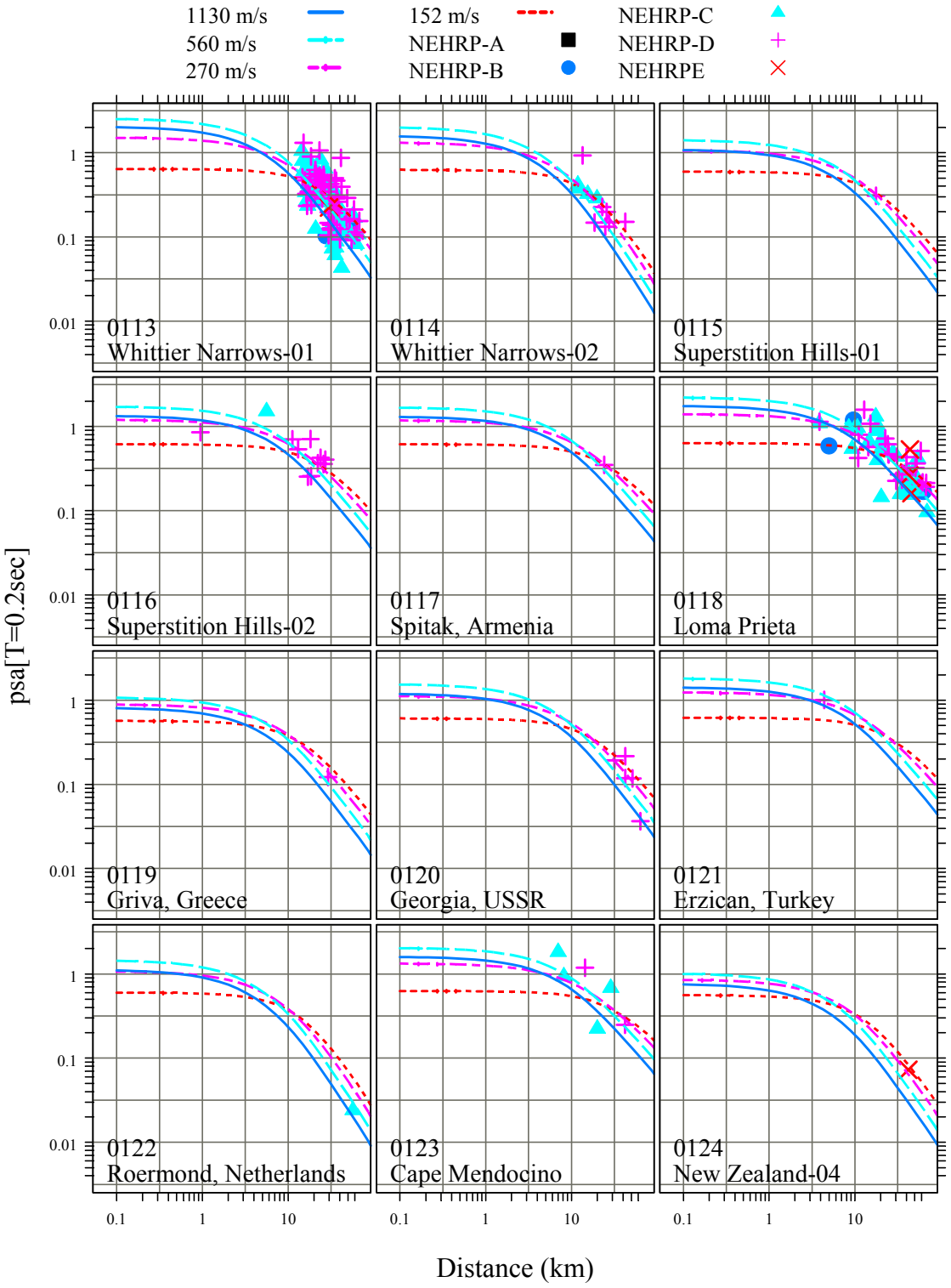
1130 m/s
560 m/s
270 m/s
152 m/s
NEHRP-A
NEHRP-B
NEHRP-C
NEHRP-D
NEHRPE
psa[T=0.2sec]
Distance (km)
0113
Whittier Narrows-01
0114
Whittier Narrows-02
0115
Superstition Hills-01
0116
Superstition Hills-02
0117
Spitak, Armenia
0118
Loma Prieta
0119
Griva, Greece
0120
Georgia, USSR
0121
Erzican, Turkey
0122
Roermond, Netherlands
0123
Cape Mendocino
0124
New Zealand-04

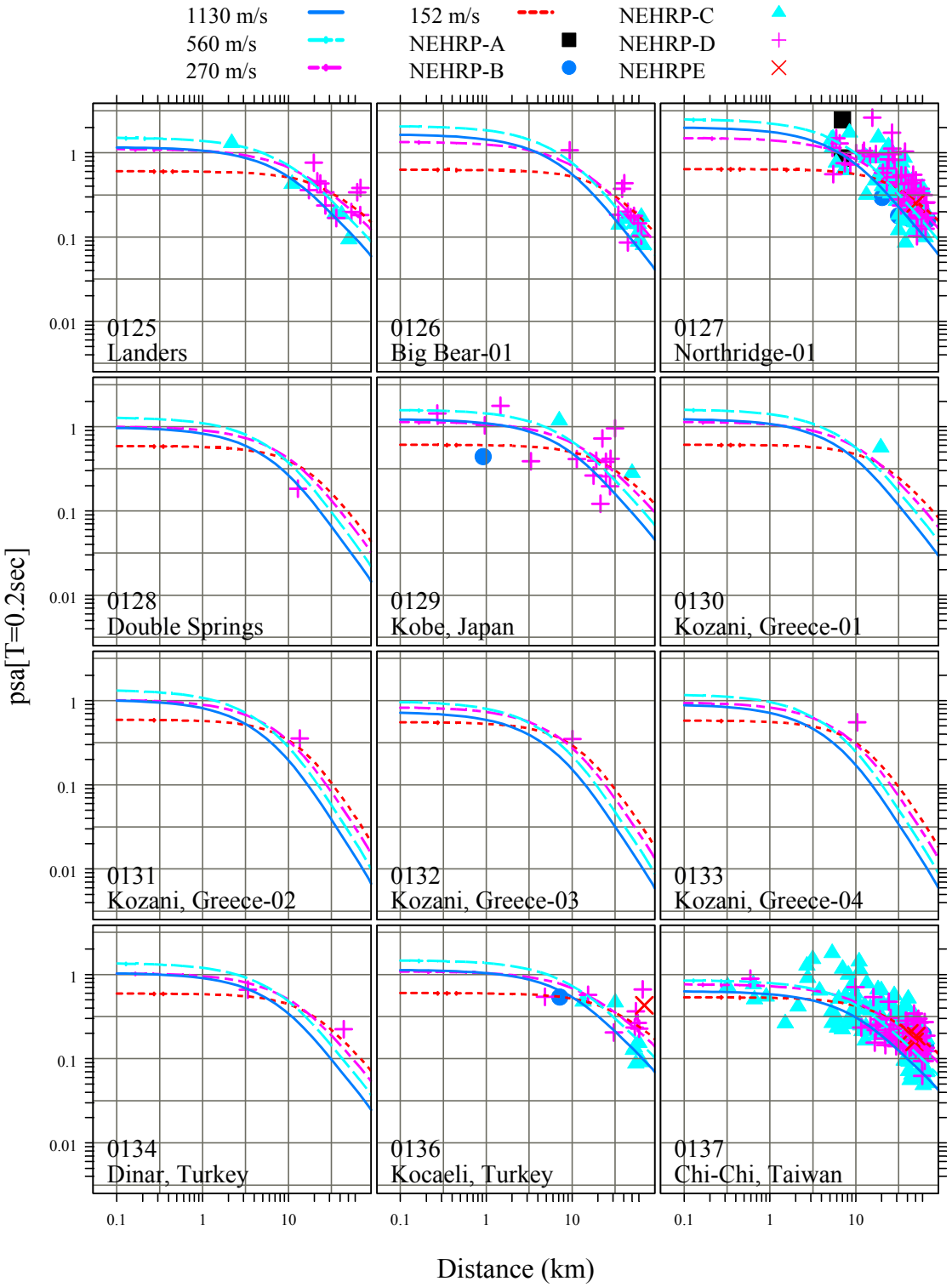
1130 m/s
560 m/s
270 m/s
152 m/s
NEHRP-A
NEHRP-B
NEHRP-C
NEHRP-D
NEHRPE
psa[T=0.2sec]
Distance (km)
0125
Landers
0126
Big Bear-01
0127
Northridge-01
0128
Double Springs
0129
Kobe, Japan
0130
Kozani, Greece-01
0131
Kozani, Greece-02
0132
Kozani, Greece-03
0133
Kozani, Greece-04
0134
Dinar, Turkey
0136
Kocaeli, Turkey
0137
Chi-Chi, Taiwan

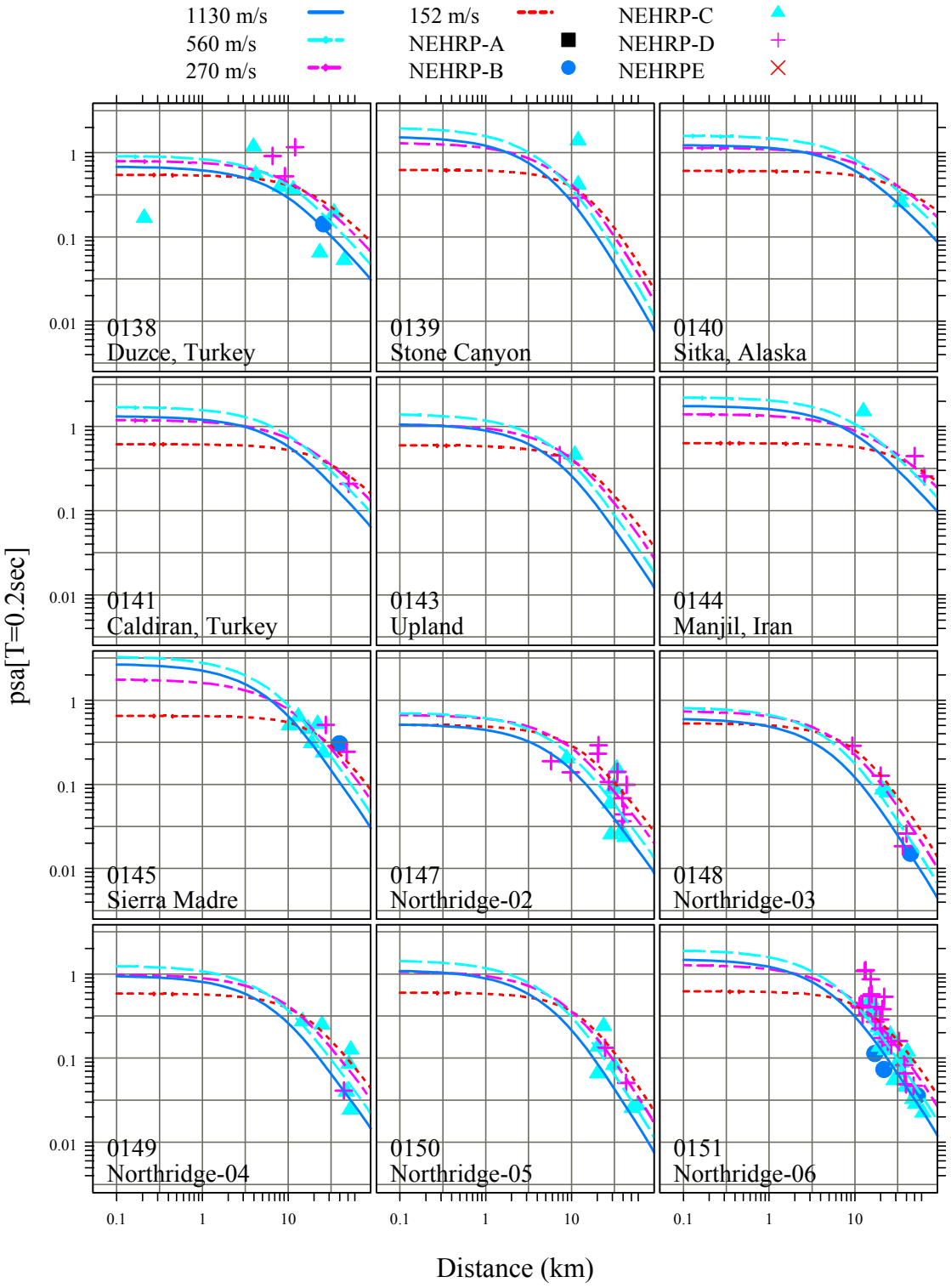
1130 m/s
560 m/s
270 m/s
152 m/s
NEHRP-A
NEHRP-B
NEHRP-C
NEHRP-D
NEHRPE
psa[T=0.2sec]
Distance (km)
0138
Duzce, Turkey
0139
Stone Canyon
0140
Sitka, Alaska
0141
Caldiran, Turkey
0143
Upland
0144
Manjil, Iran
0145
Sierra Madre
0147
Northridge-02
0148
Northridge-03
0149
Northridge-04
0150
Northridge-05
0151
Northridge-06

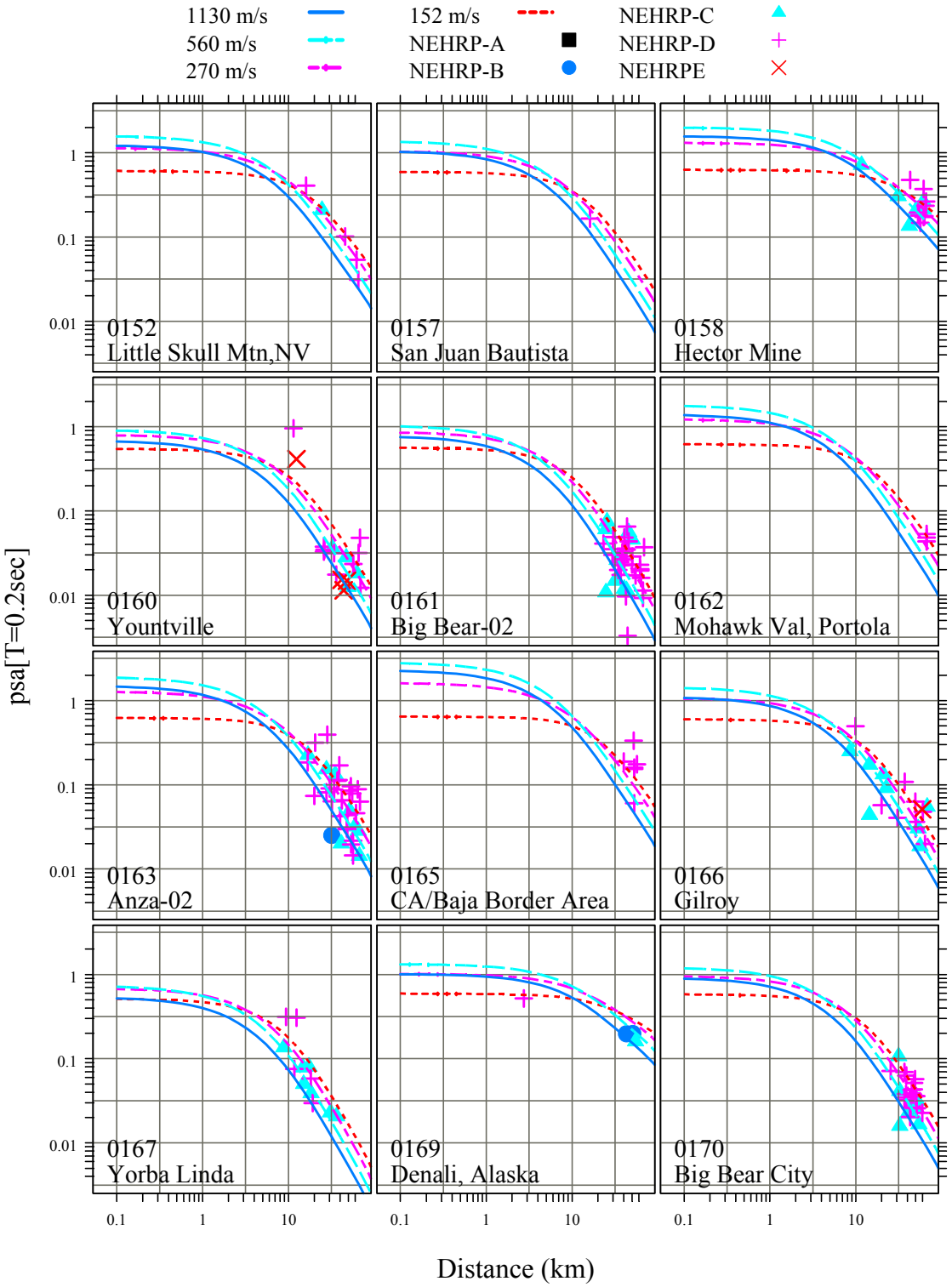
1130 m/s
560 m/s
270 m/s
152 m/s
NEHRP-A
NEHRP-B
NEHRP-C
NEHRP-D
NEHRPE
psa[T=0.2sec]
0152
Little Skull Mtn,NV
0157
San Juan Bautista
0158
Hector Mine
0160
Yountville
0161
Big Bear-02
0162
Mohawk Val, Portola
0163
Anza-02
0165
CA/Baja Border Area
0166
Gilroy
0167
Yorba Linda
0169
Denali, Alaska
0170
Big Bear City
1
0.1
0.01
0.1
1
10
Distance (km)

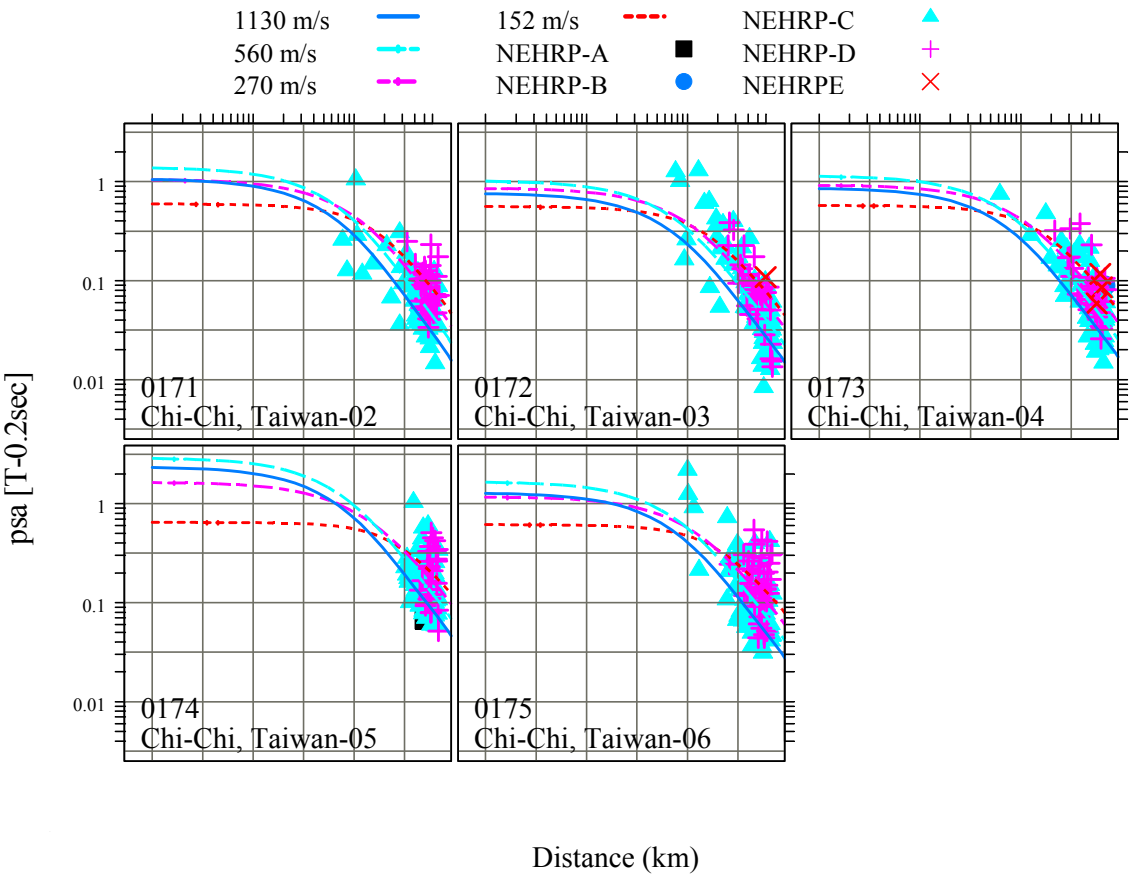
1130 m/s
560 m/s
270 m/s
152 m/s
NEHRP-A
NEHRP-B
NEHRP-C
NEHRP-D
NEHRPE
psa [T-0.2sec]
1
0.1
0.01
0171
Chi-Chi, Taiwan-02
0172
Chi-Chi, Taiwan-03
0173
Chi-Chi, Taiwan-04
0174
Chi-Chi, Taiwan-05
0175
Chi-Chi, Taiwan-06
Distance (km)

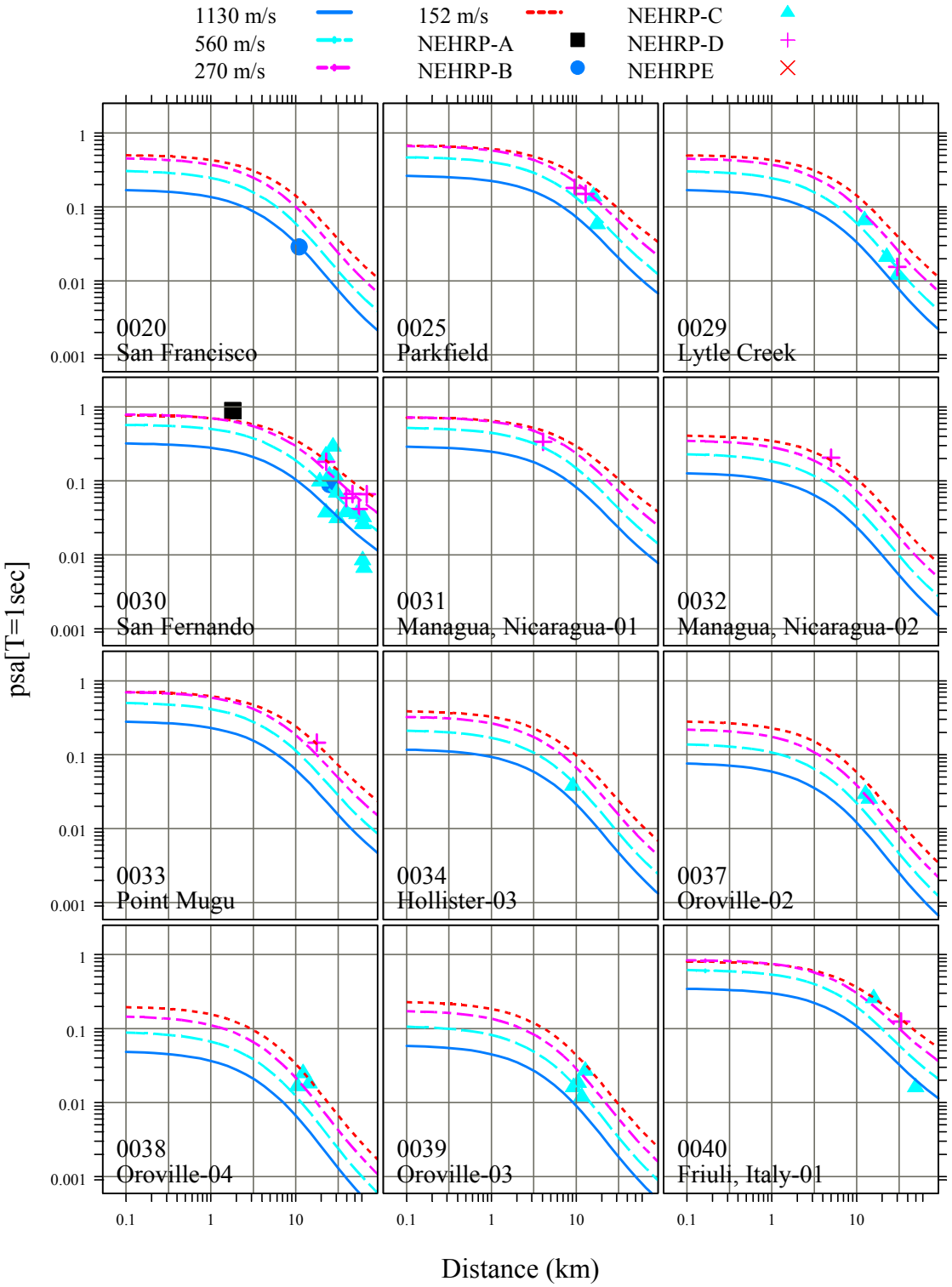
1130 m/s
560 m/s
270 m/s
152 m/s
NEHRP-A
NEHRP-B
NEHRP-C
NEHRP-D
NEHRPE
psa[T=1sec]
Distance (km)
0020
San Francisco
0025
Parkfield
0029
Lytle Creek
0030
San Fernando
0031
Managua, Nicaragua-01
0032
Managua, Nicaragua-02
0033
Point Mugu
0034
Hollister-03
0037
Oroville-02
0038
Oroville-04
0039
Oroville-03
0040
Friuli, Italy-01

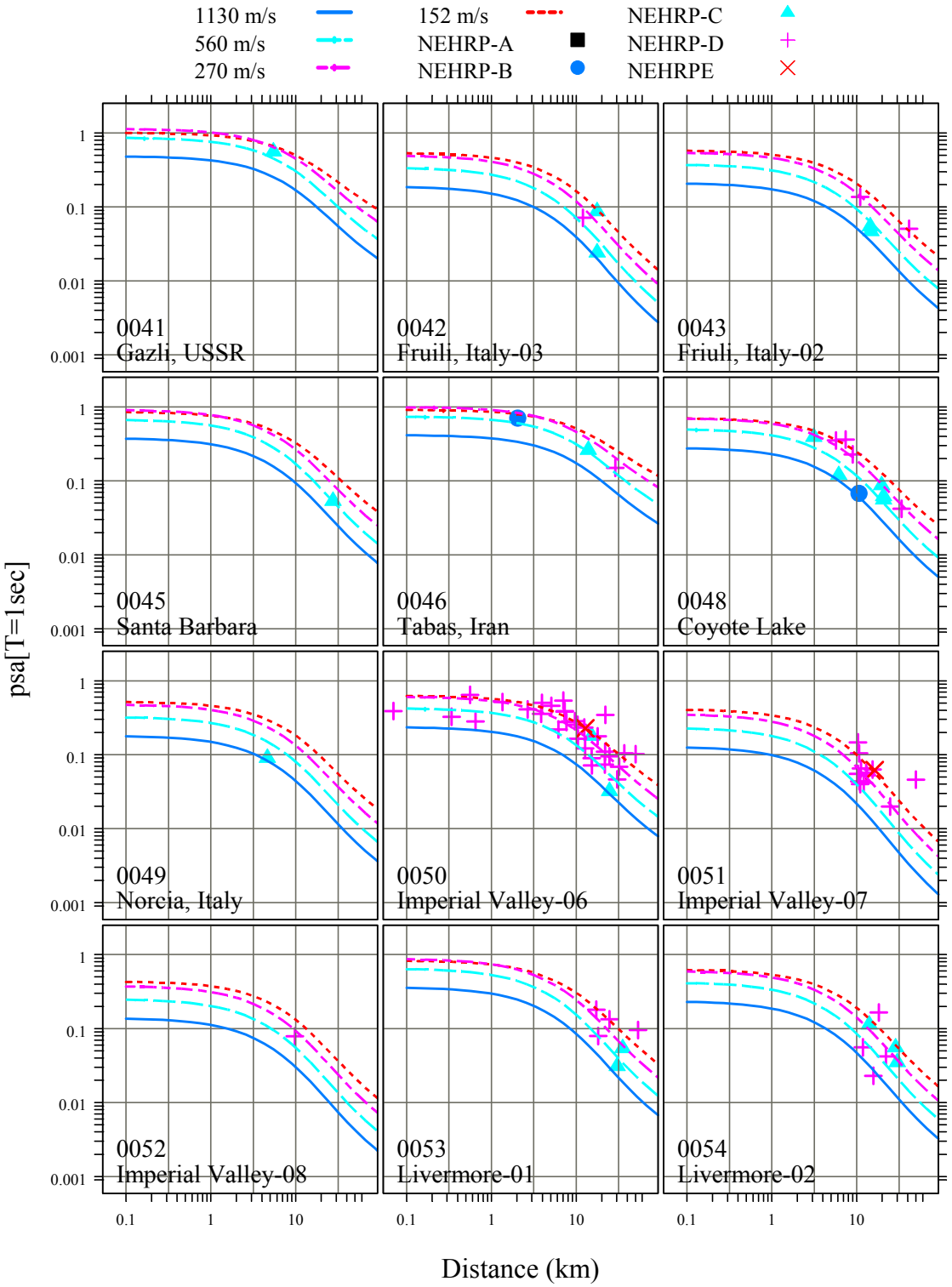
1130 m/s
560 m/s
270 m/s
152 m/s
NEHRP-A
NEHRP-B
NEHRP-C
NEHRP-D
NEHRPE
psa[T=1sec]
0041
Gazli, USSR
0042
Fruili, Italy-03
0043
Friuli, Italy-02
0045
Santa Barbara
0046
Tabas, Iran
0048
Coyote Lake
0049
Norcia, Italy
0050
Imperial Valley-06
0051
Imperial Valley-07
0052
Imperial Valley-08
0053
Livermore-01
0054
Livermore-02
1
0.1
0.01
0.001
0.1
1
10
Distance (km)

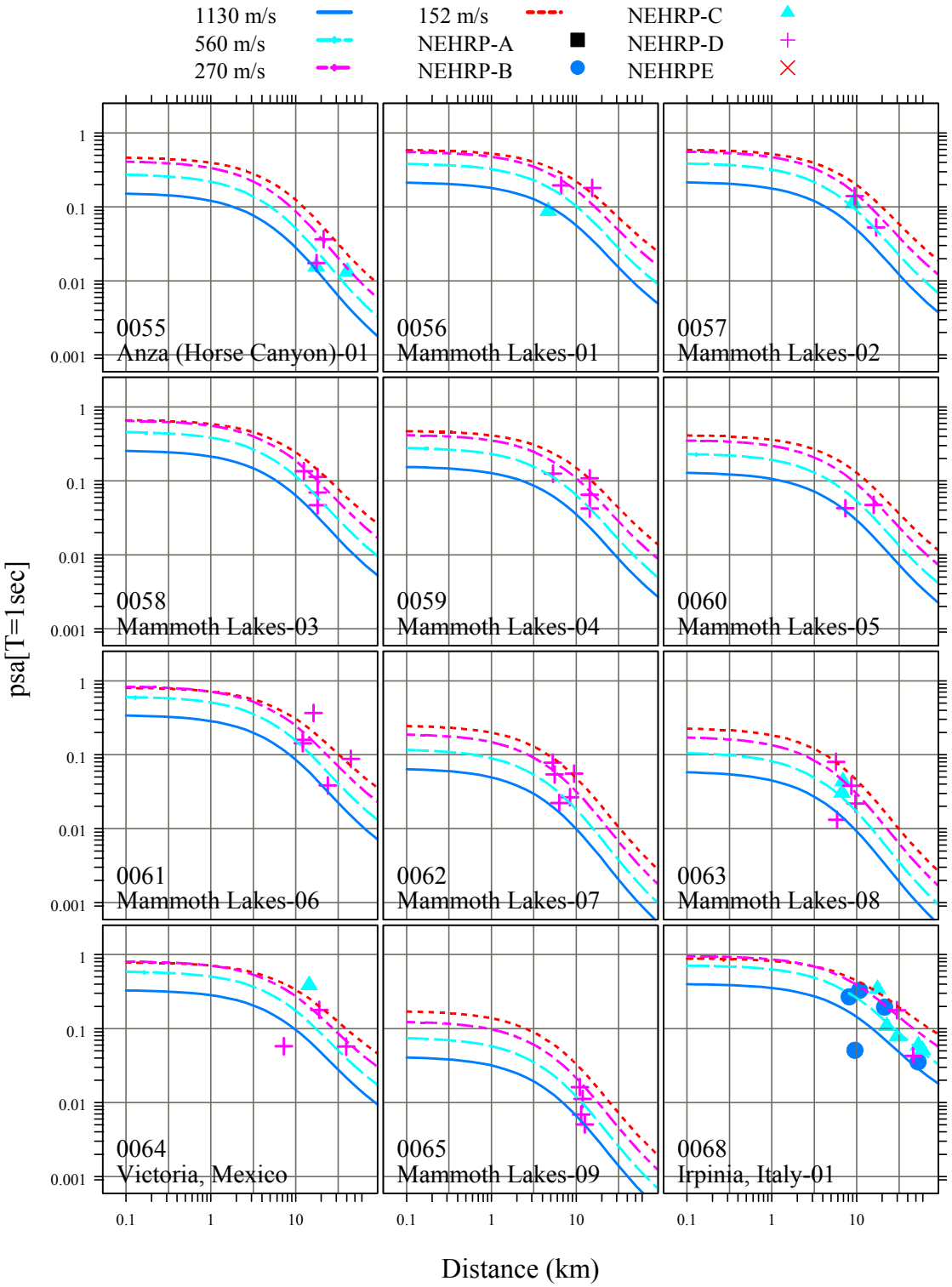
1130 m/s
560 m/s
270 m/s
152 m/s
NEHRP-A
NEHRP-B
NEHRP-C
NEHRP-D
NEHRPE
psa[T=1sec]
Distance (km)
0055
Anza (Horse Canyon)-01
0056
Mammoth Lakes-01
0057
Mammoth Lakes-02
0058
Mammoth Lakes-03
0059
Mammoth Lakes-04
0060
Mammoth Lakes-05
0061
Mammoth Lakes-06
0062
Mammoth Lakes-07
0063
Mammoth Lakes-08
0064
Victoria, Mexico
0065
Mammoth Lakes-09
0068
Irpinia, Italy-01

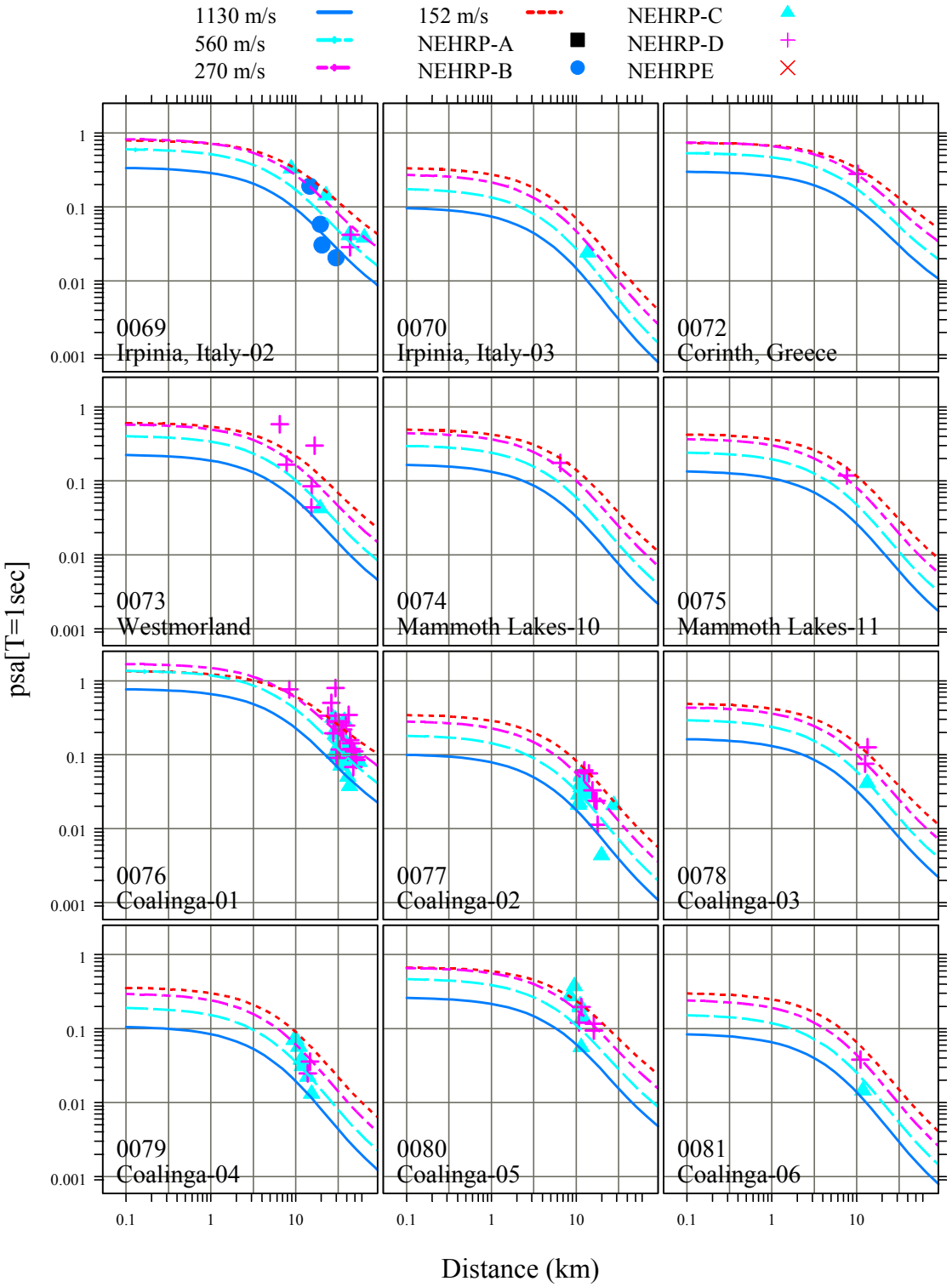
1130 m/s
560 m/s
270 m/s
152 m/s
NEHRP-A
NEHRP-B
NEHRP-C
NEHRP-D
NEHRPE
0069
Irpinia, Italy-02
0070
Irpinia, Italy-03
0072
Corinth, Greece
0073
Westmorland
0074
Mammoth Lakes-10
0075
Mammoth Lakes-11
0076
Coalinga-01
0077
Coalinga-02
0078
Coalinga-03
0079
Coalinga-04
0080
Coalinga-05
0081
Coalinga-06
psa[T=1sec]
Distance (km)

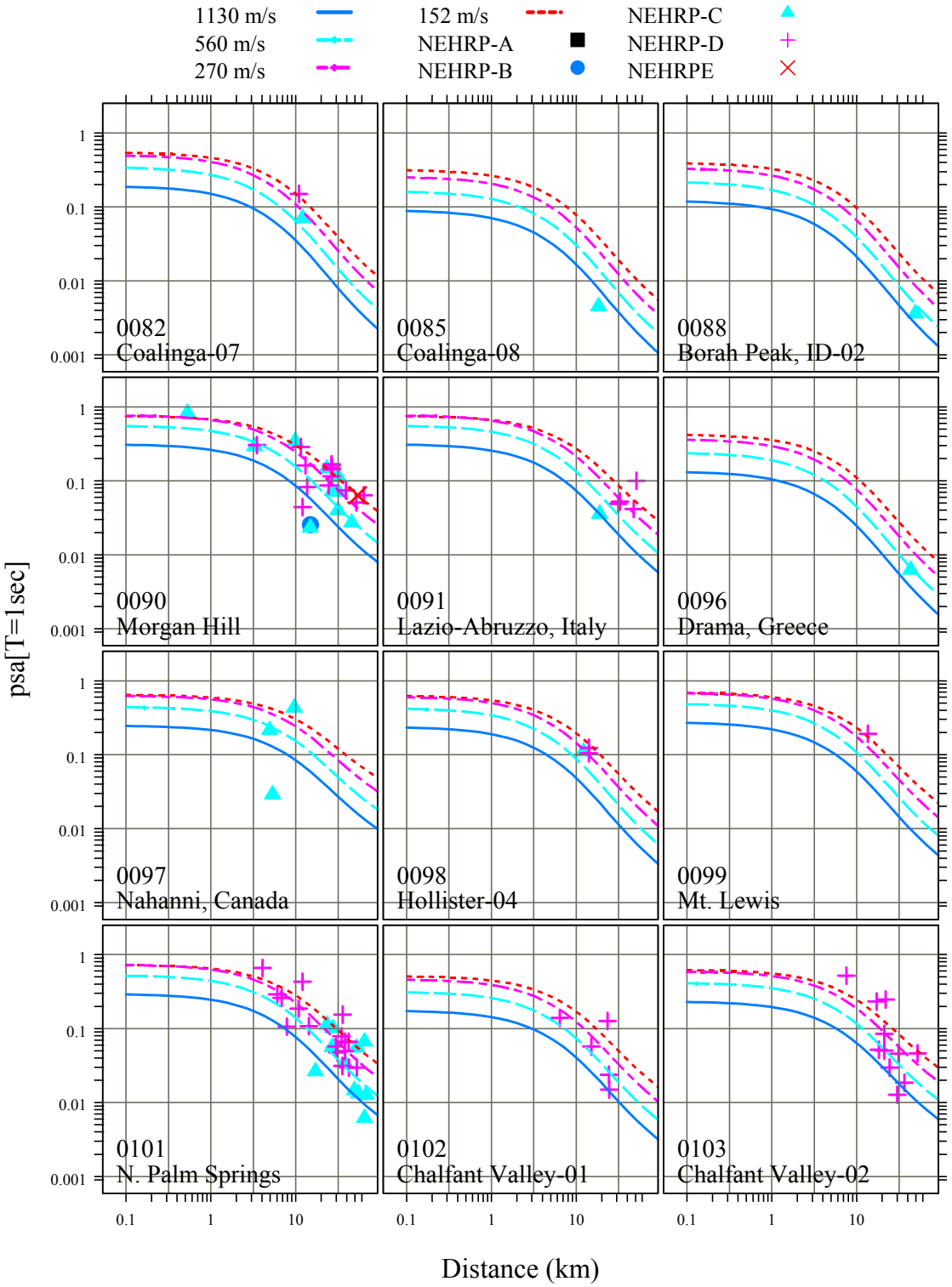
1130 m/s
560 m/s
270 m/s
152 m/s
NEHRP-A
NEHRP-B
NEHRP-C
NEHRP-D
NEHRPE
psa[T=1sec]
Distance (km)
0082
Coalinga-07
0085
Coalinga-08
0088
Borah Peak, ID-02
0090
Morgan Hill
0091
Lazio-Abruzzo, Italy
0096
Drama, Greece
0097
Nahanni, Canada
0098
Hollister-04
0099
Mt. Lewis
0101
N. Palm Springs
0102
Chalfant Valley-01
0103
Chalfant Valley-02

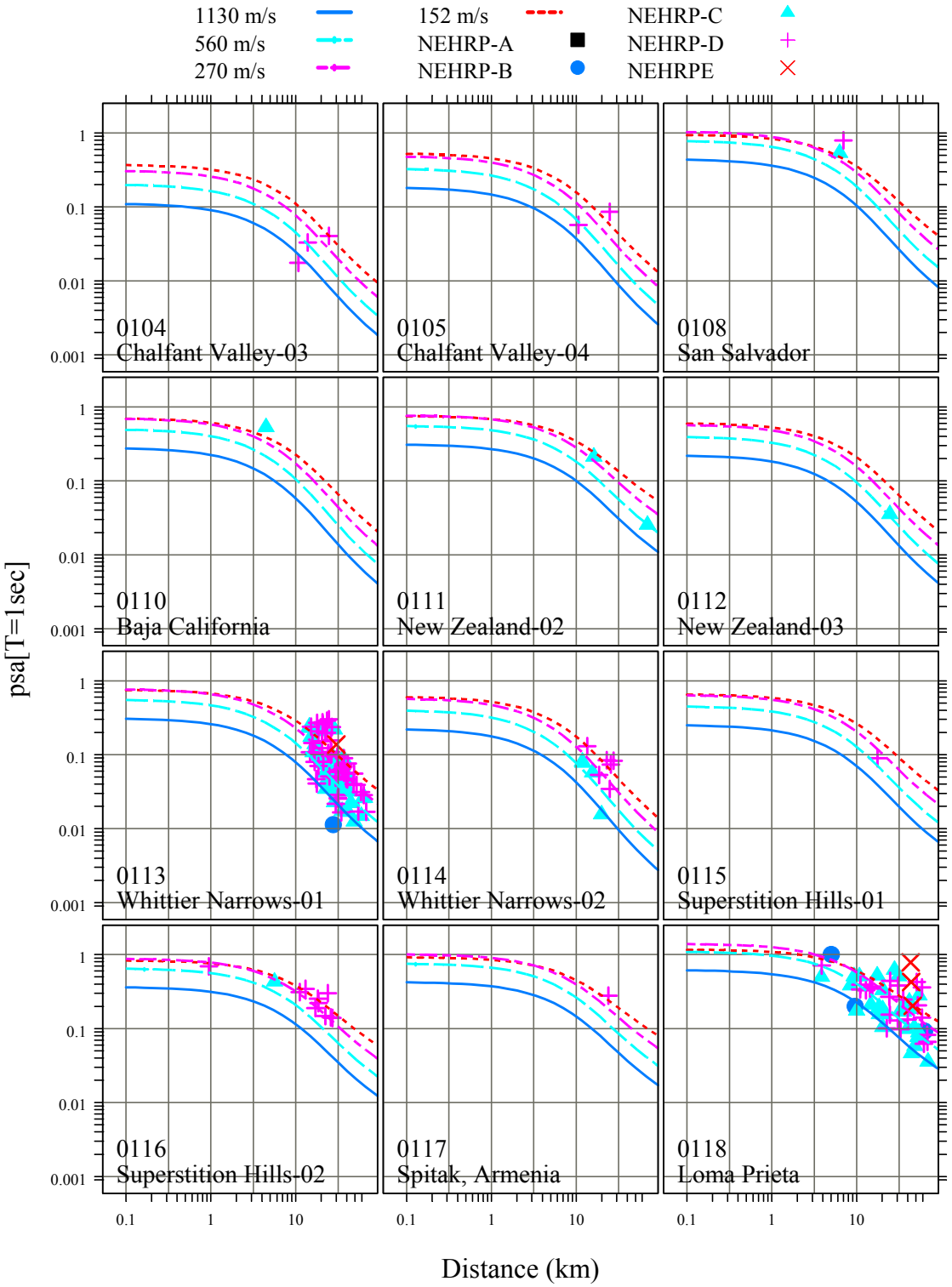
1130 m/s
560 m/s
270 m/s
152 m/s
NEHRP-A
NEHRP-B
NEHRP-C
NEHRP-D
NEHRPE
psa[T=1sec]
Distance (km)
0104
Chalfant Valley-03
0105
Chalfant Valley-04
0108
San Salvador
0110
Baja California
0111
New Zealand-02
0112
New Zealand-03
0113
Whittier Narrows-01
0114
Whittier Narrows-02
0115
Superstition Hills-01
0116
Superstition Hills-02
0117
Spitak, Armenia
0118
Loma Prieta

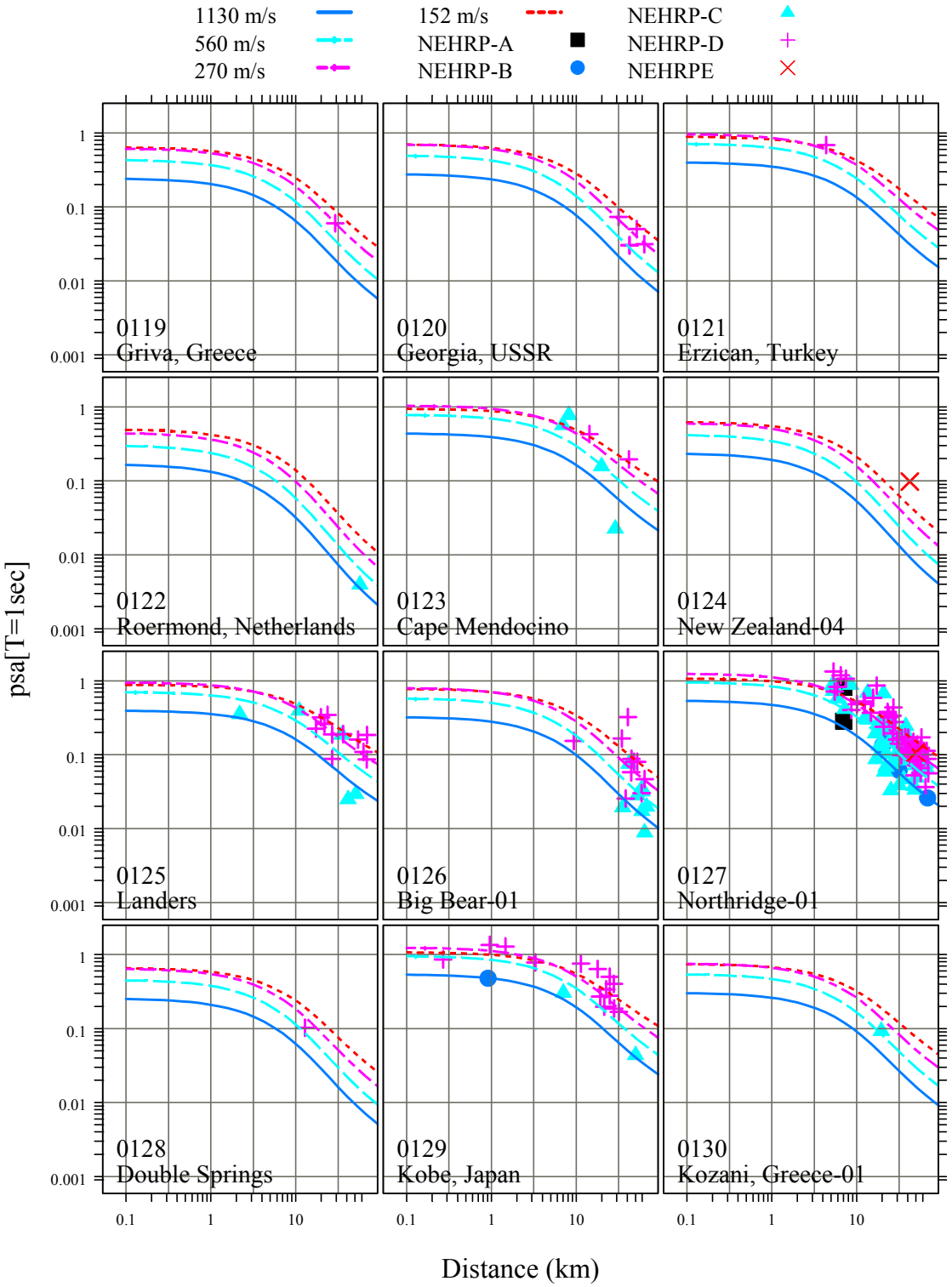
1130 m/s
560 m/s
270 m/s
152 m/s
NEHRP-A
NEHRP-B
NEHRP-C
NEHRP-D
NEHRPE
psa[T=1sec]
Distance (km)
0119
Griva, Greece
0120
Georgia, USSR
0121
Erzican, Turkey
0122
Roermond, Netherlands
0123
Cape Mendocino
0124
New Zealand-04
0125
Landers
0126
Big Bear-01
0127
Northridge-01
0128
Double Springs
0129
Kobe, Japan
0130
Kozani, Greece-01

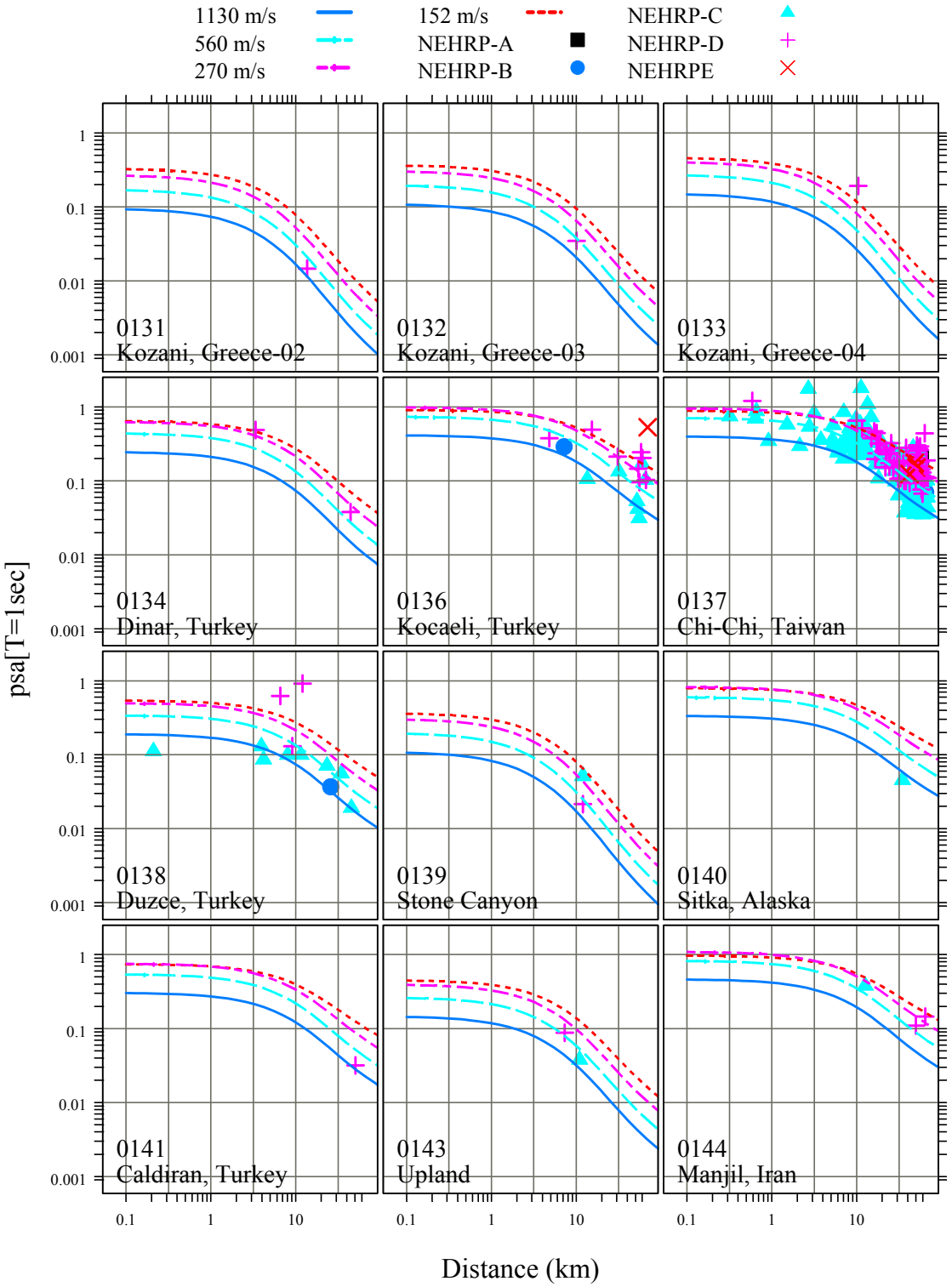
1130 m/s
560 m/s
270 m/s
152 m/s
NEHRP-A
NEHRP-B
NEHRP-C
NEHRP-D
NEHRPE
psa[T=1sec]
Distance (km)
0131
Kozani, Greece-02
0132
Kozani, Greece-03
0133
Kozani, Greece-04
0134
Dinar, Turkey
0136
Kocaeli, Turkey
0137
Chi-Chi, Taiwan
0138
Duzce, Turkey
0139
Stone Canyon
0140
Sitka, Alaska
0141
Caldiran, Turkey
0143
Upland
0144
Manjil, Iran

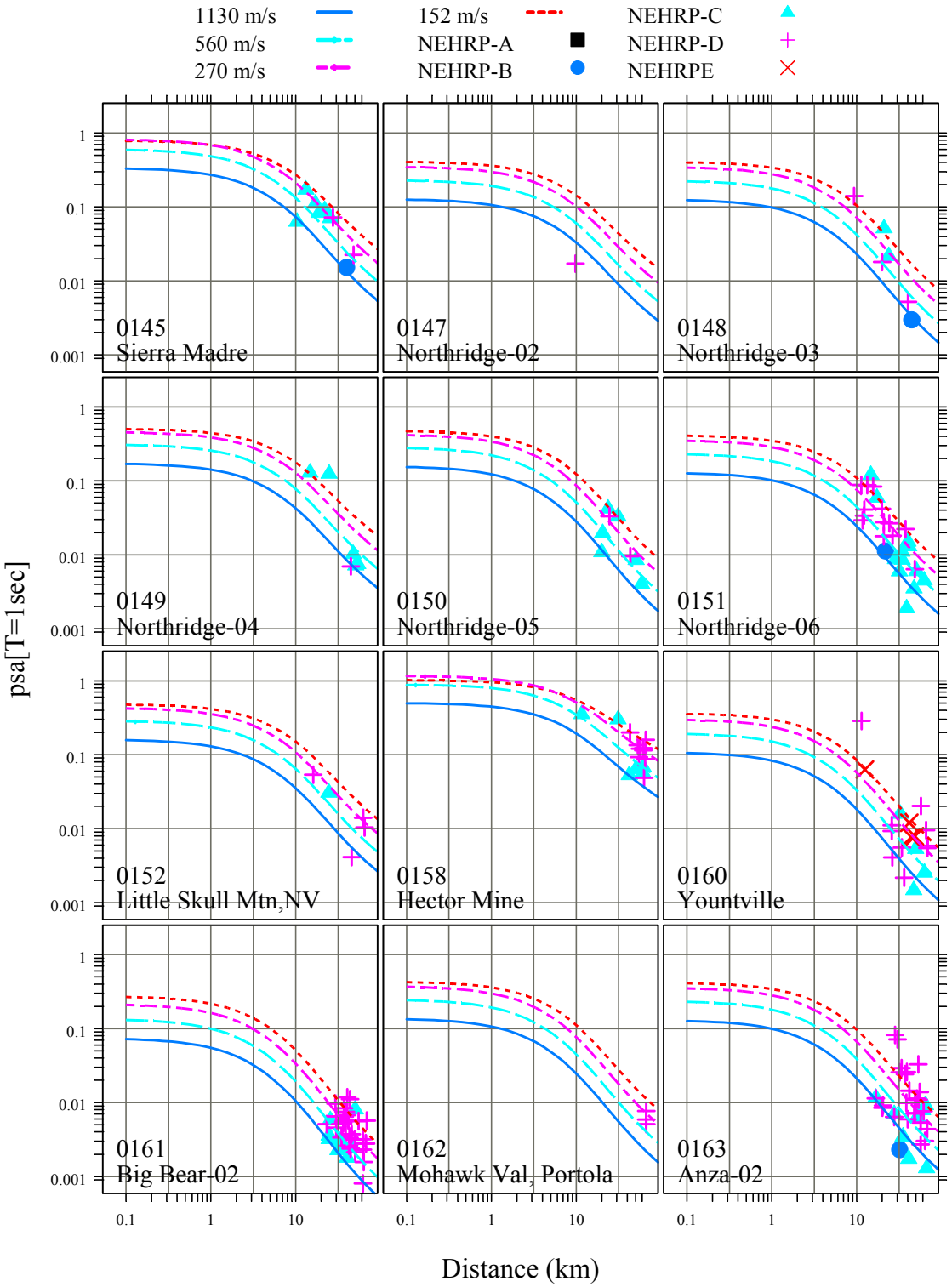
1130 m/s
560 m/s
270 m/s
152 m/s
NEHRP-A
NEHRP-B
NEHRP-C
NEHRP-D
NEHRPE
psa[T=1sec]
Distance (km)
0145 Sierra Madre
0147 Northridge-02
0148 Northridge-03
0149 Northridge-04
0150 Northridge-05
0151 Northridge-06
0152 Little Skull Mtn,NV
0158 Hector Mine
0160 Yountville
0161 Big Bear-02
0162 Mohawk Val, Portola
0163 Anza-02

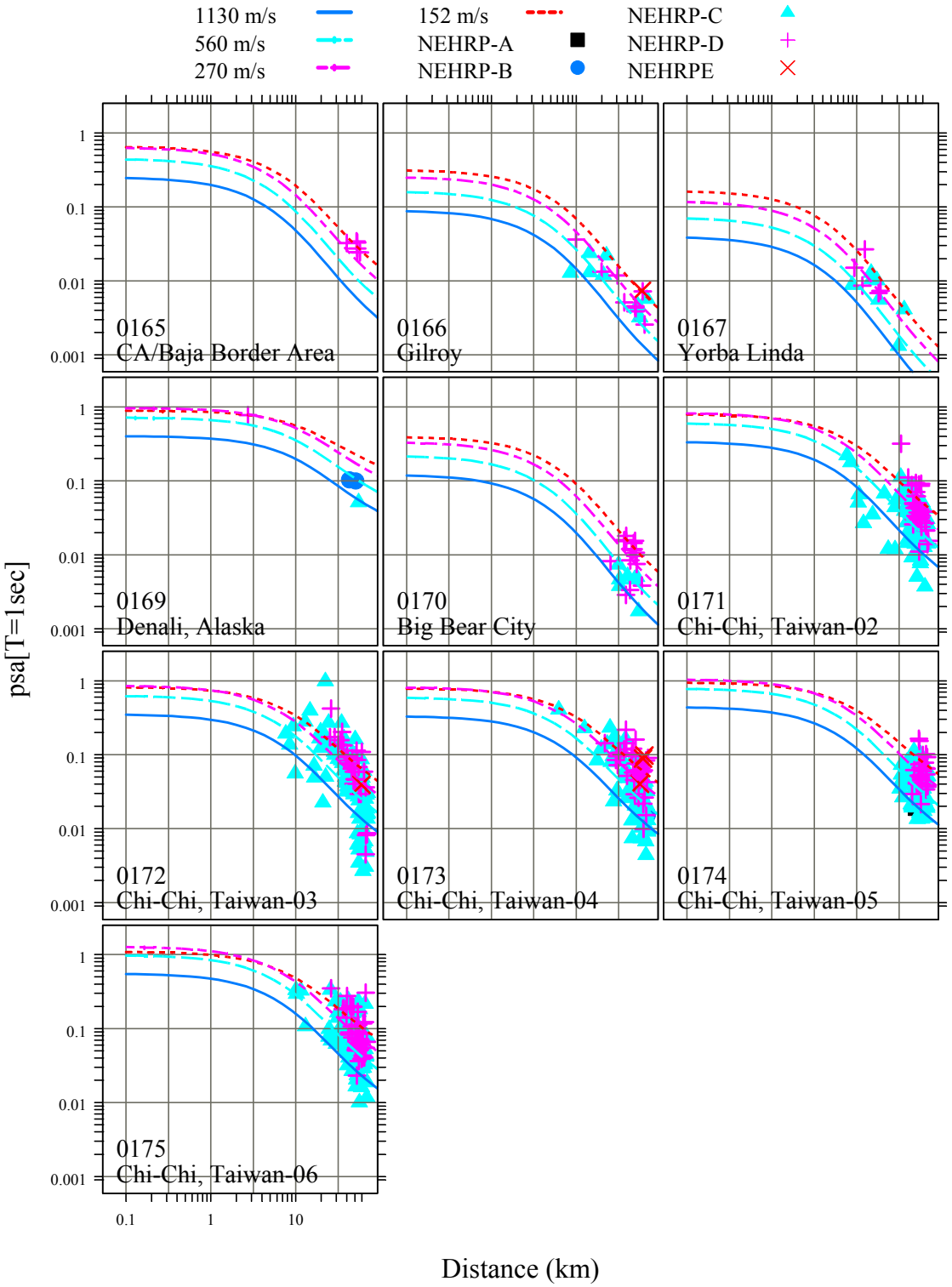
1130 m/s
560 m/s
270 m/s
152 m/s
NEHRP-A
NEHRP-B
NEHRP-C
NEHRP-D
NEHRPE
psa[T=1sec]
Distance (km)
0165
CA/Baja Border Area
0166
Gilroy
0167
Yorba Linda
0169
Denali, Alaska
0170
Big Bear City
0171
Chi-Chi, Taiwan-02
0172
Chi-Chi, Taiwan-03
0173
Chi-Chi, Taiwan-04
0174
Chi-Chi, Taiwan-05
0175
Chi-Chi, Taiwan-06

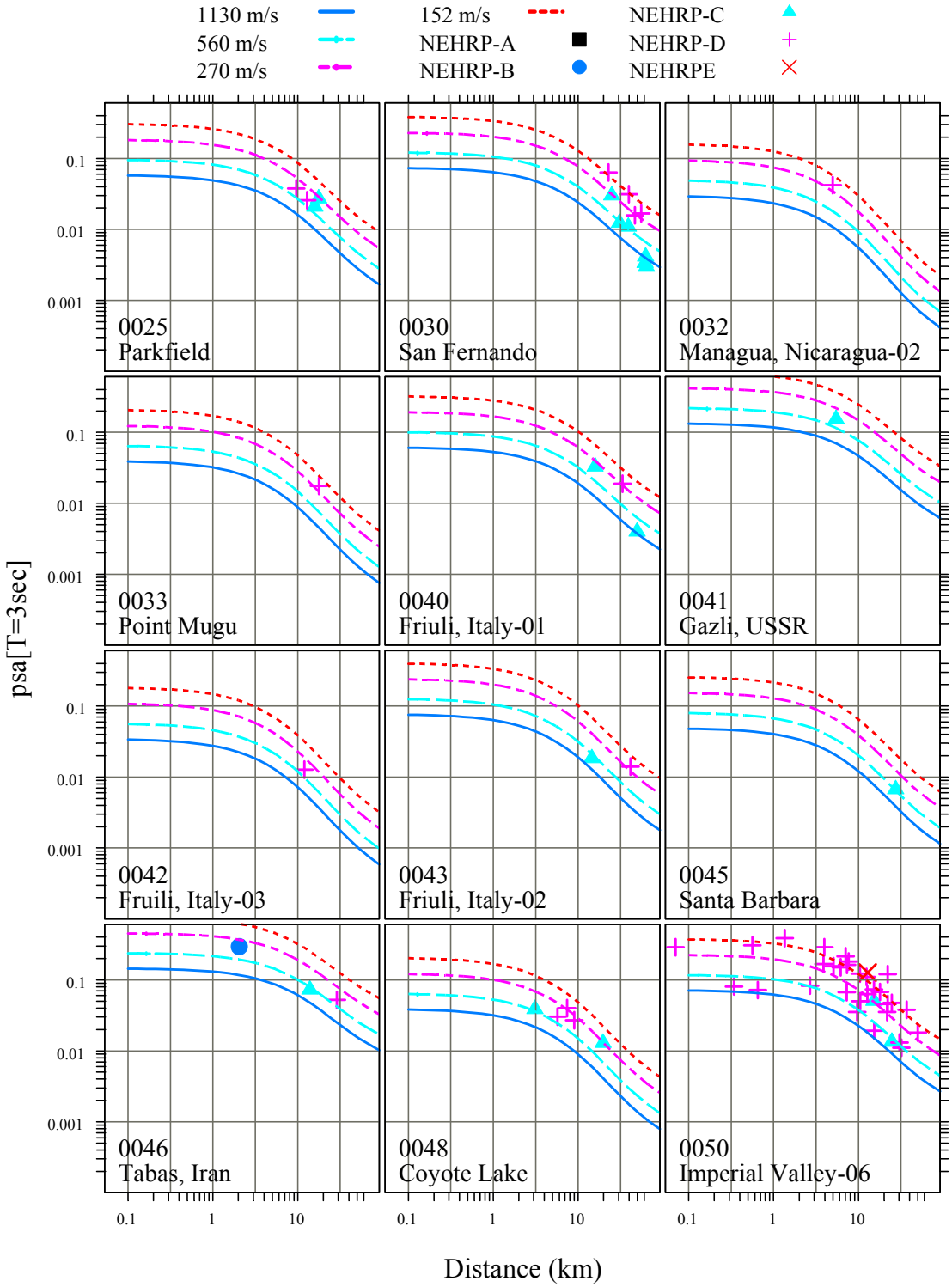
1130 m/s
560 m/s
270 m/s
152 m/s
NEHRP-A
NEHRP-B
NEHRP-C
NEHRP-D
NEHRPE
psa[T=3sec]
0.1
0.01
0.001
0025
Parkfield
0030
San Fernando
0032
Managua, Nicaragua-02
0033
Point Mugu
0040
Friuli, Italy-01
0041
Gazli, USSR
0042
Fruili, Italy-03
0043
Friuli, Italy-02
0045
Santa Barbara
0046
Tabas, Iran
0048
Coyote Lake
0050
Imperial Valley-06
0.1
1
10
Distance (km)

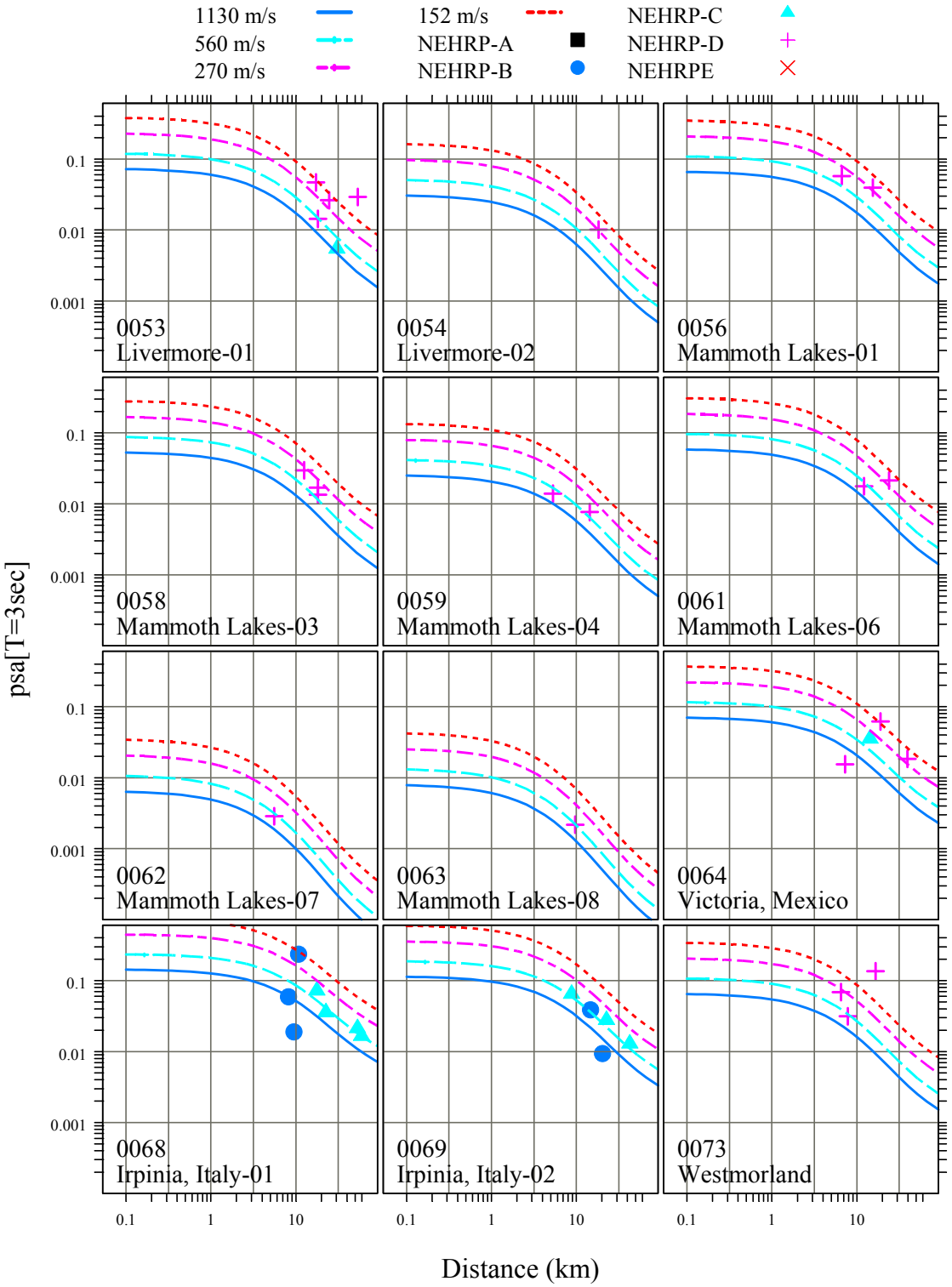
1130 m/s
560 m/s
270 m/s
152 m/s
NEHRP-A
NEHRP-B
NEHRP-C
NEHRP-D
NEHRPE
psa[T=3sec]
0.1
0.01
0.001
0053
Livermore-01
0054
Livermore-02
0056
Mammoth Lakes-01
0058
Mammoth Lakes-03
0059
Mammoth Lakes-04
0061
Mammoth Lakes-06
0062
Mammoth Lakes-07
0063
Mammoth Lakes-08
0064
Victoria, Mexico
0068
Irpinia, Italy-01
0069
Irpinia, Italy-02
0073
Westmorland
0.1
1
10
Distance (km)

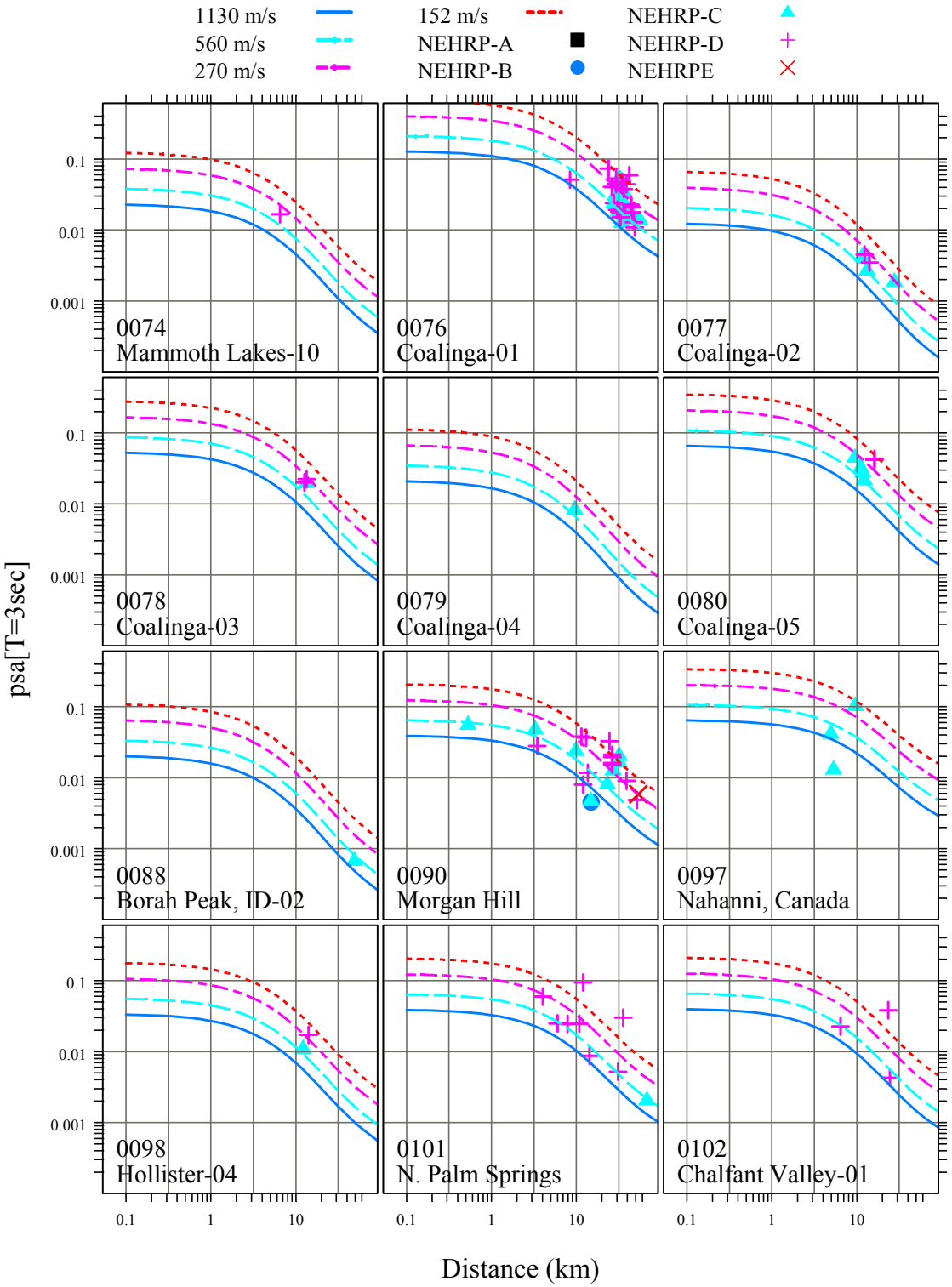
1130 m/s
560 m/s
270 m/s
152 m/s
NEHRP-A
NEHRP-B
NEHRP-C
NEHRP-D
NEHRPE
psa[T=3sec]
0.1
0.01
0.001
0074
Mammoth Lakes-10
0076
Coalinga-01
0077
Coalinga-02
0078
Coalinga-03
0079
Coalinga-04
0080
Coalinga-05
0088
Borah Peak, ID-02
0090
Morgan Hill
0097
Nahanni, Canada
0098
Hollister-04
0101
N. Palm Springs
0102
Chalfant Valley-01
0.1
1
10
Distance (km)

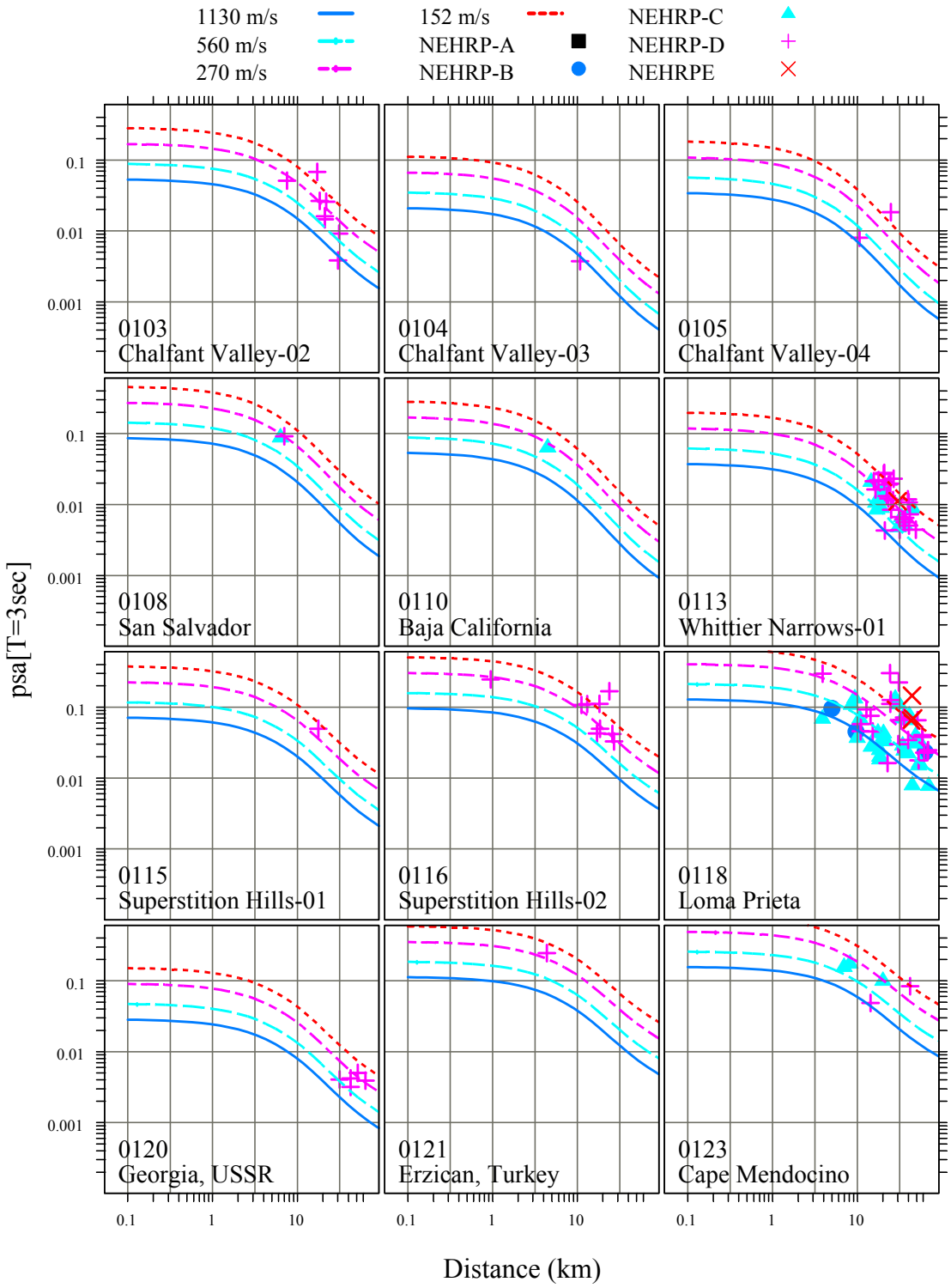
1130 m/s
560 m/s
270 m/s
152 m/s
NEHRP-A
NEHRP-B
NEHRP-C
NEHRP-D
NEHRPE
psa[T=3sec]
0.1
0.01
0.001
0103
Chalfant Valley-02
0104
Chalfant Valley-03
0105
Chalfant Valley-04
0108
San Salvador
0110
Baja California
0113
Whittier Narrows-01
0115
Superstition Hills-01
0116
Superstition Hills-02
0118
Loma Prieta
0120
Georgia, USSR
0121
Erzican, Turkey
0123
Cape Mendocino
0.1
1
10
Distance (km)

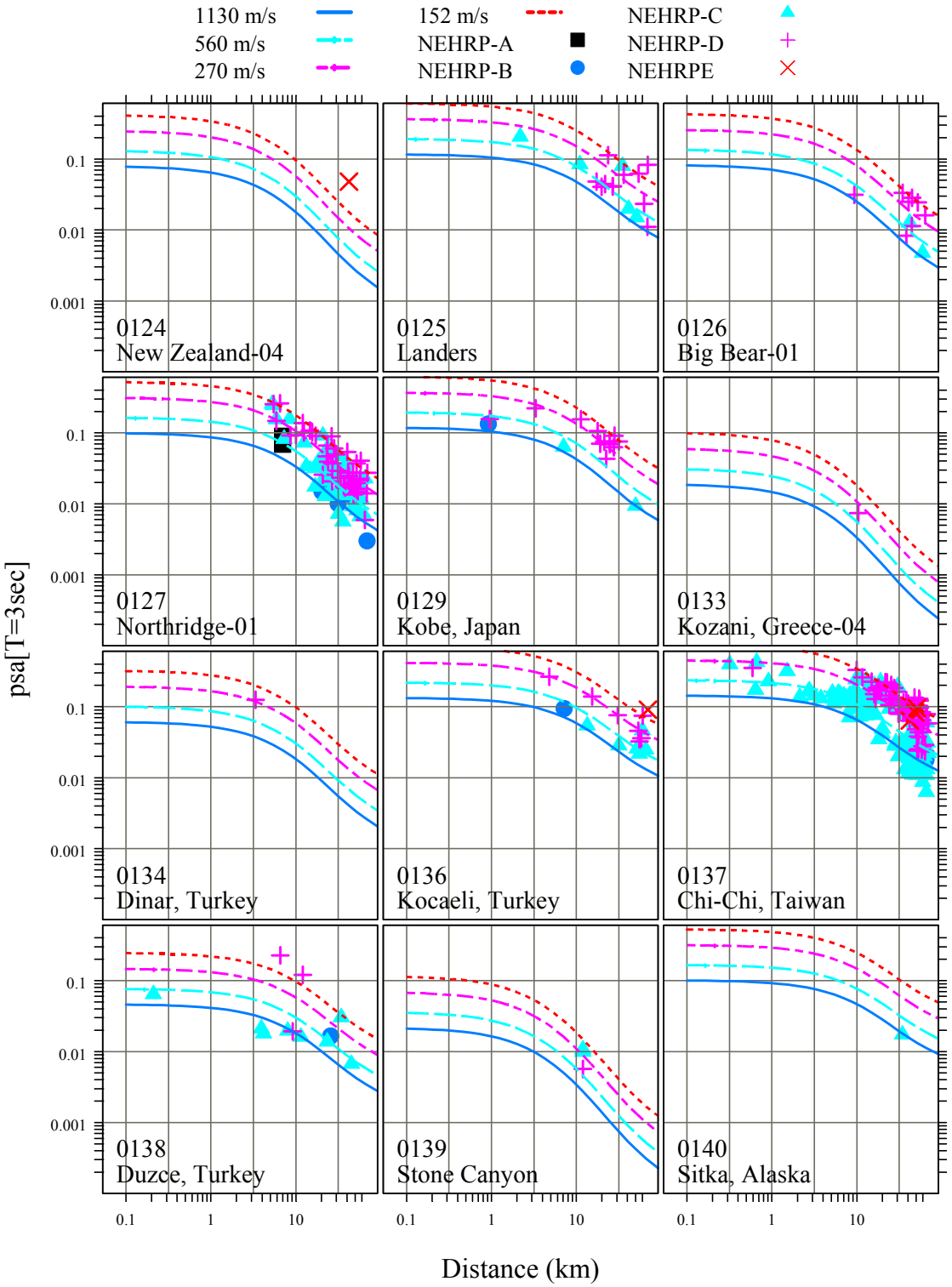
1130 m/s
560 m/s
270 m/s
152 m/s
NEHRP-A
NEHRP-B
NEHRP-C
NEHRP-D
NEHRPE
psa[T=3sec]
0124
New Zealand-04
0125
Landers
0126
Big Bear-01
0127
Northridge-01
0129
Kobe, Japan
0133
Kozani, Greece-04
0134
Dinar, Turkey
0136
Kocaeli, Turkey
0137
Chi-Chi, Taiwan
0138
Duzce, Turkey
0139
Stone Canyon
0140
Sitka, Alaska
0.1
0.01
0.001
0.1
1
10
Distance (km)

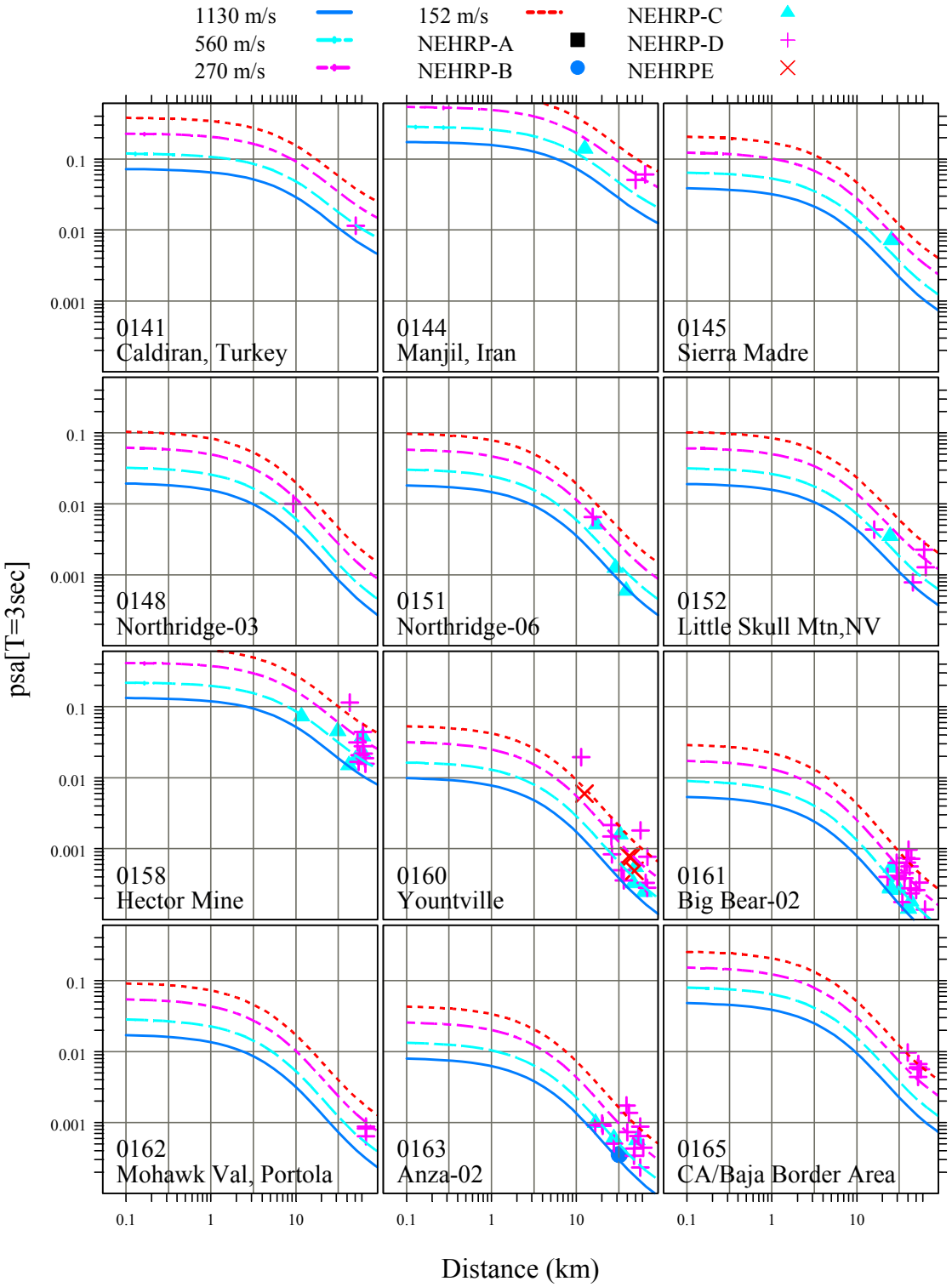
1130 m/s
560 m/s
270 m/s
152 m/s
NEHRP-A
NEHRP-B
NEHRP-C
NEHRP-D
NEHRPE
psa[T=3sec]
0.1
0.01
0.001
0141
Caldiran, Turkey
0144
Manjil, Iran
0145
Sierra Madre
0148
Northridge-03
0151
Northridge-06
0152
Little Skull Mtn,NV
0158
Hector Mine
0160
Yountville
0161
Big Bear-02
0162
Mohawk Val, Portola
0163
Anza-02
0165
CA/Baja Border Area
0.1
1
10
Distance (km)

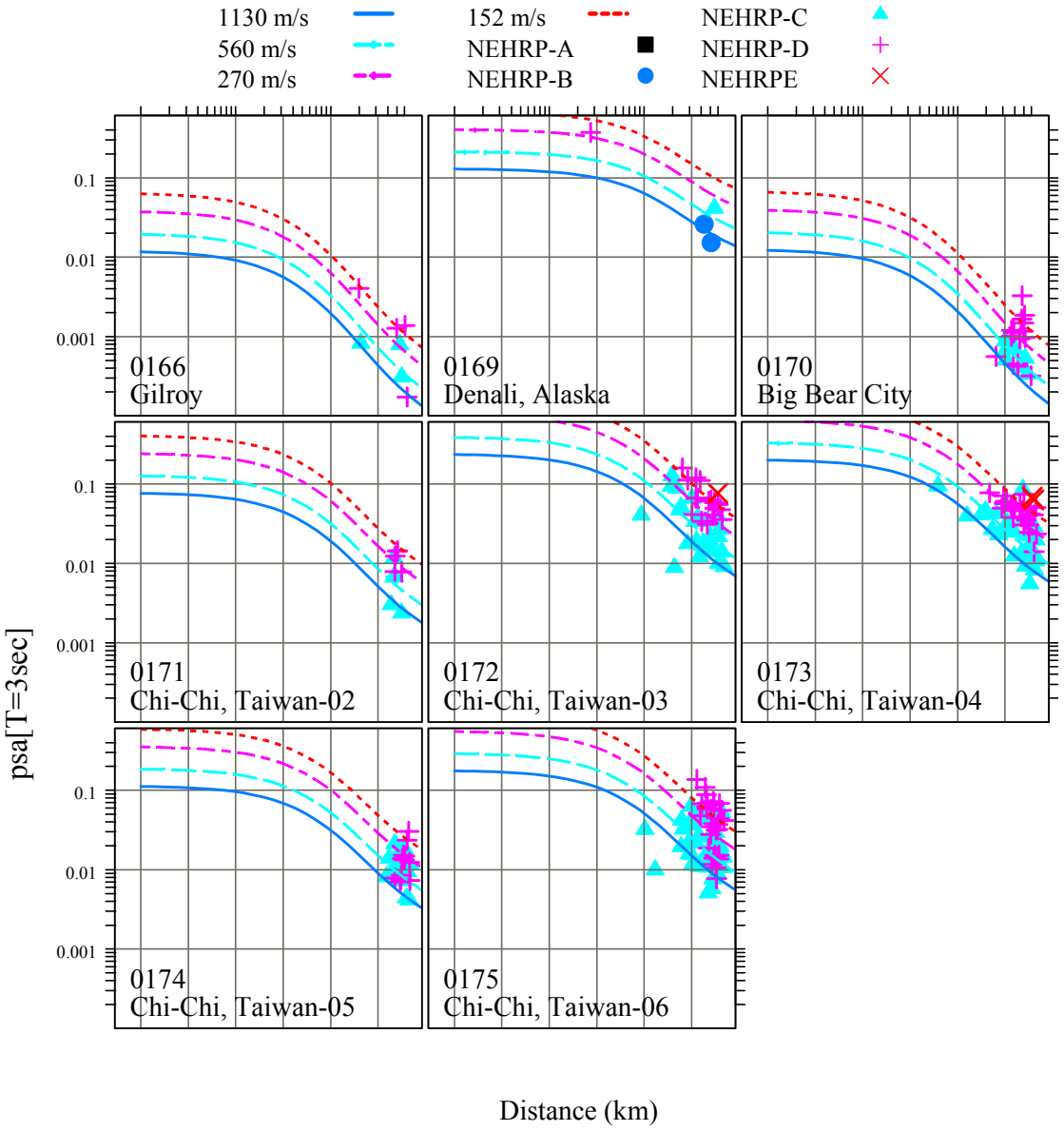
1130 m/s
560 m/s
270 m/s
152 m/s
NEHRP-A
NEHRP-B
NEHRP-C
NEHRP-D
NEHRPE
0166
Gilroy
0169
Denali, Alaska
0170
Big Bear City
0171
Chi-Chi, Taiwan-02
0172
Chi-Chi, Taiwan-03
0173
Chi-Chi, Taiwan-04
0174
Chi-Chi, Taiwan-05
0175
Chi-Chi, Taiwan-06
0.1
0.01
0.001
psa[T=3sec]
Distance (km)

Appendix F: Model SAO2006—Update of Attenuation Model of Sadigh and Others (1997), Using PEER-NGA Dataset of Chiou and Youngs (2006)

INTRODUCTION

Comparisons of predicted median motions from CY2006[4] to those from Sadigh and others (1997) (SAO97) are shown in Figures 39–44 of Chiou and Youngs (2006). It appears that there are substantial differences between the two models at **M** > 5.5, particularly for the rock conditions. The large differences are expected because SAO97 was developed more than 10 years ago with less reliable data[5] and without the benefits of the ground motion research (particularly in the area of soil response) accomplished in the last 10 years. To allow for a more meaningful comparison with CY2006, SAO97 is updated to include the current NGA dataset and to implement a few modeling concepts that do not require changing SAO97's functional form. We'll focus on the model for rock condition because agreement between the rock models is worse than agreement between the soil models. This update is not aimed to provide a complete attenuation model that can be used in engineering practice. Rather, it is used only to understand the substantial difference in *"rock"* motion between CY2006 and SAO97.

We'll show that median predictions of the updated SAO97 model are no longer substantially different from those of CY2006. We attribute the good agreement to the improved fits of updated SAO97 to NGA data.

---

[4] This appendix was written in 2006 using the preliminary model CY2006 and it has not been updated to the current model CY2008. However, the conclusions given in this appendix are not likely to be affected by the switch to CY2008.

[5] For example, spectral shape data, instead of spectral acceleration data, were used in the development of SAO97. Also, the old site classification has undergone extensive revision and as a result some rock sites are re-classified as soil sites, and vice versa.

STRONG-MOTION DATASET AND THE EQUIVALENT V_{S30} FOR ROCK AND SOIL CONDITIONS

We use the same dataset that was selected and used by Chiou and Youngs (2006). The CY2006 dataset consists of 1087 data points from main shocks at distances less than 70 km. It's important to note that, although the recent large-magnitude data from Taiwan and Turkey are included in this dataset, the bulk of data still comes from California, as shown on Figure F.1a.

As SAO97, the updated attenuation model is developed for two general site conditions of soft rock and soil. The soft rock condition consists of Geomatrix site class A (very thin soil, < 5m, over rock) and B (shallow stiff soil, 5 to 20 m, over rock). The soil condition includes Geomatrix site class C and D (deep firm soil conditions). Site condition of each recording station is assigned according to the Geomatrix site code (C_3) given in the PEER-NGA database.

Summary statistics of Vs_{30} for the rock and soil categories are listed in Table F.1 and the histograms are shown on Figures F.1b and F.1c. Because the weak-motion soil response in CY2006 is modeled by $ln(V_{S30}/1130)$, we'll use the geometric mean of V_{S30} as the reference point for comparison with CY2006. The geometric mean is slightly different between *pga* and 1-sec *PSA* because their V_{S30} distributions are different due to the minimum usable frequency requirement. However, the difference is not large enough to make a difference and we'll use 500 m/sec as a compromise[6].

We also want to point out that the V_{S30} distribution of California rock data is bimodal with a geometric mean of 485 m/sec, lower than the full-set value of 505 m/sec. The first mode of the rock V_{S30} data is similar to the geometric mean *of* soil V_{S30} data. One explanation of this observation is that many of these rock sites happen to be within geological units (such as *Qal*) where Geomatrix classification is ambiguous in the absence of reliable information on soil depth.

As in CY2006, footwall and hanging-wall sites are included in the regression analysis. Excluding FW/HW sites will impact the style of faulting effect for reverse event in a manner similar to that described in the "Modeling Steps" section of Chiou and Youngs (2006).

[6] We used V_{S30}=520 m/sec as the point of comparison in Figures 39–44 of our main text. We'll update these figures to V_{S30}=500m/sec when we revise the report in the future.

MODEL EQUATION:

To update SAO97, we combine the rock and soil model equations and use one random earthquake effect ($\tau \cdot z_i$) per earthquake. One could consult the paper by Sadigh and others (1997) to connect the new equation with the two original equations. The combined model equation is

$$
\begin{aligned}
\ln(y_{ij}) = \\
& Z_r \left(C^r{}_1 + C^r{}_2 M_i + C^r{}_{2a}(M_i - 6.5,0)_{\min} + C^r{}_3 (8.5 - M_i)^{2.5} + C^r{}_4 \ln\left(R_{rup_{ij}} + \exp\left(C^r{}_5 + C^r{}_6 M_i + C^r{}_{6a}(M_i - 6.5,0)_{\min} \right) \right) \right) \\
& + Z_s \left(C^s{}_1 + C^s{}_2 M_i + C^s{}_3 (8.5 - M_i)^{2.5} + C^s{}_4 \ln\left(R_{rup_{ij}} + \exp\left(C^s{}_5 + C^s{}_6 M_i + C^s{}_{6a}(M_i - 6.5,0)_{\min} \right) \right) \right) \\
& + C_{RV} Z_{RV} \\
& + \tau \cdot z_i + \sigma \cdot z_{ij}
\end{aligned}
$$

where Z_r (the rock condition flag) is equal to 1 if site is on rock and 0 otherwise. Z_s (the soil condition flag) is equal to 1 if site is on soil and 0 otherwise. Z_{RV} (the reverse faulting flag) is equal to 1 if $30^o \le \lambda \le 150^o$ and 0 otherwise.

MODEL DEVELOPMENT:

Followings are descriptions of model development for *pga* and pseudo spectral acceleration at 1-sec period. Each model is developed in multiple steps. For convenience of reference, each step is labeled by affixing a lower case letter to "SAO2006." (e.g., SAO2006.a, SAO2006.b, etc.).

Peak Ground Acceleration (Spectral Acceleration at Period of 0.01 Sec)

Step #1: SAO2006.a: Mixed-Effects Version of SAO97

In Step #1 all fixed-effects coefficients are set to the SAO97 values, except for coefficients $C^r{}_1$, $C^s{}_1$, and C_{RV}. The resulting coefficients $C^r{}_1$ and $C^s{}_1$ are nearly identical to those of SAO97 (probably not a coincidence). SAO2006.a is thus effectively the mixed-effects version of SAO97. Models SAO2006.a and SAO97 can be used interchangeably as far as predicting median *pga* goes.

The magnitude scaling of SAO2006.a (and SAO97) is appropriate for the NGA dataset (Fig. F.2a), therefore modifications of coefficients $C^r{}_2$, $C^r{}_{2a}$, and $C^s{}_2$ are not necessary. This finding is consistent with the c_2 value in CY2006.

SAO2006.a also adequately models the distance attenuation of soil *pga* (Fig. F.2b). But, under-prediction of rock *pga* is noted at $R_{RUP} > 50$ km. A hint of overprediction of rock *pga* in the distance range of 5 and 15 km is also noted.

Median predictions from SAO2006.a are shown in Figure F.2c. There are substantial differences between SAO2006.a (SAO97) and CY2006. These discrepancies were also noted by Art Frankel (Comment #5 of his June-27-2006 list) in his review of the NGA model.

Step # 2 (SAO2006.b):

The lack of fits noted in Step #1 suggests that an increase (less negative in value) of coefficient C^r_4 is needed. There is another (more) compelling reason to modify C^r_4. A large difference between C^r_4 and C^s_4, such as that seen in CY2006.a and SAO97, implies strong distance dependence in soil amplification even at large distances where soil response is linear and the soil amplification factor is expected to depend weakly on distance. To hamper the continuous increase of soil amplification with distance, we impose the equality constraint $C^r_4 = C^s_4$ and modify coefficients C^r_5 and C^s_5 to allow for nonlinear response at short distances. Furthermore, with the equality constraint, a large increase of C^r_4 is expected and, consequently, the associated near-source magnitude scaling will be stronger than the scaling for near saturation as implied by SAO2006.a (and SAO1997). But a stronger near-fault magnitude scaling is not supported by the NGA dataset. On the contrary, in lights of the low motions recorded from the recent Turkey and Taiwan earthquakes, one could even make the case for negative near-fault magnitude scaling (i.e., oversaturation). We think allowing for oversaturation is a dramatic change in modeling concept and in engineering practice that its acceptance requires more careful studies. Therefore, we maintain the same near-fault magnitude saturation as SAO1997 by imposing C^r_6=1.1/ C^r_4 and C^s_6=1.0/ C^s_4. Changes to C^r_6 and C^s_6 also trigger the needs to modify near-fault magnitude scaling for M < 6.5 (C^r_{6a} and C^s_{6a}).

In summary, all coefficients except C^r_2 and C^s_2 are modified in this step, with coefficients C^s_4, C^r_6 and C^s_6 being constrained by the conditions explained above. The resulting coefficients for soil model are close to the old values in SAO97, as expected. The new estimate of C^r_4 is -1.6, close to the old soil value of -1.7 in SAO97. Thanks to the new coefficients, we notice better fits to data in the distance range of 5 km ≤ R_{RUP} ≤ 15 km and $R_{RUP} > 50$ km (Fig. F.3a). We also see a slight drop in intra-event standard error.

Median predictions from SAO2006.b are shown on Figure F.3b. Also shown on Figure F3.b are median predictions from CY2006 (solid lines). The discrepancies of rock predictions noted in the previous step and by Art Frankel are now much smaller. For **M** = 6.5, the magnitude mentioned in Art's comments, SAO2006.b and CY2006 are within 5% of each other.

Note that SAO2006.b still has problem with the near-fault prediction for **M** = 5.5 and smaller. This problem can be fixed by implementing a better magnitude scaling for lower **M**, such as the one used by CY2006. But we feel the analysis so far have already met the goals stated in the introduction. Therefore we will stop here and move on to the model development for 1-sec spectral acceleration.

Spectral Acceleration at Period of 1 Sec

Model development of the 1-sec spectral acceleration is similar in concept to that of *pga*, but the process is a lot simpler because the main update is related to magnitude scaling, which does not significantly affect other coefficients.

Step #1 (SAO2006.a:, A Mixed-Effects Version of SAO97

This is the first of a sequence of regression analysis. All fixed-effects coefficients are set to the SAO97 values, except for coefficients C^r_1, C^s_1, and C_{RV}. The resulting coefficients C^r_1 and C^s_1 are nearly identical to those of SAO97 (another coincidence?). SAO2006.a is effectively a mixed-effects version of SAO97. SAO2006.a and SAO97 can be used interchangeably as far as predicting median motion goes.

We notice a lack of fit in inter-event terms (Fig. F.4a), suggesting SAO97's magnitude scaling for spectral acceleration at 1-sec period needs to be revised. The predicted median rock motions differ from those of CY2006 by about 20% to 50% (Fig. F.4b). This large discrepancy is also noted and questioned by Art Frankel (2006) in his review of the NGA model.

Step #2 (SAO2006.b):

To improve the magnitude scaling, coefficients C^r_3 and C^s_3 are added to the list of free coefficients and the regression is repeated. The resulting inter-event terms are shown on Figure F.5a. The magnitude trend noted in Step #1 is not present. As a result, the inter-event standard error (τ) is about 16 % smaller than the value in previous step.

The predicted medina motion is shown on Figure F.5b. Discrepancy with CY2006 in the distance range of 10 km ≤ R_{RUP} ≤ 50 km and **M** ≥ 5.5 is now less than 5%. There are still large differences between the two models at R_{RUP} < 10 km and at R_{RUP} > 70 km. Adjustment to coefficients C^{r}_{5} and C^{s}_{5} is conducted next to improve the overall fits at R_{RUP} < 10 km.

Step #3 (SA2006.c):

In this step, coefficients C^{r}_{5} and C^{s}_{5} are added to the list of free coefficients. The resulting model significantly improves the fits at R_{RUP} < 10 km (Fig. F.6a). As a result, the agreement in median rock prediction (Fig. F.6b) is also much closer than the agreement achieved in previous steps.

CONCLUSIONS

We've shown that median predictions of the updated SAO97 model are not substantially different from those of CY2006. We attribute the good agreement to the improved fits of updated SAO97 to NGA data.

Table F.1a Summary statistics of V_{S30} in CY2006's *pga* dataset.

Geomatrix Site Class	Arithmetic Mean of V_{S30} (m/sec)	Geometric Mean of V_{S30} (m/sec)	Number of Data
Soft Rock (A+B)	543	506	419
Deep Soil (C+D)	371	316	633
E			35

Table F.1b Summary statistics of V_{S30} in CY2006's 1-sec dataset.

Geomatrix Site Class	Arithmetic Mean of V_{S30} (m/sec)	Geometric Mean of V_{S30} (m/sec)	Number of Data
Soft Rock (A+B)	537	500	407
Deep Soil (C+D)	328	315	625
E			35

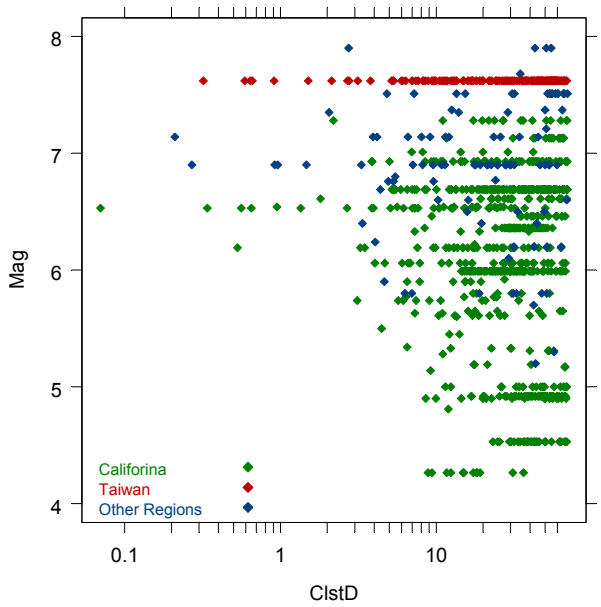

Fig. F.1a Magnitude-distance-region distribution of data used in the development of CY2006 and in this study.

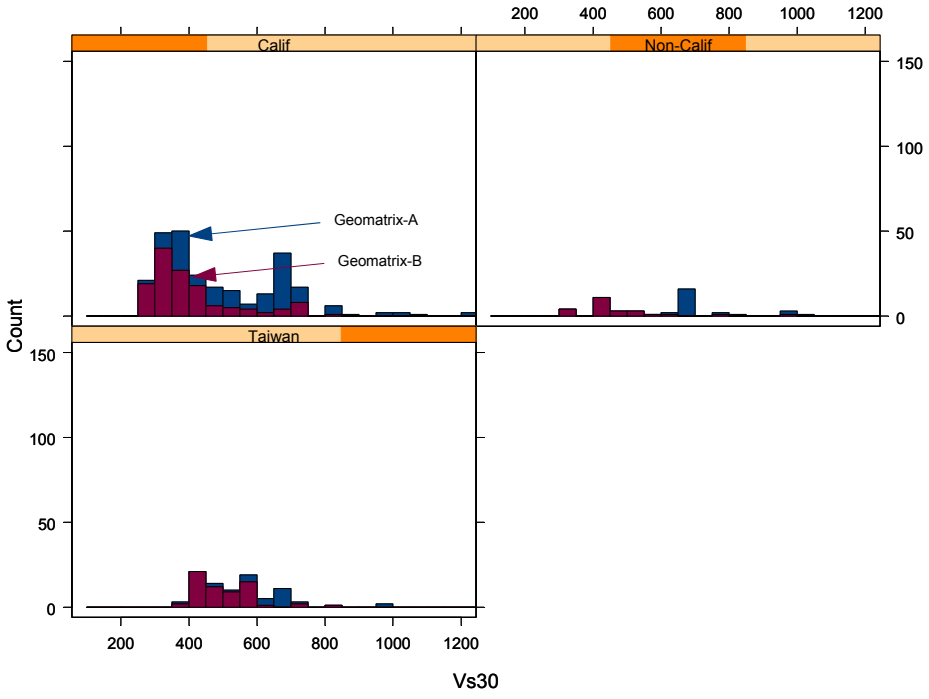

Fig. F.1b V_{S30} histogram of rock (Geomatrix A+B category) *pga* data.

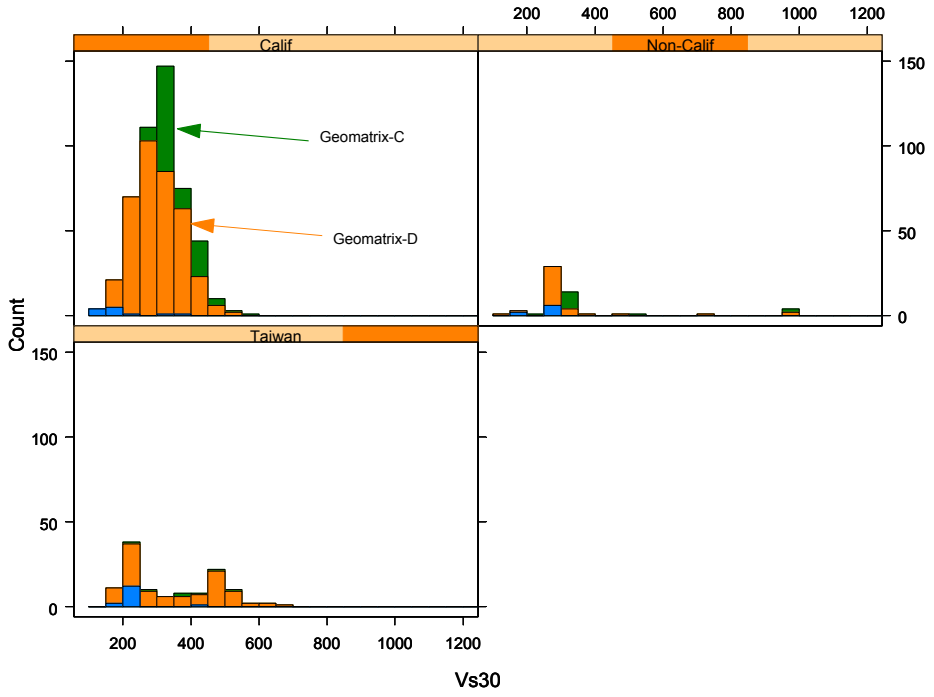

Fig. F.1c V_{S30} **histograms of soil (Geomatrix C+D)** *pga* **data. Geomatrix's E category is denoted by blue color.**

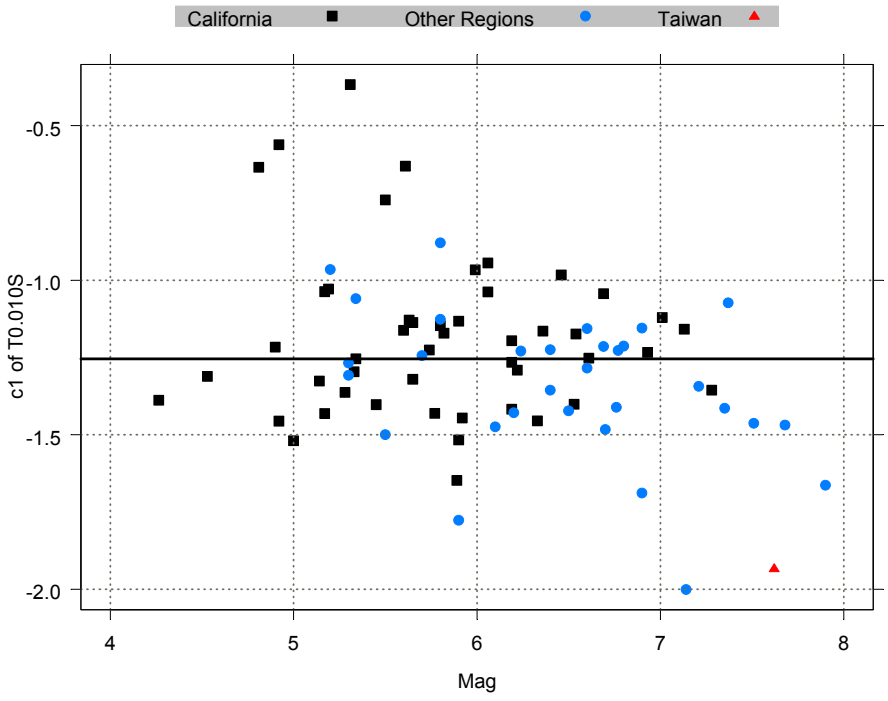

Fig. F.2a Random earthquake effects of *pga* **from SAO2006.a. Horizontal line denotes population mean. Difference between population mean and individual value represents random inter-event residual.**

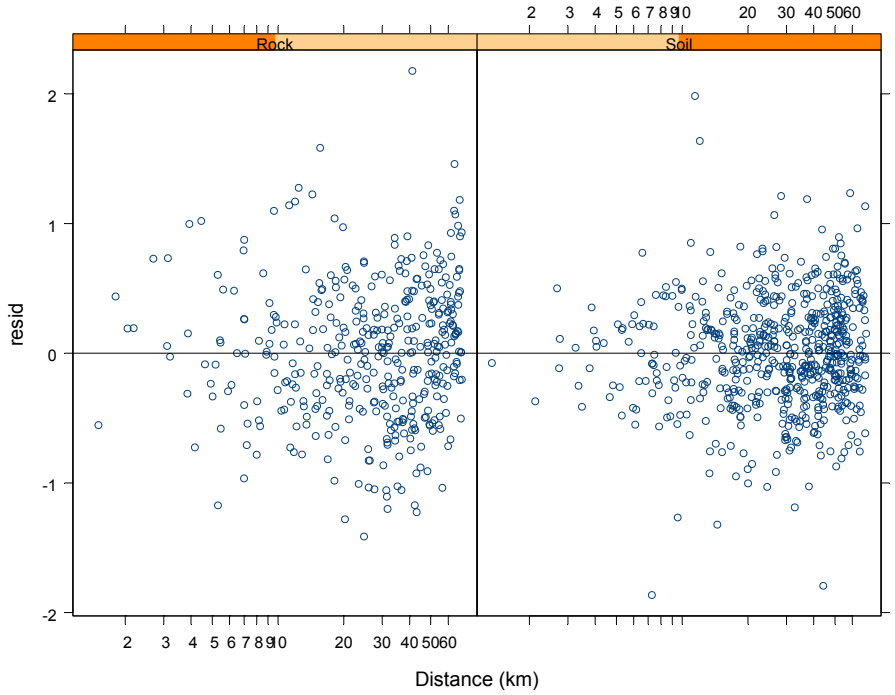

Fig. F.2b Intra-event residuals from SAO2006.a for *pga*.

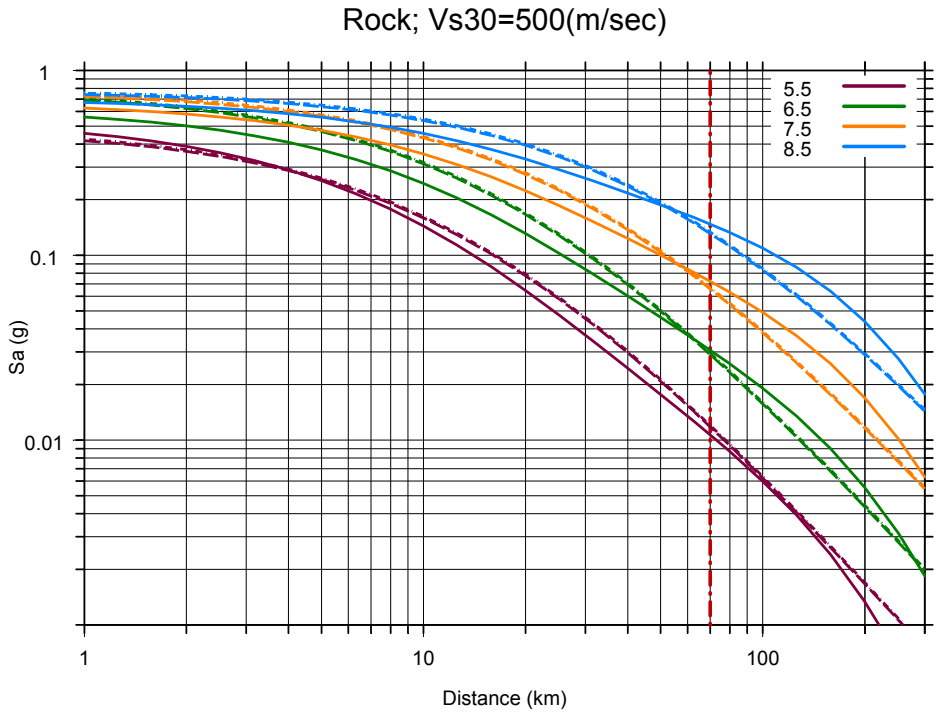

Fig. F.2c Comparison of predicted median rock *pga* by CY2006 (solid curves), SAO2006.a (dotted-dashed lines), and SAO97 (dashed lines). The read vertical line denotes the cut-off distance of the dataset.

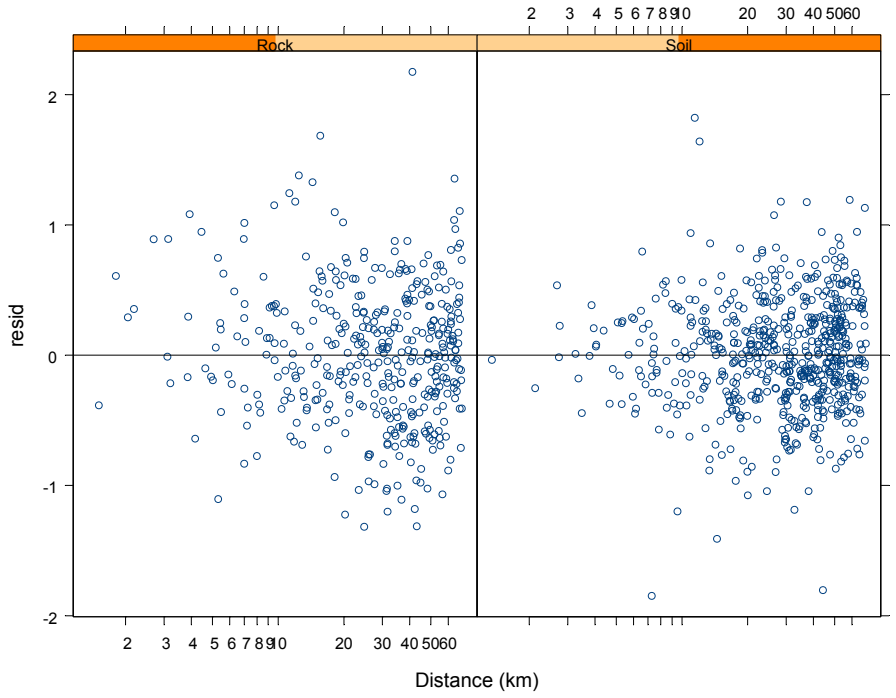

Fig. F.3a Intra-event residuals from SAO2006.b for *pga*.

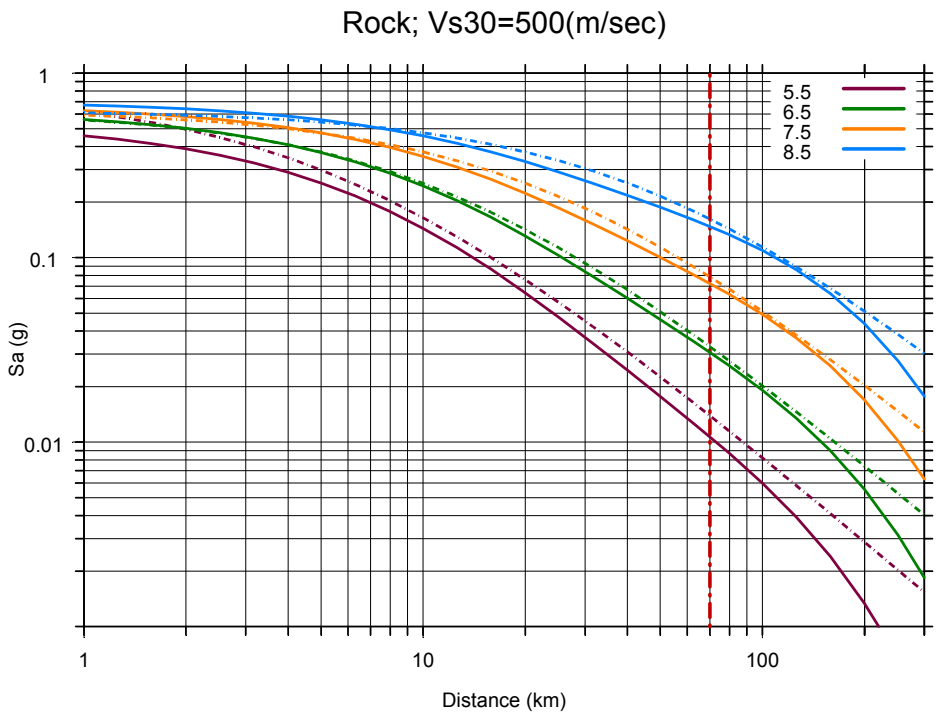

Fig. F.3b Comparison of predicted median rock *pga* by CY2006 (solid curves) and SAO2006.b (dotted-dashed lines). The red vertical line denotes the cut-off distance of the dataset.

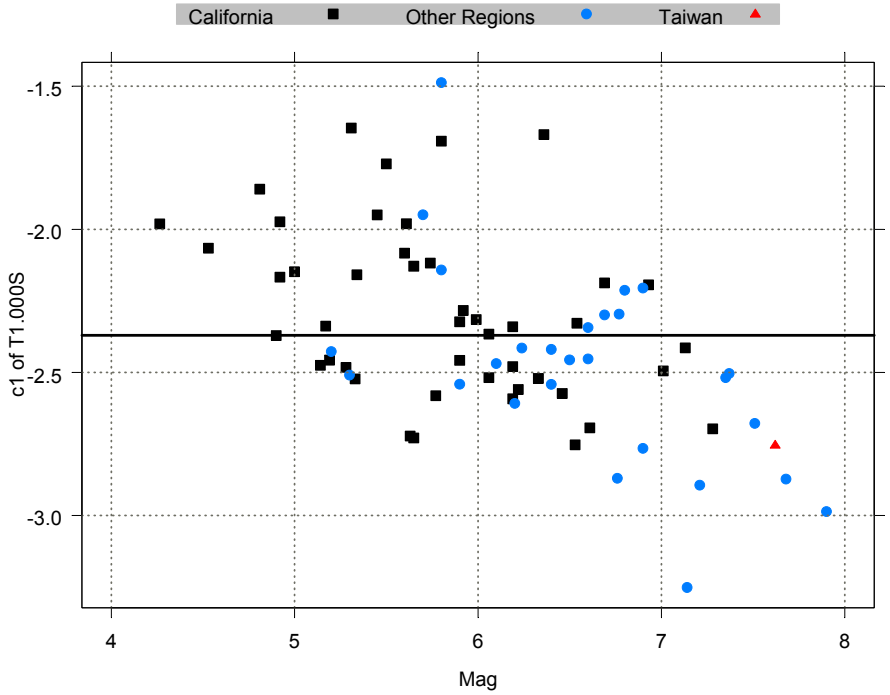

Fig. F.4a Random earthquake effects of 1-sec spectral acceleration from SAO2006.a. Horizontal line denotes population mean. Difference between population mean and individual value represents random inter-event residual.

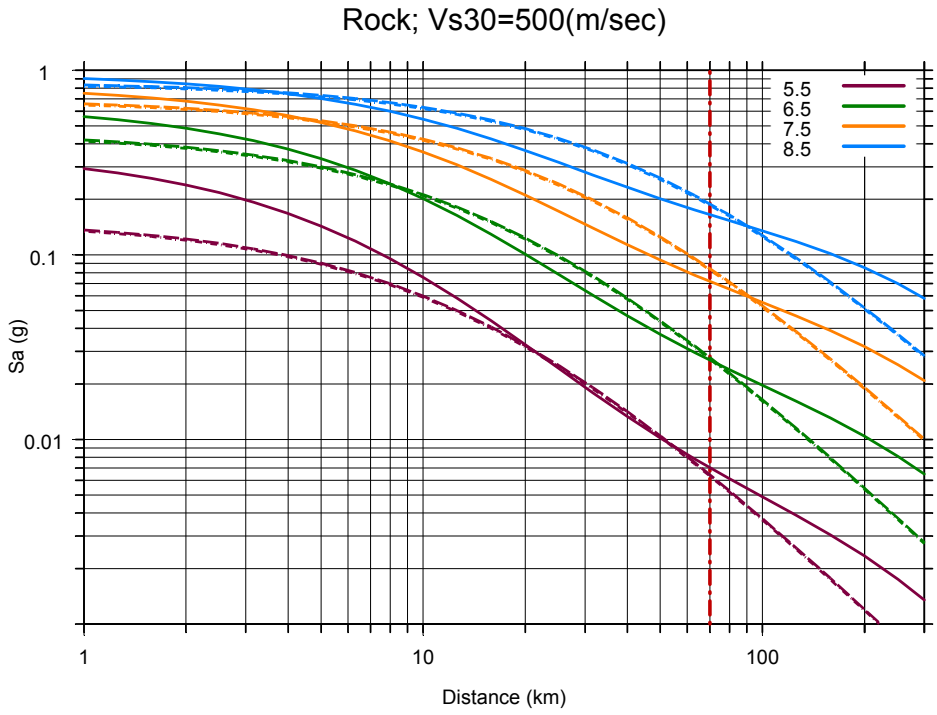

Fig. F.4b Comparison of 1-sec rock spectral accelerations predicted by the CY2006 model (solid curves), by the baseline model SAO2006.a (dotted-dashed curves), and SAO97 (long dashed curves). The read vertical line indicates the cut-off distance of the dataset.

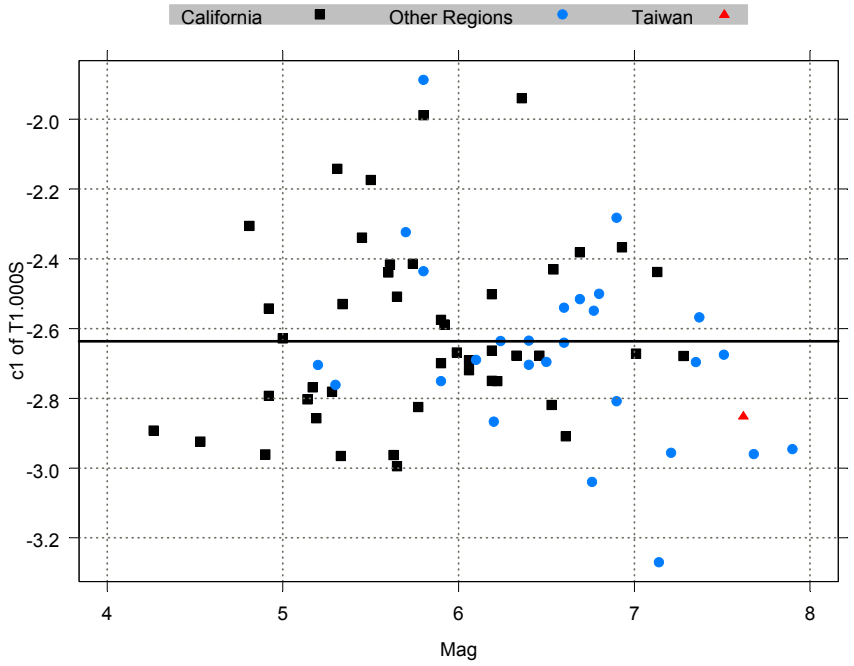

Fig. F.5a Random earthquake effects of 1-sec spectral acceleration from SAO2006.b. Horizontal line denotes population mean. Difference between population mean and individual value represents random inter-event residual.

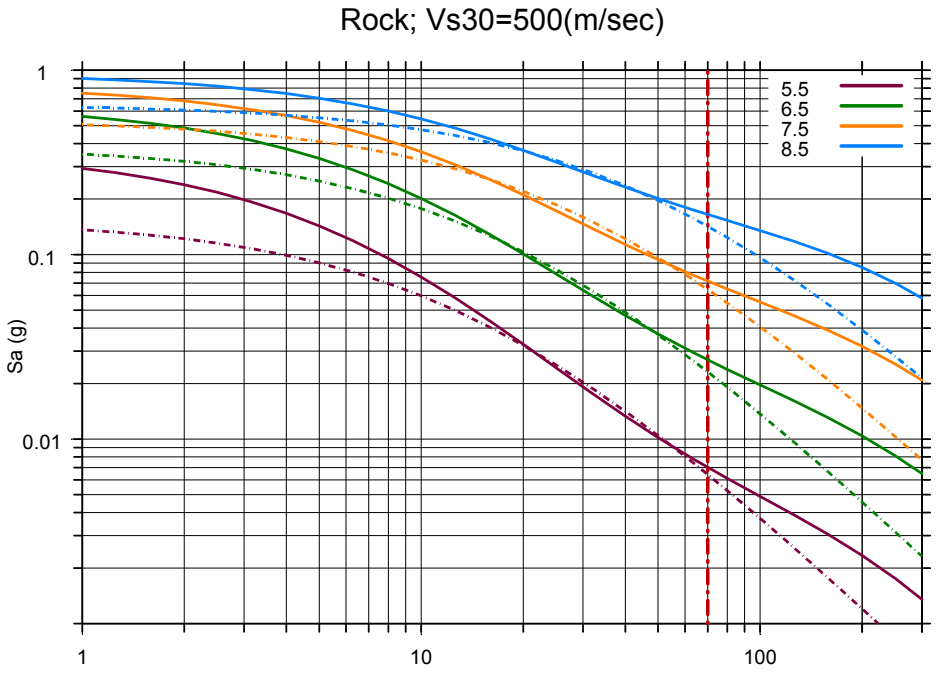

Fig. F.5b Comparison of predicted median 1-sec spectral acceleration by CY2006 (solid curves) and by SAO2006.b (dotted-dashed curves) for soft rock condition. The red vertical line indicates cut-off distance of dataset.

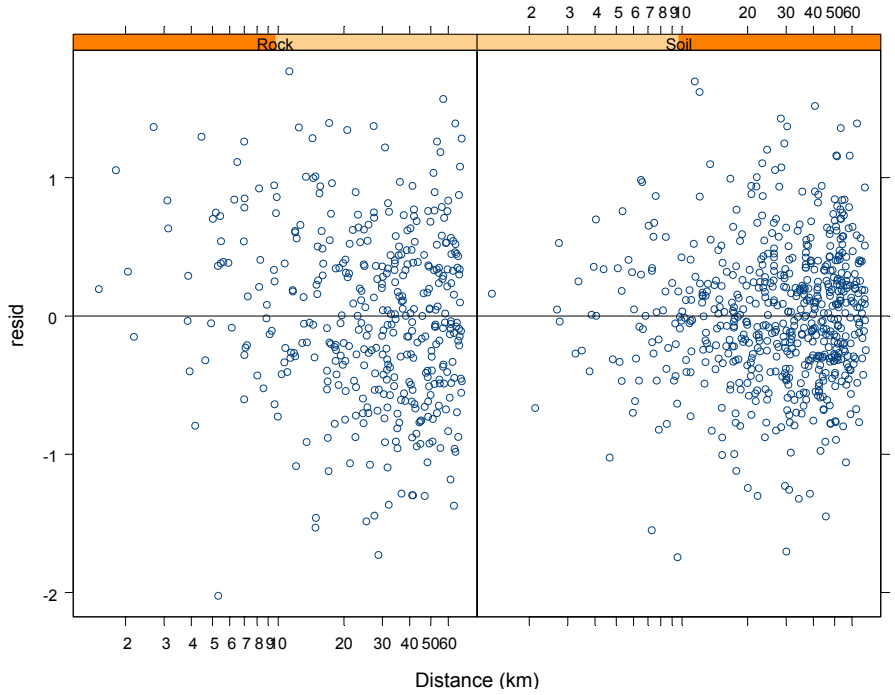

Fig. F.5c Intra- event residuals from SAO2006.b for 1-sec spectral acceleration.

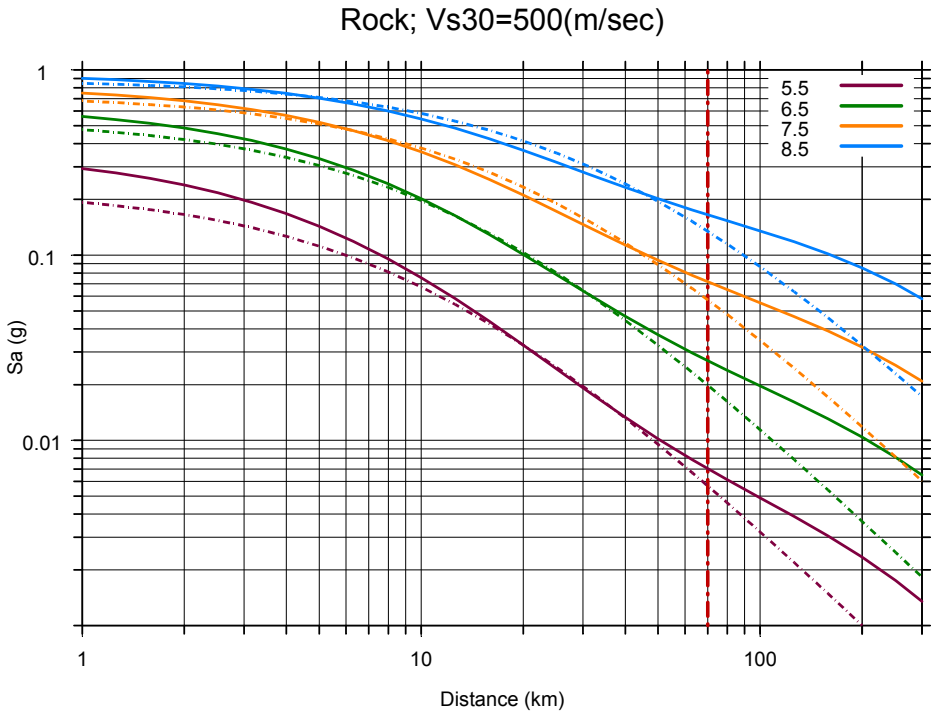

Fig. F.6a Comparison of predicted median 1-sec spectral acceleration by CY2006 (solid curves) and by SAO2006.c (dotted-dashed curves) for soft rock condition. Red vertical line indicates cut-off distance of dataset.

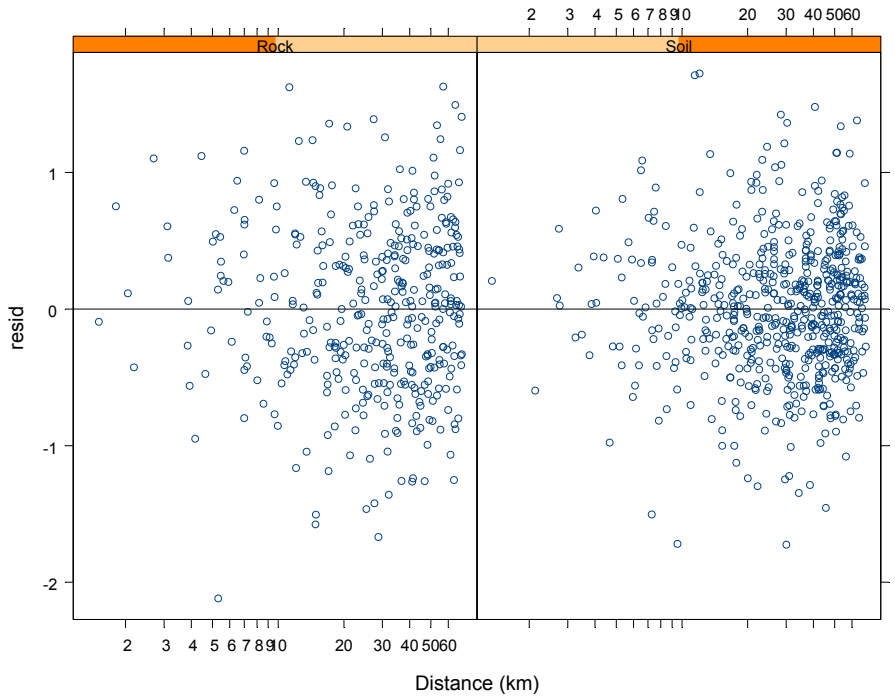

Fig. F.6b Intra-event residuals from SAO2006.c for 1-sec spectral acceleration.

Appendix G: Response to Questions by U.S. Geological Survey (USGS) and California Geological Survey (CGS)[7]

[7] USGS and CGS's comments were made with respect to a preliminary model developed in 2006 (Chiou and Youngs, 2006). However, we expect that our responses would also be valid with respect to the 2008 final model described in this report.

Art Frankel's Comment #1: Buried rupture versus surface rupture. *Somerville and Pitarka (2006) find no significant difference in source terms, on average, between surface and buried ruptures for periods of 0.2 sec and shorter. Yet the NGA relations that do include terms for depth to top of rupture, predict significant differences between surface faulting and buried faulting at all periods. This discrepancy should be explained. It appears to me that the difference in surface and buried ruptures cited in Somerville and Pitarka (2006) may be at least partly due to the differences in the period of the forward directivity pulses. The buried ruptures used in their paper have magnitudes between 6.4 and 7.0, whereas the surface rupture events have magnitudes between 6.5 and 7.6 and produce forward directivity pulses with longer periods, on average.*

RESPONSE FROM CHIOU AND YOUNGS

It is not clear whether Somerville and Pitarka intend to use their Figure 2 as an authoritative estimate of the difference in ground motion between surface and buried ruptures. They may merely use it as a compelling evidence of the existence of such difference.

We believe the ZTOR (depth to top of rupture) effects in the CY2006 model are consistent with the NGA mainshock data. Below, we present plots of earthquake terms from the CY2006 model with the ZTOR effect turned off to verify our claim. We'll also show that the ZTOR effect is responsible for a 15% to 20% reduction of the inter-event standard error (τ) at high frequencies. The large variance reduction highlights the importance of including ZTOR effort in the CY2006 model.

Earthquake Terms as a Function of Z_{TOR}

To obtain earthquake terms with the Z_{TOR} effect turned off, we take the CY2006 model, set coefficient c_7 (the coefficient of the Z_{TOR} term) to zero, and rerun the regression. The new earthquake terms, grouped into three magnitude bins, are plotted against Z_{TOR} on Figure 1. We use the pseudo-standard error $\sigma/\sqrt{n_i}$ [8] of each earthquake term as an approximation for estimation uncertainty. The red (long dashed) line is the predicted Z_{TOR} effect from the CY2006 model.

[8] n_i is the number of records in an earthquake.

Figure 1 indicates a clear Z_{TOR} dependence in the earthquake terms, with some indication that the linear trend for earthquakes with $M \leq 5.5$ is weaker than that for earthquakes with $M > 5.5$. We tested the significance of magnitude dependence in the early stage of our model development and found it to be not statistically significant. We conducted the test against our final model again and also found the dependence to be not significant. Moreover, we cannot think of a physical basis for an increase in the Z_{TOR} effect with increasing magnitude. Based on these two reasons, we feel that we can't justify including magnitude dependence in Z_{TOR} effort in our model.

Is the CY2006 model inconsistent with Somerville and Pitarka (2006) at high frequency?

The average Z_{TOR} is 0.2 km for the 6 surface rupture events used by Somerville and Pitarka, and 3 km for the 4 buried rupture events. Note that Kobe earthquake was treated by Somerville and Pitarka as having a buried rupture, but its Z_{TOR} is 0.0 km. Using the CY2006 model, the expected difference between these two groups of earthquakes is about 0.15, not very different from the difference shown by Somerville and Pitarka[9].

In fact, it's the depth effects at long periods that are quite different between the two studies. At 1-sec period, the difference between the two types of rupture is about 0.6 in Somerville and Pitarka, but only 0.12 is predicted by CY2006. To understand this striking difference, earthquake terms of 1-sec spectral acceleration is plotted on Figure 2. It turns out the 4 buried earthquakes picked by Somerville and Pitarka happen to have much larger event terms than other buried earthquakes with similar Z_{TOR}. The CY2006 model has a weaker depth effect because it was fit to all the earthquakes in the NGA dataset.

Reduction of Inter-Event Standard Error due to Z_{TOR}

As another confirmation of the importance of Z_{TOR} effect at high frequency, we compute the amount of reduction of the inter-event standard error due to including the Z_{TOR} effect. The results are shown on Figure 3 for every period in the CY2006 model. The reduction of inter-event

[9] The average curve for shallow crustal earthquakes plotted on Figure 2 of Somerville and Pitarka may be in error. For example, at 0.1 sec period, the average of the 6 earthquake terms is more negative than what is indicated by the plotted curve.

standard error is large (by about 15% to 20%) at high frequency. It diminishes as the Z_{TOR} effect becomes smaller toward longer periods.

Future Refinement of the Z_{TOR} term

The recent paper by Shearer et al (2006) indicates that the stress drops of southern California earthquakes show an increase with increasing depth up to a depth of ~8 km, and no trend below this depth. In our model development, we did not find that a change in the slope of the depth trend at large depths was statistically significant. However, we have very limited data for Z_{TOR} > 8 km. Our data cannot reject the trends seen by Shearer et al (2006). Based on their results we plan to change the depth trend to level off at a depth of about 8 to 10 km. We will have this adjustment by the time of the meeting on the 25th.

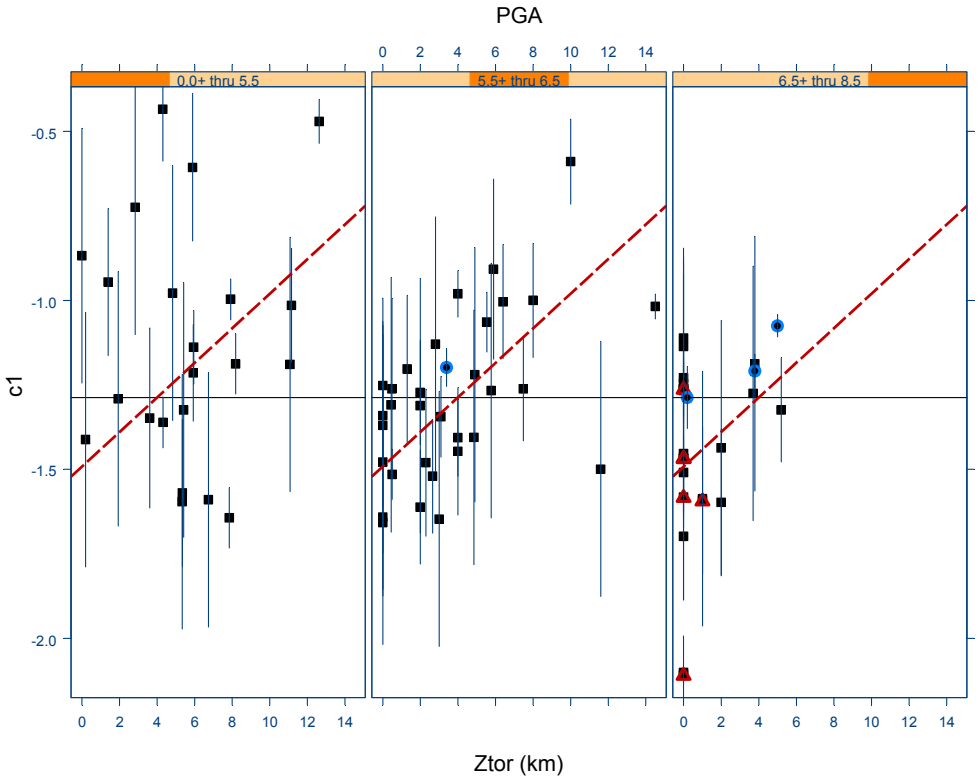

Fig. 1a Earthquake event terms of *pga* from CY2006 with effect of Z_{TOR} turned off. Red line is predicted effect of Z_{TOR} from CY2006. Earthquakes used by Somerville and Pitarka are red triangles (shallow rupture) and blue circles (buried rupture).

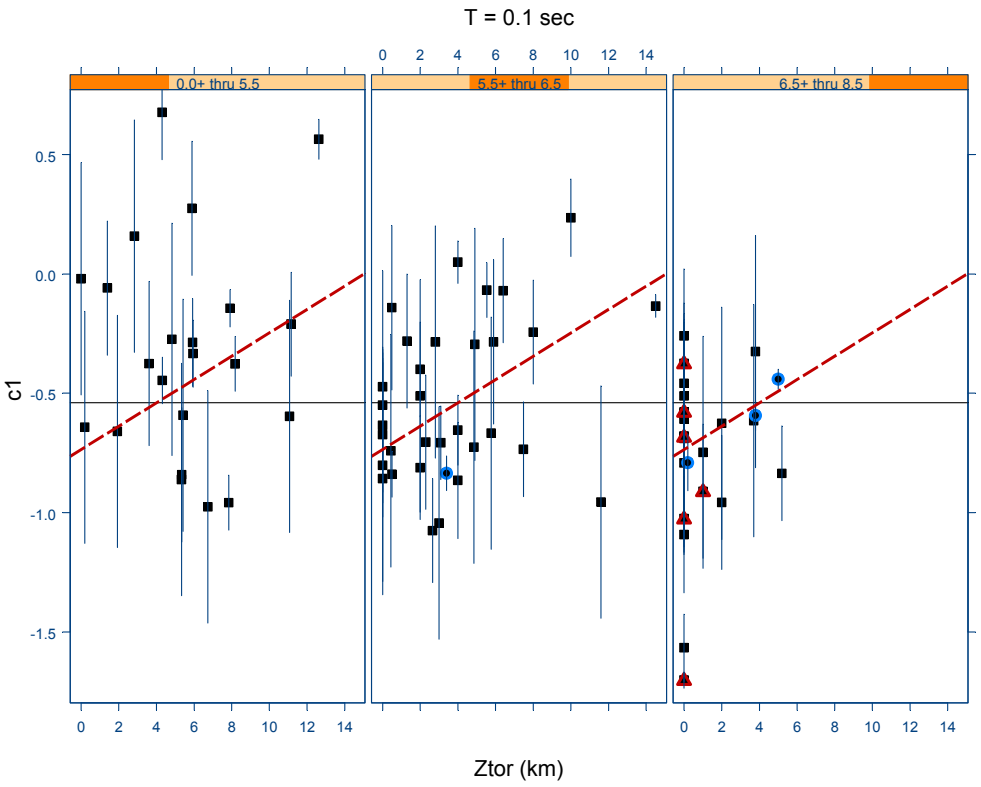

Fig. 1b Same as Fig. 1a, but for 0.1-sec period.

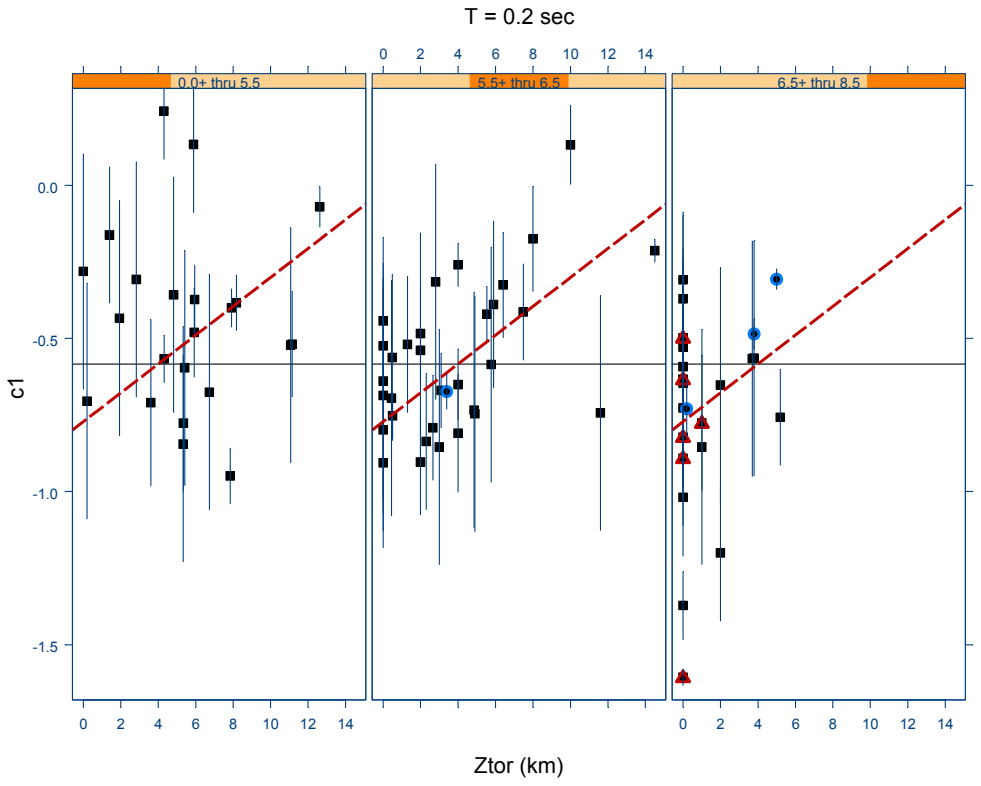

Fig. 1c Same as Fig. 1a, but for 0.2-sec period.

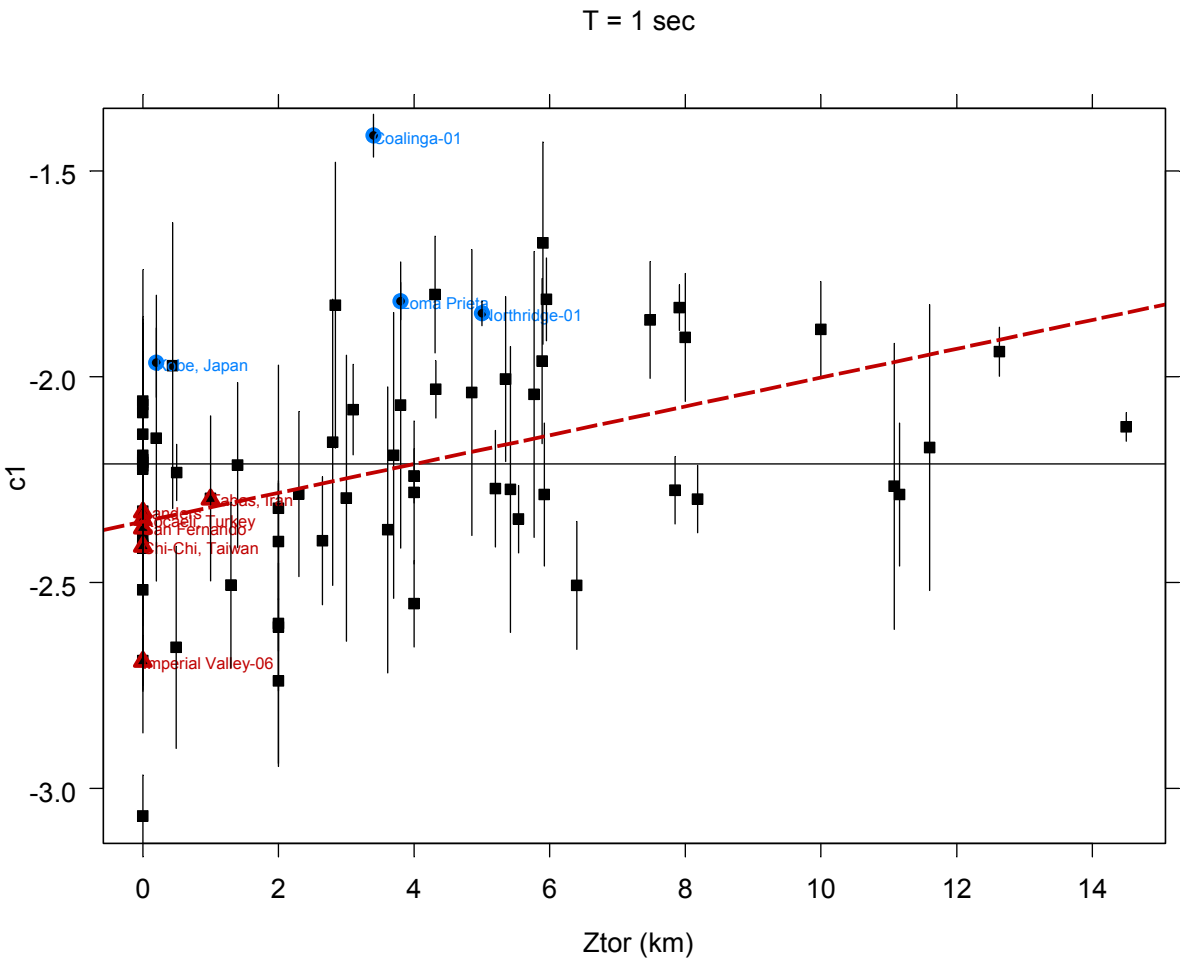

Fig. 2 Same as Fig. 1, but for 1-sec period.

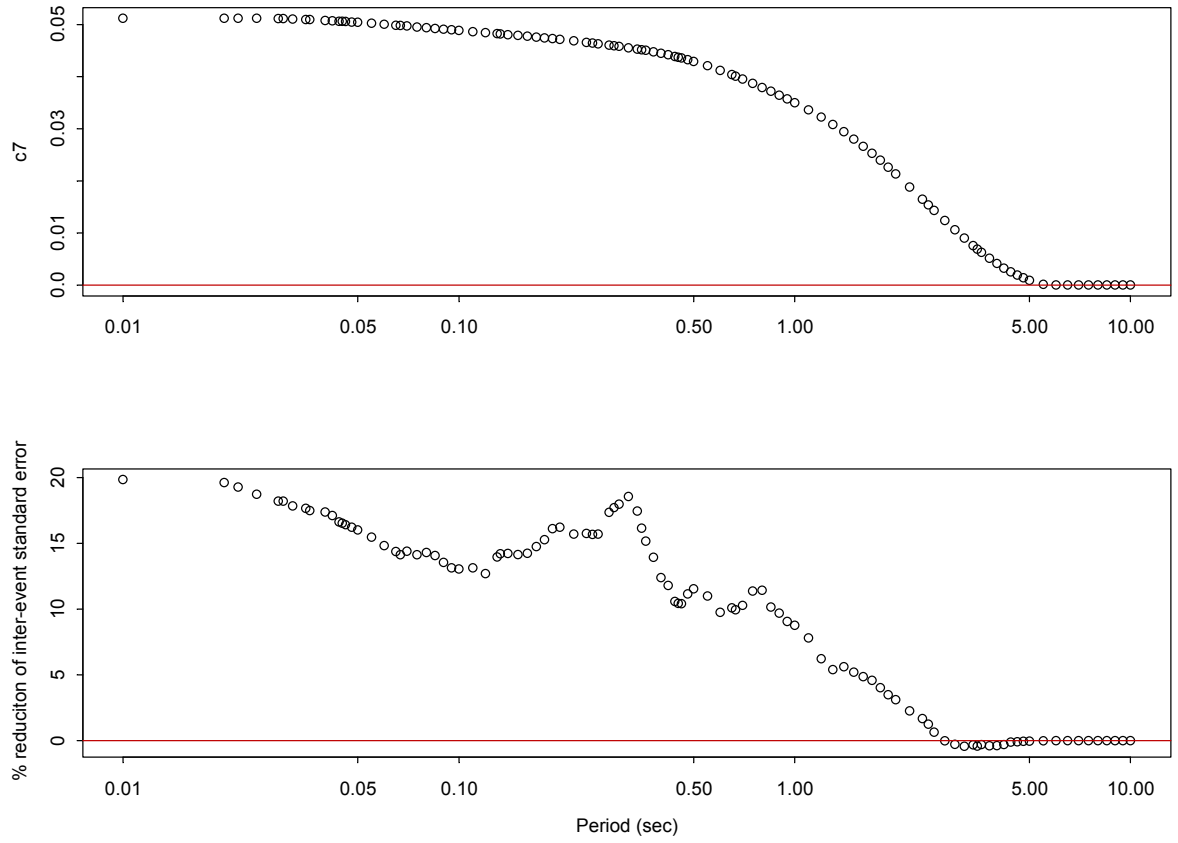

Fig. 3 (a) Coefficient c_7 (estimated effect of Z_{TOR}) as function of period. (b) Percentage of reduction of τ (standard error of inter-event error) due to Z_{TOR} effect.

Art Frankel's Comment #2: Too many predictive variables: *The above paragraph points out the danger of using too many predictive variables. For example, magnitude-dependent effects may be confused with a depth to top of faulting effect. Larger events are more likely to rupture the surface. Also, rupture aspect ratio is correlated with magnitude, so it is not obvious these two effects can be separated using the available data.*

CHIOU AND YOUNGS'S RESPONSE

Question of Confusing Magnitude-Dependent Effects with Z_{TOR} Effect

Our response to this question is already in the response to Frankel's Comment #1, in which we demonstrated that, given the magnitude scaling of Chiou and Youngs, there is a clear and significant effect of Z_{TOR}.

Too many predictors in the Chiou and Youngs's model?

We include in our model terms to address six basic trends in residuals: magnitude, distance (including magnitude effects), style of faulting, hanging wall, depth to top of rupture (addressed in our response to 1), and site condition effects. We believe that all of these trends are observed in the data and should be included in the model. Our formulation attempts to model these trends with smooth functions to avoid sharp "corners", rather than magnitude and distance ramps. This leads to somewhat complicated model equations, but not necessarily more parameters.

Frankel's Comment #3: Foot wall term. *Chang et al. (BSSA Dec. 2004) shows that there is a dip in residuals of the Chi-Chi footwall motions (at distances less than 15 km) when they are plotted as a function of nearest distance to rupture. This is caused by the fact that the distance to the center of the rupture is farther than the nearest distance for footwall sites. Is this relative dip of footwall ground motions accommodated in the functional forms used in NGA? If not, this could artificially lower ground motions in the distance ranges greater than 15 km. The dip in Chi Chi ground motions is also observed when using RJB. This dip does not appear to be present in the Northridge data. This calls into question the utility of the Chi Chi records for predicting ground motions for large events in other regions (see below).*

RESPONSE FROM CHIOU AND YOUNGS

We agree with Ken's comment; the dip in residuals of the footwall motions at distances less than 15km is an artifact resulting from not having a hanging wall term in Chang et al.'s equation. To verify this claim and to elaborate on the impact of hanging wall term on footwall residuals, we

take the same subset of Chi-Chi mainshock data used by Chang et al. and fit two equations to these data. The first equation $ln\, y = a + b\, ln(R_{RUP} + c)$ is identical in form to the equation used by Chang et al. The 2nd equation includes the hanging wall term developed by Chiou and Youngs (2006),

$$ln\, y = a + b\, ln(R_{RUP} + c) + \mathrm{d} \cdot cos^2 \delta_i \cdot tanh\left(\frac{R_{RUPij}}{2}\right) tan^{-1}\left(\frac{W_i \cos \delta_i}{2(Z_{TORi} + 1)}\right) \frac{1}{\pi / 2} \left\{1 - \frac{R_{JBij}}{R_{RUPij} + 0.001}\right\}$$

The resulting coefficients are listed in Table 1.

Median predictions from these two equations are shown on Figure 1. The hanging wall term has a large influence on parameter *c* because it stops the hanging wall data from pulling the distance curve upward. The larger *c* value in equation 2 results in lower motions at $R_{RUP} < 20$ km, and therefore the dip is no longer present in footwall residuals (Fig. 2).

We also want to add that the general form of our distance attenuation model was developed with HW data removed for all earthquakes (this was done only in phase 1 of our model development; see the "Modeling Steps" section of our report). That decision was motivated by findings similar to the above re-analysis of Chang et al. Removing the hanging wall data helps prevent them from biasing the distance scaling of near-source motions.

Table 1 Coefficients of Eqs. 1 and 2.

Equation	a	b	c	d	σ
1	3.776	-1.576	19.1	0	0.4123
2	3.926	-1.576	24.6	1.274	0.3097

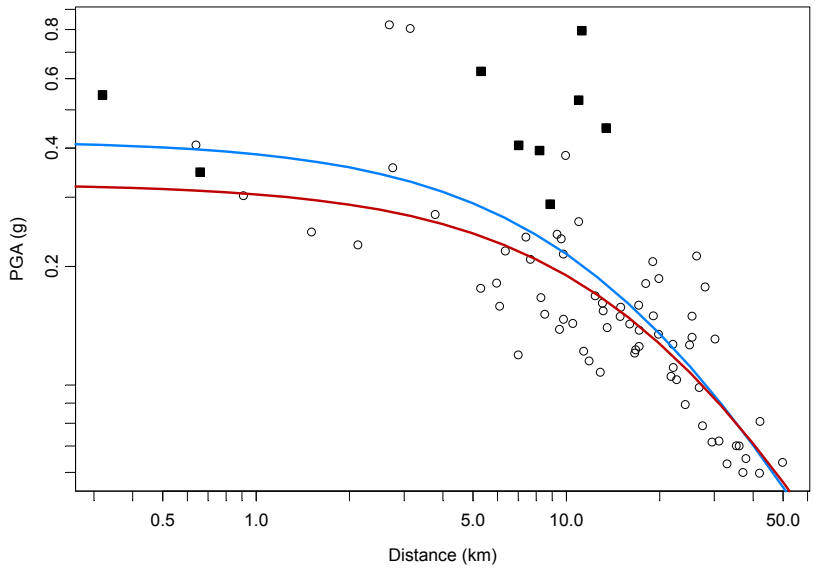

Fig. 1 Data and median predictions from equation 1 (blue) and equation 2 (red) for non-hanging wall sites. The hanging wall data are shown as solid squares.

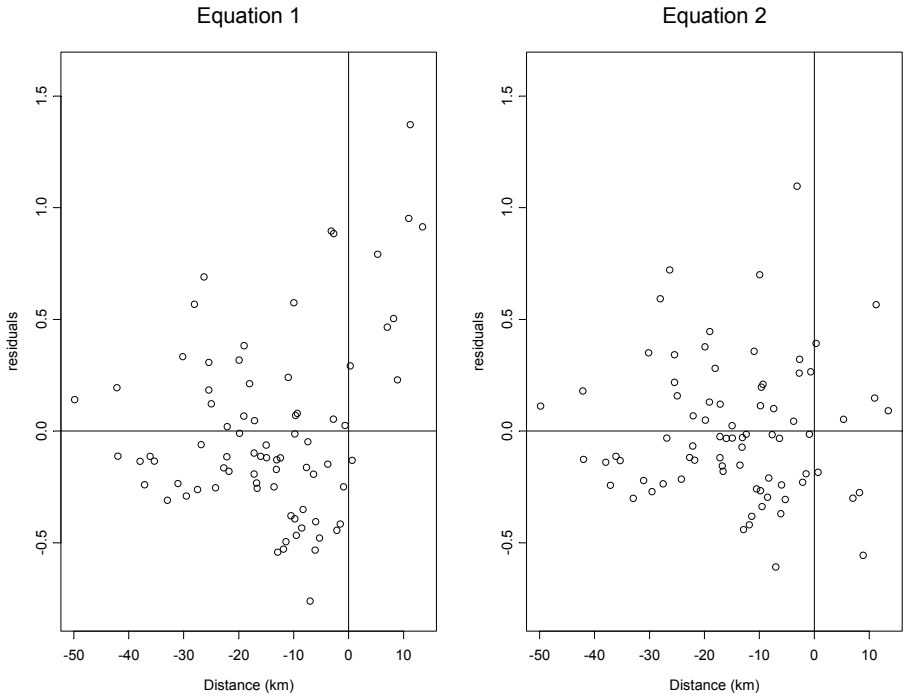

Fig. 2 Residuals from equations 1 and 2.

Art Frankel's Comment #4: Scaling with magnitude. *For high frequencies (≥ 5hz), the spectral accelerations for close-in sites (< 10 km JB distance) are far higher for Superstition Hills, Landers, and Kobe earthquakes, than for the Kocaeli earthquake. Here I have chosen only strike-slip earthquakes. This suggests there are regional differences in stress drop for strike-slip earthquakes.*

RESPONSE FROM CHIOU AND YOUNGS

We concur with Ken's comment that comparison of a few earthquakes is not really sufficient to derive general conclusion.

Following Ken's response, plots of intra-event residuals for these four earthquakes are provided below to allow checking of systematic bias or trend. Close-in sites with JB distance less than 10 km are plotted in red.

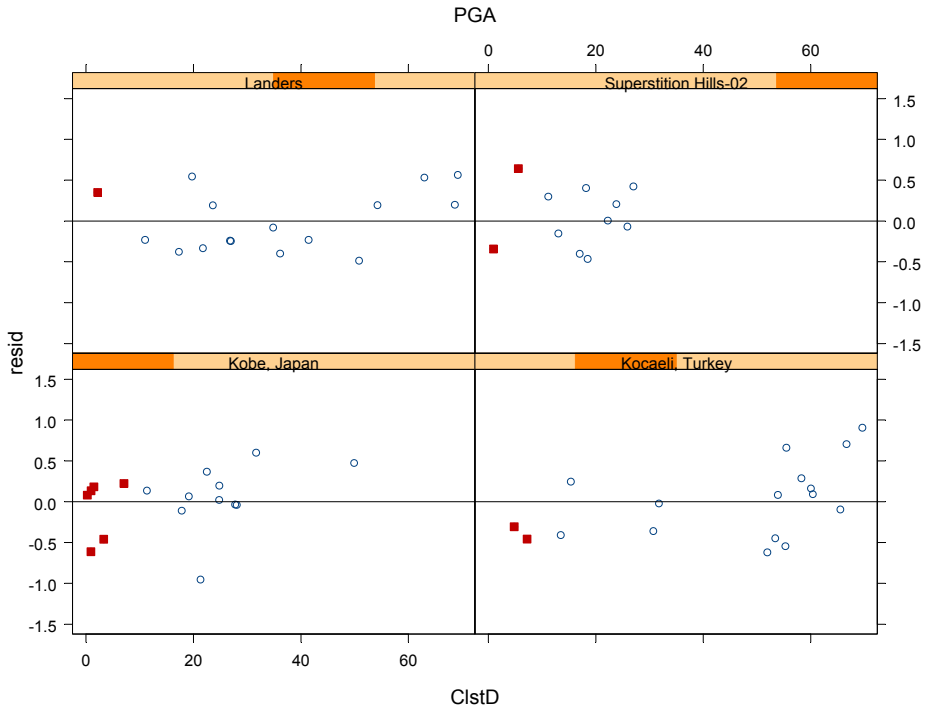

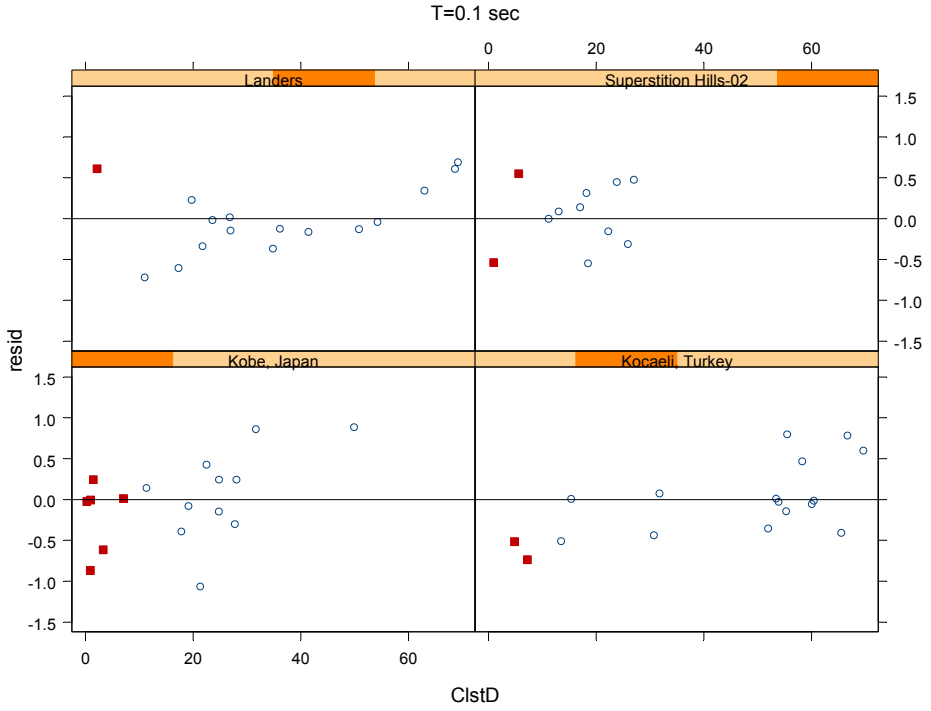
T=0.1 sec
Landers
Superstition Hills-02
Kobe, Japan
Kocaeli, Turkey
resid
ClstD

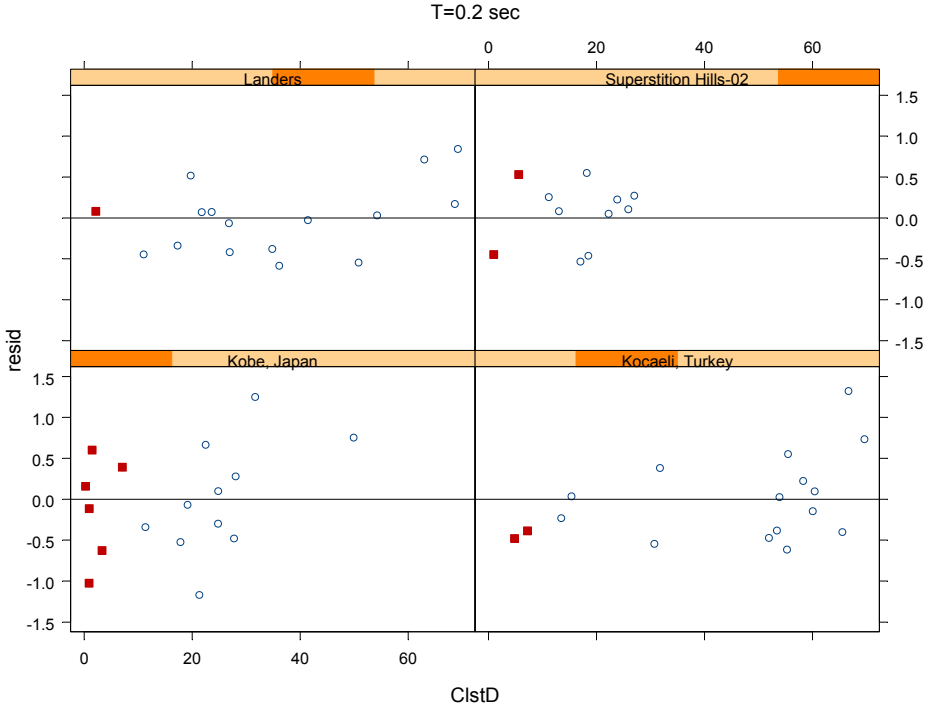
T=0.2 sec
Landers
Superstition Hills-02
Kobe, Japan
Kocaeli, Turkey
resid
ClstD

Art Frankel's comment #5: Changes from previous attenuation relations. *There are substantial differences in ground motions from moderate-sized (M6.5) earthquakes at distances of 15-30 km between the NGA relations and the previous relations from the same authors (using the same site conditions). Since there doesn't appear to be very much new data in this magnitude and distance range, why the large differences? An egregious example is Boore-Atkinson (2006) compared to Boore, Joyner and Fumal (1996) for 1 sec S.A. for RJB=0 and M=6.5. There is about a factor of two decrease for BA (2006) compared to Boore et al. 1996. Why?*

RESPONSE FROM CHIOU AND YOUNGS

We believe the large differences noted by Art can be attributed to the lack of fit of the SAO97 model to the NGA dataset. After SAO97 is updated and the trend in residuals is removed, the median rock motion from the updated SAO97 model is not substantially different from CY2006's prediction. This is particularly true in the case of the 1-sec spectral acceleration. Details are given in Appendix F.

Art Frankel's Comment #7: Unique aspects of Chi Chi mainshock. *The fact that the Chi-Chi aftershocks do not show the same anomalously low high-frequency excitation in the near-source region (< 30 km) as the mainshock (Wang et al., Dec. 2004 BSSA) combined with the observation that regional and teleseismic spectra of the aftershocks and mainshock scale as expected for a constant stress drop model (Frankel, 2006, SSA annual meeting), indicates that there is a bias in the near-source recordings of the Chi-Chi earthquake. This may be due to the low accelerations near the north end of the rupture and/or footwall effects described above. We have previously noted the possible bias introduced by a higher number of stations located near the north end of the rupture compared to the south end. It is worth noting that Kanno et al. (June 2006 BSSA) exclude the Chi Chi mainshock data from their new attenuation relations for Japan (which include some California data), citing propagation differences between Taiwan and Japan. The Kanno et al. (2006) relations appear to be significantly higher than the NGA ones, for large magnitudes and close-in distances.*

RESPONSE FROM CHIOU AND YOUNGS

Are there propagation differences between Taiwan and California?

"Propagation differences" between Taiwan and Japan were speculated by Kanno et al. (2006), not demonstrated. In fact, based on the evidences described below, we believe differences in magnitude scaling and distance attenuation between Taiwan and California are not likely to be significant. First, we did not find significant difference in Chi-Chi mainshock's γ (anelastic damping) once we account for truncation/incomplete data (Fig. 29 of our report is included). Second, we see similarity in *pga* attenuation (Fig. 1) between the model of Wu et al. (2001)[10], which was derived from Taiwan data only, and the model of Chiou and Youngs (2006), which was derived mainly from California data. Finally, we also see similarity in magnitude scaling between the two models at $R_{RUP} > 50$ km and $M < 6.5$.

However, large differences do exist at $M > 6.5$ and $R_{RUP} < 20$km, where the dataset of Wu et al. is poorly populated (Fig. 2). These differences shouldn't be construed as proof of regional difference in near-source motions because the parameter (*h)* controlling the near-source prediction was fixed in Wu at al. [11], whereas the corresponding parameters (c_5 and c_6) in Chiou and Youngs were estimated from strong-motion data.

Unique Aspects of Chi-Chi Mainshock High-Frequency Motions and Their Effect on the Chiou-Youngs's Model

Several unique aspects of the Chi-Chi high-frequency motions were identified by the reviewers and they were also used by the reviewers to call into questions the utility of the Chi-Chi mainshock data for predicting ground motions of large magnitude event in California.

Some of the Chi-Chi motions are addressed in our responses to Mark's question #1 and Art's questions #3. To confirm and provide scientific explanations of the remaining issues would require additional ground motion data and more in-depth analysis. These studies may be of great

---

[10] Wu, Y.M., T.C. Shin, and C.H. Chang (2001). Near real-time mapping of peak ground acceleration and peak ground velocity following a strong earthquake, *Bull. Seism. Soc. Am.* **91**, 1218 – 1228.

[11] The Wu et al. model is $log_{10}(PGA)=0.00215+0.581M_w-log_{10}(R_{RUP}+h) -0.00414R_{RUP}$. Parameter $h=0.00871 x10^{0.5Mw}$ is fixed to the square root of the rupture area determined from a simple relationship between rupture area and M_w.

scientific interests, but from the standpoint of ground motion prediction the more relevant question to ask is: do the unique Chi-Chi data bias the estimates of key model parameters?

Throughout our model development we made an attempt to prevent any one earthquake from having a major effect on the estimates of model parameters. For example, we estimated the style of faulting effect with the Chi-Chi mainshock data removed. Another example, the general form of our distance attenuation model was developed with footwall (and hanging) data removed for all earthquakes so that the unique Chi-Chi footwall data will not affect these terms.

The outcome of this practice, we believe, is a model that is not unduly biased by the Chi-Chi data.

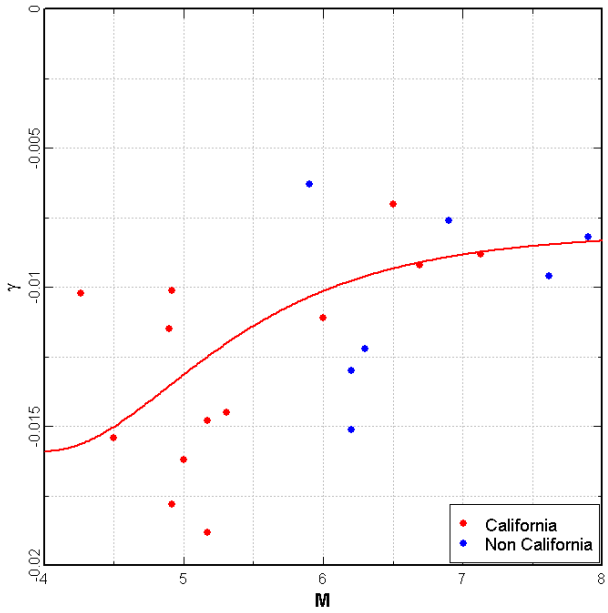

Fig. 29 (Chiou and Youngs 2006) Estimates of γ from analysis of extended datasets (Table 4). Red curve shows model developed by a fit to combined California earthquake data set.

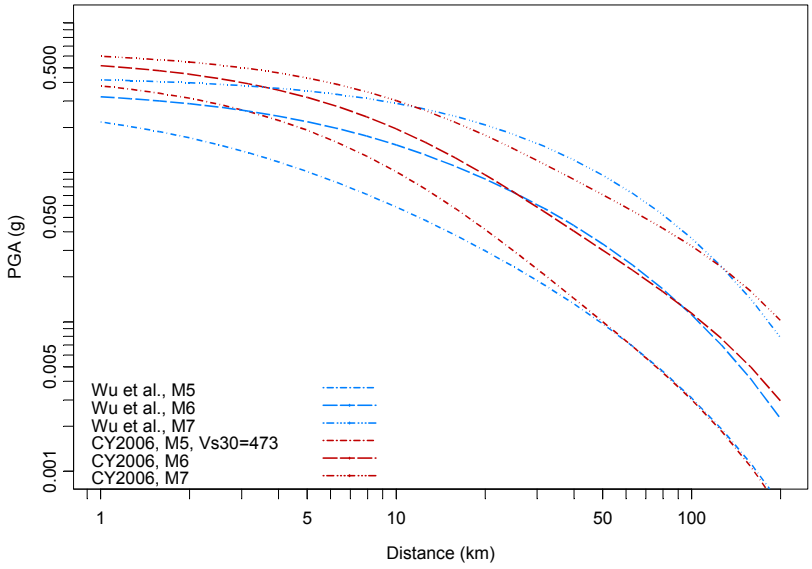

Fig. 1 Comparison of median motions predicted by models of Wu et al. (2001) and Chiou and Youngs (2006). A V_{S30} of 474 m/sec was used to compute motions from Chiou and Youngs.

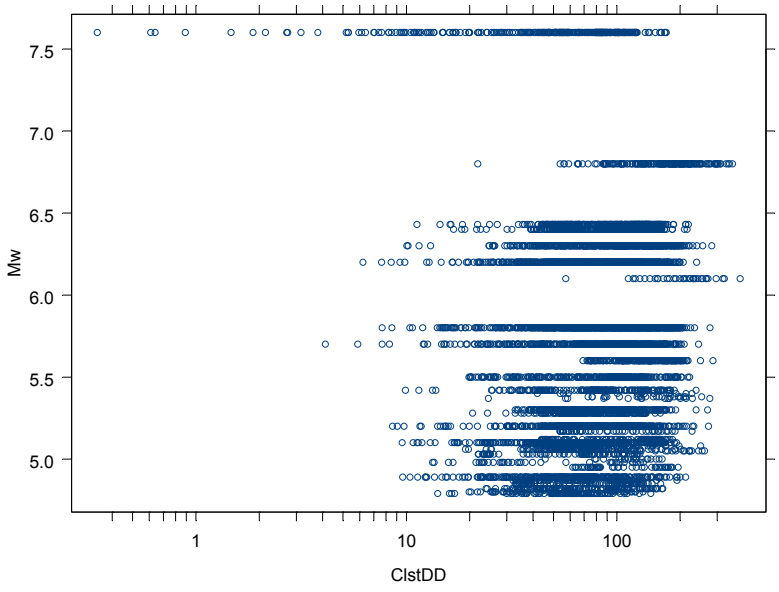

Fig. 2 Magnitude-distance distribution of dataset used in regression of *pga* model by Wu et al. (2001). Note regression dataset consists of *pga* data from 60 earthquakes recorded at 75 telemetered strong-motion stations in Taiwan, plus data recorded by TSMIP stations at distance less than 30km from source.

MARK PETERSEN'S QUESTION #1

Do you consider your ground motion prediction equations appropriate for seismic hazard assessments of California and throughout the western U.S.? Please explain. If you had left out international data and only used California data would you get a significantly different answer? Please explain.

Response to the Question of Applicability to California

This question arises from the concern about undue influence of non-California data on the regression results. A good way to address this concern is to examine the residuals of California only data. we'll show that significant trends can not be detected in California residuals. Thus, the NGA models are not biased relative to California data and the concern of undue influence of non-California data is not justified.

Before the residual plots are presented, we need to point out several important factors that work in favor of reaching an attenuation model that is California-like. First, the majority of the data selected for use in NGA model development is from California. As an example, the magnitude-distance-region distribution of data used in the Chiou and Youngs's model is shown in Figure 1. California data dominate the dataset at magnitude less than 7.2 and they play an important role in shaping the NGA model. Second, formulation of the NGA models and the constraints imposed on the model coefficients were mainly based on California data or on models derived from California data. For example, the Atkinson and Silva (1997, 2000) California-based seismic source models were used by Chiou and Youngs to generate synthetic motions, which were then used to formulate the form of magnitude scaling model. Another example is the use of California TriNet data by Boore and Atkinson and Chiou and Youngs to constrain the anelastic parameters. Thirdly, the developers were given the scope to develop models suitable for use in California. This goal strongly influenced developers' decisions and judgment made during model development.

Residuals plots for *pga*, T=0.2, 1 and 3 sec, are provided to facilitate the examination of model applicability to California in terms of magnitude scaling, distance attenuation, and site effect. In the following, we'll use plots from Chiou and Youngs to demonstrate the appropriateness of NGA model for California.

Inter-event errors are shown in Figure 2 and there is no significant bias relative to California earthquakes. In fact, the magnitude scaling model fits both the California and non-California earthquakes well except in the cases of *pga* and 0.2 sec the low values of several non-California earthquakes with M ≥ 7.2. The magnitude scaling model was not dragged down to fit the low values. The non-California earthquakes do not have a major influence on magnitude scaling because it was constrained to follow an earthquake source model derived from largely California data. One might argue that the low values could still drag down the intercept C_1 (and hence the overall level of median motion). This will be addressed later.

Intra-event residuals in six magnitude bins are plotted against distance on Figure 2 Intra-event residuals plotted against Vs30 are shown on Figure 3. Fits to the California data are very good. It is difficult to argue there is significant bias relative to California data.

Based on the above observations, we conclude that, despite the use of some non-California earthquakes in the development of NGA models, the NGA models are appropriate for seismic hazard assessments of California.

Response to the Question of Applicability Throughout the Western U.S.

There are only a few data from the rest of western U.S. This makes it difficult to evaluate the applicability. Some developers warned that modifications of the NGA model may be needed in certain region. This applicability question is addressed in the Applicability Section of C&Y's report. Use of C&Y model in the rest of the WUS may require some modification if the anelastic attenuation (Q) is significantly different from California (e.g., in the Intermountain region).

Response to the Question of Using California Data Only

Given the good fits of C&Y model to California data, it is reasonable to state that if we were to develop a model using only California data the C & Y model would already be an excellent candidate. Some may suggest that the low values of several non-California earthquakes (Fig. 2) could still have a significant influence on coefficient C_1 and therefore C_1 should be re-estimated. Responding to this suggestion, we rerun the regression analysis using only California data with C_1 being the only free fixed-effect coefficient. The differences between the resulting C_1 and C&Y's C_1 are shown in Figure 5. The consequences of removing the non-California data are: an increase of C_1 (and hence the predicted median motion) by 5% to 10% at high frequencies

(T<0.2 sec), and a decrease of C_1 by less than 5% at long periods (T>3 sec). Such changes are not considered to be significant.

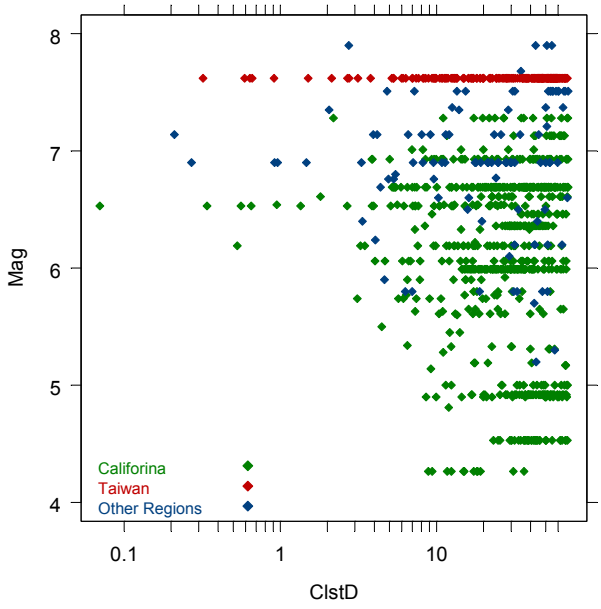

Fig. 1 Magnitude-distance-region distribution of data used in development of Chiou and Youngs model.

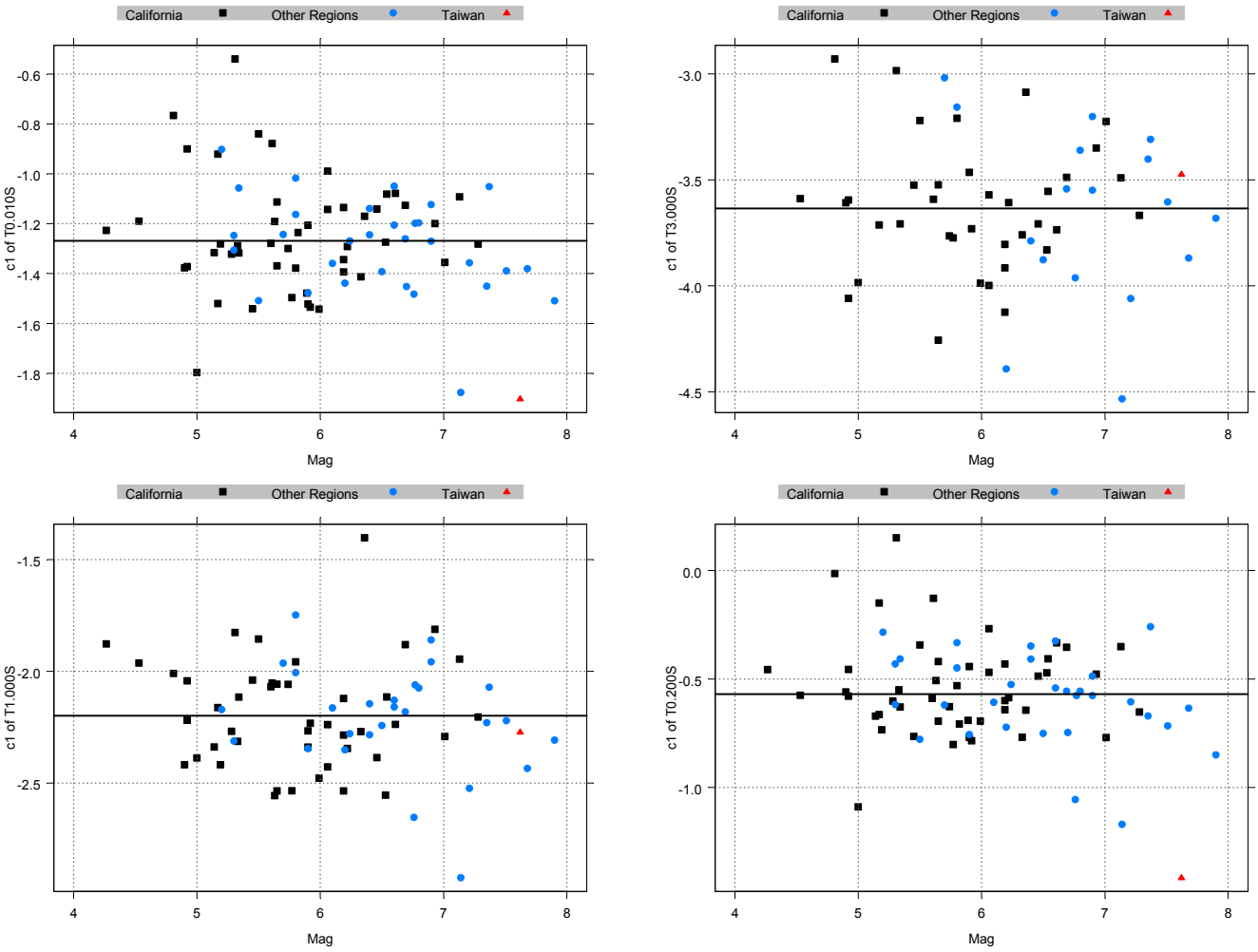

Fig. 2 Random earthquake effects for *pga* and the 0.2, 1, and 3 sec spectral periods of Chiou and Youngs. Horizontal line denotes coefficient C_1 (population mean of random earthquake effects). Difference between population mean and individual value represents random inter-event error.

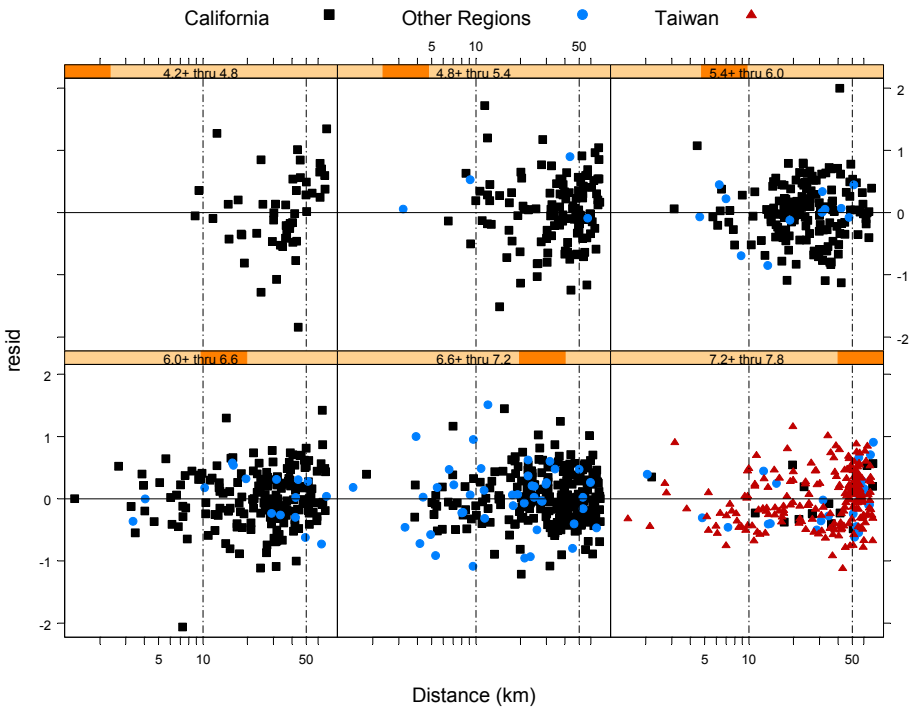

Fig. 3a Intra-event residuals from Chiou and Youngs for *pga* are plotted against distance.

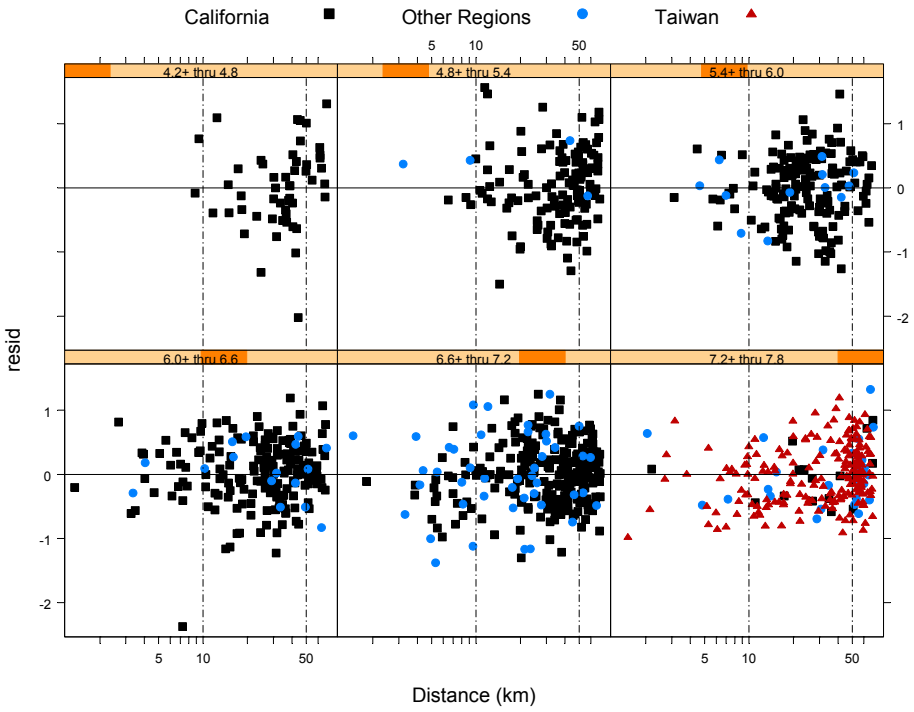

Fig. 3b Intra-event residuals from Chiou and Youngs for spectral period of 0.2 sec plotted against distance.

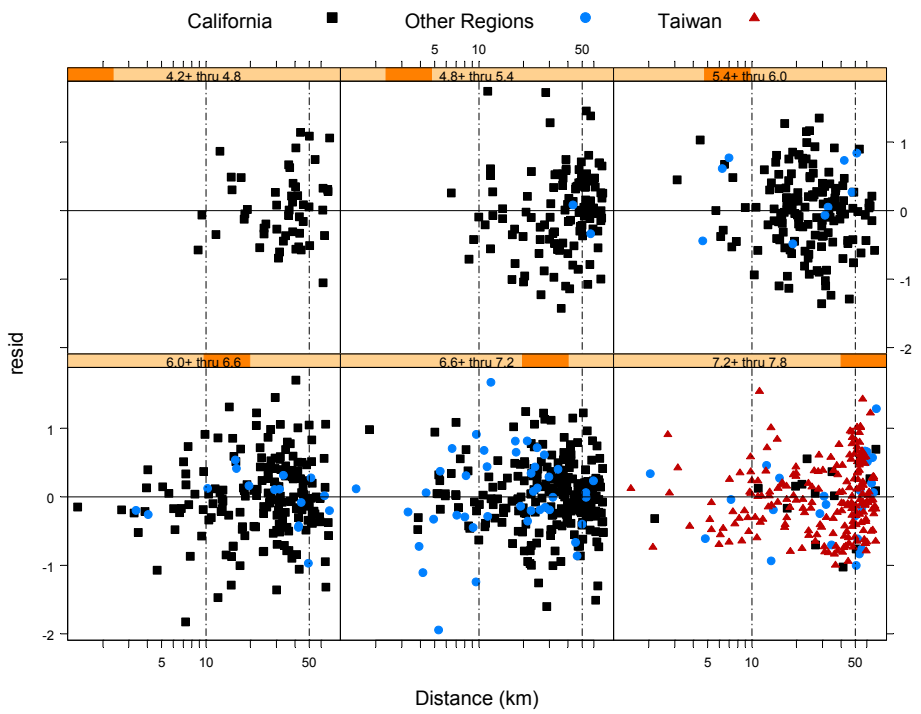

Fig. 3c Intra-event residuals from Chiou and Youngs for spectral period of 1 sec plotted against distance.

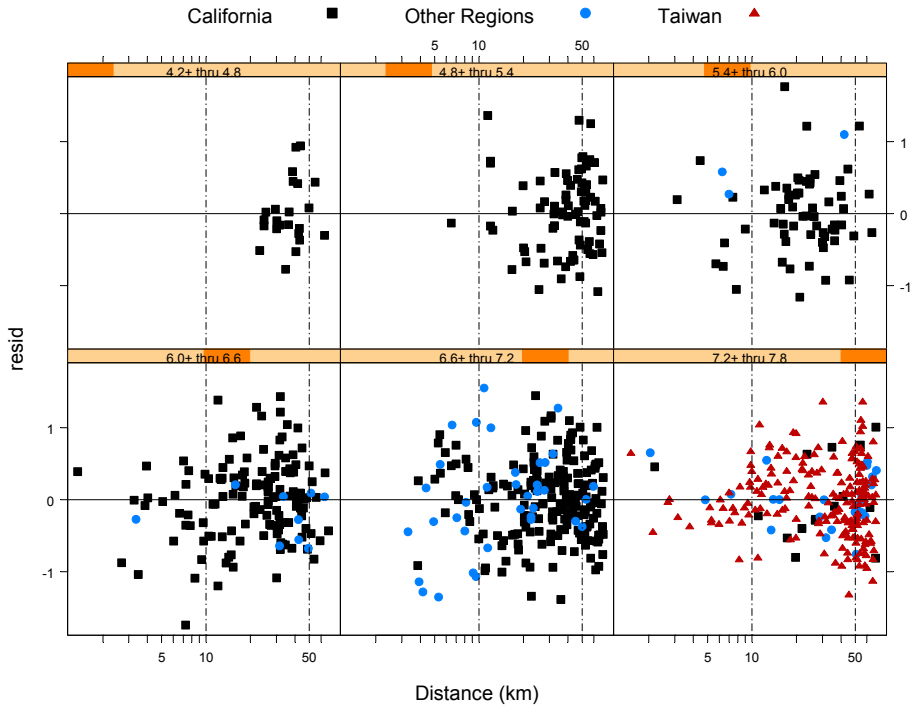

Fig. 3d Intra-event residuals from Chiou and Youngs for spectral period of 3 sec plotted against distance.

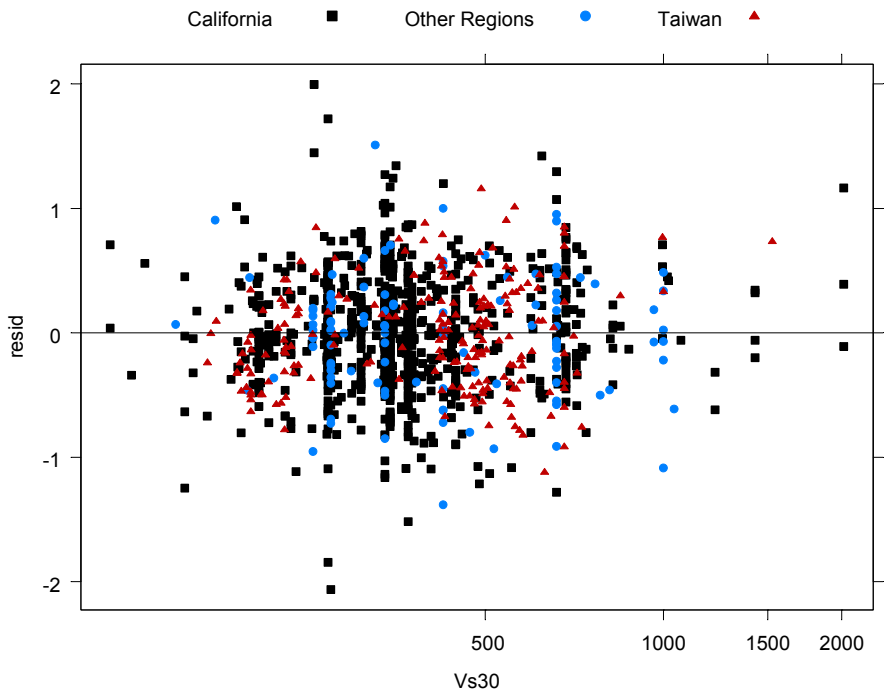

Fig. 4a Intra-event residuals from Chiou and Youngs for *pga* are plotted against Vs30 (m/sec).

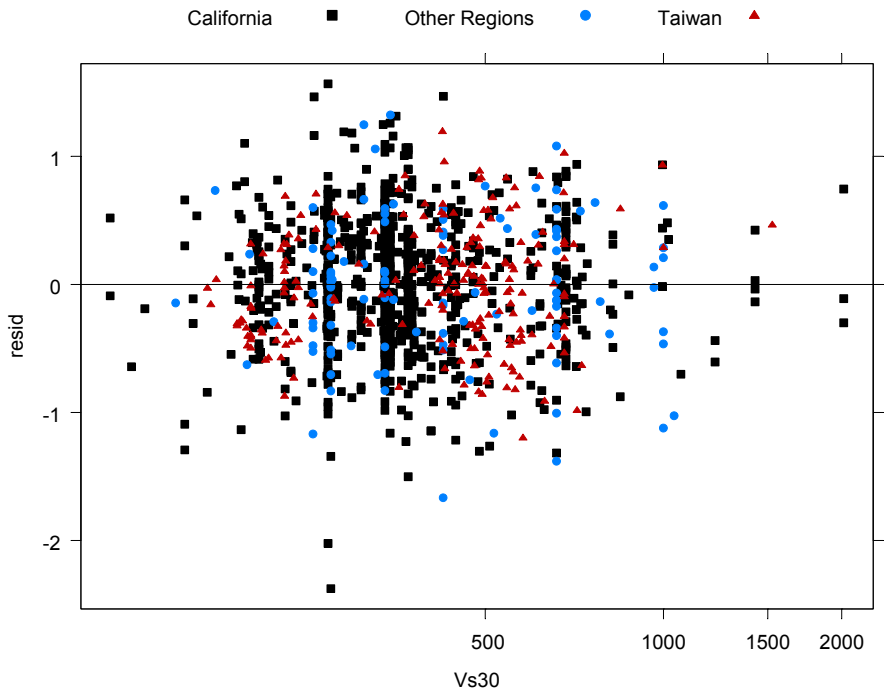

Fig. 4b Intra-event residuals from Chiou and Youngs for spectral period of 0.2 sec plotted against Vs30 (m/sec).

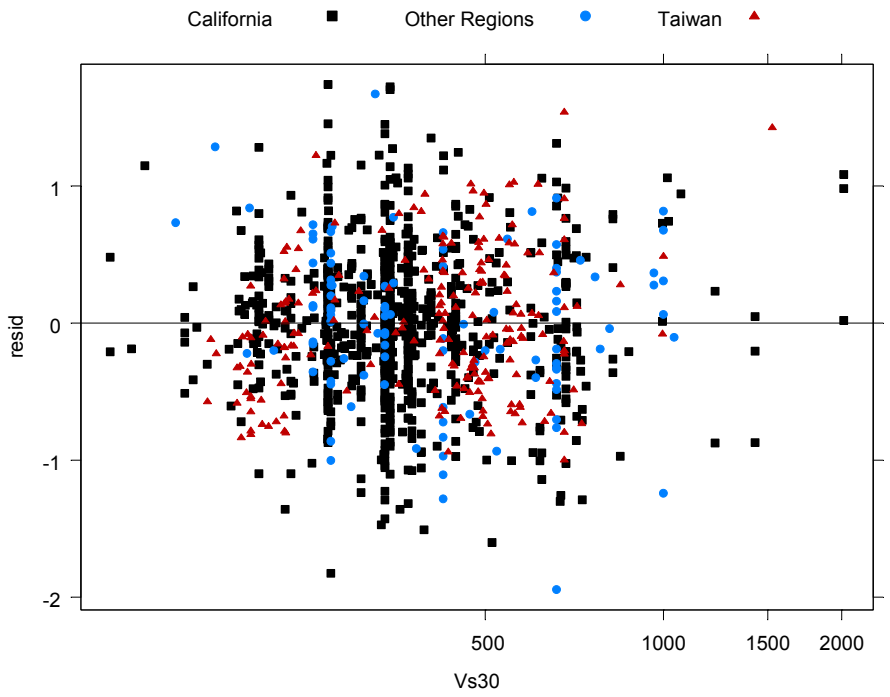

Fig. 4c Intra-event residuals from Chiou and Youngs for spectral period of 1 sec plotted against Vs30 (m/sec).

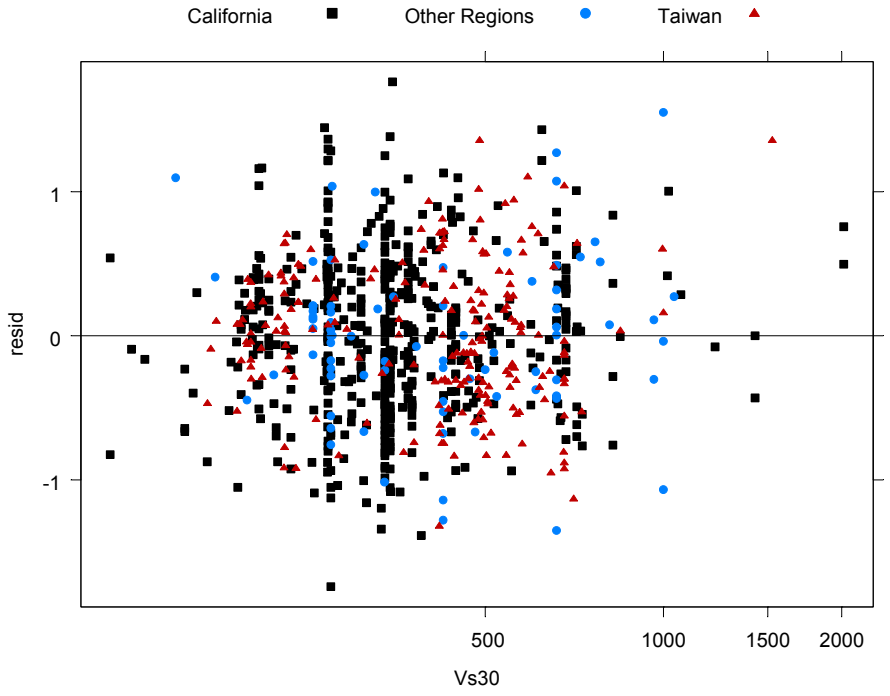

Fig. 4d Intra-event residuals from Chiou and Youngs for spectral period of 3 sec are plotted against Vs30 (m/sec).

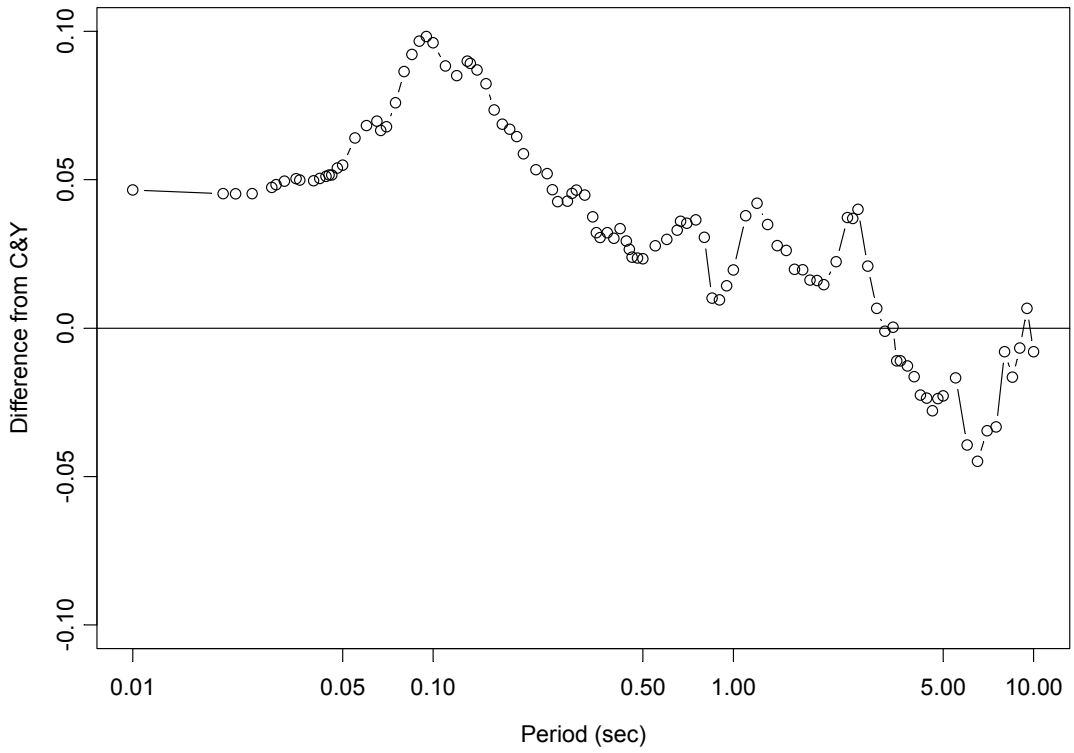

Fig. 5 Differences between C_1 estimated from California data and C_1 of Chiou and Youngs, which also used non-California earthquakes.

MARK PETERSEN'S QUESTION #2

Do you feel that your equations have adequately accounted for epistemic and aleatory uncertainties to be used for public policy? Please explain. How do you suggest that the USGS account for the epistemic uncertainties in the ground motion relations in the national maps?

Preliminary Epistemic Uncertainty Model

The epistemic uncertainty in the median ground motions has a number of components, including:

- Uncertainty in selecting the appropriate database
- Uncertainty in selecting the appropriate model formulation
- Uncertainty in estimating the population mean with a finite data set
- Uncertainty in estimating the population mean due to uncertainty in the predictor variables in the dataset (magnitude, distance, V_{S30}, etc.)

The first two items are addressed (to some degree) by the alternative model forms and databases use by the five development teams. Presented below is an assessment of the uncertainty in the C&Y model due to the second two items.

Uncertainty in Estimation of Model from Finite Data Set

A simple first order estimate of the uncertainty in the median (mean log) estimates of ground motion for an individual model can be made using the standard statistical estimate of the uncertainty in the mean, $\bar{x}$, of a sample of size n :

$$\sigma_{\bar{x}} = \sqrt{\frac{\sigma_x^2}{n}} \tag{1}$$

where σ_x^2 is the sample variance.

The parameters of the PEER-NGA ground motion models are defined by mixed effects regression (or equivalently two-stage regression) such that the total variance in the log of ground motion amplitude is partitioned into an inter-event component τ^2 and an intra-event component σ^2. For this case, an equivalent form of Equation (1) is

$$\sigma_{\overline{\ln[PGA]}} = \sqrt{\frac{\tau^2}{n_{Eq}} + \frac{\sigma^2}{n_{Sites}}} \tag{2}$$

where n_{Eq} is the number of earthquakes and n_{Sites} is the number of recordings. Equation (2) can be used to qualitatively assess the estimation uncertainty in ground motion for different magnitude and distance intervals.

Figure 1 shows the magnitude-distance distribution of the data used to develop the C&Y model. The magnitude range was divided into four intervals, $\mathbf{M} < 5$, $5 \le \mathbf{M} < 6$, $6 \le \mathbf{M} < 7$, and $\mathbf{M} \ge 7$ and the distance range was divided into three intervals, $R_{RUP} < 10$, $10 \le R_{RUP} < 30$, and $R_{RUP} \ge 30$. Table 1 lists the values of n_{Eq} and n_{Sites} for the C&Y data set and values of $\sigma_{\overline{\ln[PGA(m,r)]}}$ computed using $\tau = 0.288$ and $\sigma = 0.515$.

Table 1 Application of equation (2) to C&Y dataset.

M and R_{RUP} Range	Average **M**	Median R_{RUP}	n_{Eq}	n_{Sites}	$\sigma_{\overline{\ln[PGA(m,r)]}}$
M < 5 R_{RUP} < 10	4.7	7.3	6	25	0.156
M < 5 10 ≤ R_{RUP} < 30	4.7	15.7	12	47	0.112
M < 5 R_{RUP} ≥ 30	4.8	45.4	5	98	0.139
5 ≤ **M** < 6 R_{RUP} < 10	5.6	7.0	23	32	0.109
5 ≤ **M** < 6 10 ≤ R_{RUP} < 30	5.5	16.9	50	263	0.052
5 ≤ **M** < 6 R_{RUP} ≥ 30	5.7	46.5	26	241	0.065
6 ≤ **M** < 7 R_{RUP} < 10	6.5	4.4	24	78	0.083
6 ≤ **M** < 7 10 ≤ R_{RUP} < 30	6.5	20.1	26	210	0.067
6 ≤ **M** < 7 R_{RUP} ≥ 30	6.3	48.8	23	670	0.063
M ≥ 7 R_{RUP} < 10	7.5	4.1	7	45	0.133
M ≥ 7 10 ≤ R_{RUP} < 30	7.5	17.9	8	71	0.119
M ≥ 7 R_{RUP} ≥ 30	7.5	50.3	10	170	0.099

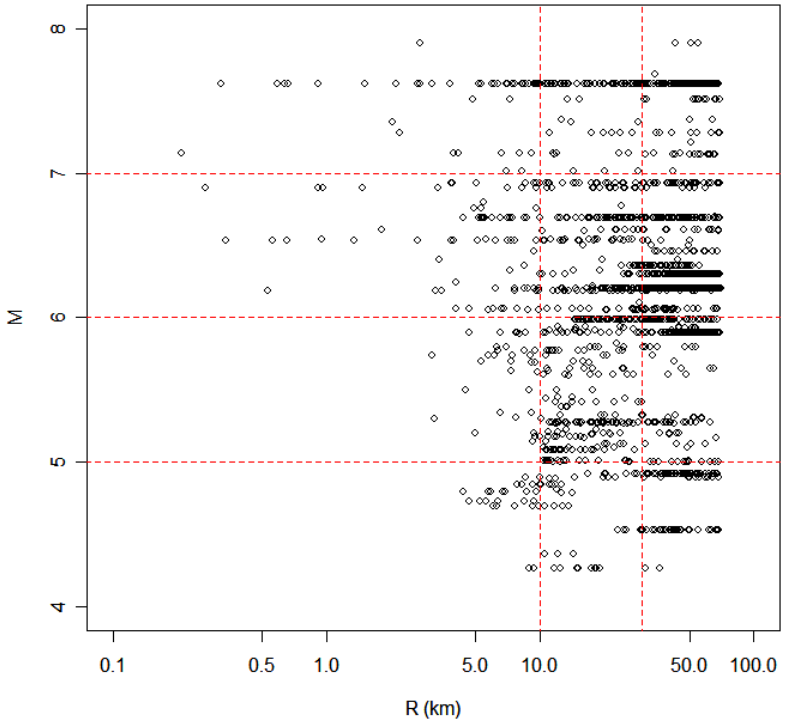

Fig. 1 Magnitude-distance distribution of C&Y dataset for *pga*.

The magnitude and distance ranges selected above are arbitrary but they provide an indication of the variation of uncertainty in the estimate of $\overline{\ln[PGA(m,r)]}$ as a function the amount of data.

The uncertainty estimates illustrated above do not incorporate the structure of the regression model and any external constraints imposed in the fitting. For linear regression models there are standard formulations for the uncertainty in the mean estimate as a function of the location of the estimation point with respect to the mean of the predictor variables. The uncertainty is smallest near the mean of the predictors and grows as the estimation point moves to the edges of the data used to fit the model. For non-linear, mixed effect regression models, explicit formulation of the uncertainty becomes much more difficult.

An alternative is to use non-parametric methods to estimate the uncertainty in the median prediction. One method that is widely employed is the bootstrap (Efron and Tibshirana, 1993). In the standard bootstrap, repeated random samples of size n_{Total} are drawn with replacement from the original data set. Each bootstrap sample is fit and the resulting model used to estimate $\overline{\ln[PGA(m,r)]}$ for a range of magnitudes and distances. The process is repeated multiple times and the resulting variability in $\overline{\ln[PGA(m,r)]}$ provides an estimate of uncertainty. The bootstrap process draws repeated samples from the unknown true distribution of the data using the empirical distribution as a substitute.

Unfortunately, application of the bootstrap to a mixed effects regression model is not straight forward because of the assumed nested nature of the data (correlation of ground motions from the same earthquake) and there is very little in the literature on how to proceed. As a first step, bootstrapping of the intra-event data was performed. This involved sampling with replacement from the recordings for each earthquake to build a data set of the same size as the original. Figures 2 and 3 show the resulting range and 90% interval in $\overline{\ln[PGA(m,r)]}$ for 100 bootstrap samples. It should be noted that Efron and Tibshirani (1993) recommend on the order of 1000 samples for confidence intervals. However, the results presented in Figures 2 and 3 indicate the magnitude of the estimation uncertainty for $\overline{\ln[PGA(m,r)]}$.

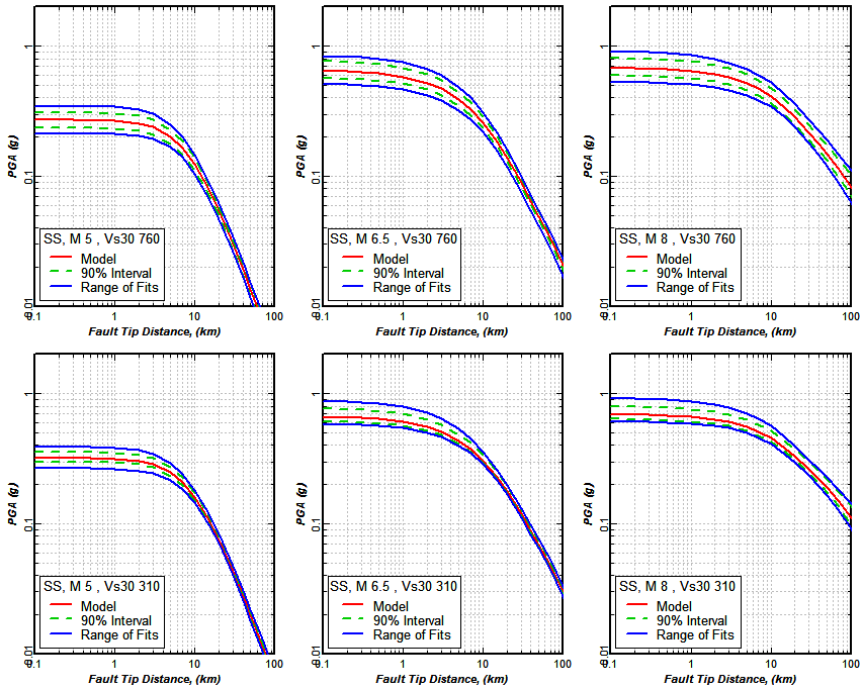

Fig. 2 Bootstrap 90% intervals for $\overline{\ln[PGA(m,r)]}$ for strike-slip earthquake ground motions. Bootstrapping restricted to intra-event samples. (Z_{TOR} = 5, 0, 0; dip = 90º)

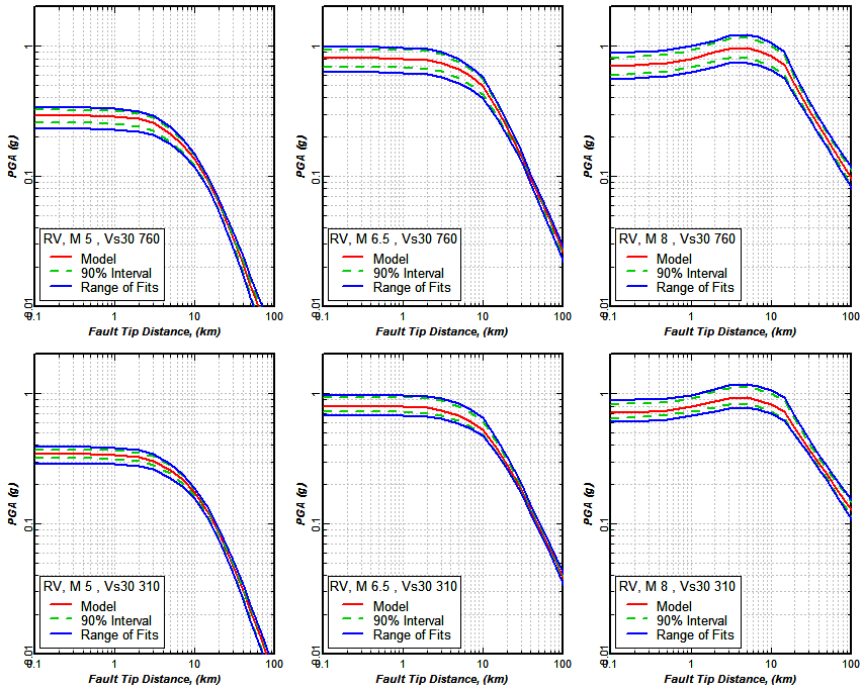

Fig. 3 Bootstrap 90% intervals for $\overline{\ln[PGA(m,r)]}$ for reverse earthquake ground motions. Bootstrapping restricted to intra-event samples. (Z_{TOR} = 5, 2, 0; dip = 45º; widths 3, 15, 21.21 km)

The examples presented above provide an estimate of uncertainty by sampling from the empirical distribution of the intra-event terms. An estimate of uncertainty from sampling from the inter-event terms can be provided by employing another non-parametric technique, the jackknife. The standard jackknife technique uses repeated samples in which one data point is left out each time. For a data set of size n, n samples are created leaving out each data point in turn. We adapted this concept by creating 125 data sets for the C&Y model, each set has one of the 125 earthquakes removed. Figures 4 and 5 show the resulting range of values for $\overline{\ln[PGA(m,r)]}$. Ninety percent of the estimates lie very close to the model prediction and the 90% interval is not shown.

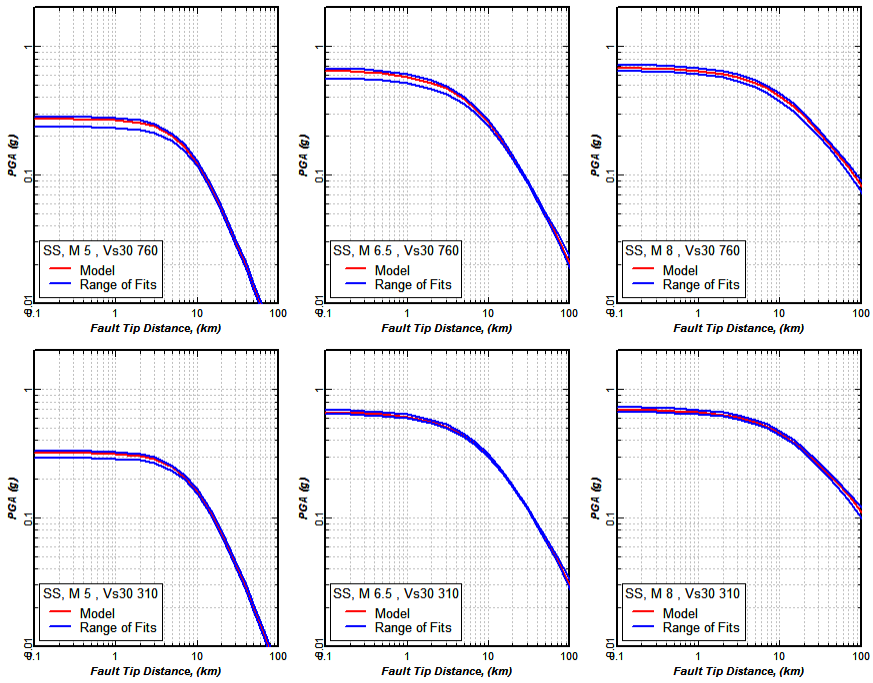

Fig. 4 Range of $\overline{\ln[PGA(m,r)]}$ for strike-slip faulting from jackknife (on earthquakes) fits to C&Y database (Z_{TOR} = 5, 0, 0; dip = 90º)

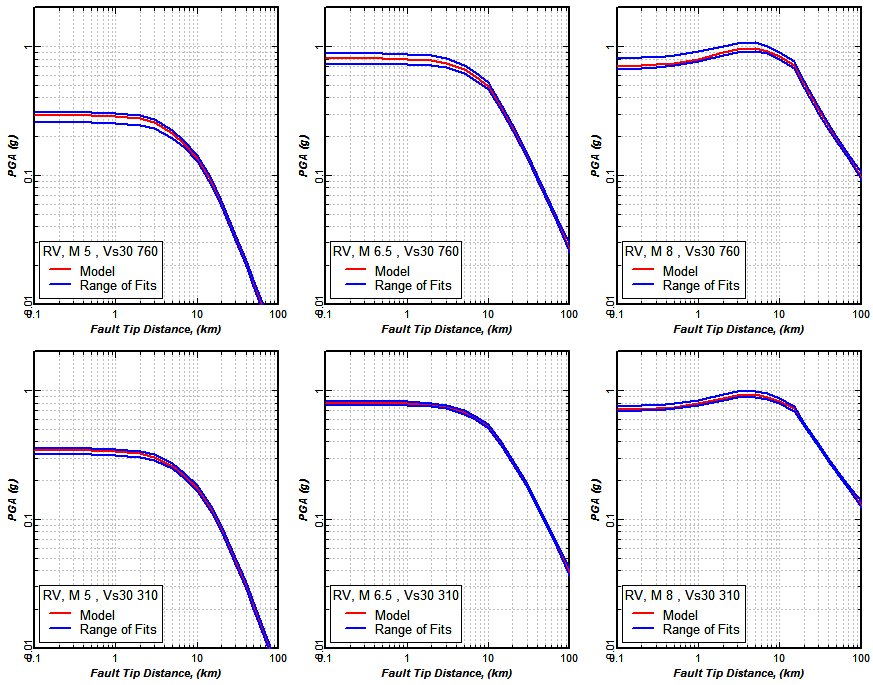

Fig. 5 Range of $\overline{\ln[PGA(m,r)]}$ for reverse faulting from jack knife (on earthquakes) fits to C&Y database (Z_{TOR} = 5, 2, 0; dip = 45°; widths 3, 15, 21.21 km).

We believe that some combination of the uncertainties shown on Figures 2 and 3 with that shown on Figures 4 and 5 provides a reasonable estimate of the uncertainty in $\overline{\ln[PGA(m,r)]}$ derived from fitting the ground motion model to the selected data base.

Effect of Uncertainty in Predictor Variables

The fourth contribution to uncertainty in $\overline{\ln[PGA(m,r)]}$ is from uncertainty in the predictor variables (**M**, R, Z_{TOR}, V_{S30}). We estimate this using simulation. One hundred data sets are simulated with random errors added to the predictor variables. The standard deviations for the individual values of **M** and V_{S30} given in the flat file were used for these variables. Approximate errors for R and Z_{TOR} were included based on judgment (these will need to be refined). Figures 6 and 7 show the resulting uncertainties in $\overline{\ln[PGA(m,r)]}$.

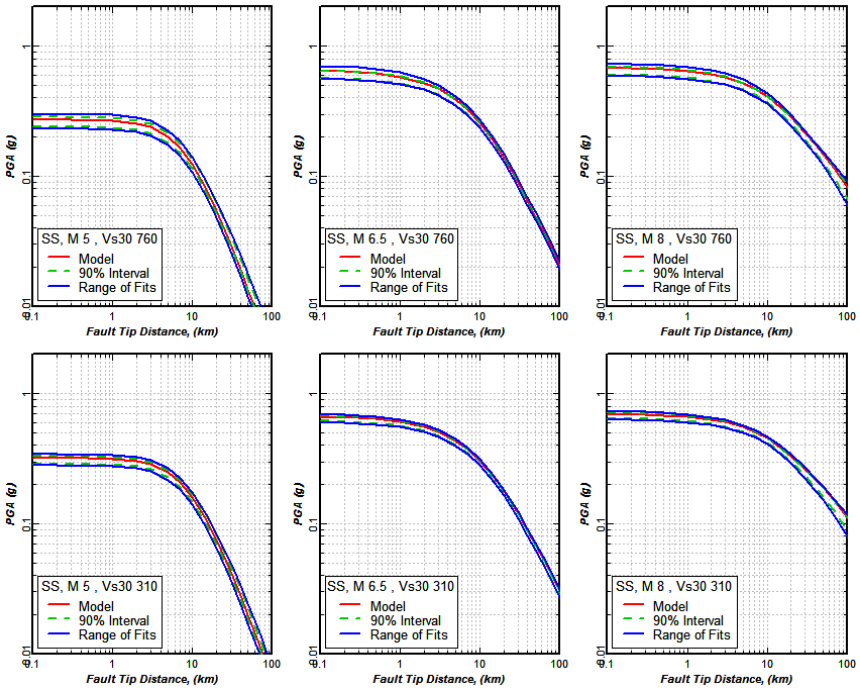

Fig. 6 Uncertainty in $\overline{\ln[PGA(m,r)]}$ for strike-slip earthquake ground motions due to uncertainty in predictor variables.

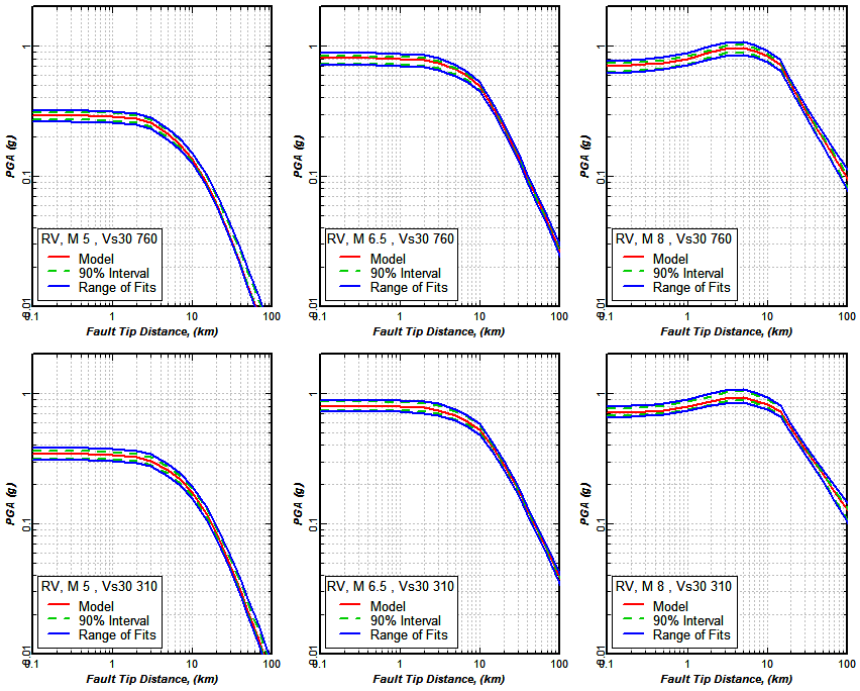

Fig. 7 Uncertainty in $\overline{\ln[PGA(m,r)]}$ for reverse earthquake ground motions due to uncertainty in predictor variables.

Suggested Uncertainty Model(s)

The uncertainties presented above on Figures 2 through 5, combined with the uncertainty resulting from predictor variable uncertainty shown on Figures 6 and 7, provide an estimate of the uncertainty in $\overline{\ln[PGA(m,r)]}$ for the C&Y model. This can be parameterized as a set of (three) alternative median models. Similar calculations can be done for each of the other models, leading to 3×5 ground motion estimation equations. Alternatively, a combined uncertainty across all models could be developed and a reduced number of relationships developed to represent that uncertainty.

REFERENCES

Efron, B., and R.J. Tibshirani, 1993, *An Introduction to the Bootstrap*, Monographs on Statistics and Applied Probability 57, Chapman Hall, 436 p.

Appendix H: Full Set of Model Coefficients

Table H.1 Period-independent fixed-effect coefficients for model of ln(y_{ref})—Eq. (3.12a).

c_2	c_3	c_4	c_{4a}	c_{RB}	c_{HM}	$c_{\gamma 3}$
1.06	3.45	-2.1	-0.5	50	3	4

Table H.2 Period-dependent fixed-effect coefficients of model for ln(y_{ref})—Eq. (3.12a)[1].

Spectral Period (sec)	Raw c_1	c_1	c_{1a}	c_{1b}	c_n	c_M	c_5	c_6	c_7	c_{7a}	c_9	c_{9a}	c_{10}	$c_{\gamma 1}$	$c_{\gamma 2}$
Pga	-1.2687	-1.2687	0.1	-0.2550	2.996	4.1840	6.1600	0.4893	0.0512	0.0860	0.7900	1.5005	-0.3218	-0.00804	-0.00785
Pgv	2.2884	2.2884	0.1094	-0.0626	1.648	4.2979	5.1700	0.4407	0.0207	0.0437	0.3079	2.6690	-0.1166	-0.00275	-0.00625
0.01	-1.2687	-1.2687	0.1	-0.2550	2.996	4.1840	6.1600	0.4893	0.0512	0.0860	0.7900	1.5005	-0.3218	-0.00804	-0.00785
0.02	-1.2480	-1.2515	0.1	-0.2550	3.292	4.1879	6.1580	0.4892	0.0512	0.0860	0.8129	1.5028	-0.3323	-0.00811	-0.00792
0.022	-1.2337	-1.2381	0.1	-0.2550	3.352	4.1828	6.1580	0.4892	0.0512	0.0860	0.8188	1.5035	-0.3339	-0.00816	-0.00796
0.025	-1.2131	-1.2164	0.1	-0.2550	3.429	4.1734	6.1570	0.4891	0.0512	0.0860	0.8280	1.5046	-0.3361	-0.00823	-0.00804
0.029	-1.1805	-1.1842	0.1	-0.2550	3.501	4.1593	6.1558	0.4891	0.0511	0.0860	0.8407	1.5067	-0.3388	-0.00835	-0.00815
0.03	-1.1715	-1.1744	0.1	-0.2550	3.514	4.1556	6.1550	0.4890	0.0511	0.0860	0.8439	1.5071	-0.3394	-0.00839	-0.00819
0.032	-1.1524	-1.1545	0.1	-0.2550	3.533	4.1485	6.1545	0.4890	0.0511	0.0860	0.8502	1.5082	-0.3406	-0.00845	-0.00826
0.035	-1.1225	-1.1233	0.1	-0.2550	3.551	4.1382	6.1530	0.4889	0.0510	0.0860	0.8594	1.5104	-0.3424	-0.00856	-0.00836
0.036	-1.1118	-1.1119	0.1	-0.2550	3.555	4.1351	6.1530	0.4889	0.0509	0.0860	0.8624	1.5110	-0.3430	-0.00860	-0.00840
0.04	-1.0661	-1.0671	0.1	-0.2550	3.563	4.1226	6.1508	0.4888	0.0508	0.0860	0.8740	1.5138	-0.3453	-0.00875	-0.00855
0.042	-1.0410	-1.0431	0.1	-0.2550	3.563	4.1174	6.1497	0.4887	0.0507	0.0860	0.8795	1.5157	-0.3463	-0.00883	-0.00862
0.044	-1.0157	-1.0188	0.1	-0.2550	3.561	4.1123	6.1487	0.4887	0.0506	0.0860	0.8848	1.5177	-0.3473	-0.00891	-0.00870
0.045	-1.0036	-1.0066	0.1	-0.2550	3.559	4.1104	6.1477	0.4886	0.0506	0.0860	0.8874	1.5186	-0.3478	-0.00895	-0.00873
0.046	-0.9917	-0.9943	0.1	-0.2550	3.557	4.1084	6.1470	0.4886	0.0505	0.0860	0.8899	1.5195	-0.3483	-0.00898	-0.00877
0.048	-0.9681	-0.9702	0.1	-0.2550	3.553	4.1038	6.1459	0.4885	0.0505	0.0860	0.8949	1.5214	-0.3493	-0.00905	-0.00884
0.05	-0.9457	-0.9464	0.1	-0.2550	3.547	4.1011	6.1441	0.4884	0.0504	0.0860	0.8996	1.5230	-0.3502	-0.00912	-0.00891
0.055	-0.8832	-0.8895	0.1	-0.2550	3.531	4.0940	6.1409	0.4883	0.0502	0.0860	0.9105	1.5297	-0.3522	-0.00929	-0.00907
0.06	-0.8265	-0.8361	0.1	-0.2550	3.513	4.0892	6.1362	0.4880	0.0500	0.0860	0.9204	1.5359	-0.3540	-0.00943	-0.00921
0.065	-0.7731	-0.7873	0.1	-0.2547	3.493	4.0867	6.1314	0.4878	0.0499	0.0860	0.9292	1.5428	-0.3555	-0.00956	-0.00934
0.067	-0.7566	-0.7694	0.1	-0.2540	3.484	4.0860	6.1294	0.4876	0.0498	0.0860	0.9325	1.5464	-0.3561	-0.00960	-0.00938
0.07	-0.7332	-0.7440	0.1	-0.2540	3.471	4.0860	6.1260	0.4875	0.0497	0.0860	0.9371	1.5516	-0.3568	-0.00966	-0.00943
0.075	-0.6912	-0.7051	0.1	-0.2540	3.448	4.0860	6.1200	0.4872	0.0495	0.0860	0.9442	1.5597	-0.3579	-0.00973	-0.00950

Table H.2—*Continued*

Spectral Period (sec)	Raw c_1	c_1	c_{1a}	c_{1b}	c_n	c_M	c_5	c_6	c_7	c_{7a}	c_9	c_{9a}	c_{10}	$c_{\gamma 1}$	$c_{\gamma 2}$
0.08	-0.6600	-0.6708	0.1	-0.2540	3.423	4.0873	6.1144	0.4869	0.0494	0.0860	0.9505	1.5678	-0.3587	-0.00978	-0.00955
0.085	-0.6302	-0.6409	0.1	-0.2540	3.397	4.0899	6.1072	0.4865	0.0492	0.0860	0.9559	1.5792	-0.3594	-0.00981	-0.00958
0.09	-0.6027	-0.6151	0.1	-0.2540	3.369	4.0938	6.1007	0.4862	0.0491	0.0860	0.9606	1.5901	-0.3598	-0.00981	-0.00958
0.095	-0.5799	-0.5931	0.1	-0.2530	3.341	4.0985	6.0929	0.4858	0.0490	0.0860	0.9645	1.6005	-0.3602	-0.00979	-0.00956
0.1	-0.5612	-0.5747	0.1	-0.2530	3.312	4.1030	6.0850	0.4854	0.0489	0.0860	0.9677	1.6104	-0.3604	-0.00975	-0.00952
0.11	-0.5363	-0.5453	0.1	-0.2529	3.255	4.1144	6.0683	0.4846	0.0486	0.0860	0.9718	1.6384	-0.3603	-0.00963	-0.00940
0.12	-0.5125	-0.5276	0.1	-0.2520	3.199	4.1277	6.0494	0.4837	0.0484	0.0860	0.9733	1.6645	-0.3599	-0.00946	-0.00924
0.13	-0.5029	-0.5200	0.1	-0.2510	3.145	4.1416	6.0296	0.4828	0.0482	0.0860	0.9725	1.6927	-0.3591	-0.00927	-0.00905
0.133	-0.5017	-0.5203	0.1	-0.2510	3.129	4.1459	6.0237	0.4825	0.0482	0.0860	0.9719	1.7023	-0.3587	-0.00921	-0.00899
0.14	-0.5079	-0.5227	0.1	-0.2504	3.093	4.1565	6.0087	0.4818	0.0481	0.0860	0.9699	1.7246	-0.3579	-0.00905	-0.00884
0.15	-0.5180	-0.5309	0.1	-0.2500	3.044	4.1717	5.9871	0.4808	0.0479	0.0860	0.9660	1.7549	-0.3565	-0.00883	-0.00862
0.16	-0.5324	-0.5447	0.1	-0.2490	2.997	4.1871	5.9647	0.4797	0.0477	0.0860	0.9609	1.7848	-0.3548	-0.00861	-0.00841
0.17	-0.5486	-0.5630	0.1	-0.2480	2.952	4.2023	5.9416	0.4787	0.0476	0.0860	0.9549	1.8194	-0.3530	-0.00840	-0.00820
0.18	-0.5734	-0.5847	0.1	-0.2470	2.910	4.2172	5.9177	0.4776	0.0474	0.0860	0.9482	1.8528	-0.3510	-0.00818	-0.00799
0.19	-0.5970	-0.6090	0.1	-0.2460	2.870	4.2323	5.8942	0.4765	0.0473	0.0860	0.9410	1.8848	-0.3490	-0.00798	-0.00779
0.2	-0.6229	-0.6352	0.1	-0.2449	2.831	4.2476	5.8699	0.4755	0.0471	0.0860	0.9334	1.9157	-0.3470	-0.00778	-0.00759
0.22	-0.6849	-0.6893	0.1	-0.2428	2.760	4.2759	5.8231	0.4735	0.0468	0.0860	0.9179	1.9806	-0.3431	-0.00740	-0.00722
0.24	-0.7452	-0.7465	0.1	-0.2400	2.692	4.3042	5.7767	0.4715	0.0466	0.0860	0.9023	2.0415	-0.3395	-0.00704	-0.00688
0.25	-0.7720	-0.7766	0.1	-0.2382	2.658	4.3184	5.7547	0.4706	0.0464	0.0860	0.8946	2.0709	-0.3379	-0.00688	-0.00671
0.26	-0.7983	-0.8068	0.1	-0.2370	2.626	4.3320	5.7335	0.4698	0.0463	0.0860	0.8871	2.0982	-0.3364	-0.00672	-0.00656
0.28	-0.8598	-0.8666	0.0999	-0.2343	2.564	4.3584	5.6917	0.4680	0.0460	0.0860	0.8726	2.1505	-0.3336	-0.00641	-0.00626
0.29	-0.8916	-0.8972	0.0999	-0.2328	2.533	4.3712	5.6719	0.4673	0.0459	0.0860	0.8657	2.1758	-0.3324	-0.00626	-0.00612
0.3	-0.9216	-0.9278	0.0999	-0.2313	2.505	4.3844	5.6527	0.4665	0.0458	0.0860	0.8590	2.2005	-0.3314	-0.00612	-0.00598
0.32	-0.9819	-0.9877	0.0999	-0.2275	2.449	4.4086	5.6163	0.4651	0.0455	0.0860	0.8462	2.2468	-0.3295	-0.00586	-0.00572

Table H.2—*Continued*

Spectral Period (sec)	Raw c_1	c_1	c_{1a}	c_{1b}	c_n	c_M	c_5	c_6	c_7	c_{7a}	c_9	c_{9a}	c_{10}	$c_{\gamma 1}$	$c_{\gamma 2}$
0.34	-1.0464	-1.0469	0.0999	-0.2247	2.397	4.4323	5.5832	0.4638	0.0453	0.0850	0.8342	2.2846	-0.3281	-0.00561	-0.00548
0.35	-1.0748	-1.0764	0.0998	-0.2226	2.372	4.4441	5.5681	0.4632	0.0452	0.0850	0.8284	2.3030	-0.3276	-0.00550	-0.00537
0.36	-1.1044	-1.1055	0.0998	-0.2214	2.348	4.4557	5.5528	0.4626	0.0450	0.0850	0.8228	2.3210	-0.3271	-0.00539	-0.00526
0.38	-1.1586	-1.1623	0.0998	-0.2180	2.303	4.4768	5.5252	0.4616	0.0448	0.0850	0.8121	2.3558	-0.3264	-0.00518	-0.00505
0.4	-1.2124	-1.2176	0.0997	-0.2146	2.261	4.4979	5.4997	0.4607	0.0445	0.0850	0.8019	2.3886	-0.3256	-0.00498	-0.00486
0.42	-1.2663	-1.2714	0.0996	-0.2107	2.222	4.5172	5.4764	0.4598	0.0442	0.0847	0.7922	2.4126	-0.3248	-0.00480	-0.00469
0.44	-1.3196	-1.3235	0.0995	-0.2073	2.185	4.5361	5.4555	0.4591	0.0439	0.0840	0.7830	2.4356	-0.3237	-0.00463	-0.00452
0.45	-1.3452	-1.3490	0.0995	-0.2054	2.167	4.5452	5.4458	0.4587	0.0437	0.0840	0.7786	2.4468	-0.3231	-0.00455	-0.00445
0.46	-1.3717	-1.3740	0.0994	-0.2037	2.150	4.5545	5.4362	0.4583	0.0436	0.0840	0.7743	2.4579	-0.3225	-0.00448	-0.00437
0.48	-1.4217	-1.4226	0.0993	-0.2008	2.118	4.5712	5.4189	0.4578	0.0432	0.0830	0.7659	2.4794	-0.3208	-0.00433	-0.00423
0.5	-1.4672	-1.4695	0.0991	-0.1972	2.087	4.5881	5.4029	0.4571	0.0429	0.0830	0.7578	2.5000	-0.3189	-0.00420	-0.00410
0.55	-1.5708	-1.5790	0.0986	-0.1889	2.017	4.6273	5.3697	0.4560	0.0421	0.0810	0.7391	2.5337	-0.3123	-0.00390	-0.00381
0.6	-1.6792	-1.6786	0.0978	-0.1814	1.957	4.6632	5.3431	0.4550	0.0412	0.0792	0.7221	2.5646	-0.3036	-0.00365	-0.00357
0.65	-1.7723	-1.7691	0.0968	-0.1744	1.904	4.6959	5.3213	0.4542	0.0404	0.0760	0.7065	2.5893	-0.2934	-0.00344	-0.00335
0.667	-1.7990	-1.7979	0.0963	-0.1722	1.887	4.7071	5.3149	0.4540	0.0401	0.0756	0.7015	2.5953	-0.2897	-0.00337	-0.00329
0.7	-1.8520	-1.8516	0.0954	-0.1680	1.855	4.7276	5.3045	0.4536	0.0395	0.0730	0.6922	2.6065	-0.2821	-0.00325	-0.00317
0.75	-1.9238	-1.9278	0.0936	-0.1620	1.812	4.7571	5.2900	0.4531	0.0387	0.0690	0.6788	2.6224	-0.2702	-0.00308	-0.00301
0.8	-1.9982	-1.9988	0.0914	-0.1564	1.773	4.7851	5.2788	0.4528	0.0379	0.0647	0.6662	2.6366	-0.2577	-0.00293	-0.00286
0.85	-2.0275	-2.0655	0.0887	-0.1511	1.737	4.8114	5.2692	0.4524	0.0372	0.0601	0.6540	2.6456	-0.2449	-0.00280	-0.00273
0.9	-2.0856	-2.1285	0.0853	-0.1472	1.704	4.8362	5.2607	0.4522	0.0364	0.0552	0.6423	2.6538	-0.2319	-0.00267	-0.00261
0.95	-2.1510	-2.1883	0.0813	-0.1432	1.675	4.8597	5.2537	0.4519	0.0357	0.0505	0.6308	2.6615	-0.2189	-0.00256	-0.00250
1	-2.2133	-2.2453	0.0766	-0.1400	1.648	4.8820	5.2480	0.4517	0.0350	0.0450	0.6196	2.6690	-0.2059	-0.00246	-0.00241
1.1	-2.3182	-2.3521	0.0651	-0.1337	1.605	4.9245	5.2387	0.4514	0.0336	0.0357	0.5975	2.6773	-0.1801	-0.00229	-0.00223
1.2	-2.4031	-2.4519	0.0512	-0.1282	1.572	4.9641	5.2321	0.4511	0.0322	0.0282	0.5756	2.6851	-0.1550	-0.00214	-0.00209

Table H.2—*Continued*

Spectral Period (sec)	Raw c_1	c_1	c_{1a}	c_{1b}	c_n	c_M	c_5	c_6	c_7	c_{7a}	c_9	c_{9a}	c_{10}	$c_{\gamma 1}$	$c_{\gamma 2}$
1.3	-2.4982	-2.5474	0.0355	-0.1246	1.546	5.0013	5.2266	0.4510	0.0308	0.0216	0.5538	2.6910	-0.1308	-0.00201	-0.00196
1.4	-2.5798	-2.6401	0.0188	-0.1214	1.526	5.0367	5.2224	0.4508	0.0294	0.0168	0.5320	2.6947	-0.1075	-0.00190	-0.00185
1.5	-2.6740	-2.7307	0.0022	-0.1184	1.511	5.0697	5.2194	0.4507	0.0280	0.0134	0.5101	2.6985	-0.0852	-0.00180	-0.00176
1.6	-2.7681	-2.8189	-0.0135	-0.1166	1.498	5.1019	5.2166	0.4506	0.0266	0.0100	0.4877	2.7015	-0.0637	-0.00172	-0.00168
1.7	-2.8081	-2.9044	-0.0275	-0.1140	1.489	5.1325	5.2140	0.4505	0.0253	0.0080	0.4649	2.7034	-0.0429	-0.00164	-0.00160
1.8	-2.8932	-2.9868	-0.0399	-0.1125	1.481	5.1623	5.2125	0.4504	0.0240	0.0065	0.4412	2.7053	-0.0227	-0.00158	-0.00154
1.9	-2.9805	-3.0659	-0.0504	-0.1111	1.474	5.1905	5.2111	0.4504	0.0227	0.0050	0.4169	2.7069	-0.0031	-0.00152	-0.00148
2	-3.0635	-3.1413	-0.0591	-0.1100	1.470	5.2173	5.2099	0.4504	0.0213	0.0040	0.3917	2.7085	0	-0.00147	-0.00143
2.2	-3.1823	-3.2815	-0.0722	-0.1080	1.463	5.2691	5.2080	0.4503	0.0188	0.0028	0.3390	2.7101	0	-0.00138	-0.00135
2.4	-3.3153	-3.4096	-0.0808	-0.1070	1.458	5.3173	5.2060	0.4502	0.0165	0.0020	0.2833	2.7118	0	-0.00131	-0.00128
2.5	-3.3717	-3.4698	-0.0840	-0.1060	1.456	5.3393	5.2060	0.4502	0.0154	0.0012	0.2546	2.7123	0	-0.00128	-0.00125
2.6	-3.4236	-3.5277	-0.0866	-0.1060	1.456	5.3610	5.2050	0.4502	0.0144	0.0010	0.2262	2.7129	0	-0.00126	-0.00123
2.8	-3.4997	-3.6378	-0.0905	-0.1050	1.455	5.4013	5.2043	0.4502	0.0124	0.0010	0.1722	2.7137	0	-0.00121	-0.00118
3	-3.6126	-3.7413	-0.0931	-0.1040	1.456	5.4385	5.2040	0.4501	0.0106	0.0010	0.1244	2.7145	0	-0.00117	-0.00115
3.2	-3.7158	-3.8390	-0.0949	-0.1040	1.457	5.4737	5.2030	0.4501	0.0090	0.0005	0.0846	2.7150	0	-0.00114	-0.00112
3.4	-3.7921	-3.9314	-0.0962	-0.1030	1.458	5.5069	5.2030	0.4501	0.0076	0	0.0538	2.7153	0	-0.00112	-0.00109
3.5	-3.8241	-3.9759	-0.0967	-0.1030	1.459	5.5229	5.2030	0.4501	0.0069	0	0.0420	2.7156	0	-0.00111	-0.00108
3.6	-3.8682	-4.0192	-0.0971	-0.1030	1.461	5.5382	5.2024	0.4501	0.0063	0	0.0322	2.7158	0	-0.00110	-0.00107
3.8	-3.9599	-4.1025	-0.0978	-0.1020	1.463	5.5687	5.2020	0.4501	0.0052	0	0.0177	2.7161	0	-0.00108	-0.00105
4	-4.0481	-4.1814	-0.0982	-0.1020	1.465	5.5977	5.2020	0.4501	0.0041	0	0.0086	2.7164	0	-0.00107	-0.00104
4.2	-3.9518	-4.2560	-0.0986	-0.1020	1.468	5.6252	5.2020	0.4501	0.0033	0	0.0031	2.7167	0	-0.00105	-0.00103
4.4	-4.0160	-4.3268	-0.0989	-0.1020	1.470	5.6518	5.2017	0.4501	0.0025	0	0.0004	2.7167	0	-0.00104	-0.00102
4.6	-4.0841	-4.3939	-0.0991	-0.1020	1.473	5.6776	5.2010	0.4501	0.0019	0	0	2.7169	0	-0.00103	-0.00101
4.8	-4.1450	-4.4577	-0.0993	-0.1010	1.475	5.7027	5.2010	0.4500	0.0014	0	0	2.7169	0	-0.00102	-0.00100

Table H.2—*Continued*

Spectral Period (sec)	Raw c_1	c_1	c_{1a}	c_{1b}	c_n	c_M	c_5	c_6	c_7	c_{7a}	c_9	c_{9a}	c_{10}	$c_{\gamma 1}$	$c_{\gamma 2}$
5	-4.2100	-4.5187	-0.0994	-0.1010	1.478	5.7276	5.2010	0.4500	0.0010	0	0	2.7172	0	-0.00102	-0.00099
5.5	-4.3352	-4.6606	-0.0996	-0.1010	1.483	5.7855	5.2010	0.4500	0.0002	0	0	2.7175	0	-0.00100	-0.00098
6	-4.4778	-4.7894	-0.0998	-0.1010	1.488	5.8404	5.2010	0.4500	0	0	0	2.7175	0	-0.00099	-0.00096
6.5	-4.5752	-4.9079	-0.0998	-0.1010	1.492	5.8924	5.2010	0.4500	0	0	0	2.7177	0	-0.00098	-0.00095
7	-4.6771	-5.0183	-0.0999	-0.1010	1.496	5.9422	5.2010	0.4500	0	0	0	2.7177	0	-0.00097	-0.00095
7.5	-4.7827	-5.1224	-0.0999	-0.1010	1.498	5.9891	5.2000	0.4500	0	0	0	2.7177	0	-0.00096	-0.00094
8	-4.8795	-5.2215	-0.0999	-0.1000	1.499	6.0339	5.2000	0.4500	0	0	0	2.7180	0	-0.00096	-0.00093
8.5	-4.8221	-5.3166	-0.1000	-0.1000	1.500	6.0770	5.2000	0.4500	0	0	0	2.7180	0	-0.00095	-0.00093
9	-4.9113	-5.4082	-0.1000	-0.1000	1.501	6.1172	5.2000	0.4500	0	0	0	2.7180	0	-0.00095	-0.00092
9.5	-5.0032	-5.4968	-0.1000	-0.1000	1.501	6.1561	5.2000	0.4500	0	0	0	2.7180	0	-0.00094	-0.00092
10	-5.1102	-5.5872	-0.1000	-0.1000	1.502	6.1930	5.2000	0.4500	0	0	0	2.7180	0	-0.00094	-0.00091

[1]Units are g's for *pga* and *PSA* , and cm/sec for *pgv*

Table H.3 Fixed-effect coefficients of site response model for ln(y)—Eq. (3.12b).

Spectral Period (sec)	ϕ_1	ϕ_2	ϕ_3	ϕ_4	ϕ_5	ϕ_6	ϕ_7	ϕ_8
pga	-0.4417	-0.1417	-0.007010	0.102151	0.2289	0.014996	580.0	0.0700
pgv	-0.7861	-0.0699	-0.008444	5.41000	0.2899	0.006718	459.0	0.1138
0.01	-0.4417	-0.1417	-0.007010	0.102151	0.2289	0.014996	580.0	0.0700
0.02	-0.4340	-0.1364	-0.007279	0.108360	0.2289	0.014996	580.0	0.0699
0.022	-0.4313	-0.1361	-0.007301	0.110372	0.2289	0.014996	580.0	0.0699
0.025	-0.4267	-0.1365	-0.007364	0.113710	0.2289	0.014996	580.0	0.0700
0.029	-0.4196	-0.1392	-0.007378	0.118600	0.2289	0.014996	580.0	0.0700
0.03	-0.4177	-0.1403	-0.007354	0.119888	0.2289	0.014996	580.0	0.0701
0.032	-0.4139	-0.1430	-0.007281	0.122493	0.2289	0.014996	580.0	0.0701
0.035	-0.4082	-0.1482	-0.007162	0.126540	0.2289	0.014996	580.0	0.0702
0.036	-0.4064	-0.1502	-0.007129	0.127926	0.2289	0.014996	580.0	0.0702
0.04	-0.4000	-0.1591	-0.006977	0.133641	0.2289	0.014996	579.9	0.0702
0.042	-0.3973	-0.1641	-0.006878	0.136572	0.2289	0.014996	579.9	0.0702
0.044	-0.3949	-0.1694	-0.006765	0.139596	0.2290	0.014996	579.9	0.0702
0.045	-0.3939	-0.1721	-0.006710	0.141112	0.2290	0.014996	579.9	0.0702
0.046	-0.3930	-0.1748	-0.006656	0.142659	0.2290	0.014996	579.9	0.0702
0.048	-0.3914	-0.1804	-0.006556	0.145774	0.2290	0.014996	579.9	0.0702
0.05	-0.3903	-0.1862	-0.006467	0.148927	0.2290	0.014996	579.9	0.0701
0.055	-0.3892	-0.2008	-0.006279	0.157001	0.2290	0.014996	579.8	0.0700
0.06	-0.3903	-0.2153	-0.006117	0.165249	0.2290	0.014996	579.8	0.0698
0.065	-0.3934	-0.2291	-0.005970	0.173635	0.2291	0.014996	579.8	0.0696
0.067	-0.3951	-0.2344	-0.005914	0.177001	0.2291	0.014996	579.7	0.0694
0.07	-0.3981	-0.2420	-0.005835	0.182082	0.2291	0.014996	579.7	0.0692
0.075	-0.4040	-0.2538	-0.005734	0.190596	0.2292	0.014996	579.6	0.0686
0.08	-0.4108	-0.2644	-0.005670	0.199129	0.2293	0.014996	579.6	0.0679
0.085	-0.4182	-0.2739	-0.005632	0.207505	0.2294	0.014996	579.5	0.0671
0.09	-0.4261	-0.2819	-0.005607	0.215628	0.2295	0.014996	579.4	0.0662
0.095	-0.4341	-0.2887	-0.005597	0.223398	0.2296	0.014996	579.3	0.0654
0.1	-0.4423	-0.2943	-0.005604	0.230662	0.2297	0.014996	579.2	0.0646
0.11	-0.4585	-0.3025	-0.005644	0.243315	0.2302	0.014994	578.8	0.0635
0.12	-0.4743	-0.3077	-0.005696	0.253169	0.2305	0.014994	578.6	0.0625
0.13	-0.4892	-0.3106	-0.005744	0.260175	0.2311	0.014993	578.2	0.0602
0.133	-0.4935	-0.3111	-0.005758	0.261767	0.2313	0.014993	578.0	0.0592
0.14	-0.5032	-0.3118	-0.005794	0.264504	0.2319	0.014991	577.7	0.0560
0.15	-0.5162	-0.3113	-0.005845	0.266468	0.2326	0.014988	577.2	0.0494
0.16	-0.5283	-0.3093	-0.005901	0.266468	0.2334	0.014987	576.7	0.0407

Table H.3—*Continued*

Spectral Period (sec)	ϕ_1	ϕ_2	ϕ_3	ϕ_4	ϕ_5	ϕ_6	ϕ_7	ϕ_8
0.17	-0.5396	-0.3062	-0.005959	0.265060	0.2348	0.014981	576.0	0.0306
0.18	-0.5502	-0.3022	-0.006019	0.262501	0.2361	0.014975	575.2	0.0199
0.19	-0.5602	-0.2976	-0.006080	0.259163	0.2374	0.014970	574.6	0.0089
0.2	-0.5697	-0.2927	-0.006141	0.255253	0.2386	0.014964	573.9	-0.0019
0.22	-0.5873	-0.2823	-0.006262	0.246252	0.2433	0.014928	571.6	-0.0223
0.24	-0.6034	-0.2716	-0.006381	0.236525	0.2477	0.014895	569.5	-0.0401
0.25	-0.6109	-0.2662	-0.006439	0.231541	0.2497	0.014881	568.5	-0.0479
0.26	-0.6182	-0.2609	-0.006495	0.226570	0.2533	0.014832	566.9	-0.0548
0.28	-0.6319	-0.2505	-0.006604	0.216796	0.2606	0.014731	563.6	-0.0665
0.29	-0.6383	-0.2455	-0.006655	0.211993	0.2641	0.014684	562.0	-0.0713
0.3	-0.6444	-0.2405	-0.006704	0.207277	0.2674	0.014639	560.5	-0.0756
0.32	-0.6559	-0.2310	-0.006795	0.198077	0.2746	0.014513	557.3	-0.0825
0.34	-0.6665	-0.2220	-0.006882	0.189304	0.2847	0.014239	552.6	-0.0875
0.35	-0.6715	-0.2177	-0.006923	0.185074	0.2895	0.014110	550.4	-0.0895
0.36	-0.6762	-0.2135	-0.006965	0.180920	0.2942	0.013985	548.3	-0.0912
0.38	-0.6850	-0.2053	-0.007047	0.172976	0.3032	0.013747	544.1	-0.0939
0.4	-0.6931	-0.1975	-0.007125	0.165464	0.3120	0.013493	540.0	-0.0960
0.42	-0.7005	-0.1901	-0.007194	0.158358	0.3227	0.012938	534.0	-0.0975
0.44	-0.7072	-0.1830	-0.007259	0.151662	0.3329	0.012429	528.4	-0.0987
0.45	-0.7104	-0.1795	-0.007290	0.148466	0.3378	0.012190	525.7	-0.0991
0.46	-0.7135	-0.1762	-0.007320	0.145352	0.3427	0.011962	523.0	-0.0994
0.48	-0.7193	-0.1696	-0.007378	0.139415	0.3520	0.011532	517.8	-0.0998
0.5	-0.7246	-0.1633	-0.007435	0.133828	0.3610	0.011133	512.9	-0.0998
0.55	-0.7365	-0.1487	-0.007579	0.121226	0.3810	0.009769	497.1	-0.0983
0.6	-0.7468	-0.1353	-0.007720	0.110339	0.3993	0.008660	482.7	-0.0948
0.65	-0.7557	-0.1232	-0.007863	0.100842	0.4142	0.007829	468.7	-0.0896
0.667	-0.7585	-0.1194	-0.007911	0.097891	0.4180	0.007620	463.9	-0.0876
0.7	-0.7636	-0.1124	-0.008001	0.092504	0.4252	0.007244	454.8	-0.0834
0.75	-0.7708	-0.1028	-0.008120	0.085153	0.4353	0.006739	441.9	-0.0765
0.8	-0.7773	-0.0943	-0.008223	0.078622	0.4444	0.006325	429.9	-0.0693
0.85	-0.7833	-0.0869	-0.008313	0.072788	0.4494	0.006163	419.5	-0.0620
0.9	-0.7888	-0.0805	-0.008381	0.067563	0.4542	0.006014	409.8	-0.0549
0.95	-0.7941	-0.0748	-0.008423	0.062850	0.4587	0.005876	400.5	-0.0479
1	-0.7990	-0.0699	-0.008444	0.058595	0.4629	0.005749	391.8	-0.0412
1.1	-0.8082	-0.0617	-0.008500	0.051206	0.4668	0.005678	379.6	-0.0285

Table H.3—*Continued*

Spectral Period (sec)	ϕ_1	ϕ_2	ϕ_3	ϕ_4	ϕ_5	ϕ_6	ϕ_7	ϕ_8
1.2	-0.8165	-0.0552	-0.008478	0.045054	0.4703	0.005613	368.5	-0.0167
1.3	-0.8243	-0.0501	-0.008307	0.039879	0.4729	0.005573	359.8	-0.0057
1.4	-0.8315	-0.0459	-0.008042	0.035504	0.4743	0.005558	353.7	0.0045
1.5	-0.8382	-0.0425	-0.007707	0.031787	0.4756	0.005544	348.1	0.0140
1.6	-0.8445	-0.0395	-0.007317	0.028613	0.4767	0.005533	343.1	0.0229
1.7	-0.8504	-0.0369	-0.006862	0.025890	0.4772	0.005529	340.2	0.0313
1.8	-0.8560	-0.0346	-0.006265	0.023537	0.4777	0.005527	337.5	0.0393
1.9	-0.8613	-0.0323	-0.005541	0.021496	0.4781	0.005524	334.9	0.0469
2	-0.8663	-0.0302	-0.004792	0.019716	0.4785	0.005521	332.5	0.0544
2.2	-0.8755	-0.0262	-0.003555	0.016771	0.4789	0.005519	330.0	0.0687
2.4	-0.8836	-0.0225	-0.002764	0.014434	0.4792	0.005518	327.8	0.0826
2.5	-0.8874	-0.0207	-0.002497	0.013436	0.4793	0.005518	326.7	0.0895
2.6	-0.8909	-0.0190	-0.002292	0.012534	0.4794	0.005518	326.1	0.0963
2.8	-0.8974	-0.0159	-0.002007	0.010962	0.4795	0.005517	325.1	0.1098
3	-0.9032	-0.0129	-0.001828	0.009643	0.4796	0.005517	324.1	0.1232
3.2	-0.9083	-0.0102	-0.001713	0.008521	0.4797	0.005517	323.3	0.1366
3.4	-0.9130	-0.0077	-0.001636	0.007561	0.4798	0.005517	322.9	0.1498
3.5	-0.9151	-0.0066	-0.001608	0.007130	0.4798	0.005517	322.7	0.1562
3.6	-0.9170	-0.0055	-0.001585	0.006730	0.4798	0.005517	322.5	0.1625
3.8	-0.9205	-0.0036	-0.001549	0.006008	0.4798	0.005517	322.1	0.1746
4	-0.9231	-0.0016	-0.001523	0.005379	0.4799	0.005517	321.7	0.1859
4.2	-0.9249	0	-0.001501	0.004830	0.4799	0.005517	321.6	0.1964
4.4	-0.9257	0	-0.001483	0.004349	0.4799	0.005517	321.4	0.2060
4.6	-0.9255	0	-0.001467	0.003925	0.4799	0.005517	321.2	0.2147
4.8	-0.9243	0	-0.001453	0.003553	0.4799	0.005517	321.1	0.2225
5	-0.9222	0	-0.001440	0.003223	0.4799	0.005517	320.9	0.2295
5.5	-0.9129	0	-0.001416	0.002551	0.4800	0.005517	320.7	0.2435
6	-0.8982	0	-0.001397	0.002047	0.4800	0.005517	320.6	0.2532
6.5	-0.8791	0	-0.001384	0.001662	0.4800	0.005517	320.4	0.2595
7	-0.8572	0	-0.001375	0.001366	0.4800	0.005517	320.4	0.2635
7.5	-0.8346	0	-0.001369	0.001134	0.4800	0.005517	320.3	0.2660
8	-0.8126	0	-0.001364	0.000952	0.4800	0.005517	320.2	0.2675
8.5	-0.7914	0	-0.001362	0.000806	0.4800	0.005517	320.2	0.2683
9	-0.7711	0	-0.001360	0.000689	0.4800	0.005517	320.2	0.2686
9.5	-0.7517	0	-0.001360	0.000593	0.4800	0.005517	320.1	0.2685
10	-0.7332	0	-0.001361	0.000515	0.4800	0.005517	320.1	0.2682

Table H.4 Coefficients of variance model—Eqs. (5.1) and (5.2).

Spectral Period (sec)	τ_1	τ_2	σ_1	σ_2	σ_3	σ_4
pga	0.3437	0.2637	0.4458	0.3459	0.8	0.0663
pgv	0.2539	0.2381	0.4496	0.3554	0.7504	0.0133
0.01	0.3437	0.2637	0.4458	0.3459	0.8	0.0663
0.02	0.3471	0.2671	0.4458	0.3459	0.8	0.0663
0.022	0.3505	0.2705	0.4476	0.3477	0.8	0.0663
0.025	0.3538	0.2738	0.4500	0.3502	0.8	0.0663
0.029	0.3571	0.2771	0.4529	0.3530	0.8	0.0663
0.03	0.3603	0.2803	0.4535	0.3537	0.8	0.0663
0.032	0.3633	0.2833	0.4547	0.3549	0.8	0.0663
0.035	0.3663	0.2863	0.4564	0.3566	0.8	0.0663
0.036	0.3691	0.2891	0.4569	0.3572	0.8	0.0663
0.04	0.3718	0.2918	0.4589	0.3592	0.8	0.0663
0.042	0.3744	0.2944	0.4598	0.3602	0.8	0.0663
0.044	0.3768	0.2968	0.4607	0.3611	0.8	0.0663
0.045	0.3791	0.2991	0.4611	0.3615	0.8	0.0663
0.046	0.3811	0.3011	0.4615	0.3619	0.8	0.0663
0.048	0.3831	0.3031	0.4623	0.3627	0.8	0.0663
0.05	0.3848	0.3048	0.4630	0.3635	0.8	0.0663
0.055	0.3863	0.3063	0.4647	0.3654	0.8	0.0663
0.06	0.3876	0.3076	0.4663	0.3670	0.8	0.0663
0.065	0.3877	0.3095	0.4677	0.3686	0.8	0.0663
0.067	0.3881	0.3106	0.4682	0.3692	0.8	0.0663
0.07	0.3883	0.3118	0.4690	0.3700	0.8	0.0663
0.075	0.3878	0.3129	0.4702	0.3713	0.8	0.0663
0.08	0.3872	0.3138	0.4712	0.3726	0.8	0.0663
0.085	0.3865	0.3145	0.4722	0.3738	0.8	0.0663
0.09	0.3856	0.3149	0.4731	0.3749	0.8	0.0663
0.095	0.3846	0.3151	0.4740	0.3759	0.8	0.0663
0.1	0.3835	0.3152	0.4747	0.3769	0.8	0.0663
0.11	0.3816	0.3154	0.4761	0.3787	0.8	0.0660
0.12	0.3795	0.3153	0.4773	0.3804	0.8	0.0652
0.13	0.3775	0.3151	0.4782	0.3819	0.8	0.0640
0.133	0.3761	0.3143	0.4785	0.3824	0.8	0.0636
0.14	0.3742	0.3135	0.4791	0.3834	0.8	0.0627
0.15	0.3719	0.3128	0.4798	0.3847	0.8	0.0612
0.16	0.3696	0.3120	0.4803	0.3859	0.8	0.0596

Table H.4—*Continued*

Spectral Period (sec)	τ_1	τ_2	σ_1	σ_2	σ_3	σ_4
0.17	0.3672	0.3110	0.4808	0.3871	0.8	0.0579
0.18	0.3649	0.3100	0.4811	0.3882	0.8	0.0563
0.19	0.3626	0.3089	0.4814	0.3893	0.8	0.0546
0.2	0.3601	0.3076	0.4816	0.3902	0.8	0.0530
0.22	0.3572	0.3068	0.4817	0.3921	0.7999	0.0499
0.24	0.3543	0.3060	0.4816	0.3938	0.7999	0.0470
0.25	0.3522	0.3047	0.4815	0.3946	0.7999	0.0457
0.26	0.3500	0.3034	0.4813	0.3953	0.7998	0.0444
0.28	0.3474	0.3026	0.4808	0.3967	0.7998	0.0420
0.29	0.3455	0.3015	0.4805	0.3974	0.7997	0.0408
0.3	0.3438	0.3005	0.4801	0.3981	0.7997	0.0398
0.32	0.3417	0.2999	0.4794	0.3993	0.7996	0.0377
0.34	0.3398	0.2993	0.4786	0.4005	0.7994	0.0359
0.35	0.3386	0.2988	0.4781	0.4010	0.7993	0.0350
0.36	0.3375	0.2983	0.4777	0.4016	0.7992	0.0342
0.38	0.3362	0.2983	0.4768	0.4026	0.7990	0.0326
0.4	0.3351	0.2984	0.4758	0.4036	0.7988	0.0312
0.42	0.3344	0.2987	0.4748	0.4046	0.7983	0.0299
0.44	0.3339	0.2993	0.4738	0.4054	0.7979	0.0287
0.45	0.3340	0.2999	0.4734	0.4059	0.7976	0.0281
0.46	0.3344	0.3008	0.4729	0.4063	0.7974	0.0275
0.48	0.3346	0.3021	0.4719	0.4071	0.7970	0.0265
0.5	0.3353	0.3036	0.4710	0.4079	0.7966	0.0255
0.55	0.3354	0.3060	0.4688	0.4098	0.7940	0.0234
0.6	0.3360	0.3085	0.4667	0.4114	0.7917	0.0215
0.65	0.3369	0.3113	0.4650	0.4130	0.7884	0.0200
0.667	0.3390	0.3139	0.4644	0.4135	0.7867	0.0195
0.7	0.3409	0.3169	0.4634	0.4144	0.7836	0.0186
0.75	0.3429	0.3205	0.4621	0.4157	0.7792	0.0175
0.8	0.3452	0.3243	0.4610	0.4170	0.7747	0.0164
0.85	0.3478	0.3283	0.4600	0.4181	0.7681	0.0155
0.9	0.3508	0.3326	0.4592	0.4192	0.7619	0.0147
0.95	0.3541	0.3371	0.4586	0.4203	0.7560	0.0140
1	0.3577	0.3419	0.4581	0.4213	0.7504	0.0133
1.1	0.3608	0.3472	0.4555	0.4213	0.7400	0.0122

Table H.4—*Continued*

Spectral Period (sec)	τ_1	τ_2	σ_1	σ_2	σ_3	σ_4
1.2	0.3644	0.3527	0.4535	0.4213	0.7304	0.0112
1.3	0.3682	0.3584	0.4518	0.4213	0.7230	0.0104
1.4	0.3725	0.3643	0.4505	0.4213	0.7182	0.0096
1.5	0.3769	0.3703	0.4493	0.4213	0.7136	0.0090
1.6	0.3816	0.3765	0.4484	0.4213	0.7097	0.0085
1.7	0.3865	0.3828	0.4476	0.4213	0.7080	0.0080
1.8	0.3916	0.3892	0.4469	0.4213	0.7064	0.0075
1.9	0.3968	0.3957	0.4463	0.4213	0.7049	0.0071
2	0.4023	0.4023	0.4459	0.4213	0.7035	0.0068
2.2	0.4085	0.4085	0.4451	0.4213	0.7025	0.0062
2.4	0.4149	0.4149	0.4444	0.4213	0.7017	0.0057
2.5	0.4212	0.4212	0.4442	0.4213	0.7012	0.0054
2.6	0.4277	0.4277	0.4440	0.4213	0.7011	0.0052
2.8	0.4341	0.4341	0.4436	0.4213	0.7008	0.0049
3	0.4406	0.4406	0.4433	0.4213	0.7006	0.0045
3.2	0.4470	0.4470	0.4430	0.4213	0.7004	0.0043
3.4	0.4534	0.4534	0.4428	0.4213	0.7003	0.0040
3.5	0.4598	0.4598	0.4427	0.4213	0.7003	0.0039
3.6	0.4661	0.4661	0.4426	0.4213	0.7002	0.0038
3.8	0.4723	0.4723	0.4425	0.4213	0.7002	0.0036
4	0.4784	0.4784	0.4424	0.4213	0.7001	0.0034
4.2	0.4845	0.4845	0.4423	0.4213	0.7001	0.0032
4.4	0.4904	0.4904	0.4422	0.4213	0.7001	0.0031
4.6	0.4962	0.4962	0.4421	0.4213	0.7001	0.0030
4.8	0.5019	0.5019	0.4420	0.4213	0.7001	0.0028
5	0.5074	0.5074	0.4420	0.4213	0.7	0.0027
5.5	0.5128	0.5128	0.4418	0.4213	0.7	0.0025
6	0.5181	0.5181	0.4417	0.4213	0.7	0.0023
6.5	0.5232	0.5232	0.4417	0.4213	0.7	0.0021
7	0.5281	0.5281	0.4416	0.4213	0.7	0.0019
7.5	0.5328	0.5328	0.4416	0.4213	0.7	0.0018
8	0.5374	0.5374	0.4415	0.4213	0.7	0.0017
8.5	0.5419	0.5419	0.4415	0.4213	0.7	0.0016
9	0.5461	0.5461	0.4415	0.4213	0.7	0.0015
9.5	0.5502	0.5502	0.4415	0.4213	0.7	0.0014
10	0.5542	0.5542	0.4414	0.4213	0.7	0.0014